Modélisation cinétique de la photo-thermo-oxydation du polypropylène

Alexandre Francois Heude

ParisTech
INSTITUT DES SCIENCES ET TECHNOLOGIES
PARIS INSTITUTE OF TECHNOLOGY

ARTS ET MÉTIERS ParisTech

2014-ENAM-0017

École doctorale n° 432 : Sciences des Métiers de l'Ingénieur

Doctorat ParisTech

T H È S E

pour obtenir le grade de docteur délivré par

l'École Nationale Supérieure d'Arts et Métiers

Spécialité " Mécanique - Matériaux "

présentée et soutenue publiquement par

Alexandre FRANCOIS-HEUDE

le 19 Juin 2014

KINETIC MODELING OF THE POLYPROPYLENE PHOTOTHERMAL OXIDATION

Directeur de thèse : **Xavier COLIN**
Co-encadrement de la thèse : **Emmanuel RICHAUD**

Jury

M. Jean-Luc GARDETTE	Professeur, Université Blaise-Pascal, Clermont-Ferrand	Président
M. Jozef RYCHLY	Directeur de Recherche, Polymer Institute, Bratislava	Rapporteur
M. Mathiew CELINA	Directeur de Recherche, Sandia National Laboratories, Albuquerque	Rapporteur
Mme. Michele EDGE	Directrice de Recherche, Manchester Metropolitan University	Examinateur
M. Xavier COLIN	Professeur, PIMM, Arts et Métiers ParisTech	Examinateur
M. Emmanuel RICHAUD	Maître de Conférences HDR, PIMM, Arts et Métiers ParisTech	Examinateur
M. Eric DESNOUX	Ingénieur R&D, Référent Vieillissement Matériaux, DETC-A, Renault	Examinateur

T H È S E

Arts et Métiers ParisTech - Centre de Paris
Laboratoire de Procédés et Ingénierie en Mécanique et Matériaux

ACKNOWLEDGMENTS

First, I would like to acknowledge Dr. Jozef RYCHLY and Dr. Matthiew CELINA for having accepted to be referees and thus, to carefully check my PhD manuscript. Dr. Michele EDGE and Pr. Jean-Luc GARDETTE are also greatly acknowledged as assessors for their deep examination of this work. Their remarks were very complementary and thus enabled to discuss many challenging issues and perspectives of the thesis and its approach in general.

Thereafter, I would like to thank my supervisors for having given me this PhD opportunity which turned out to provide both very comfortable working conditions and a very challenging and multidisciplinary topic. More particularly, I would like to express my gratefulness to Pr. Xavier COLIN for our trustful relationship, its very constructive criticism and for having lent your continuous support to my project of article-based manuscript. I also thank Dr. Emmanuel RICHAUD for its warm welcome in the laboratory, its supervision as predecessor in the line of scientist oriented on polypropylene aging and its assistance in experiments (especially for Gel Permeation Chromatography experiments). I am also very gratefully to Mr. Eric DESNOUX as industrial supervisor and project leader for its very concerned project monitoring. I have really appreciated its efforts for making me acquainted with the industrial concerns without encroaching on time dedicated on PhD topic. It has enabled to meet as much as possible the theoretical academic aspects with the value-oriented requirements of industry.

Then, I would like to gratefully acknowledge the scientists and technicians whose mentioned contributions have made this work possible:

- Dr. Narcisse SIAMPIRINGUE, from the Centre National d'Evaluation et de Photoprotection (CNEP, Clermont-Ferrand), for UV-light exposure and careful control of irradiation conditions.
- Pr. Helene MESDAGH, Dr. Michel HENINGER and Mr. Julien LEPROVOST from University of Orsay/Alyxan, for real-time analysis of VOCs emissions.
- Dr. Alain GUINAULT from PIMM (CNAM), for his contribution and expertise in permeability measurements.
- Mr. Paulo FERRERA and Mrs. Anne GRANDMONTAGNE for their assistance in processing specimens.

- Mrs. Audrey PIERRE, Sonia ACHARD and Mr. Frederic RATEAU from Renault, Microscopy and Chemical Analysis Department, for STEM and NMR measurements.
- Mr. Christian FOURCADE, from Renault, Numerical Methods Department, for his assistance in getting acquainted with Open Modelica software for the numerical solving of systems of differential-algebraic equations,

and obviously to Pr. Jacques VERDU for the tremendous scientific heritage he has handed down to the polymer aging team.

Afterwards, I would like to thank my colleagues from my teams at the Material Department of Renault, with a specific dedication to those of my previous modeling team "IPOM Forever" who helped me to keep confidence -sometimes faith- in benefits of numerical simulation but also for the very amicable work environment. Many thanks to Eric, Véronique, Lucas, Cécile, Emmanuelle, Alain, Camille and Alessandra! Similarly, I would like to show my thankfulness to my colleagues of the PIMM laboratory for the very friendly atmosphere which has always made me enjoying going at work, in particular Sophie, Camilo, Fidèle, Fatma, Paulo, Virginie, Denis, Magali, Julie, Yahya, Ines, Wissam, Amin, Octavie, Sebastian, Nidal, Adrien, Esteve and not forgetting my friend Nicolas. I cannot help to dedicate special thanks to my office colleagues, now friends, first my great friend Mouna and more recently Emilie, for having shared the inescapable timing of stress along PhD studies –and maybe for having endured my talkativeness ;-).

I will finish by expressing my deepest gratitude to my old friend Josephine for our indestructible bond of friendship, to my family for lending unconditional support. More specifically, I express my eternal recognition to to my parents who have urged me to embark on a scientific career up to the PhD and, above all, who have never desisted in doing their utmost for me.

CONTENTS

General introduction

1. Context

Polypropylene-based materials are widespread in the automotive industry due to their low cost, chemical resistance, good mechanical properties or even recyclability. Thermo-Plastic Olefins (TPO), which refer to blend of polypropylene with ethylene-propylene rubber (EPR) in order to confer scratch and impact resistance, are particularly used in exterior parts such as bumpers and side protectors. Nowadays, these TPO are commonly synthesized by multistage polymerization, which improves compatibility of phases and thereby enhances their mechanical properties as well as their processability (high Melt Flow Rate). They still account for more than 50% in volume and 25% in value of the polymer amount in a car and their use, including in thermoplastic composites, is intended to be increasingly popular in the perspective of lightening vehicles. Indeed, this is an important leverage in order to satisfy the requirements of the European regulation (N° 443/2009) in terms of CO_2 emissions for light-duty vehicles (95 g CO_2/km before 2020).

The main drawback of polypropylene is its degradation under the combined effects of oxygen with temperature (thermal oxidation) or UV-light (photooxidation). Indeed, most of the alteration of both mechanical and aspect properties (loss of gloss, whitening, chalking…) has been ascribed to the occurrence of macromolecular chain scissions and the subsequent formation of a lattice of micro-cracks [1-3]. Today, it is widely accepted, in the scientific community of polymer degradation, that the relevant scale to investigate these phenomena is the chemistry of oxidation. The subsequent alteration of upper-scale properties can theoretically be calculated provided that the structure-properties relationships have been identified. The issue is thus to ensure the durability of materials specifications, particularly in terms of perceived quality, and thereby focusing on aspect properties.

In a demanding context of time-to-market reduction, the challenge for R&D departments is to shorten validation periods while aging tests in real conditions are very time-consuming. Different strategies can be envisaged:

(i) The choice of materials (and their suppliers) can be restricted to a shortened list which has passed validations test upstream, at the expense of the innovation responsiveness.

(ii) The aging tests can be accelerated by applying harsher conditions in terms of UV-light intensity, temperature or frequency of rainfalls for instance. However, these

accelerated test methods must be representative of the real-use conditions in order to be reliable: in other words, the relative importance of the different phenomena under competition must be kept unchanged. This point has been particularly emphasized in the so-called mechanistic approach, supported by Lemaire, Gardette and coworkers (Clermont-Ferrand), which consists in ensuring that the mechanisms of degradation are similar in natural (outdoor) and accelerated exposure conditions [4, 5].

(iii) The impact of the various factors (environmental stresses and materials constituents) on polymer aging can be capitalized (feedback). This can be done by "statistical modeling": lifetimes relative to a given property are interpolated generally using polynomials. The other possibility is to simulate the chemical changes depending upon the aging factors, namely the composition of the material and the harshness of the environmental factors. This can be done by applying an approach of kinetic modeling. The main advantage of this latter approach is its heuristic feature thereby enabling extrapolation of the model to longer durations or softer aging conditions.

To date, there is still a long way to go before obtaining a tool viable for lifetime prediction of commercial materials in real-use conditions. Many physicochemical phenomena are involved as a consequence of the complex industrial formulations containing stabilizers [6] –additives conferring the long term stability- fillers or pigments [3, 7, 8]. Modeling their effects on aging requires understanding the impact of each environmental factor and material constituent, their possible interactions depending on the initial state (amount of structural defaults [6, 9] and thermal history given by the processing conditions [10]). The scope of this thesis has thus been restricted to the case of the unstabilized TPO, free of any additive or filler.

This study is the result of the collaboration between the laboratory of Processing and Engineering in Mechanics and Materials (PIMM, Arts et Metiers ParisTech, CNRS) and the automotive company Renault in the framework of the project POLAR (POLymer Aspect Reliability).

2. Objectives

The aim of this thesis thus consists in designing a kinetic model for the photothermal oxidation of isotactic polypropylene and its impact copolymers. This approach has been initiated for two decades in the PIMM laboratory by investigating alternately the effect of

temperature [11], UV-light [12] or oxygen partial pressure [13] on the oxidation kinetics of polypropylene and its subsequent properties changes [14]. An important stake will be to upgrade the numerical tool established for thermal oxidation to the case of the photothermal oxidation. Besides a tool for lifetime prediction, numerical simulation must be above all considered as a research tool, a way to put to the test various mechanistic assumptions and thus to elucidate the impact of the exposure conditions on the oxidation kinetics. A particular attention will be also dedicated to the aging methodology and their reliability.

3. Structure of the dissertation

The literature overview, given in chapter aims at making an inventory of the involved mechanisms in photothermal oxidation, focusing particularly on additional mechanisms induced by the UV-light mainly initiation processes. A particular attention will be dedicated to the mechanistic considerations which lay the foundations of the kinetic modeling approach. Chapter 2, will focus on methodological aspects in relation with the sources of errors, both experimental and numerical, which is necessary in order to apprehend the reliability of the proposed model.

The first results chapter will be dedicated to thermal oxidation which constitutes the core and a subset of the photothermal model since temperature is an intensive quantity in any system. However, the thermal model has been established in very different conditions from solid [8, 11, 14, 15] to molten states [16], thereby resulting in slight predictive discrepencies depending upon the mechanistic and kinetic assumptions. Thus, the challenge will consist in unifying the different proposals of thermal model and checks its validity whatever the temperature, oxygen pressure or material thickness. In chapter 3, the emissions of volatile organic compounds (VOCs) during the thermal oxidation of polypropylene at 140°C will be monitored in real-time by using Fourier transform ion cyclotron resonance mass spectrometry. This original method enables to investigate the impact of VOCs emissions on the mechanisms of polypropylene thermal oxidation and its kinetic modeling. Following these complementary mechanistic considerations, chapter 4 and 5 will be dedicated to establishing a unique kinetic model for thermal oxidation, mainly focusing on the impact of oxygen transport properties. In chapter 4, the oxygen solubility will be shown to be a critical parameter to report the whole diversity of iPP oxidation behaviors, in close connection with the effect of oxygen partial

pressure. Chapter 5 is then devoted to the competitive effect of oxygen diffusion when applying the modeling approach to thick specimens.

Once the thermal core established, it will be possible to introduce in the model new sources of extrinsic initiation, in a similar way as performed by Khelidj et al for describing the impact of γ-radiations in the PE radiothermal oxidation [17-19]. However, the case of the photo-oxidation is more complex because of the wavelength dependence of the UV-light effects and the existence of additional physical phenomena such as light attenuation in the material thickess. The chapter 6 will aim at formalizing the light contribution to initiation basing on the polymer photochemistry. A criterion will thus be proposed to report for the contribution of UV-light to the polypropylene degradation and tested in analytical models. In chapter 7, this criterion will be introduced into the numerical model in order to test various photochemical mechanisms of degradation including the relative contributions of various initiating species. In chapter 8, the model is tentatively extended to the case of thick specimens by introducing aspects of geometrical optics, such as the effect of opacity (screen effect). In chapter 9, the general discussion enables to precise the model validity range in terms of exposure condition and time-domain as well as to detail perspectives of improvements in order to treat commercial formulations.

This manuscript has been the subject of a collection of papers published or submitted in international refereed journals.

4. Introduction générale [Translation in French]

Contexte

Les matériaux à base polypropylène sont très répandus dans l'industrie automobile de part leur coût attractif, leur résistance chimique (aux bases et solvants), leurs propriétés mécaniques ou encore leur recyclabilité. Les polyolefines thermoplastiques (TPO) désignent ainsi des alliages de polypropylène istotactique et de copolymères ethylène-propylène élastomères sous forme de nodules conférant au matériau des propriétés de résistance au choc ou aux éraflures. Ils sont particulièrement utilisés dans les pièces automobiles extérieures telles que les pare-chocs ou les baguettes de protection latérales par exemple. De nos jours, ces alliages TPO sont majoritairement synthétisés par copolymérisation multi-étapes, ce qui améliore la compatibilité des différentes phases et donc leurs propriétés mécaniques ou encore leur processabilité (faible MFR/MFI). Ils représentent déjà plus de 50% en volume et

25% en valeur des polymères présents sur un véhicule et leur usage est amené à croître encore dans la perspective d'alléger les véhicules, en incluant leur usage dans les composites thermoplastiques. En effet, ces matériaux représentent un levier intéressant pour satisfaire les exigences de la régulation européenne relative aux émissions de CO_2 des véhicules particuliers (N° 443/2009), soit 95 g de CO_2/km à l'horizon 2020.

Le principal inconvénient du polypropylène réside dans sa dégradation sous les effets combinés du dioxygène, et de la température (thermooxydation) ou de la lumière UV-visible (photooxydation). En effet, la plupart des altérations des propriétés mécaniques et d'aspect (perte de brillant, blanchissement, farinage,…) ont été attribuées à la production de coupures macromoléculaires et à la formation consécutive d'un réseau de microfissures [1-3]. Il est aujourd'hui largement accepté dans la communauté scientifique que ces phénomènes relèvent de la chimie de l'oxydation. L'altération des propriétés aux échelles supérieures peut théoriquement être déduite de ces modifications chimiques moyennant l'emploi de relations structure-propriétés adéquates. L'enjeu est alors d'assurer la durabilité des propriétés définies dans le cahier des charges, en s'intéressant plus particulièrement à l'évolution des propriétés d'aspect qui ont un impact direct sur la qualité perçue par le client.

Face aux exigences de réduction des délais de mise sur le marché, le défi pour les départements R&D est de raccourcir les durées de validation alors que les essais en conditions d'usage sont très chronophages. Différentes stratégies peuvent être envisagées :

(i) La sélection d'une liste de matériaux (et de fournisseurs) ayant réussi les essais de validations en amont, au détriment de l'innovation.

(ii) L'emploi de conditions accélérées dans des conditions d'expositions sévérisées en termes d'intensité lumineuse, de température ou de fréquence des aspersions (simulant les précipitations). Toutefois, ces méthodes d'essai accéléré doivent être représentatives des conditions d'usage pour être fiables. En d'autres mots, le poids relatif des différents phénomènes en compétition doit rester le même. Cette problématique a été tout particulièrement soulignée dans l'approche dite mécanistique, portée par l'équipe des professeurs Lemaire et Gardette (Clermont-Ferrand), qui s'attache à s'assurer que les mécanismes de dégradation sont similaires en conditions naturelles et accélérées [4, 5].

(iii) L'impact des différents facteurs (contraintes environnementales et constituants des matériaux) sur le vieillissement des polymères peut être capitalisée (retour d'expérience). Cela peut être fait par modélisation statistique : les durées de vies définies par rapport à une propriété donnée sont généralement interpolées. L'autre

possibilité est de simuler les modifications chimiques en fonction des facteurs de vieillissement, notamment les éléments de la formulation et la sévérité des facteurs environnementaux, en utilisant une approche de modélisation cinétique. Le principal avantage de cette dernière réside dans son caractère heuristique qui autorise l'utilisation du modèle en mode extrapolation, typiquement en conditions d'usage, plus douces et impliquant des durées plus longues.

A l'heure actuelle, il reste encore un long chemin à parcourir avant d'obtenir un outil viable pour la prédiction de durée de vie de formulations commerciales en conditions d'usage. De nombreux phénomènes physico-chimiques sont en effet impliqués en raison de la complexité des formulations industrielles contenant des stabilisants, des charges et des pigments [3, 7, 8]. Modéliser leurs effets sur le vieillissement nécessite d'en comprendre les mécanismes propres, leur dépendandance aux facteurs environnementaux ainsi qu'aux caractéristiques du matériau (y-compris ses défauts de structure [6, 9]) ou encore des conditions de mise en œuvre [10]). Le périmètre de cette thèse a donc été restreint au cas des matériaux à base polypropylène ne contenant ni stabilisant (ou autre additif), ni charge ou pigment.
Cette étude est le produit de la collaboration entre le Laboratoire de Procédés et Ingénierie en Mécanique et Matériaux (PIMM, Arts et Metiers ParisTech, CNRS) et du constructeur automobile Renault dans le cadre du projet POLAR (*Polymer Aspect Reliability*).

Objectifs

Cette thèse vise ainsi à concevoir un modèle cinétique pour l'oxydation photothermique du polypropylène isotactique et de ses copolymères résistants. Cette approche a été initiée au laboratoire PIMM depuis deux décennies en étudiant alternativement les effets de la température [11], de la lumière UV-visible [12] ou de la pression partielle en oxygène [13] sur les cinétiques d'oxydation du polypropylène et ses conséquences sur l'altération des propriétés [14]. Un enjeu important sera alors d'adapter l'outil numérique, mis au point pour la thermooxydation, au cas de la photooxydation. Outre son utilisation potentielle pour la prédiction de durée de vie, la simulation numérique doit avant tout être considérée comme un outil de Recherche, un moyen d'éprouver les différentes hypothèses mécanistiques et d'appréhender les effets des conditions d'exposition sur les cinétiques d'oxydation.

Structure du manuscrit

La synthèse bibliographique, qui constitue le chapitre 1, vise à faire un inventaire des mécanismes impliqués dans la photooxydation, en se focalisant particulièrement sur les mécanismes additionnels induit par la lumière UV, c'est-à-dire majoritairement les processus d'amorçage. Une attention particulière sera consacrée aux considérations mécanistiques qui sont à la base de l'approche de modélisation cinétique. Dans le chapitre 2, les aspects méthodologiques seront détaillés en lien avec les différentes sources d'erreur, de variabilité, à la fois expérimentales et numériques. Ceci permettra de mieux appréhender la fiabilité du modèle proposé.

Ensuite, les premiers chapitres de résultats regrouperont les travaux portant sur la thermooxydation qui constitue le cœur du modèle et un sous-groupe du modèle photo-thermique puisque la température est une grandeur intensive de tout système. Le modèle thermique a déjà été établi dans des conditions très différentes, depuis l'état solide [8, 11, 14, 15] jusqu'à l'état fondu [16], en introdusant progressivement des réactions négligées jusqu'alors. Il en résulte de légères différences de prédiction selon les hypothèses mécanistiques et cinétiques. Ainsi, le défi consistera à unifier les différentes propositions de modèle thermique et à vérifier sa validité quelles que soient la température, la pression partielle en dioxygène et l'épaisseur du matériau. Dans le chapitre 3, les émissions de composés organiques volatils (COVs) pendant la thermooxydation du polypropylène à 140°C seront suivies en temps réel par spectroscopie de masse par résonance cyclotron d'ions à transformée de Fourier. Cette méthode originale permet d'étudier en temps réel l'impact des émissions de COVs sur le processus de thermooxydation et sa modélisation. En complément de ces considérations, les chapitres 4 et 5 seront consacrés à l'influence des propriétés de transport du dioxygène sur l'établissement d'un modèle cinétique unique pour la thermooxydation du polypropylène, respectivement aux échelles locales et de la pièce épaisse. Dans le chapitre 4, il sera mis en évidence que la solubilité au dioxygène constitue le paramètre critique pour décrire l'intégralité des comportements à l'oxydation des iPP, en relation étroite avec l'effet de la pression partielle en dioxygène. Le chapitre 5 est dédié à la compétition diffusion-réaction observable lorsque le modèle est étendu aux échantillons épais.

Une fois le « cœur » thermique validé, il est possible d'introduire dans le modèle de nouvelles sources d'amorçage extrinsèque comme cela a été fait pour les radiations γ en radio-oxydation

du polyéthylène [17-19]. Cependant, le cas de la photooxydation est plus complexe du fait de l'amorçage sélectif, la dépendance des effets de la lumière UV à la longueur d'onde ou encore l'atténuation de la lumière dans l'épaisseur du matériau. Le chapitre 6 visera à formaliser la contribution de la lumière à l'amorçage en se basant sur la photochimie des polymères. Un critère décrivant la quantité d'énergie absorbable par le polymère sous une source lumineuse donnée, sera ainsi proposé pour décrire la contribution des rayonnements UV à la dégradation du polypropylène et testé dans des modèles analytiques. Dans le chapitre 7, ce critère sera introduit dans le modèle numérique de manière à tester différents mécanismes photochimiques de dégradation, y-compris les contributions relatives des différentes espèces amorceuses. Dans le chapitre 8, le modèle est étendu au cas des pièces épaisses en introduisant notamment des aspects d'optique géométrique afin de décrire l'atténuation de la lumière dans l'épaisseur du matériau (effet d'écran). En chapitre 9, la discussion générale s'emploie à préciser le domaine de validité du modèle en termes de conditions d'exposition et de fenêtre temporelle ainsi qu'à détailler les perspectives d'amélioration pour traiter les formulations commerciales, y compris l'extension du modèle polypropylène aux alliages.

Ce manuscrit fait l'objet d'une série d'articles publiés ou soumis dans des journaux internationaux à comités de lecture.

References

[1] B. Fayolle, L. Audouin, J. Verdu, A critical molar mass separating the ductile and brittle regimes as revealed by thermal oxidation in polypropylene, Polymer, 45 (2004) 4323-4330.
[2] B. Fayolle, X. Colin, L. Audouin, J. Verdu, Mechanism of degradation induced embrittlement in polyethylene, Polymer Degradation and Stability, 92 (2007) 231-238.
[3] D. Vaillant, Etude du comportement a long terme du polypropylene. Influence de pigments mineraux et organiques, de stabilisants et de charges, in, Université Blaise-Pascal, Clermont-Ferrand, 1993.
[4] O. Haillant, Analyse de méthodes d'étude du comportement à long terme de matériaux polymères en usage extérieur, in: G. Jean-Luc (Ed.), Université Blaise-Pascal, Clermont-Ferrand, 2002.
[5] X. Jouan, Etude de mecanismes de photooxydation de materiaux polymeres en conditions d'ultra-acceleration, in, Université Blaise-Pascal, Clermont-Ferrand, 1990.
[6] P. Gijsman, The Long-Term Stability of Polyolefins. Wibro Dissertatiedrukkerij, Helmond., in, Technische Universiteit Eindhoven 1994, pp. 176 p.
[7] P. Delprat, Etude du mecanisme de photooxydation de copolymeres polypropylene/polyethylene. Influence de pigments photocatalytiques, photostabilisants et colorants organiques et inorganiques, in, Université Blaise-Pascal, Clermont-Ferrand, 1993.
[8] G.G. Gutiérrez, Oxydation des nanocomposites à matrice polyoléfinique in, Arts et metiers ParisTech, Paris, 2010.
[9] W.B.H. Leeming, Thermal and photolytic degradation of polypropylene, in, University of Glasgow, 1973.
[10] C. Frechou, Influence des conditions d'injection sur le comportement photochimique des polypropylènes in, 1994, pp. 215 P.

[11] L. Achimsky, Etude cinétique de la thermooxydation du polypropylène, in: Mécanique et Matériaux, Université Pierre et Marie-Curie (Paris VI), Paris, 1996.
[12] S. Girois, Photooxydation du polypropylène : aspects cinétiques in: Mécanique et Matériaux, Ecole Nationale Supérieure des Arts et Métiers, 2001.
[13] E. Richaud, Durabilité des géotextiles en polypropylène [PhD thesis], in: Mécanique et Matériaux, Arts et Métiers ParisTech, Paris, 2006.
[14] B. Fayolle, Fragilisation du polypropylène induite par fragilisation [In French], in: Mécanique et Matériaux, Ecole Nationale Supérieure des Arts et Métiers, Paris, 2001.
[15] E. Richaud, X. Colin, B. Fayolle, L. Audouin, J. Verdu, Induction period in the low-temperature thermal oxidation of saturated hydrocarbons: Example of polyethylene, International Journal of Chemical Kinetics, 40 (2008) 769-777.
[16] S. Sarrabi, Vers une approche mécanistique du vieillissement thermique du polypropylène à l'état fondu au cours du rotomoulage, in, 2009, pp. 1 vol. (190 p.).
[17] X. Colin, E. Richaud, J. Verdu, C. Monchy-Leroy, Kinetic modelling of radiochemical ageing of ethylene-propylene copolymers, in: I.R.a. Polymers (Ed.) Proceedings of the 8th International Symposium on Ionizing Radiation and Polymers, Elsevier, Angra dos Reis, Rio de Janeiro, Brazil, 12-17 October 2008, 2008, pp. 6.
[18] N. Khelidj, X. Colin, L. Audouin, J. Verdu, C. Monchy-Leroy, V. Prunier, Oxidation of polyethylene under irradiation at low temperature and low dose rate. Part II. Low temperature thermal oxidation, Polymer Degradation and Stability, 91 (2006) 1598-1605.
[19] N. Khelidj, X. Colin, L. Audouin, J. Verdu, C. Monchy-Leroy, V. Prunier, Oxidation of polyethylene under irradiation at low temperature and low dose rate. Part I. The case of "pure" radiochemical initiation, Polymer Degradation and Stability, 91 (2006) 1593-1597.

CHAPTER I. Overview of the literature

From mechanistic considerations to kinetic modeling

Résumé [Summary in French]

Les processus de thermo-, photo- ou radio-oxydation des polyoléfines sont communément considérés, en cinétique chimique, comme des variantes d'un même mécanisme radicalaire en chaîne se distinguant les unes des autres essentiellement au travers de leurs réactions d'amorçage spécifiques. L'idée est alors d'inventorier les mécanismes rapportés dans la littérature en thermo- et photo- oxydation du polypropylène pour mettre en lumière ceux qui leurs sont communs (notamment dans les étapes de propagation et de terminaison) ainsi que ceux spécifiques à la photooxydation, relevant essentiellement des étapes d'amorçage.

Le cas de la photooxydation présente en outre des difficultés inhérentes à son amorçage extrinsèque très sélectif. Celui-ci est susceptible d'impliquer un grand nombre d'espèces dont la nature, la concentration (souvent à l'état de trace dans le polymère natif) et donc le pouvoir amorceur sont mal connus. Ces impuretés et défauts de structure peuvent être des résidus de catalyseur, des insaturations, des produits d'oxydation (cétones, peroxydes, …) voire des radicaux. L'étude des mécanismes d'amorçage est toutefois largement centrée sur les mécanismes impliquant des espèces photosensibles et clivables générées par l'oxydation elle-même, à savoir les hydroperoxydes et les cétones, qui deviennent très rapidement majoritaires.

A partir du rensensement relativement exhaustif des mécanismes impliqués, y compris ceux *a priori* secondaires, il a d'abord été question de formaliser les séquences réactionnelles, relativement complexes, en schémas généraux. Ceux-ci, dits « en boucle fermée », relatent la formation d'espèces instables (de type peroxydes) et leur décomposition en produits d'accumulation pour les différents types de sites réactifs potentiels (cf. figure 17).

Toutefois, le schéma mécanistique ainsi représenté reste complexe et implique de nombreuses réaction chimiques (et autant de paramètres cinétiques). Celui-ci est alors simplifié (figure 18) via une approche de cinétique formelle avec deux approximations majeures : (i) la prise en compte d'un unique site réactif, les unités méthyne (hydrogène labile porté par un carbone tertiaire) ; cela

revient à considérer que les radicaux méthyls, primaires et secondaires s'isomérisent totalement et rapidement en radicaux tertiaires. (ii) il n'y a pas de réactions de co-oxydation, de propagation ou de terminaison croisées (entre radicaux ou sites secondaires et tertiaires par exemple). En cinétique formelle, cela se traduit par un schéma simplifié avec des paramètres cinétiques apparents pour les réactions pseudo-élémentaires représentatives d'un ensemble de réactions. L'avantage de cette approche est de fournir une bonne description de la chimie à l'origine des coupures de chaîne, lesquelles régissent l'évolution des propriétés du matériau.

L'objectif est alors multiple :

- Mieux comprendre les hypothèses sous-jacentes de l'approche modélisation cinétique et leurs implications sur la validité du modèle, en particulier lors d'extrapolation en dehors du domaine de l'étude (typiquement aux basses températures d'usage) ou sur son évolutivité (lors de l'ajout de phénomènes physiques ou chimiques additionnels).
- Evaluer dans quelle mesure l'approche modélisation cinétique est applicable à l'oxydation photo-thermique du polypropylene.

En mettant ainsi en évidence que la photo-thermo-oxidation du polypropylène peut être décrite au moyen de la cinétique formelle, on en déduit la possibilité d'ajouter des réactions d'amorçage photochimique au « cœur thermique » du modèle. On justifie ainsi la stratégie incrémentale de résolution du problème : déterminer les paramètres cinétiques propres au cas de la thermooxydation puis ceux relatifs aux réactions photochimiques.

Introduction

Right from the very first kinetic studies, the different kinds of oxidative degradations (thermo-, photo- and radio-oxidation) have been considered as variants of a single mechanistic scheme, constituted by the same propagation and termination steps but mainly differing from their initiation processes [1, 2]. Such a kinetic modeling approach has been recently put forward and improved basing on the critical path of oxidation [3, 4]. These mechanistic considerations have been extensively justified elsewhere [5] but it is probably as well important to detail the impact of secondary reactions and the reasons for neglecting them.

The present chapter aims at reviewing main mechanisms to be considered for applying the kinetic model to the photothermal oxidation. The first issue lies in the nature of the predominant

initiating species, which has been deeply reviewed by Carlsson and Wiles [6]. Are these species and their relative contribution similar whatever the exposure conditions? What are the main photoinduced reactions? The second issue lays undoubtedly in the multiplicity of reactive sites in polypropylene compared to polyethylene for instance. Starting from these mechanistic considerations, we will justify the relevant of proposing a general kinetic model for photothermal oxidation.

1. Macromolecular mechanisms of oxidation

1.1. Initiation processes: multiplicity and predominance of species

1.1.1. Extrinsic initiation

Metal species- Catalyst residues

Metal species such as titanium, copper, cobalt, chromium, manganese and iron can be present in the very different forms of chelates [7-10], salts -including stearates- [11-14], metal ions [15, 16], catalyst-supported residues [9, 10, 16-21] or fillers and pigments. According to Carlsson and Wiles [6], transition metals would have a first order contribution to the initiation of PP oxidation by promoting or inhibiting the oxidation of polyolefins depending on their oxido-reduction potential, the nature of their ligand or counter-ion or even their concentration as reviewed by Kamiya and Niki [22]. In thermal oxidation, it was reported that they have in solution a prodegradant action below, and an inhibiting action above a critical concentration [9, 12], as modeled by Black basing on the formation of a metal/hydroperoxide complex [23]. The prodegradant effect of catalyst residues was reported for solid state at low temperatures, typically 50°C, for concentrations lower than 180 ppm [24]. They would promote hydroperoxide decomposition according to the so-called" Haber Weiss cycle" thus lowering the its activation energy, which would result in a curvature on the Arrhenius graph of induction times [11, 24-26].

$$M^{n+} + POOH \rightarrow PO^{\circ} + M^{(n+1)+} + HO^{-}$$

$$M^{(n+1)+} + POOH \rightarrow POO^{\circ} + M^{n+} + H^{+}$$

$$POOH + POOH \rightarrow PO^{\circ} + POO^{\circ} + H_2O$$

Recently, Goss et al. have reported that the induction time depends upon the concentration of catalyst [Mn] only though its pre-exponential factor, proportional to $[Mn]^{-0.33}$, but not in term of activation energy [27]. This is in noticeable agreement with the results of Gijsmanfor titanium

concentrations ranging between 2 and 180 ppm [24]. This observation was numerically checked for concentrations up to 200 ppm basing on the "infection model", which was proposed by Georges and co-workers to account for the heterogeneity of the oxidation initiation of polypropylene [28-30]. The photosensitizing action of transition metals was attributed to (i) the oxidation of the "ligand" and the subsequent radical transfer to the polymer [10], (ii) photocatalytic reactions generating hydroxyl radicals at the surface of TiO_2 nanoparticles or (iii) to the chemistry of the transition metal prooxidant [31]. The stabilizing action of metal chelates would be due to their ability to scavenge macroalkyl radicals or to the stabilizing action of their degradation products [32] rather than their role of quencher [33].

Ethylenic and aromatic impurities

Unsaturations would have a strong effect on the induction period in both thermal [34] and photooxidation [35, 36], mainly due to the high lability of the α-ethylenic hydrogen atom by reaction with triplet oxygen leading to an α-ethylenic hydroperoxide, or either by formation of a complex between an unsaturation and singlet oxygen (figure 1) [37, 38]. Indeed, the reactivity of oxygen –a biradical at its triplet ground state- would be still increased at the singlet state due to the existence of non-bonding lone pair [39], [40]. However, such a reaction would be minoritary at low temperature according to Mill, Richardson et Mayo as compared with high temperatures in processing conditions [41]. The validity of this assumption was checked by hexane extraction, a well-known technique to remove α-β unsaturated carbonyl species or polynuclear aromatic species (PNA), as suggested by Carlsson and Wiles [6].

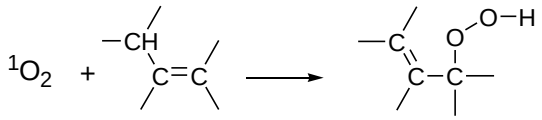

Figure 1: Reaction between an unsaturation and singlet oxygen

These latter species, such as naphtalene, phenanthrene or anthracene, would thus react with singlet oxygen to generate endoperoxides and finally anthraquinones, widely known to be highly photosensitive.

Oxygen-reactive species

Singlet oxygen was believed for a long time to be a noticeable initiation species in photooxidation due to the formation of a highly photosensitive charge-transfer complex. Its

contribution was however moderated by Carlsson et al. [6] basing on the very low concentration of singlet oxygen. This latter was estimated to 10^{-3} ppm despite its formation by peroxy radical recombination, reaction with ozone or quenching of excited ketones. It must be compared with the value of 50 ppm for triplet oxygen. Although reconsidered by Gijsman [42], kinetic considerations lead to dismiss this assumption, since this type of process is incompatible with the observation of an induction period. On the contrary, the fast addition of ozone to double bonds is widely established [6]. It first generates an instable primary ozonide -or molozonide- and then leads to a secondary ozonide or to a polyperoxide which finally transform into a ketone (figure 2).

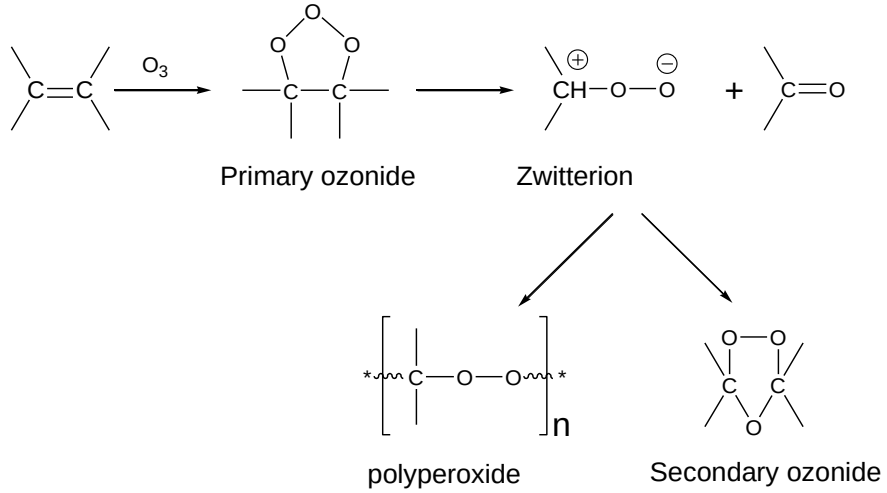

Figure 2: Reaction of ozone with an unsaturation

All these structural defects are considered as extrinsic initiating species and their contribution is expected to be predominant only in the early period of oxidation as compared with intrinsic sources, generated by the polymer oxidation itself.

1.1.2. Role of peroxides

The first-order role of peroxide species, including hydroperoxides, in oxidation of hydrocarbons has been established for a long time by eminent scientists such as Semenov, Tobolsky and Mesrobian [1, 2]. Indeed, these species are extremely cleavable due to the low dissociation energy of the O-O bond -150 kJ/mol), largely lower than the energy of UV-light quanta (~ 95 kcal/Einstein at 300 nm) [43]. The issue of their nature in polypropylene oxidation arises from the studies of Chien *et al* [44] and Zolatova *et al* [45] who evidenced the existence of a fast and a slow-rate decomposing fractions of hydroperoxides, both confirmed by Billingham et al [46]

using chemiluminescence. The auto-accelerated character of their decomposition, as well as the competition between both unimolecular and bimolecular decomposition reactions in thermal oxidation, were highlighted by Schyapnikov et al. [47].

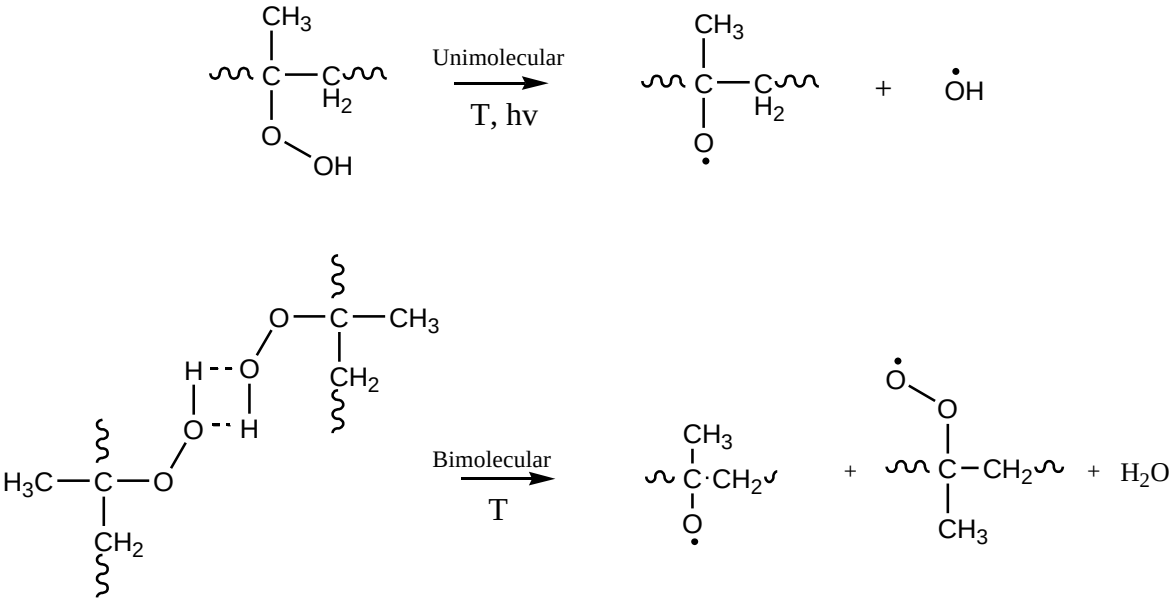

Figure 3: Unimolecular and bimolecular mechanisms of hydroperoxides decomposition

According to Chien et al. and Zolotova et al., the fast-decomposing fraction would consist in the association of hydroperoxides in pairs [45, 47-49] or longer sequences through hydrogen bonds [50], as shown by the FTIR absorption at 3400 cm^{-1} and 3550 cm^{-1} for associated and isolated hydroperoxides respectively. The competition between unimolecular and bimolecular decomposition reactions was reconsidered by Verdu and coworkers [5, 51]. These latter finally conclude to the predominance of the bimolecular decomposition, except in molten state [52-55] in consistency with the findings of Gugumus [56]. In contrast, in photooxydation,, the highly photo-cleavable nature of hydroperoxides mimlitates in favor of the predominance of the unimolecular process [57, 58].

The very instable alkoxy radicals quickly rearrange by hydrogen abstraction or β scission [59] resulting in tertiary alcohols or macro-ketones respectively. These latter species could consist in middle chain (denoted ketones A) and end-chain ketones (or methyl ketones B).

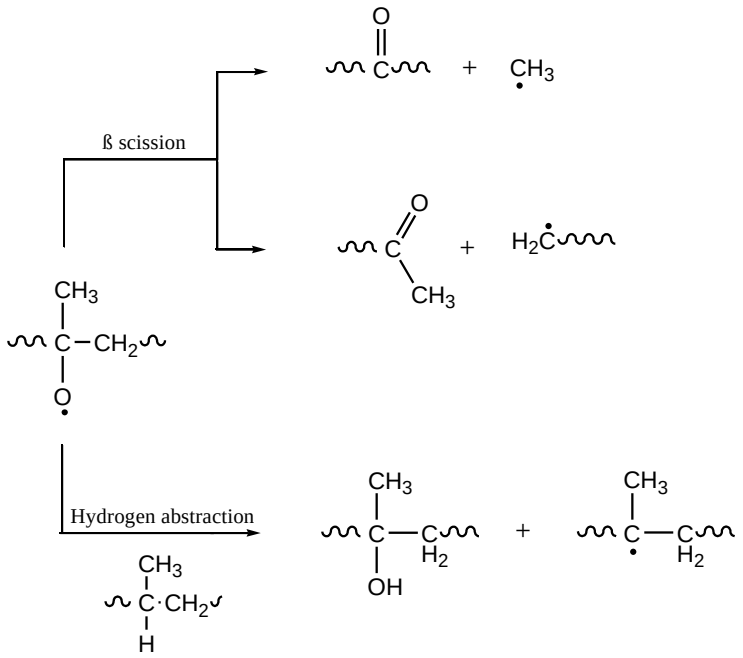

Figure 4: Rearrangement of alkoxy radicals. Competition between β scission and hydrogen abstraction

In parallel, Gijsman et al. [60] first suggested that the fast-decomposing fraction would mainly consist in peresters and the slow-decomposing fraction in tertiary hydroperoxides, whereas Zahradnickova [61] attributed this latter to peracids (peroxy-acids) basing on titration with dimethylsulfide. Despite questionings on the titration method [62], Gijsman et al. [63] finally validated these findings and explained them by the oxidation of primary radicals resulting from the β scission of hydroperoxides. In the case of polyethylene, peracids come from the oxidation of aldehydes (carrying a very labile hydrogen) as suggested by Gugumus [64], or from acyl radicals through the Norrish I reaction which competes with decarbonylation [65]. However, the photolysis of aldehydes is expected to be minority because of the reactivity of the involved hydrogen [64]. Let us notice that this overall path would also enable to explain the formation of α-methylated carboxilic acid consistently with the mechanism of Delprat *et al* [66].

1) Oxidation of primary radicals

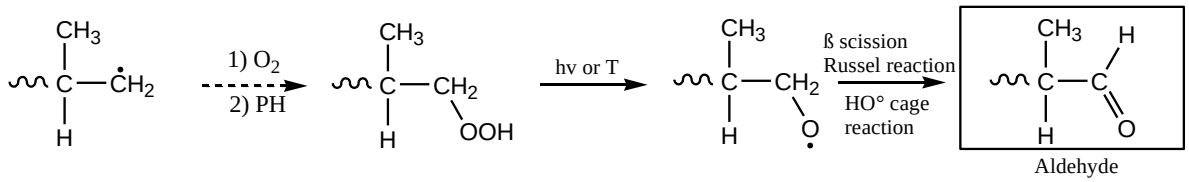

2) Oxidation of aldehydes

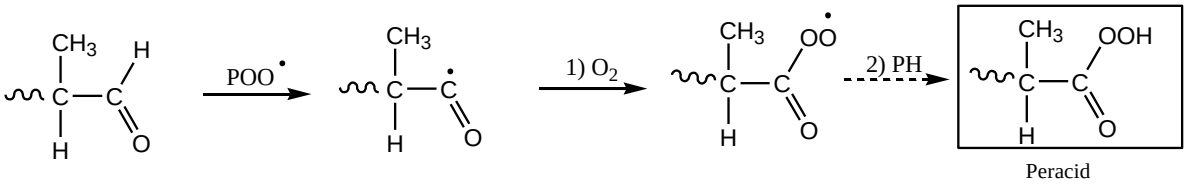

3) Decomposition of peracids

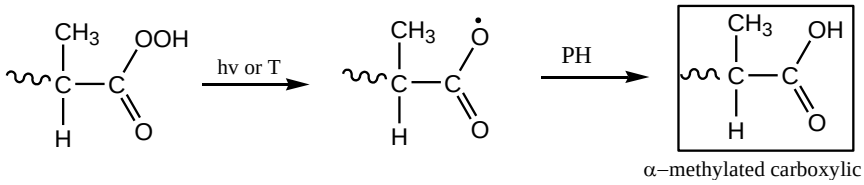

Figure 5: Mechanism of peracids formation and decomposition in polypropylene

Similarly, this mechanism would explain the formation of γ-lactones though the cyclic rearrangement of carboxylic acids (intramolecular esterification) as reported by Adams in the case of polypropylene [67] (figure 6) and Gugumus in the case of polyethylene [68, 69].

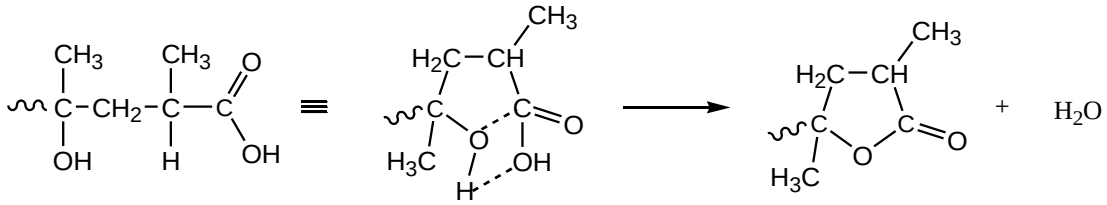

Figure 6: Mechanism of γ-lactone formation in polypropylene

1.1.3. Photolysis of ketones through Norrish reactions

Ketones have been considered as the key initiating species, i.e. the main source of alkyl radicals, in the photooxidation of polyolefins due their high photosensitivity. The Norrish I reactions consists in the scission of the bond in α-position of the carbonyl group. In contrast, Norrish II reaction consists in the abstraction of the hydrogen atom in γ-position through a mechanism

involving a six-membered strcuture, thus generating a vinylene group and an enol, which rapidly isomerizes in ketone.

Middle-chain ketones- Ketones A

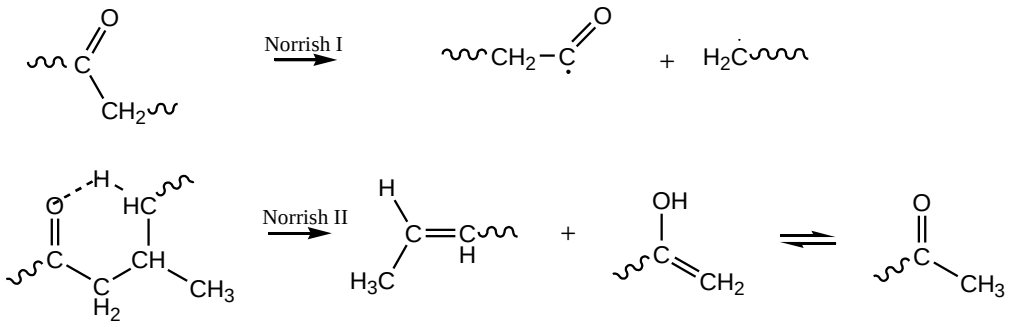

End-chain ketones- Methyl ketones B

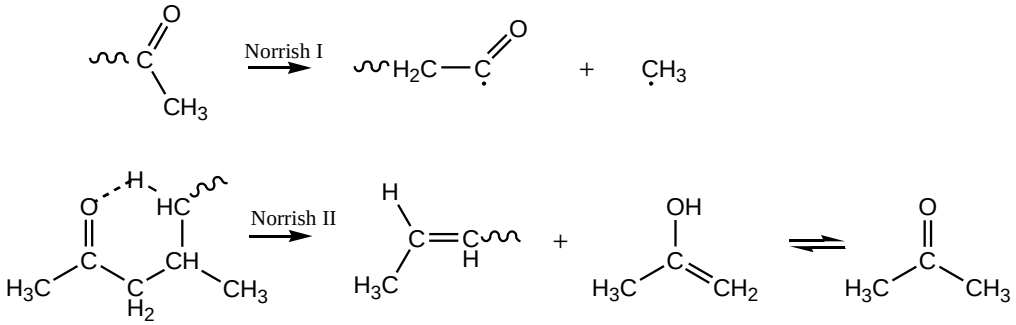

Figure 7: Photolysis of ketones A and B through the Norrish I and II reactions

Their contribution was tentatively determined by Carlsson and Wiles from photolysis experiments [70]. The middle-chain and end-chain ketones were respectively found to undergo Norrish I and II photolysis. The low occurrence of the Norrish II reaction on ketone A can be understood since requiring specific conformation despite the poor mobility of its macro-substituents. On the contrary, the absence of Norrish I reaction on ketone B is more difficult to understand, except if considering the quenching of end-chain ketones by singlet oxygen. Eventually, Norrish reactions would have a lower contribution to the formation of alkyl radicals than hydroperoxide photolysis [43, 70]. The photolysis of aldehydes is expected to be minority due to the high reactivity of the hydrogen and would mainly occur though the Norrish 1 process [64].

1.1.4. Dual/joint initiation by the formation of ketone/peroxide complexes

The possibility of an energy transfer from an excited ketone to an adjacent hydroperoxide was reported in polyolefins by several authors [43, 71-73]. Since termolecular reactions are expected to have a low probability of occurrence, Guillet suggested the formation of an exciplex between these species, benefiting from the photosensitive feature of ketones and the cleavability of hydroperoxides [72]. In such a molecule association, different kinds of energy transfer were reported including coulombian, resonance or radiative transfers [74]. This would constitutes a potential explanation of the particular high quantum yields of hydroperoxide photolysis founded by Carlsson et al. [43], which should not theoretically exceed unity for primary processes. According to Geuskens and Kabamba [75], both species involved in the complex would react together in a kind of reactive energy transfer. The complex would be responsible for a new chain scission mechanism, in addition to the photosensitized decomposition of hydroperoxides. The formation of the complex could occur between various peroxide species (including hydroperoxides, alkyl peroxides, peracids and peresters) and ketones thus generating acids, esters or peresters [76] (cf. figure 8).

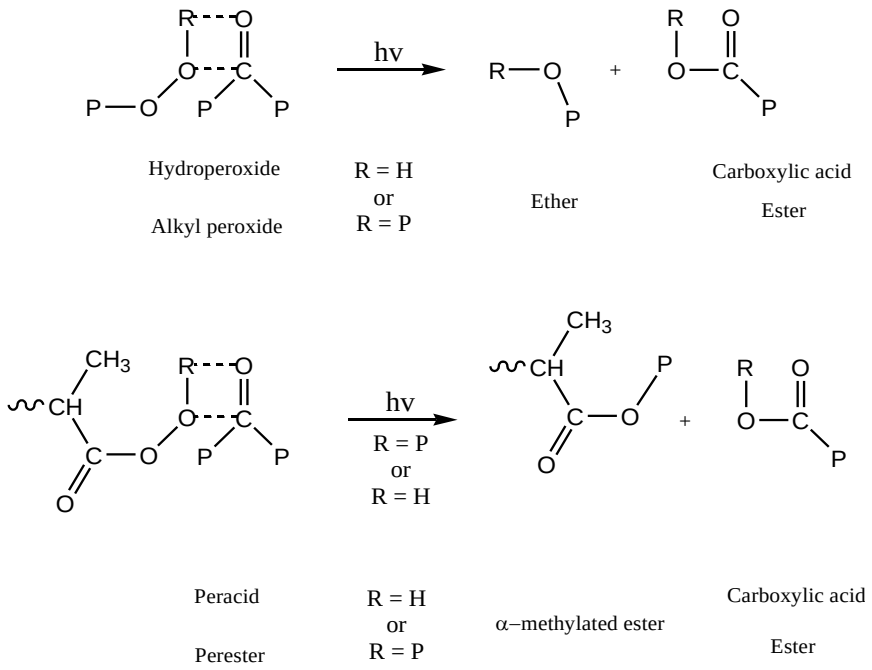

Figure 8: Decomposition of peroxyde-type complexes activated by ketone species

1.2. Propagation and multiplicity of reactive sites

According to Bolland and Gee [77], the propagation stage would involve two steps: the addition of oxygen on alkyl radical and the subsequent abstraction of labile hydrogens on polymer substrate by peroxy radicals. Tertiary carbons (methyne units) would be more reactive than secondary carbons (methylene units) and largely more reactive than primary carbons (methyl groups) [78] (figure 11).

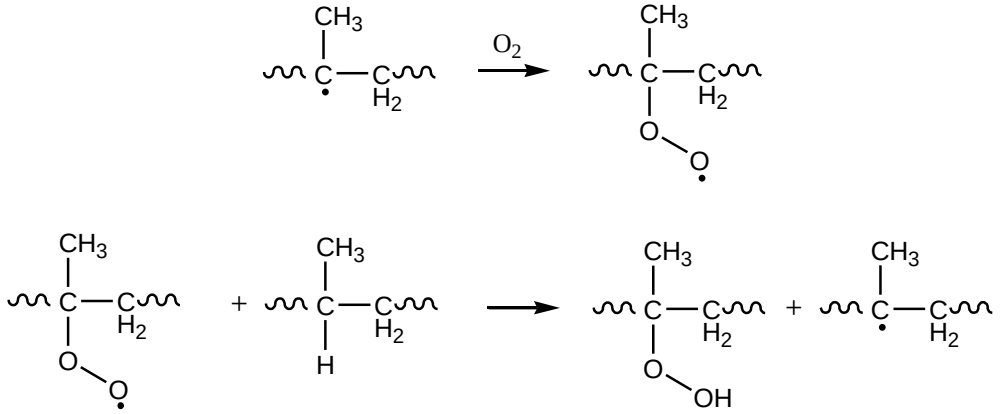

Figure 9: Intermolecular propagation of oxidation

Looking at the association of hydroperoxides in pairs or sequences though hydrogen bonds, the propagation step could also happen through an intramolecular step [49] favored by a six-membered stabilizing structure in close relationship with the 3^1 helicoidal structure of isotactic polypropylene [39].

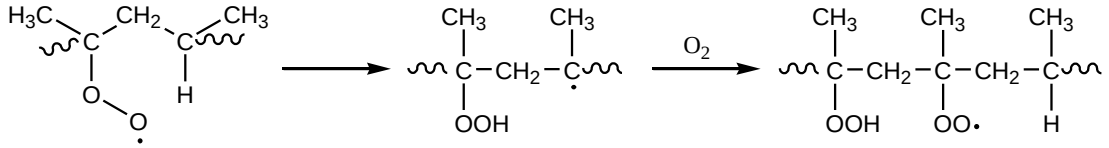

Figure 10: Intramolecular propagation of oxidation

Nonetheless, this kind of pairs association would hinder further propagation steps [79]. Despite this contradiction with the observation of longer sequences by Chien, it would explain the lower oxidation rate of isotactic polypropylene compared to atactic PP.

1.3. Termination

Termination reactions can occur by recombination (coupling) or disproportionation by abstraction of hydrogen atoms in α-position of alkyl radicals. The coupling reactions would be responsible for polypropylene crosslinking due to the generation of alkyl-alkyl and alkyl-peroxy (peroxide) bridges, these latter being particularly instable in photooxidation conditions. Disproportionation would generate vinylidene function and, in the case of the alkyl-peroxy disproportionation, hydroperoxides undergoing further thermal or photochemical decomposition (figure 11).

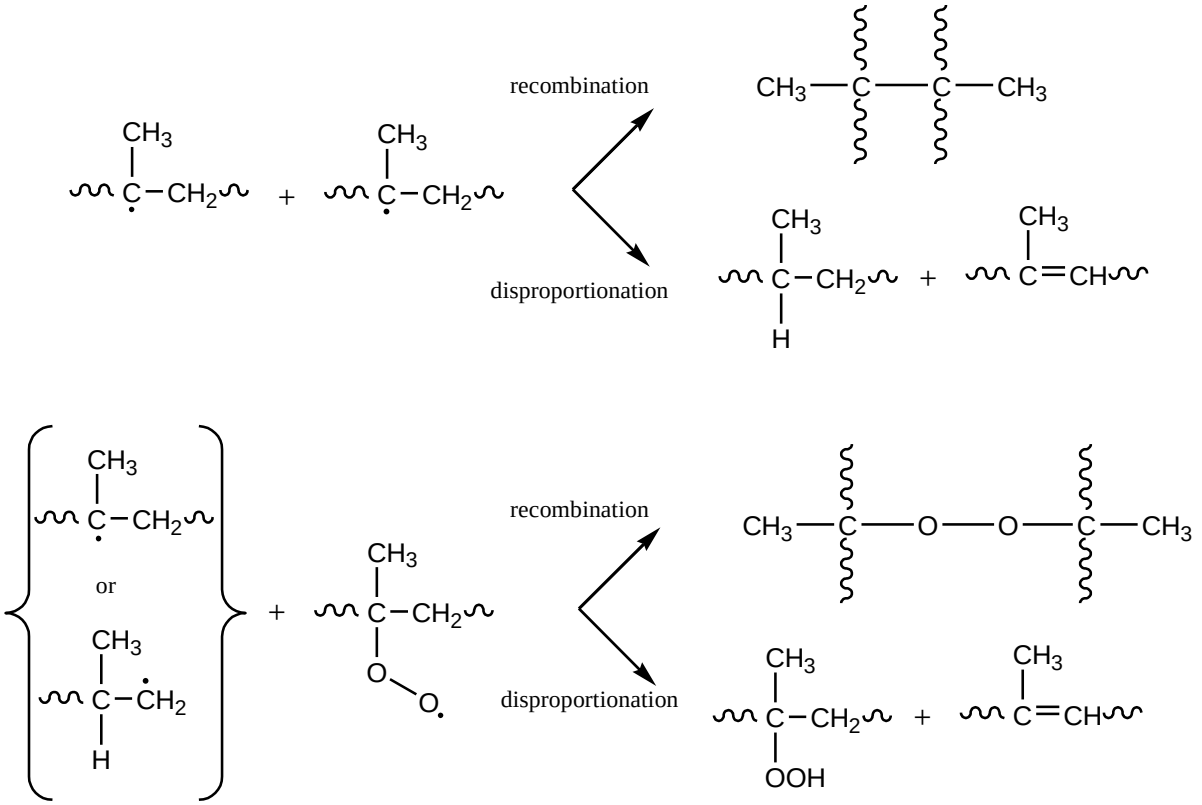

Figure 11: Termination of alkyl + alkyl and alkyl + peroxy radicals

In contrast, peroxy radicals would only terminate through recombination and thus, this latter constitutes the majority of the termination process in oxygen excess [60].

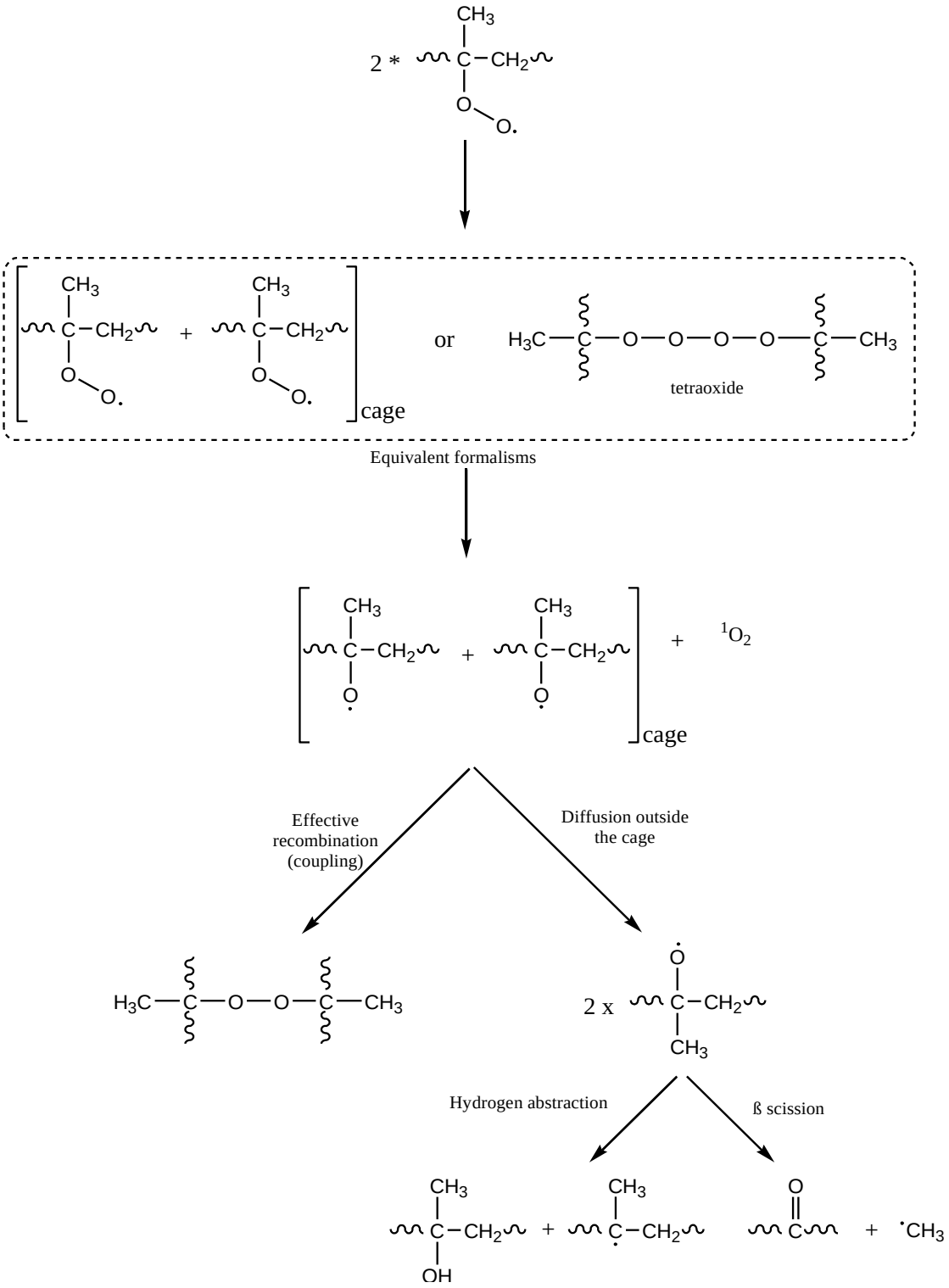

Figure 12: Recombination reactions of peroxy radicals

Decker *et al* have investigated the termination process involving peroxy radicals in polypropylene thermal oxidation, as initiated by the di-*tert*-butylperoxy oxalate between 25°C and 55°C [80] or γ-radiation between 22°C and 45°C [81]. They evidenced the predominance of recombination accounting for 80% of the overall termination steps. About 30% of the alkoxy radicals would diffuse outside the cage, whereas 50% would couple into the cage and thus lead to alkyl peroxides.

The remaining 20% would result from a Russel reaction involving a secondary radical and evidenced in the case of polyethylene. This reaction would be particularly favored at low temperature due to its weak activation energy (17 $kJ.mol^{-1}$) [22] and the high efficiency of primary peroxy radicals in the termination process [60].

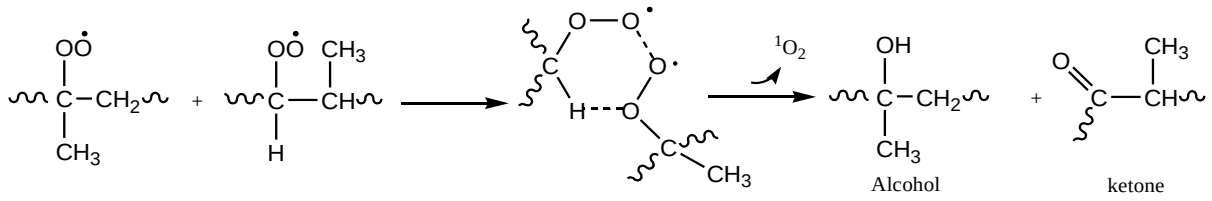

Figure 13: Russel's reaction in polypropylene

This termination process was also studied in an atmosphere composed of the $^{32}O_2$ and $^{36}O_2$ oxygen isotopes in photooxidation at 60°C [82] and thermal oxidation at 95°C and 140°C [83]. The formation of $^{34}O_2$ was found in photooxidation, thus evidencing the cage mechanism (with tetraoxide as intermediate), but not in thermal oxidation which would be attributed to a lower probability of peroxy radicals recombination or the consumption of singlet oxygen by unsaturations, suspected to be favored at high temperature.

2. Kinetic treatment

2.1. Formalism of the closed- loop scheme

In order to describe the oxidation of polyolefins, Verdu and coworkers proposed to focus on the critical paths of oxidation formalized into the so-called "closed-loop" mechanistic scheme (CLMS) according to the following general principles:

(i) The key species are those which are generated and decomposed along the oxidation process (mainly hydroperoxides and potentially ketones in photooxidation).

(ii) Balance equation can account for pseudo-elementary steps basing on the rate-determining steps such as in the case of the hydroperoxide decomposition where the dissociation of the O-O bond is the limiting step as compared to the subsequent rearrangement of alkoxy radicals.

(iii) The probability of a chemical reaction is all the more probable that the lifetime of its reactant is long. As a consequence, the radical fragments would only recombine into the cage. Also, the formation of oxidation products would rather happen though subsequent oxidation reactions than though recombination of molecular radicals (such as hydroxyl radical for generating carboxylic acids for instance).

The CLMS has been written for both tertiary and secondary hydroperoxides accounting respectively for the oxidation of polypropylene and polyethylene. Below, radicals $P_t^{\bullet}$, $P_s^{\bullet}$ and $P_p^{\bullet}$ denote tertiary, secondary and primary alkyl radicals produced by hydrogen abstraction from methyne P_tH, methylene P_sH and methyl P_pH reactive sites. $R^{\bullet}$ accounts for methyl radical. It is reminded for convenience:

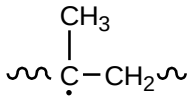

Tertiary radical $P_t°$

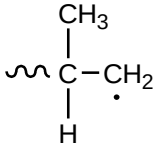

Tertiary radical $P_s°$

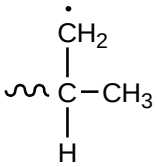

Tertiary radical $P_p°$

Methyl radical R°

Figure 14 reports the closed-loop due to the propagation of oxidation on tertiary sites (methyne units) including its termination processes. These will not be indicated anymore in order to overload schemes.

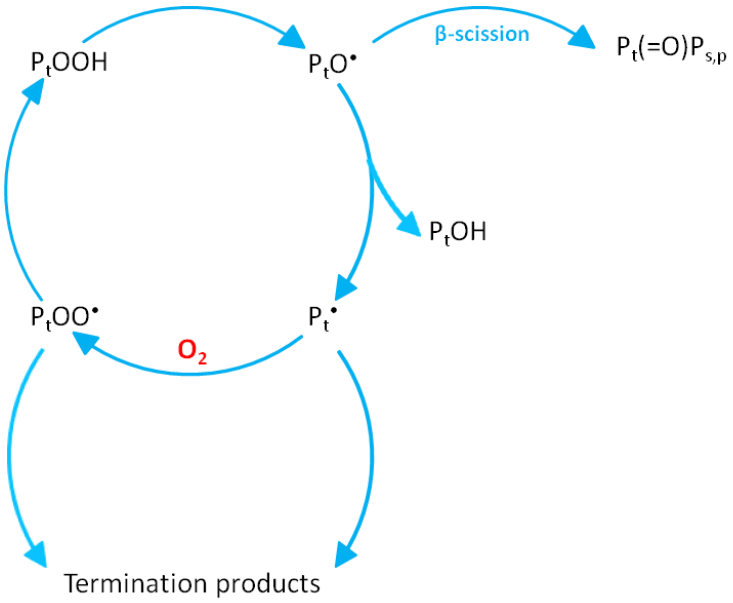

Figure 14: Closed-loop formalism for the thermal oxidation of methyne units P_tH

This formalism can be extended to the case of multiple reactive sites in polypropylene. Non tertiary alkyl radicals are generated by secondary reactions, in particular though β-scission of alkoxy radicals. Thus, primary alkyl radicals oxidize to generate secondary highly reactive aldehydes (figure 15).

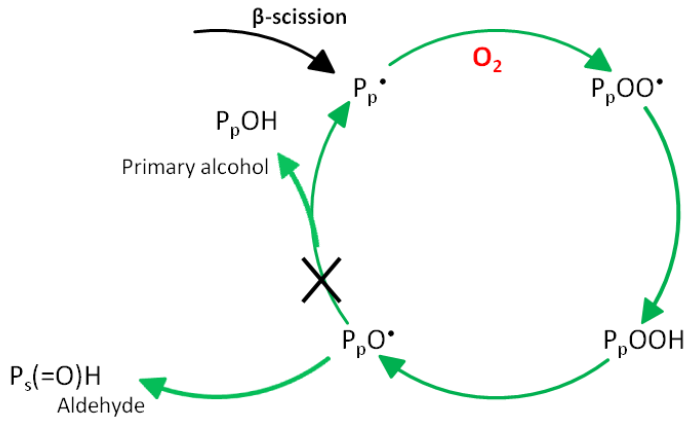

Figure 15: Closed-loop formalism for the oxidation of primary alkyl radicals P_pH

Aldehydes can then be oxidized into peracids and subsequent oxidation products according to the mechanism reported by Gijsman [60]. The mechanism of oxidation of methylene units, describing for instance the oxidation of polyethylene, involves two imbricated loops where the peroxidic nature of peracids is clearly highlighted (figure 16). Adehydes are here analogous to

alkyl radicals due to their high reactivity, which is in consistency with the absence of their accumulation into the polymer matrix (at least in the case of polypropylene).

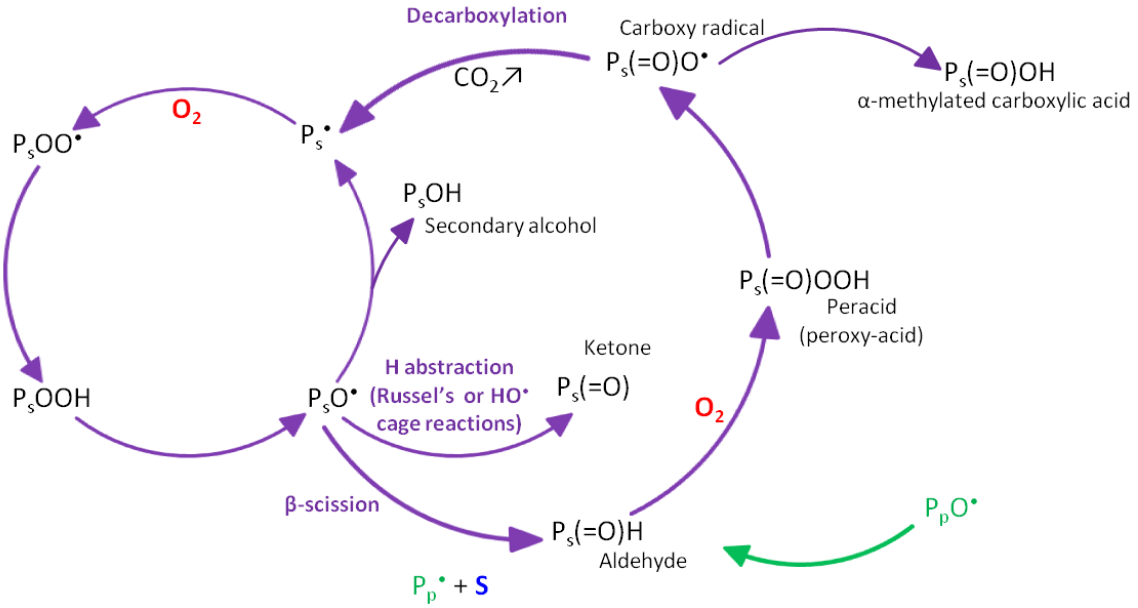

Figure 16: Closed-loop formalism for the oxidation of methylene units P_sH

Methyl fragments, although they are not presented, can abstract tertiary hydrogens to generate methane or undergo further oxidation to give methanol as volatile products. These species, as well as other volatile compounds, would not be detailed here since involving only scission at the chain extremities but wille be treated in the first thermal oxidation chapter.

At this stage, it is shown that it is possible to describe very rigorously the oxidation of polyolefins by applying the closed-loop mechanistic scheme to each potential site of oxidation. Most of these reactions have been considered in order to propose a model for the oxidation of ethylene-propylene copolymers without simplifying mechanistic assumptions [84]. However, such a work has highlighted the limitations of solving the inverse problem by introducing many chemical reactions (i.e. many adjustable parameters).

In contrast, in the case of polypropylene, it has been considered for a long time that the tertiary carbon (methyne unit) is the main site of oxidation. This consideration is reasonable regarding at the activation energies of the propagation step Ea_3 which could occur in polypropylene

(calculated by Korcek et al. [78] and reported in table 1). However, this consideration leads to neglect crossed reactions such as :

(i) The propagation steps on non tertiary carbons, in particular, the abstraction of hydrogen atoms from methylene units by tertiary peroxy radicals whose relative importance is expected to increase with temperature due to their higher activation energies.

(ii) The crossed-termination reactions. However, it is noteworthy that primary radicals are about one thousand more reactive than tertiary radicals, so their probability of occurrence should be higher [80, 85].

Table 1: Energies of activation for the propagation step (3), the termination step involving peroxy radicals (6) and the maximal rate of oxygen consumption

Type pf peroxy radicals	**Type of reactive sites**	Ea_3 [a]		Ea_6 [b]	$Ea_s=2E_3-E_6$
		kcal.mol^{-1}	*kJ.mol^{-1}*	*kJ.mol^{-1}*	*kJ.mol^{-1}*
t-POO°	P_pH	18.2	76.0	40.0	111.9
	P_sH	16.5	69.1		98.1
	P_tH	14.9	62.2		84.3
s-POO°	P_pH	19.5	81.7	20.0	143.4
	P_sH	17.9	74.8		129.6
	P_tH	16.2	67.9		115.8
p-POO°	P_pH	20.9	87.5	10.0	165.0
	P_sH	19.3	80.6		151.1
	P_tH	17.6	73.7		137.3

a These activation energies are calculated according to the relationships proposed by Korcek [78]

b These activation energies are estimated from literature [80, 81, 85]

The overall oxidation scheme for poypropylene thus consists in multiple imbricated loops (figure 17). In this manner, the polypropylene oxidation is not decribed by a mechanistic scheme of co-oxidation but rather by the oxidation series of its multiple oxidation sites. Also, what is particularly striking is the key role of isomerization reactions undergone by non tertiary radicals, in competition with their propagation. By assuming their complete izomzrisation of non tertiary radicals into tertiary ones, it is possible describe the polypropylene oxidation though a simplified CLMS involving only tertiary hydroperoxides. This strong assumption is not necessarily erroneous, at least for moderate conversion ratio of the oxidation reaction. Indeed, the products

arising from the oxidation of methylene units such as peracids or VOCs (including carbon monoxide and dioxide) have been evidenced in significant amounts only for advanced state of degradation [63, 86-90].

This latter assumption of complete izomerization, characterizing the formal kinetic approach and leading to a simplified CLMS, would come down to variable consumptions in oxygen and substrate (PH sites) according to a quantitative assessment. Eventually, such a demarche would result in determining apparent values for the kinetic rate constants of elementary reactions, especially termination reactions.

2.2. Extension to the photothermal oxidation case

The polypropylene photothermal oxidation can be described by introducing photo-induced chemical reactions into the thermal scheme (as indicated in orange) in figure 14. Here also, only the predominant mechanism must be considered in a first approach.

The first issue consists in the selectivity of Norrish reactions for ketones A or B. It requires their differentiation and so the quantitative determination of products resulting from the rearrangement of alkoxy radicals. In the matter, literature is rather scarce and results are rarely corroborating. The ratio between the yield of hydrogen abstraction and β scission ranges between 0.1 and 0.3 which is rather consistent with the results obtained in thermo- and photo-oxidation or in photolysis by Carlsson or Lacoste [6, 43, 70, 87, 91]. However, it is noticeable that Adams and Mowery found much higher values (up to 0.7) [67, 88, 92], presumably because of the instability of hydroperoxides along titration [90]. Besides, Carlsson [43, 70] and Adams [67, 92] found equivalent amount of middle-chain and end chain ketones (assuming assignments of FTIR peaks at 1718 cm^{-1} and 1726 cm^{-1} for ketones A and B respectively), while Mowery found that middle-chain ketones result only from the oxidation of the methylene unit.

The second main issue lies in the relative importance of the reactions proposed by Geuskens and Kabamba compared to the common hydroperoxides and ketones photolysis reactions. Considering ester groups (including peresters), the literature indicates that they results from both the oxidation of methyne and methylene units [88, 90], thus making difficult to conclude without introducing kinetic aspects. However, ester groups can also be formed by condensation of acid and alcohol groups [93] due to the low activation energy, although tertiary alcohols are expected

to be less reactive than primary or secondary ones. Moreover, acids and esters do not absorb light above 300 nm and so, would not undergo photolysis reactions as already seen for ketones [92]. The mechanism of Geuskens and Kabamba would be in line with the stoechiometric changes in the carbonyl oxidation products depending on the exposure conditions observed by Philippart *et al* [94]. Indeed, these latter observed a significant increase in the concentration of esters relative to carboxilic acids, when increasing the ratio light intensity/temperature.

1.1. The heterogeneity of oxidation: a scale issue

Different kinds of heterogeneities were reported in the case of polypropylene depending on their scale: (i) Heterogeneities due to the competition between the oxygen reaction and its diffusion in the specimen thickness (diffusion controlled oxidation) [26, 95-99], (ii) heterogeneities at the morphological scale since crystalline phase does not undergo oxidation [100, 101], (iii) heterogeneities at the micron scale which would be due to the spreading and accumulation of oxidation products in highly oxidized domains mainly due to catalyst residues or atactic material [28, 29, 63, 102, 103]. This theory was investigated through an heterogeneous model by Gugumus [104, 105] or George and coworkers [30, 106-108]. In parallel, Meekev and coworkers [109-111] proposed a heterogeneous model accounting for the micro-heterogeneous physical organisation of amorphous polymers. The validity of these theories of heterogeneous kinetics was tentatively checked from literature experimental results [112, 113].

Actually, heterogeneous models would be more consistent with the fact that initiation theoretically occurs randomly. The work of George and coworkers is hence particularly valuable in the comprehension of the role of transition metal in the initiation stage of oxidation. Nonetheless, the existence of an induction period or the monomodal distribution of the molecular weight even after degradation is a strong argument in favor of the homogeneity of the oxidation process. It can be thus assumed that oxidation propagates fast enough so that the process is homogeneous in the very beginning of the induction period. For instance, the distance between two metal particles can be estimated between 50 and 120 nm for current catalyst concentrations (ranging from 0.2 to 4 ppm), which is not so far from the radius of gyration of a polymer chain (about 30 nm).

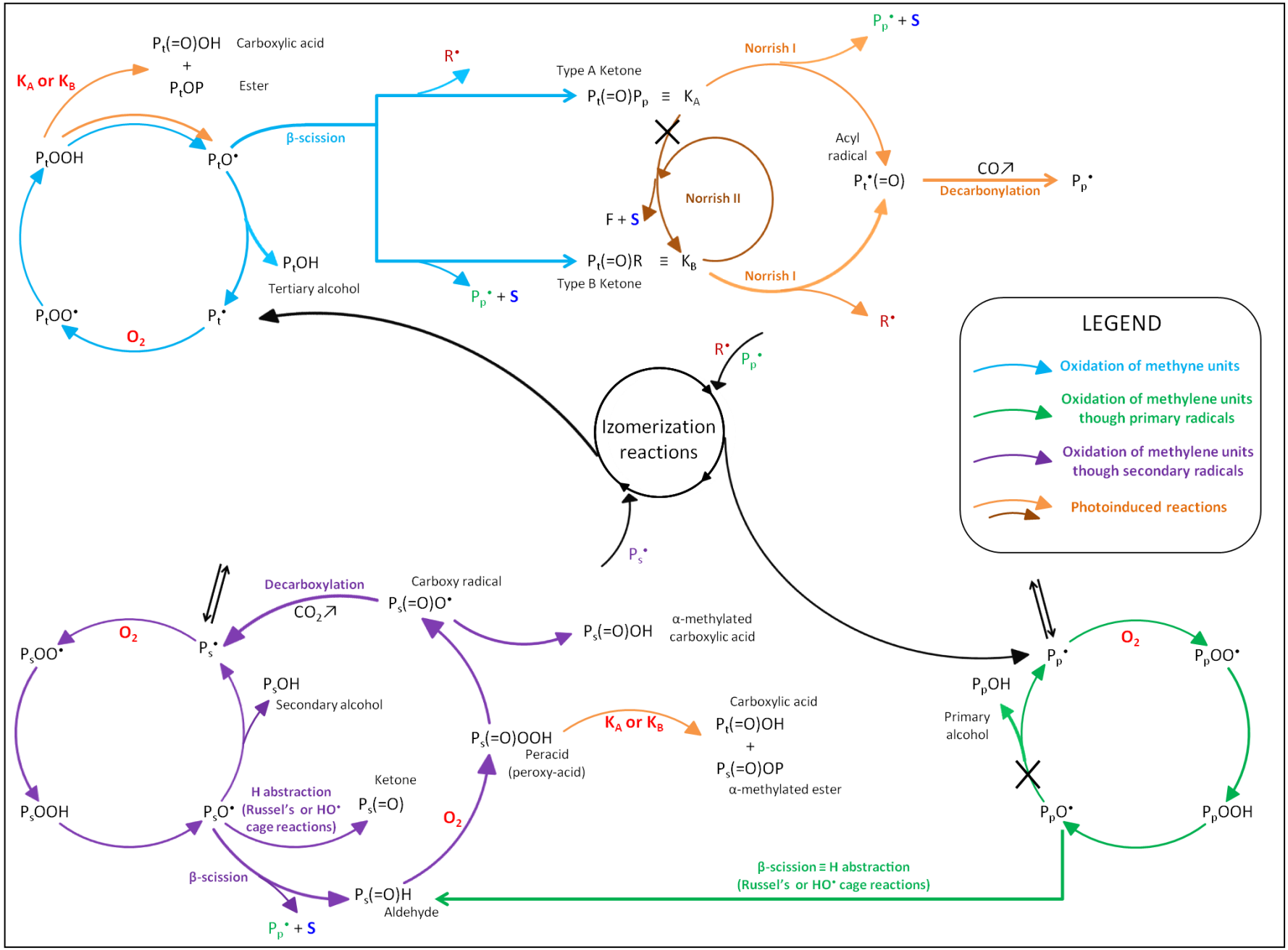

Figure 17: Generalization of the closed loop scheme to multiple reactive sites in polypropylene (double arrows indicates the ability of radical to isomerizes

Conclusion: general strategy and research survey

From this literature review, a large scope of reactions can be involved, but it appears that the most important mechanisms have been elucidated thus allowing the modeling of the global oxidation process. The predominant mechanisms have been tentatively organized in a comprehensive scheme by generalizing the "closed-loop" formalism to the case of multiple oxidation sites in polypropylene.

Admittedly, this scheme is still based on the strong simplifying assumption that the propagation steps only occurs on methyne units, but it has the merit of explaining the formation of all the oxidation products. Based on this assumption, this scheme thus clearly evidences that the critical issue is the competition between the propagation of non tertiary radicals with their isomerization into tertiary ones. If assuming that this latter is total, the mechanistic scheme can be considerably simplified into a simple Closed-Loop mechanistic scheme for thermal oxidation. Eventually, these assumptions lead to underestimate the oxygen consumption (as well as the substrate consumption).

In a so-called "formal kinetic approach", the contribution of the neglected reactions is thus taken into account by attributing average values to the kinetic rate constants of the elementary steps. The changes in reactive species are then translated into a system of ordinary differential equations though the classical theory of the chemical kinetics.

The determination of these apparent kinetic rate constants can be advantageously carried out by applying an inverse resolution method to the optimization procedure. Nonetheless, the more numerous the parameters are, the more difficult the numerical determination of parameters is, mainly because of the high number of parameters combinations to test. It is thus advisable to simplify the system in order to minimize the number of adjustable parameters. Actually, we start from the simplest mechanistic scheme. Chemical reactions or physical phenomena are then added stepwise for simulating all the experimental results. Finally, the principle of parsimony (*lex parsimoniae*), also called as the Ockham's razor, constitutes the guiding line in the optimization procedure. It was formulated in different ways:

Numquam ponenda est pluralitas sine necessitate

[Plurality must never be posited without necessity]

'Sentences of Peter Lombard', in *Quaestiones et decisiones in quattuor libros Sententiarum Petri Lombardi* (ed. Lugd., 1495), i, dist. 27, qu. 2, K).

The main advantage of this approach is its upgradability: (i) This is compatible with the introduction/coupling of physical phenomena (e.g. oxygen diffusion, light absorption, etc.); (ii) New chemical reactions can be added in order to account for the impact of other additives (e.g. stabilizers, fillers, etc.) in the formulation. This principle is at the core of our strategy for modeling the photothermal aging of stabilized polypropylene impact copolymers. In this perspective, the model must be implemented in terms of exposure conditions (accounting for the effect of light) and in terms of components, among them the impact of elastomer nodules and additives in future developments.

For these reasons, a great attention was paid in the literature overview to the additional mechanisms induced by the UV-light, particularly those which generate chain scissions. Finally, most of them concern the initiation stage. Considering their relative predominance, only the photolysis of hydroperoxides and ketones can be considered in a first approach, thus resulting in the following mechanistic scheme of imbricated loops.

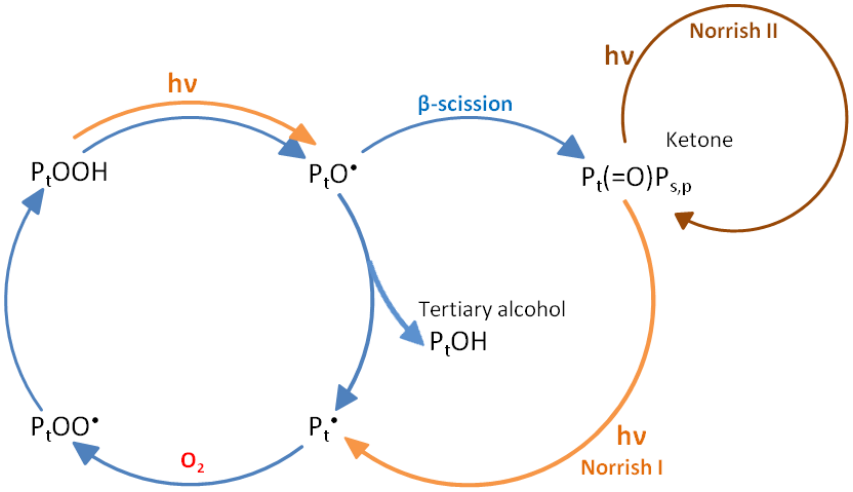

Figure 18: Simplified CLMS for the photothermal oxidation of polypropylene

The photosensitizing actions of catalyst residues or ketones on the decomposition of peroxides species would be envisaged to account for additional effects of light.

The burning issue that arises is: how is this upgradability impacted by the formal kinetic approach? Indeed, the system must be described at the suitable scale in order to enable introduction of the new relevant interactions of the new component with the existing system.

In concrete terms, it requires that the oxidation products, neglected in a first approach, will not have some decisive interactions with a potential additional component. Otherwise, it will be necessary to adjust the entire model according to the “Back and Forward” (trial an error) procedure.

Besides, it is legitimate to wonder in which extent the model remains valid in terms of time-domain, i.e. up to which conversion ratio of oxidation process, but also in terms of exposure conditions. Obviously, the thermal scheme is expected to remain valid in photothermal oxidation, at least in the range of experimented exposure conditions. The underlying question consists in its validity when extrapolating outside the range of investigation. Actually, its validity is thought to be ensured in the close vicinity of this domain due to its high heuristic value, all the more that is valid in a wide range of exposure conditions (generalized mechanism).

References

[1] A.V. Tobolsky, Oxidative degradation of polymeric material, Discussions of the Faraday Society, 2 (1947) 384-388.
[2] A.V. Tobolsky, D.J. Metz, R.B. Mesrobian, Low temperature autoxidation of hydrocarbons: The phenomenon of maximum rates, Journal of the American Chemical Society, 72 (1950) 1942-1952.
[3] L. Audouin, V. Gueguen, A. Tcharkhtchi, J. Verdu, "Closed loop" mechanistic schemes for hydrocarbon polymer oxidation, Journal of Polymer Science Part A: Polymer Chemistry, 33 (1995) 921-927.
[4] S. Verdu, J. Verdu, A new kinetic model for polypropylene thermal oxidation at moderate temperatures, Macromolecules, 30 (1997) 2262-2267.
[5] L. Audouin, L. Achimsky, J. Verdu, Kinetic modelling of low-temperature oxidation of hydrocarbon polymers., in: e. Hamid SH (Ed.) Handbook of polymer degradation. 2nd ed, Marcel Dekker, New York, 2000, pp. 734.
[6] D.J. Carlsson, D.M. Wiles, The Photooxidative Degradation of Polypropylene. Part I. Photooxidation and Photoinitiation Processes, Journal of Macromolecular Science, Part C, 14 (1976) 65-106.
[7] A.W. Benbow, C.F. Cullis, H.S. Laver, Effects of metal chelates on the oxidation of polyolefins at high temperatures, Polymer, 19 (1978) 824-828.
[8] J. Holcik, M. Kosik, A.W. Benbow, C.F. Cullis, The oxidative thermal degradation of polypropylene and the influence of transition metal chelates, European Polymer Journal, 14 (1978) 769-772.
[9] O. Cicchetti, R. De Simone, F. Gratani, Titanium-catalysed-inhibited autoxidation of polypropylene and of its models, European Polymer Journal, 9 (1973) 1205-1229.
[10] O. Cicchetti, F. Gratani, The effect of titanium compounds on photo-oxidation of 2,4,6,8-tetramethylnonane (a liquid model of polypropylene), European Polymer Journal, 8 (1972) 561-573.
[11] M. Koutný, T. Václavkováa, L. Matisová-Rychlá, J. Rychlý, Characterization of oxidation progress by chemiluminescence: A study of polyethylene with pro-oxidant additives, Polymer Degradation and Stability, 93 (2008) 1515-1519.
[12] Z. Osawa, T. Saito, The Effect of Transition Metal Compounds on the Thermal Oxidative Degradation of Polypropylene in Solution, in: Stabilization and Degradation of Polymers, AMERICAN CHEMICAL SOCIETY, 1978, pp. 159-174.
[13] P.K. Roy, P. Surekha, R. Raman, C. Rajagopal, Investigating the role of metal oxidation state on the degradation behaviour of LDPE, Polymer Degradation and Stability, 94 (2009) 1033-1039.
[14] J.L. Pablos, C. Abrusci, I. Marin, J. Lopez-Marin, F. Catalina, E. Espi, T. Corrales, Photodegradation of polyethylenes: Comparative effect of Fe and Ca-stearates as pro-oxidant additives, Polymer Degradation and Stability, 95 2057-2064.
[15] G. Gutiérrez, F. Fayolle, G. Régnier, J. Medina, Thermal oxidation of clay-nanoreinforced polypropylene, Polymer Degradation and Stability, 95 (2010) 1708-1715.
[16] J. Scheirs, S.W. Bigger, N.C. Billingham, Effect of chromium residues on the stability of gas-phase high-density polyethylene produced by supported catalysts, Journal of Polymer Science Part A: Polymer Chemistry, 30 (1992) 1873-1889.
[17] Z. Osawa, Role of metals and metal-deactivators in polymer degradation, Polymer Degradation and Stability, 20 (1988) 203-236.
[18] S. Sack, S. Schär, E. Steger, H. Wagner, Studies on the mechanism of the copper-catalyzed thermal oxidation of low-density polyethylene, Polymer Degradation and Stability, 7 (1984) 193-203.
[19] E. Epacher, C. Kröhnke, B. Pukánszky, Effect of catalyst residues on the chain structure and properties of a Phillips type polyethylen, Polymer Engineering & Science, 40 (2000) 1458-1468.
[20] J. Tocháček, J. Jančář, J. Kalfus, S. Hermanová, Processing stability of polypropylene impact-copolymer during multiple extrusion â€“ Effect of polymerization technology, Polymer Degradation and Stability, 96 491-498.
[21] E.M. Hoàng, N.S. Allen, C.M. Liauw, E. Fontán, P. Lafuente, The thermo-oxidative degradation of metallocene polyethylenes. Part 1: Long-term thermal oxidation in the solid state, Polymer Degradation and Stability, 91 (2006) 1356-1362.

[22] Y. Kamiya, E. Niki, Oxidative degradation, in: e. Jellinek H (Ed.) Aspects of degradation and stabilization of polymers, Elsevier Science, New York, 1978, pp. 80.
[23] J.F. Black, Metal-catalyzed autoxidation. The unrecognized consequences of metal-hydroperoxide complex formation, Journal of the American Chemical Society, 100 (1978) 527-535.
[24] P. Gijsman, J. Hennekens, J. Vincent, The influence of temperature and catalyst residues on the degradation of unstabilized polypropylene, Polymer Degradation and Stability, 39 (1993) 271-277.
[25] L. Achimsky, L. Audouin, J. Verdu, J. Rychly, L. Matisova-Rychla, On a transition at 80 °C in polypropylene oxidation kinetics, Polymer Degradation and Stability, 58 (1997) 283-289.
[26] F. Gugumus, Thermooxidative degradation of polyolefins in the solid state - 7. Effect of sample thickness and heterogeneous oxidation kinetics for polypropylene, Polymer Degradation and Stability, 62 (1998) 245-257.
[27] B.G.S. Goss, H. Nakatani, G.A. George, M. Terano, Catalyst residue effects on the heterogeneous oxidation of polypropylene, Polymer Degradation and Stability, 82 (2003) 119-126.
[28] M. Celina, G.A. George, A heterogeneous model for the thermal oxidation of solid polypropylene from chemiluminescence analysis, Polymer Degradation and Stability, 40 (1993) 323-335.
[29] M. Celina, G.A. George, Heterogeneous and homogeneous kinetic analyses of the thermal oxidation of polypropylene, Polymer Degradation and Stability, 50 (1995) 89-99.
[30] B.G.S. Goss, I. Blakey, M.D. Barry, G.A. George, Modelling of infectious spreading in heterogeneous polymer oxidation II. Refinement of stochastic model and calibration using chemiluminescence of polypropylene, Polymer Degradation and Stability, 74 (2001) 523-532.
[31] M. Nikolic, E. Gauthier, K. George, G. Cash, M.D. de Jonge, D.L. Howard, D. Paterson, B. Laycock, P.J. Halley, G. George, Antagonism between transition metal pro-oxidants in polyethylene films, Polymer Degradation and Stability, 97 1178-1188.
[32] N.S. Allen, A. Chirinos-Padron, J.H. Appleyard, Photo-stabilising action of metal chelates in polypropylene. Part II: Photolysis versus photo-sensitised oxidation under monochromatic irradiation, Polymer Degradation and Stability, 5 (1983) 29-41.
[33] N.S. Allen, A. Chirinos-Padron, J.H. Appleyard, Photo-stabilising action of metal chelates in polypropylene. Part I: Excited state quenching versus UV antioxidant action under polychromatic irradiation, Polymer Degradation and Stability, 4 (1982) 223-237.
[34] N. Hisayuki, et al., Degradation behavior of polymer blend of isotactic polypropylenes with and without unsaturated chain end group, Science and Technology of Advanced Materials, 9 (2008) 024401.
[35] N.S. Allen, K.O. Fatinikun, J. Luc-Gardette, J. Lemaire, Photo-oxidation of polypropylene: Relationship between unsaturation and induction period, Polymer Degradation and Stability, 4 (1982) 95-100.
[36] G. Teissedre, J.F. Pilichowski, S. Chmela, J. Lacoste, Ageing of EPDM--I: Photo and thermal stability of EPDM hydroperoxides, Polymer Degradation and Stability, 53 (1996) 207-215.
[37] F. Delor, G. Teissedre, M. Baba, J. Lacoste, Ageing of EPDM. 2. Role of hydroperoxides in photo- and thermo-oxidation, Polymer Degradation and Stability, 60 (1998) 321-331.
[38] A.M. Trozzolo, F.H. Winslow, A Mechanism for the Oxidative Photodegradation of Polyethylene, Macromolecules, 1 (1968) 98-100.
[39] G.a.C.D. Geuskens, The photo-oxydation of polymers. A comparison with low molecular weight compounds, Pure and Applied Chemistry, 51 (1979) 233-240.
[40] J. Pospísil, S. Nespurek, J. Pilar, Impact of photosensitized oxidation and singlet oxygen on degradation of stabilized polymers, Polymer Degradation and Stability, 93 (2008) 1681-1688.
[41] M. Theodore, R. Harold, R.M. Frank, Aging and degradation of polyolefins. IV. Thermal and photodecompositions of model peroxides, Journal of Polymer Science: Polymer Chemistry Edition, 11 (1973) 2899-2907.
[42] P. Gijsman, Reply to "comment on oxygen charge-transfer complexes as peroxidation initiators in polymers" • , Polymer Degradation and Stability, 60 (1998) 217-219.
[43] D.J. Carlsson, D.M. Wiles, The photodegradation of Polypropylene Films. III. Photolysis of polypropylene hydroperoxydes, Macromolecules, 2 (1969) 597-606.
[44] J.C.W. Chien, Jabloner, H. , Polymer reactions. IV. Thermal decomposition of polypropylene hydropéroxydes, Journal of Polymer Science Part A-1: Polymer Chemistry, 6 (1968) 393-402.
[45] N.V. Zolotova, E.T. Denisov, J., Journal of Polymer Science, Part A-l, 9 (1971) 3311.

[46] N.C. Billingham, E.T.H. Then, P.J. Gijsman, Chemiluminescence from peroxides in polypropylene. Part I: Relation of luminescence to peroxide content, Polymer Degradation and Stability, 34 (1991) 263-277.
[47] Y.A. Shlyapnikov, T.A. Bogaevskaya, S.G. Kiryushkin, T.V. Monakhova, Specific features of formation and properties of hydroperoxides of polyolefins, European Polymer Journal, 15 (1979) 737-742.
[48] C. Walling, L. Heaton, Journal of the American Chemical Society, 87 (1968) 48.
[49] C.W.C. James, E.J. Vandenberg, H. Jabloner, Polymer reactions. III. Structure of polypropylene hydroperoxide, Journal of Polymer Science Part A-1: Polymer Chemistry, 6 (1968) 381-392.
[50] J.C.W. Chien, Jabloner, H. , Polymer reactions. IV. Thermal decomposition of polypropylene hydroperoxides, Journal of Polymer Science Part A-1: Polymer Chemistry, 6 (1968) 393-402.
[51] L. Achimsky, L. Audouin, J. Verdu, Kinetic study of the thermal oxidation of polypropylene, Polymer Degradation and Stability, 57 (1997) 231-240.
[52] X. Colin, B. Fayolle, L. Audouin, J. Verdu, About a quasi-universal character of unstabilised polyethylene thermal oxidation kinetics, Polymer Degradation and Stability, 80 (2003) 67-74.
[53] E. Richaud, X. Colin, B. Fayolle, L. Audouin, J. Verdu, Induction period in the low-temperature thermal oxidation of saturated hydrocarbons: Example of polyethylene, International Journal of Chemical Kinetics, 40 (2008) 769-777.
[54] E. Richaud, F. Farcas, B. Fayolle, L. Audouin, J. Verdu, Hydroperoxide build-up in the thermal oxidation of polypropylene - A kinetic study, Polymer Degradation and Stability, 92 (2007) 118-124.
[55] J. Rychly, L. Matisova-Rychla, K. Csmorova, L. Achimsky, L. Audouin, A. Tcharkhtchi, J. Verdu, Kinetics of mass changes in oxidation of polypropylene, Polymer Degradation and Stability, 58 (1997) 269-274.
[56] F. Gugumus, Thermolysis of polyethylene hydroperoxides in the melt. Part 9: Re-examination of the experimental kinetics of hydroperoxide decomposition, Polymer Degradation and Stability, 92 (2007) 2121-2134.
[57] J.G. Calvert, J.N. Pitts, Jr., Photochemistry, American Chemical Society, 1966.
[58] S. Girois, Photooxydation du polypropylène : aspects cinétiques in: Mécanique et Matériaux, Ecole Nationale Supérieure des Arts et Métiers, 2001.
[59] R. Mill T., H., Mayo, F.R., Journal of Polymer Science, Polym. Chem., 11 (1973) 2899.
[60] P. Gijsman, J. Hennekens, J. Vincent, The mechanism of the low-temperature oxidation of polypropylene, Polymer Degradation and Stability, 42 (1993) 95-105.
[61] A. Zahradnícková, J. Sedlár, D. Dastych, Peroxy acids in photo-oxidized polypropylene, Polymer Degradation and Stability, 32 (1991) 155-176.
[62] S. Falicki, D.J. Carlsson, D.J. Gosciniak, J.M. Cooke, Reactions of dimethyl sulfide with oxidized polypropylene, Polymer Degradation and Stability, 41 (1993) 205-210.
[63] P. Gijsman, M. Kroon, M. van Oorschot, The role of peroxides in the thermooxidative degradation of polypropylene, Polymer Degradation and Stability, 51 (1996) 3-13.
[64] F. Gugumus, Contribution to the role of aldehydes and peracids inpolyolefin oxidation1. Photolysis and photooxidation of aldehydes in polyethylene, Polymer Degradation and Stability, 65 (1999) 259-269.
[65] G. Oster, Photochemistry (Calvert, Jack G.; Pitts, James N., Jr.), Journal of Chemical Education, 43 (1966) 564.
[66] P. Delprat, X. Duteurtre, J.-L. Gardette, Photooxidation of unstabilized and HALS-stabilized polyphasic ethylene-propylene polymers, Polymer Degradation and Stability, 50 (1995) 1-12.
[67] J.H. Adams, Analysis of the nonvolatile oxidation products of polypropylene I. Thermal oxidation, Journal of Polymer Science Part A-1: Polymer Chemistry, 8 (1970) 1077-1090.
[68] F. Gugumus, Physico-chemical aspects of polyethylene processing in an open mixer. Part 29: Experimental kinetics and mechanisms of [gamma]-lactone formation, Polymer Degradation and Stability, 92 (2007) 143-157.
[69] F. Gugumus, Physico-chemical aspects of polyethylene processing in an open mixer. Part 30: Formal kinetics of [gamma]-lactone formation at a constant rate, Polymer Degradation and Stability, 92 (2007) 158-175.
[70] D.J. Carlsson, D.M. Wiles, The Photodegradation of Polypropylene Films. II. Photolysis of Ketonic Oxidation Products, Macromolecules, 2 (1969) 587-597.

[71] G. Geuskens, F. Debie, M.S. Kabamba, G. Nedelkos, New aspects of the photooxidation of polyolefins, Polymer Photochemistry, 5 (1984) 313-331.
[72] E. Guillet J, Studies of energy transfer and molecular mobility in polymer photochemistry, Pure and Applied Chemistry, 49 (1977) 249-258.
[73] N.L. Maecker, D.B. Priddy, Photodegradation of ethylene–propylene copolymer and ethylene–propylene–ethylidene norbornene terpolymer, Journal of Applied Polymer Science, 42 (1991) 21-33.
[74] N.J. Turro, Energy Transfer Processes, Pure and Applied Chemistry, 49 (1977) 405-429.
[75] G. Geuskens, M.S. Kabamba, Photo-oxidation of polymers--Part V: A new chain scission mechanism in polyolefins, Polymer Degradation and Stability, 4 (1982) 69-76.
[76] G. Geuskens, M.S. Kabamba, Photo-oxidation of polymers: Part IX--Additional comments about a new chain scission mechanism in polyolefins, Polymer Degradation and Stability, 5 (1983) 399-401.
[77] J.L. Bolland, G. Gee, Kinetic studies in the chemistry of rubber and related materials. II. The kinetics of oxidation of unconjugated olefins, Transactions of the Faraday Society, 42 (1946) 236-243.
[78] S. Korcek, J.H.B. Chenier, Howard J.A., I. K.U., Absolute rate constants for hydrocarbon auto-oxidation- Activation energies for propagation and the correlation of propagation rate constants, Canadian Journal of Chemistry, (1972) 2285-2297.
[79] D.J. Carlsson, J. Lacoste, A critical comparison of methods for hydroperoxide measurement in oxidized polyolefins, Polymer Degradation and Stability, 32 (1991) 377-386.
[80] E. Niki, C. Decker, F. Mayo, Aging and degradation of polyolefins. I. Peroxide-initiated oxidations of atactic polypropylene, Journal of Polymer Science: Polymer Chemistry Edition, 11 (1973) 2813-2845.
[81] C. Decker, F. Mayo, Aging and degradation of polyolefins. II. gamma-initiated oxidations of atactic polypropylene, Journal of Polymer Science: Polymer Chemistry Edition, 11 (1973) 2847-2877.
[82] J.L. Philippart, J.L. Gardette, Photochemical behavior of isotactic-polypropylene irradiated in 32O2-36O2, Polymer Degradation and Stability, 71 (2000) 189-194.
[83] J.L. Philippart, J.L. Gardette, Thermo-oxidation of isotactic polypropylene in 32O2-36O2: comparison of the mechanisms of thermo- and photo-oxidation, Polymer Degradation and Stability, 73 (2001) 185-187.
[84] X. Colin, E. Richaud, J. Verdu, C. Monchy-Leroy, Kinetic modelling of radiochemical ageing of ethylene-propylene copolymers, in: I.R.a. Polymers (Ed.) Proceedings of the 8th International Symposium on Ionizing Radiation and Polymers, Elsevier, Angra dos Reis, Rio de Janeiro, Brazil, 12-17 October 2008, 2008, pp. 6.
[85] J.A. Howard, K.U. Ingold, Absolute rate constants for hydrocarbon autoxidation. VI. Alkyl aromatic and olefinic hydrocarbons, Canadian Journal of Chemistry, 45 (1967) 793-802.
[86] R. Bernstein, S.M. Thornberg, R.A. Assink, A.N. Irwin, J.M. Hochrein, J.R. Brown, D.K. Derzon, S.B. Klamo, R.L. Clough, The origins of volatile oxidation products in the thermal degradation of polypropylene, identified by selective isotopic labeling, Polymer Degradation and Stability, 92 (2007) 2076-2094.
[87] J. Lacoste, D. Vaillant, D.J. Carlsson, Gamma-, photo-, and thermally-initiated oxidation of isotactic polypropylene, Journal of Polymer Science Part A: Polymer Chemistry, 31 (1993) 715-722.
[88] D.M. Mowery, R.A. Assink, D.K. Derzon, S.B. Klamo, R.L. Clough, R. Bernstein, Solid-State 13C NMR Investigation of the Oxidative Degradation of Selectively Labeled Polypropylene by Thermal Aging and Î³-Irradiation, Macromolecules, 38 (2005) 5035-5046.
[89] J.-L. Philippart, F. Posada, J.-L. Gardette, Mass spectroscopy analysis of volatile photoproducts in photooxidation of polypropylene, Polymer Degradation and Stability, 49 (1995) 285-290.
[90] D. Vaillant, J. Lacoste, G. Dauphin, The oxidation mechanism of polypropylene: contribution of 13C-NMR spectroscopy, Polymer Degradation and Stability, 45 (1994) 355-360.
[91] R. Arnaud, J.-L. Gardette, J. Lacoste, A. Rivaton, Evolution photochimique des macromolécules organiques naturelles et synthétiques- Photoprotection des matériaux polymères synthétiques, L'Actualité Chimique [In french], N°7 (suppl.) (12/94) (1994) 132-210.
[92] J.H. Adams, Analysis of nonvolatile oxidation products of polypropylene. III. Photodegradation, Journal of Polymer Science Part A-1: Polymer Chemistry, 8 (1970) 1279-1288.
[93] F. Gugumus, Formation of ester functional groups in oxidizing polymers, Polymer Degradation and Stability, 65 (1999) 5-13.

[94] J.-L. Philippart, C. Sinturel, R. Arnaud, J.-L. Gardette, Influence of the exposure parameters on the mechanism of photooxidation of polypropylene, Polymer Degradation and Stability, 64 (1999) 213-225.
[95] L. Audouin, V. Langlois, J. Verdu, J.C.M. de Bruijn, Role of oxygen diffusion in polymer ageing: kinetic and mechanical aspects, Journal of Materials Science, 29 (1994) 569-583.
[96] A.V. Cunliffe, A. Davis, Photo-oxidation of thick polymer samplesâ€"Part II: The influence of oxygen diffusion on the natural and artificial weathering of polyolefins, Polymer Degradation and Stability, 4 (1982) 17-37.
[97] S. Girois, P. Delprat, L. Audouin, J. Verdu, Oxidation thickness profiles during photooxidation of non-photostabilized polypropylene, Polymer Degradation and Stability, 56 (1997) 169-177.
[98] K.M.B. Jansen, Analytical approximation of degradation profiles in polymer products, Polymer Engineering & Science, 34 (1994) 1619-1627.
[99] L.M. Rincon-Rubio, B. Fayolle, L. Audouin, J. Verdu, A general solution of the closed-loop kinetic scheme for the thermal oxidation of polypropylene, Polymer Degradation and Stability, 74 (2001) 177-188.
[100] N.C. Billingham, P. Prentice, T.J. Walker, Some effects of morphology on oxidation and stabilization of polyolefins, Journal of Polymer Science: Polymer Symposia, 57 (1976) 287-297.
[101] J.B. Knight, P.D. Calvert, N.C. Billingham, Localization of oxidation in polypropylene, Polymer, 26 (1985) 1713-1718.
[102] M. Celina, G.A. George, N.C. Billingham, Physical spreading of oxidation in solid polypropylene as studied by chemiluminescence, Polymer Degradation and Stability, 42 (1993) 335-344.
[103] M.L. Castejon, P. Tiemblo, J.M. Gomez-Elvira, Photo-oxidation of thick isotactic polypropylene films I. Characterisation of the heterogeneous degradation kinetics, Polymer Degradation and Stability, 70 (2000) 357-364.
[104] F. Gugumus, Thermooxidative degradation of polyolefins in the solid state. 4: Heterogeneous oxidation kinetics, Polymer Degradation and Stability, 53 (1996) 161-187.
[105] F. Gugumus, Thermooxidative degradation of polyolefins in the solid state. Part 2: Homogeneous and heterogeneous aspects of thermal oxidation, Polymer Degradation and Stability, 52 (1996) 145-157.
[106] G.A. George, M. Celina, C. Lerf, G. Cash, D. Weddell, A spreading model for the oxidation of polypropylene, Macromolecular Symposia, 115 (1997) 69-92.
[107] B.G.S. Goss, M.D. Barry, D. Birtwhistle, G.A. George, Modelling of infectious spreading in heterogeneous polymer oxidation I. Development of a stochastic model, Polymer Degradation and Stability, 74 (2001) 271-282.
[108] G.A. George, M. Ghaemy, Hydroperoxide formation in the early stages of polypropylene photo-oxidation, Polymer Degradation and Stability, 33 (1991) 411-428.
[109] Y.V. Makedonov, A.L. Margolin, N.Y. Raporort, L.S. Shibryayeva, Reasons for the change in the effective reaction constants of chain propagation and termination in the induction period of oxidation of isotropic and oriented isotactic polypropylene Polymer science USSR, 28 (1987) 1536-1543.
[110] Y.A. Mikheev, L.N. Guseva, G.E. Zaikov, An analysis of the kinetic models of polyolefin oxidation, Polymer Science - Series B, 39 (1997) 241-256.
[111] Y.A. Mikheev, L.N. Guseva, G.E. Zaikov, Comments on structural-kinetic models of oxidation of polyolefins, Polymer Degradation and Stability, 63 (1999) 509-523.
[112] L. Audouin, X. Colin, B. Fayolle, E. Richaud, J. Verdu, Le vieillissement thermo-oxydant des polymères est-il modélisable ? [In french], 98 (2010) 347-360.
[113] J. Verdu, On the autoaccelerated character of the branched oxidation of polyolefins, Macromolecular Symposia, 115 (1997) 165-180.

CHAPTER II. Materials and Methods- Methodological aspects

Résumé [Summary in French]

La partie Matériaux et Méthodes est dédiée à l'identification et au traitement des sources de variabilité ou d'erreurs, d'origine expérimentale (reproductibilité des essais en enceintes), méthodologique (traitement des résultats) ou numérique (simulations) :

(i) La variabilité matériaux, issus de différences de méthodes de synthèse, de mise en œuvre ou de préparation. Dans le cas des échantillons d'iPP étudiés sans cette thèse, les différences de comportement proviennent majoritairement de la qualité d'extraction des additifs stabilisants. Cette variabilité entre les lots d'échantillons a est inévitable et a été évaluée par des tests non-paramétriques (contrôle qualité).

(ii) Les incertitudes sur les conditions d'exposition, la température ou l'intensité lumineuse. Ainsi, la température a été contrôlée en surface de l'échantillon, laquelle peut différer notablement de la température dans la chambre climatique ou au panneau noir en photooxydation. De même, un soin particulier a été apporté à la mesure des irradiances pour les différentes géométries d'enceinte utilisées. Cette problématique du contrôle des conditions d'exposition se pose en particulier en termes de stabilité temporelle : les fluctuations de températures observées lors des prélèvements effectués pour mesure peuvent induire une incertitude sur les temps réels d'exposition et donc sur sur la cinétique d'oxydation et la détermination des conatantes. Cette difficulté a été contournée en optimisant la fréquence d'échantillonnage des prélèvements en conséquence.

(iii) Le choix des indicateurs de l'oxydation ainsi que la méthode de suivi. Il a été montré que la vitesse maximale d'oxydation observée par spectroscopie FT-IR peut être notablement plus faible que la valeur théorique si l'état quasi-stationnaire n'est pas atteint, et ainsi générer un biais entre la valeur expérimentale et la valeur numérique simulée par le modèle.

(iv) Les erreurs numériques (convergence et stabilité de l'intégration). Elles résultent des approximations numériques et dépendent du conditionnement du problème

(notamment les conditions d'initialisation), ou encore de l'algorithme de résolution choisi. En effet, les problèmes traités dans cette étude sont particulièrement raides du fait des temps caractéristiques très différents des différents phénomènes impliqués (notamment les réactions chimiques) et nécessitent l'usage d'algorithmes spécifiques.

1. Introduction

Since the PhD dissertation will be based on articles, in which the experimental procedures will be detailed, this chapter will just focus on the metrology in polymer aging which is usually not evoked in the experimental sections of papers.

Indeed, a great attention must be paid to the numerous factors impacting the results along aging experiments. The response Y, accounting for a relevant end-of-life criterion (e.g. oxidation induction period) is a function of different environmental factors, e.g. temperature (T) and UV-light exposure (I), the material preparation (Mat), the sensitivity of analytical methods (Met) or mean of measurement (Mea), etc:

$$Y = f(T, I, Mat, Met, Mea\ \ldots.)$$

Then, according to the principle of variance partition, the overall uncertainty can be expressed as:

$$u(Y) = f(u(T), u(I), u(Mat), u(Met), u(Mea)\ \ldots.)$$

In a general rule, it will be considered that the repeatability mainly derives from the sensitivity and/or accuracy of the analytical methods, whereas the other sources of variability (including the material quality) will mainly impact the reproducibility.

All the resulting uncertainties can involve noticeable scattering or even incoherencies of the results which is incompatible with an approach of kinetic modeling. All the errors cannot be eliminated but they must be minimized as much as possible.

The first part will tackle general considerations of metrology in the field of polymer aging. The second part will be dedicated to the variability on material and its impact on the methodology. Finally, the choice of the experimental conditions will be discussed as well as the procedure to control the exposure conditions in photothermal aging.

2. Metrology: general considerations in aging experiments

2.1. The criteria for oxidation monitoring

Kinetics of oxidation are commonly characterized though two main indicators: (i) the steady-state oxidation rate R_{ox}, which applies to the slope of the maximal oxidation rate (ii) the induction period t_{ind}, also called Oxidation Induction Time, which can be mathematically defined as the intercept of the maximal oxidation rate with the time abscissa (figure 1).

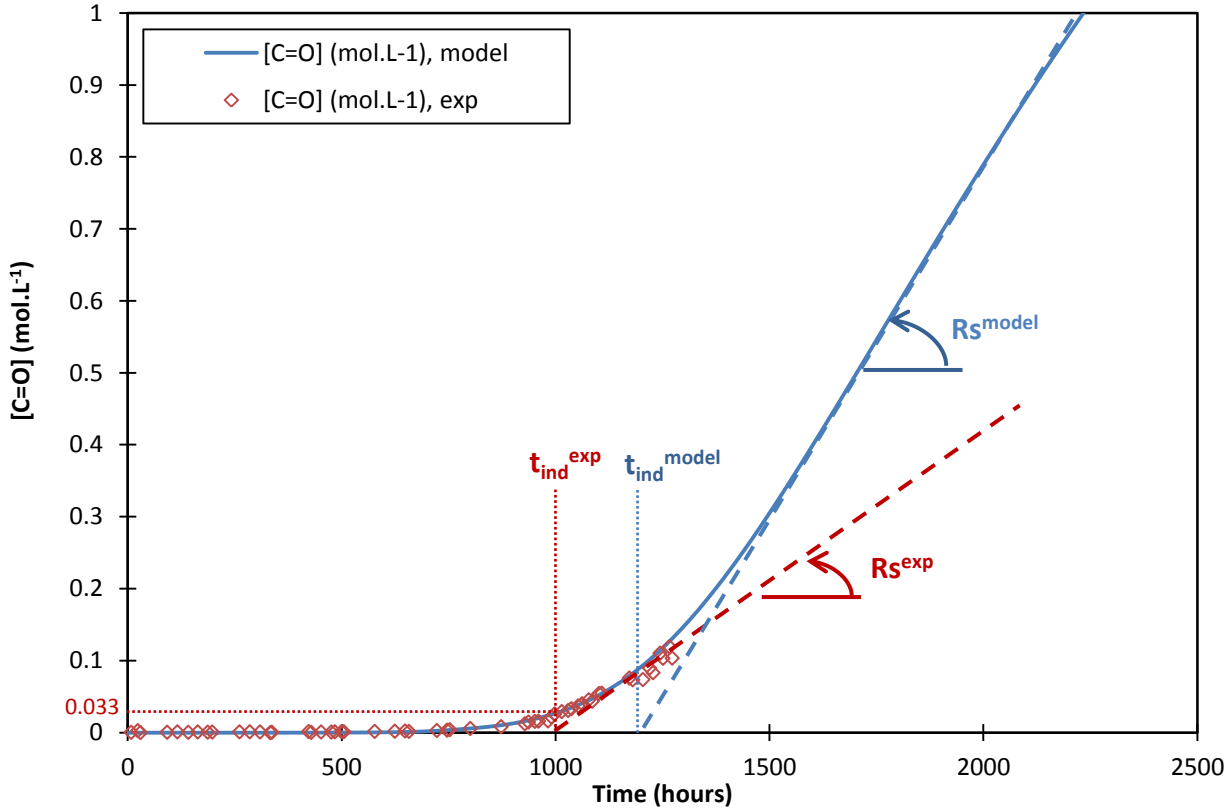

Figure 1: Determination of two oxidation indicators: namely the induction period (or Oxidation Induction Time) and the maximal oxidation rate. The example applies to the thermal oxidation of iPP at 60°C in air. Symbols: experimental. Solid line: kinetic modeling. Dashed line: intercept from slopes of the experimental datas (in red) and the simulation (in blue).

The observed maximal oxidation rate theoretically applies to the steady-state oxidation rate provided that this state was reached, i.e. that the duration of monitoring was long enough. For most of analyses -e.g. oxygen uptake, chemiluminescence or thermal analyses-, this condition is fulfilled, but not systematically in the case of FTIR carbonyl products monitoring (especially at low temperatures). Indeed, the test run duration was limited by film fracture,

well before reaching the steady-state, for instance in the case of thermal aging at 60°C as depicted in figure 1. Since the model enables to simulate the whole curve, the numerically estimated value is correct but noticeably differs from the experimental one. This discrepancy also concerns induction periods if they are measured through the intercept of the maximal oxidation rate with the x-abscissa. It results in a statistical bias between the numerical and the experimental values, which can let believe that the model is unsuitable. It is suspected that this phenomenon could be responsible for discontinuities in the Arrhenius graphs of oxidation rates and induction periods besides mechanistic explanations basing on effects of catalyst residues [1-4]. This apparent gap (or systematic error) must be corrected in agreement with the Guide for Uncertainties Measurements [5] recommendations in order to account for the agreement of the model with experimental data.

2.2. Estimation of uncertainties and "error" bars

2.2.1. Uncertainties on measurements

This kind of uncertainties was particularly important to calculate in the case of chemical species titration. In the case of hydroperoxide titration, this uncertainty was estimated by logarithmic differentiation to be of 7.5 mol%, mainly coming from the sequence of tasks rather than due to the sensitivity and/or resolution of the analytical apparatus. This uncertainty must be compared to the variability induced by the sample batch which largely exceeds this value –particularly in the case of a thermal aging campaign- and degrade the reproducibility of induction without impacting theoretically steady-state oxidation rates.

2.2.2. Expanded uncertainties

Considering the different random variabilities, experimental values were given with their expanded uncertainties -in agreement with GUM specifications [5]- using the conventional reliability threshold of 95% usually in bilateral test. The uncertainties of induction times or oxidation rates were calculated from errors on least-squares methods applied to the whole cluster of values.

3. Material preparation and characterization

3.1. Isotactic polypropylene morphological features

The reference material was an isotactic homo-polypropylene h-PP injection grade (Mw=250 kg.mol^{-1} g/mol, Mn = 67 kg.mol^{-1}) supplied by Aldrich. Thin films of 80 µm and 135 µm

were processed by compression molding. The cristallinity was found equal to 45 ± 3 wt% by DSC in a TA Q1000 device, taking a melting enthalpy of ΔH_m^0 = 209 $J.g^{-1}$ for crystalline lamellae.

3.2. Procedure of purification in Soxhlet

Different characteristics of the material can induce a variability of its oxidation behavior such as its morphological features, its content in metal chelates from catalysis residues and, above all, the residual concentration in stabilizers whose even trace amounts dramatically impact resistance to oxidation. These latter must thus be quantitatively removed prior exposure.

The iPP films were purified from their antioxidants in Soxhlet with dichloromethane for 48 hours at room temperature prior to aging experiments. Dichloromethane was chosen as a good compromise due to its high efficiency (even at low temperature) and its low boiling point which ensure minimal pre-oxidation of samples. Obviously, the quality of the stabilizers extraction depends on the nature and flow rate of solvent, the duration of the extraction or even, the amount and the thickness of the samples introduced into the Soxhlet apparatus. These different parameters were difficult to control, thus resulting in a potential scattering between different batches. In order to control the purity of iPP samples, Oxidation Induction Times experiments were performed in pure oxygen under atmospheric pressure (P_{O2}=1 bar) at 140°C. Before sample exposure to photothermal aging, $OIT_{140°C}$ obtained for a first batch (non-destructive analyses) were respectively 30, 26 and 24 minutes (three replicates). Results obtained for a second batch (destructive analyses) are depicted in Figure 2.

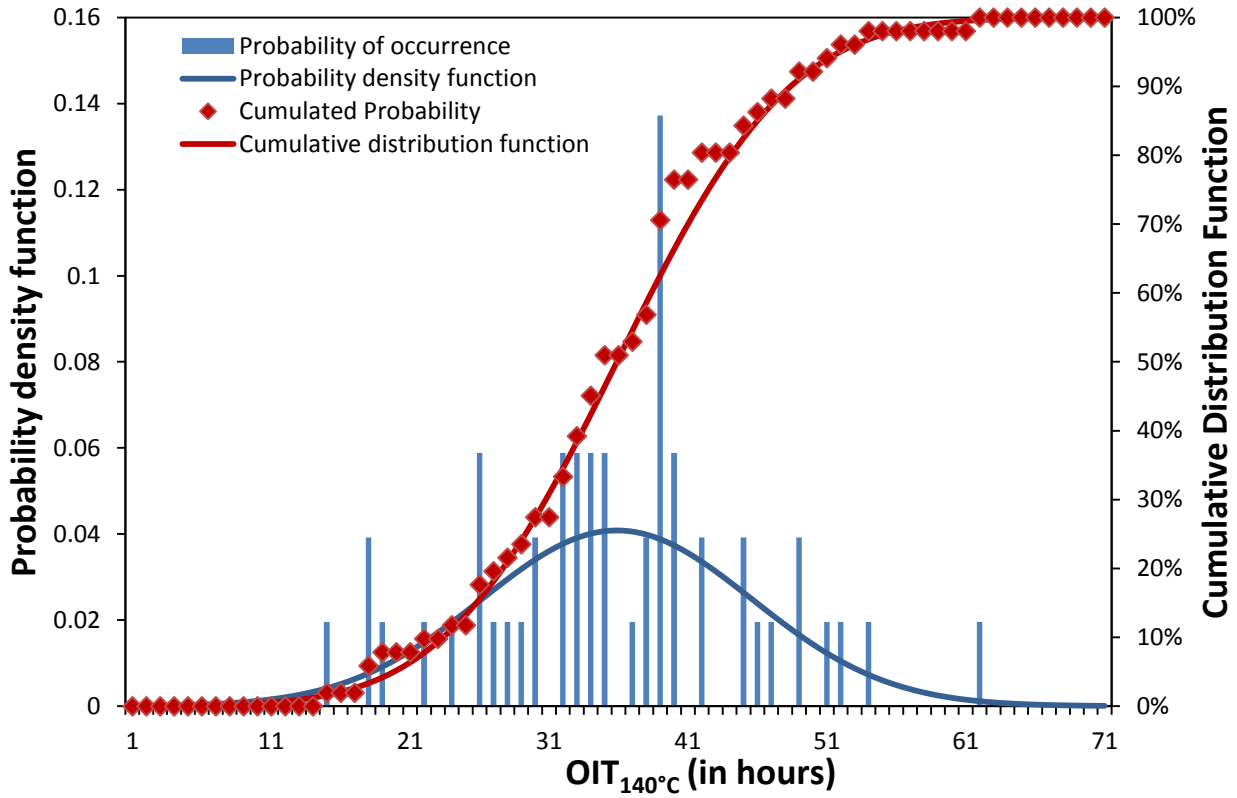

Figure 2: Probability density and cumulative distribution functions of the OIT of purified iPP samples batch

The distribution of OIT from the second batch is clearly normal (gaussian) according to the Jarque-Bera test (excess kurtosis equal to 0.345, asymmetry of 0.025, Jarque-Bera's criterion of 0.67). The probability density and cumulative distribution functions are depicted in Figure 2. So, the impact of the efficacy of the stabilizers extraction is a random variable.

The results from these two batches do not obey to the same kind of distribution according to the Fisher-Snedecor test. It enables to choose the suitable Student's test for testing the means equality and to find no statistical bias between the two batches. This result enables to highlight statistical bias, at least in thermal oxidation, which must be corrected once differentiated from ramdom error.

Ideally, samples of a same batch should be exposed in all the aging conditions in order to minimize scattering but the scheduled analyses would require a great amount of material which would come necessarily from different batches. As a consequence, the methodology was to proceed in two phases: (i) the exposure of sample from a same batch in all the aging conditions (with three replicates in the case of the photothermal oxidation) followed by a non-destructive FTIR monitoring (ii) the exposure of numerous samples, necessarily from different batches, which are dedicated to destructive analyses. Thus, there is no scattering

between the different aging conditions due to the material variability in the results of the first stage and their aging monitoring can be used as kinds of calibration curves.

4. Control of the exposure conditions in photothermal aging

4.1. Design of the tests matrix: an incremental approach

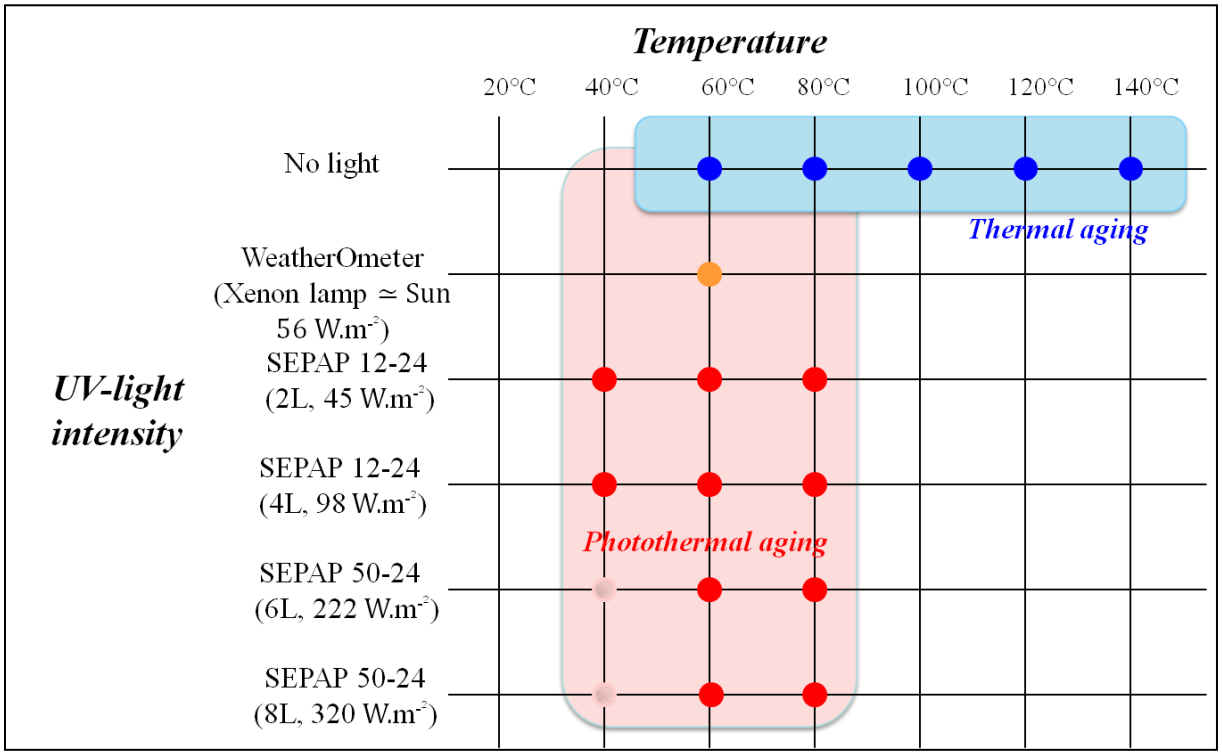

Figure 3: Test matrix for investigating the effect of light and temperature on polypropylene ageing

In photothermal aging, it will be necessary to decouple thermal and photochemical effects and the test matrix must be crossed. In thermal oxidation, the temperature range was chosen to study iPP at the solid-state and temperature as close of real-use as possible but with reasonable aging durations. In photothermal aging, exposure conditions were determined according to device possibilities and normalized testing methodologies (including different types of light sources) in order to cover domain as large as possible.

It would enable to check that there is no interaction terms between the two effects and that they are additive.

4.2. Specification of irradiation devices

UV-light exposures and measurements of irradiance and sources spectra have been performed by Narcisse Siampiringue, from *Centre National d'Evaluation et de Photoprotection (CNEP), Clermont-Ferrand.*

4.2.1. SEPAP: a suitable device for polymer aging monitoring

Most of the irradiation tests were carried out in SEPAP 12/24 or SEPAP 50/24 devices respectively equipped with 4 and 8 medium-pressure mercury arc lamps equipped with borosilicate filters. The specimens (8 mm x 25 mm) were positioned on a rotating carousel (4 laps per minute) at respectively 200 and 80 mm of the lamps' axes according to the devices' geometry depicted in figures 2 and 3 (Figure 4 and 5). The temperature is controlled by a thermocouple type Pt1000 at the ambient humidity (currently between 45 and 80% with expected minor influence).

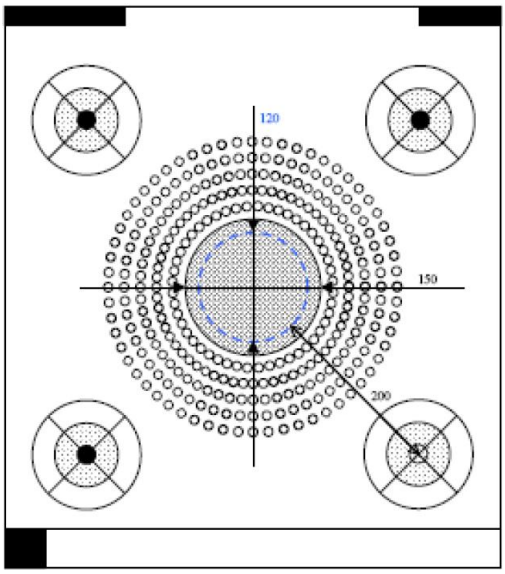

Figure 4: Geometric specifications of the "accelerated" SEPAP 12/24 device (4 lamps)

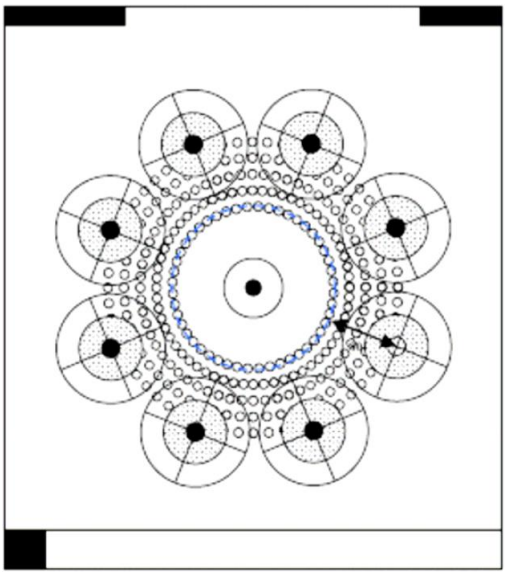

Figure 5: Geometric specifications of the "ultra-accelerated" SEPAP 50/24 device (8 lamps)

This kind of device, as the reference instrument of the Renault's method D27 3064, was chosen because mercury arc lamps have a very low emission in the infrared region which minimizes the additional heating of the sample by irradiation, facilitates the temperature regulation and enables to accelerate aging much more than other common aging devices. This kind of device is slightly richer in high-energy photons (λ < 280 nm) as discussed in the ISO/DIS 10640 standard (Plastics -- Methodology for assessing polymer photoageing by FTIR and UV/visible spectroscopy).

The light intensity was adjusted by varying the number of lamps from 2 to 4 in a SEPAP 12/24 and from 6 to 8 in a SEPAP 50/24.

4.2.2. Weather-OMeter

In order to obtain complementary results with a different light source, an additional test was led in a WeatherOMeter CI4000 device, equipped with a Xenon lamp using a S/S Boro/Boro filter. This light source is well-know to simulate the spectral power distribution of the natural sunlight and is thus close to the real-life conditions. The conditions were fixed according to the specifications of the Renault method D271911. The illuminance was fixed at 0.55 $W.m^{-2}$ at 340 nm. The black panel (BPT) and chamber temperatures were fixed at 70°C and 50°C respectively. Contrarily to the mercury lamp of SEPAP, the xenon lamp has a non-negligible emission in the infrared wavelength domain, thereby causing overheating of the specimen depending upon its opacity. The effective sample temperature is thus intermediary between the chamber and black panel temperatures. The humidity in the chamber was of 50 ± 10% with no water spaying.

4.3. Irradiation and sources' spectra

The emission spectra of the different light sources were recorded using an Avantes spectroradiometer (AvaSpec 2048x14-USB2 – optical fiber, probe temperature of 26°C, calibrated in terms of wavelength and irradiance) in the 200-720nm spectral range with a minimal resolution of 0.7 nm. The spectra of the Xenon and medium pressure mercury lamps are depicted in figure 6.

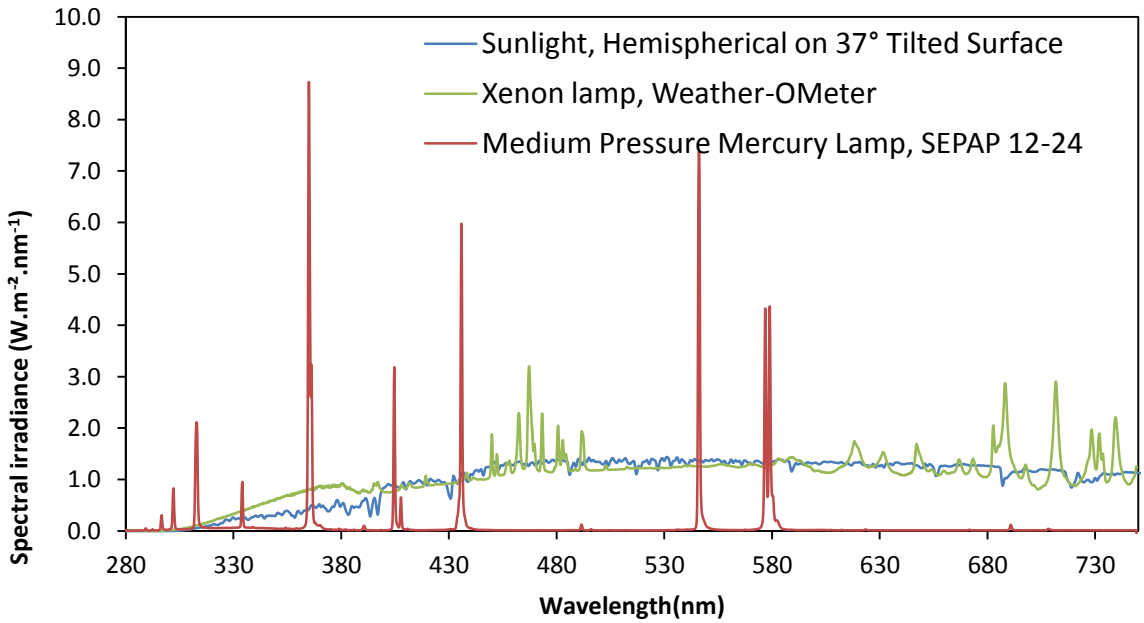

Figure 6: Sources spectra of Sunlignt (direct + circumsolar according to ASTM G-173-03, National Renewable Energy Laboratory) and of the Xenon and Medium Pressure Mercury lamps in WeatherOMeter and SEPAP c12-24 devices respectively

The irradiance measurements in SEPAP were performed using a wireless IL390C radiometer in a spectral range from 250 to 415 nm) at the same distance from the source as specimens. The UV-light dose was averaged over 8 laps (2 minutes) with an accuracy of 10%.

Table 1: Irradiances on specimens in the different configurations

Device	Number of lamps	Irradiance ($W.m^{-2}$)
SEPAP 12/24	2	45
SEPAP 12/24	4	98
SEPAP 50/24	6	233 ± 10
SEPAP 50/24	8	310 ± 10

In the SEPAP 50/24 device, it was checked that the irradiance was proportional to the number of lamps and thus, not impacted by the device geometry (Figure 7).

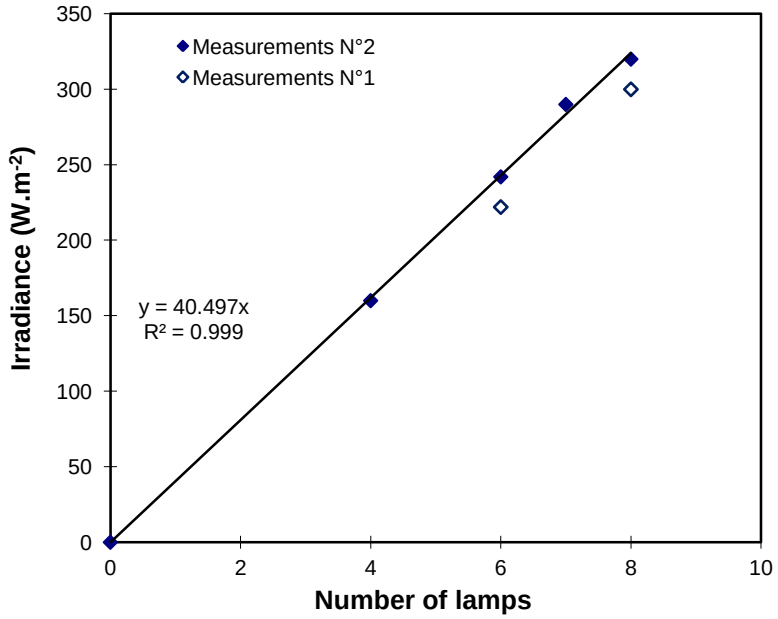

Figure 7: Influence of the number of lamps on the SEPAP 50/24 irradiance (the empty lamps locations were diametrically opposed)

4.4. Control of the temperature: difficulty in monitoring fast aging kinetics

The regulation of the temperature turned out to be somewhat difficult in the case of ultra-accelerated aging at 60°C since the regulation system of the air flow is designed to reach a set point of about 70°C. The other difficulty in regulating the temperature lies in the frequency of sampling in the case of fast aging kinetics. Indeed, specimens' analyses required periodical interruptions of the device and thus, to wait small durations after its relighting to rebalance the temperature of the desired value. This time needed to regulate the temperature can be too long to be neglected face to the exposure duration between two samplings and such durations must be subtracted from the total duration of irradiation. This phenomenon was all the more pronounced that heating rate was low, particularly in the case of irradiation with 6 lamps at 60°C and 80°C in a minor extent. These reasons led us to perform a direct temperature monitoring on the sample using a thermobutton type sensor, in contact with the studied specimen.

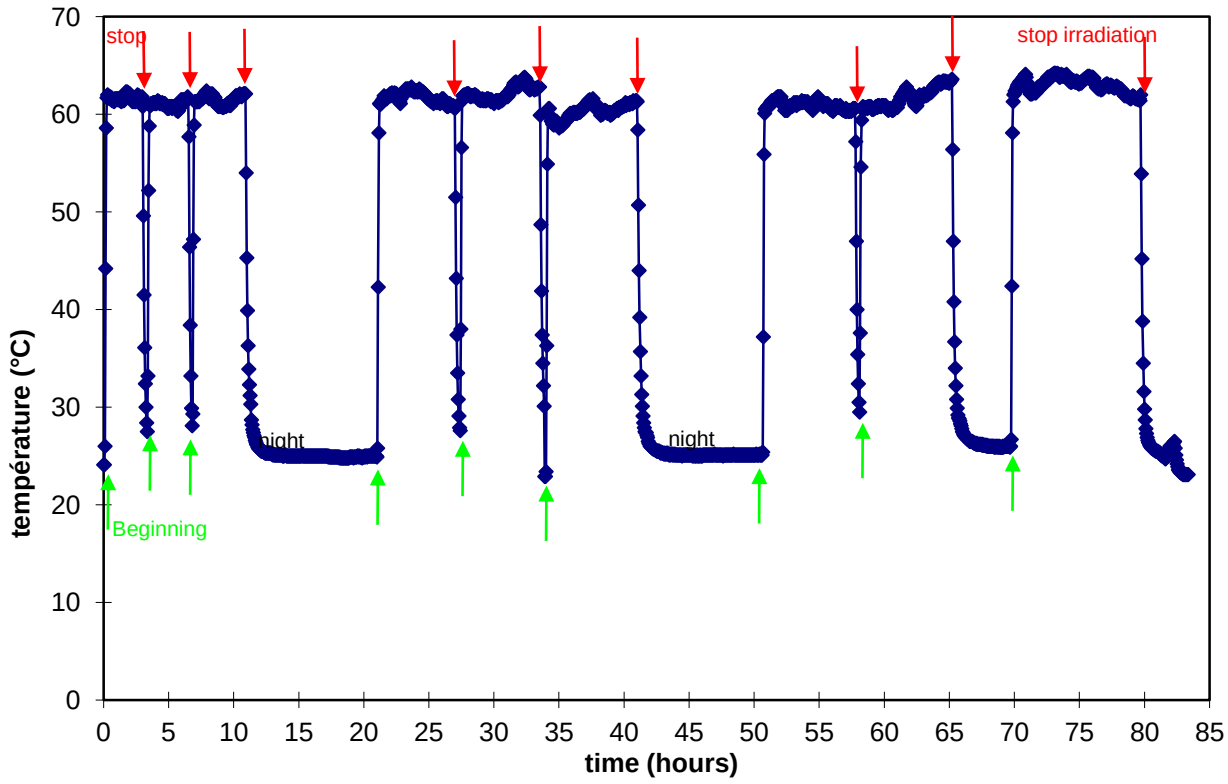

Figure 8: Example of temperature monitoring on the specimens' surface, at 60°C with 8 UV lamps. Arrows in green and red respectively indicate the beginnings and interruptions of light irradiation

During the time to equilibrate temperature, specimens were submitted to the effect of light irradiation at moderate temperature. Thus, the correction of the exposure duration is not trivial. Since, the variation of temperature can accidentally reach up to 10°C (during very small periods), it was found to be relevant to subtract the period of exposure when the temperature was 10°C under the target temperature. The time between two samplings was also adjusted in order to eliminate the gap in exposure duration induced by frequent sampling in fast aging kinetics.

5. Errors in numerical simulations

In part 2.1, an example of interpretation mistake resulting from the common simplifying assumptions in the analytical resolution of differential equation of chemical kinetics. In this case, it was shown that it is preferable to determine the kinetic rate constants by simulating the whole oxidation kinetics than from indicators such as the induction time or the maximal oxidation rate from analytical relationships.

Despite being powerful tools, numerical integration techniques also exhibit specific limitations and difficulties in solving the equations describing the kinetics of oxidation.

Indeed, such systems imply phenomena with very different time scales (for instance, reactions with kinetic rate constants having different orders of magnitude) and they are consequently very stiff. This specificity of the differential equations in chemical kinetics can generate errors when using numerical integration methods exhibiting instability in the solutions, e.g. Runge-Kutta or multisteps methods.

In this work, the numerical solving is performed using the ODE15s and ODE23s algorithms of the Matlab library, which are recommended for solving very stiff problem of chemical kinetics [6-8]. The former is a variable order solver based either on the numerical differentiation formulas (NDFs) or optionally on the backward differentiation formulas (BDFs, also known as Gear's method [9]). The latter is a one step solver based on a modified Rosenbrock formula of order 2. Practically, the choice of an integration method is a compromise between the stability and the efficiency of the method. ODE15s enables a significant decrease of the calculation time, which is useful in a trial and error procedure of optimization. However, its lower stability requires additional tests to check a suitable convergence. This can be easily operated by adjusting the absolute and relative tolerance of calculation steps. It is also useful to use the option relative to the Jacobian sparsity particularly in the case of ODE 15s.

These Matlab's routines are not suitable in the case of the photooxidation model which implies solving of differential algebraic equations systems of index higher than 1 (that ODE15s can solve [10]). The order of the DAE applies to the minimal number of analytical differentiations in order to extract an explicit ordinary differential equations system.

Basically, indexes higher than 1 implies hidden constrains which present difficulties for solvers. It is necessary to reduce this index which can be operated by symbolic differential (usually not trivial) or by using index reduction algorithms (basically included in higher index solvers).

In the present work, the DAE system has been written in the semi-explicit form of index-2:

$$\begin{cases} \dot{y} = f(y, x, t) \\ 0 = g(y, x) \end{cases}$$

It has been solved by using the software Open Modelica by using the DASSL method [11, 12] and the Pantelides index reduction algorithm [7].

Actually, the main issue consists in finding consistent for DAE of index higher than 1. Indeed, initial conditions must satisfy all intermediate algebraic equation:

$$\frac{\partial g}{\partial y} f = 0$$

The initialization of the problem has turned out to be awkward for simulations involving a high number of space discretizations. The Open Modelica software includes by default several high index capable DAE solvers which might be more efficient for solving the present problem. These numerical aspects are here off-topic but would hopefully undergo deeper investigation in the laboratory in the future.

The second issue lays probably in finding a suitable formalism for writing the equations (differential or algebraic) which involve vectors as far as it is applied to the case of polychromatic light sources. Basically, it consists in precomputing the relevant quantities which describes the influence of the light wavelength and then to introduce them in the DAE system. This approach facilitates their formalization and saves their calculation at each integration step.

References

[1] Achimsky L, Audouin L, Verdu J, Rychly J, Matisova-Rychla L. On a transition at 80 °C in polypropylene oxidation kinetics. Polymer Degradation and Stability. 1997;58:283-9.

[2] Celina M, Gillen KT, Assink RA. Accelerated aging and lifetime prediction: Review of non-Arrhenius behaviour due to two competing processes. Polymer Degradation and Stability. 2005;90:395-404.

[3] Gijsman P, Hennekens J, Vincent J. The influence of temperature and catalyst residues on the degradation of unstabilized polypropylene. Polymer Degradation and Stability. 1993;39:271-7.

[4] Gugumus F. Effect of temperature on the lifetime of stabilized and unstabilized PP films. Polymer Degradation and Stability. 1999;63:41-52.

[5] JCGM. Evaluation of measurement data – Guide to the expression of uncertainty in measurement. Joint Committee for Guides in Metrology, Bureau International des Poids et Mesures (CEI, IFCC, ILAC, ISO, UICPA, UIPPA and OIML). 100; 2008.

[6] Hairer E, Wanner G. Stiff and Differential-Algebraic Problems1996.

[7] Pantelides C. The Consistent Initialization of Differential-Algebraic Systems. SIAM Journal on Scientific and Statistical Computing. 1988;9:213-31.

[8] Shampine L, Reichelt M. The MATLAB ODE Suite. SIAM Journal on Scientific Computing. 1997;18:1-22.

[9] Gear C. Simultaneous Numerical Solution of Differential-Algebraic Equations. Circuit Theory, IEEE Transactions on. 1971;18:89-95.

[10] Shampine L, Reichelt M, Kierzenka J. Solving Index-1 DAEs in MATLAB and Simulink. SIAM Review. 1999;41:538-52.

[11] Gear C, Petzold L. ODE Methods for the Solution of Differential/Algebraic Systems. SIAM Journal on Numerical Analysis. 1984;21:716-28.

[12] Petzold L. Differential/Algebraic Equations are not ODE's. SIAM Journal on Scientific and Statistical Computing. 1982;3:367-84.

PART 1/ THERMAL OXIDATION

Thermooxydation du polypropylene [Summary in French]

Effet de paramètres morphologiques sur la cinétique d'oxydation

La modélisation cinétique de la thermooxydation du polypropylène isotactique (iPP), et plus généralement des polyoléfines, a été reconsidérée au début des années 1990 en se basant sur le rôle clé des hydroperoxydes, produits d'oxydation primaires bien connus pour se former et se décomposer au cours de l'oxydation. L'hypothèse sous-jacente est que la décomposition des hydroperoxydes (amorçage intrinsèque) devient rapidement la source majoritaire de radicaux en comparaison des défauts de structure (produits d'oxydation, coupures de chaines issues de contraintes thermomécaniques, résidus de catalyseur). L'idée générale de ce schéma simplifié, dit en « boucle fermée », consiste à identifier le chemin critique, prépondérant auquel on applique une démarche de cinétique formelle pour en déduire les lois générales reliant les conditions d'exposition à l'état de dégradation du matériau. La valeur des constantes cinétiques, ou des coefficients des lois d'Arrhenius qui les régissent, dépendent alors du matériau mais sont sensées rester valides lors de leur extrapolation aux températures d'usage (plus basses) ou encore lors de l'ajout de réactions chimiques accompagnant la complexification du système d'étude (ajout de facteurs environnementaux/conditions d'exposition ou de constituants à la formulation).

Les travaux de ces deux dernières décennies se sont attachés à décrire l'influence de la température et de la pression partielle en dioxygène sur les processus chimiques (réactions oxygène-polymère) et physiques (diffusion d'O_2) impliqués dans l'oxydation. Les différents travaux impliqués ont ainsi conduit à valider un schéma mécanistique commun (séquence de réactions chimiques) mais en appliquant des jeux de paramètres légèrement différents selon les conditions de l'étude et le matériau. Un paramètre ajustable, matérialisé par la concentration initiale en hydroperoxydes $[POOH]_0$, a été introduit pour décrire la variabilité de comportement au sein de la famille des iPP.

Néanmoins, les tentatives d'unification de ces travaux en un modèle universel, c'est-à-dire faisant appel à un jeu de constantes unique, s'avèrent infructueuses car le paramètre $[POOH]_0$ s'avère

incapable de rendre compte de l'intégralité de la variabilité constatée comme dans le cas du polyéthylène (une partie de cette variabilité étant en fait noyée dans les légers ajustements de constantes cinétiques opérés entre les différentes études préexistantes).

Les épaisseurs de couches oxydées (ECO) peuvent également être très variables en fonction du matériau et des conditions d'exposition, avec des valeurs dispersées entre quelques dizaines et quelques centaines de microns dans des conditions très proches. L'intérêt porté à ce phénomène s'explique par : (i) la relation étroite entre ces épaisseurs de couches oxydées et les propriétés mécaniques de la pièce (fragilisation des couches de surface avec amorces de fissures susceptibles de se propager au cœur de la pièce), ou (ii) les évolutions symétriques des profils d'oxydation/ dégradation et les profils de concentration en antioxydants.

In fine, la thermooxydation du polypropylène peut être résumée via un triangle d'interactions polymère/température/concentration en O_2. Cette dernière est gouvernée par les propriétés de transport du dioxygène, à savoir la diffusivité D_{O2} et la solubilité du dioxygène S_{O2} ainsi que leur produit, la perméabilité Pe_{O2} :

$$Pe_{O_2} = S_{O_2} \cdot D_{O_2} \qquad \text{Eq. R1}$$

A l'échelle locale, pour un volume élémentaire en équilibre avec l'atmosphère, la concentration en dioxygène dans le matériau, est supposée obéir à la loi de Henry, et fait donc intervenir la solubilité:

$$C_s = P_{O_2} \times S_{O_2} \qquad \text{Eq. R2}$$

La compétition de la consommation du dioxygène et de son apport depuis la surface vers le cœur de l'échantillon (communément dénommée « compétition diffusion-réaction ») est supposée respecter la relation de la forme :

$$\partial[O_2]/\partial t = D_{O_2}\, \partial^2[O_2]/\partial z^2 - r(C) \qquad \text{Eq. R3}$$

où r(C) décrit le terme de consommation chimique, et s'exprime au moyen de la théorie de la cinétique classique (homogène) en fonction des constantes cinétiques et concentrations en espèces pertinentes.

Jusqu'à présent, l'attention s'était focalisée essentiellement sur la détermination des constantes cinétiques tandis que ces paramètres caractéristiques du matériau avaient été estimés approximativement à partir de quelques valeurs la littérature. Toutefois, ces grandeurs ont le

grand avantage d'être aisément mesurables en comparaison des constantes cinétiques. Leur connaissance précise devrait donc permettre de calibrer le modèle, avec comme perspective de tendre vers un modèle quasi-universel.

La problématique qui émerge est d'obtenir un degré du raffinement du modèle au juste nécessaire afin de : (i) rationnaliser les ressources, (ii) favoriser la lisibilité du modèle, (iii) obtenir un modèle raisonnablement fiable (en tenant compte de la variabilité des résultats) pour envisager de le complexifier sans propager dramatiquement les incertitudes.

1. Universalité et auto-cohérence du modèle

Pour estimer au mieux la valeur de ces paramètres, la démarche employée consiste à les mesurer dans les domaines de température autorisées par l'appareillage (typiquement 10-45°C) et de décrire leur évolution dans l'ensemble de la gamme de température considérée (60-140°C) par extrapolation suivant une loi d'Arrhenius. La pertinence de cette dernière hypothèse est vérifiée en cohérence avec une compilation exhaustive des données de la littérature réalisée pour chacun des paramètres de transport du dioxygène, à savoir, la solubilité (cf. figure 2 du chapitre IV ; les valeurs de solubilité ont été rapportées à la fraction amorphe puisque l'oxygène est insoluble en phase cristalline) ainqi que la diffusivité et la perméabilité (figures 1 et 2 du chapitre V).

D'autre part, les différentes compilations révèlent des dispersions des valeurs s'étendant sur plus d'une décade, particulièrement dans le cas de la solubilité et de la diffusivité du dioxygène. Ces variabilités peuvent résulter :

(i) D'erreur de mesure ou biais (erreurs d'appareillage répétables), notamment à cause du temps de retard instrumental caractéristique de l'appareil qui ne serait pas négligeable par rapport au « time-lag » obtenu par mesure en régime transitoire.

(ii) De variabilités matériaux se traduisant un changement, soit réel, soit apparent des paramètres de transport du dioxygène. Après élimination des données erronées, les dispersions de valeurs restent ainsi importantes et semblent compatibles avec l'introduction d'une variabilité sur ces paramètres.

1.1. Dépendance à la pression partielle en O_2 (échelle locale)

Au moyen d'une démarche rigoureuse d'optimisation des constantes cinétiques par étapes, après avoir mesuré les paramètres de transport, il apparait impossible de modéliser les résultats expérimentaux au moyen d'une unique valeur de solubilité au dioxygène pour différents iPPs. En effet, leur résistance à l'oxydation (en termes de temps d'induction et de vitesse d'oxydation) semble suivre des évolutions différentes avec la pression partielle en dioxygène.

$$P_{O_2}{}^{c} = {[O_2]_c}/{S_{O_2}} = K \cdot {k_3\, k_5\, [PH]}/{k_2\, k_6\, S_{O_2}} \quad \text{Eq. R4}$$

Au contraire, l'introduction d'une variation de la solubilité au dioxygène dans un rapport 6 permet de bien rendre compte de leurs comportements respectifs avec la pression en dioxygène et est compatible avec la dispersion des valeurs de solubilité rapportée précédemment (cf. figure 9 du chapitre IV).

L'observation de ces comportements différents avec la pression en dioxygène semblent donc constituer une preuve convaincante de la variabilité de la solubilité. A défaut d'une variation effective de la solubilité, cela pourrait être interprété : soit (i) comme une déviation de l'évolution de la concentration en O_2 par rapport à la loi de Henry, laquelle serait toutefois valable jusqu'à 50 bars pour N_2 et CO_2 d'après Kimaya et al. (J. Polm. Sci., Polym. Phys. Ed., 24, 1525 (1986) quoted by Hedenqvist and Gedde, Progress in Polymer Science, 21 (1996) 299-333), soit (ii) comme un effet de microstructure modifiant la réactivité polymère-O_2 mais, *in fine*, descriptible par une variabilité de la solubilité apparente.

1.2. Modélisation multi-échelles du système

La démarche consiste à modéliser les évolutions chimiques du matériau et à en déduire changements de propriétés aux échelles supérieures, moyennant de connaître les relations structure-propriétés pertinentes. Le modèle permet ainsi de simuler les évolutions de concentrations en produits d'oxydation primaires, i.e., les hydroperoxydes POOH (Figure IV.3), et secondaires, i.e. les espèces carbonylées (Figure IV.4), ou encore en coupures de chaînes et nœuds de réticulation. A partir de ces derniers et en utilisant la loi de Saito, il est possible de calculer les masses moléculaires théoriques en nombre (Figure IV.6) et en poids (Figure IV.7), lesquelles ont été comparées aux valeurs mesurées par chromatographie d'exclusion stérique.

1.3. Simulation de la variabilité des comportements

L'introduction de la solubilité au dioxygène comme un paramètre ajustable dans le modèle permet en outre de rendre compte de la majeure partie de la diversité des comportements à l'oxydation en termes de temps d'induction (Figure IV.11) et de vitesse d'oxydation (Figure IV.12). Tout cela forme un scénario cohérent qui permet de conclure à l'unification du modèle.

L'attribution de ces variations de solubilité à l'oxygène à des caractéristiques microstructurales ou morphologiques particulières est néanmoins délicate car repose uniquement sur des conjectures.

1.4. Domaine de validité et pouvoir prédictif

Ainsi le modèle proposé permet de simuler les cinétiques d'oxydation du polypropylène avec une certaine cohérence générale, à savoir : (i) un schéma mécanistique pertinent, (ii) des paramètres physiques mesurables, (iii) des constances cinétiques avec des valeurs sensées. C'est ce caractère heuristique, basé sur la compréhension des phénomènes physico-chimiques, qui confère au modèle sa valeur prédictive en dehors du domaine de l'étude et autorise son extrapolation. Toutefois, cela nécessite une modélisation fine des phénomènes qui peut être très exigeante pour des phénomènes complexes. Il est alors possible d'introduire des rendements qualifiés apparents lorsque qu'ils sont présumés dépendre des conditions d'exposition, du choix de l'espèce/propriété suivie ou de sa mesure. Ces derniers perdent alors leur caractère prédictif et se résument à des paramètres de capitalisation.

Pour appréhender les limites « raisonnables » de l'approche, nous avons notamment procédé au suivi en temps réel des émissions de produits volatils par spectrométrie de masse haute résolution générées à 140°C pour des pressions partielles en O_2 de 0.02 et 0.1 MPa.

Parmi les paramètres apparents, on distingue :

(i) Le rendement en produits carbonylés γ_1, du fait de (a) le relargage partiel des produits volatils en dehors de la matrice conduit à omettre une partie de ces fonctions dans le décompte effectué par dosage FTIR, (b)les variations de stœchiométrie des différents produits d'oxydation en fonction des conditions d'exposition, (c) les modifications morphologiques (chimicristallisation) qui peuvent induire des variations apparentes de vitesse d'oxydation.

(ii) Le rendement apparent en coupures de chaînes γ_s résultant de la compétition entre les réactions de réticulation et de coupures en β « efficaces », c'est-à-dire se produisant sur la chaîne macromoléculaire principale. Une analyse fine des rendements en coupures de chaîne et en produits carbonylés suggèrent que les coupures en β se produisant sur les groupes méthyles latéraux ou en bout de chaîne (générant des volatils) ont une contribution négligeable à la chute des masses moléculaires.

(iii) La masse moléculaire M_v du produit volatil moyen généré. S'agissant d'une moyenne pondérée, elle va être très dépendante de la distribution des produits volatils. Elle peut être utilisée pour calculer la perte de masse du matériau lors de la dégradation.

Bien qu'apparents, les deux premiers rendements ont l'avantage de varier très peu dans l'intervalle de température considéré, laissant penser que ce rendement unique est en effet caractéristique de la thermooxydation du polymère à l'état solide. En revanche, ce rendement est affecté par les variations de pression, passant de 0.2 (5 MPa) en excès à 0.5 en défaut d'oxygène (0.02 MPa). Ceci est à mettre en relation avec les changements importants de distribution en produits volatils que l'on peut observer pour de faibles variations de pression partielle en O_2 (0.02 à 0.1 MPa). De même, la pression en O_2 à un effet important sur les distributions de produits d'oxydation volatils, tout particulièrement sur les émissions de fragments volatils tels que les mono et dioxyde de carbone. Il en résulte une forte variabilité de M_v, qui devient très difficilement prédictive pour des variations importantes de température et/ou de pression partielle en dioxygène.

2. Altération des propriétés au cours du vieillissement et conséquences en modélisation

L'importance des caractéristiques morphologiques a été mise en évidence sur la variabilité des paramètres de transport du dioxygène initiaux (avant vieillissement). Toutefois, l'utilisation du modèle en résolution inverse pour simuler les profils d'oxydation renvoie des valeurs apparentes bien plus faibles que les valeurs initiales pour les coefficients de perméabilité, lesquels représentent le paramètre pertinent (car invariant) pour décrire les profils d'oxydation.

A l'échelle locale, les cinétiques locales d'oxydation ont pu être modélisées via un coefficient de solubilité du dioxygène unique et indépendant du temps, et ce malgré la mise en évidence de modifications morphologiques au cours de l'oxydation, en particulier les modifications de la nature des phases cristallines ou de microstructure (longueur de séquences isotactiques) mises en évidence via les formes des endothermes de fusion obtenues par DSC. En conséquence, la chute de perméabilité est portée par la diffusivité et ainsi attribuée aux modifications structurales (densification du matériau par greffage de l'oxygène) ou morphologiques en termes de taux de cristallinité, de tailles/forme/orientation des lamelles de cristallites ou de couches amorphes interlamellaires.

Cette diminution drastique de la diffusivité doit nécessairement être prise en compte via une relation structure-propriété spécifique pour pouvoir simuler les profils d'oxydation de manière fiable. Il est à noter que dans certains cas, on observe l'apparition marquée d'épaulement dans le profil d'oxydation (plateau de concentration en produits d'oxydation) sur plusieurs centaines de microns traduisant généralement l'apparition de fissures. Cette altération des propriétés de transport du dioxygène restreint considérablement l'applicabilité du modèle au-delà de la période d'induction, c'est-à-dire pour des degrés d'oxydation importants. On notera que cela est sans répercutions sur la simulation de profils d'antioxydants de type inhibiteur (phénols, phosphites, etc…) mais pas sur ceux de type retardateurs d'oxydation (HALS par exemple). Egalement, cela conduit inévitablement à imposer des critères de fin de vie plus restrictifs.

Après avoir introduit l'effet de caractéristiques microstructurales et morphologiques dans les modèles cinétiques et mis en évidence les effets direct sur la durée de vie (période d'induction), il est clair que le vieillissement physique a également une influence, certes bien moindre, sur le vieillissement chimique du matériau (cf. graphical abstract au chapitre V).

CHAPTER III. Real-time quantitative analysis of volatile products generated during solid-state polypropylene thermal oxidation

Alexandre François-Heude[1, 3 1], Emmanuel Richaud[1], Julien Leprovost[2], Michel Heninger[2, 4], Helene Mestdagh[4], Eric Desnoux[3], and Xavier Colin[1]

1) PIMM, UMR CNRS 8006, ARTS ET METIERS ParisTech, Paris, France
2) ALYXAN, Orsay, France
3) DREAM-DIMAT department, RENAULT, Guyancourt, France
4) LCP, UMR8000, Bât 350, Université Paris-Sud, 91405 Orsay cedex

Abstract

Analysis of volatile organic compounds (VOCs) during PP thermal oxidation under three oxygen partial pressures (0%, 21% and 100% of atmospheric pressure) at 140°C was performed by proton transfer reaction coupled with Fourier transform ion cyclotron resonance mass spectrometry. Six main VOCs were identified: acetone, acetic acid, 2,4-pentanedione, acetaldehyde, formaldehyde and methyl acrolein. Their formation was shown to obey two main reaction pathways, both involving methyne units as driving oxidation sites: (i) the widely accepted chain scission mechanism of tertiary alkoxy radicals, which generates primary radicals undergoing secondary reactions leading to the oxidation of methylene units; (ii) the chain scission mechanism occurring on tertiary alkyl radical, which is proposed here as a realistic path leading to methyl acrolein. The relative proportions of the six main VOCs depend on the oxygen partial pressure which mostly impacts the oxidation of methylene units rather than the competition between the two previous paths.

Keywords

[1] Corresponding author : Email: Alexandre.FRANCOIS-HEUDE@ensam.eu
Tel/ Fax: +33 1 44 24 64 13/ +33 1 44 24 63 82

Polypropylene Oxidation; Volatile Organic Compounds; Mass spectrometry; Chain Scission Mechanisms;

1. Introduction

Analysis of Volatile Organic Compounds (VOCs) emitted during degradation of polypropylene (PP) has been widely studied during the last three decades under various exposure conditions such as photo-oxidation [1-3], radio-oxidation [4-6] and thermal oxidation in both solid and molten state [7-14]. Many VOCs were identified, particularly in thermal oxidation by Hoff et al. [15] or more recently by Bernstein et al. [8]. Moreover, except for a recurrent group of VOCs, multiple products were identified by the different authors even for similar ageing conditions, possibly due to:

(i) The existence of a potential degradation of primary VOCs occurring between the sample and the detector,

(ii) The presence of residues or degradation products from "contaminants" such as additives,

(iii) The use of different ageing conditions generating a large range of minor products.

Most of the previous authors tried to quantify VOCs by trapping them and subsequently performing titration by gas chromatography often coupled with mass spectrometry (GC-MS).

Identification and quantification of VOCs brought valuable information, about the prevailing mechanisms of polypropylene oxidation, consistent with their precursory macromolecular oxidation products [1, 3-5, 7, 16, 17]. VOCs analysis was particularly applied to the determination of the relative sensitivities to oxidation of methyne and methylene -besides methyl- units to oxidation [8]. It was confirmed that methyne units are about 10 times more reactive than the methylene ones, as in previous results obtained on macromolecular oxidation products by derivatization methods [18] or isotope labeling [17]. Basing on such mechanistic considerations, i.e. only considering the oxidation of methyne units in a first approach, a "closed loop" mechanistic scheme was proposed to describe the general oxidation path [19]. Using kinetic modeling, such an approach enables determination of the amount of chain scission generated and its impact on the polypropylene mechanical properties [20] or mass loss [21]. In the case of kinetic modeling of ethylene-propylene copolymers, the reactivities of both methyne and

methylene sites were considered mainly due to the higher content of methylene units [22]. However, these results are not transposable to the case of isotactic polypropylene where the tacticity –and the subsequent conformational effect- would change the relative reactivities of both sites [23]. The impact of methylene units on the oxidation in polypropylene, although considered as minority in a first approach, is thus questionable.

A reliable quantitative analysis of volatiles is expected to give additional information about the prevalence of the PP oxidation mechanisms, among them the minority impact of methylene oxidation, but also about their impact on the subsequent property changes. Recently, Chemical Ionization (analyte ionization through chemical reaction with a specific ionic precursor) associated with Fourier Transform Ion Cyclotron Resonance Mass Spectrometry (CI-FTICR) was shown to be a powerful technique to perform quantitative and real-time analysis of VOCs emission during the thermal oxidation of PP in the molten state (256°C) [24].

The aim of this study was to apply VOCs real-time analysis to the study of PP thermal oxidation in the solid state (140°C) under different oxygen partial pressures (0%, 21% or 100% of atmospheric pressure), since it was shown that this last factor can significantly influence the overall oxidation kinetics of PP [25]. More precisely, the issue here is the impact of oxygen pressure on both methylene and methyne site reactivities polyethylene and polypropylene having been shown to have very different critical oxygen pressures and hence, different oxygen pressure dependencies [26]. The consequences of oxygen pressure on the released VOC will be interpreted in terms of competitive pathways, established from a comprehensive review of mechanistic schemes proposed for prevailing VOCs.

2. Experimental Section

2.1. Materials

Isotactic polypropylene (M_W = 250 kg/mol and M_n = 67 kg/mol) was supplied by Aldrich and processed to produce 80-150 µm films by compression molding. All films were purified from antioxidants by Soxhlet extraction with dichloromethane for 48 h prior to thermal ageing experiments.

2.2. Analysis

The thermal oxidation kinetics of PP was followed at 140°C under air and pure oxygen by three analytical techniques: (i) CI-FTICR as described below, using proton transfer reaction (PTR) as specific CI reaction; (ii) Fourier Transformed Infrared Spectroscopy (FTIR), performed with a Perkin-Elmer device (16 scans, minimal resolution of 4 cm^{-1}); (iii) thermogravimetric analyses (TGA) performed on samples of about 14-16 mg with a TA Instruments TGA Q50 apparatus equipped with an Alytech GasMix unit.

2.3. PTR-FTICR: apparatus & methods

Under air and pure oxygen, samples of 158.7 mg and 30.2 mg (i.e. slices of 80 to 150 µm thickness) were put into a small quartz vessel and introduced into the preheated oven at zero time. The temperature was stabilized at 140°C. The sample was swept by a controlled gas mixture flow generated by the AlyTech GasMix device. The gas flow was continuously sampled by the mass spectrometer, providing real time analysis of VOCs emission. VOCs analysis were performed with a BTrap mass spectrometer device, the specifications and analysis procedure of which were described in detail in a previous publication [24]. The experimental setup is schematized in Figure 1.

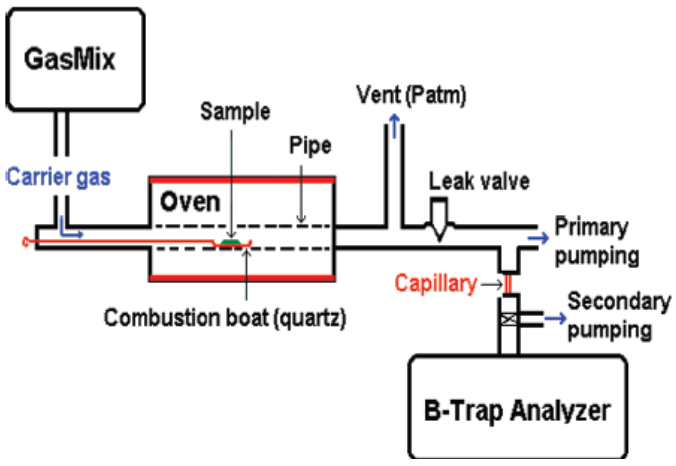

Figure 1 : PTR-FTICR experimental setup.

Briefly, BTrap instruments are compact and transportable mass spectrometers based on the FTICR technique, allowing trapping of ions and detecting them by their mass-to-charge (*m/z*)

ratio. The strong and homogeneous magnetic field required by this technique is generated by a structured permanent magnet [27], providing a 1T magnetic field for the instrument used in the present work.

Each recorded mass spectrum results from a programmed sequence including successive precursor ion generation, sample introduction, ion-molecule reaction during a controlled time, and ion detection. The whole sequence is performed in the FTICR cell, with a total duration that does not exceed 1 s. The cell is maintained at a pressure in the range from ≤ 10^{-8} mbar during ion detection to 10^{-6} mbar during sample introduction.

In the present study, the CI precursor consists of H_3O^+ ions. These ions are generated by electron ionization of H_2O, followed by ion-molecule reaction leading to H_3O^+ terminal ions. On sample introduction, these ions react with each VOC denoted M_i by proton transfer, leading to the protonated ion M_iH^+:

$$H_3O^+ + M_i \rightarrow H_2O + M_iH^+$$

This reaction occurs rapidly for any VOC bearing unsaturation and/or a N or O atom. Therefore the resulting mass spectrum contains a peak corresponding to unreacted H_3O^+, and a variable number of peaks corresponding to M_iH^+ ions arising from protonation of M_i molecules. Recorded intensities of the ions, along with knowledge of the operating parameters and the rate constant of the PTR reaction, allow VOC quantification as explained in the following.

According to the classical theory of chemical kinetics:

$$\frac{d[H_3O^+]}{dt} = -[H_3O^+]S$$

where $S = \sum k_i[M_i]$ is the sum of all $k_i[M_i]$ terms corresponding to the molecules M_i undergoing protonation by H_3O^+ and:

$$\frac{d[M_iH^+]}{dt} = k[M_i]\,[H_3O^+]$$

The resolution of the system of differential equations leads to the expression:

$$[M_i] = \frac{\ln(H_3O^+) \times (M_iH^+)}{k_i\tau\,(1 - (H_3O^+))}$$

where τ is the reaction time, (H_3O^+) and (M_iH^+) the relative intensities of the corresponding ions, normalized to the sum of all ion intensities.

The gas pulse of analytes was adjusted to 250 ms to increase the sensitivity. Under these conditions, the conversion rate of the reaction is kept under 30% to avoid secondary reactions.

The concentration C_i in the gas flow for the component M_i is derived from its concentration $[M_i]$ in the ICR cell according to:

$$C_i = [M_i] \frac{P_{flow}}{P_{cell}}$$

In the present work, the corrected cell pressure was 1.99×10^{-5} and 2.13×10^{-5} Torr under air and pure oxygen respectively.

With P_{flow} = 1 bar, the following relationship is obtained:

$$C_i(mol/L) = 1{,}26\ 10^{-18} \frac{[M_i]\ (cm^{-3})}{P_{cell}\ (torr)}$$

The total amount N_i of a compound M_i emitted by pyrolysis of a sample at a given time t is expressed as:

$$N_i(t) = \int dn_i = \int_0^t C_i(t)\ dt$$

where $C_i(t)$ (in mol/L) is the instantaneous concentration of M_i in the gas flow and F (L/min) is the volume flow rate of the carrier gas.

Adjusting the carrier gas flow F to 50 mL/min, the resulting transport time is 1.50 min. This time was systematically subtracted from the time measured from sample introduction.

An example of real-time data acquisition is depicted in Figure 2.

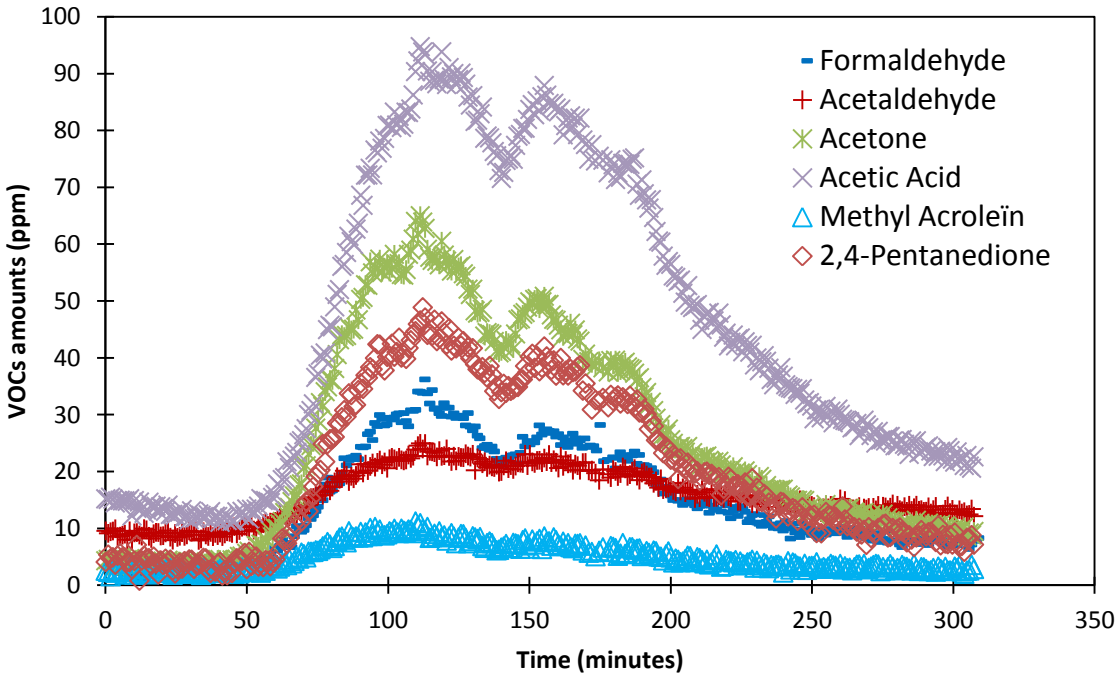

Figure 2 : Real-time monitoring of VOCs generation in pure oxygen at 140°C.

Since the previous work, several technical improvements have been brought to the instrument, resulting in increased sensitivity, easier software, and real-time pressure measurement in the FTICR cell. This direct pressure monitoring provides reliable control of the sample amount introduced into the mass spectrometer during each gas pulse. The uncertainty of this absolute quantification method is 25%, mainly due to the uncertainty on the rate constant, ranging between 15% (for acetone) and 30% for the quantitative mode, whereas the semi-quantitative mode gives the right order of magnitude. It was shown that the amount of VOCs is a linear function of the initial sample mass.

3. Results and discussion

3.1. Real-time analysis: identification and quantification of VOCs

PTR-FTICR analysis evidences numerous VOCs during PP thermal oxidation in air and pure oxygen. They only differ by their relative proportions. No trace of VOCs is found in nitrogen atmosphere at the same temperature, even for extended duration (up to 1000 min) and high initial sample mass. This confirms that thermolysis reactions alone do not initiate the degradation of polypropylene at the working temperature. The use of high resolution mass spectrometry enables determination of the precise molecular formula besides the mass spectra themselves. When several attributions are possible, results are systematically compared to an extensive literature review. It is thus possible to differentiate two compounds of the same nominal molecular mass, but with different exact masses (Table 1). For instance, the peak here observed at 72 g/mol must be assigned to acrylic acid instead of butanone [4, 7] or 2-methyl-2-propen-1-ol [6, 8] as previously reported in the literature. For a sake of simplicity, six main VOCs, each representing more than 5 mol% of the total amount of VOCs, are considered in this study (Table 1). Among the minor products, acrylic acid, 1-hydroxy-2-propanone, crotonic acid, 2,4-dimethylfurane and 4-methyl-3-penten-2-one have been identified. Propylene and hept-3-ene have also been detected as non-oxygenated compounds.

Table 1: Attribution of VOCs according to high-resolution mass spectrometry

Calculated M+1 peak (in g.mol^{-1})	Measured M+1 peak (in g.mol^{-1})	| Error | (%)	M+1 Formula	M Formula	Attribution	Attribution according to references	Protonation kinetic constant rate (in cm^3.s^{-1})
101.0535	101.0603	0.007	$C_5H_9O_2$	$C_5H_8O_2$	2,4-pentanedione	[6, 8, 9, 14, 15]	1.85E-09
71.0419	71.0497	0.011	C_4H_7O	C_4H_6O	Methyl acrolein	[6-8, 15, 24]	3.80E-09
61.0211	61.029	0.013	$C_2H_5O_2$	$C_2H_4O_2$	Acetic acid	[1-3, 6-10, 13-15]	2.60E-09
59.0421	59.0497	0.013	C_3H_7O	C_3H_6O	Acetone	[1-4, 6-15, 24]	3.92E-09
45.027	45.034	0.016	C_2H_5O	C_2H_4O	Acetaldehyde	[4, 7, 10, 13, 15, 24]	3.78E-09
31.0143	31.0184	0.013	CH_3O	CH_2O	Formaldehyde	[3, 11, 12, 15, 24]	3.32E-09

As volatile emissions are reported to be responsible for the mass changes, VOCs releases can be advantageously compared to thermogravimetric data. The whole releases apply to the cumulated emissions along time and are thus obtained by integration of real-time monitoring data (as depicted in figure 2). The curves are presented in Figure 3.

a) Air

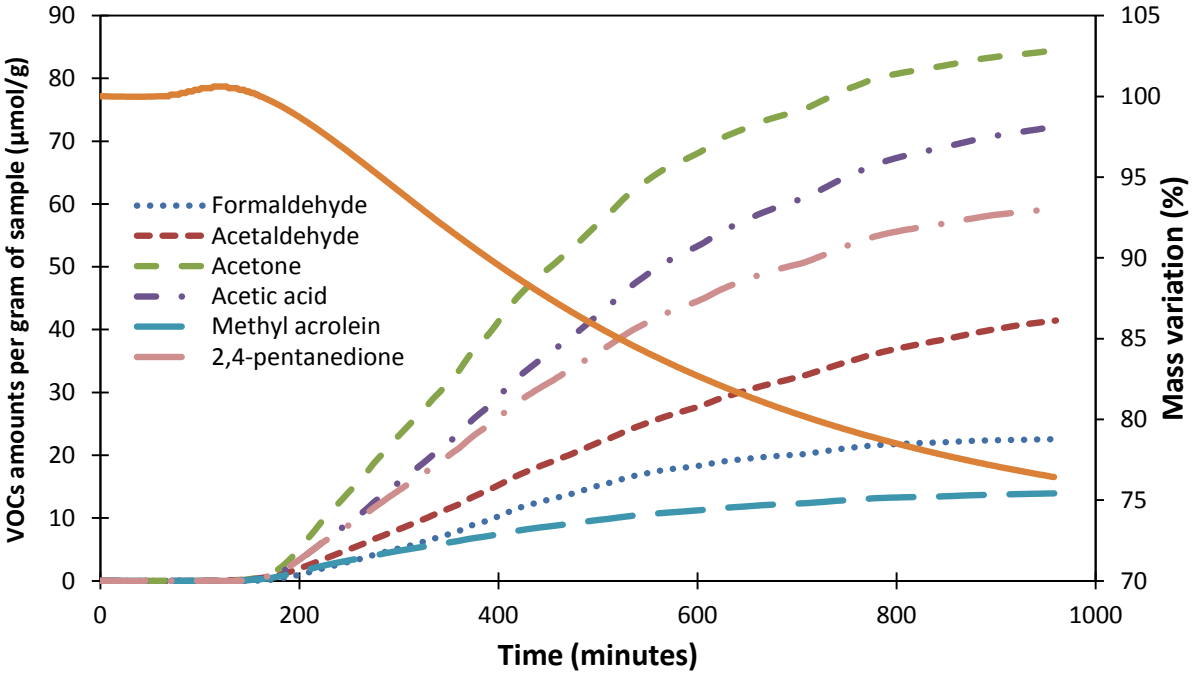

b) Oxygen

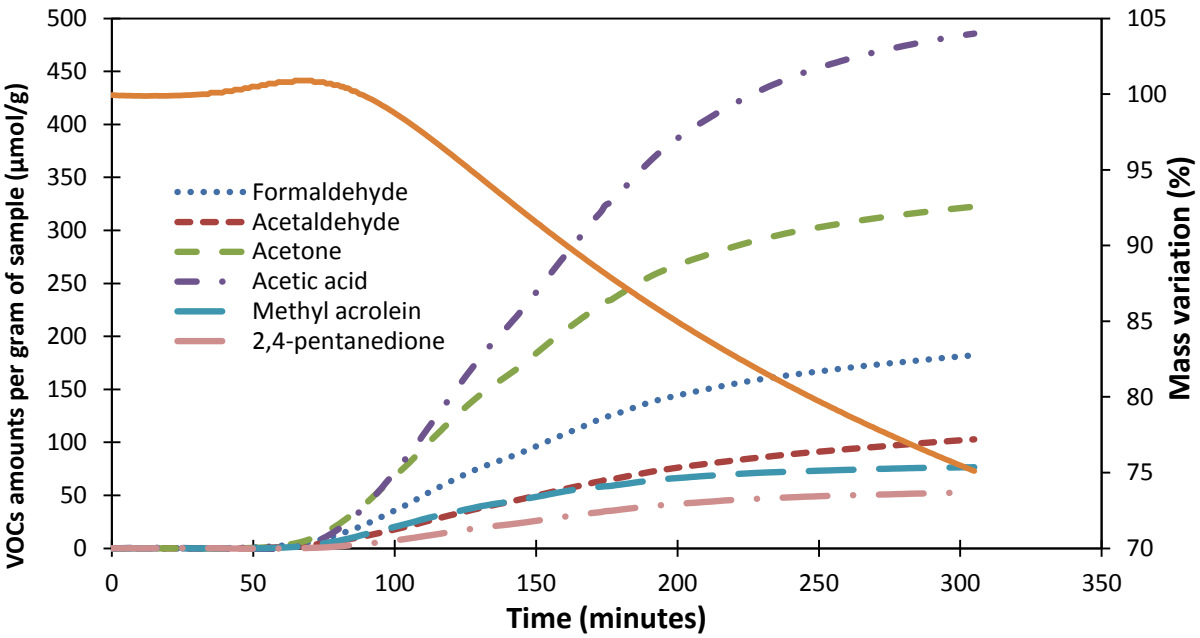

Figure 3 : Cumulated VOCs amounts normalized by the sample initial mass (left caption) and correlation with thermo-gravimetric analysis at 140°C (right caption) in air (fig. a) and pure oxygen (fig. b)

Real time monitoring techniques allow determination of three different characteristic times:

- The onset time corresponding to the first detectable VOCs emission, mass changes and build-up of macromolecular carbonyl products.
- The induction time corresponding to the establishment of the steady-state regime in these three kinetic curves. In general, it is arbitrarily determined by intercepting the steady-state straight-line with the x-abscissa.
- The time of maximal mass gain corresponding to the position of the maximum value in thermogravimetric curves.

Their values, determined at 140°C under both air and pure oxygen, are summarized in Table 2.

Table 2: Characteristic times (in minutes) for the kinetic curves of VOCs emission, mass changes and build-up of macromolecular carbonyl products (see text) at 140°C in air and pure oxygen. Close values to the induction time relative to VOCs release and the time of maximal mass gain are highlighted in bold.

In air	VOCs	Mass	>C=O
Onset time (min)	140	53	30
Induction time (min)	**158**	78	**66**
Time of maximal mass gain (min)	–	**129**	-

In O_2	VOCs	Mass	>C=O
Onset time (min)	60	31	–
Induction time (min)	**73 to 78**	44	–
Time of maximal mass gain (min)	–	**78**	–

VOCs emission clearly starts after mass increase and formation of the first macromolecular carbonyl products but, as expected, when mass loss becomes predominant over mass gain. Obviously, this is a coarse grained tendency since the three physico-chemical techniques under consideration have not been coupled in this study. However, given the low scattering of experimental results, no doubt it is a real characteristic of the PP thermal oxidation kinetics [21].

These results are consistent with the previous assumption on PP thermal oxidation mechanism [28]. First, the initial mass increase results from the "closed loop" character of the oxidation reaction: the initiation rate increases and the kinetic chain length decreases with time. Mass increase, due to oxygen incorporation and thus hydroperoxides accumulation, is essentially linked to propagation and predominates at the beginning of the induction period. In contrast, the build-up of macromolecular carbonyl products is due to β scissions of alkoxy radicals induced by initiation (i.e. hydroperoxides decomposition) or non-terminating combination of (peroxy) radical pairs. Moreover, VOCs are formed when chain scissions occur at polymer chain extremities, i.e. at advanced degradation states of PP. Therefore, it is not surprising to observe the formation of macromolecular carbonyl products and the predominance of mass gain in the early period of exposure and VOCs emissions and mass loss later (when the kinetic chain length tends towards unity).

However, the emission of VOCs begins before the end of the formation of macromolecular carbonyl products. As suggested in the literature [3], any release of carbonyl fragments (in

particular pentanedione, methyl acrolein, acetic acid, acetone, acetaldehyde, formaldehyde, etc.) can affect significantly the carbonyl index measurement because VOCs are currently not measured using conventional FTIR methods following oxidation. Nonetheless, the impact of this was not clearly evaluated. Thanks to real-time VOCs analysis, it is now possible to precisely quantify the impact of volatile products on the -underestimation of carbonyl concentration. At 140°C in air, for instance, the amount of released carbonyl functions -including carboxyl ones- has been obtained by cumulating VOCs, considering their functionality. It has then been added to the concentration of macromolecular carbonyl products measured at 1713 cm^{-1} by FTIR spectrophotometry. The theoretical concentration in carbonyl oxidation products without any VOC emission has been calculated and plotted in figure 4. In this case, it can be seen that VOCs emission clearly impacts the steady-state oxidation rate measured on carbonyl species, by about 70%.

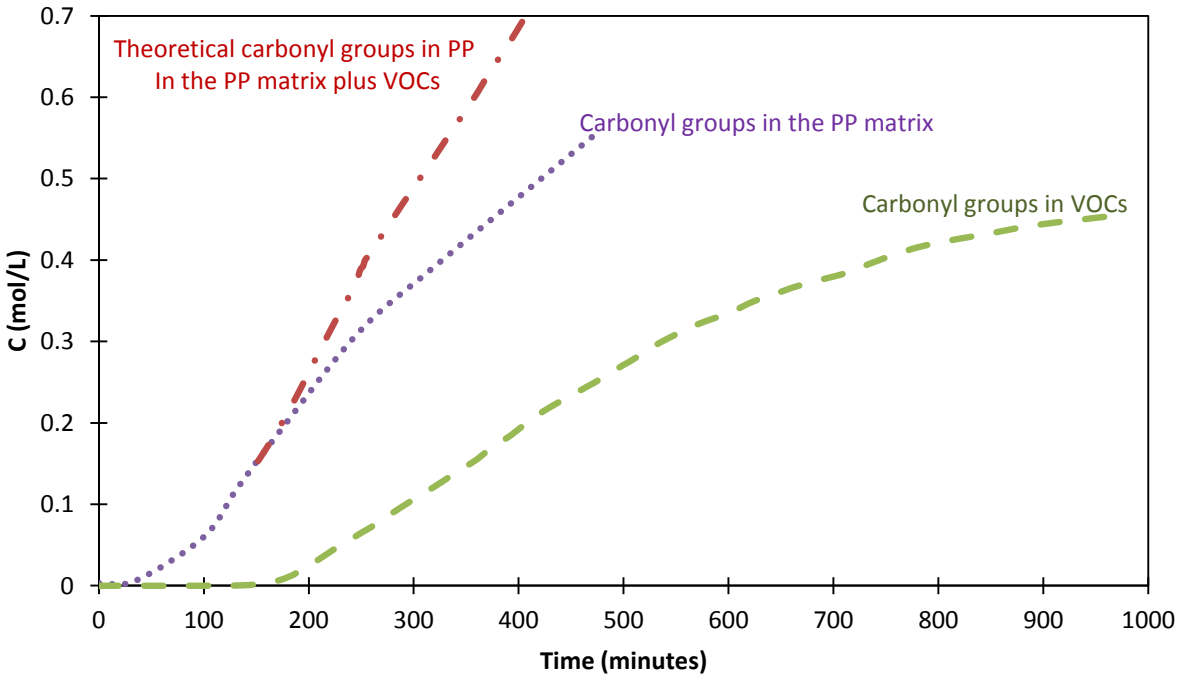

Figure 4 : Changes in the concentration of carbonyl groups in the PP matrix and VOCs at 140°C in air. Comparison to the hypothetical concentration of carbonyl groups if no VOC was formed.

Moreover, carbon assessment between the mass loss and VOCs release provides evidence of some missing material: other volatile compounds would not be detected by PTR-FTICR. These molecules would mainly consist of carbon monoxide, carbon dioxide, and methane in addition to water, which is a well-known by-product of initiation reactions by hydroperoxides decomposition. The contribution of each kind of volatiles to the overall weight loss, under both air (a) and oxygen exposure (b) are depicted in figure 5.

a) Air

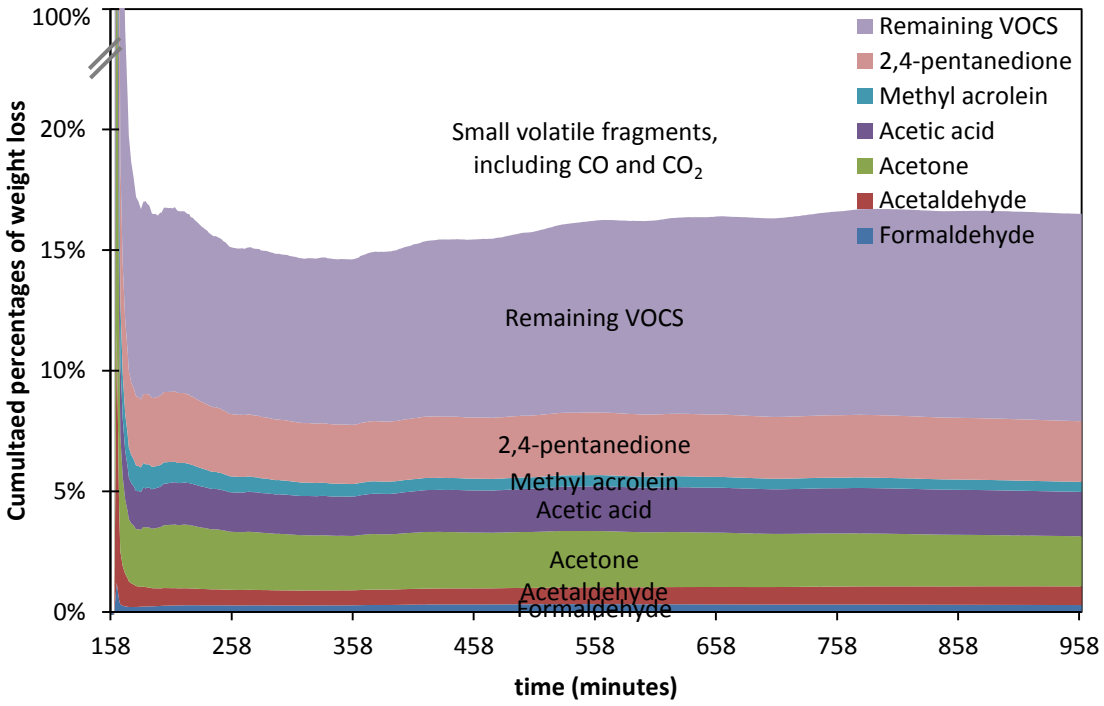

b) Oxygen

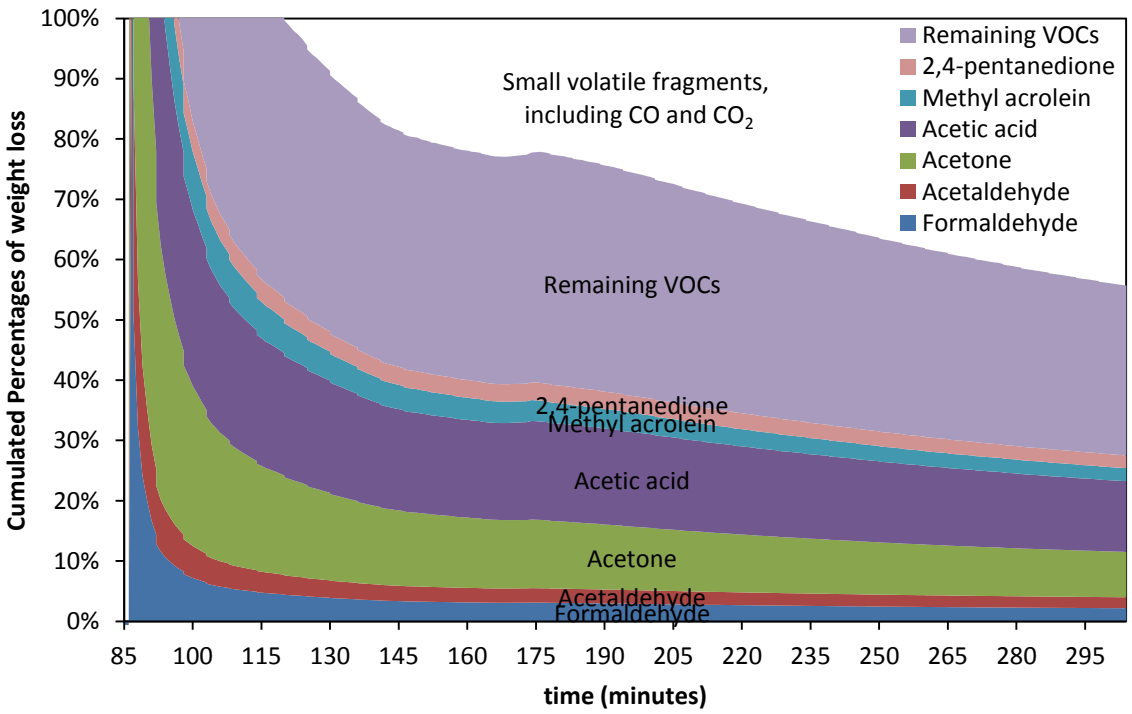

Figure 5 : Mass contribution of VOCs to PP weight loss in air (fig. a) and pure oxygen (fig. b); Results are only plotted after the beginning of VOCs release, as reported in table 2.

Under air, VOCs emission accounts for 17 wt% of the initial material mass, i.e. 9 ± 2 mol%, whereas the small fragments account for 83 wt%. As a consequence, the theoretical oxidation rate measured by FTIR would be still strongly underestimated. Moreover, these amounts remain almost unchanged along the entire course of PP thermal oxidation, which would suggests that mechanisms of VOCs formation do not much change even for extended state of degradation. Under pure oxygen, however, the mass loss due to VOCs emission exceeds 55 wt%, i.e. 30 ± 5 mol%. In both cases, PTR-FTICR does not detect high prevailing organic fragments of key importance for mass loss.

3.2. Effects of oxygen pressure

During experiments under 0.2 and 1 bar oxygen pressure, no difference in the VOCs nature is detected. In contrast, significant differences in their relative proportions of VOCs are detected (Figures 3).

First, this phenomenon is tentatively explained by investigating the changes in reactivity of methyne and methylene units with the oxygen pressure. All VOCs, including minor ones, are

classified depending on their(s) own oxidation site(s) in order to evaluate the relative proportions of reactive sites oxidized at 140°C. The oxidation site for each molecule is determined from the results in our extended review of published works. As shown in Figure 7, the percentages of oxidized methyne and methylene sites remain largely unchanged along the entire course of oxidation whatever the aging atmosphere (air or pure oxygen). In air, methyne sites account for almost 90 mol% of the oxidation sites in VOCs, which is consistent with analyses performed on macromolecular oxidation products by NMR spectrometry [5, 17]. Indeed, according to these authors, PP thermal oxidation would affect: 90 mol% of methyne units, 9 mol% of methylene units and 1 mol% of methyl units. In pure oxygen, however, methylene sites account for a higher proportion of oxidation sites: about 17 mol%. Thus, the reactivity of methylene sites would be also enhanced when increasing the oxygen partial pressure, which is contrary to what was expected.

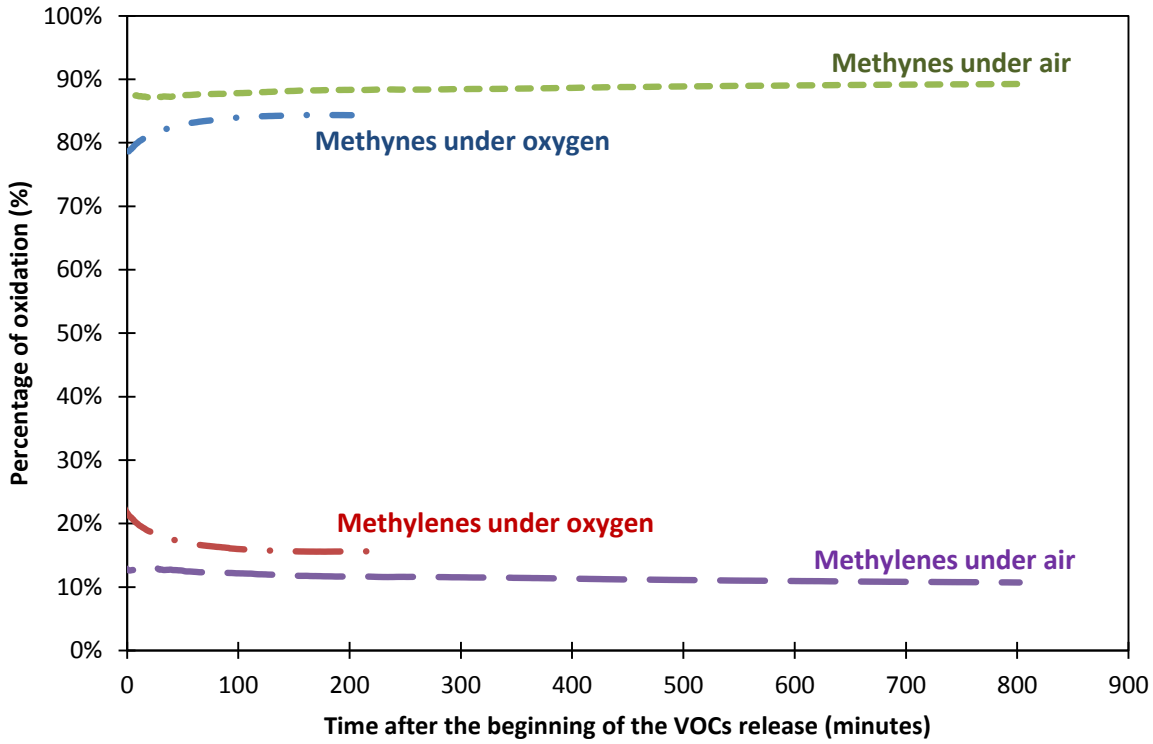

Figure 6: Oxidation sites in volatile products in both air and pure oxygen (The initial time applies to the beginning of VOCs release for each oxygen atmosphere).

To compare the impact of an increase in the oxygen partial pressure on the formation paths of volatile compounds, the ratios of their generation rates in oxygen and air have been calculated

(Figure 7). Considering a single elementary generation path for each molecular species, ratios of macroscopic rates are equal to the ratio of elementary kinetic rate constants. The macroscopic generation rates have been determined at the inflexion point on the plot of their cumulated concentrations presented in figure 3. The higher this ratio is for a species, the higher its sensitivity to oxygen pressure is.

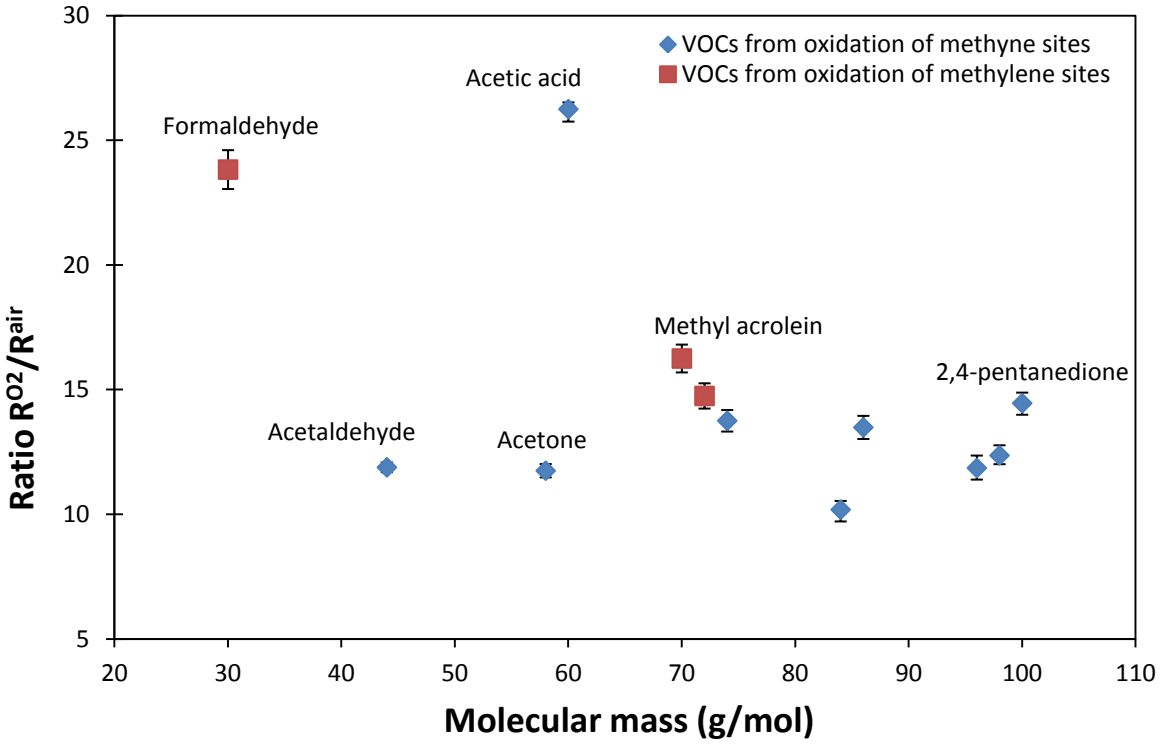

Figure 7: Ratio between the formation rates of VOCs in pure oxygen and air versus their molecular mass. Values are determined for maximal VOCs emission rates.

As expected, for all VOCs, the ratio exceeds a value of 10, indicating that a small increase in oxygen partial pressure (by a factor 5) induces a high increase in oxidation rate (by a factor higher than 10). This result is consistent with the previous assumption on PP thermal oxidation mechanism [28]. Indeed, it was recently shown that the critical oxygen partial pressure for oxygen excess is about 2 MPa at 60°C for PP and is a slow decreasing function of temperature [25]. Thus, even far below this critical pressure, PP thermal oxidation kinetics is very sensitive to oxygen partial pressure. Nonetheless, all VOCs do not undergo similar effects of oxygen partial pressure, since their respective ratios range from 10 to 26. Only formaldehyde and acetic acid seem to be highly impacted by the change in oxygen partial pressure. It is noteworthy that these

species were evidenced by Eriksson et al. to be gas-phase contributors to the spreading of oxidation in polypropylene [29].

3.3. Mechanistic discussion

In order to explain both the nature and the relative proportions of VOCs, an interpretation in terms of mechanisms is required. The most probable mechanisms, for the six main VOCs detected by PTR-FTICR as well as the evidenced carbon oxides, have been arbitrarily selected basing on kinetic considerations such as probabilities of molecules collisions or lifetime of transition states and on published experimental evidences such as isotope labeling [5, 30].
However, a new mechanism is proposed to explain the formation of methyl acrolein as well as carbon oxides resulting from the oxidation of tertiary carbons, whose published mechanisms are considered unrealistic. The selected mechanisms are organized in two global schemes (one dedicated to the detected VOCs and a second one dedicated to carbon oxides) to give a good insight of the different reactive paths, as summarized in figure 8 and 9.

Thus, the "zip" mechanism proposed by Delprat [2] allows explanation of the high amounts of acetone rather than further reactions undergone by methyl ketones. However, according to Bernstein et al [8] , the radical attack in γ position of a methyl ketone would explain the generation of 2,4 pentanedione. Formaldehyde generation is reported according to the mechanism of Hoff and Jacobsson which consists of the oxidation of primary alkyl radicals [11, 12].
Concerning methyl acrolein, although a mechanism was already proposed [8], its low probability led us to consider an alternative reaction generating a chain scission directly from alkyl radicals. The resulting allylic methylenes are highly reactive. Their rapid oxidation would explain the detected amounts of methyl acrolein detected by PTR-FTICR. Finally, secondary alkyl radicals, generated in the same reactions as methyl acrolein and formaldehyde, would lead to the formation of secondary hydroperoxides, whose β-scission would result to acetaldehyde according to Hoff and Jacobsson [11, 12]. As a competitive route, these secondary alkyl radicals would also lead to macro-aldehydes whose oxidation followed by a radical attack in γ position is preferred to explain the formation of acetic acid rather than the complex recombination of methyl ketone with an hydroxyl radical HO° proposed by Geuskens [31, 32].

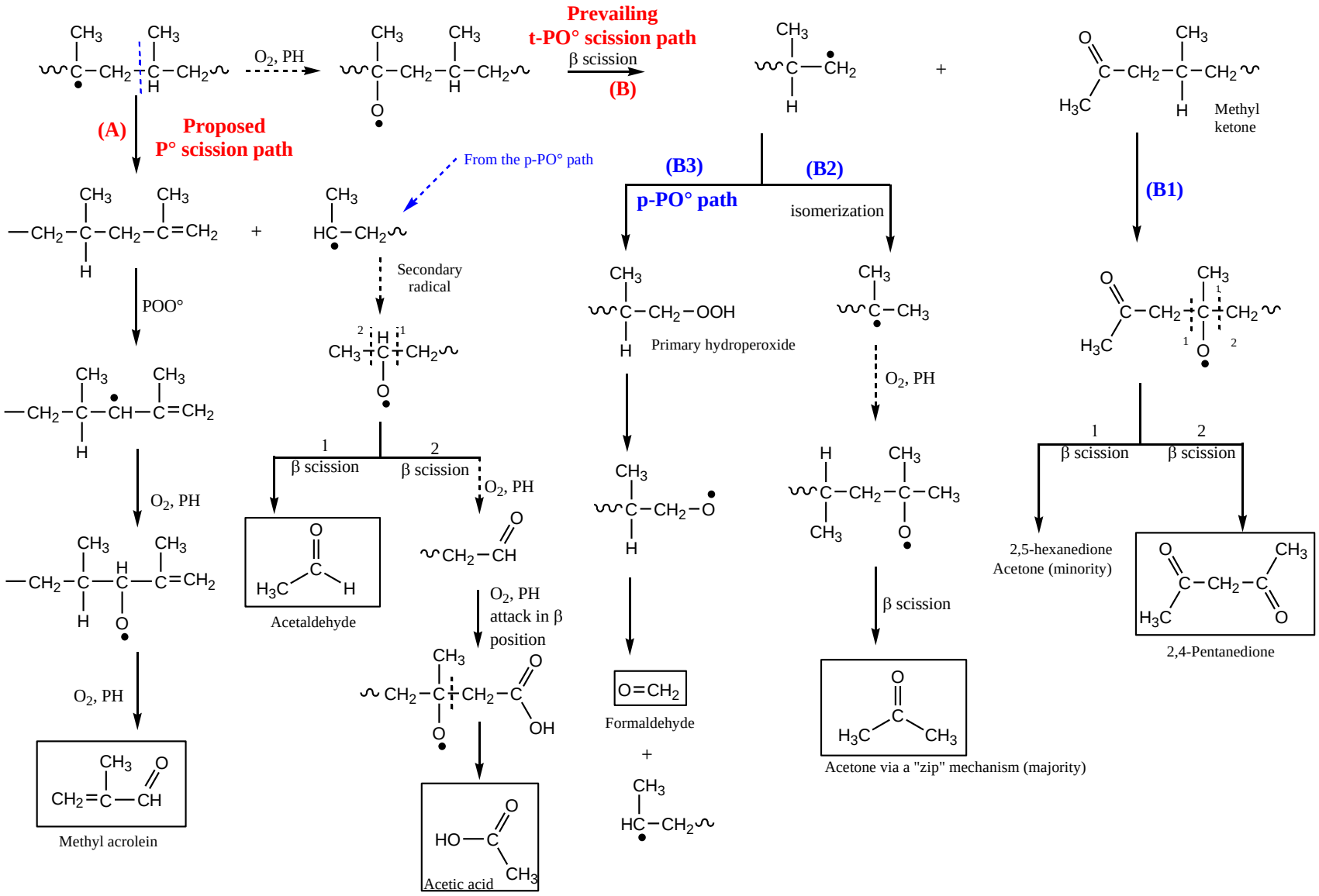

Figure 8: Mechanistic scheme of formation for the six main VOCs

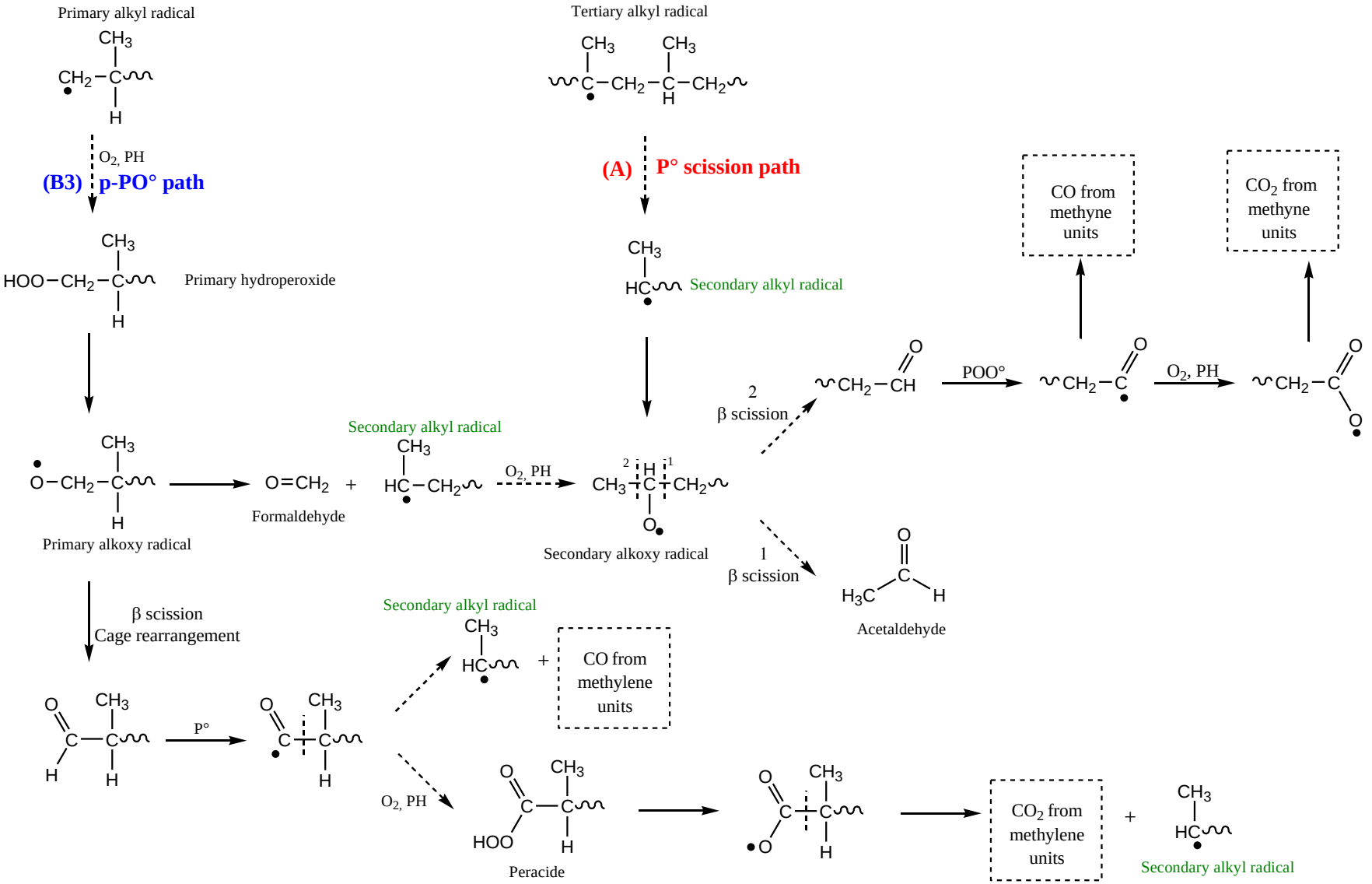

Figure 9: Mechanisms of carbon oxides formation

Concerning the formation of carbon monoxide and dioxide, the present work does not enable identification of the reactive sites (methyne or methylene units) responsible for this generation, so it is relevant to comprehend it on the basis of the very valuable work of Thornberg et al [33]. By NMR on C^{13} isotope labeled PP aged at 140°C at air, they showed that methylene units generate about 66 mol% of CO_2 and more than 80 mol% of CO, whereas methyne units generate only 33 mol% of CO_2 and 5-15 mol% of CO. Thus, carbon oxides come mainly from oxidation of methylene units but the part coming from oxidation of methyne units cannot be neglected. The high amounts of carbon oxides resulting from the oxidation of methylene units evidence the prevalence of their formation path involving primary hydroperoxides. This is consistent with the generation of high concentrations of peroxy-acids reported in polypropylene oxidation [34, 35]. However, in the case of methyne oxidized unit, the proposed mechanism seems unlikely as written, even if the isotope labeling is unarguable. Consistent with the latter published isotope labeling results, we propose a route for the formation of these later compounds from secondary alkyl radical, as proposed above in the cases of acetaldehyde and acetic acid.

Finally, all these chemical mechanisms can be organized into two competitive pathways:

(i) The "t-P° scission path", noted (A): the decomposition of tertiary alkyl radicals results in relatively unstable allylic methylenes and leads to methyl acrolein. This mechanism enables explanation of additional chain scission and generating carbon dioxide and monoxide from methyne units (Figure 9). Anyway, these mechanisms would account for a low exten of PP thermal degradation, and require a radical initiation.

(ii) The "t-PO° scission path", noted (B): the decomposition of tertiary alkoxy radicals generates methyl ketones and primary alkyl radical. The former species can undergo further vicinal oxidation to give 2,4-pentanedione (B1). The latter species can isomerize in tertiary alkyl radicals to lead to acetone (B2), or undergo directly an oxidation to generate formaldehyde, denoted as p-PO° sub-path (B3).

Along these reactions, acetaldehyde can be produced by cleavage of secondary hydroperoxides according to the paths (A) and (B3).

The general mechanistic scheme of Figure 5 allows explanations of the amounts of the six main VOCs, in particular the high amounts of acetone, acetic acid, formaldehyde and, in a minor extent, of acetaldehyde can be correlated to the high amounts of radicals formed in the various reaction paths. In both air and pure oxygen, the amount of methyl acrolein remains

rather low compared to other VOCs, thus indicating that the “t-P° path” is secondary compared to the “t-PO° path”.

When considering the previous mechanisms organized in main paths, it is now possible to comment on the changes of VOCs distribution depending on the oxygen pressure. Ranking VOCs by their relative proportions gives an idea of the prevailing mechanisms in both air and pure oxygen. Surprisingly, the predominance of the “t-PO° scission path” over the “t-P°” one is not dramatically enhanced when increasing the oxygen partial pressure. This would result from the fact that the pressure increase is very low in comparison to the high increase required to reach the critical oxygen partial pressure. On the contrary, such an increase seems to favor “p-PO° path” over “t-PO°”. Indeed, oxygen addition to primary alkyl radicals seems to be dramatically enhanced when increasing the oxygen partial pressure. At this stage of investigation, it is important to underline that nowhere, in the previous proposal of mechanistic scheme (Figure 5) do methylene units undergo a radical attack. The radical attack only occurs on methyne units, leading to the formation of t-PO° radicals of which the β scission generates primary alkyl radicals. Thus, the depletion of methylene units would be an indirect consequence of the PP thermal oxidation.

Previous results obtained in the molten state [24] can also be analyzed on the basis of the proposed global scheme. Indeed, amounts of acetone, acetaldehyde, formaldehyde and to a lower extent, of methyl acrolein are considerably enhanced above the melting point at 256°C in the molten state whereas acetic acid and 2,4-pentanedione are really minority products. The higher proportion of methyl acrolein indicates that the t-P° path (A) becomes more important with temperature, which is consistent with a thermolysis reaction. Simultaneously, the formation of acetone through the “zip” mechanism (B2) and formation of primary hydroperoxides (B3) are enhanced at the expense of the further reactions undergone by methyl ketones (B1). Similarly, the secondary radicals produced by decomposition of primary hydroperoxides mostly convert into acetaldehyde and carbon oxides rather than acetic acid.

4. Conclusion

PTR-FTICR was successfully used to detect, identify and quantify a large number of VOCs generated during PP thermal oxidation. Six main VOCs were clearly evidenced at 140°C under both air and pure oxygen, consistent with previous literature. In air, they were, from the major to the minor, acetone, acetic acid, 2,4-pentanedione, acetaldehyde, formaldehyde and

methyl acrolein. Real time monitoring of VOCs allowed us to describe a general thermal oxidation scenario, which remains in perfect agreement with thermogravimetric and FTIR analyses. The high amounts of VOCs including small volatile molecules would lead to underestimate the overall oxidation rate determined by a factor from 2 up to 5, as determined by these two latter complementary techniques.

In terms of mechanisms, it was shown that only methyne units undergo radical attacks, through a majority t-PO° path and a minority t-P° path. Oxidation of methylene units only results from subsequent reactions of the former path. The influence of oxygen pressure on the relative proportions of VOCs does not express itself into the competition between the t-PO° and t-P° scission paths, but rather from the its competition with the PO° path. In particular, oxygen addition to primary alkyl radicals leading to primary hydroperoxides seems to be highly impacted by a small increase in oxygen partial pressure far below the critical oxygen pressure. This would lead us to fear considerable changes on the equivalence and/or validity of the oxidation monitoring criteria depending on oxygen pressure.

Regarding these conclusions, several outlooks can be outlined in terms of kinetic modeling. It seems relevant to consider methyne units as the unique driving oxidation sites, thus strengthening the relevancy of the “closed loop” mechanistic scheme while demarcating its limits to tackle modeling of advanced state of degradation. Indeed, there are few incentives to model such complex imbrications of reactions with their own oxygen pressure dependence. Instead, it is possible from the present results to suitably estimate apparent parameters for common oxidation monitoring indicators, such as the yield in carbonyl products or the equivalent molecular mass of volatiles respectively for carbonyl index and mass loss.

References

[1] S. Commereuc, D. Vaillant, J.L. Philippart, J. Lacoste, J. Lemaire, D.J. Carlsson, Photo and thermal decomposition of iPP hydroperoxides, Polymer Degradation and Stability, 57 (1997) 175-182.
[2] P. Delprat, X. Duteurtre, J.-L. Gardette, Photooxidation of unstabilized and HALS-stabilized polyphasic ethylene-propylene polymers, Polymer Degradation and Stability, 50 (1995) 1-12.
[3] J.-L. Philippart, F. Posada, J.-L. Gardette, Mass spectroscopy analysis of volatile photoproducts in photooxidation of polypropylene, Polymer Degradation and Stability, 49 (1995) 285-290.
[4] Bernstein, Robert, Thornberg, M. Steven, Irwin, N. Adriane, Hochrein, M. James, Derzon, K. Dora, Klamo, B. Sara, Dough, L. Roger, Radiation-oxidation mechanisms : Volatile organic degradation products from polypropylene having selective C-13 labeling studied by GC/MS, Polymer Degradation and Stability, 93 (2008) 854-870.
[5] R. Bernstein, S.M. Thornberg, R.A. Assink, D.M. Mowery, M. Kathleen Alam, A.N. Irwin, J.M. Hochrein, D.K. Derzon, S.B. Klamo, R.L. Clough, Insights into oxidation mechanisms in gamma-irradiated polypropylene, utilizing selective isotopic labeling with analysis by GC/MS, NMR and FTIR, Nuclear Instruments and Methods in Physics Research Section B: Beam Interactions with Materials and Atoms, 265 (2007) 8-17.
[6] R. Buchalla, C. Boess, K.W. Bögl, Analysis of volatile radiolysis products in gamma-irradiated LDPE and polypropylene films by thermal desorption-gas chromatography-mass spectrometry, Applied Radiation and Isotopes, 52 (2000) 251-269.
[7] K. Barabás, M. Iring, S. László-Hedvig, T. Kelen, F. Tüdos, Study of the thermal oxidation of polyolefines--VIII : Volatile products of polypropylene thermal oxidation, European Polymer Journal, 14 (1978) 405-407.
[8] R. Bernstein, S.M. Thornberg, R.A. Assink, A.N. Irwin, J.M. Hochrein, J.R. Brown, D.K. Derzon, S.B. Klamo, R.L. Clough, The origins of volatile oxidation products in the thermal degradation of polypropylene, identified by selective isotopic labeling, Polymer Degradation and Stability, 92 (2007) 2076-2094.
[9] Z. Czégény, E. Jakab, A. Víg, B. Zelei, M. Blazsó, Thermal decomposition of photooxidized isotactic polypropylene, Journal of Analytical and Applied Pyrolysis, 56 (2000) 229-242.
[10] J.-i. Hayashi, T. Nakahara, K. Kusakabe, S. Morooka, Pyrolysis of polypropylene in the presence of oxygen, Fuel Processing Technology, 55 (1998) 265-275.
[11] A. Hoff, S. Jacobsson, Thermal oxidation of polypropylene close to industrial processing conditions, Journal of Applied Polymer Science, 27 (1982) 2539-2551.
[12] A. Hoff, S. Jacobsson, Thermal oxidation of polypropylene in the temperature range of 120–280°c, Journal of Applied Polymer Science, 29 (1984) 465-480.
[13] S.G. Kiryushkin, A.P. Mar'in, Y.A. Shlyapnikov, Annular reactor for chromatographic analysis of gases formed by thermal breakdown of polymers, Polymer Science U.S.S.R., 22 (1980) 1570-1574.
[14] Willoughby, G. B, Golby, A, Davies, J, Cain, R, Volatile component analysis as a routine characterisation tool: an approach to fingerprinting polyolefin type and process history using ATD-GC/MS, Anglais, 22 (2003) 553-570.
[15] H.A. Frostling H, Jacobsson S, Pfäffli P, Vainiotalo S, Zitting A., Analytical, occupational and toxicologic aspects of the degradation products of polypropylene plastics, Scand J Work Environ Health, 10 (1984) 163-169.
[16] D.J. Carlsson, D.M. Wiles, The Photooxidative Degradation of Polypropylene. Part I. Photooxidation and Photoinitiation Processes, 14 (1976) 65 - 106.
[17] D.M. Mowery, R.A. Assink, D.K. Derzon, S.B. Klamo, R.L. Clough, R. Bernstein, Solid-State 13C NMR Investigation of the Oxidative Degradation of Selectively Labeled Polypropylene by Thermal Aging and Î³-Irradiation, Macromolecules, 38 (2005) 5035-5046.
[18] J. Lacoste, D. Vaillant, D.J. Carlsson, Gamma-, photo-, and thermally-initiated oxidation of isotactic polypropylene, Journal of Polymer Science Part A: Polymer Chemistry, 31 (1993) 715-722.
[19] L. Audouin, V. Gueguen, A. Tcharkhtchi, J. Verdu, Close loop mechanistic schemes for hydrocarbon polymer oxidation, Journal of Polymer Science Part A: Polymer Chemistry, 33 (1995) 921-927.

[20] B. Fayolle, L. Audouin, J. Verdu, A critical molar mass separating the ductile and brittle regimes as revealed by thermal oxidation in polypropylene, Polymer, 45 (2004) 4323-4330.
[21] J. Rychly, L. Matisova-Rychla, K. Csmorova, L. Achimsky, L. Audouin, A. Tcharkhtchi, J. Verdu, Kinetics of mass changes in oxidation of polypropylene, Polymer Degradation and Stability, 58 (1997) 269-274.
[22] Colin, Xavier, Richaud, Emmanuel, Verdu, Jacques, L. Monchy, Carole, Kinetic modelling of radiochemical ageing of ethylene-propylene copolymers, Radiation Physics and Chemistry, 79 (2010) 365–370.
[23] J.C.W. Chien, Jabloner, H. , Polymer reactions. IV. Thermal decomposition of polypropylene hydroperoxydes, Journal of Polymer Science Part A-1: Polymer Chemistry, 6 (1968) 393-402.
[24] S. Sarrabi, X. Colin, A. Tcharkhtchi, M. Heninger, J. Leprovost, H.l.n. Mestdagh, Real Time Analysis of Volatile Organic Compounds from Polypropylene Thermal Oxidation Using Chemical Ionization Fourier Transform Ion Cyclotron Resonance Mass Spectrometry, Analytical Chemistry, 81 (2009) 6013-6020.
[25] E. Richaud, F. Farcas, P. Bartoloméo, B. Fayolle, L. Audouin, J. Verdu, Effect of oxygen pressure on the oxidation kinetics of unstabilised polypropylene, Polymer Degradation and Stability, 91 (2006) 398-405.
[26] X. Colin, L. Audouin, J. Verdu, Determination of thermal oxidation rate constants by an inverse method. Application to polyethylene, Polymer Degradation and Stability, 86 (2004) 309-321.
[27] G. Mauclaire, J. Lemaire, P. Boissel, G. Bellec, M. Heninger, MICRA: A compact permanent magnet Fourier transform ion cyclotron resonance mass spectrometer, European Journal of Mass Spectrometry, 10 (2004) 155-162.
[28] L. Matisova-Rychla, J. Rychly, J. Verdu, L. Audouin, K. Csomorova, Chemiluminescence and thermogravimetric study of thermal oxidation of polypropylene, Polymer Degradation and Stability, 49 (1995) 51-55.
[29] P. Eriksson, T. Reitberger, B. Stenberg, Gas-phase contribution to the spreading of oxidation in polypropylene as studied by imaging chemiluminescence, Polymer Degradation and Stability, 78 (2002) 183-189.
[30] D. Vaillant, J. Lacoste, G. Dauphin, The oxidation mechanism of polypropylene: contribution of 13C-NMR spectroscopy, Polymer Degradation and Stability, 45 (1994) 355-360.
[31] G. Geuskens, M.S. Kabamba, Photo-oxidation of polymers--Part V: A new chain scission mechanism in polyolefins, Polymer Degradation and Stability, 4 (1982) 69-76.
[32] G. Geuskens, M.S. Kabamba, Photo-oxidation of polymers: Part IX--Additional comments about a new chain scission mechanism in polyolefins, Polymer Degradation and Stability, 5 (1983) 399-401.
[33] S.M. Thornberg, R. Bernstein, A.N. Irwin, D.K. Derzon, S.B. Klamo, R.L. Clough, The genesis of CO2 and CO in the thermooxidative degradation of polypropylene, Polymer Degradation and Stability, 92 (2007) 94-102.
[34] P. Gijsman, J. Hennekens, J. Vincent, The mechanism of the low-temperature oxidation of polypropylene, Polymer Degradation and Stability, 42 (1993) 95-105.
[35] P. Gijsman, M. Kroon, M. van Oorschot, The role of peroxides in the thermooxidative degradation of polypropylene, Polymer Degradation and Stability, 51 (1996) 3-13.

CHAPTER IV. On the impact of oxygen transport properties on polypropylene thermal oxidation. Part I: Effect of oxygen solubility

Alexandre François-Heude[a,b 2], Emmanuel Richaud[a], Alain Guinault[a], Eric Desnoux[b], Xavier Colin[a]

[a]PIMM Laboratory, CNRS UMR 8006, Arts et Metiers ParisTech, Paris, France

[b]Renault, DETC-A, Guyancourt, France

Abstract

A general kinetic model is proposed to describe the polypropylene thermal oxidation of thin polypropylene films in a wide range of temperatures (from 60 to 200°C) and oxygen partial pressures (from 0.02 to 5 MPa) using a single set of parameters. This model was calibrated with several series of experimental data including analyses of primary (hydroperoxides) and secondary oxidation products (carbonyl species), and subsequent changes in macromolecular properties (average molecular masses). It predicts the experimental data previously published in the literature in terms of induction times and maximal oxidation rates. The variability of the oxygen solubility coefficient allows to explain the scattering of induction times and oxidation rates among the whole iPP family, but also the dependence of this latter quantity with oxygen partial pressure. This variability is presumably due to iPP polymorphism in the temperature range where oxygen permeability is commonly measured. It is concluded that the kinetic model can be used to study the direct effect of iPP morphology on its thermal oxidation kinetics (chemistry of oxidation).

Keywords

Polypropylene; Thermal oxidation; Oxygen solubility; Oxygen partial pressure; Chain scissions.

[2] Corresponding author : Email: Alexandre.FRANCOIS-HEUDE@ensam.eu
Tel/ Fax: +33 1 44 24 64 13/ +33 1 44 24 63 82

1. Introduction

In the early 1990s, a formal kinetic approach which consists in focusing on the critical oxidation path, i.e. basing on the rate determining step (RDS), was proposed at the laboratory in order to get around the overcomplexity of radical chain oxidation mechanisms. The main propagation product: hydroperoxide, was shown to be the key initiating species. Indeed, its decomposition leads to the generation of a vast majority of alkyl and peroxy radicals then reacting with oxygen. This closed-loop character describes well the auto-accelerated behavior of polypropylene thermal oxidation from the end of the induction period [1].

Major advances were made in kinetic modeling. Efforts were brought about the eradication of the usual simplifying hypotheses (long oxidation kinetic chains, Bodenstein-Semenov steady-state, oxygen excess and existence of an interrelationship between the termination rate constants) which are necessary for any analytical treatment, but lead to serious inaccuracies when the results have to be extrapolated to longer times or lower temperatures. This first numerical model [2] enabled to simulate accurately the control of oxidation kinetics by oxygen diffusion. It substantiated the overall consistency of the postulated mechanistic scheme, but the kinetic rate constants were mainly estimated from model compounds. Further developments were about the impact of oxygen partial pressure on polypropylene thermal oxidation kinetics at solid [3] and molten states [4]. In both cases, the rate constants were determined by applying an inverse resolution method in order to facilitate the model convergence with a unique set of parameters values, as done successfully for instance for polyethylene [5]. This approach has been generalized in our laboratory to determine all unknown parameters, essentially rate constants, for a given kinetic model and to simulate the experimental results with minimum deviation. If not possible, the postulated mechanistic scheme and the corresponding kinetic model are progressively complexified by adding stepwise new elementary reactions, and the parameters values are readjusted through a trial and error procedure.

Despite these encouraging results, this approach seems to have limitations, in particular in the controversial case of isotactic polypropylene (iPP). Indeed, reading of previous kinetic literature works, it turns out to be impossible to converge towards a unique set of parameters values, which raises the question of the model “universality” in respect with the wide scattering of thermal oxidation behaviors among the whole iPP family. This apparent

variability has been largely attributed to the presence of impurities or structural defects such as catalysis residues, traces of stabilizers, chemical irregularities (including oxidation products) generated during processing or storage [6, 7]. All these defects are in a very low concentration, analytically out of reach, and thus are currently assimilated to an initial concentration of hydroperoxides $[POOH]_0$ as adjustable parameter [8]. This quantity represents a hypothetical (but kinetically equivalent) value accounting for all the radical-producing species initially present into the polymer sample. Indeed, all these extrinsic sources of radicals are expected to vanish while hydroperoxides accumulate in the early periods of exposure, thus becoming quickly negligible compared to hydroperoxides decomposition. $[POOH]_0$ values, usually ranged between 10^{-5} and 10^{-1} $mol.L^{-1}$, were shown to describe properly the scattering of induction times for polyethylene which spreads over only one decade [9, 10]. The upper limit (10^{-1} $mol.L^{-1}$) would simply correspond to the threshold above which the polymer samples could be considered "dirty" and thus, should be rejected. In comparison, iPP induction times [11-20] range over two decades (Figure 1) and thus, cannot be fully described by such a variation range of $[POOH]_0$. This result may suggest additional sources of variabilities which will be tentatively elucidated in the present study.

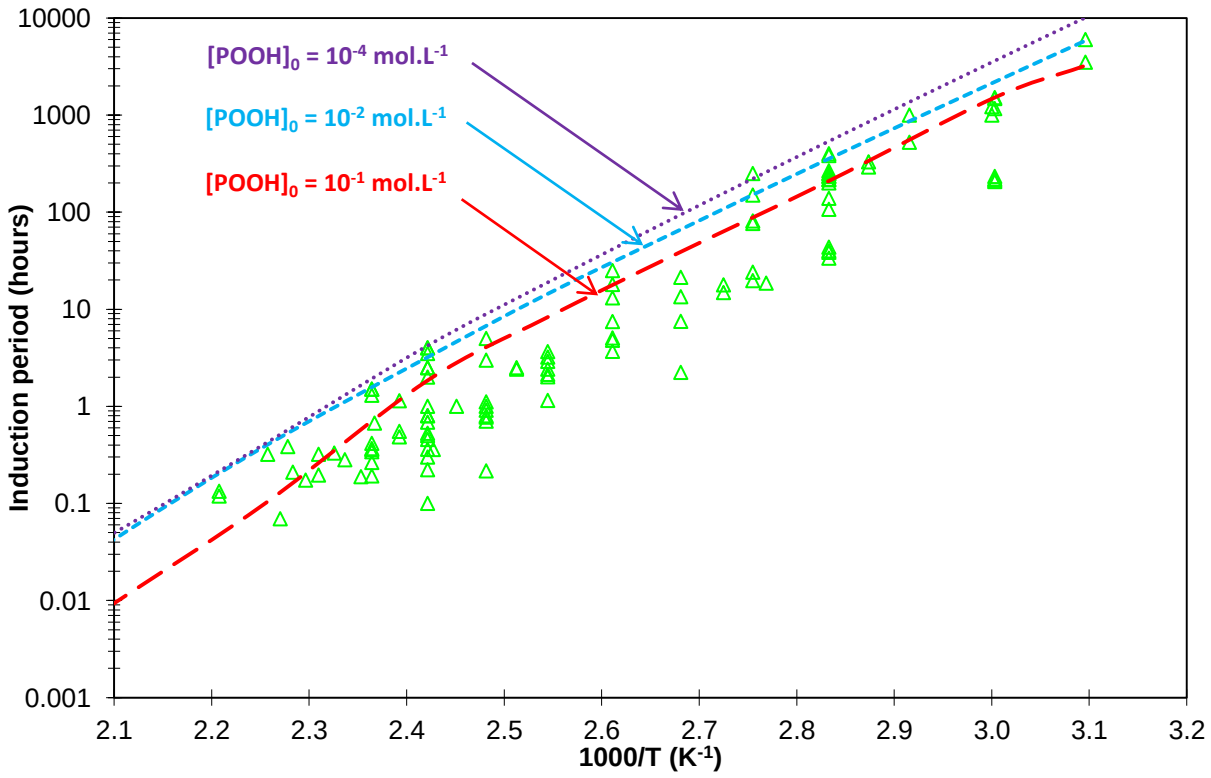

Figure 1: Arrhenius plot of the oxidation induction times compiled from the literature between 50 and 190°C in air. Dotted lines are simulations made with the kinetic model described in reference [3] for various values of $[POOH]_0$ (and a unique value of solubility of $4.2 \cdot 10^{-7}$ exp (-6700/RT) $mol.L^{-1}.Pa^{-1}$.

Symbols (△): compilation of literature data measured by oxygen uptake, carbonyl index, microcalorimetry or chemiluminescence in air.

The objective of the present article is to consider the crystalline morphology as another source of variability which could affect oxygen transport properties, in particular oxygen solubility. Of course, such an assumption will be considered as satisfactory only if it allows modeling all the thermal oxidation behaviors among the whole iPP family with a single set of parameters values.

2. Experimental part

2.1. Materials

A reference isotactic polypropylene, supplied by Aldrich (ref. 427888) as pellets and denoted iPP1, has been chosen for this study in order to properly calibrate the kinetic model. Its thermo-oxidative behavior has been compared with those previously reported in the literature for two other isotactic polypropylenes, denoted iPP2 and iPP3 [3, 12]. Their respective physico-chemical characteristics are reported in table 1.

Table 1: Specifications of investigated iPPs

Material	Reference iPP1	iPP2 [3]	iPP3 [12]
Supplier/grade	Aldrich	BIDIM geosynthetics	Montell/Profax 6501
MFI [230°C, 2.16 kg] (g/10min)	12	-	4
Mw (kg.mol^{-1})	250	170	165
Mn (kg.mol^{-1})	67	70	44
Polydispersity index	3.7	2.5	3.8
Crystallinity ratio (wt%)	45	35	50

IPP1 films of 80-130 µm thick were obtained by compression molding with a Gibitre laboratory press under a pressure of 20 MPa during 30 s at 200°C. Additives were removed by Soxhlet extraction for 48 hours using dichloromethane as solvent without altering the film integrity. The crystallinity was found equal to 45 ± 3 wt% by Differential Scanning Calorimetry (TA Q1000 apparatus) taking a melting enthalpy for crystalline lamellae of ΔH_m^0=209 J/g.

2.2. Thermal aging conditions and FTIR aging monitoring

iPP1 samples were thermally aged at temperatures ranged between 60°C and 140°C in air-ventilated ovens regulated at ±1 °C. Aging monitoring was done with a Perkin-Elmer FTIR spectrophotometer (16 scans, resolution 4 cm^{-1}), basing on the peak of carbonyls at 1713 cm^{-1} (ε=300 $L.mol^{-1}.cm^{-1}$). Low residual concentrations of stabilizers may induce a significant scattering on data between different batches of purification. As a consequence, we proceeded in two steps. Firstly, films stemming from a single batch were submitted to a non-destructive FTIR monitoring at 60, 70, 80, 90, 100, 120 and 140°C in air. These results were considered as standards (as a kind of calibration curve depending on temperature) in order to correct the statistical bias in terms of induction times (due to the presence of stabilizer residues) for the subsequent destructive analyses on films coming from other batches.

2.3. Characterization by complementary destructive analyses

The iodine method was chosen to perform hydroperoxides titration, instead of the sulfide dioxide or ferrous cyanate reactive methods, due to its better reliability for polypropylene [21, 22]. This former is based on the reduction of hydroperoxides by sodium iodide in an acidic medium according to the reaction:

$$R_3COOH + 3I^- + 2H^+ \rightarrow R_3COH + I_3^- + H_2O$$

The concentration of I_3^- ions was titrated by UV spectrophotometry at 355 nm using a Perkin-Elmer Lambda 35 device and a molar extinction coefficient of ε = 25000 $L.mol^{-1}.cm^{-1}$. About 10 mg of PP sample and 7 ml of a solution of isopropanol and acetic acid solvents mixture (10:1) were introduced into a two neck glass flask equipped with a bulb condenser. When refluxing, 2 ml of sodium iodide dissolved in isopropanol (200 g/L) was added with a syringe throughout the side neck. After 10 minutes, the mixture was quenched up to room temperature with 25 ml of distilled water. It is noteworthy that the previous iodometry procedure does not enable discrimining between hydroperoxides, peracids and peresters. Dialkyl peroxides would

not be titrated in theory except if chlorhydric acid is used instead of acetic acid as catalyst. The accuracy on concentration measurement was estimated to be ± 7.5 mol%.

2.4. Molecular weight measurements

Gel Permeation Chromatography (GPC) experiments were performed with a PL-GPC 220 high temperature device commercialized by Agilent Technologies. The GPC was equipped with a guard colomn and two columns branded PLGel Olexis as well as a refractive index detector. The eluent was 1,2,4-trichlorobenzene (Chromasolv, Sigma-Aldrich) stabilized with 0.03 wt% of 2,6-di-*tert*-butyl-4-methylphenol (BHT, Fluka). It was filtered with a 0.2 µm pore size membrane (in PTFE, Whatman) before use. The injection volume was 200 µl and the flow rate was 1.0 ml/min. PP samples were dissolved in 1,2,4-trichlorobenzene/BHT (0.3 wt%) using a PL-SP 260-VS high temperature sample preparation system (PL Ltd.) at 135 °C during 20 minutes. The calibration curve was established from four Polystyrene Shodex narrow standards of respective molecular weights of 1470000, 257000, 46500 and 7210 $g.mol^{-1}$. Results were then corrected using the so-called "universal calibration", based on the well-known Mark-Houwink's relationship (Eq. 1) with the coefficient values reported in table 2.

$$[\eta] = K \bullet M^{\alpha} \qquad \textbf{Eq. 1}$$

Table 2: Coefficients used for universal calibration.

Materials	K (10^3 $ml.g^{-1}$)	α	References
Polystyrene standards	13.8	0.70	[23, 24]
Polypropylene	15.2	0.76	[25]

2.5. Oxygen permeability

Oxygen permeability measurements were performed with a Systech 8001 device on films of about 130 µm thick at 10, 23 or 45°C and 0 % of relative humidity. Their active surface area was equal to 50 cm^2. The time-lag method was chosen to measure oxygen transport properties (see for instance [26]). This analysis mode required a complete purge of the system (including detector, pipes and samples) under a pure nitrogen flow, up to 0.4 ppm as baseline, prior to introduce pure oxygen gas. The diffusivity can be calculated by intercepting with the x-abscissa the straight-line describing the steady-state regime of the kinetic curve of oxygen cumulated amount Q_{O2} obtained by integrating the kinetic curve of Oxygen Transmission Rate

along time. For a semi-infinite film of thickness L, this straight-line obeys the following general equation:

$$Q = \alpha \left(t - \frac{L^2}{6D_{O_2}} \right) \qquad \textbf{Eq. 2}$$

where α is a constant.

So, the oxygen diffusivity D_{O2} is given by:

$$D_{O_2} = \frac{L^2}{6t_{Q=0}} \qquad \textbf{Eq. 3}$$

where $t_{Q=0}$ is the time-lag.

The oxygen solubility $S_{O2}$is related to the oxygen diffusivity D_{O2} and permeability Pe_{O2} according to:

$$S_{O_2} = {D_{O_2}}\Big/{Pe_{O_2}} \qquad \textbf{Eq. 4}$$

3. Theory of formal kinetic modeling

3.1. Closed-Loop Mechanistic Scheme

Most of the mechanistic schemes, used as basis to describe the general trends of oxidation kinetics, were derived from the standard scheme proposed by Bolland and Gee for ethyl linoeate [27] and then, extended to saturated and unsaturated hydrocarbon polymers, namely polyolefins and elastomers [28, 29]. As a general strategy, this scheme was progressively complexified by adding a minimal number of reactions in order to minimize the number of adjustable parameters, thus facilitating analytical or numerical solving. This strategy of formal kinetic (just like the versatile Tobolsky's model proposed in the 1950's which used a reduced number of parameters [30],[31]) differs from the approach adopted by Somersall and Guillet [32], whose mechanistic scheme included all the elementary reactions involved in the aging process. The resulting Closed-Loop Mechanistic Scheme (CLMS) for polypropylene is given below with the kinetic constant rates k_i relative to each step:

Initiation

(1u) $POOH \rightarrow 2P^{\bullet} + (1 - \gamma_1)POH + \gamma_1 P{=}O + H_2O + \gamma_s S$ (- 2PH) (k_{1u})

(1b) $2POOH \rightarrow P^{\bullet} + PO_2^{\bullet} + (1 - \gamma_1)POH + \gamma_1 P{=}O + H_2O + \gamma_s S$ (- PH) (k_{1b})

Propagation

(2) $P^{\bullet} + O_2 \rightarrow PO_2^{\bullet}$ (k_2)

(3) $PO_2^{\bullet} + PH \rightarrow POOH + P^{\bullet}$ (k_3)

Termination

(4) $P^{\bullet} + P^{\bullet} \rightarrow \gamma_4 P\text{-}P + (1 - \gamma_4)PH + (1 - \gamma_4)F + \gamma_4 B$ (k_4)

(5) $P^{\bullet} + PO_2^{\bullet} \rightarrow \gamma_5 POOP + (1 - \gamma_5)POOH + (1 - \gamma_5)F + \gamma_5 B$ (k_5)

(6a) $PO_2^{\bullet} + PO_2^{\bullet} \rightarrow [PO^{\bullet}\ {}^{\bullet}OP]_{cage} + O_2$ (k_{6a})

(6b) $[PO^{\bullet}\ {}^{\bullet}OP]_{cage} \rightarrow POOP + B$ (k_{6b})

(6d) $[PO^{\bullet}\ {}^{\bullet}OP]_{cage} \rightarrow 2P^{\bullet} + 2(1 - \gamma_1)POH + 2\gamma_1 P{=}O + 2\gamma_s S$ (- 2PH) (k_{6d})

with the following formalism:

- PH accounts for tertiary CH groups,
- $P^{\bullet}$, $PO_2^{\bullet}$, $PO^{\bullet}$account respectively for alkyl, peroxy and alkoxy radicals,
- POOH, POOP, P-OH, P=O account respectively for hydroperoxides, peroxides, alcohols and ketones as macromolecular oxidation products,
- γ_1 is the yield of β scission (leading to ketones), irrespectively of the molecularity of the initiation reaction, in competition with hydrogen abstraction (leading to alcohols):

$$\gamma_1 = \frac{k_{\beta\ scission}}{k_{\beta\ scission} + k_{H\ abstraction}} \quad \textbf{Eq. 5}$$

- γ_s is the yield in chain scission which can differ from γ_1 since only β scission occurring on the main macromolecular chain would impact molecular masses contrary to scissions occurring on side-groups or chain extremities.
- From a practical point of view, it is more convenient to consider an apparent yield γ_1^{app} for carbonyl products owing to the high uncertainty on the nature of these species and the value of their corresponding molar extinction coefficients.
- γ_4 and γ_5 are the respective yields of alkyl-alkyl and alkyl-peroxy radicals coupling (of respective rate constants k_{4r} and k_{5r}), in competition with disproportionation (of respective rate constants k_{4d} and k_{5d}):

$$\gamma_4 = \frac{k_{4_r}}{k_{4_r} + k_{4_d}} \quad \text{and} \quad \gamma_5 = \frac{k_{5_r}}{k_{5_r} + k_{5_d}} \quad \textbf{Eq. 6 and 7}$$

- F, S and B account for double bonds, chain scissions and crosslinks (i.e. covalent bridges) respectively.

Most of the justifications of these mechanistic considerations are detailed elsewhere [4, 33], but the fundamental principles and noticeable improvements of this model can be briefly detailed below:

(i) The mechanistic scheme only considers a single reactive site: the methyne unit (tertiary CH groups);

(ii) In terms of initiation processes, the hypothesis of a constant initiation rate (as considered, for instance, by Neiman and reported by Reich and Stivala [20]) was dismissed in thermal oxidation, because it does not allow to simulate the induction period. In this latter case, the main source of radicals is the hydroperoxides decomposition whose molecularity was shown to be mainly bimolecular at temperatures typically lower than 200°C [10]. It is a balance reaction since the homolysis of the O-O bond is very slow and rate determining compared with the subsequent rearrangements of the very reactive alkoxy ($PO^{\bullet}$) and hydroxy ($HO^{\bullet}$) radicals generated by this decomposition.

(iii) In terms of termination reactions, recombinations of peroxy radicals were detailed taking into account their propagation outside the cage, as supported by the kinetic analyses made by Reich and Stivala [34]. Such a consideration aims at describing the mobility hindrance of peroxy macroradical when decreasing temperature and thus, at predicting a change in kinetic regime below a critical temperature, located around 90°C for polyethylene [35].

(iv) Although the formation of volatile compounds (VOCs) is not explicited, it is taken into account though the apparent yield in carbonyl products γ_1 [36]. It is important to remind here that the VOCs generation does not modify the polymer backbone since it takes place at the chain extremities. As a result, γ_s corresponds to the real yield of chain scissions in the middle-chain which is responsible for the polymer embrittlement.

This general mechanistic scheme leads, by using the classical concepts of chemical kinetics, to a system of ordinary differential equations (SDE) describing the local concentration changes in primary products, i.e. $[P^{\bullet}]$, $[PO_2^{\bullet}]$, [POOH], $[PO^{\bullet\bullet}OP]_{cage}$, [PH] and $[O_2]$, along the course of oxidation. These quantities are the most relevant to model because their calculation does not require the use of an additional apparent yield as adjustable parameter. Actually, only the concentrations of oxygen $[O_2]$ and hydroperoxides [POOH] are currently measured. From a practical point of view, concentrations of secondary oxidation products, such as ketones, alcohols and related quantities (such as chain scissions S and crosslinking nodes B), are also very useful to check the model validity because they are easily accessible

experimentally. They are calculated in the post-treatment stage by integrating the following differential equations (**Eq. 8-11)**:

$$\frac{d[C=O]}{dt} = \gamma_1 k_{1u}[POOH] + \gamma_1 k_{1b}[POOH]^2 + 2\gamma_1 k_{6d}[PO^{\bullet\bullet}OP] \quad \textbf{Eq. 8}$$

$$\frac{d[OH]}{dt} = (1-\gamma_1)k_{1u}[POOH] + (1-\gamma_1)k_{1b}[POOH]^2 + 2(1-\gamma_1)k_{6d}[PO^{\bullet\bullet}OP] \quad \textbf{Eq. 9}$$

$$\frac{dS}{dt} = \gamma_s k_{1u}[POOH] + \gamma_s k_{1b}[POOH]^2 + 2\gamma_s k_{6d}[PO^{\bullet\bullet}OP] \quad \textbf{Eq. 10}$$

$$\frac{dB}{dt} = \gamma_4 k_4[P^{\bullet}]^2 + \gamma_5 k_5[P^{\bullet}][PO_2^{\bullet}] + k_{6b}[PO^{\bullet\bullet}OP] \quad \textbf{Eq. 11}$$

For the full detail of the mathematical treatment, the reader is invited to refer to appendix A. From both quantities S and B, subsequent multiscale properties can be then calculated, as for instance the decrease in weight M_w and number M_n average molecular masses by using the usual Saito's laws [37]:

$$\frac{S}{2} - 2B = \rho_{tot}\left(\frac{1}{\overline{M_w}} - \frac{1}{\overline{M_{wO}}}\right) \quad \textbf{Eq. 12}$$

And

$$S - B = \rho_{tot}\left(\frac{1}{\overline{M_n}} - \frac{1}{\overline{M_{nO}}}\right) \quad \textbf{Eq. 13}$$

where ρ_{tot} is the polymer density (0.91 g.cm^{-3})

3.2. Strategy for the optimization procedure

According to the model previously described, the resolution of the chemical problem implies to determine up to 9 rate constants (k_{1u}, k_{1b}, k_2, k_3, k_4, k_5, k_{6a}, k_{6b} and k_{6d}) and 4 yields (γ_1, γ_4, γ_5 and γ_s) with their respective temperature dependences considering a reliable estimate of the initial concentration of hydroperoxides $[POOH]_0$. Moreover, literature data on rate constants k_2, k_4 and k_5 are very scarce because these latter are difficult to estimate independently. The problem could thus appear as underdetermined with such a high number of parameters, thus giving access to several numerically equivalent solutions, even if a large number of complementary experimental data is available.

Considering that an inverse resolution method may be tentatively used in order to solve this problem, the simpler the model will be, the better the problem will be conditioned. Therefore, to reduce the number of adjustable parameters, the strategy consists in oversimplifying the system, which can be conveniently operated by working at high oxygen partial pressure. Indeed, in such aging conditions, alkyl radicals $P^{\bullet}$ are rapidly converted into peroxy radicals $PO_2^{\bullet}$, so that the concentration in alkyl radicals is very low comparatively to the concentration in peroxy radicals [3]. In such a case, steps (4) (alkyl-alkyl radicals recombination) and (5) (alkyl-peroxy radicals recombination) can be neglected compared to step (6) (peroxy-peroxy radicals recombination) [3, 5, 34, 38]. This kinetic regime is called "oxygen excess", as the opposite of "oxygen default" conditions. Physically, the "oxygen excess" regime corresponds to the saturation of reactive sites (PH) by oxygen.

The optimization procedure thus first consists in determining k_{1u}, k_{1b}, k_3, k_{6a}, k_{6b} and k_{6d} in oxygen excess. The value of k_3 was assumed to obey the semi-empirical Korcek's relationship [39]. Moreover, at high oxygen partial pressure, it can be assumed that $k_2[O_2]$ is much higher than $k_4[P^{\bullet}]$ or $k_5[PO_2^{\bullet}]$ (see invariant k_2/k_4 below). That is the reason why k_2 must be fixed in oxygen default as well as all other parameters neglected in oxygen excess, i.e. k_4, k_5, γ_4 and γ_5.

To facilitate the optimization of parameters determination, it is fruitful to understand their influence on the oxidation kinetics. In this perspective, kinetic relationships coming from the analytical solving are very valuable since providing a phenomenological description. They allow to understand the existence of some invariant quantities [5]:

(i) In oxygen excess, the oxidation rate is maximal:

$$r_s = \frac{k_3^2[PH]^2}{4\,k_6} \qquad \textbf{Eq. 14}$$

The ratio k_3^2/k_6 describes the competition between the propagation by hydrogen abstraction (3) and bimolecular recombination of peroxy radicals (6).

(ii) The apparent rate constant k_6 describing the bimolecular recombination of peroxy radicals does not apply to an elementary step, but is the result of the combination of several competitive steps of termination into and outside the cage. The resulting relationship describing its non arrhenian behavior is [33, 35]:

$$k_6 = \frac{k_{60}}{\left(1+\frac{k_{63}}{k_{61}}\right)\left(1+\frac{k_{63}}{2\,k_{61}}\right)} \qquad \textbf{Eq. 15}$$

Thereby, the ratio k_{63}/k_{61} appears also as an invariant quantity.

(iii) The ratio k_2/k_4 was also reported as an invariant quantity resulting from the competition between very fast reactions involving alkyl radicals: oxygen addition (2) and bimolecular recombination (4).

Actually, the kinetic rate constant k_4 for alkyl-alkyl radicals recombination has almost no influence under the investigated conditions (at P_{O2}=0.02 MPa). Thus, the latter invariant must be rather conceived as a constraint in order to preserve the heuristic value of the kinetic model, as well as the inequality postulated by Gillen and Clough, i.e. $(k_5)^2 > 4 \cdot k_4 \cdot k_6$ [40]. This latter allows to fix the orders of magnitude of termination rate constants since, it induces that $k_4 > k_5 >> k_6$ up to a temperature of about 160°C.

In a first approach, the yields γ_4 and γ_5 were fixed at zero for reporting results obtained in radio-oxidation [41] (since termination reactions are expected to be weakly impacted by ionizing radiations) in order to avoid the generation of an unrealistic crosslinking.

Therefore, the main challenge consists in the determination of the kinetic rate constant k_5 for alkyl-peroxy radical recombination (in consistency with previous literature data [13, 41, 42]) which turns out to be closely interrelated with the values of oxygen solubility S_{O2} and rate constant k_2. A last invariant combination of rate constants can be deduced from the expression of the critical oxygen concentration above which oxygen is in excess in the sample:

$$[O_2]_c = {}^{K}\!/_{\beta} = K \cdot {}^{k_3\, k_5\, [PH]}\!/_{k_2\, k_6} \qquad \textbf{Eq. 16}$$

where K is an arbitrary value depending exclusively on the physical or chemical property under consideration (e.g. oxidation rate or induction time; see appendix B).

Thus, the corresponding critical oxygen pressure is:

$$P_c = {}^{[O_2]_c}\!/_{S_{O_2}} = K \cdot {}^{k_3\, k_5\, [PH]}\!/_{k_2\, k_6\, S_{O_2}} \qquad \textbf{Eq. 17}$$

This last equation particularly evidences the existence of an interrelationship between the oxygen solubility and some kinetic rate constants, especially k_2 and k_5. Indeed, in oxygen default, the polymer is not saturated in oxygen anymore and the impact of oxygen solubility increases dramatically. A special interest was therefore dedicated to the determination of the oxygen transport properties, and to the estimation of their variability for the whole iPP family, prior to the calibration of k_5. Its accurate determination requires the knowledge of primary products concentrations, thus justifying additional experiments on the reference polypropylene (iPP1) such as hydroperoxides titration. The present work is the result of an

exhaustive back and forward procedure. For a sake of simplicity, the calibration of the model will be presented before investigating the effect of oxygen partial pressure.

4. Model calibration with iPP1 in oxygen default

4.1. Determination of the oxygen transport properties

Since oxygen transport properties are suspected to impact the polypropylene oxidation behavior, the values of oxygen permeability, diffusivity and solubility have been measured by permeametry on the reference polypropylene (iPP1) at 10, 23 and 45°C. Obviously, it would have been more relevant to measure directly these data over the higher temperature range investigated for aging, but it is unfortunately outside the device capacities. That is the reason why these three quantities were extrapolated at higher temperatures by assuming that they obey an Arrhenius' law.

In sufficiently thin PP films (typically ~100 µm thick), thermal oxidation can be considered homogeneous in the whole thickness (no diffusion limited oxidation). Indeed, oxygen diffusion until the middle of samples is quasi instantaneous and thus, only the coefficient of oxygen solubility will be relevant for modeling thermal oxidation kinetics. That is the reason why only the value of oxygen solubility is given in the present paper whereas the values of oxygen permeability and diffusivity will be discussed in a future paper dedicated to the determination of oxidation profiles in thicker PP samples (typically few millimeters thick):

$$S_{O_2}{}^{tot} = 1.48 \cdot 10^{-6} \times \exp\left(-6700/_{\mathrm{RT}}\right) \left(mol.L^{-1}.Pa^{-1}\right) \qquad \textbf{Eq. 18}$$

There is a large consensus in the literature on the fact that the oxygen solubility is proportional to the fraction of amorphous phase wherein oxygen is dissolved [43]. Thus, if $S_{O2}{}^{am}$ and $S_{O2}{}^{tot}$ are the respective oxygen solubilities in the amorphous phase and in the semi-crystalline polymer, one can write:

$$S_{O_2}^{am} = \frac{S_{O_2}^{tot}}{1-\chi_c} \frac{\rho_{am}}{\rho_{tot}} \qquad \textbf{Eq. 19}$$

with χ_c the crystallinity ratio, ρ_{am} the density of the amorphous phase (0.85 g.cm^{-3}) and ρ_{tot} the density of the semi-crystalline polymer.

Let us remind, here, that the chemical problem is solved in the amorphous phase and the structural changes in the semi-crystalline polymer are deduced in a post-treatment stage (see equation A.13 in appendix A).

The values of oxygen solubility S_{O2}^{am} determined in the iPP amorphous phase in this study are compared with the data compiled from the literature [44-56] in figure 2. S_{O2}^{am} is of the same order of magnitude and almost temperature independent for all iPPs. To illustrate, at 50°C, S_{O2}^{am} is ranged between $3 \cdot 10^{-8}$ and $2 \cdot 10^{-7}$ $mol.^{-1}.Pa^{-1}$. Its activation energy is about 0 ± 5 $kJ.mol^{-1}$ for the whole literature dataset and 7 $kJ.mol^{-1}$ for iPP1is located in the upper range of the compilation.

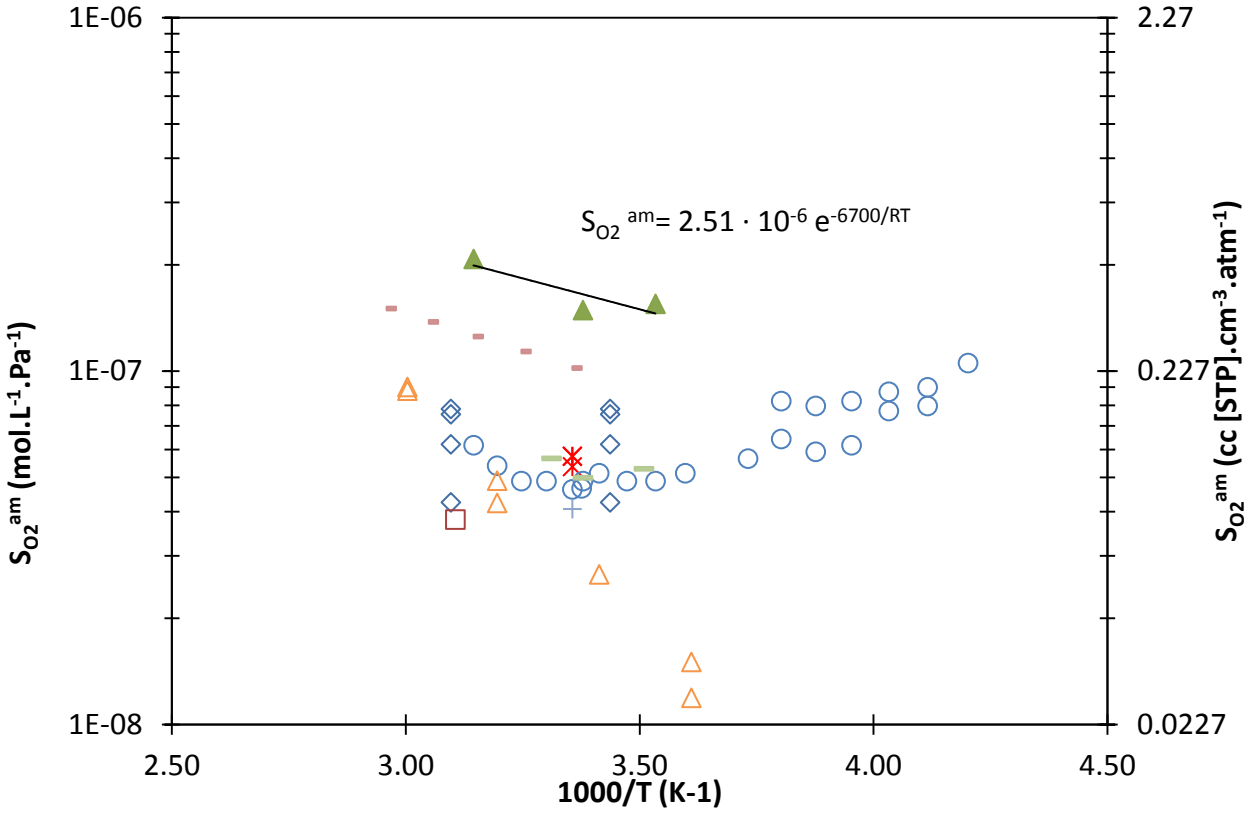

Figure 2: Comparison of the oxygen solubilities of iPPs measured in this study and compiled from the literature: ▲ iPP1 (this study). ✳ Lin [48, 49]. ○ Somlai [50]. ▬ Villaluenga [52]. ▬ Beltrame [44]. ◇ Mani [56]. ◇ Kiryushskin [46, 57]. □ Denisov [45]. + Thorlaksen [51]. △ Kurek [47].

4.2. Modeling the changes in primary oxidation products

Once the oxygen related parameters, in particular the coefficient of oxygen solubility, have been determined for the reference polypropylene (iPP1), it has been then possible to determine accurately the kinetic rate constants. The entire set of values able to describe the thermal oxidation behaviors of the three isotactic polypropylenes under study (iPPs 1, 2 and 3) is given in table 3.

Table 3: Parameters used for modeling polypropylene thermal oxidation

*k_{1u}^{0} = (2.4 ± 1.5)· 10^{13} s^{-1}, **k_{1b0} = (7.7 ± 1.5) · 10^{8} $L.mol^{-1}.s^{-1}$

	P⁰			***Ea (kJ.mol⁻¹)***
	iPP1	*iPP2*	*iPP3*	
$[POOH]_0$ $(mol.L^{-1})$	$4 \cdot 10^{-3}$	$1 \cdot 10^{-4}$	$1 \cdot 10^{-4}$	-
S_{O2}^{am} $(mol.L^{-1}.Pa^{-1})$	$2.5 \cdot 10^{-6}$	$4.2 \cdot 10^{-7}$	$2.5 \cdot 10^{-6}$	6.7
D_{O2} $(m^2.s^{-1})$	$8.7 \cdot 10^{-6}$	$8.7 \cdot 10^{-6}$	$8.7 \cdot 10^{-6}$	36.4
Pe_{O2} $(cm^3.cm.cm^{-2}.Pa^{-1}.s^{-1})$	$2.9 \cdot 10^{-6}$	-	-	43.0
k_{1u} (s^{-1})*	$2.9 \cdot 10^{13}$	$1.9 \cdot 10^{13}$ $2.9 \cdot 10^{13}$	$2.9 \cdot 10^{13}$	140.7
k_{1b} $(L.mol^{-1}.s^{-1})$**	$9.2 \cdot 10^{8}$	$6.2 \cdot 10^{8}$ $9.2 \cdot 10^{8}$	$9.2 \cdot 10^{8}$	95.0
k_2 $(L.mol^{-1}.s^{-1})$	$3.0 \cdot 10^{9}$	$3.0 \cdot 10^{9}$	$3.0 \cdot 10^{9}$	10.0
k_3 $(L.mol^{-1}.s^{-1})$	$5.1 \cdot 10^{7}$	$5.1 \cdot 10^{7}$	$5.1 \cdot 10^{7}$	62.2
k_4 $(L.mol^{-1}.s^{-1})$	$1.0 \cdot 10^{12}$	$1.0 \cdot 10^{12}$	$1.0 \cdot 10^{12}$	0.0
k_5 $(L.mol^{-1}.s^{-1})$	$4.5 \cdot 10^{10}$	$4.5 \cdot 10^{10}$	$4.5 \cdot 10^{10}$	0.0
k_{6a} $(L.mol^{-1}.s^{-1})$	$2.0 \cdot 10^{17}$	$2.0 \cdot 10^{17}$	$2.0 \cdot 10^{17}$	90.0
k_{6b} (s^{-1})	$6.7 \cdot 10^{6}$	$6.7 \cdot 10^{6}$	$6.7 \cdot 10^{6}$	5.0
k_{6d} (s^{-1})	$1.4 \cdot 10^{12}$	$1.4 \cdot 10^{12}$	$1.4 \cdot 10^{12}$	41.0
γ_1	0.5	0.5	0.5	-
γ_4	0	0	0	-
γ_5	0	0	0	-
γ_s	0.5	0.5	0.5	-

This values result from the optimization procedure detailed in part 3.3. It is relevant to remind here that modeling the changes in hydroperoxides concentration was a key step in this study because it gives access to the value of k_5 which is closely related to the values of k_2 and S_{O2}.

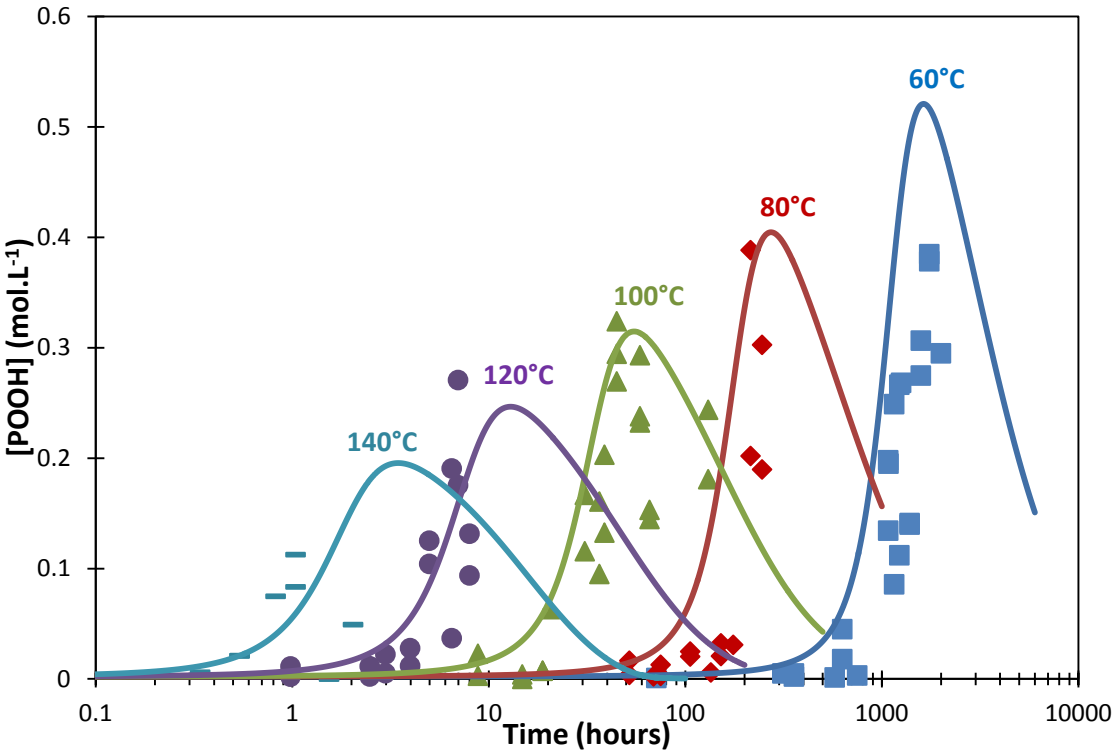

Figure 3: Changes in the hydroperoxydes concentration of iPP1 at 0.02 MPa between 60 and 140°C. Symbols: experimental data. Solid lines: kinetic modeling.

4.3. Modeling the build-up of secondary oxidation products

The simulation of the changes in carbonyls concentration is also satisfying (Figure), particularly when considering that a single apparent yield γ_1 has been used for carbonyls over the whole temperature range under investigation at the solid state.

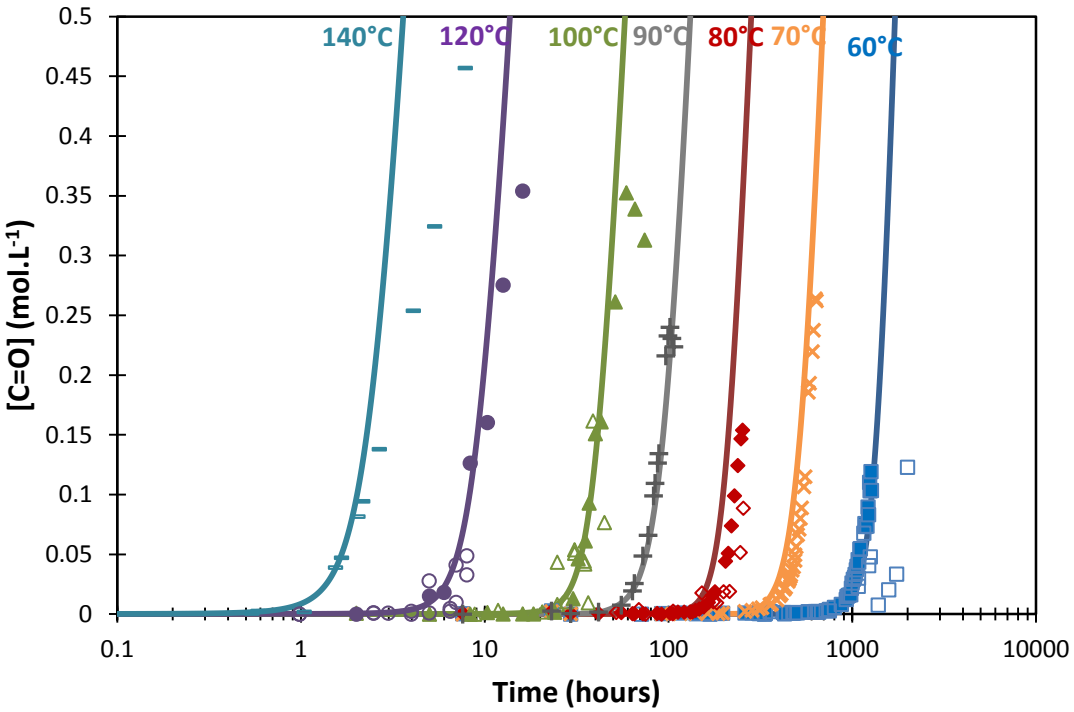

Figure 4: Changes in the carbonyls concentration of iPP1 at 0.02 MPa between 60 and 140°C. Symbols: experimental data. Solid lines: kinetic modeling.

γ_1 is prone to be dramatically impacted by:

(i) the release of volatile compounds by the matrix, which are thereby not monitored [36],

(ii) in a minor extent, the distribution of macromolecular oxidation products,

(iii) the changes in crystallinity ratio (for instance, due to annealing or chemi-crystallization).

This parameter would be weakly temperature dependent, especially at temperatures lower than 140°C where VOC emissions would be noticeably low, which is rather beneficial for extrapolation at temperatures close to ambient. Moreover, the shape of the IR absorption band of carbonyl species remains unchanged when varying the temperature, which would confirm minor changes in the distribution of these species over the whole temperature range under study. In contrast, γ_1 seems to depend more significantly on oxygen partial pressure, as discussed in part 5.

4.4. Modeling the changes in average molecular masses

From the changes in macromolecular quantities, in particular chain scission and crosslink concentrations, it is possible to calculate the changes in weight Mw and number M_n average molecular masses according to the Saito laws (equations 12 and 13). The yield of chain scissions γ_s accounts for β-scissions occurring on the polymer middle chain and resulting in methyl ketones. In other words, β-scissions on side-chain methyl groups (responsible for the generation of middle chain ketones) and chain extremities (volatile products) are not considered here.

Because of the large scattering of our experimental results, it was not possible to determine precisely a value for γ_s except at 100°C. Fortunately, values of this parameter were available in the literature [13] [58] [59] [60] [61] [62]. This yield has been divided by the apparent yield in carbonyl species γ_1, calculated at the same temperature by neglecting the occurrence of crosslinks B in a first approach. Values of the ratio γ_s/γ_1 for iPP, aPP (atactic polypropylene) and PE under various oxygen partial pressures between 90 and 160°C are reported in table 4.

Table 4: Ratio of the yield in chain scission over the yield in carbonyl species between 90 and 160°C under various oxygen partial pressures for iPP, aPP and PE.

P_{O2} (MPa)	T (°C)	Material	γ_s/γ_1	Reference
0.02	100	Bulk iPP	0.75	This study
0.01	130	Bulk iPP	0.99 ± 0.25	[58]
0.02	90	Bulk iPP	0.77	[59]
0.02	90-110	Bulk iPP	0.75 ± 0.15	[13]
1	130	Bulk iPP	0.67 ± 0.12	[60]
1	130	iPP in solution (0.56 $mol.L^{-1}$)	0.92 ± 0.23	[60]
0.02	120	Bulk aPP	0.78	[61]
1	130	Bulk aPP	1.20 ± 0.16	[60]
0.01	130	Bulk PE	1.42 ± 0.45	[58]
0.1	130-160	Bulk PE	0.99 ± 0.07	[62]

It can be seen that the mean value of γ_s/γ_1 is around 0.8 for iPP (so γ_s = 0.4) whatever the temperature and the oxygen partial pressure. This value is slightly higher in PE (~1.2) and aPP (~1.0). When considering the crosslinking reactions, the real yield in chain scissions for iPP is 0.5. The competition between chain scissions and crosslinking processes in iPP1 can be illustrated by the plot of S = f(B) reported in Figure . The model generates a ratio S/B of 6 ± 2 in rather good agreement with the general experimental trend of 9.6 ± 2.7 evidenced on iPP1 in the present study, but also on another iPP by Achimsky et al. [59].

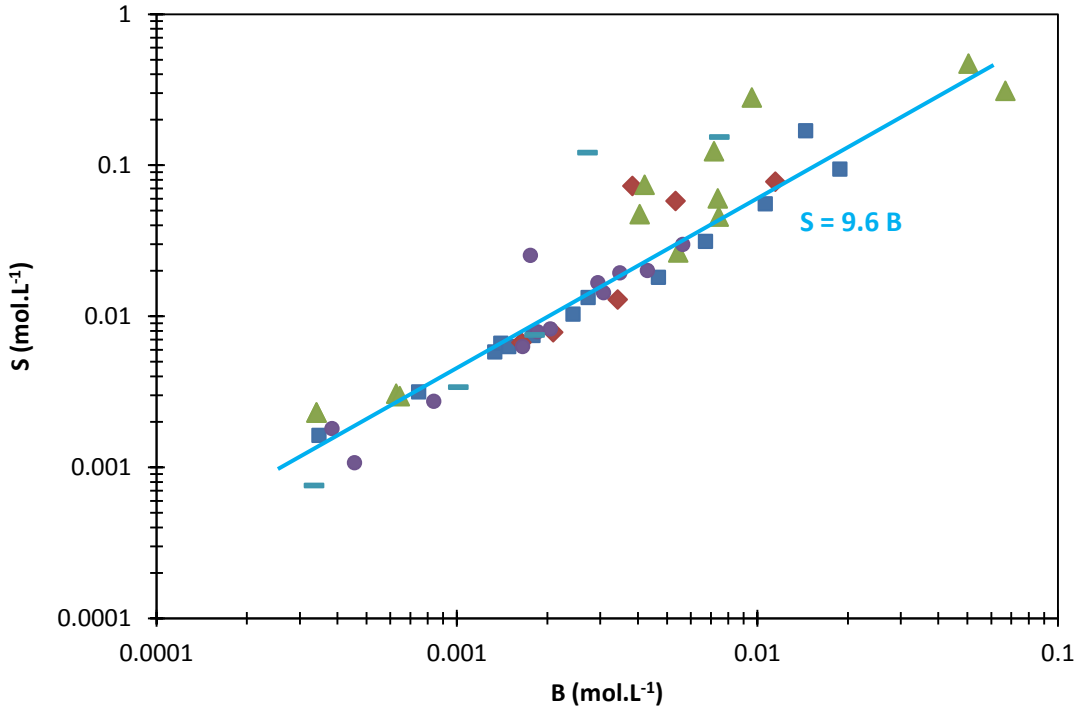

Figure 5: Number of chain scissions S versus number of crosslinks (or covalent bridges) B for iPP1 under 0.02 MPa between 60 and 140°C. Values of S and B have been obtained by solving the system of equations 8 and 9. Legend: ■ 60°C, ◆ 80°C, ▲ 100°C, ● 120°C and − 140°C.

In figures 6 and 7, numerical simulations of M_n and M_w have been compared with experimental results. As expected (see equations 12 and 13), M_w is more sensitive than M_n to crosslinking, which is materialized by the presence of an acute shoulder just before the drop of molecular masses. Thus, this observation is not a numerical artifact, but it is difficult to confirm experimentally because of the wide data scattering. Nevertheless, the model simulates the general experimental trend in the whole temperature range under study and confirms that chain scissions prevail largely over crosslinking whatever the temperature.

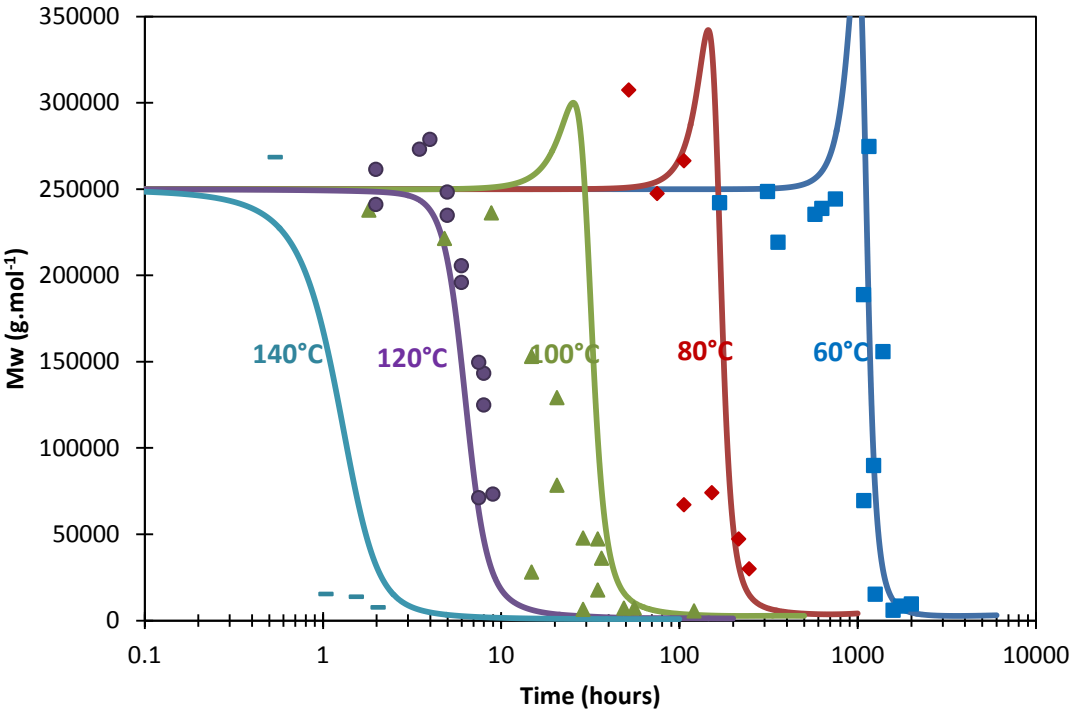

Figure 6: Changes in the weight average molecular mass of iPP1 under 0.02 MPa between 60 and 140°C. Symbols: experimental data. Solid lines: kinetic modeling.

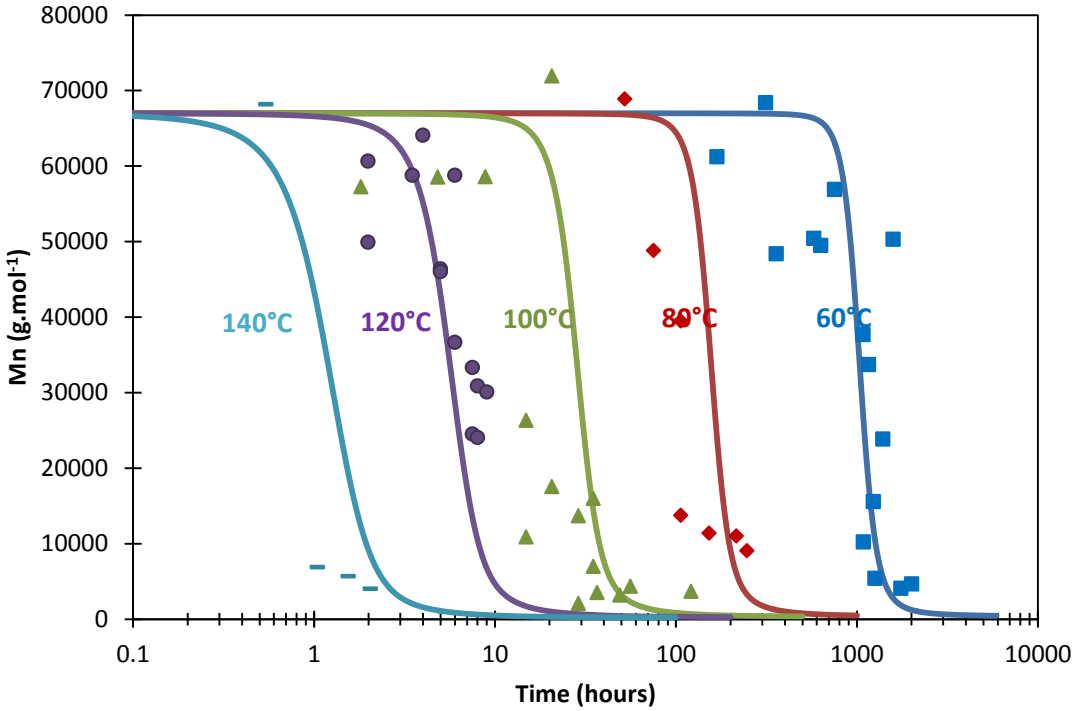

Figure 7: Changes in the number average molecular mass of iPP1 under 0.02 MPa between 60 and 140°C. Symbols: experimental data. Solid lines: kinetic modeling.

The ability of the model to predict the changes in macromolecular masses is highly valuable since the polypropylene lifetime, in terms of mechanical properties, can be determined according to a critical value of weight average molecular mass (end-of-life criterion) [63].

5. Discussion: towards a "universal" kinetic model

5.1. Common sources of variability in connection with initiation processes

The optimization of parameters determination in oxygen excess, namely k_{1u}, k_{1b}, k_3, k_{6a}, k_{6b} and k_{6d}, was the first modeling stage of the polypropylene thermal oxidation. In order to be reliable, this optimization was mostly based on titration of hydroperoxides as primary oxidation products. Indeed, a lot of information is included in the shape of their concentration changes, focusing on the induction time, but also on the maximal and final concentrations. The shape of these curves, illustrating the auto-accelerated character of thermal oxidation, has been extendedly discussed elsewhere [42]. Figure shows the best simulations used for determining the single set of parameters values (table 3).

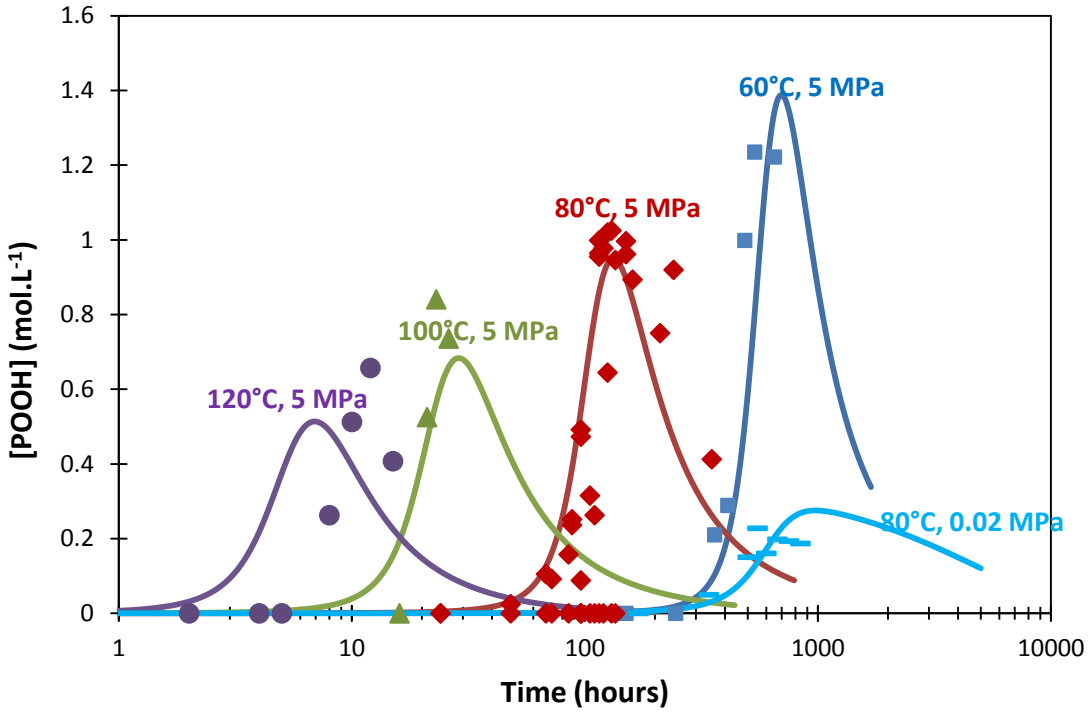

Figure 8: Changes in the hydroperoxydes concentration of iPP2 under 5 MPa between 60 and 140°C and under 0.02 MPa at 80°C. Symbols: experimental data coming from reference [3]. Solid lines: kinetic modeling.

According to assertions of part 3.3, in oxygen excess, the values of the coefficient of oxygen solubility and rate constant k_2 do not affect the oxidation kinetics. This is highly beneficial because the oxidation behavior is not diffusion-controlled and so, independent of the oxygen transport properties. Therefore, oxygen excess is particularly indicated in order to quantify the part of variability which must be attributed to the multiplicity of initiating species, e.g chemical irregularities (including oxidized functions), traces of metal chelates and residual concentration of stabilizers.

In this perspective, it is relevant to compare the oxidation behaviors of different iPPs under high partial oxygen pressure. Such experimental data have been advantageously collected from papers of Richaud et al. on iPP2 [3] and Faulker on iPP3 [11]. This latter iPP3 turns out to have close morphological features with our reference material iPP1. That is the reason why, for iPP1, the oxygen excess conditions have been considered as experimentally fulfilled under the highest oxygen partial pressure investigated by Richaud et al. (5 MPa) and Faulkner (4.24 MPa). This assumption will be checked later (see literature compilation of oxygen critical pressures in Figure).

Surprisingly, the discrepancies between the two kinds of polypropylenes cannot be described by a simple change in the initial concentration of hydroperoxides $[POOH]_0$, i.e. by a simple difference in their pre-oxidation state during processing and/or storage. It would thus require to adjust the initiation rate by slightly modifying the values of initiation rate constants (i.e. k_{1u}, k_{1b} or both). Metal particles are thought to favor unimolecular decomposition of hydroperoxides, but several arguments support the idea that the competition of both kinds of initiation processes would remain unchanged:

(i) Modifying only k_{1u} would lead to a preexponential factor k_{1u}^0 higher than the upper realistic value of 10^{13} s^{-1}.

(ii) The simulations show that the commonly accepted mechanism of hydroperoxides decomposition by catalyst residues (metal chelates) [64] partially behaves as a bimolecular process.

(iii) The bends of kinetic curves of carbonyl build-up at the end of the induction period are similar for the three different iPPs under investigation. This experimental observation suggests that the balance between both types of initiation processes must remain unchanged. In other words, the critical concentration in hydroperoxides $[POOH]_c$ must also remain unchanged [3, 5] (this notion and its use in kinetic modeling is detailed in appendix A):

$$[POOH]_c = \frac{k1_u}{k1_b} = \frac{{k1_u}^0}{{k1_b}^0} \exp\left(-\frac{E_u - E_b}{RT}\right)$$ **Eq. 20**

In this study, a unique corrective factor (of 1.5) has been applied to k_{1u} and k_{1b} in order to report the observed discrepancies. This is eventually a moderate correction which is not be sufficient to report the variability of induction times observed in oxygen default (Figure 1).

Such a behavior was previously evidenced by Georges and coworkers. They found that the amount of titanium catalyst has an impact on the pre-exponential factor of the Arrhenius law of induction time, but not on activation energy [65-67]. The effect of catalytic residues on the oxidation kinetics, already well-documented in the literature [6, 7], has been tested in a first approach. Although relevant to account for the variability of results in oxygen excess, this phenomenon is clearly insufficient to report for the oxidation behaviors of all iPPs in oxygen default.

5.2. Introduction of a variability on the coefficient of oxygen solubility

5.2.1. Dependences with oxygen partial pressure

When buckling down to the kinetic modeling of thermal oxidation in oxygen default, the main issue was to explain the differences between the oxygen partial pressures dependences of induction times for the iPPs under study, in particular iPP2 and iPP3 (knowing that iPP3 is characterized by similar features and oxidation behavior as iPP1). Indeed, in Figure , it is clear that these changes are less pronounced for iPP3 at 90°C than for iPP2 at 60, 80 or 100°C (for which they are rather homothetic). In other words, both iPP would have a different critical oxygen pressure.

According to our theoretical expectations (in particular from equation 17), this effect should be taken into account by adjusting the oxygen solubility (rather than the rate constant k_5, which would constitute a physical nonsense for a given polymer family).

The changes in the carbonyls concentrations have been simulated with the kinetic model. The resulting changes in induction times with oxygen pressure at various temperatures are depicted in Figure . It has been necessary to use a value of oxygen solubility 6 times higher for iPP3 than for iPP2 in order to report the experimental discrepancies. This variability on the oxygen solubility is in satisfactory agreement with the large scattering reported when

compiling the data of various authors [44-56] (see Figure). All these results constitute a supporting evidence of the impact of oxygen solubility on the iPP thermal oxidation kinetics.

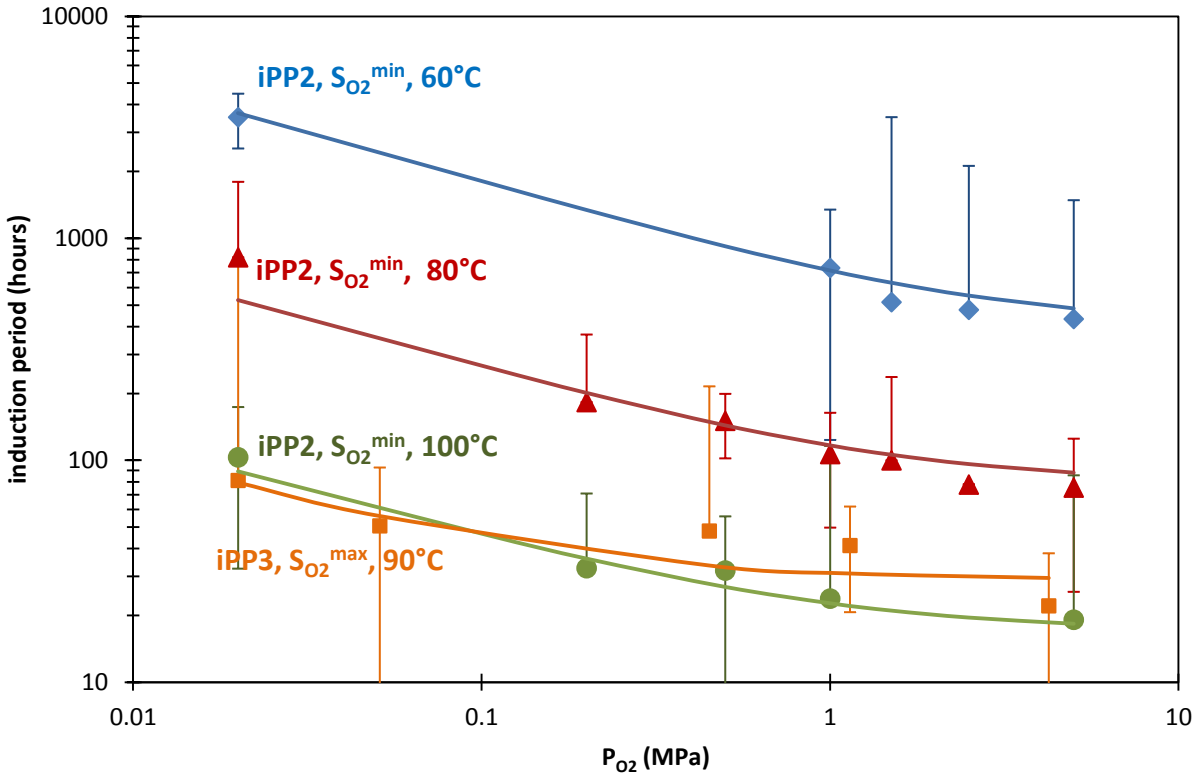

Figure 9: Dependences with oxygen partial pressure of induction time (from carbonyl species) for iPP2 and iPP3 with different oxygen solubility (respectively $S_{O2}^{min} = 4.2 \cdot 10^{-7}$ exp(-6700/RT) and $S_{O2}^{max} = 2.5 \cdot 10^{-6}$ exp(-6700/RT) mol.L^{-1}.Pa^{-1}) coefficients between 60°C and 100°C. Symbols: experimental data. Solid lines: kinetic modeling.

It is noteworthy that the activation energy of oxygen solubility undergoes uncertainty due to large data scattering over a too small interval of temperatures. But, it takes a low value in agreement with our expectations. Since the rate constant k_2 and oxygen solubility are strongly correlated, there is a compensation effect between their respective activation energies. Thus, affecting small activation energy on S_{O2} enables to minimize the value of Ea_2, as expected for very fast reactions (compared with k_4 and k_5). Eventually, Ea_2 was set at 10 kJ.mol^{-1}, in agreement with previous studies [2, 68]. In addition to the effect of oxygen solubility on its dependence with the oxygen partial pressure, it is also noteworthy that the apparent yield in carbonyl products γ_1 decreases with the oxygen partial pressure (Table 5) from a value of 0.5 in oxygen default up to 0.2 in oxygen excess. This variation can be related to the changes in the formation mechanisms of oxidation products, including VOCs, with oxygen partial

pressure [36]. This is of particular interest as source of error when determining the critical oxygen pressure from the kinetic curves of carbonyls build-up.

Table 5: Changes in the apparent yield γ_1 of carbonyl products with oxygen partial pressure. Values range gradually from 0.5 under ambient pressure to 0.2 in oxygen excess (under 5 MPa)

Material	Oxygen partial pressure (MPa)	T (°C)	γ_1
iPP1	0.02	60-140	0.5
iPP2	0.02	60-100	0.5
iPP2	0.2	80-100	0.2
iPP2	0.5	80	0.2
iPP2	1	60	0.15
iPP2	1	80	0.3
iPP2	1	100	0.4
iPP2	1.5	60	0.4
iPP2	1.5	80	0.2
iPP2	1.5	100	0.4
iPP2	2.5	60	0.2
iPP2	5	60-120	0.2
iPP3	0.02	60-90	0.5
iPP3	0.051	90	0.3
iPP3	0.45	90	0.3
iPP3	1.14	90	0.3
iPP3	4.24	60-90	0.3

5.2.2. Critical oxygen pressure

The dependence of the oxidation behavior with oxygen partial pressure can be materialized by the critical oxygen pressure Pc. This quantity has thus been tentatively determined, by using the analytical relationships reported in appendix B for all the relevant literature results between 40 and 160°C [12, 15, 69-72]. The resulting Arrhenius graph of the critical oxygen pressure has been plotted in Figure .

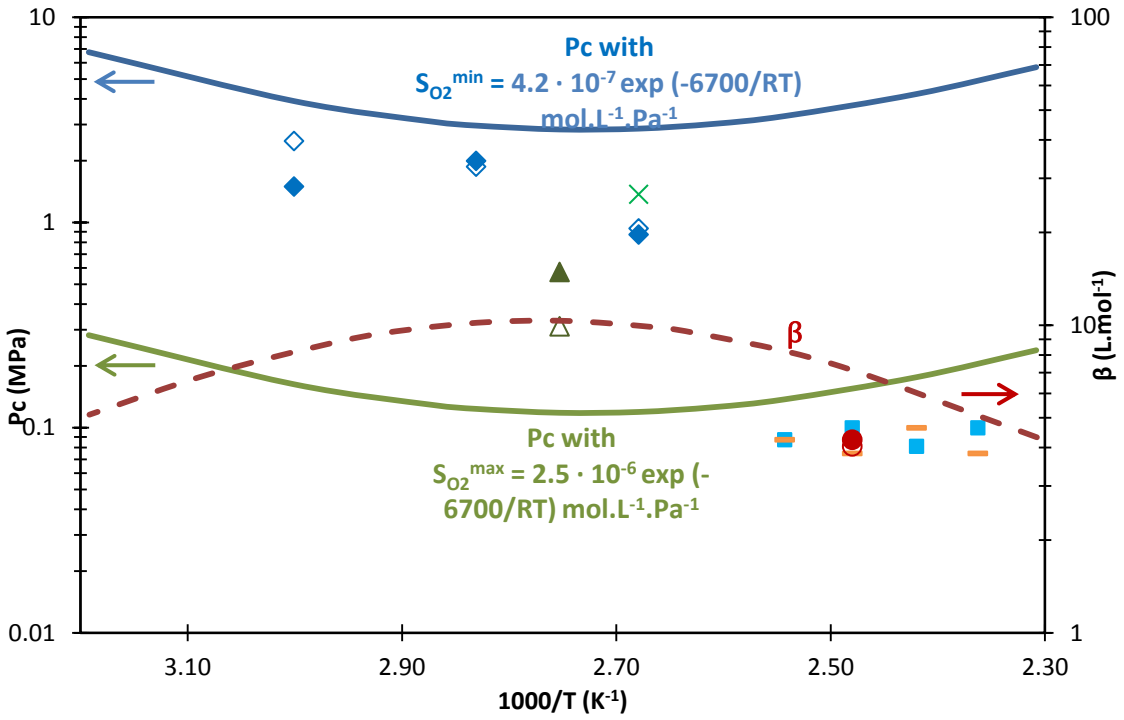

Figure 10: Arrhenius graph of the critical oxygen pressure Pc for boundary values of solubility (solid lines) and coefficient of oxygen pressure dependence β (dotted line) for iPP between 40°C and 160°C. Filled and open symbols apply to the experimental values of Pc determined from induction times and from oxidation rates respectively: ◇,◆ Richaud [3]. △,▲ Faulkner [12]. ●, ○ Bogayevskaya [15]. ■ Miller [20]. ▬ Reich [73]. × Vink [72].

First of all, the width of the cluster of Pc values is quite well described by the assumed variability of oxygen solubility. Surprisingly, the theoretical plots show some extrema instead of the expected straight-lines for an Arrhenian behavior. Actually, this singular behavior results from the detail of step (6), considering that peroxy macroradicals can escape from the cage, whose behavior is not Arrhenian anymore. The activation energy of the critical oxygen pressure can be written from equation 17 as:

$$Ea_{P_c} \approx Ea_2 + Ea_s + Ea_6^{app} - Ea_3 - Ea_5 \quad \textbf{Eq. 21}$$

When calculating the activation energy of Ea_6^{app} according to equation 11, values range from 30 to 75 kJ.mol^{-1}. Therefore, Ea_{Pc} varies between -16 and 29 kJ.mol^{-1} in the temperature range under study. This kind of graph could constitute a good way to check the existence of the cage reaction.

However, it is difficult to conclude on the Arrhenius character of the critical oxygen pressure because of the wide data scattering, which is presumably due to questionable methods of treatment for experimental results, in particular:

(i) The use of analytical relationships instead of numerical simulation to determine Pc,

(ii) The mode of calculation of the oxidation criteria which can induce errors when based on carbonyl index [3, 12] or mechanical properties [72] instead of oxygen uptake experiments,

(iii) The use of data sometimes measured at oxygen partial pressures noticeably lower than Pc, thus requiring risky extrapolation to determine Pc. Similarly, these aspects, and particularly the latter, could partly explain that no significant differences in critical oxygen pressure are observed between the various iPPs studied by Bogayevskaya et al. [15], despite their very different morphological features.

5.2.3. Consequences of the variability of S_{O2} on the iPP oxidation behavior

The variation of S_{O2} now enables to simulate the whole range of induction times compiled from the literature under 0.1 MPa [6, 12, 14, 17, 20, 33, 34, 43, 58, 60, 65, 74-98] and 0.02 MPa [11-20, 99-110], except the lowest values attributed to polypropylenes which are atactic, pre-oxidized or with a high metal content. The slope of the Arrhenius graph, i.e. the activation energy predicted by the model, is slightly lower than that given by the global trend of compiled data, but was optimized on the reference polypropylene (iPP1).

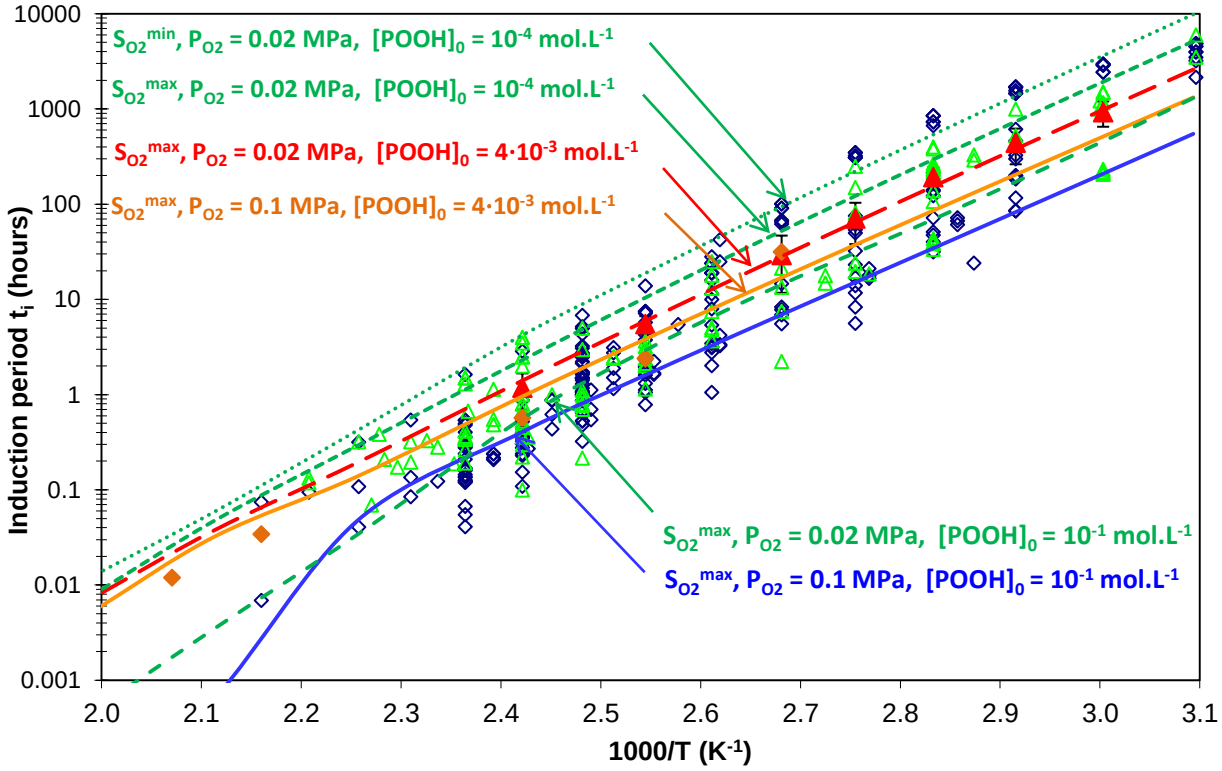

Figure 11: Arrhenius graph of oxidation induction time of iPP between 40 and 200°C. Symbols: Experimental data from several techniques (oxygen uptake, carbonyl index, microcalorimetry, thermogravimetry or chemiluminescence) under 0.1 (◇) and 0.02 MPa (△) compiled from the literature. Solid and dashed lines apply to simulations made with the indicated values of S_{O2}, P_{O2} and $[POOH]_0$ under 0.1 and 0.02 MPa respectively. The results for iPP1 are depicted in orange and red respectively.

Similarly, the variability of the oxygen solubility enables to simulate a larger cluster of maximal oxidation rates among the compilation of literature data [6, 16, 43, 58, 60, 74, 87-90, 92, 111-113] than the effect of the crystallinity ratio alone (see Figure). Moreover, the highest value of solubility, more consistent with the compilation of iPP data than the previous one, does not allow to simulate the upper range of this compilation, particularly above 110°C. This can be related to the additional oxygen consumption through secondary reactions due on the higher reactivity of labile hydrogens from secondary alcohols and ketones compared to methyne sites, as suggested by Mayo. These reactions have not been considered in the kinetic model, thus leading to a slight underestimation of the maximal oxidation rate [34].

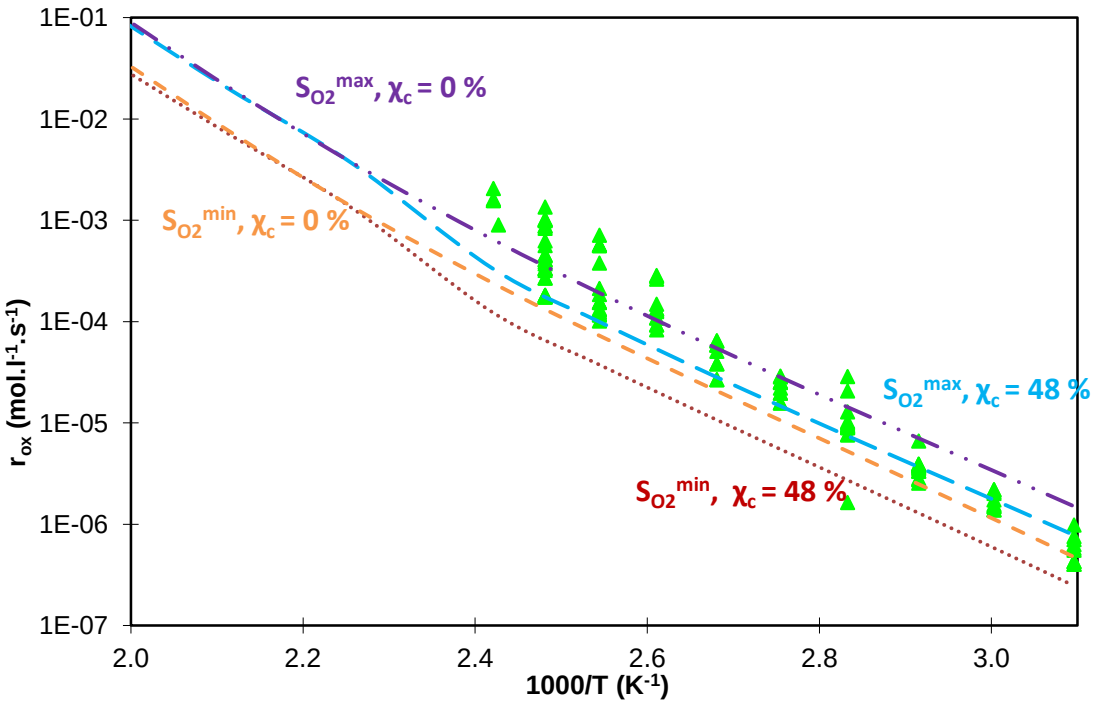

Figure 12: Arrhenius graph of the maximal oxidation rate of iPP between 40 and 230°C under 0.1 MPa. Symbols: Experimental data from oxygen uptake compiled from the literature. Solid lines: simulations made with the indicated values of S_{O2} and χ_c.

The introduction of variability on the oxygen solubility can be connected with the effect of morphology on the sensitivity to oxidation. Indeed, the induction period was reported to decrease with increasing density and crystallinity ratio [114, 115], crystallites size [15] or annealing temperature [89] as reviewed by Vink [116]. These results, somewhat conflicting in a first approach, could be the consequence of the existence of different iPP crystalline structures. Indeed, iPP crystals can exist in monoclinic (α), hexagonal/trigonal (β), orthorhombic (γ) or smectic/mesomorphic (δ) lattices (see review [117] for further details). The smectic lattice would be promoted by quenching and characterized by lower crystallinity ratios and smallest spherulithes. In contrast, the more stable (in terms of physical aging) α-monoclinic crystal lattice would be favored by annealing (especially above 90°C) and a low cooling rate, and would be associated to higher crystallinity ratios and coarsest spherulithes. Actually, the former α-monoclinic lattice would oxidize faster than the β-hexagonal or δ-smectic lattices as found by Vieth and Wurth [118] and confirmed in other studies [119-121]. In contrast, Kato, Carlsson and Wiles [122] observed no correlation between the iPP stability to oxidation and its morphology, and ascribed the discrepancy of stability to differences of molecular order, i.e. tacticity. This assertion was supported by various authors [123, 124].

However, it is now well-established that these structural and morphological features are closely intertwined since high isotacticity index would favor crystallization.

6. Conclusion

This work deals with the interrelationship between the oxygen transport properties and rate constants for modeling the iPP thermal oxidation. The resulting general kinetic model was thus calibrated on a reference material (iPP1) and was capable of simulating the concentration changes in primary (e.g. hydroperoxides) and secondary oxidation products such as carbonyl species, but also the changes in molecular masses for different iPPs.

The variability of oxygen solubility was shown to be critical in order to describe the polypropylene thermal oxidation kinetics. Indeed, the current adjustable parameter, namely the initial concentration in hydroperoxides $[POOH]_0$, was unable to report the scattering of iPP oxidation induction times, particularly in oxygen default. In contrast, the introduction of a variability on the oxygen solubility enables to explain the discrepancies of oxygen partial pressure dependences between the three different iPPs under study, as well for induction period as for oxidation rate. The meaning of this latter variability constitutes a key issue. Indeed, it can be attributed to:

(i) Either morphological differences in terms of lamellar structures. In this case, the variability of the oxygen solubility enables to introduce into the kinetic model the impact of the polymer morphology on the chemistry of oxidation. This option has been considered by default since the variability has been checked to be roughly compatible with the experimental data scattering despite the noticeable uncertainty of measurements.

(ii) Or structural features, in particular the average length of isotactic sequences, which would impact the local reactivity of oxygen with iPP. In this case, the oxygen solubility appears as an apparent and so, an adjustable parameter.

To discriminate between both options, it would be necessary to investigate the coupling between the physical/morphological and chemical agings. In this perspective, it could be relevant to perform specific analyses such as real-time SAXS and WAXS measurements along the course of oxidation. The challenge would thus be to propose, in a near future, structure/solubility relationships to reduce the number of remaining empirical steps in the kinetic model.

7. Appendices

7.1. Model equations, numerical computation and resolution

A System of Differential Equations (SDE) can be derived from the Closed-Loop Mechanistic Scheme (CLMS) for polypropylene thermal oxidation. However, in the case of relatively thick samples (typically few millimeters thick), oxidation is restricted to superficial layers: indeed, oxygen is the reactant in default in the core of the sample because its diffusion is much slower than its chemical consumption by the chemical reaction. It is thus necessary to introduce the second Fick's law in the SDE to take into account this oxidation control by oxygen diffusion (Equations A.1-A.6).

$$\frac{d[P^\bullet]}{dt} = 2k_{1u}[POOH] + k_{1b}[POOH]^2 - k_2[P^\bullet][O_2] + k_3[PO_2^\bullet][PH] - 2k_4[P^\bullet]^2 - k_5[P^\bullet][PO_2^\bullet] + 2k_{6d}[PO^{\bullet\bullet}OP] \quad \textbf{Eq. A.1}$$

$$\frac{d[PO_2^\bullet]}{dt} = k_{1b}[POOH]^2 + k_2[P^\bullet][O_2] - k_3[PO_2^\bullet][PH] - k_5[P^\bullet][PO_2^\bullet] - 2k_{6a}[PO_2^\bullet]^2 \quad \textbf{Eq. A.2}$$

$$\frac{d[POOH]}{dt} = -k_{1u}[POOH] - 2k_{1b}[POOH]^2 + k_3[PO_2^\bullet][PH] + (1 - \gamma_5)k_5[P^\bullet][PO_2^\bullet] \quad \textbf{Eq. A.3}$$

$$\frac{d[PH]}{dt} = -2k_{1u}[POOH] - k_{1b}[POOH]^2 - k_3[PO_2^\bullet][PH] + (1 - \gamma_4)k_4[P^\bullet]^2 - 2k_{6d}[PO^{\bullet\bullet}OP] \quad \textbf{Eq. A.4}$$

$$\frac{d[PO^{\bullet\bullet}OP]}{dt} = k_{6a}[PO_2^\bullet]^2 - (k_{6b} + k_{6d})[PO^{\bullet\bullet}OP] \quad \textbf{Eq. A.5}$$

$$\partial[O_2]/\partial t = D_{O_2}\,\partial^2[O_2]/\partial z^2 - k_2[P^\bullet][O_2] + k_{6a}[PO_2^\bullet]^2 \quad \textbf{Eq. A.6}$$

where [$P^\bullet$], [$PO_2^\bullet$], [POOH], [PH], [$PO^{\bullet\bullet}$ OP] and [O_2] are the respective concentrations of alkyl and peroxy radicals, hydroperoxides, tertiary CH groups, cage paired alkoxy radicals and oxygen, which are defined at each time t and depth z. D_{O2} is the coefficient of oxygen diffusion in the polymer, here considered as constant and concentration independent.

The SDE admits the following initial conditions:

$\forall z, \quad t = 0,$

$[P^{\bullet}]\ (0, z) = [PO_2^{\bullet}]\ (0, z) = [PO^{\bullet}\ {}^{\bullet}OP]\ (0, z) = 0\ mol.L^{-1}$ **Eq. A.7**

$[PH]\ (0, z) = [PH]_0 \approx 20.3\ mol.l^{-1}$ *(concentration of tertiary CH groups)* **Eq. A.8**

$$[POOH]\ (0, z) = [POOH]_0 = 10^{-5}–10^{-1}\ mol.L^{-1} \quad \textbf{Eq. A.9}$$

$$and\ [O_2]\ (0, z) = Cs \quad \textbf{Eq. A.10}$$

The boundary conditions at the sample edges (z = 0 and L) are:

$$\forall\, t > 0, \quad [O_2](t, 0) = [O_2](t, L) = C_s \quad \textbf{Eq. A.11}$$

where C_s is the oxygen concentration for a material in equilibrium with the atmosphere under a given oxygen partial pressure P_{O2}. This quantity is assumed to obey the Henry's law:

$$C_s = P_{O_2} \times S_{O_2}{}^{am} \quad \textbf{Eq. A.12}$$

where P_{O2} is the oxygen partial pressure in the atmosphere and $S_{O2}{}^{am}$ is the coefficient of oxygen solubility in the amorphous phase of the polymer.

It means that the sample has reached its equilibrium oxygen concentration C_s elsewhere before starting thermal oxidation. On the contrary, at the transitory state, only the superficial layer is in equilibrium with the surrounding atmosphere, which suggests an immediate dissolution of oxygen in the polymer.

The simultaneous solving of equations A.1 to A.6 in space (z) and time (t) with initial and boundary conditions (equations A.7 to A.12) enables to calculate the local concentration changes in chemical species directly involved in the CLMS, whatever the distance z from the sample surface. The SDE was solved numerically using the ODE15s or ODE23s MATLAB algorithms, which are the recommended semi-implicit methods for stiff problems of chemical kinetics [125]. Yet, it is noteworthy that the SDE only describes phenomena occurring in the amorphous phase where oxygen is dissolved. Therefore, the parameters relative to the local chemistry, such as oxygen consumption and solubility, must be defined in the amorphous phase. On the contrary, parameters describing physical phenomena, such as the oxygen diffusivity, are relative to the whole semi-crystalline polymer. Since oxygen is not soluble in the crystalline phase [43], the real concentrations for all chemical species have been deduced

from their concentrations calculated in the amorphous phase by multiplying them by the volumic fraction of amorphous phase V_a:

$$V_a = (1 - \chi_c) \times \frac{\rho_{tot}}{\rho_{am}} \quad \textbf{Eq. A.13}$$

with χ_c the crystallinity ratio, ρ_{am} the density of the amorphous phase (0.85 g.cm^{-3}) and ρ_{tot} the density of the semi-crystalline polymer (0.91 g.cm^{-3}).

At the molten state, the crystallinity ratio is fixed at 0, considering that the liquid state is equivalent to an amorphous phase. Clearly, the kinetic modeling of the thermal oxidation of the semi-crystalline polymer at the solid state is based on a homogenization approach at the micron scale.

In order to compare with experimental data, such as FTIR aging monitoring, average concentrations and global properties throughout the whole sample thickness were calculated by summing the local values calculated in the N-1 computational elementary sublayers:

$$Y_{global}(t) = \frac{1}{N-1} \int_{z=0}^{z=N} Y(z,t)dz \quad \textbf{Eq. A.14}$$

7.2. Analytical relationships for describing the oxygen pressure dependence of oxidation behavior

In previous papers [126], analytical expressions of oxidation rate and oxidation induction times have been derived from the CLMS and the steady state assumption in order to describe the oxygen partial pressure dependence of both physico-chemical quantities. Their respective expressions are reminded just below:

$$\frac{r_{ox}}{r_s} = 2\left(\frac{\beta[O_2]}{1+\beta[O_2]}\right)\left(1 - \frac{1}{2}\left(\frac{\beta[O_2]}{1+\beta[O_2]}\right)\right) \quad \textbf{Eq. B.1}$$

And

$$\frac{OIT}{OIT_s} = \left(1 + \frac{1}{\beta[O_2]}\right)^{1/2} \quad \textbf{Eq. B.2}$$

where r_s and OIT_s are their respective values in oxygen excess (i.e. close to oxygen saturation):

$$r_s = \frac{k_3^2[PH]^2}{4\,k_6} \qquad \textbf{Eq. B.3}$$

And

$$OIT_s = \frac{1+\psi}{k_3[PH]\left(\frac{k_1}{k_6}\right)^{1/2}} \qquad \textbf{Eq. B.4}$$

One can plot the curve of both quantities in reduced coordinates:

$r_{ox}/r_s = f(\beta[O_2])$ (Fig. B1) and $OIT/OIT_s = f(\beta[O_2])$ (Fig. B2)

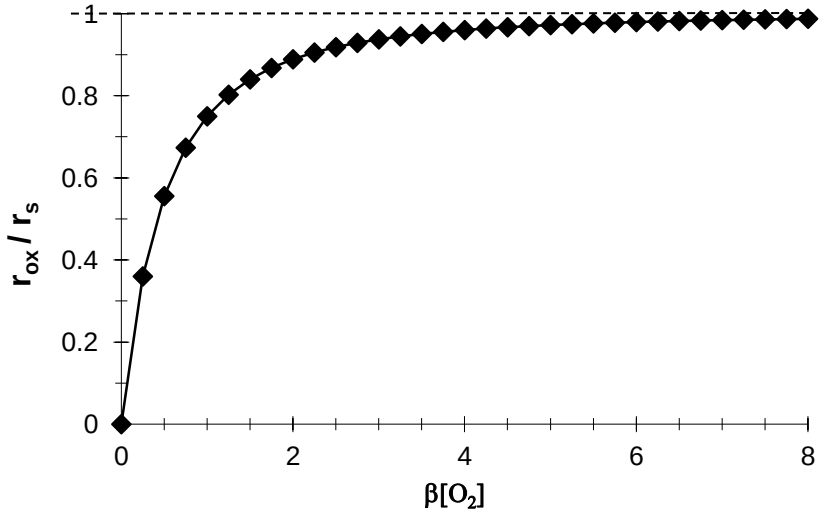

Figure B1: Oxidation rate versus oxygen partial pressure ($\beta[O_2]$ is dimensionless).

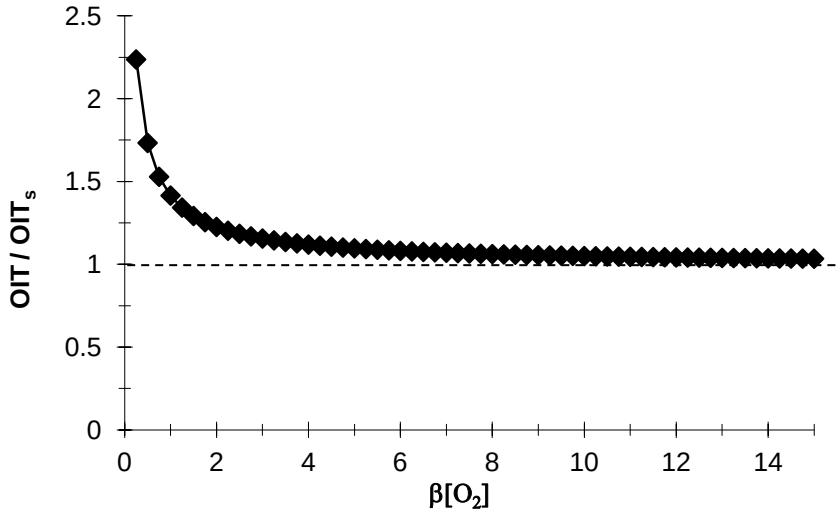

Figure B2: Oxidation induction time versus oxygen partial pressure ($\beta[O_2]$ is dimensionless)

It is clear that both oxidation indicators have clearly different dependences with the oxygen partial pressure. This appendix is thereby dedicated to the the determination of the critical oxygen pressure, delimitating “oxygen excess” from “oxygen default” regimes. Oxygen is considered in excess when its concentration reaches a saturation value in the polymer within an arbitrary tolerance or threshold, i.e. when $[O_2] \geq [O_2]_c$ with:

$$[O_2]_c = {K}/{\beta} = K \cdot {k_3\, k_5\, [PH]}/{k_2\, k_6} \qquad \textbf{Eq. B.5}$$

In terms of oxygen partial pressure, oxygen excess conditions will be considered as fulfilled when $P_{O2} \geq Pc$, with:

$$Pc = {[O_2]_c}/{S_{O_2}} = K \cdot {k_3\, k_5\, [PH]}/{k_2\, k_6\, S_{O_2}} \qquad \textbf{Eq. B.6}$$

From a practical point of view, it appears that K is an arbitrary criterion depending on the oxidation indicator under consideration (r_{ox} or OIT).
For instance, by choosing a tolerance of 5% for both quantities (which is meaningless), it implies that:

$\beta[O_2] \geq 3.5$ for r_{ox} and $\beta[O_2] \geq 10$ for OIT

i.e. K=3.5 for r_{ox} and K=10 for OIT

These considerations highlight the difficulties encountered for determining Pc from r_{ox} and OIT measurements in a wide range of oxygen partial pressure, being given the numerous sources of experimental errors. Thus, the choice of the value K will be decisive. A more accurate mathematical definition of this parameter is proposed below by using two thresholds:

$$K = \left(\frac{1}{1-\sqrt{1-\kappa}} - 1\right)^{-1} \text{ with } \kappa = r_{ox}/r_s \qquad \textbf{Eq. B.7}$$

and

$$K = (\tau^2 - 1)^{-1} \qquad \text{with } \tau = OIT/OIT_s \qquad \textbf{Eq. B.8}$$

From these equations, the values of K have been determined for both oxidation indicators in table 6. It is noteworthy that values of Pc depicted in figure 10 have been determined with κ = 0.8 and τ = 1.34, both resulting in K = 1.24.

Table 1: Correspondence between coefficient K and tolerance thresholds for induction time (κ) and oxidation rate (τ)

κ	**τ**	**K**
0.7	1.49	0.83
0.75	1.41	1.00
0.8	1.34	1.24
0.85	1.28	1.58
0.9	1.21	2.16
0.91	1.20	2.33
0.92	1.18	2.54
0.93	1.17	2.78
0.94	1.15	3.08
0.95	1.13	3.47
0.96	1.12	4.00
0.97	1.10	4.77
0.98	1.08	6.07
0.99	1.05	9.00

References

[1] L. Audouin, V. Gueguen, A. Tcharkhtchi, J. Verdu, “Closed loop” mechanistic schemes for hydrocarbon polymer oxidation, Journal of Polymer Science Part A: Polymer Chemistry, 33 (1995) 921-927.
[2] R.L.M. Rincon, B. Fayolle, L. Audouin, J. Verdu, A general solution of the closed-loop kinetic scheme for the thermal oxidation of polypropylene, Polymer Degradation and Stability, 74 (2001) 177–188.
[3] E. Richaud, F. Farcas, P. Bartoloméo, B. Fayolle, L. Audouin, J. Verdu, Effect of oxygen pressure on the oxidation kinetics of unstabilised polypropylene, Polymer Degradation and Stability, 91 (2006) 398-405.
[4] S. Sarrabi, X. Colin, A. Tcharkhtchi, Kinetic modeling of polypropylene thermal oxidation during its processing by rotational molding, Journal of Applied Polymer Science, 118 (2010) 980-996.
[5] X. Colin, L. Audouin, J. Verdu, Determination of thermal oxidation rate constants by an inverse method. Application to polyethylene, Polymer Degradation and Stability, 86 (2004) 309-321.
[6] P. Gijsman, J. Hennekens, J. Vincent, The influence of temperature and catalyst residues on the degradation of unstabilized polypropylene, Polymer Degradation and Stability, 39 (1993) 271-277.
[7] D.J. Carlsson, D.M. Wiles, The Photooxidative Degradation of Polypropylene. Part I. Photooxidation and Photoinitiation Processes, Journal of Macromolecular Science, Part C, 14 (1976) 65-106.
[8] L. Audouin, L. Achimsky, J. Verdu, Kinetic modelling of low-temperature oxidation of hydrocarbon polymers., in: e. Hamid SH (Ed.) Handbook of polymer degradation. 2nd ed, Marcel Dekker, New York, 2000, pp. 734.
[9] X. Colin, B. Fayolle, L. Audouin, J. Verdu, About a quasi-universal character of unstabilised polyethylene thermal oxidation kinetics, Polymer Degradation and Stability, 80 (2003) 67-74.
[10] E. Richaud, X. Colin, B. Fayolle, L. Audouin, J. Verdu, Induction period in the low-temperature thermal oxidation of saturated hydrocarbons: Example of polyethylene, International Journal of Chemical Kinetics, 40 (2008) 769-777.
[11] L. Achimsky, L. Audouin, J. Verdu, J. Rychly, L. Matisova-Rychla, On a transition at 80 °C in polypropylene oxidation kinetics, Polymer Degradation and Stability, 58 (1997) 283-289.
[12] D.L. Faulkner, Effects of high oxygen pressure and temperature on the aging of polypropylene, Polymer Engineering and Science, 22 (1982) 466-471.
[13] B. Fayolle, Fragilisation du polypropylène induite par fragilisation [In French], in: Mécanique et Matériaux, Ecole Nationale Supérieure des Arts et Métiers, Paris, 2001.
[14] N.C. Billingham, B.D. C., A.S. Manke, Developments in Polymer Degradation, Applied Science, London, 1981.
[15] T.A. Bogayevskaya, B.A. Gromov, V.B. Miller, T.V. Monakhova, Y.A. Shlyapnikov, Effect of the supermolecular structure of polypropylene on its oxidation kinetics, Polymer Science U.S.S.R., 14 (1972) 1741-1746.
[16] C.R. Boss, J.C.W. Chien, Oxygen diffusion limitation in autoxidation of polypropylene, Journal of Polymer Science Part A-1: Polymer Chemistry, 4 (1966) 1543-1551.
[17] D. Forsstrom, M. Hamskog, P. Eriksson, B. Terselius, Oxidation of unstabilised polypropylene particles as studied by microcalorimetry and chemiluminescence techniques, Polymer Degradation and Stability, 81 (2003) 81-88.
[18] F. Gugumus, Thermooxidative degradation of polyolefins in the solid state. Part 2: Homogeneous and heterogeneous aspects of thermal oxidation, Polymer Degradation and Stability, 52 (1996) 145-157.
[19] F. Gugumus, Thermooxidative degradation of polyolefins in the solid state - 7. Effect of sample thickness and heterogeneous oxidation kinetics for polypropylene, Polymer Degradation and Stability, 62 (1998) 245-257.
[20] F.A. Miller, M.B. Neiman, Y.A. Shlyapnikov, Vysokomolekul. Soedin, 1 (1959) 1703.
[21] D.J. Carlsson, R. Brousseau, D.M. Wiles, Reactions of sulfur dioxide with oxidized polyolefins, Polymer Degradation and Stability, 15 (1986) 67-79.

[22] D.J. Carlsson, J. Lacoste, A critical comparison of methods for hydroperoxide measurement in oxidized polyolefins, Polymer Degradation and Stability, 32 (1991) 377-386.
[23] J.M. Evans, Gel permeation chromatography: A guide to data interpretation, Polymer Engineering & Science, 13 (1973) 401-408.
[24] W.W. Yau, J.J. Kirkland, D.D. Bly, Modern Size-Exclusion Liquid Chromatography: Practice of Gel Permeation and Gel Filtration Chromatography, 2nd Edition, John Wiley and Sons, 1979.
[25] S. Mori, H.G. Barth, Size Exclusion Chromatography, Springer, 1999.
[26] S.W. Rutherford, D.D. Do, Review of time lag permeation technique as a method for characterisation of porous media and membranes, Adsorption, 3 (1997) 283-312.
[27] J.L. Bolland, Kinetic Studies in the Chemistry of Rubber and Related Materials. I. The Thermal Oxidation of Ethyl Linoleate, Proceedings of the Royal Society of London. Series A. Mathematical and Physical Sciences, 186 (1946) 218-236.
[28] J.L. Bolland, G. Gee, Kinetic studies in the chemistry of rubber and related materials. II. The kinetics of oxidation of unconjugated olefins, Transactions of the Faraday Society, 42 (1946) 236-243.
[29] J.L. Bolland, G. Gee, Kinetic studies in the chemistry of rubber and related materials. III. Thermochemistry and mechanisms of olefin oxidation, Transactions of the Faraday Society, 42 (1946) 244-252.
[30] A.V. Tobolsky, D.J. Metz, R.B. Mesrobian, Low temperature autoxidation of hydrocarbons: The phenomenon of maximum rates, Journal of the American Chemical Society, 72 (1950) 1942-1952.
[31] A.V. Tobolsky, P.M. Norling, N.H. Frick, H. Yu, On the mechanism of autoxidation of three vinyl polymers: Polypropylene, ethylene-propylene rubber, and poly (ethyl acrylate), Journal of the American Chemical Society, 86 (1964) 3925-3930.
[32] A. Somersall, C., J. Guillet, E., Computer Modeling Studies of Polymer Photooxidation and Stabilization, in: Polymer Stabilization and Degradation, American Chemical Society, 1985, pp. 211-234.
[33] S. Sarrabi, X. Colin, A. Tcharkhtchi, Isothermal Oxidation Kinetics of Unstabilized Polypropylene in the Molten State, Journal of Applied Polymer Science, 110 (2008) 2030–2040.
[34] L. Reich, S.S. Stivala, Kinetics and mechanism of oxidative degradation of polymers, in: McGraw-Hill (Ed.) Elements of polymer degradation 1971, pp. 229-293.
[35] N. Khelidj, X. Colin, L. Audouin, J. Verdu, C. Monchy-Leroy, V. Prunier, Oxidation of polyethylene under irradiation at low temperature and low dose rate. Part II. Low temperature thermal oxidation, Polymer Degradation and Stability, 91 (2006) 1598-1605.
[36] A. François-Heude, E. Richaud, J. Leprovost, M. Heninger, H. Mestdagh, E. Desnoux, X. Colin, Real-time quantitative analysis of volatile products generated during solid-state polypropylene thermal oxidation, Polymer Testing, 32 (2013) 907-917.
[37] O. Saito, On the Effect of High Energy Radiation to Polymers I. Cross-linking and Degradation., Journal of the Physical Society of Japan, 13 (1958) 198-206.
[38] T. Kelen, M. Iring, Tüdo, F. s, Study of the thermal oxidation of polyolefins--III: Pressure and temperature dependence of the rate of oxygen absorption, European Polymer Journal, 12 (1976) 35-39.
[39] S. Korcek, J.H.B. Chenier, Howard J.A., I. K.U., Absolute rate constants for hydrocarbon auto-oxidation- Activation energies for propagation and the correlation of propagation rate constants, Canadian Journal of Chemistry, (1972) 2285-2297.
[40] K.T. Gillen, J. Wise, R.L. Clough, General solution for the basic autoxidation scheme, Polymer Degradation and Stability, 47 (1995) 149-161.
[41] X. Colin, E. Richaud, J. Verdu, C. Monchy-Leroy, Kinetic modelling of radiochemical ageing of ethylene-propylene copolymers, in: I.R.a. Polymers (Ed.) Proceedings of the 8th International Symposium on Ionizing Radiation and Polymers, Elsevier, Angra dos Reis, Rio de Janeiro, Brazil, 12-17 October 2008, 2008, pp. 6.
[42] E. Richaud, F. Farcas, B. Fayolle, L. Audouin, J. Verdu, Hydroperoxide build-up in the thermal oxidation of polypropylene - A kinetic study, Polymer Degradation and Stability, 92 (2007) 118-124.
[43] J.B. Knight, P.D. Calvert, N.C. Billingham, Localization of oxidation in polypropylene, Polymer, 26 (1985) 1713-1718.
[44] P.L. Beltrame, C. Citterio, G. Testa, A. Seves, Oxygen permeation through films of compatibilized polypropylene/polyamide 6 blends, Journal of Applied Polymer Science, 74 (1999) 1941-1949.

[45] E.T. Denisov, I.B. Afanas'ev, Oxidation and Antioxidants in Organic Chemistry and Biochemistry. , Taylor and Francis 2006.
[46] S.G. Kiryushkin, Dissertation, Institute Chemical Physics, Moscow,, (1975).
[47] M. Kurek, D. Klepac, M. Ščetar, K. Galić, S.k. Valić, Y. Liu, W. Yang, Gas barrier and morphology characteristics of linear low-density polyethylene and two different polypropylene films, Polymer Bulletin, 67 (2011) 1293-1309.
[48] Y.J. Lin, P. Dias, H.Y. Chen, S. Chum, A. Hiltner, E. Baer, Oxygen permeability of biaxially oriented polypropylene films, Polymer Engineering & Science, 48 (2008) 642-648.
[49] Y.J. Lin, P. Dias, H.Y. Chen, A. Hiltner, E. Baer, Relationship between biaxial orientation and oxygen permeability of polypropylene film, Polymer, 49 (2008) 2578-2586.
[50] L.S. Somlai, R.Y.F. Liu, L.M. Landoll, A. Hiltner, E. Baer, Effect of orientation on the free volume and oxygen transport of a polypropylene copolymer, Journal of Polymer Science Part B: Polymer Physics, 43 (2005) 1230-1243.
[51] P. Thorlaksen, J. Abildskov, G.M. Kontogeorgis, Fluid Phase Equilibria, 211 (2003) 17-33.
[52] J.P.G. Villaluenga, M. Khayet, M.A. Lopez-Manchado, J.L. Valentin, B. Seoane, J.I. Mengual, Gas transport properties of polypropylene/clay composite membranes, European Polymer Journal, 43 (2007) 1132-1143.
[53] V. Stannet, Diffusion in polymers, in: J.C.G.S. PARK (Ed.), Academic Press, New York, 1968, pp. 41.
[54] D.W. Van Krevelen, Properties of polymers, 1976.
[55] G.G. Gutiérrez, Oxydation des nanocomposites à matrice polyoléfinique in, Arts et metiers ParisTech, Paris, 2010.
[56] R. Mani, R.P. Singh, S. Sivaram, J. Lacoste, J. Lemaire, Effect of UV irradiation on gas permeability in heterophasic ethylene-propylene copolymer films, Journal of Macromolecular Science - Pure and Applied Chemistry, 33 (1996) 783-787.
[57] S.G. Kiryushkin, Y.A. Shlyapnikov, Diffusion-controlled polymer oxidation, Polymer Degradation and Stability, 23 (1989) 185-192.
[58] F. Tüdos, M. Iring, T. Kelen, Oxidation of Polyolefins, in: E.A.V. Patsis (Ed.) International conference on advances in the stabilization and controlled degradation of polymers, 1985.
[59] L. Achimsky, Etude cinétique de la thermooxydation du polypropylène, in: Mécanique et Matériaux, Université Pierre et Marie-Curie (Paris VI), Paris, 1996.
[60] M. Iring, S. László-Hedvig, F. Tüdos, T. Kelen, Study of the thermal oxidation of polyolefins--XII : Thermal oxidation of isotactic and atactic polypropylene in the condensed phase and in solution, Polymer Degradation and Stability, 5 (1983) 467-480.
[61] N.C. Billingham, Die Makromol. Chem., Macromol. Symp., 28 (1989) 145-163.
[62] F. Tüdős, M. Iring, Polyolefine oxidation: Rates and products, Acta Polymerica, 39 (1988) 19-26.
[63] B. Fayolle, L. Audouin, J. Verdu, A critical molar mass separating the ductile and brittle regimes as revealed by thermal oxidation in polypropylene, Polymer, 45 (2004) 4323-4330.
[64] Y. Kamiya, E. Niki, Oxidative degradation, in: e. Jellinek H (Ed.) Aspects of degradation and stabilization of polymers, Elsevier Science, New York, 1978, pp. 80.
[65] M. Celina, G.A. George, A heterogeneous model for the thermal oxidation of solid polypropylene from chemiluminescence analysis, Polymer Degradation and Stability, 40 (1993) 323-335.
[66] B.G.S. Goss, I. Blakey, M.D. Barry, G.A. George, Modelling of infectious spreading in heterogeneous polymer oxidation II. Refinement of stochastic model and calibration using chemiluminescence of polypropylene, Polymer Degradation and Stability, 74 (2001) 523-532.
[67] B.G.S. Goss, H. Nakatani, G.A. George, M. Terano, Catalyst residue effects on the heterogeneous oxidation of polypropylene, Polymer Degradation and Stability, 82 (2003) 119-126.
[68] S.S. Stivala, J. Kimura, S.M. Gabbay, Thermal degradation and oxidative processes, in: N.S. Allen (Ed.) Degradation and Stabilization of Polyolefins, Appl. Sci. Publ., London, 1983, pp. 63–185.
[69] V.B. Miller, M.B. Neiman, I.A. Shliapnikov, Thermal oxidative degradation of polyppropylene-II. The kinetics of the initial oxidation stage, Polymer Science U.S.S.R., 2 (1961) 129-132.
[70] L. Reich, S.S. Stivala, Autoxidation of hydrocarbons and polyolefins: kinetics and mechanisms, Marcel Dekker, Inc., New York, 1969.
[71] E. Richaud, Durabilité des géotextiles en polypropylène [PhD thesis], in: Mécanique et Matériaux, Arts et Métiers ParisTech, Paris, 2006.

[72] P. Vink, H.F.N. Fontijn, Testing the resistance to oxidation of polypropylene geotextiles at enhanced oxygen pressures, Geotextiles and Geomembranes, 18 (2000) 333-343.
[73] L. Reich, S.S. Stivala, Investigation of polyolefin oxidation by various techniques, in: M.D. Inc. (Ed.) Auto-oxidation of Hydrocarbons ans Polyolefins, Kinetics and Mechanisms, New-York, 1969, pp. 455-504.
[74] P. Gijsman, The Long-Term Stability of Polyolefins. Wibro Dissertatiedrukkerij, Helmond., in, Technische Universiteit Eindhoven 1994, pp. 176 p.
[75] D.M. Mowery, R.A. Assink, D.K. Derzon, S.B. Klamo, R.L. Clough, R. Bernstein, Solid-State 13C NMR Investigation of the Oxidative Degradation of Selectively Labeled Polypropylene by Thermal Aging and Î³-Irradiation, Macromolecules, 38 (2005) 5035-5046.
[76] H.J. Oswald, E. Turi, The deterioration of polypropylene by oxidative degradation, Polymer Engineering & Science, 5 (1965) 152-158.
[77] P. Richters, Initiation process in the oxidation of polypropylene, Macromolecules, 3 (1970) 262-264.
[78] J. Rychly, L. Matisova-Rychla, P. Tiemblo, J. Gomez-Elvira, The effect of physical parameters of isotactic polypropylene on its oxidisability measured by chemiluminescence method. Contribution to the spreading phenomenon, Polymer Degradation and Stability, 71 (2001) 253-260.
[79] G. Ahlblad, P. Gijsman, B.r. Terselius, A. Jansson, K. Möller, Thermo-oxidative stability of PP waste films studied by imaging chemiluminescence, Polymer Degradation and Stability, 73 (2001) 15-22.
[80] M. Celina, G.A. George, Heterogeneous and homogeneous kinetic analyses of the thermal oxidation of polypropylene, Polymer Degradation and Stability, 50 (1995) 89-99.
[81] P. Gijsman, F. Verdun, The influence of polymer type, stabilizers and sample geometry on the relationship between chemiluminescence and oxygen uptake, Polymer Degradation and Stability, 74 (2001) 533-542.
[82] L. Matisova-Rychla, J. Rychly, New approach to understanding chemiluminescence from the decomposition of peroxidic structures in polypropylene, Polymer Degradation and Stability, 67 (2000) 515-525.
[83] L. Matisova-Rychla, J. Rychly, J. Verdu, L. Audouin, K. Csomorova, Chemiluminescence and thermogravimetric study of thermal oxidation of polypropylene, Polymer Degradation and Stability, 49 (1995) 51-55.
[84] T. Schwarz, G. Steiner, J. Koppelmann, Diffusion of antioxidants in sheets and plates of isotactic polypropylene measured by isothermal differential-thermal-analysis, Journal of thermal analysis, 35 (1989) 481-496.
[85] L. Reich, B.R. Jadrnicek, S.S. Stivala, Effect of oxidation-reduction potential on the metal salt-catalyzed autoxidation of atactic polypropylene, Journal of Polymer Science Part A-1: Polymer Chemistry, 9 (1971) 231-233.
[86] M. Celina, G.A. George, N.C. Billingham, Physical spreading of oxidation in solid polypropylene as studied by chemiluminescence, Polymer Degradation and Stability, 42 (1993) 335-344.
[87] R.H. Hansen, C.A. Russell, T. De Benedictis, W.M. Martin, J.V. Pascale, Inhibition of the copper-catalyzed oxidation of polypropylene, Journal of Polymer Science Part A: General Papers, 2 (1964) 587-609.
[88] M. Iring, S. László-Hedvig, K. Barabás, T. Kelen, F. Tüdos, Study of the thermal oxidation of polyolefins--IX : Some differences in the oxidation of polyethylene and polypropylene, European Polymer Journal, 14 (1978) 439-442.
[89] N.Y. Rapoport, S.I. Berulava, A.L. Kovarskii, I.N. Musayelyan, Y.A. Yershov, V.B. Miller, The kinetics of thermo-oxidative degradation of oriented polypropylene in relation to the structure and molecular mobility of the polymer, Polymer Science U.S.S.R., 17 (1975) 2901-2909.
[90] N.Y. Rapoport, N.M. Livanova, V.B. Miller, On the influence of internal stress on the kinetics of oxidation of oriented polypropylene, Polymer Science U.S.S.R., 18 (1976) 2336-2341.
[91] L. Zlatkevich, Chemicluminescence apparatus and method for studying thermal oxidative stability of polymers Polymer Engineering and Science, 24 (1984) 1421-1428.
[92] T.H. Meltzer, J.J. Kelley, R.N. Goldey, Absorption of oxygen by supported films of polyethylene, Journal of Applied Polymer Science, 3 (1960) 84-89.

[93] L. Matisova-Rychla, J. Rychly, Inherent Relations of Chemiluminescence and Thermooxidation of Polymers, in: Polymer Durability, American Chemical Society, 1996, pp. 175-193.
[94] M. Celina, G.A. George, N.C. Billingham, Physical Spreading and Heterogeneity in Oxidation of Polypropylene, in: R.L. Clough, N.C. Billingham, K.T. Gillen (Eds.) Polymer Durability: Degradation, Stabilization, and Lifetime Prediction, American Chemical Society, 1996, pp. 159-174.
[95] G.A. George, M. Celina, Handbook of Polymer Degradation, in: M.D.I. S. Halim Hamid (Ed.) Handbook of Polymer Degradation, Second Edition, New-York, 2000, pp. 277.
[96] M. Kato, Z. Osawa, Effect of stereoregularity on the thermo-oxidative degradation of polypropylenes, Polymer Degradation and Stability, 65 (1999) 457-461.
[97] R. Setnescu, S. Jipa, Z. Osawa, Chemiluminescence study on the oxidation of several polyolefinsâ€"I. Thermal-induced degradation of additive-free polyolefins, Polymer Degradation and Stability, 60 (1998) 377-383.
[98] H. Bergenudd, P. Eriksson, C. DeArmitt, B. Stenberg, E. MalmstrÃ¶m Jonsson, Synthesis and evaluation of hyperbranched phenolic antioxidants of three different generations, Polymer Degradation and Stability, 76 (2002) 503-509.
[99] W.L. Hawkins, W. Matreyek, F.H. Winslow, The morphology of semicrystalline polymers. Part I. The effect of temperature on the oxidation of polyolefins, Journal of Polymer Science, 41 (1959) 1-11.
[100] P. Eriksson, B. Stenberg, T. Reitberger, D. ForsstrÃ¶m, The simultaneous detection of heat flow and chemiluminescence intensity during oxidation of unstabilised polypropylene particles, Polymer Testing, 22 (2003) 915-921.
[101] J. Lemaire, J.-L. Gardette, J. Lacoste, P. Delprat, D. Vaillant, Mechanisms of Photooxidation of Polyolefins: Prediction of Lifetime in Weathering Conditions, in: Polymer Durability, American Chemical Society, 1996, pp. 577-598.
[102] J.T. Henman, Characterisation of Oxidised Polyolefines by Reaction with Sulphur Dioxide, in: E. N. Grassie (Ed.) Developments in polymer degradation – 6, Elsevier Applied Science London, 1985, pp. 124.
[103] Z. Osawa, T. Shibamiya, K. Matsuzaki, Thermal Oxidative Degradation of Polypropylene and the Decomposition of tert-Butyl Hydroperoxide Catalysed by Metallic Salts of Fatty Acids, The Journal of the Society of Chemical Industry, Japan, 71 (1968) 552-556.
[104] G. Scott, M.F. Yusoff, Mechanisms of antioxidant action: autosynergistic antioxidants containing chain-breaking and peroxidolytic functions, European Polymer Journal, 16 (1980) 497-501.
[105] S. Al-Malaika, Mechanisms of antioxidant action and stabilisation technologyâ€"The Aston experience, Polymer Degradation and Stability, 34 (1991) 1-36.
[106] S. Al-Malaika, G. Scott, P. Huczkowski, Mechanisms of antioxidant action: Effect of benzophenone-substituted xanthates on the stability of polypropylene, Polymer Degradation and Stability, 7 (1984) 95-107.
[107] P. Tiemblo, J. Manuel GÃ³mez-Elvira, G. Teyssedre, F. Massines, C. Laurent, Chemiluminescence spectral evolution along the thermal oxidation of isotactic polypropylene, Polymer Degradation and Stability, 65 (1999) 113-121.
[108] L. Matisova-Rychla, J. Rychy, M. Vavrekova, Chemiluminescence in thermo-oxidation of polypropylene, European Polymer Journal, 14 (1978) 1033-1037.
[109] S. Jipa, R. Setnescu, T.a. Setnescu, T. Zaharescu, Efficiency assessment of additives in thermal degradation of i-PP by chemiluminescence I. Triazines, Polymer Degradation and Stability, 68 (2000) 159-164.
[110] N.C. Billingham, P.D. Calvert, chapter 5, in: G. Scott (Ed.) Developments in Polymer stabilisation - 3, Applied Science, London, 1980.
[111] Y.A. Mikheev, L.N. Guseva, G.E. Zaikov, Comments on structural-kinetic models of oxidation of polyolefins, Polymer Degradation and Stability, 63 (1999) 509-523.
[112] M. Iring, S. Laszlo-Hedvig, T. Kelen, F. Tudos, L. Fuzes, G. Gamey, G. Bodor, Journal of Polymer Science, 57 (1976) 55-63.
[113] N.Y. Rapoport, A.S. Goniashvili, M.S. Akutin, V.B. Miller, Vysokomol. Soed., 21A (1979) 2071.
[114] F.H. McTigue , M. Blumberg, Modern Plastics, 44 (1967) 145.
[115] P. Vink, Photooxidation of polypropylene Journal of Applied Polymer Science: Applied Polymer Symposium, 35 (1979) 265-273.

[116] P. Vink, The Photo-Oxidation of Polyolefins - Structural and Morphological Aspects, in: e.N.S. Allen (Ed.) Degradation and Stabilisation of Polyolefins, Applied Science Publishers, London, 1983, pp. 213-246.
[117] S. Brückner, S.V. Meille, V. Petraccone, B. Pirozzi, Polymorphism in isotactic polypropylene, Progress in Polymer Science, 16 (1991) 361-404.
[118] W. Vieth, W.F. Wuerth, Transport properties and their correlation with the morphology of thermally conditioned polypropylene, Journal of Applied Polymer Science, 13 (1969) 685-712.
[119] S. Nishimoto, T. Kagiya, Y. Watanabe, M. Kato, Material design of radiation resistant polypropylene: Part II-Importance of the smectic structure produced by quenching treatment, Polymer Degradation and Stability, 14 (1986) 199-208.
[120] M. Obadal, R. Cermak, M. Raab, V. Verney, S. Commereuc, F. Fraïsse, Structure evolution of α- and beta-polypropylenes upon UV irradiation: A multiscale comparison, Polymer Degradation and Stability, 88 (2005) 532-539.
[121] M. Obadal, R. Cermak, M. Raab, V. Verney, S. Commereuc, F. Fraïsse, Study on photodegradation of injection-moulded Î²-polypropylenes, Polymer Degradation and Stability, 91 (2006) 459-463.
[122] Y. Kato, D.J. Carlsson, D.M. Wiles, The photo-oxidation of polypropylene: Some effects of molecular order, Journal of Applied Polymer Science, 13 (1969) 1447-1458.
[123] H. Nakatani, S. Suzuki, T. Tanaka, M. Terano, New kinetic aspects on the mechanism of thermal oxidative degradation of polypropylenes with various tacticities, Polymer, 46 (2005) 12366-12371.
[124] S. Suzuki, Y. Nakamura, A.T.M.K. Hasan, B. Liu, M. Terano, H. Nakatani, Dependence of tacticity distribution in thermal oxidative degradation of polypropylene, Polymer Bulletin, 54 (2005) 311-319.
[125] E. Hairer, G. Wanner, Stiff and Differential-Algebraic Problems, 1996.
[126] J. Verdu, X. Colin, L. Audouin, J. Rychly, L. Matisova-Rychla, Chemiluminescence from the thermal oxidation of polyisoprene and polybutadiene I. Influence of oxygen pressure on the chemiluminescence of polyisoprene during its oxidation, Polymer Degradation and Stability, 91 (2006) 1387-1394.

CHAPTER V. On the impact of oxygen transport properties on the kinetic modeling of polypropylene thermal oxidation. Part II: effect of oxygen diffusivity

Alexandre François-Heude[a,b 3], Emmanuel Richaud[a], Alain Guinault[a], Eric Desnoux[b], Xavier Colin[a]

[a]PIMM Laboratory, CNRS UMR 8006, Arts et Metiers ParisTech, Paris, France

[b]Renault, DETC-A, Guyancourt, France

Abstract

The kinetic model, established in a previous paper [1] to predict the homogeneous oxidation in iPP films typically thinner than 100 µm, is now extended to simulate the oxidation profiles in thicker plates by coupling the oxygen diffusion and its consumption by the chemical reaction. In this perspective, oxygen transport properties (namely oxygen solubility, diffusivity and permeability) are measured by permeametry on a reference iPP. These values are compared with an exhaustive compilation of literature data in order to evaluate their variability among the whole iPP family, reasonably ascribed to initial differences in polymer morphology, but also their consistency, especially their temperature dependence between 20 and 140°C. Failing to simulate oxidation profiles, the kinetic model is then used as an inverse resolution method for estimating more satisfactory values of oxygen transport properties. It is thus evidenced that the crystallinity changes induced by thermal oxidation largely explains the dramatic decrease in oxygen penetration towards the sample core just after the induction period. A strategy for introducing the complex relationship between the polymer crystalline morphology and oxygen transport properties into the kinetic model is given in the graphical abstract, although the effect of polymer polarity remains to be established prior this implementation.

[3] Corresponding author : Email: Alexandre.FRANCOIS-HEUDE@ensam.eu
Tel/ Fax: +33 1 44 24 64 13/ +33 1 44 24 63 82

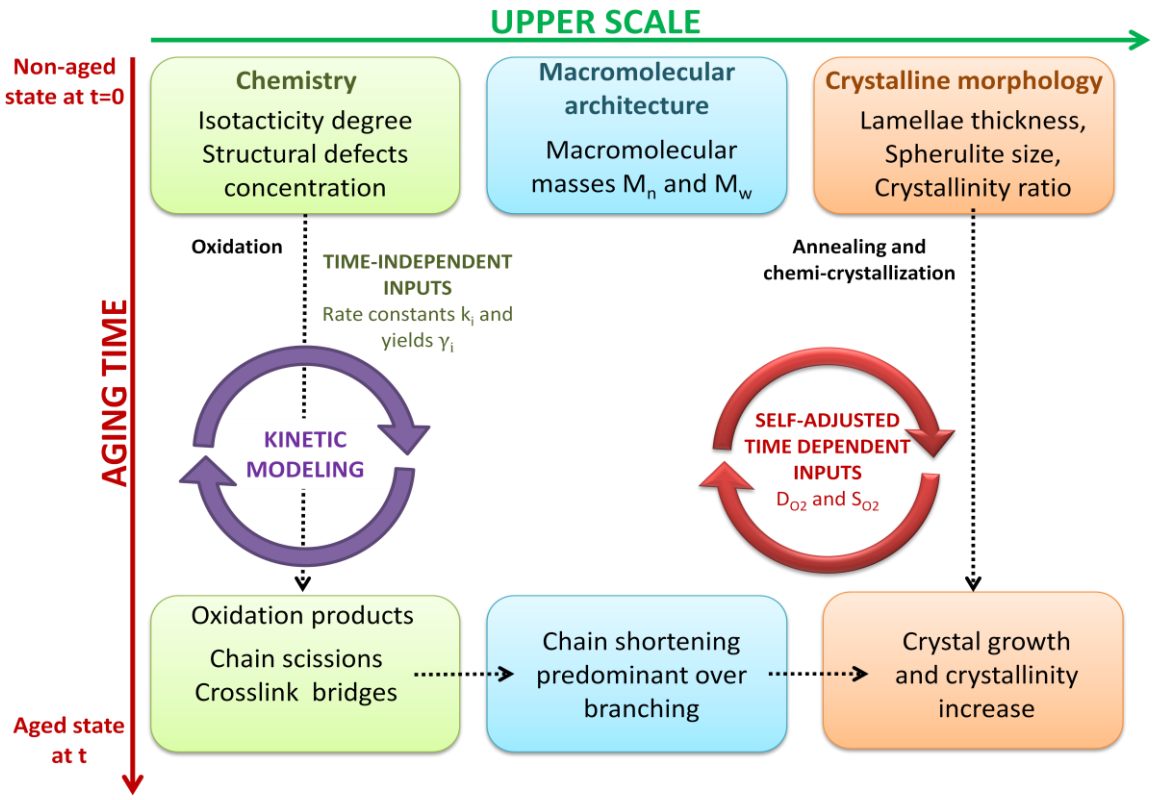

Graphical abstract: Strategy for kinetic modeling of thermal aging of semi-crystalline polymers. Influence of crystalline morphology on oxygen transport properties.

Keywords

Oxygen diffusivity and permeability; Crystalline morphology; Oxidation products profiles; Kinetic Modeling.

1. Introduction

It is well known that the oxidative degradation of thick polymer plates (typically few mm thick) is restricted to a superficial layer whose thickness impacts their mechanical properties (in particular their fracture properties) when it reaches a critical value [2] which is, for instance, of the order of one hundred of microns for polyethylene (see [3, 4]). Based on this observation, several authors have attempted to determine the thickness of oxidized layer (TOL) in polymers by using a large variety of analytical techniques, for instance: optical microscopy, FTIR spectrophotometry, nano-indentation, etc… The reader may consult reference [5] for an outstanding review on these techniques. The simplest method consists in determining the overall oxidation rate of polymer samples of different thicknesses in order to

deduce the critical thickness (L_c) above which oxidation gradients appear. Indeed, L_c is presumably equal to twice of TOL. At this time, many doubts exist on the real order of magnitude of TOL in isotactic polypropylene (iPP) for which values ranging from ten to hundred microns have been reported in the literature as well for thermal [6-12] as for photothermal aging [13] in air (see table 1).

Table 1: Thicknesses of oxidized layer reported in the literature for iPP thermal oxidation

Reference	**Exposure conditions**	**TOL = L_c / 2**
Boss et al. [11]	150°C	> 75 µm
Kiryushskin et al. [9]	130°C	20 µm
Guttierez et al. [8]	110°C	10 µm
Gugumus et al. [12]	80°C	60 µm
Fayolle et al. [6]	70C	20 µm

Oxidation products profiles result from the diffusion control of the oxidation kinetics. These profiles can be satisfactorily predicted as well by analytical [3, 4, 9, 11, 14, 15] as by numerical kinetic models [7] in which the Fick's second law (for oxygen diffusion) has been introduced into the balance equation governing the oxygen chemical consumption by the polymer. Assuming that the oxygen diffusivity (D_{O2}) is independent of the conversion degree of oxidation or time, this equation can be written:

$$\partial[O_2]/\partial t = D_{O_2}\,\partial^2[O_2]/\partial z^2 - r([O_2]) \qquad \textbf{Eq. 1}$$

with r([O_2]) the term accounting for the oxygen consumption by the polymer in an elementary sublayer at the depth z in the sample thickness

Oxygen diffusivity could thus appear as the relevant parameter governing the oxygen supply from the surface towards the specimen core. However, the realistic description of the oxygen consumption is a crucial step in the lifetime prediction approach: indeed, the better the description of oxidation reaction is, the more accurate the simulation of oxidation profiles will be. This connection between the shape of oxidation profiles and the local polymer reactivity in respect to oxygen was particularly highlighted by Boss and Chien [11] who evidenced a misleading attribution of the changes in the overall oxidation rate to the limiting effect of oxygen diffusion instead of the effect of oxygen partial pressure. This consideration can be illustrated by the interrelationship between the three oxygen transport properties, namely permeability Pe_{O2}, diffusivity D_{O2} and solubility S_{O2}, in the semi-crystalline polymer:

$$Pe_{O_2} = D_{O_2} \cdot S_{O_2} \quad \textbf{Eq. 2}$$

This is the reason why it was decided to study separately both phenomena (i.e. oxygen diffusion and chemical consumption), first by focusing on the polymer reactivity at the local scale, i.e. on homogeneously degraded iPP films [1]. This approach requires an accurate measurement of oxygen transport properties, from the transitory and steady-state regimes of permeation using the time-lag method, on a reference iPP. It is advisable to compare these values to an exhaustive compilation of literature data, as started with S_{O2} in the first part [1], and extended to D_{O2} and Pe_{O2} in this second part of this study. The main objective consists in apprehending the validity of the Arrhenius law for describing their temperature dependence, since these parameters are extrapolated to simulate the PP thermal oxidation at temperatures higher than for their measurement.

The introduction into the kinetic model of a variability on S_{O2} allowed to account for the large scattering of induction periods and oxidation rates, as well as for their oxygen pressure dependences, reported in the literature for the whole iPP family [1]. This variability wasfound to be in line with the scattering of S_{O2} values compiled from literature, which can be reasonably ascribed to differences in iPP morphology, i.e. in its ability to crystallize into different structures (polymorphism), or to the presence of stereo-defects distribution materialized by an average length of isotactic sequences. The issue is now to quantify the variability of D_{O2} over the whole iPP family, since it is well-known that this coefficient is also impacted by morphological differences, such as: crystallinity ratio; nature, size, shape and orientation of crystallites; and chain orientation in amorphous phase (i.e. segmental mobility of the constrained tie-molecules) [16]. The reader may consult reference [17] for an outstanding review. In addition, it was shown by permeametry that the oxygen transport properties change along the course of photothermal oxidation [18]. However, these experiments were performed at ambient temperature after thermal aging to prevent further oxidation during the permeability measurements themselves.

From this rapid literature survey, the questions that arise are: Can this variability on D_{O2} explain the scattering of iPP oxidation behaviors evidenced in the literature? Can these morphological differences explain the variability of TOL? The kinetic modeling approach is proposed here as an original tool to overcome the experimental difficulties in determining the oxygen transport properties of aged samples. Values of D_{O2} and S_{O2} will be determined by inverse resolution method in order to simulate the oxidation profiles of the reference iPP, but

also of other iPPs investigated in the literature. Then, it will be interesting to check in which extent the kinetic modeling approach remains valid and how can be integrated themorphological differences into the kinetic model.

2. Experimental part

2.1. Materials

The isotactic polypropylene under investigation was supplied by Aldrich (under the reference 427888). Its main physico-chemical characteristics are MFI [230°C, 2.16 kg] = 12 g/10min, M_w = 250 kg.mol^{-1}, M_n = 67 kg.mol^{-1} and PI = 3.7. IPP plates with a thickness of 2 mm were made by stacking of about 25 thin iPP films (with a thickness of 80 µm) in a Gibitre press during 2 min at 140°C under 20 MPa. These films were previously obtained by compression molding (during 1 min at 200°C under 20 MPa) and purified from their stabilizers (Soxhlet extraction for 48 hours using dichloromethane as solvent). Plates were transparent, without bubble, free of most of their additives and without any change in crystalline morphology. Despite a careful purification, the low residual concentration of stabilizers required a correction of the statistical bias in OIT.

2.2. Thermal aging and physico-chemical characterization

Plates were thermally aged between 60°C and 140°C in air-ventilated ovens regulated at ±1 °C. After aging, they were delaminated with a cutter and each elementary film was analyzed separately by FTIR spectrophotometry in transmission mode (Perkin-Elmer spectrophotometer, 16 scans, resolution of 4 cm^{-1}) basing on the carbonyl peak at 1713 cm^{-1} (ε = 300 L.mol^{-1}.cm^{-1}).

Differential scanning calorimetry (DSC) was performed on 10 mg sample weight with a TA Q1000 calorimeter under a nitrogen flow. A temperature ramp of 10°C.min^{-1} from 30 to 200°C was applied in order to minimize the annealing phenomena. Crystallinity ratios were calculated taking a melting enthalpy for crystalline lamellae of ΔH_m^0 = 209 J.g^{-1}. The initial crystallinity value was 45 ± 3 %wt.

No significant changes in crystallinity ratio were observed by DSC along the course of thermal oxidation, but increases up to 25% were observed by FTIR spectrophotometry on iPP samples of 80 µm thickness (see appendix A) basing on the following correlation [19], beforehand checked to give similar results than WAXS:

$$\chi_c(\%) = 109 * \left(\frac{A_{997}-A_{917}}{A_{973}-A_{917}}\right) - 31.4 \quad \textbf{Eq. 3}$$

where A_{997}, A_{973} and A_{917} are the respective optical densities at 997, 973 and 917 cm^{-1}.

2.3. Oxygen permeability tests

Oxygen permeability was performed with a Systech 8001 device on films of about 130 µm thick at 10, 23 and 45°C and 0 % of relative humidity. Their active surface area was equal to 50 cm^2. The time-lag method was chosen to measure oxygen transport properties (see for instance reference [20]). This analysis mode required a complete purge of the system (including detector, pipes and samples) under a pure nitrogen flow, up to 0.4 ppm as baseline, prior to introduce pure oxygen gas. The diffusivity can be calculated by intercepting, with the x-abscissa, the straight-line describing the steady-state regime of the kinetic curve of cumulated oxygen amount Q_{O2} obtained by integrating the kinetic curve of Oxygen Transmission Rate along time. For a semi-infinite film of thickness L, this straight-line obeys the following general equation:

$$Q = \alpha \left(t - \frac{L^2}{6D_{O_2}}\right) \quad \textbf{Eq. 4}$$

where α is a constant.

So, the oxygen diffusivity D_{O2} is given by:

$$D_{O_2} = \frac{L^2}{6t_{Q=0}} \quad \textbf{Eq. 5}$$

where $t_{Q=0}$ is the time-lag.

Oxygen solubility S_{O2} is related to oxygen diffusivity D_{O2} and permeability Pe_{O2} by equation 2.

3. Kinetic modeling

Since the kinetic model has been detailed in the first part of this study [1], its main features will be briefly reminded here. The chemistry of oxidation is described by a simplified mechanistic scheme by assuming that methyne units are the main reactive sites. At low to moderate temperature (typically at T < 200°C), oxidation is initiated by the decomposition of its main propagation products: hydroperoxides.

Initiation

(1u) $POOH \rightarrow 2P^{\bullet} + (1 - \gamma_1)POH + \gamma_1 P{=}O + H_2O + \gamma_s S$ (- 2PH) (k_{1u})

(1b) $2POOH \rightarrow P^{\bullet} + PO_2^{\bullet} + (1 - \gamma_1)POH + \gamma_1 P{=}O + H_2O + \gamma_s S$ (- PH) (k_{1b})

Propagation

(2) $P^{\bullet} + O_2 \rightarrow PO_2^{\bullet}$ (k_2)

(3) $PO_2^{\bullet} + PH \rightarrow POOH + P^{\bullet}$ (k_3)

Termination

(4) $P^{\bullet} + P^{\bullet} \rightarrow \gamma_4 P\text{-}P + (1 - \gamma_4)PH + (1 - \gamma_4)F + \gamma_4 B$ (k_4)

(5) $P^{\bullet} + PO_2^{\bullet} \rightarrow \gamma_5 POOP + (1 - \gamma_5)POOH + (1 - \gamma_5)F + \gamma_5 B$ (k_5)

(6a) $PO_2^{\bullet} + PO_2^{\bullet} \rightarrow [PO^{\bullet}\ {}^{\bullet}OP]_{cage} + O_2$ (k_{6a})

(6b) $[PO^{\bullet}\ {}^{\bullet}OP]_{cage} \rightarrow POOP + B$ (k_{6b})

(6d) $[PO^{\bullet}\ {}^{\bullet}OP]_{cage} \rightarrow 2P^{\bullet} + 2(1 - \gamma_1)POH + 2\gamma_1 P{=}O + 2\gamma_s S$ (- 2PH) (k_{6d})

with the following formalism and initial conditions (concentrations at $t = 0$ for any depth z):

- PH accounts for the tertiary CH groups of the polymer chain as unique reactive site, with $[PH](0, z) = [PH]_0 \approx 20.3$ mol.l^{-1}
- $P^{\bullet}$, $PO_2^{\bullet}$, $PO^{\bullet}$account respectively for alkyl, peroxy and alkoxy radicals, with $[P^{\bullet}](0, z) = [PO_2^{\bullet}](0, z) = [PO^{\bullet}\ {}^{\bullet}OP]_{cage}(0, z) = 0$ mol.L^{-1}
- POOH, POOP, P-OH, P=O account respectively for hydroperoxides, peroxides, alcohols and ketones as macromolecular oxidation products. The initial concentration of POOH is kinetically equivalent to the amount of structural defects initially present in the polymer: $[POOH](0, z) = [POOH]_0 = 10^{-5}$–$10^{-1}$ mol.L^{-1} [21].
- F, S and B account respectively for double bonds, chain scissions and C-C crosslinks (i.e. covalent bridges).

Each elementary reaction is characterized by its rate constant k_i. Various yields for products formation have been introduced:

- γ_1 is the yield of β scission (leading to ketones) in competition with hydrogen abstraction (leading to alcohols). It does not depend on the molecularity of initiation reactions. From a practical point of view, it is more convenient to determine an apparent yield γ_1 for carbonyl products owing to the high uncertainty on their nature and the values of their molar extinction coefficients.
- γ_s is the yield in chain scission which can differ from γ_1 since only β scission occurring on the main macromolecular chain would impact molecular masses contrary to scissions occurring on side-groups or chain extremities.

- γ_4 and γ_5 are the yields for coupling of alkyl-alkyl and alkyl-peroxy radicals in competition with disproportionation.

In this scheme, the bimolecular recombination of peroxy radicals has been detailed. They react together to give cage paired radicals which can recombine to give a peroxide bridge (reaction 6a) or leave the cage to initiate new oxidation cycles (reaction 6d). Only the oxygen diffusion has been considered through the second Fick's law as limiting process for the oxidation reaction:

$$\partial[O_2]/\partial t = D_{O_2}\,\partial^2[O_2]/\partial z^2 - k_2[P^\bullet][O_2] + k_{6a}[PO_2^\bullet]^2 \qquad \textbf{Eq. 6}$$

where D_{O2} is the coefficient of oxygen diffusion into the semi-crystalline polymer.

The oxygen concentrations (in the amorphous phase) throughout the plate thickness before aging, and at the plate surfaces along the course of oxidation, obey the Henry's law:

$$\forall\, z,\quad t = 0,\quad [O_2](0,z) = C_s \qquad \textbf{Eq. 7}$$

$$\forall\, t > 0,\ z = 0,\ [O_2](t,0) = [O_2](t,L) = C_s \qquad \textbf{Eq. 8}$$

where C_s is the oxygen concentration in the polymer in equilibrium with the atmosphere under an oxygen partial pressure P_{O2}:

$$C_s = P_{O_2} \times S_{O_2}^{am} \qquad \textbf{Eq. 9}$$

with S_{O2}^{am} the coefficient of oxygen solubility in the polymer, here taken in the amorphous phase, i.e. only where oxygen is soluble.

The concentration changes in the involved chemical species are described by a system of ordinary differential equations (SDE) derived from the previous mechanistic scheme by applying the classical kinetics theory. This system was solved numerically using the ODE15s algorithm of Matlab software recommended for stiff problems of chemical kinetics [22]. All simulations were performed with a unique set of parameters, determined in the first part of this study [1] and reminded in table 2.

Table 2: Parameters used for kinetic modeling of iPP thermal oxidation

Parameters	***Units***	P^0	***Ea (kJ.mol^{-1})***
$[POOH]_0$	$mol.L^{-1}$	$4 \cdot 10^{-3}$	-
S_{O2}^{am}	$mol.L^{-1}.Pa^{-1}$	$2.5 \cdot 10^{-6}$	6.7
D_{O2}	$m^2.s^{-1}$	$8.7 \cdot 10^{-6}$	36.4
Pe_{O2}	$cm^3.cm.cm^{-2}.Pa^{-1}.s^{-1}$	$2.9 \cdot 10^{-6}$	43.0

k_{1u}	s^{-1}	$2.9 \cdot 10^{13}$	140.7
k_{1b}	$L.mol^{-1}.s^{-1}$	$9.2 \cdot 10^{8}$	95.0
k_2	$L.mol^{-1}.s^{-1}$	$3.0 \cdot 10^{9}$	10.0
k_3	$L.mol^{-1}.s^{-1}$	$5.1 \cdot 10^{7}$	62.2
k_4	$L.mol^{-1}.s^{-1}$	$1.0 \cdot 10^{12}$	0
k_5	$L.mol^{-1}.s^{-1}$	$4.5 \cdot 10^{10}$	0
k_{6a}	$L.mol^{-1}.s^{-1}$	$2.0 \cdot 10^{17}$	90.0
k_{6b}	s^{-1}	$6.7 \cdot 10^{6}$	5.0
k_{6d}	s^{-1}	$1.4 \cdot 10^{12}$	41.0
γ_1	%	50	-
γ_4	%	0	-
γ_5	%	0	-
γ_s	%	50	-

The real concentrations of all chemical species in the semi-crystalline polymer have been deduced from the concentrations calculated in the amorphous phase by multiplying them by the volumic fraction of amorphous phase V_a:

$$V_a = \chi_a \times \frac{\rho_{tot}}{\rho_a} = (1 - \chi_c) \times \frac{\rho_{tot}}{\rho_a} \qquad \textbf{Eq. 10}$$

with χ_c the crystallinity ratio, ρ_{am} the density of the amorphous phase (0.85 $g.cm^{-3}$) and ρ_{tot} the density of the semi-crystalline polymer (0.91 $g.cm^{-3}$).

4. Results and discussion

4.1. Variability of oxygen transport properties

Prior to properly calibrate the model, it has been required to determine accurately the input parameters which are accessible experimentally, i.e. the oxygen transport properties, namelyoxygen permeability Pe_{O2}, solubility S_{O2} and diffusivity D_{O2}. In particular, determining S_{O2} was mandatory to determine the different rate constants by inverse resolution method. Permeametry measurements have thus been carried out in the 10-45°C temperature range. In this domain, these three parameters reveal an Arrhenian behavior despite a fairly large experimental scattering:

$$P_{O_2} = 2.87 \cdot 10^{-6} \times \exp\left(-43100/_{RT}\right) (cm^3.cm.cm^{-2}.Pa^{-1}.s^{-1}) \qquad \textbf{Eq. 11}$$

$$S_{O_2} = 1.48 \cdot 10^{-6} \times \exp\left(-6700/_{RT}\right) (mol.L^{-1}.Pa^{-1}) \qquad \textbf{Eq. 12}$$

$$D_{O_2} = 8.65 \cdot 10^{-6} \times \exp\left(-36400/_{RT}\right) (m^2.s^{-1}) \qquad \textbf{Eq. 13}$$

However, physical transformations can affect the chain mobility and thus lead to discontinuities in Arrhenius graphs, such as the α-crystalline phase transitions occurring around 70°C as evidenced for instance by DMA [23]. Owing to these potential deviations from the Arrhenius law, extrapolating at temperatures outside the range of permeation measurement would induce a misestimation of oxygen transport properties. It is thus relevant to position our experimental values among an exhaustive compilation of literature data, as performed for oxygen solubility in the first part of this study [1]. It can be now fulfilled in the case of the oxygen permeability [16, 18, 24-34] and diffusivity [18, 24, 30, 31, 33-41], of which the respective Arrhenius graphs have been depicted in figures 1 and 2.

In the case of oxygen permeability, our results are fully consistent with the data compiled from the literature [16, 18, 24-34] since both datasets are overlapped (figure 1). This result suggests that our samples were of suitable quality in terms of thickness and morphological features. The rather low scattering (over only one decade) of literature data would result from differences in morphologies between the different iPP samples.

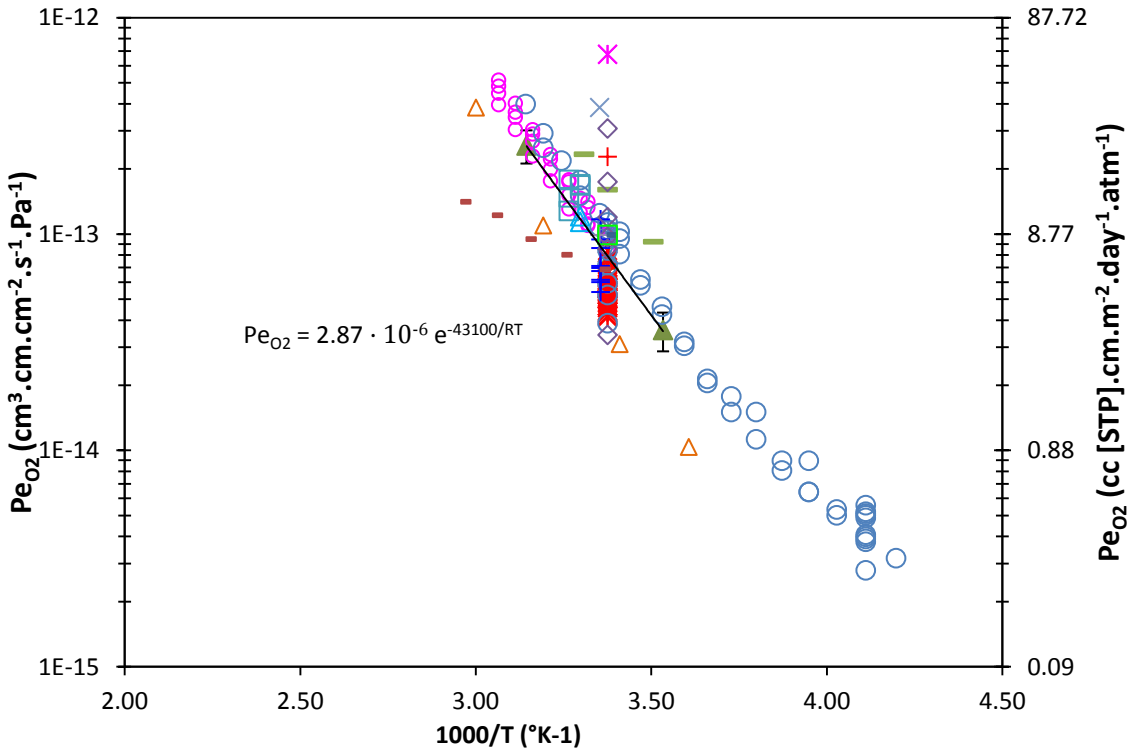

Figure **1**: Arrhenius graph of oxygen permeability of iPP between -10 and 60°C: ▲This work, ✳Lin [30, 31], ○ Somlai [33], ○ Sezi [32], ▬ Villaluenga [34], ▬ Beltrame [24], ◇ Mani [18], ◇ Kiryushskin [9, 36], □ Denisov [35], □ Modern Plastic Encyclopedia in [25], + Taraiya [16], ×Kanehashi [28], ✳ Frounchi [26], △ Incarnato [27], + Katsura [29], ▬ Vladimirov [42], □ Bikiaris [43], △ Kurec [37] and + Guttierez [8].

In contrast, the values of oxygen diffusivity compiled from the literature [18, 24, 30, 31, 33-41] show a significantly higher scattering ranging over two decades, as previously evidenced for oxygen solubility (figure 2). The simplest scenario would assume that this additional experimental scattering only stems from additional systematic error (instrumental delay effect) in the time-lag measurements which can occur when this latter is of the same order of magnitude as the characteristic time of the permeameter (i.e. the time needed for gas transport in the lines up to the detector, which depends on the device technology) [33]. In such conditions, the experimental scattering on permeability would be more relevant to apprehend the variability due to initial differences in iPP morphology. However, it can be also envisaged that variation of morphological features would have a reverse effect one oxygen solubility and diffusivity, thereby explaining their higher experimental scattering compared with permeability.

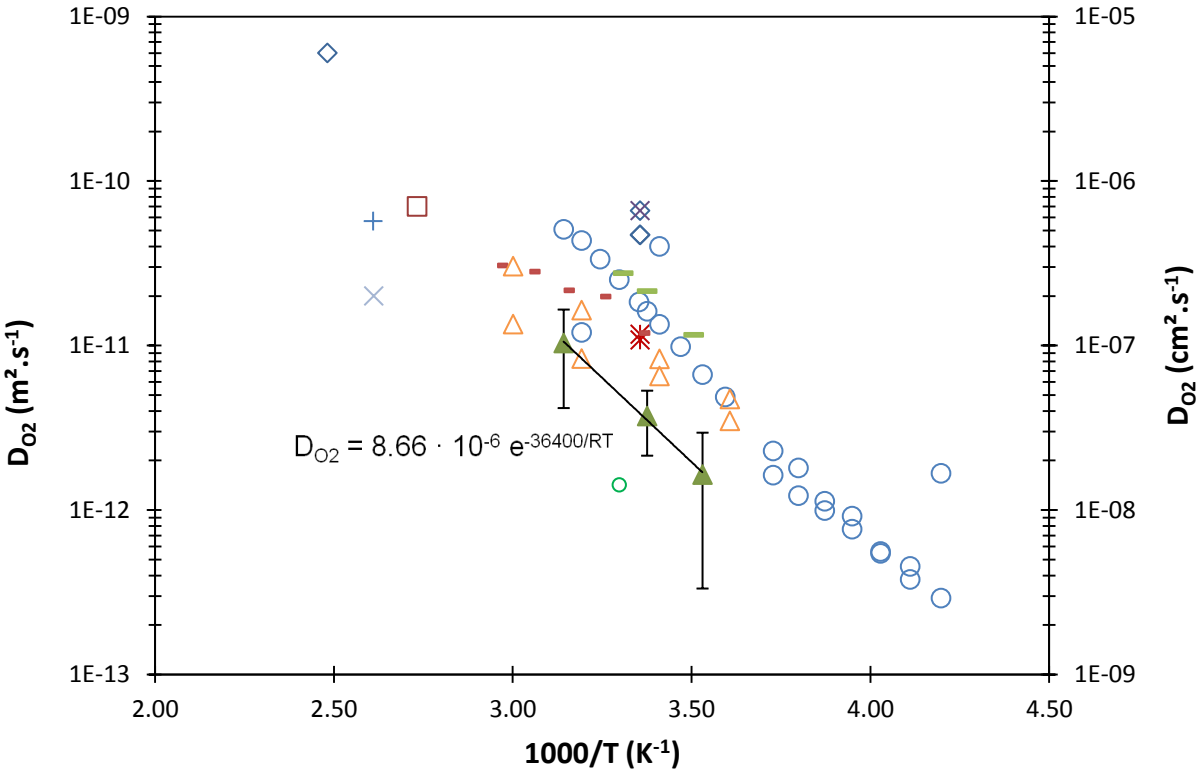

Figure **2**: Arrhenius graph of oxygen diffusivity for polypropylene between -10 and 130°C: ▲ This work, ✳Lin [30, 31], ○ Somlai [33], ▬ Villaluenga [34], ▬ Beltrame [24], ◇ Kiryushskin [9, 36], □ Denisov [35], + Van Krevelen [40], △ Kurek [37], ○ Stannet [39], × G.A. George in ref. [44] and ×Felder [45].

Despite this experimental scattering, the activation energy of oxygen diffusivity seems to remain unchanged in a large range of temperatures, going from glass transition temperature (~ -10°C) up to 135°C, and thus appears consistent with the assumption of Arrhenian behavior for oxygen transport properties.

4.2. Simulation of oxidation profiles - Impact of oxidation on oxygen transport properties

The oxidation profiles have been tentatively simulated by introducing in the kinetic model the oxygen transport properties determined in the previous section (equations 11 to 13). As an example, figure 3 reports examples of simulated and experimental oxidation profiles at 60°C and 140°C in air.

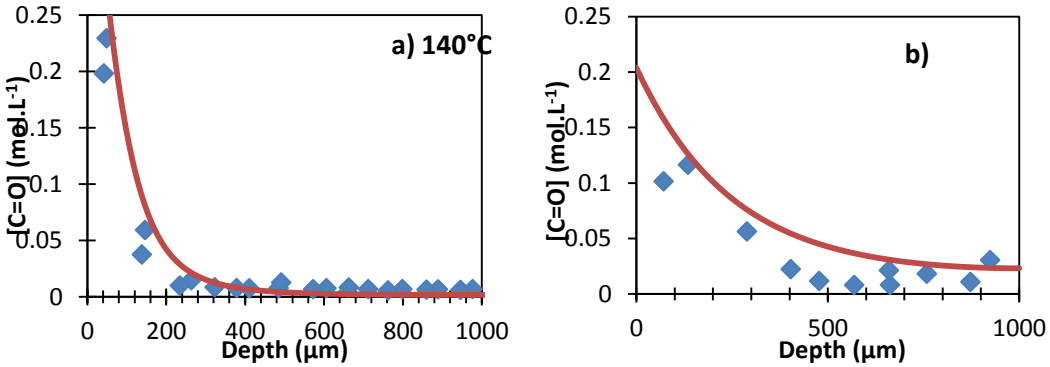

Figure 3: Profiles of carbonyl products in the sample thickness after 3.5 hours at 140°C (a) and 1400 hours at 60°C in air (b). Symbols: Experimental data. Solid lines: kinetic modeling with D_{O2} obeying equation 13.

Clearly, experimental results reveal an oxidation profile more acute than simulated which implies that the oxygen permeability (and so, the diffusivity) is lower than stated from permeametry measurements. This result confirms the drop in oxygen transport properties during iPP oxidation.

It is thus proposed to determine by inverse resolution method an average value of the oxygen diffusivity, which will enable to simulate more satisfactorily the same oxidation products profile as observed at time t. This demarche implies that the entire drop in oxygen permeability is ascribed to the diffusion component, thus keeping oxygen solubility constant. Indeed, the model relevancy at the local scale (goodness-of-fit) suggests that the oxygen

solubility is properly calibrated and will thereby enable to determine accurately the coefficient of oxygen diffusion.

For various oxidation degrees and temperatures ranged between 60 and 140°C, oxygen diffusivity was found to be divided by a factor 7 compared to the nominal value D_{O2} measured on the reference iPP, despite the scattering of experimental data (see equation 13). All the fits at 60, 80, 100 and 140°C in air are depicted in figure 4. The uncertainty is partly due to the lack of measurements in the first dozens of microns. Our attempts to obtain additional values for smaller depths, by delaminating superficial layers of more oxidized iPP or by performing an ATR-FTIR analysis at the extreme plate surface, turns out to be unsuccessful.

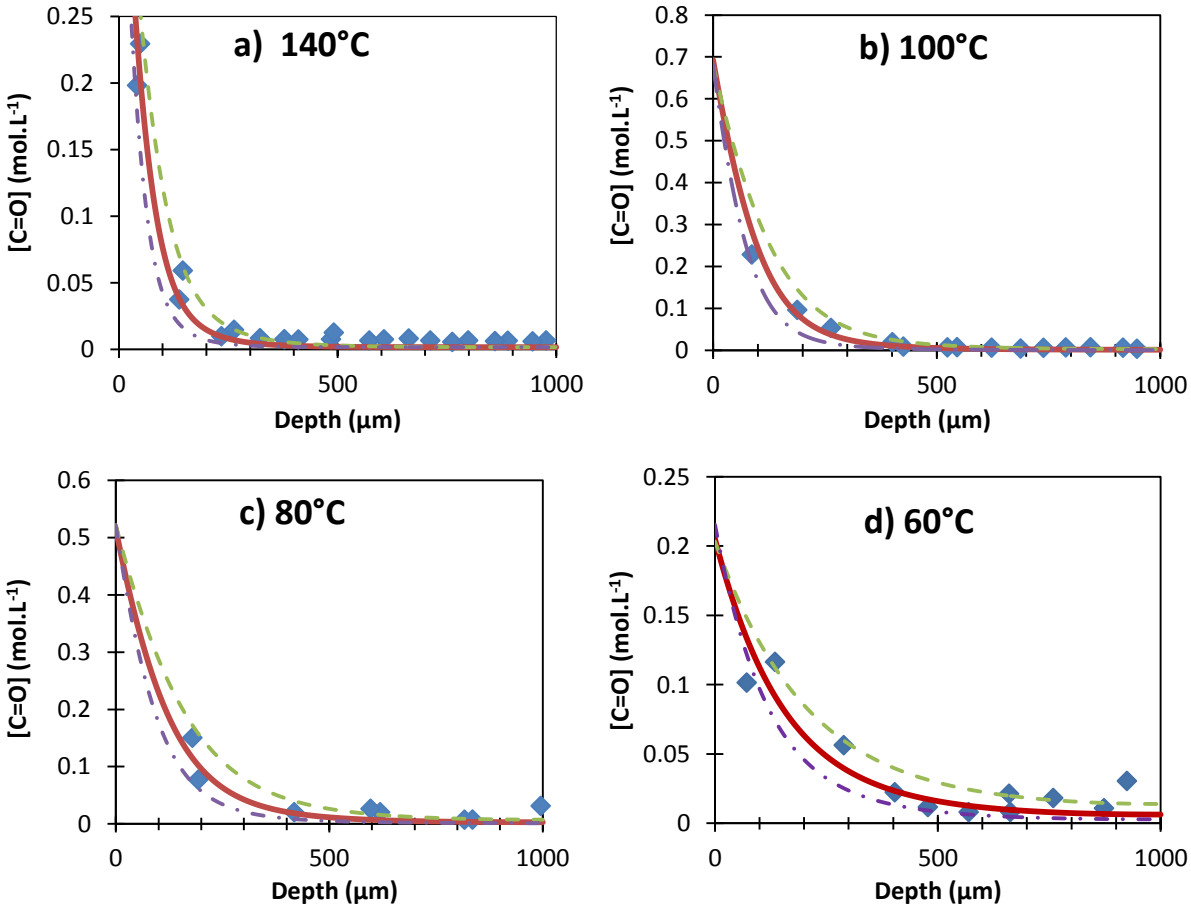

Figure 4: Profiles of carbonyl products in the sample thickness after 3.5 h at 140°C (a), 70 h at 100°C (b), 300 h at 80°C (c) and 1400 hours at 60°C in air (b) Symbols: Experimental data. Solid lines: kinetic modeling, best fits for $0.14*D_{O2}$ (given by equation 15). Dotted lines: parametric tests with various multipliers (0.08 and 0.25) of the nominal value of D_{O2} (given in equation 13)

Despite the drop of oxygen transport properties, it is possible by a worst-case approach to assert that TOL is about 40 µm at 140°C for the reference iPP and thereby higher at lower

temperatures. Thus, films of 80 µm thickness would undergo a homogeneous oxidation in the temperature range under investigation.

It is relevant to highlight that this observation is not the consequence of any bias introduced by the kinetic modeling approach, since both parameters which govern the oxidation process, denoted below as "invariant quantities", are calibrated on experimental results.

(i) The ratio $k_2 \cdot S_{O2}^{am}/k_5$ governs the oxygen pressure dependence of a given polypropylene sample. Thereby, any bias on the determination of the oxygen solubility would be compensated by the adjustment of kinetic rate constants k_2 or k_5. In other words, different combinations of k_2, k_5 and S_{O2}^{am} will enable to simulate the results for the given invariant quantity.

(ii) The permeability is the relevant quantity which governs the shape of oxidation profiles. Thus, according to equation 2, there are also various combinations of S_{O2} and D_{O2} which generate the suitable oxidation profiles. This assertion has been checked by testing different combinations of k_5, S_{O2}^{am} and D_{O2} leading to a same value of Pe_{O2} and generating an identical oxidation profile.

Values of parameters giving the same values of both invariant quantities are reported in table 3.

Table 3: Values of parameters allowing to simulate oxidation profiles (the most relevant values are gived in bold).

Pe_{O2} ($cm^3.cm.cm^{-2}.Pa^{-1}.s^{-1}$)	**D_{O2} ($m^2.s^{-1}$)**	**S_{O2} ($mol.L^{-1}.Pa^{-1}$)**	**S_{O2}^{am} ($mol.L^{-1}.Pa^{-1}$)**	**k_5 ($mol.L^{-1}.s^{-1}$)**
$2.87 \cdot 10^{-6}$ exp(-43000/RT)	$8.65 \cdot 10^{-6}$ exp(-36400/RT)	$1.48 \cdot 10^{-6}$ exp(-6700/RT)	$2.51 \cdot 10^{-6}$ exp(-6700/RT)	$4.50 \cdot 10^{10}$
$2.87 \cdot 10^{-6}$ exp(-43000/RT)	$8.65 \cdot 10^{-7}$ exp(-36400/RT)	$1.48 \cdot 10^{-5}$ exp(-6700/RT)	$2.51 \cdot 10^{-5}$ exp(-6700/RT)	$4.50 \cdot 10^{11}$
$2.87 \cdot 10^{-6}$ exp(-43000/RT)	$8.65 \cdot 10^{-8}$ exp(-36400/RT)	$1.48 \cdot 10^{-4}$ exp(-6700/RT)	$2.51 \cdot 10^{-4}$ exp(-6700/RT)	$4.50 \cdot 10^{12}$

Since oxygen permeability governs the shape of oxidation profiles, it was selected as the relevant parameter for evaluating the competition between oxygen diffusivity and its chemical consumption by the polymer. To account for the wide range of TOL values reported in the literature, the oxidation profiles available in the literature [6, 10-12, 41, 46] have been collected and have undergone the previous numerical treatment. These latter can be

advantageously compared to those obtained for the reference iPP. All the permeability values thus determined by using the kinetic model as an inverse resolution method have been reported in the Arrhenius plot depicted in figure 5.

It is noteworthy that the inverse resolution method allows determining apparent values of oxygen permeability at temperatures higher than the ambient temperature: it seems that only the pre-exponential factor of Pe_{O2} varies over one decade on both sides of the melting point, whereas the activation energy is weakly impacted.

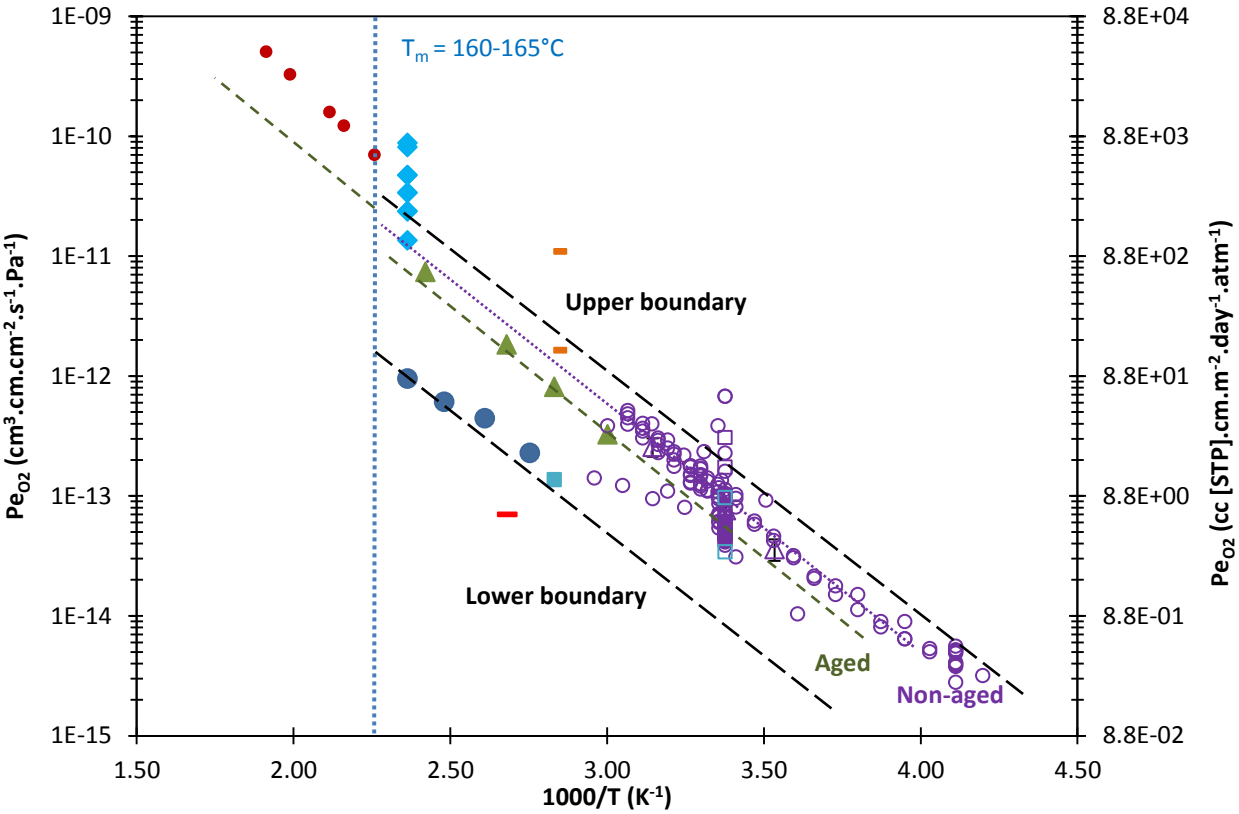

Figure 5: Arrhenius graph of oxygen permeability determined for iPP by permeametry (○ literature, △ reference iPP, □ By Mani on aged and, □ unaged specimens [18]) or by inverse resolution method from experimental oxidation profiles (▲ reference iPP, ● Fayolle [6], ● Sarrabi [46], ▬ Guttierez [8], ◆ Boss [11], ▬ Gugumus [12], ■ Singh [10]). The discontinuity at 160-165°C is ascribed to melting point.

Generally, the values obtained by the inverse resolution method from oxidation profiles of aged specimens are lower than for non-aged specimens. It is clear that a noticeable part of the Pe_{O2} scattering, materialized by the upper and lower boundaries, stems from the alteration of oxygen transport properties. This result is particularly evidenced on the reference iPP with a decrease in Pe_{O2} by a factor 7, in rather good agreement with the literature data [28]. Mani et

al. [18] observed that the polypropylene permeability of various gases -namely carbon dioxide, nitrogen and oxygen- can decrease by a factor ranged between 3 and 10 along the course of oxidation. They attributed this result to a change in crystallinity, the occurrence of chain scissions and crosslinking, or the formation of photoproducts. Guttierez and coworkers [41] observed a similar trend for semicrystalline PE (although Mani et al. observed the reverse trend in amorphous LDPE and EPR) that they attributed to chemi-crystallisation, i.e. crystalline rearrangements of the short macromolecular segments created by chain scissions in the amorphous phase [47-49].

Among the different explanations for the drop in oxygen transport properties, i.e. chain scissions and crosslinking, crystallinity ratio changes and photoproducts formation, we will first focus on the two former. According to Rabello and White [47], chain scissions and crosslinking would not directly contribute to the decrease in Pe_{O2} but promote chemi-crystallization, i.e. increases in crystallinity ratio. In our case, no significant change in crystallinity was observed by DSC, whereas FTIR measurements revealed an increase of about 20%, i.e. 9 index points (see appendix A).

Basically, this phenomenon is expected to mostly impact oxygen diffusivity whereas photoproducts formation would induce an increase in polymer polarity affecting oxygen solubility. At this stage of investigation, the relationship between χ_c and oxygen solubility S_{O2} is not yet available, so this issue is left aside in a first approach.

The ideal strategy for kinetic modeling would consist in expressing the oxygen diffusivity as a function of the amount of chain scissions, as proposed by Guttierez et al. [41] . In a first coarse-grained approach, this would require at first to calculate the variation of χ_c from the concentration changes in chain scissions [50] and then, to deduce the impact of this change on D_{O2} by using well-established relationships in the literature.

Even for diffusivity of simple gases, a linear correction of the oxygen diffusivity by the volume fraction of the amorphous phase V_a is not sufficient to describe such a complex behavior:

$$D_{O_2}^{cr} = D_{O_2}^{am} \cdot {V_a}^{-n} \quad with\ n = 1 \qquad \textbf{Eq. 14}$$

Indeed, the most widespread models of the literature, developed by Michaels and Bixler [51] and Peterlin [52, 53], attempt to describe the influence of crystallites through phenomenological relationships of the form:

$$D_{O_2}^{cr} = {D_{O_2}^{am}}/{\tau\beta} \qquad \textbf{Eq. 15}$$

where τ is the tortuosity factor accounting for the increase in the diffusive pathway owing to the bypass of crystallites, and β is the immobilization factor reporting the lowering of the segmental mobility in the amorphous regions near the crystallites (i.e. of constrained tie-molecules), which depends on the penetrant size.

According to Michaels and Bixler, in semi-crystalline polymers, only the tortuosity factor would depend on the volume fraction amorphous phase according to a power law: V_a^{-n} [51], with n = 1.61 for iPP [54], compared with n ranging from 1.08 to 1.88 for PE synthesized according to Ziegler-Natta and Philips procedures [51, 55]. This relationship between *n* and the morphological characteristics cited above has been tentatively established through empirical [56] or semi-empirical relationships, such as the Fricke's theory adapted by Michaels and Bixler [51], or numerical models involving Monte-Carlo algorithms [57, 58] [56, 59]. From these studies, a particular result can be reminded: the relevant impermeable structure are lamellae whose aspect ratio (i.e. shape) and orientation impact the oxygen transport properties, as checked experimentally [60] and numerically [56, 59]. Therefore, spherulitic structures would have a second order of influence owing to the specific spatial arrangement that they confer to lamellae [59].

From this standpoint, it is clear that any accurate description of the diffusivity dependence on morphological features would require demanding characterization procedures. Admittedly, it remains possible to use the empirical power law: $V_a^{-1.61}$ [54], but without acquaintance of its validity range. In contrast, the approach of Compañ et al. [61] consists in giving expressions for the tortuosity and immobilization factors respectively from thermodynamic and free volume theory considerations. Since β is closed to unity ($\beta = 1.2$ compared with $\tau = 3.2$ for HDPE [51]), it is generally neglected and oxygen diffusivity only depends on the crystallinity ratio χ_c:

$$D_{O_2} \approx D_{O_2}^{am} \exp(-A(T) \cdot \chi_c) \qquad \textbf{Eq. 16}$$

with *A(T)* a weakly temperature dependent constant characteristic of a given material (equal to 3.16 for HDPE [51] and 1.34 for octane based HDPE [61] at 25°C)

This kind of relationship has a physical meaning and is easier to use than other models which require data on lamellae features (aspect ratio and orientation).

Our theoretical change in oxygen diffusivity (and so, in permeability) have been calculated with these kinds of relationships, namely according to equation 14(with n = 1 and n = 1.61) and equation 16 (with A = 2.2 for iPP and A = 1.77 and 3.51 for HDPE). It is important to precise here that the value of 2.2 has been determined for A by minimizing the gap between equations 16 and 14 for the unaged reference iPP (i.e. for χ_c = 0.45).

Whatever the relationship considered, the increase in crystallinity ratio of about 20% induces a drop in the ratio D_{O2}^{am}/D_{O2} which would not exceed 25%, which is very far from the previous observation (divided by a factor 7). Thus, chemi-crystallization alone cannot explain the observed drop in oxygen transport properties.Therefore, the remaining part of this drop could be ascribed to a change in the polymer polarity induced by oxygen grafting onto macromolecules, thus impacting oxygen solubility.

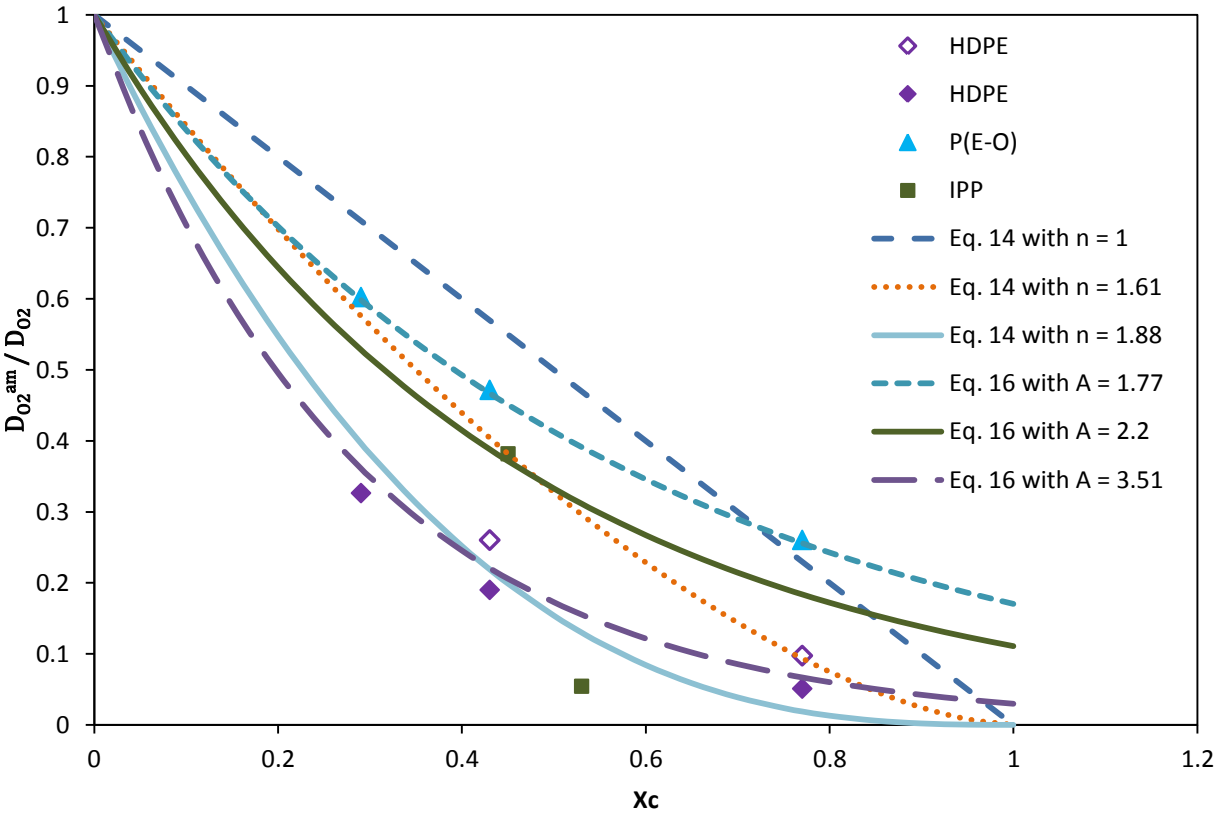

Figure 6: Changes in the ratio D_{O2}^{am}/D_{O2} with crystallinity

4.3. Impact of iPP thermal oxidation on the kinetic modeling

Anyway, the morphology changes during oxidation are not restricted to crystallinity ratio alone. The specimens underwent crystalline structure modifications as revealed by the shape of melting endotherm [47, 62-64], which becomes broader and is shifted toward lower temperatures (figure 6). The reader can refer to review [65] for further information about iPP polymorphism. These observations can be assigned to the formation of the β-hexagonal/trigonal or δ-smectic phase (T_m = 150°C) at the expense of the initial monoclinic α-phase (T_m = 165°C), mainly because chain scissions and oxidation products act as structural defects which promote nucleation of the metastable trigonal or smectic phases. On the contrary, annealing would favor the recrystallization of the α-phase as a competitive process [63, 66, 67]. The difference in the melting temperatures between both phases would be due to the decrease in the lamellae thickness [68] or the increase in the interfacial energy of lamellae induced by the presence of oxidation products, in better consistency with the scenario of chemi-crystallization [47, 63, 66, 67]. At the microstructural scale, this decrease in melting temperature would be ascribed to the distribution of stereo-defects materialized by the length of crystallisable isotactic sequences rather than to the isotacticity itself [69-74].

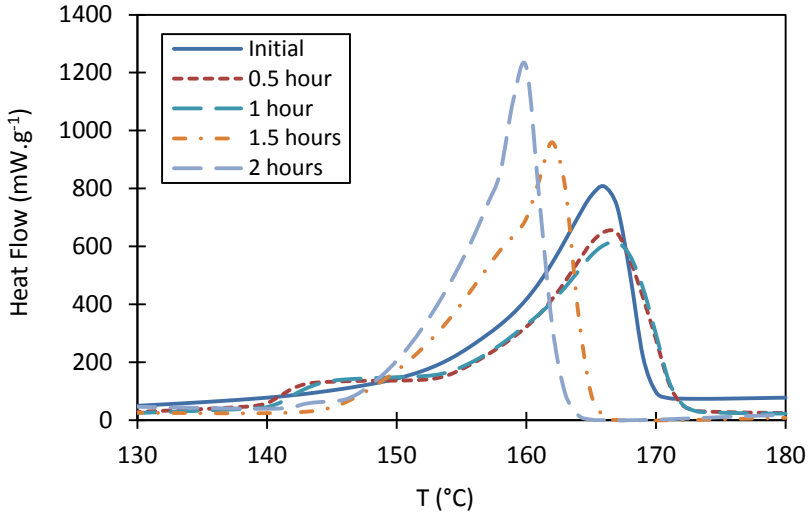

Figure 7: Changes in the shape of melting endotherm at 140°C in air (the oxidation induction time is 1 hour in such aging conditions)

These considerations have two important implications. First, the determination of the structure/property relationship between the changes in oxygen diffusivity and crystallinity could be more complicated than expected if only considering the crystallinity ratio. Second,

this must be connected with the presumed impact of polymorphism on the apparent value of oxygen solubility. If the variability of solubility is ascribed to the multiplicity of crystal lattices, its value would be affected by the previous morphological changes. This aspect would be a specificity of polypropylene due to the multiplicity of crystalline phases compared with polyethylene. However, the oxygen solubility was kept unchanged considering that the impact on this quantity is of second order. If necessary, it could be described in the kinetic model through the yields in carbonyl products γ_1 and chain scission γ_s. Undoubtly, this would deserve further considerations.

5. Conclusion

The main objective of this second part of our study was to tentatively explain the wide range of TOL values reported in the literature, i.e. to check the ability of the kinetic model to predict the competition between the oxygen diffusion and its chemical consumption by the polymer.

First, the impact of the initial polymer morphology has been evidenced in an exhaustive literature compilation of oxygen transport properties, i.e. permeability, diffusivity and solubility. Actually, the experimental scattering on oxygen solubility and diffusivity is significantly higher than the scattering on oxygen permeability. This observation is ascribed to:

(i) Cumulative errors in the determination of D_{O2} and S_{O2} by the time-lag method.

(ii) The changes in both coefficients during thermal exposure due to morphological transformations.

The existence of multiple explanations could hinder the elucidation of structure/transport properties relationships. However, oxygen permeability has been identified as the effective invariant quantity which governs the shape of oxidation profiles and thus TOL values.

The literature compilation also enabled to check the relevancy of the Arrhenius behavior observed for Pe_{O2}, D_{O2} and S_{O2} in the 10-45°C temperature range (by oxygen permeametry measurements) and postulated at higher temperatures (up to 130°C).

Anyway, the experimental scattering on oxygen permeability gives a first idea of the impact of the initial polymer morphology on oxygen transport properties. But, it does not enable to report variability on TOL for the whole iPP family. It was thus attempted to determine the apparent value of diffusivity by using the kinetic model as an inverse resolution method on

our reference iPP whose oxygen solubility is known. Surprisingly, this latter value was significantly lower than the value measured by permeametry, but seems to still obey an Arrhenius behavior. This observation indicates changes in properties, which would essentially impact the pre-exponential factor, but not the activation energy. This increase in oxygen barrier properties along the course of oxidation is in satisfactory agreement with the permeability values collected in the literature for iPP photooxidation.

These changes would be ascribed to the polymer densification in superficial oxidized layers (oxygen grafting) and to the occurrence of morphological changes, such as recrystallization and chemicrystallization phenomena which would respectively result from physical (annealing) and chemical aging (chain scissions).

From this standpoint, it is clear that properly simulating oxidation profiles requires to establish the dependence of oxygen transport properties with crystallinity ratio and oxidation conversion degree. In the absence of such a relationship, the validity of the kinetic model would be restrained to moderate degree of oxidation, i.e. for exposure durations just longer than the induction period.

References

[1] A. François-Heude, E. Richaud, A. Guinault, E. Desnoux, X. Colin, On the impact of oxygen transport properties on the polypropylene thermal oxidation. Part I: Effect of oxygen solubility in, Arts et Metiers ParisTech, Renault (France), 2014.

[2] G.E. Schoolenberg, H.D.F. Meijer, Ultra-violet degradation of polypropylene: 2. Residual strength and failure mode in relation to the degraded surface layer, Polymer, 32 (1991) 438-444.

[3] A.V. Cunliffe, A. Davis, Photo-oxidation of thick polymer samples" Part II: The influence of oxygen diffusion on the natural and artificial weathering of polyolefins, Polymer Degradation and Stability, 4 (1982) 17-37.

[4] G.C. Furneaux, K.J. Ledbury, A. Davis, Photo-oxidation of thick polymer samples" Part I: The variation of photo-oxidation with depth in naturally and artificially weathered low density polyethylene, Polymer Degradation and Stability, 3 (1981) 431-442.

[5] K.T. GIllen, R.L. Clough, Techniques for monitoring heterogeneous oxidation of polymers, in: M. Dekker (Ed.) Handbook of Polymer Science and Technology, Cheremisinoff N.P. (ed.), New York, 1989.

[6] B. Fayolle, Fragilisation du polypropylène induite par fragilisation [In French], in: Mécanique et Matériaux, Ecole Nationale Supérieure des Arts et Métiers, Paris, 2001.

[7] R.L.M. Rincon, B. Fayolle, L. Audouin, J. Verdu, A general solution of the closed-loop kinetic scheme for the thermal oxidation of polypropylene, Polymer Degradation and Stability, 74 (2001) 177–188.

[8] G. Gutiérrez, F. Fayolle, G. Régnier, J. Medina, Thermal oxidation of clay-nanoreinforced polypropylene, Polymer Degradation and Stability, 95 (2010) 1708-1715.

[9] S.G. Kiryushkin, Y.A. Shlyapnikov, Diffusion-controlled polymer oxidation, Polymer Degradation and Stability, 23 (1989) 185-192.

[10] R.P. Singh, R. Mani, S. Sivaram, J. Lacoste, J. Lemaire, Thermo-oxidative degradation of heterophasic ethylene-propylene copolymers and their fractions, Polymer International, 32 (1993) 189-196.
[11] C.R. Boss, J.C.W. Chien, Oxygen diffusion limitation in autoxidation of polypropylene, Journal of Polymer Science Part A-1: Polymer Chemistry, 4 (1966) 1543-1551.
[12] F. Gugumus, Thermooxidative degradation of polyolefins in the solid state - 7. Effect of sample thickness and heterogeneous oxidation kinetics for polypropylene, Polymer Degradation and Stability, 62 (1998) 245-257.
[13] S. Girois, P. Delprat, L. Audouin, J. Verdu, Oxidation thickness profiles during photooxidation of non-photostabilized polypropylene, Polymer Degradation and Stability, 56 (1997) 169-177.
[14] K.M.B. Jansen, Analytical approximation of degradation profiles in polymer products, Polymer Engineering & Science, 34 (1994) 1619-1627.
[15] L. Audouin, V. Langlois, J. Verdu, J.C.M. de Bruijn, Role of oxygen diffusion in polymer ageing: kinetic and mechanical aspects, Journal of Materials Science, 29 (1994) 569-583.
[16] A.K. Taraiya, G.A.J. Orchard, I.M. Ward, The effect of amorphous orientation on the oxygen permeability of polypropylene films, Journal of Polymer Science Part B: Polymer Physics, 31 (1993) 641-645.
[17] M. Hedenqvist, U.W. Gedde, Diffusion of small-molecule penetrants in semicrystalline polymers, Progress in Polymer Science, 21 (1996) 299-333.
[18] R. Mani, R.P. Singh, S. Sivaram, J. Lacoste, J. Lemaire, Effect of UV irradiation on gas permeability in heterophasic ethylene-propylene copolymer films, Journal of Macromolecular Science - Pure and Applied Chemistry, 33 (1996) 783-787.
[19] A. Perlin, Structured polymer properties, The identification, interpretation, and application of crystalline polymer structure, Journal of Polymer Science: Polymer Letters Edition, 13 (1975) 61-62.
[20] S.W. Rutherford, D.D. Do, Review of time lag permeation technique as a method for characterisation of porous media and membranes, Adsorption, 3 (1997) 283-312.
[21] E. Richaud, X. Colin, B. Fayolle, L. Audouin, J. Verdu, Induction period in the low-temperature thermal oxidation of saturated hydrocarbons: Example of polyethylene, International Journal of Chemical Kinetics, 40 (2008) 769-777.
[22] E. Hairer, G. Wanner, Stiff and Differential-Algebraic Problems, 1996.
[23] J.M. Gomez-Elvira, P. Tiemblo, M. Elvira, L. Matisova-Rychla, J. Rychly, Relaxations and thermal stability of low molecular weight predominantly isotactic metallocene and Ziegler-Natta polypropylene, Polymer Degradation and Stability, 85 (2004) 873-882.
[24] P.L. Beltrame, C. Citterio, G. Testa, A. Seves, Oxygen permeation through films of compatibilized polypropylene/polyamide 6 blends, Journal of Applied Polymer Science, 74 (1999) 1941-1949.
[25] J. Brandrup, E.H. Immergut, E.A. Grulke, Polymer Handbook, 4th Edition, , 1998
[26] M. Frounchi, S. Dadbin, Z. Salehpour, M. Noferesti, Gas barrier properties of PP/EPDM blend nanocomposites, Journal of Membrane Science, 282 (2006) 142-148.
[27] L. Incarnato, P. Scarfato, O. Motta, D. Acierno, Properties of films from polypropylene and thermotropic liquid crystalline polymer blends, Polymer Composites, 21 (2000) 354-360.
[28] S. Kanehashi, A. Kusakabe, S. Sato, K. Nagai, Analysis of permeability; solubility and diffusivity of carbon dioxide; oxygen; and nitrogen in crystalline and liquid crystalline polymers, Journal of Membrane Science, 365 (2010) 40-51.
[29] T. Katsura, M.R. Kamal, L.A. Utracki, Some properties of polypropylene filled with metal fibers, Polymer Composites, 6 (1985) 282-295.
[30] Y.J. Lin, P. Dias, H.Y. Chen, S. Chum, A. Hiltner, E. Baer, Oxygen permeability of biaxially oriented polypropylene films, Polymer Engineering & Science, 48 (2008) 642-648.
[31] Y.J. Lin, P. Dias, H.Y. Chen, A. Hiltner, E. Baer, Relationship between biaxial orientation and oxygen permeability of polypropylene film, Polymer, 49 (2008) 2578-2586.
[32] R. Sezi, J. Springer, Gaspermeabilität von Polypropylen, Colloid and Polymer Science, 259 (1981) 1170-1176.
[33] L.S. Somlai, R.Y.F. Liu, L.M. Landoll, A. Hiltner, E. Baer, Effect of orientation on the free volume and oxygen transport of a polypropylene copolymer, Journal of Polymer Science Part B: Polymer Physics, 43 (2005) 1230-1243.

[34] J.P.G. Villaluenga, M. Khayet, M.A. Lopez-Manchado, J.L. Valentin, B. Seoane, J.I. Mengual, Gas transport properties of polypropylene/clay composite membranes, European Polymer Journal, 43 (2007) 1132-1143.
[35] E.T. Denisov, I.B. Afanas'ev, Oxidation and Antioxidants in Organic Chemistry and Biochemistry. , Taylor and Francis 2006.
[36] S.G. Kiryushkin, Dissertation, Institute Chemical Physics, Moscow,, (1975).
[37] M. Kurek, D. Klepac, M. Ščetar, K. Galić, S.k. Valić, Y. Liu, W. Yang, Gas barrier and morphology characteristics of linear low-density polyethylene and two different polypropylene films, Polymer Bulletin, 67 (2011) 1293-1309.
[38] P. Thorlaksen, J. Abildskov, G.M. Kontogeorgis, Fluid Phase Equilibria, 211 (2003) 17-33.
[39] V. Stannet, Diffusion in polymers, in: J.C.G.S. PARK (Ed.), Academic Press, New York, 1968, pp. 41.
[40] D.W. Van Krevelen, Properties of polymers, , 1976.
[41] G.G. Gutiérrez, Oxydation des nanocomposites à matrice polyoléfinique in, Arts et metiers ParisTech, Paris, 2010.
[42] V. Vladimirov, C. Betchev, A. Vassiliou, G. Papageorgiou, D. Bikiaris, Dynamic mechanical and morphological studies of isotactic polypropylene/fumed silica nanocomposites with enhanced gas barrier properties, Composites Science and Technology, 66 (2006) 2935-2944.
[43] D. Bikiaris, A. Vassiliou, K. Chrissafis, K.M. Paraskevopoulos, A. Jannakoudakis, A. Docoslis, Effect of acid treated multi-walled carbon nanotubes on the mechanical, permeability, thermal properties and thermo-oxidative stability of isotactic polypropylene, Polymer Degradation and Stability, 93 (2008) 952-967.
[44] H.H.G. Jellinek, Developments in polymer degradation – 3, N. Grassie, Ed., Applied science publishers, London, 1981, 321 pp. [45] R.M. Felder, R.D. Spence, J.K. Ferrel, A Method for the Dynamic Measurement of Diffusivities of Gases in Polymers, Journal of Applied Polymer Science, 19 (1975) 3193.
[46] S. Sarrabi, X. Colin, A. Tcharkhtchi, Kinetic modeling of polypropylene thermal oxidation during its processing by rotational molding, Journal of Applied Polymer Science, 118 (2010) 980-996.
[47] M.S. Rabello, J.R. White, Crystallization and melting behaviour of photodegraded polypropylene -- I. Chemi-crystallization, Polymer, 38 (1997) 6379-6387.
[48] I.H. Craig, J.R. White, P.C. Kin, Crystallization and chemi-crystallization of recycled photo-degraded polypropylene, Polymer, 46 (2005) 505-512.
[49] F.H. Winslow, C.J. Aloisio, W.L. Hawkins, W. Matreyek, Chem. Ind., (1963) 1465.
[50] B. Fayolle, E. Richaud, X. Colin, J. Verdu, Review: degradation-induced embrittlement in semi-crystalline polymers having their amorphous phase in rubbery state, Journal of Materials Science, 43 (2008) 6999-7012.
[51] A.S. Michaels, H.J. Bixler, Flow of gases through polyethylene, Journal of Polymer Science, 50 (1961) 413-439.
[52] A. Peterlin, Transport properties as an extremely sensitive indicator of the status of the amorphous component in the elastically and plastically deformed semicrystalline polymer, in: Materials Science Monographs, Elsevier, Athens, Greece, 1984, pp. 585-604.
[53] A.J. Peterlin, Macromol. Sci. Rev. Macromol. Chem. Phys., 11 B (1975) 57.
[54] W. Vieth, W.F. Wuerth, Transport properties and their correlation with the morphology of thermally conditioned polypropylene, Journal of Applied Polymer Science, 13 (1969) 685-712.
[55] A.S. Michaels, H.J. Bixler, H.L. Fein, Gas transport in thermally conditioned linear polyethylene, Journal of Applied Physics, 35 (1964) 3165-3178.
[56] P.M. Hadgett, G. Goldbeck-Wood, A.H. Windle, Lattice modelling of penetrant diffusion through heterogeneous polymers, Polymer, 41 (2000) 6151-6160.
[57] F. Müller-Plathe, Towards a computational approach to penetrant diffusion in semicrystalline polymers, Chemical Physics Letters, 177 (1991) 527-535.
[58] F. Müller-Plathe, Molecular dynamics simulation of gas transport in amorphous polypropylene, The Journal of Chemical Physics, 96 (1992) 3200-3205.
[59] A. Mattozzi, P. Serralunga, M.S. Hedenqvist, U.W. Gedde, Mesoscale modelling of penetrant diffusion in computer-generated polyethylene spherulite-like structures, Polymer, 47 (2006) 5588-5595.

[60] A.S. Michaels, H.J. Bixler, Solubility of gases in polyethylene, Journal of Polymer Science, 50 (1961) 393-412.
[61] V. Compañ, L.F. Del Castillo, S.I. Hernández, M.M. López-González, E. Riande, Crystallinity effect on the gas transport in semicrystalline coextruded films based on linear low density polyethylene, Journal of Polymer Science Part B: Polymer Physics, 48 (2010) 634-642.
[62] R. Mani, R.P. Singh, S. Sivaram, J. Lacoste, Effect of UV irradiation on the structure of heterophasic ethylene-propylene copolymers, Polymer Journal, 26 (1994) 1132-1141.
[63] M. Elvira, P. Tiemblo, J.M. Gómez-Elvira, Changes in the crystalline phase during the thermo-oxidation of a metallocene isotactic polypropylene. A DSC study, Polymer Degradation and Stability, 83 (2004) 509-518.
[64] P. Tiemblo, J.M. Gómez-Elvira, S. García Beltrán, L. Matisova-Rychla, J. Rychly, Melting and α relaxation effects on the kinetics of polypropylene thermooxidation in the range 80-170°C, Macromolecules, 35 (2002) 5922-5926.
[65] S. Brückner, S.V. Meille, V. Petraccone, B. Pirozzi, Polymorphism in isotactic polypropylene, Progress in Polymer Science, 16 (1991) 361-404.
[66] J. Guisández, P. Tiemblo, J.M. Gómez-Elvira, Change of thermal and dynamic-mechanical behaviour of a metallocene isotactic polypropylene during low-temperature thermo-oxidation, Polymer Degradation and Stability, 87 (2005) 543-553.
[67] M.S. Rabello, J.R. White, Crystallization and melting behaviour of photodegraded polypropylene. II. Re-crystallization of degraded molecules, Polymer, 38 (1997) 6389-6399.
[68] S.A.S. Alariqi, A.P. Kumar, B.S.M. Rao, R.P. Singh, Effect of [gamma]-dose rate on crystallinity and morphological changes of [gamma]-sterilized biomedical polypropylene, Polymer Degradation and Stability, 94 (2009) 272-277.
[69] J.J. Janimak, S.Z.D. Cheng, A. Zhang, E.T. Hsieh, Isotacticity effect on crystallization and melting in polypropylene fractions: 3. Overall crystallization and melting behaviour, Polymer, 33 (1992) 728-735.
[70] V. Virkkunen, P. Laari, P. Pitkänen, F. Sundholm, Tacticity distribution of isotactic polypropylene prepared with heterogeneous Ziegler-Natta catalyst. 2. Application and analysis of SSA data for polypropylene, Polymer, 45 (2004) 4623-4631.
[71] V. Virkkunen, P. Laari, P. Pitkänen, F. Sundholm, Tacticity distribution of isotactic polypropylene prepared with heterogeneous Ziegler-Natta catalyst. 1. Fractionation of polypropylene, Polymer, 45 (2004) 3091-3098.
[72] R. Paukkeri, A. Lehtinen, Thermal behaviour of polypropylene fractions: 1. Influence of tacticity and molecular weight on crystallization and melting behaviour, Polymer, 34 (1993) 4075-4082.
[73] S. Qian, T. Igarashi, K.-H. Nitta, Influence of Thermo-degradation on the Crystallization Kinetics of Isotactic Polypropylene with a Beta Nucleating Agent, Journal of Macromolecular Science, Part B, 52 (2013) 48-64.
[74] J. Kang, J. Li, S. Chen, H. Peng, B. Wang, Y. Cao, H. Li, J. Chen, J. Gai, F. Yang, M. Xiang, Investigation of the crystallization behavior of isotactic polypropylene polymerized with different Ziegler-Natta catalysts, Journal of Applied Polymer Science, 129 (2013) 2663-2670.

PART 2/ PHOTOTHERMAL OXIDATION

Photooxydation du polypropylène [Summary in french]

1. Introduction

La théorie commune en cinétique chimique de l'oxydation considère qu'il existe un schéma général de l'oxydation, observé en thermooxydation (la température étant une grandeur intensive), auquel on ajoute des réactions supplémentaires décrivant l'amorçage extrinsèque, par exemple sous l'effet d'un rayonnement γ en radio-oxydation ou UV-visible en photo-oxydation [1, 2]. En se basant sur ce principe, on comprend mieux l'absolue nécessité de disposer d'un « cœur » thermique universel, i.e. décrivant le comportement en thermooxydation de l'intégralité de la famille des iPP, et fiable, i.e. établi de manière rigoureuse. On évite ainsi d'introduire, via la méthode de résolution inverse, un biais dans les paramètres photochimiques pour compenser un éventuel défaut d'ajustement du modèle de thermooxydation. En radio-oxydation, les photons γ de haute énergie sont absorbés indifféremment (sans sélectivité particulière) par les sites methynes et méthylène et la vitesse d'amorçage est directement proportionnelle au débit de dose [3]. Dans le cas de la photooxydation, les réactions d'amorçage extrinsèque consistent en la photolyse des espèces chromophores (aptes à absorber la lumière) et clivables dans les conditions d'exposition (c'est-à-dire présentant des liaisons dont l'énergie de dissociation est inférieure à celle apportée par les photons incidents). Il en résulte la génération de radicaux susceptibles d'induire une réaction d'oxydation en chaîne.

Pour exprimer la vitesse d'amorçage photolytique, plusieurs possibilités sont envisageables :

(1) Utiliser une loi semi-empirique ou des coefficients propres à chaque source lumineuse, éventuellement identifiée par résolution inverse [4].

(2) Proposer une loi heuristique de quantification de l'énergie lumineuse efficace pour une espèce chromophore exposée à une source lumineuse donnée. En définissant un critère objectif et comparable entre sources de différentes distributions spectrales et intensités, il est envisageable de comparer différentes sources lumineuses en vue d'optimiser les méthodologies d'essai. En l'occurrence, ce critère serait défini pour chaque espèce

photosensible et potentiellement clivable. Selon leur nature, il est possible d'induire des mécanismes supplémentaires responsables des coupures de chaînes et affectant ainsi les propriétés d'usage (notamment mécaniques et d'aspect). C'est cette seconde option qui a été choisie pour la présente étude.

Outre la sélectivité de la lumière UV-visible comparée aux rayonnements γ, la photooxydation des polyolefines présente une seconde difficulté, à savoir l'incertitude qui persiste quand à la nature exacte, la concentration (bien souvent très faible) et le « pouvoir amorceur » des défauts de structure. En effet, les polyoléfines n'absorbant pas dans le domaine du spectre solaire (λ>295 nm), seuls certains défauts de structure, non constitutifs du matériau polymère, peuvent constituer des sources d'amorçage dans les toutes premières étapes de l'oxydation. Le mode d'amorçage est donc doublement extrinsèque (en termes de rayonnement et de défauts de structure) contrairement à la radio-oxydation où les sites d'amorçage (absorbant l'énergie) sont les liaisons chimiques elles-mêmes dès le début de l'oxydation. En outre, l'activité, le « pouvoir amorceur » de ces différents défauts de strucure serait suceptibles de différer selon les différents types de vieillissement oxydant. En thermooxydation, l'activité globale des défauts extrinsèques est traduite par une concentration équivalente en hydroperoxydes $[POOH]_{0,}$ qui constitue alors un paramètre ajustable. Comment ces difficultés vont-elles se répercuter sur la démarche de détermination des paramètres cinétiques par résolution inverse, et en particulier, la valeur de $[POOH]_0$?

L'amorçage photolytique impose donc de prendre en compte deux sources additionnelles de complexité par rapport à la radio-oxydation : la sélectivité de l'absorption des photons et la méconnaissance des espèces photosensibles. Il y a donc un véritable enjeu sur la description du paramètre d'exposition « lumière ».

2. Introduction de l'effet de la lumière

D'après la première loi de la photochimie, seule la lumière qui est absorbée par une molécule peut induire une réaction photochimique. Il est donc nécessaire de définir une fonction sélective déterminant la part de l'énergie environnante, dispensée par la source lumineuse, qui va être

absorbée par une molécule chromophore. La collision efficace (inélastique) avec le photon engendre une transition électronique (généralement depuis la plus haute orbitale occupée HOMO vers la plus basse vacante LUMO) avec une dispersion due aux différents états vibrationnels. La distribution de probabilités qu'une telle transition se produise est traduite par le coefficient d'extinction molaire ε (en $L.mol^{-1}.cm^{-1}$). La quantité d'énergie absorbée peut donc être calculée à partir du recouvrement du spectre de la source lumineuse et de la distribution spectrale du coefficient d'extinction molaire.

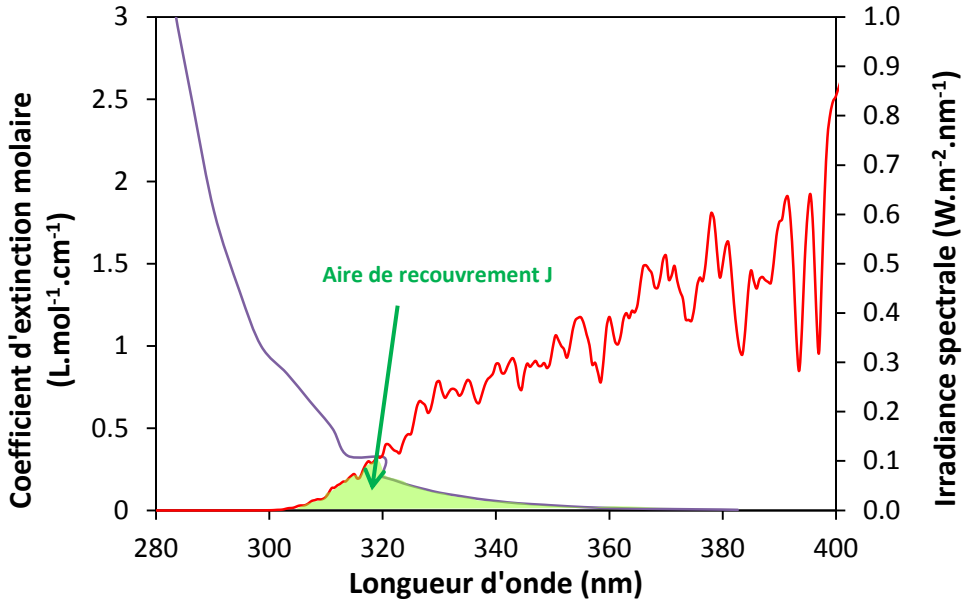

Figure R1: Recouvrement du spectre d'émission d'un spectre de lampe Xenon en WeatherO'Meter et du spectre d'absorption du ter-butyl hydroperoxyde

La vitesse d'amorçage photolytique s'exprime alors comme la fraction efficace, matérialisée par le rendement quantique, de l'énergie absorbée pour dissocier la liaison chimique et amorcer la réaction d'oxydation en générant un radical:

$$\left.\frac{d[X_j]}{dt}\right|^{photolysis} = -\Phi(\lambda)_X \times I_{abs_v} = -\Phi(\lambda)_X \cdot [X_j] \cdot J_X \qquad \textbf{Eq. R1}$$

Avec $[X_j]$ *la concentration en espèce* X_j *(en* $mol.L^{-1}$*),*

$\Phi(\lambda)$ *le rendement quantique de photolyse (en* $mol.Einstein^{-1}$*), et*

$I_{abs.v}$ *l'intensité lumineuse (énergie) volumique absorbée (en* $Einstein.L^{-1}.s^{-1}$*) qui s'exprime elle-même comme le produit de la concentration en chromophore* $[X_j]$ *(en* $mol.L^{-1}$*) et de l'intégrale de recouvrement spectral J (en* $Einstein.mol^{-1}.s^{-1}$*)*

$$J_X = \frac{I_{abs_p}}{[X_j]} = \int_{\lambda_{min}}^{\lambda_{max}} \frac{\ln(10)}{10} \frac{E(\lambda)}{N_a} \frac{\lambda}{hc} \varepsilon_X(\lambda)\ d\lambda \quad \textbf{Eq. R2}$$

avec E(λ) l'irradiance lumineuse de la source filtrée (en $W.m^{-2}.nm^{-1}$),
N_a la constante d'Avogadro,
h la constante de Planck égale à $6.623 \cdot 10^{-34}$ J.s,
c la célérité de la lumière (en $m.s^{-1}$), λ la longueur d'onde (en m),
$\varepsilon_X(\lambda)$ le coefficient d'extinction molaire du chromophore (en $L.mol^{-1}.cm^{-1}$).

On remarquera que l'intégrale de recouvrement spectral a été définie comme une grandeur indépendante du mode d'accumulation des produits chromophores dans la matrice. De cette manière, on différencie en quelque sorte les deux problématiques à savoir la fonction de sélectivité (et donc le pouvoir absorbant du chromophore) et l'incertitude sur sa nature et sa concentration. Cette quantité apparait donc comme un critère pertinent pour décrire la sévérité des conditions d'exposition lumineuse et présente une dimension adéquate pour être introduite dans les modèles analytiques et numériques. Notons ainsi que ΦJ est homogène à la constante cinétique d'une étape élémentaire unimoléculaire (s^{-1}). La validation de ce critère a été effectuée au moyen de modèles analytiques simples (loi de réciprocité ou Schwarzschild et modèle cinétique détaillé ci-dessous) appliqués aux résultats de notre campagne expérimentale menée sur iPP non stabilisé dans des enceintes SEPAP (source à vapeur de mercure) pour plusieurs intensités et avec un point de contrôle en WeatherO'Meter (source xénon simulant le spectre solaire). Pour chacun des modèles analytiques utilisés, l'introduction du critère énergétique basé sur le recouvrement spectral permet de décrire l'évolution des durées de vie de matériaux iPP non stabilisés au moyen de lois communes aux différentes sources lumineuses et comparables à celle obtenue sur des séries d'essais provenant de la litérature menées avec un seul type de source.

2.1. **Modèle analytique**

Les modèles cinétiques décrivent l'évolution chimique du système par un système d'équations différentielles couplées. Sous couvert qu'il soit suffisamment simple et/ou d'hypothèses simplificatrices, il est possible d'établir des relations analytiques simples entre les indicateurs de

suivi de l'oxydation (période d'induction, vitesse d'oxydation), sur lesquels sont généralement définis les critères de fin de vie, et les conditions d'exposition (contraintes environnementales). Dans le modèle analytique considéré ici, on suppose (i) l'existence d'une unique (i.e. prépondérante) espèce chromophore et clivable, à savoir les hydroperoxydes, et (ii) l'unimolécularité de la décomposition des hydroperoxydes par voie thermique et photochimique. La période d'induction s'exprime alors en fonction des deux quantités homogènes à des constantes cinétiques élémentaires qui décrivent les vitesses d'amorçage selon les deux voies en compétition:

$$t_{ind} = \frac{C}{\Phi J + k_{1u}{}^{0} \exp(\frac{-E_{a1u}}{RT})} \qquad \textbf{Eq. R3}$$

Dans cette loi, C représente une constante propre à l'espèce chimique titrée (C = 3 pour les espèces carbonylées et C = 0.383 pour les hydroperoxydes),
Φ et J sont respectivement le rendement quantique de photolyse et l'intégrale de recouvrement spectral relatifs aux hydroperoxydes, $k_{1u}{}^{0}$ et Ea_{1u} sont respectivement le facteur préexponentiel et l'énergie d'activation de leur décomposition unimoléculaire.

La résolution inverse du problème à partir de nos résultats expérimentaux a permis d'identifier un rendement de photolyse des hydroperoxydes $\Phi_{POOH} = 8$, dont la valeur est évidemment dénuée de sens physique car ne devant excéder 1. Il est bon de préciser que la démarche de calculer l'énergie absorbée pour exprimer la vitesse de photolyse a déjà été employée par Carlsson et Wiles dans les années 1970. Leur résolution inverse à partir d'essais de photolyse en atmosphère inerte avait conduit à une valeur de $\Phi_{POOH} = 4$ et constitue donc notre valeur cible. Celle-ci, déjà trop haute par rapport à la théorie, avait été attribuée à la mésestimation du pouvoir chromophore des espèces photosensibles macromoléculaires à partir de composés modèles. L'écart entre la valeur constatée et la valeur cible illustre les effets des hypothèses simplificatrices et les limites heuristiques des modèles analytiques. Ces derniers présentent plutôt l'intérêt de décrire des phénomènes complexes via une loi très générale et facilitent la constitution d'outils méthodologiques (voir abaque en figure R2).

L'une des retombées pratiques de l'introduction de notre critère a été d'estimer la compétion des deux types d'amorçage, thermique et photochimique, pour différentes conditions d'essais

accélérés et sur site. La prépondérance de l'un des types d'amorçage est indiquée au moyen de courbes dites de représentativité. Dans le cas de l'iPP non stabilisé et non chargé, l'équilibre entre l'amorçage thermique et photochimique est plus représentatif des conditions naturelles dans la méthode SEPAP que dans la méthode WeatherO'Meter (sans aspersion d'eau), dont la source est pourtant de distribution spectrale très similaire à celle du soleil. Notons que la connaissance des conditions d'expositions est sujette à incertitude, notamment la température de l'échantillon, sensible non seulement aux cycles jour/nuit et d'aspersion d'eau mais aussi à la charge pigmentaire du matériau, etc.

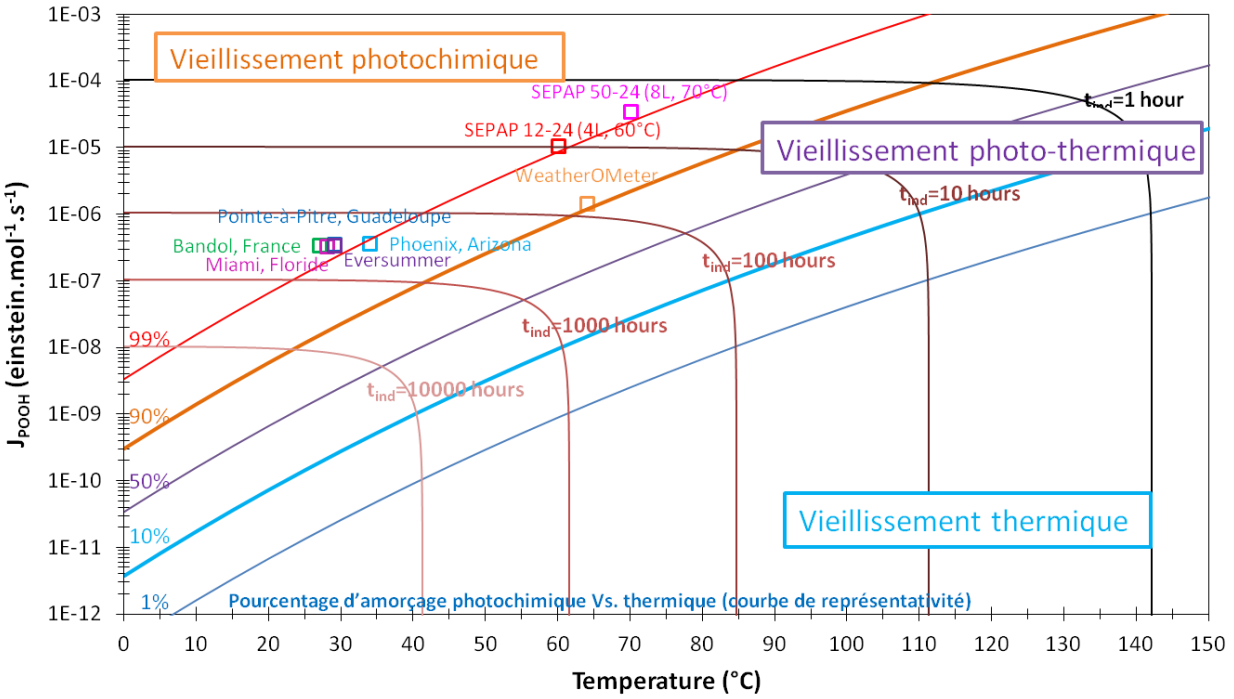

Figure R2: Abaque décrivant la compétition de l'amorçage thermique et photochimique de l'oxydation du polypropylène (iPP non stabilisé) en fonction des conditions d'exposition. Différentes méthodes Renault et sites de vieillissements naturels ont été positionnés. Les courbes de représentativité donnent les pourcentages d'amorçage de chaque type. Les courbes d'iso-durée de vie permettent d'apprécier les facteurs d'accélération entre méthodes.

2.2. **Modèle numérique**

L'apport des modèles numériques réside quant à lui dans:

(i) la précision de la résolution, sans recourir à des hypothèses simplificatrices: il est alors préférable de simuler directement la cinétique d'oxydation du matériau au lieu de se focaliser sur des indicateurs de suivi.

(ii) la diversité des phénomènes que l'on peut prendre en compte tels que l'existence de multiples espèces initiatrices (notamment les hydroperoxydes et les cétones), les phénomènes de transferts d'énergie assimilés à des processus photophysiques termoléculaires ou encore les couplages multiphysiques avec la diffusion des espèces réactives et l'atténuation de la lumière dans l'épaisseur du matériau).

Il est alors possible de bénéficier au mieux de l'approche de cinétique formelle pour tester la cohérence de nombreux scénarii et écarter ceux conduidant à des contradictions ou incompatibles avec les résultats expérimentaux. Les modèles numériques ont ainsi pu être éprouvés dans des conditions très différentes en température (40-80°C) et en irradiation (avec des intensités absorbées s'étalant sur plus de deux décades) en se basant sur des variables à la fois chimiques (hydroperoxydes et produits carbonylés en tant que produits d'oxydation primaires et secondaires) et macromoléculaires (masses moléculaires en poids et en nombre consécutives aux coupures de chaînes). En figure R3, les résultats sont représentés dans les conditions correspondant aux méthodes d'essai normalisées Renault c'est à dire la SEPAP 12-24 à 60°C et le WeatherO'Meter à 64°C (i.e. BPT = 70°C).

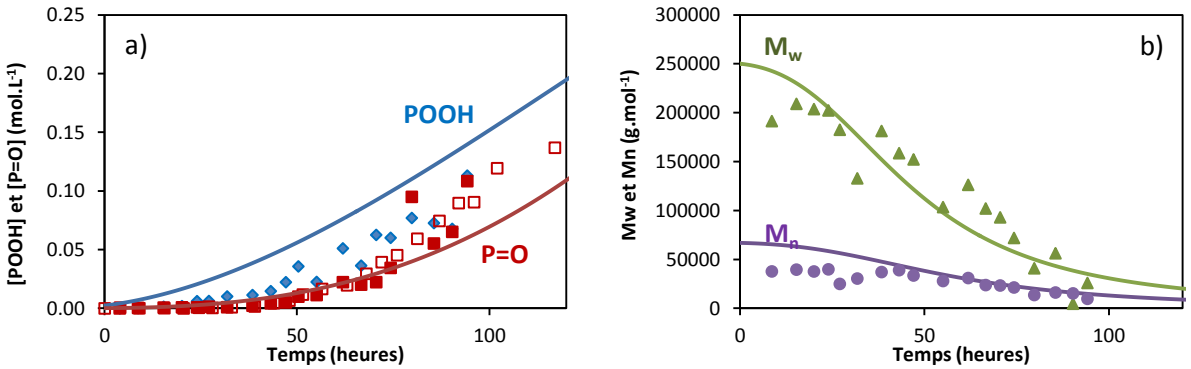

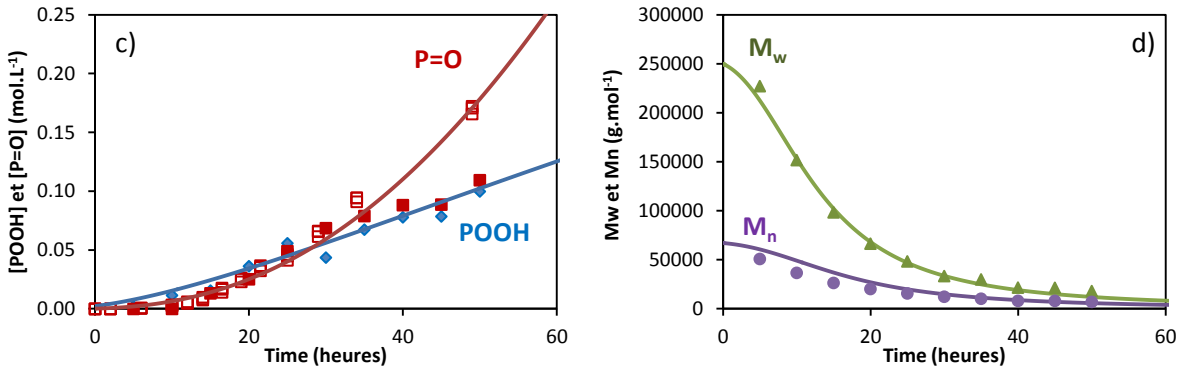

Figure R3: Simulations des cinétiques de degradation de l'iPP and Weather O'Meter à 64°C (figures a et b) et en SEPAP 12-24 à 60°C (figures c et d). Les lignes continues et les symboles représentent respectivement le modèle et les résultats expérimentaux: ◆ hydroperoxydes; ■□ produits carbonylés; ▲masses moléculaires en poids et ●en nombre.

Il a ainsi été possible, via une petite étude paramétrique, de mettre en évidence la contribution négligeable des réactions de Norrish sur les cétones à l'amorçage photochimique de l'oxydation en comparaison de la photolyse des hydroperoxydes.

Les valeurs de rendements quantiques de photolyse des hydroperoxydes dans les différentes conditions d'essai (dont 11 essais issus de notre campagne et 3 essais, menés à plus faible température, tirés de la littérature) sont représentées en figure R4. De manière générale, on remarquera des valeurs de rendement égales à 4 ± 1 dans la plupart de la gamme d'intensités lumineuses absorbées, en accord avec les valeurs cibles héritées de Carlsson et Wiles [5, 6]. Une tendance à la baisse avec l'irradiance se dessine toutefois, conduisant à limiter la validité du modèle à des intensités inférieures à $2 \cdot 10^{-5}$ Einstein.mol^{-1}.s^{-1}. Au-delà, les valeurs plus faibles de rendements quantiques sont attribuées à l'apparition d'excitations multiphotoniques ou de processus photophysiques termoléculaires (impliquant 2 molécules et de la lumière) tels que les transferts d'énergie ou l'absorption par des complexes, lesquels sont favorisés par les hautes intensités. On soupçonne plus particulièrement les phénomènes de photosensibilisation des hydroperoxydes par les résidus catalytiques ou encore la décomposition d'hydroperoxydes associés en séquences. Néanmoins, le coût pour prendre en compte ces phénomènes et améliorer le modèle est excessif au regard des difficultés que cela engendrerait.

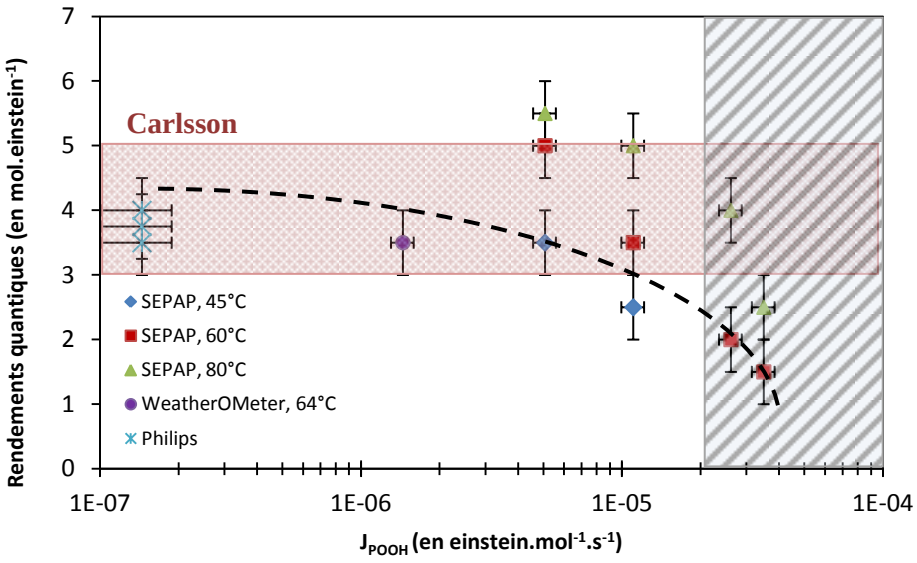

Figure R4: Evolution du rendement quantique de photolyse des hydroperoxydes avec l'intensité absorbée. Le domaine colorié en rose correspond à la gamme de valeurs trouvée par Carlsson et Wiles. Le domaine hachuré correspond à des intensités absorbées où le modèle n'est plus considéré comme valide.

3. Le cas de la pièce épaisse : couplage avec le transport des réactifs migrants

Pour étendre le modèle de photooxydation à la pièce épaisse, il est nécessaire d'introduire le transport des espèces réactives en particulier (i) la diffusion du dioxygène, de manière analogue au thermique, et (ii) l'atténuation de la lumière dans l'épaisseur du matériau. En effet, le profil de photooxydation ou photo-dégradation résulte du couplage de chacun de ces profils. Comme pour la thermooxydation, la diffusion du dioxygène est décrite par une loi de Fick dont les paramètres de transport initiaux sont donnés par les mesures de perméamétrie. L'atténuation de la lumière est, quant-à-elle, décrite par un modèle à un flux dont le coefficient d'atténuation est décomposé en :

(i) un coefficient d'absorption linéique $\alpha(\lambda)$ supposé fixe dans le temps et sensé refléter l'opacité du matériau.

(ii) Une composante variable correspondant à l'absorption de la lumière par les espèces chromophores susceptibles de réagir chimiquement (y compris par photolyse) ou soumises aux phénomènes de perte physique (évaporation, extraction, lessivage,

etc…). Cette composante est négligeable dans le cas de films de polypropylène non stabilisé mais trouve son intérêt dans le cas de matériaux additivés notamment par des stabilisants anti-UV.

Pour pouvoir être couplée avec le système d'équations différentielles ordinaires dérivées dans le temps, l'équation différentielle ordinaire dérivée dans l'espace est transformée en une équation algébrique par différence finie. Quelle que soit la longueur d'onde λ, il est possible d'écrire l'atténuation de la lumière entre les pas z et z+dz :

$$E_{z+dz}(\lambda) = E_z(\lambda)\left[1 - \left(\alpha(\lambda) + \ln(10) \sum_{\substack{j \\ chromophoric \\ species\ X_j}} \varepsilon_j(\lambda)\,[X_j]\right)\Delta z\right] \qquad \textbf{Eq. R4}$$

Avec $E_z(\lambda)$ l'irradiance spectrale (en $W.m^{-2}.nm^{-1}$) à une prodondeur z (en m) de la surface irradiée (notons que E est un vecteur dont les valeurs sont données à différentes longueurs d'onde), $\alpha(\lambda)$ le coefficient d'absorption linéique (en m^{-1}), $\varepsilon_j(\lambda)$ la distribution spectrale du coefficient d'extinction molaire (en $L.mol^{-1}.m^{-1}$) et $[X_j]$ *la concentration en espèce chromophore j (en $mol.L^{-1}$).*

Comme précédemment, le paramètre d'atténuation initial est obtenu à partir de la mesure des propriétés optiques globales (transmittance, réflectance, absorbance) d'un échantillon de 3 mm.
De manière générale, les profils de photooxydation sont de qualités très variables et le recalage du modèle à partir des résultats expérimentaux est difficile. Dans plusieurs cas, on obtient par résolution inverse des rendements quantiques supérieurs d'un facteur 2 à 3 par rapport aux valeurs identifiées sur film mince. Cela laisse penser que l'énergie effectivement absorbée par le matériau est sous-estimée.
On notera ainsi plusieurs sources d'erreur ou de variabilité, au premier rang desquelles **l'incertitude sur les conditions d'expositions** tant en intensité lumineuse qu'en température. En effet, des erreurs sur les énergies absorbées par le matériau peuvent résulter d'incertitudes sur les intensités lumineuses ou les géométries d'irradiance, par exemple à cause de, l'existence de réflexion spéculaire en surface de l'échantillon ou de réflexions secondaires induisant une exposition sur le revers de l'échantillon. Concernant la température, les sources d'erreur sont

encore plus nombreuses ; bien souvent, l'irradiation dans l'infrarouge de l'échantillon peut induire un échauffement de l'échantillon dont la température est alors supérieure à la température de la chambre mais inférieure à celle du panneau noir. Aussi, les problématiques de régulation de température, éventuellement du fait des cycles d'éclairement et surtout d'aspersion d'eau empêche bien souvent de connaître précisément la température en surface de l'échantillon. Aussi, dans le cas de programme cycliques à fréquence élevée, les problématiques de transfert thermique dans les pièces épaisses ne sont probablement plus négligeables.

Une deuxième source de perturbation résulte des **variations de morphologie**, souvent méconnues, dans l'épaisseur du matériau. En particulier, les problématiques de couche de « peau » amorphes en surface d'une plaque injectée peuvent conduire à des rendements quantiques apparents deux fois plus importants que dans un matériau cristallin à 50% par exemple car seule la fraction amorphe peut être oxydée. D'autre part, les caractéristiques morphologiques sont présumées affecter à la fois les propriétés optiques et les propriétés de transport du dioxygène dans le matériau.

De même que les variations spatiales de morphologies et de propriétés, il faut prendre en compte les **variations temporelles de ces propriétés en particulier celles induites par le vieillissement du matériau**. L'altération des propriétés de transport du dioxygène, qui avait été particulièrement mise en évidence par résolution inverse en thermooxydation, se confirme en photooxydation. L'évolution temporelle du coefficient de perméabilité avec le degré d'oxydation en surface a été représentée en cumulant les données obtenues initialement par perméamétrie et les données apparentes obtenues par résolution inverse en thermooxydation et en photooxydation jusqu'à dessiner une tendance très claire à la baisse (cf. figure 12 in chapitre XIII), du moins jusqu'à des degrès d'oxydation modérés. La différentiation d'une éventuelle altération des propriétés optiques, dont les effets sur le profil sont présumés moins marqués que pour les propriétés de transport, s'avère toutefois difficile par résolution inverse compte tenu des incertitudes sur les données expérimentales des profils. Aussi, l'intégralité des différences constatées sont attribuées par défaut aux propriétés de transport. Pour des d'avancements de l'oxydation plus élevés (typiquement à partir de concentrations en carbonyles de l'ordre de 0.1 à 0.2 $mol.L^{-1}$, les modifications consécutives à la dégradation du matériau peuvent générer des contraintes résiduelles conduisant à la génération de fissures modifiant ainsi la profondeur du front

d'alimentation en oxygène. Ce phénomène modifie en profondeur la forme des profils d'oxydation faisant apparaître un épaulement similaire à celui généré dans le cas d'échantillon vieillis en excès d'oxygène. Pour décrire ce phénomène, il est envisageable, bien que délicat, d'introduire une cinétique de propagation du front d'alimentation en O_2. Néanmoins, le modèle heuristique proposé présente l'avantage d'éviter de générer ce type de profils avec des paramètres irréalistes à contrario de certains modèles analytiques.

Enfin, si la loi de Fick est adaptée pour rendre compte de la diffusion des gaz dans les polymères, un modèle à un flux relativement simple a été considéré en première approche pour décrire l'atténuation de la lumière dans l'épaisseur du matériau. Toutefois, ce type de loi ne permet pas de rendre compte des phénomènes de réflexions multiples que l'on pourrait rencontrer dans des semi-cristallins présentant une certaine turbidité par essence, voire dans des matériaux pigmentés ou polyphasiques. Elles sont également limitées dans leur facultées à rendre compte des géométries d'exposition lumineuses complexes, ne permettant pas de rendre compte d'exposition secondaires par exemple. Dans le cas présent, ce qui nous intéresse, c'est la fraction des photons qui est rétro-diffusée, ce qui implique une augmentation de la longueur du chemin optique réel. Or, la probabilité de rencontre entre un photon et une espèce chromophore est directement proportionnelle au chemin optique. Cela a pour conséquence l'augmentation de l'énergie effectivement absorbée par les chromophores et donc un gain dans le rendement quantique apparent déterminé par résolution inverse. En effet, cette fraction rétrodiffusée va être d'autant plus grande que l'échantillon est épais et va donc marquer la différence entre le film et l'échantillon épais.

Or, les expérimentations ont révélé de sérieux indices de l'existence de cette diffraction multiple ou rétrodiffusion sur les plaques puisque la réflectance (essentiellement diffuse) passe de 10 % pour un film à 15% pour une plaque (3 mm) d'iPP, et de 10% pour un film à 40% pour une plaque (3 mm) de TPO. Ces phénomènes ont été étudiés dans la partie discussions générale. Ils ont été modélisés dans le cas d'un matériau non vieillis au moyen de modèles de transfert radiatif simples de type Kubelka-Munk (avec la correction de Saunderson selon les conditions de réfraction en surface). Le modèle à 2 flux a également été modifié pour rendre compte de l'effet de la distribution spectrale de sources polychromatiques, en l'occurrence de lampe xenon et à vapeur de mercure. L'importance de ces phénomènes a été discutée en fonction de la turbidité du matériau.

Références

[1] A.V. Tobolsky, Oxidative degradation of polymeric material, Discussions of the Faraday Society, 2 (1947) 384-388.
[2] A.V. Tobolsky, D.J. Metz, R.B. Mesrobian, Low temperature autoxidation of hydrocarbons: The phenomenon of maximum rates, Journal of the American Chemical Society, 72 (1950) 1942-1952.
[3] N. Khelidj, X. Colin, L. Audouin, J. Verdu, C. Monchy-Leroy, V. Prunier, Oxidation of polyethylene under irradiation at low temperature and low dose rate. Part I. The case of "pure" radiochemical initiation, Polymer Degradation and Stability, 91 (2006) 1593-1597.
[4] S.r. Kiil, Model-based analysis of photoinitiated coating degradation under artificial exposure conditions, Journal of Coatings Technology and Research, 9 375-398.
[5] D.J. Carlsson, D.M. Wiles, The photodegradation of Polypropylene Films. III. Photolysis of polypropylene hydroperoxydes, Macromolecules, 2 (1969) 597-606.
[6] D.J. Carlsson, D.M. Wiles, The Photodegradation of Polypropylene Films. II. Photolysis of Ketonic Oxidation Products, Macromolecules, 2 (1969) 587-597.

CHAPTER VI. Influence of temperature, UV-light wavelength and intensity on polypropylene photothermal oxidation

Alexandre François-Heude[a,b 4], Emmanuel Richaud[a], Eric Desnoux[b], Xavier Colin[a]
[a]PIMM Laboratory, CNRS UMR 8006, Arts et Metiers ParisTech, Paris, France
[b]Renault, DETC-A, Guyancourt, France

Abstract

A criterion based on the energy absorbed by photosensitive species was proposed to describe the contribution of UV-light to the initiation of the polypropylene photothermal oxidation whatever the light source. The calculation of this energy was performed using the widely accepted quantum theory. The criterion was then introduced in two different types of analytical models commonly used to describe the combined effects of UV light and temperature on induction time, namely: the reciprocity law and kinetic model. The limitations of both types of analytical models were then investigated: the latter, derived from a realistic mechanistic scheme, was found to be much more relevant than the former, which is presumably valid in a restricted range of light intensities, essentially due to its empirical origin.

Keywords

Polypropylene Photodegradation; Lifetime Prediction; Reciprocity Law; Actinometry; Oxidation Kinetics

1. Introduction

It is well-known that polypropylene (PP) oxidation depends on both light and temperature in current outdoor aging conditions. The influence of temperature, commonly described with an

[4] Corresponding author : Email: Alexandre.FRANCOIS-HEUDE@ensam.eu
Tel/ Fax: +33 1 44 24 64 13/ +33 1 44 24 63 82

Arrhenius law, was widely investigated in the case of thermal oxidation, but rarely in the case of photothermal oxidation [1, 2]. The quantitative effects of the UV light intensity on the photodegradation were studied for various type of polymers including coatings [3, 4], polycarbonates [5-7], poly(vinyl chloride) [8] and also polyolefins [2, 9-14]. Most of these studies were based on empirical reciprocity laws (usually applied to the induction period or time to embrittlement), which have been recently reviewed by Martin et al. [15] for a wide range of materials including polymeric ones. For polypropylene, the dependence of the induction period with the UV-light irradiance was I^n with n = -1/2 for unstabilized PP using filtered high pressure mercury [12] or fluorescent lamps [13]. Both references also reported values of n up to -1 for stabilized PP depending on the type of stabilizer and its concentration [12, 13]. However, Philippart [11] also found a dependence of the induction time with the inverse of irradiance for only weakly stabilized PP using filtered medium pressure mercury lamps. The steady-state oxidation rate was found to vary with the square root of the irradiance in agreement with the analytical solution of the basic auto-oxidation scheme [9, 12, 16] Cumulated exposure energy is usually chosen as the key variable to follow the polymer degradation because it is very convenient for natural weathering where the exposure parameters undergo temporary fluctuations such as daily/seasonal temperature or UV light variations.

Nonetheless, not only the light intensity but also its wavelength and, in particular, the light source spectral distribution must be considered since specific spectral sensitivities were evidenced for various polymers (see reviews [17, 18]), including polypropylene [19-21]. This notion of polymer light sensitivity can be correlated with the first law of photochemistry attesting that only absorbed quanta can initiate reactions, if they have a sufficient energy to dissociate a chemical bond [22, 23].

As an example, the initiation rate by hydroperoxides photolysis can be written as:

$$v_{POOH} = \frac{d[POOH]}{dt} = -\Phi(\lambda)_{POOH} \times I_{abs_v} \quad \textbf{Eq. 1}$$

with [POOH] the concentration in hydroperoxides (in mol.L^{-1}),

$\Phi(\lambda)_{POOH}$ the quantum yield of photolysis (in mol.Einstein^{-1}, dimensionless)

and $I_{abs.v}$ the volumic absorbed energy (in Einstein.L^{-1}.s^{-1})

The quantum yield -or quantum efficiency- Φ represents the probability that a quantum absorbed by a molecule causes its decomposition. The quantum yield is defined as:

$$\Phi = \frac{Number\ of\ molecules\ X\ having\ reacted\ per\ time\ unit}{Number\ of\ photons\ absorbed\ per\ time\ unit} = \frac{dX/dt}{dn_p/dt} = \frac{d[X]/dt}{I_{abs_v}} \qquad \textbf{Eq. 2}$$

with [X] the concentration of molecule X (in mol.L^{-1}),
n_p the number of quanta,
and $I_{abs.v}$ the volumic absorbed energy (in Einstein.L^{-1}.s^{-1}).

However, molecules only absorb photons with a quantum of energy satisfying the authorized electronic transitions, i.e. if the incident photon presents a quantum of energy equal to the difference between a vibrational level of the excited state and the ground state. The probability of occurrence of this phenomenon is taken into account through the molar extinction coefficient –or cross section– in the Beer Lambert's law. It is thus necessary to consider a coupling between the emission spectrum of the polychromatic source and the absorption spectra of the different chromophoric species. Martin and Lechner [24, 25] proposed a formalism for the light dependence and chosed the dose as relevant criterion:

$$D = \int_0^t D_{eff}(t)\, dt = \iint_{\lambda_{min}}^{\lambda_{max}} E(\lambda) \left(1 - e^{-\ln(10) * A(\lambda)}\right) \Phi(\lambda)\, d\lambda\ dt \qquad \textbf{Eq. 3}$$

with D the dose, i.e. the amount of energy absorbed by the chromophoric species during a duration t (in J.m^{-2}), D_{eff}(t) the absorbed irradiance (in W.m^{-2}), Φ(λ) the spectral quantum yield, A(λ) the absorbance, and E(λ) the spectral irradiance (in W.m^{-2}.nm^{-1}).

Such an approach was previously applied for lifetime prediction of coatings [26-28]. Yet, the dose calculation requires the knowledge of the concentration of chromophoric species along the course of degradation. Then, focusing on the dose rate appears to be more convenient. Indeed, the absorbed energy by a photosensitive species (analogous to the dose rate D_{eff}(t)) can be explicated locally. As an example, in the case of hydroperoxides, it can be written:

$$I_{abs_v} = \int_{\lambda_{min}}^{\lambda_{max}} \frac{\ln(10)}{10} \frac{E(\lambda)}{N_a} \frac{\lambda}{hc} \frac{\varepsilon(\lambda)_{POOH} \Delta z\,[POOH]}{\Delta z} d\lambda \qquad \textbf{Eq. 4}$$

With E(λ) the spectral irradiance of the light source including filters (in W.m^{-2}.nm^{-1}),
N_a the Avogadro's constant,
h the Planck constant equal to 6.623·10^{-34} J.s,
c the light celerity (in m.s^{-1}), λ the wavelength (in m),
ε(λ) $_{POOH}$the spectral distribution of the molar extinction coefficient (in L.mol^{-1}.cm^{-1}),
[POOH] the hydroperoxide concentration (in mol.L^{-1}),
and Δz the sample thickness (in m).

In order to suppress the concentration dependence, we decide to calculate the spectral overlap integral (or so-called in a shortened form, "overlap function") J_{POOH} (in Einstein.mol^{-1}.s^{-1}), chosen here as the relevant criterion to describe oxidation, and defined as:

$$J_{POOH} = \frac{I_{abs_v}}{[POOH]} = \int_{\lambda_{min}}^{\lambda_{max}} \frac{\ln(10)}{10} \frac{E_\lambda}{N_a} \frac{\lambda}{hc} \varepsilon(\lambda)_{POOH}\, d\lambda \qquad \textbf{Eq. 5}$$

Provided that the quantum yield is a constant in the whole spectral range –i.e. its spectral distribution can be neglected–, the absorbed energy appears as the relevant criterion controlling the oxidation kinetics. Such a hypothesis is not unrealistic considering that the efficient wavelength range is restricted to few decades of nanometers in current photochemical aging conditions (bandwidth of the molar absorptivity multiplied by the bandwidth of the light source, usually filtered below 300 nm).

Such an approach was already used by Carlsson and Wiles in order to calculate the quantum yields of ketone [29] –according to Norrish I and II– and hydroperoxide [30] photolysis by an inverse method. In this article, we will start from these theoretical concepts to tentatively explain the oxidation behavior of PP under the combined effects of temperature and UV light, regardless the type of the UV light source under consideration.

2. Experimental part

2.1. Materials

The reference material was an isotactic homo-polypropylene injection molding grade (Mw = 250 $kg.mol^{-1}$, Mn = 67 $kg.mol^{-1}$) supplied by Aldrich. Thin films of 80 µm and 135 µm were processed by compression molding and then purified from their antioxidants in Soxhlet with dichloromethane for 48 hours prior to aging experiments. The polymer was checked to be unstabilized with an Oxidation Induction Time of 27 ± 3 min at 140°C in a pure oxygen flow. The crystallinity was calculated equal to 45 ± 3 wt% from the melting enthalpy measured by DSC in a TA Q1000 device, taking a melting enthalpy of ΔH_m^0 = 209 $J.g^{-1}$ for crystalline lamellae.

2.2. Light and/or thermal exposure

In order to decouple the light effects from the thermal ones, PP films were exposed under different UV light intensities and temperatures, always in dry conditions. Photothermal aging experiments were mostly performed on films of 80 µm thickness in a series of SEPAP devices equipped with 80 W medium pressure arc mercury lamps having a borosilicate filter. To vary the light intensity, the number of lamps was changed from 2 to 4 lamps in a SEPAP 12-24 device, and from 6 to 8 lamps in a SEPAP 50-24 device. Both light intensity and emission spectrum were measured using respectively a IL390C radiometer in the 295-415 nm range and a Avantes spectro-radiometer (AvaSpec 2048x14-USB2, resolution 0.7 nm) in the 250-750 nm range. Temperature was fixed at 45°C, 60°C or 80°C according to the apparatus specifications and directly monitored on sample surfaces using a thermo-button temperature logger. A photothermal aging test was also performed on films of 135 µm thickness in a WeatherO'Meter device (WOM), equipped with a Xenon Lamp and Borosilicate S/S filters. Black Panel (BPT) and chamber (~ White Panel Temperature) temperatures were respectively fixed at 70°C and 55°C. The temperature of the sample was found to be intermediary at 64°C, whereas the irradiance at 340 nm was measured at 0.46 $W.m^{-2}.nm^{-1}$, without water spraying. The thermal oxidation (in the absence of light) was also investigated in air-ventilated ovens for temperatures ranging from 60°C to 140°C.

2.3. Spectrophotometry measurements

Polypropylene oxidation was monitored using the carbonyl peak centered at 1713 cm^{-1} with a FTIR Nicolet 510 FTIR-spectrophotometer. All optical densities were normalized by the film thickness and a global carbonyl concentration was calculated through the classical Beer-Lambert's law using a molar extinction coefficient of 300 $L.mol^{-1}.cm^{-1}$.

3. Results and discussion

3.1. Impact of exposure conditions on lifetime

As shown in figure 1, the results were reproducible for all the tests in SEPAP. A great attention was paid to the temperature regulation which was shown to significantly affect the quality of the results. Indeed, when periodically removing the films from UV chambers for monitoring the course of oxidation, a certain time which depends on the exposure conditions was required to stabilize the temperature at the sample surface. This is due to the heating induced by the irradiation although minimized in SEPAP devices with low infrared emissions. Thanks to the monitoring of the sample temperature, these durations were subtracted to the global duration spent by samples in the UV chambers to deduce the effective duration at the target temperature.

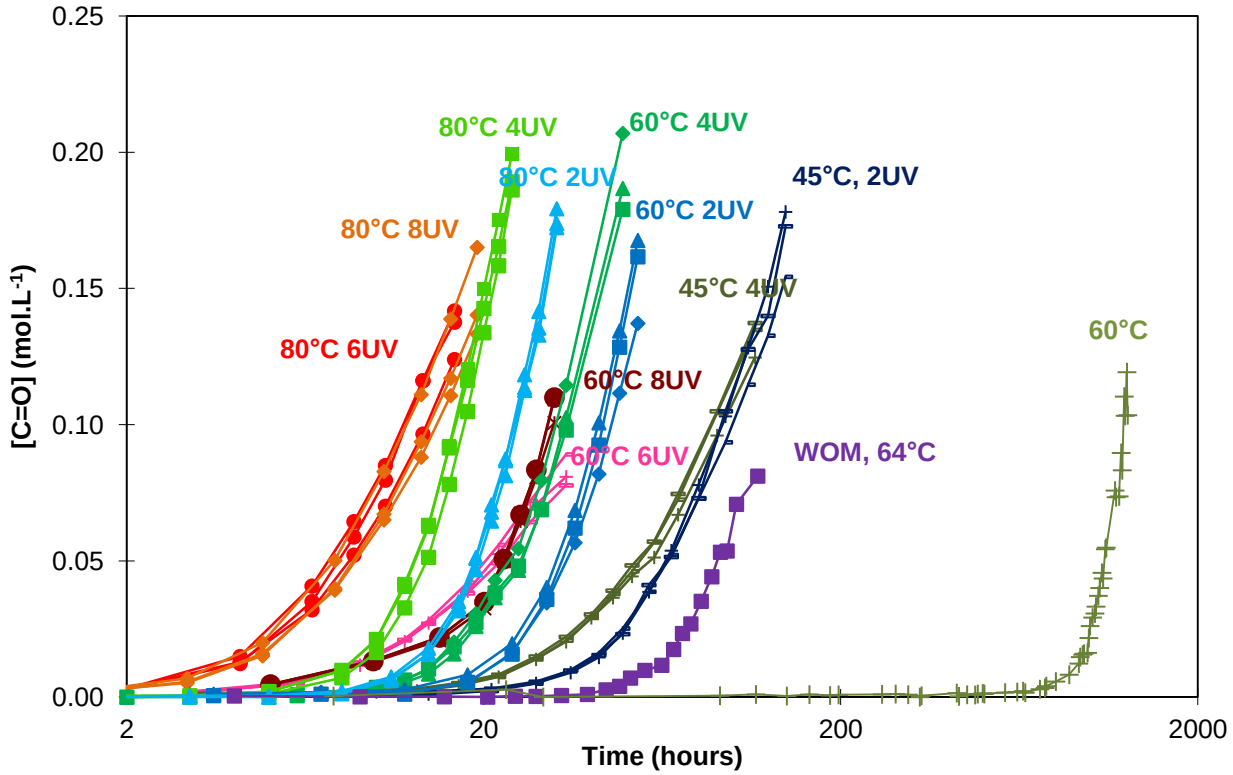

Figure 1: Change in the carbonyl concentration during thermal (at 60°C) and photo-thermal oxidation of polypropylene (The temperature and number of UV lamps are indicated for test in SEPAP; the test in WeatherOMeter is denoted WOM)

To describe the effect of light on polypropylene photooxidation, it is conventionnal to consider as key variable the irradiance between 300 and 400 nm which roughly apply to the range of polypropylene sensitivity under sunlight –or equivalent artificial light sources- exposure. Considering the irradiances of our tests in WeatherO'Meter (WOM) and in SEPAP with two lamps (2 UV-lamps) respectively equal to 55 and 38 $W.m^{-2}$ (at close temperatures) the oxidation induction time of the former would be lower than the latter, but the opposite trend is observed. The theory previously explained suggests that a fine description and quantification of the efficient energy to trigger oxidation, i.e. the absorbed energy, would explain this phenomenon. Among all the photosensitive species, two were reported to be particularly critical in the case of polypropylene oxidation: hydroperoxides and ketones [29, 31].

3.2. Cross sections of photosensitive species and calculation of the overlap function

Spectral distribution of the molar extinction coefficient –also called cross section– was compiled from literature for peroxide (figure 2) and ketone (figure 3) type's model compounds.

Tert-butyl hydroperoxide in hexane solution was chosen as representative of polypropylene hydroperoxides. Its whole spectrum was obtained from two continuous sets of data by different authors in different wavelength ranges [31, 32] and compared to those of other compounds of the same family, such as hydrogen peroxide [33], methyl hydroperoxide [34-38], dimethyl peroxide [39] and ditertbutyl peroxide [23, 31], mostly in a gas phase. Absorption spectra have similar spectral distribution and are rather homothetic depending on the compounds and their chemical environment. Besides, peroxide type compounds have cross section usually lower than analogous hydroperoxides, except t-BuOOH compared to tBuOOtBu above 260 nm. Consequently, dialkyl peroxides are neglected here as photosensitive species in comparison with hydroperoxides because of their assumed low concentration.

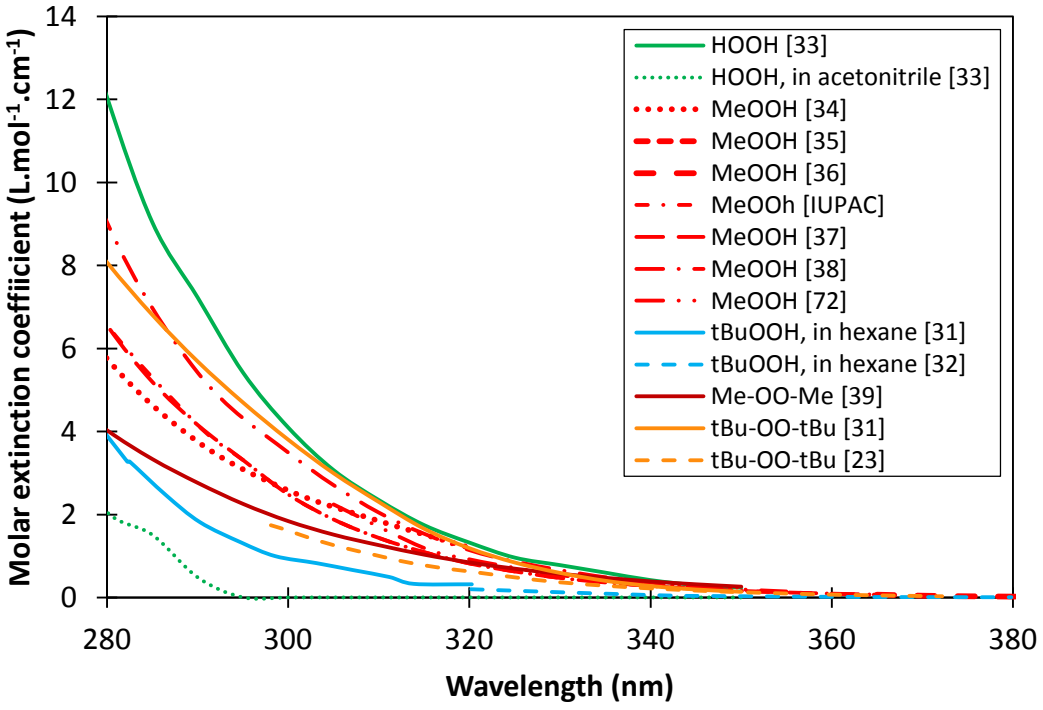

Figure 2: Absorption cross section spectra for various peroxide compounds including hydrogen peroxide [33], methyl hydroperoxide [34-38, 40], tert-butyl hydroperoxide [31, 32] (Two sets of data from different authors were required to obtain the molar absorptivity in the whole range of wavelength under

consideration), dimethyl peroxide [39] and ditert-butyl peroxide from Carlsson [31] and MicMillan (reported in [23], p 443) (colors are available online).

Absorption cross section spectra were reported for various ketones:

(i) 4-methyl-2-pentanone accounting for methyl ketones, which results from the oxidation of methyne units (i.e. tertiary carbon) along polypropylene oxidation [41].

(ii) 2,4-dimethyl-3-pentanone accounting for ketones which results from the oxidation of methylene units (i.e. secondary carbon) [41].

(iii) Various model compounds accounting for ketones on non-branched chains [33, 41-43], such as acetone, butanone and pentanone, some of them being 2-alkanone similar to so-called end-chain ketones in PP.

(iv) Ketones from polyethylene-co-carbon monoxide which is a ketone carried by a non-branched macromolecular chains. The present values are consistent with those previously published by Guillet et al. [44]. Cross sections of poly(ethylene-co-vinyl acetate) or poly(ethylene-co-methalcrylic acid) were also measured experimentally and shown that both carbonyl species are considerably less photosensitive than ketones in the investigated wavelength range.

The first two model compounds, i.e. 4-methyl-2-pentanone and 2,4-dimethyl-3-pentanone, were already chosen by Carlsson and Wiles as PP substitutes in solid state [29], and found to be similar in hexane solutions. The spectrum is reported below, but it looks more to that of 4-methyl-2-pentanone than 2,4-dimethyl-3-pentanone in gas phase. Anyway, the former compound is predominant since oxidation is known to occur mainly on tertiary carbons in PP [45]. The Carlsson's spectrum was chosen for this study because it seems rather consistent with all spectra recorded for ketones, but also with data measured on polyethylene-co-carbon monoxide polymer. Moreover, aldehyde spectra also reveal high cross sections, thus indicating that they may also absorb in the wavelength range under study, all the more that their absorption maxima are shifted towards higher wavelengths [43, 46, 47].

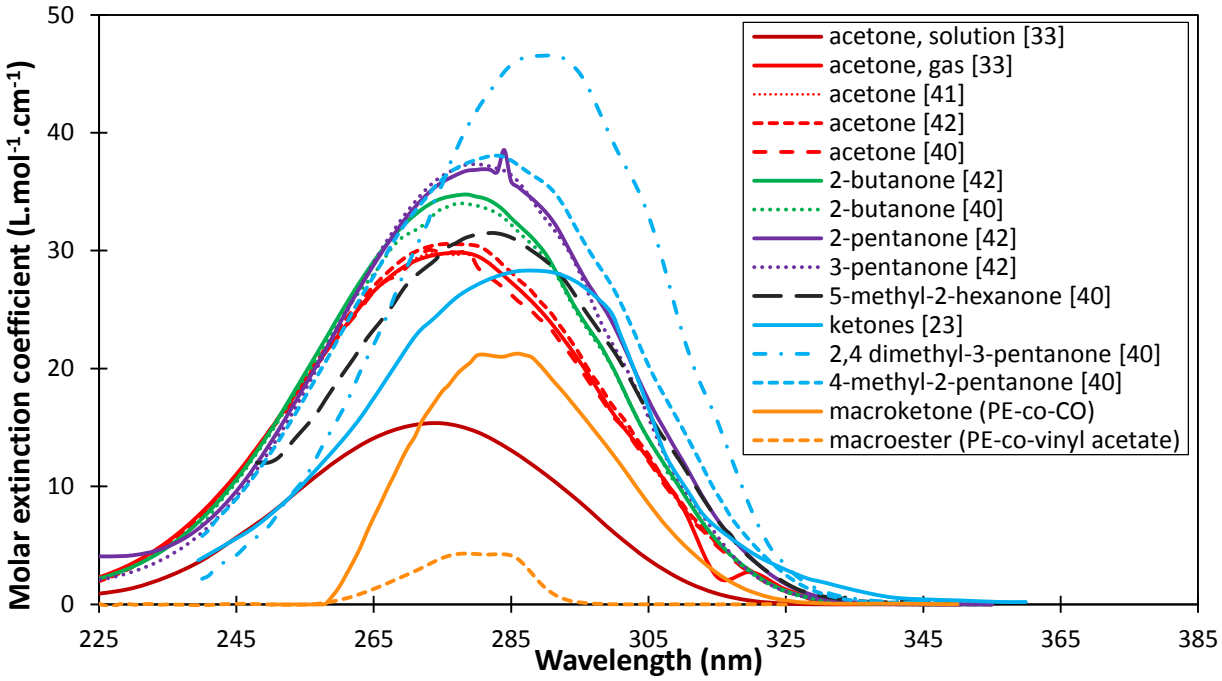

Figure 3: Spectral distribution of the molar extinction coefficient of ketone compounds including acetone [33, 41-43], 2-butanone [41, 43], 2 and 3-pentanone [43], 5-methyl-2-hexanone [41], model ketones [29], 2,4 dimethyl-3-pentanone and 4-methyl-2-pentanone [41] and model makroketones for polyethylene [this work] (colors are available online).

However, they are neglected due to their presumed low concentrations owing to their high reactivity. In contrast, carboxylic acids and esters are neglected because they are not or very weakly photosensitive to irradiance above 290 nm (as an example, the molar absorptivity of esters is depicted in figure 3).

As detailed in introduction, the overlap function $J_{species}$ for a given species, is obtained by integrating over the whole wavelength range (here 250-800 nm) the product $dJ_{species}$ of the radiation source's spectrum with the absorption cross sections spectrum. It thus applies to the area under the curve depicted in figure 4. Results are reported in the case of hydroperoxides or ketones as initiating species for an arc mercury lamp (for a SEPAP 12-24 device), a xenon lamp (WOM) and sun as radiation sources. According to the theory developed here, some interesting parallels can be drawn between the spectral distribution of the molar extinction coefficients (figures 2 and 3) and the action spectrum on one side, and between the spectral distribution of the absorbed quanta (in figures 4a and 4b) and the activation spectrum of the polymer on the other

side. Indeed, the action and activation spectra represent the wavelength dependence of a photo-process effectiveness and of the extent of degradation (damages) respectively (for further details, refer to the following reviews [17, 18]). Therefore, they only differ from the spectral distributions of the molar extinction coefficient and absorbed quanta by the spectral distribution of the quantum yield for the involved photoprocess. It turns out that the spectral distribution of the absorbed quanta for a Xenon lamp (or sunlight) is effective in the range 300-360 nm with a maximum at 315-335 nm. This result is in full agreement with the activation spectra of the literature reporting quanta activity in the interval 300-350 nm [19] and 315-360 nm with maximum between 315 and 330 nm [48]. This interval could undergo shifts to 335-360 in presence of a photostabilizer [48] or for the highest conversion degree of the oxidation [19]. This later finding can be connected with relevancy to the the fast-decomposing fraction of hydroperoxide ascribed to peracids by GijsmanGijsman [49]. However, these results corroborate the validity of the present approach (and so the mode of calculation of the criterion J) at least during the induction period up to moderate conversion degrees of oxidation.

Theoretically, both hydroperoxides and ketones may initiate oxidation and should be taken into account. Yet, since hydroperoxides and ketones have a rather similar absorption cross section, functions dJ and activation spectra are almost homothetic comparing both species. One can thus consider a unique initiating species, in this case hydroperoxides, instead of a linear combination of both contributions.

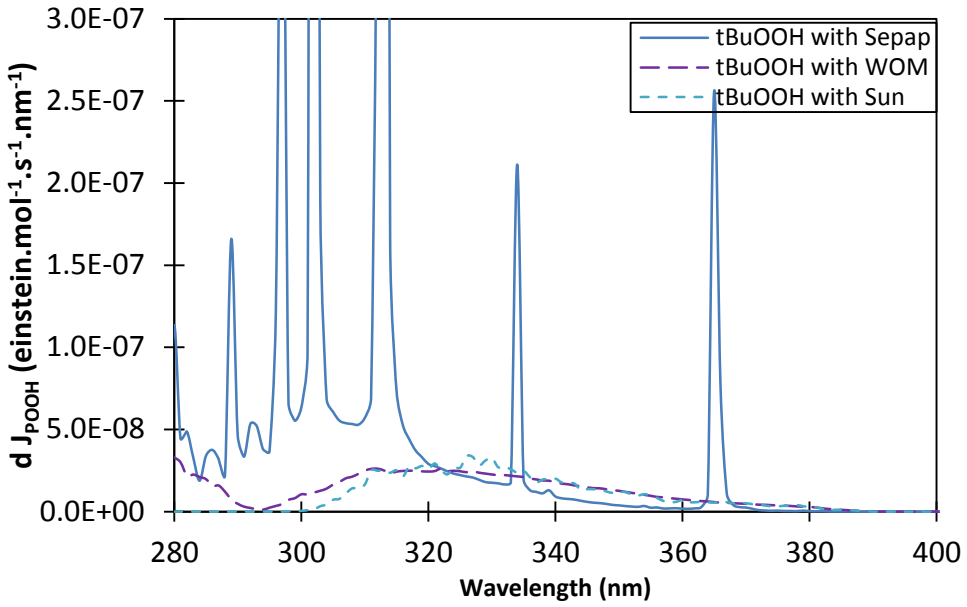

a)

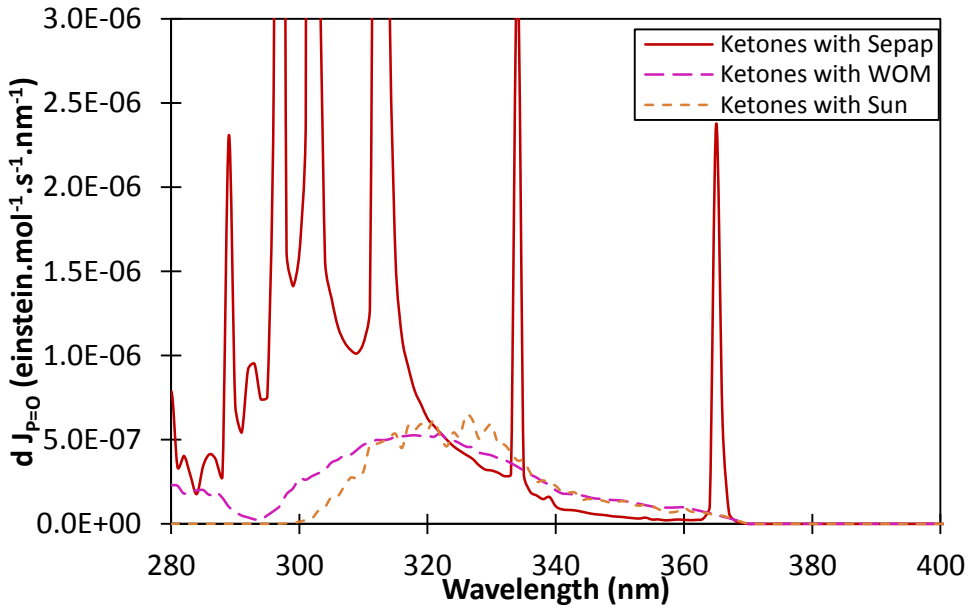

b)

Figure 4: Plot of the overlap function between the spectra of various UV light sources and the absorption spectra of hydroperoxides (a) and ketones (b).

Table 1: Dependence of the oxidation induction times (OIT) with exposure parameters

Exposure conditions					Induction Times		
T (°C)	***Light Source***	***Irradiance ($W.m^{-2}$) †*** *Between 300 and 400 nm*	***Overlap with hydroperoxides ($Einstein.mol^{-1}.s^{-1}$)***	***Overlap with ketones ($Einstein.mol^{-1}.s^{-1}$)***	***OIT (in hours) ††***	***OIT calculated at 60°C (in hours) †††***	***References***
45	Xenon lamp	35	9.45E-07	1.47E-05	83.1	55.0	[50]
25	UVA-351	82	2.84E-06	4.75E-05	33.2	11.9	[51]
25	UVA-351	163	5.66E-06	9.47E-05	19.8	7.1	[51]
25	UVA-351	325	1.13E-05	1.89E-04	0.8	0.3	[51]
21	Sunlight. Shanghai	3.0	8.92E-08	1.51E-06	1170.6	365.4	[51]
60	UVA Philips TL 40W/05	68	1.11E-07	1.78E-06	16.6	16.6	[52]
40	UVA Philips TLK 40W/05	6	1.45E-07	2.31E-06	823.1	471.2	[1]
55	UVA Philips TLK 40W/05	6	1.45E-07	2.31E-06	455.2	398.5	[1]
70	UVA Philips TLK 40W/05	6	1.45E-07	2.31E-06	196.6	253.5	[1]
45	Xenon lamp with λ>266nm	48	1.13E-06	1.77E-05	48.4	32.0	[19]
45	Xenon lamp with λ>289nm	42	7.87E-07	1.20E-05	51.5	34.1	[19]
45	Xenon lamp with λ>327nm	34	2.71E-07	2.76E-06	64.9	43.0	[19]
45	Xenon lamp with λ>346nm	28	1.13E-07	7.24E-07	98.0	64.9	[19]
45	Xenon lamp with λ>366nm	14	2.39E-08	3.58E-08	131.6	87.2	[19]
45	Xenon lamp with λ>378nm	6.5	6.17E-9	8.56E-9	138.6	91.8	[19]
45	Xenon lamp with λ>395nm	1.5	7.64E-10	4.04E-9	139.6	92.5	[19]
45	Xenon lamp with λ>430nm	0.0	0.00E+00	0.00E+00	139.6	92.5	[19]
60	SEPAP 14/24	23	2.88E-06	4.27E-05	175.7	175.7	[11]
60	SEPAP 14/24	37	4.68E-06	6.95E-05	107.1	107.1	[11]
60	SEPAP 12/24, 2 Lamps	42	5.34E-06	7.92E-05	72.6	72.6	[11]
60	SEPAP 14/24	66	8.45E-06	1.25E-04	57.3	57.3	[11]
60	SEPAP 12/24, 4 Lamps	84	1.07E-05	1.59E-04	53.3	53.3	[11]
60	SEPAP 12/24, 4 Lamps	84	1.07E-05	1.59E-04	42.7	42.7	[11]
60	SEPAP 12/24, 4 Lamps	84	1.07E-05	1.59E-04	37.4	37.4	[20]
60	SEPAP 12/24, 4 Lamps	84	1.07E-05	1.59E-04	36.4	36.4	[53]
60	SEPAP 14/24	86	1.10E-05	1.64E-04	44.4	44.4	[11]
60	SEPAP 14/24	86	1.10E-05	1.64E-04	39.5	39.5	[11]
65	SEPAP 50/24, 8 Lamps	265	3.39E-05	5.03E-04	24.6	28.0	[20]
60	SEPAP 14/24	86	1.10E-05	1.64E-04	23.3	23.3	[11]
45	SEPAP 12/24, 2 Lamps	38	4.92E-06	7.30E-05	31.9	21.1	This work.
45	SEPAP 12/24, 4 Lamps	84	1.07E-05	1.59E-04	19.1	12.7	This work.
60	SEPAP 12/24, 2 Lamps	38	4.92E-06	7.30E-05	24.1	24.1	This work.
60	SEPAP 12/24, 4 Lamps	84	1.07E-05	1.59E-04	16.5	16.5	This work.
60	SEPAP 50/24, 6 Lamps	198	2.54E-05	3.76E-04	5.2	5.2	This work.
60	SEPAP 50/24, 8 Lamps	265	3.39E-05	5.03E-04	14.8	14.8	‡This
80	SEPAP 12/24, 2 Lamps	38	4.92E-06	7.30E-05	14.0	22.9	This work.
80	SEPAP 12/24, 4 Lamps	84	1.07E-05	1.59E-04	9.5	15.5	This work.
80	SEPAP 50/24, 6 Lamps	198	2.54E-05	3.76E-04	2.8	4.5	This work.
80	SEPAP 50/24, 8 Lamps	265	3.39E-05	5.03E-04	2.8	4.6	This work.
64	Xenon lamp	55	1.45E-06	2.25E-05	56.2	62.3	This work.

Notes: † Irradiances have been calculated in the interval 300-400 nm by convention. †† Induction times from this work and literature have been calculated using the same method from native points. †††

Induction times at 60°C have been calculated from equation 6 to draw the master curve. ‡ This condition has been dismissed in applying the analytical models presumably because of an unsuitable control of the temperature.

Thus, overlap functions for both hydroperoxides and ketones were calculated for each aging condition (SEPAP and WOM). Complementary data were also extracted from the literature and underwent a similar treatment. All the results are reported in table 1. To characterize the oxidation behavior, induction time was considered as the relevant indicator, in a first approach, and was determined by intercepting the slope of the maximal oxidation rate with the abscissa axis.

3.3. Interpretation according to an empirical Schwarzschild's law

As reported in introduction, reciprocity laws are commonly used to describe the effect of light intensity on hydrocarbon polymers using empirical parameters. As reviewed by Martin et al. [15], the dependence is not always with the reciprocal of the irradiance. Indeed, the law exponent can deviate from its default value of -1 up to values of -0.7, according to a so-called Schwarzschild's law. Besides, it has been shown as more relevant to replace the irradiance by the overlap function J, basing on the comprehension of initiation processes. To correct the effect of temperature in such a photothermal aging, the induction time is empirically supposed to obey an Arrhenius law, as kinetically determined for the maximal oxidation rate [1]. Similar approaches were already proposed to correlate failure criteria with temperature and light exposure parameters, but with the irradiance as key variable instead of the proposed J overlap criterion [28, 54, 55]. Our improvements lead to the following empirical relationship (equation 6):

$$t_{ind} = K\, J^{\gamma} \exp\left(-\frac{Ea_{ind}}{RT}\right) \qquad \textbf{Eq. 6}$$

Assuming that this law is fulfilled, the activation energy Ea_{ind} can be determined by regression from our factorial testing matrix (surface response for different couples of light intensity and temperature) in SEPAP. Using a mean squares minimization criterion, the activation energy Ea_{ind} is found to be equal to 27 kJ.mol^{-1}. This activation energy is higher than the value of 15 kJ.mol^{-1}

found by Balaban for aPP [9] but in agreement with the estimation of 25 to 50 $kJ.mol^{-1}$ [1] made from the data of Mayo [56].

By using equation 6 with the determined activation energy, a kind of master curve can be defined at a given temperature from data obtained at various temperatures. The induction times were then calculated at 60°C according to equation 6, as reported in table 1. The corresponding master curve is depicted in figure 5.

Following this approach, the parameters of the Schwarzschild's law have been determined from the induction times obtained in our experiments, i.e. under both SEPAP and WOM exposure, but also from analogous experiments carried out by Gardette and coworkers in SEPAP devices only [11, 20, 53]. The two sets of data showed light dependences with a power of $\gamma = 0.86$, and a power of $\gamma = 0.77$ respectively (figure 5). So, results obtained by Gardette and coworkers gave rather comparable dependence on the light intensity while all tests were performed in SEPAP at the unique temperature of 60°C [11, 20, 53]. So, the temperature correction could be considered as valid in the investigated range. The gap of about one decade on pre-exponential factors K was ascribed to the fact that these previous samples were weakly stabilized, as suggested by the aging test of a purified control sample [11], whose induction time is close to the master curve established from our results.

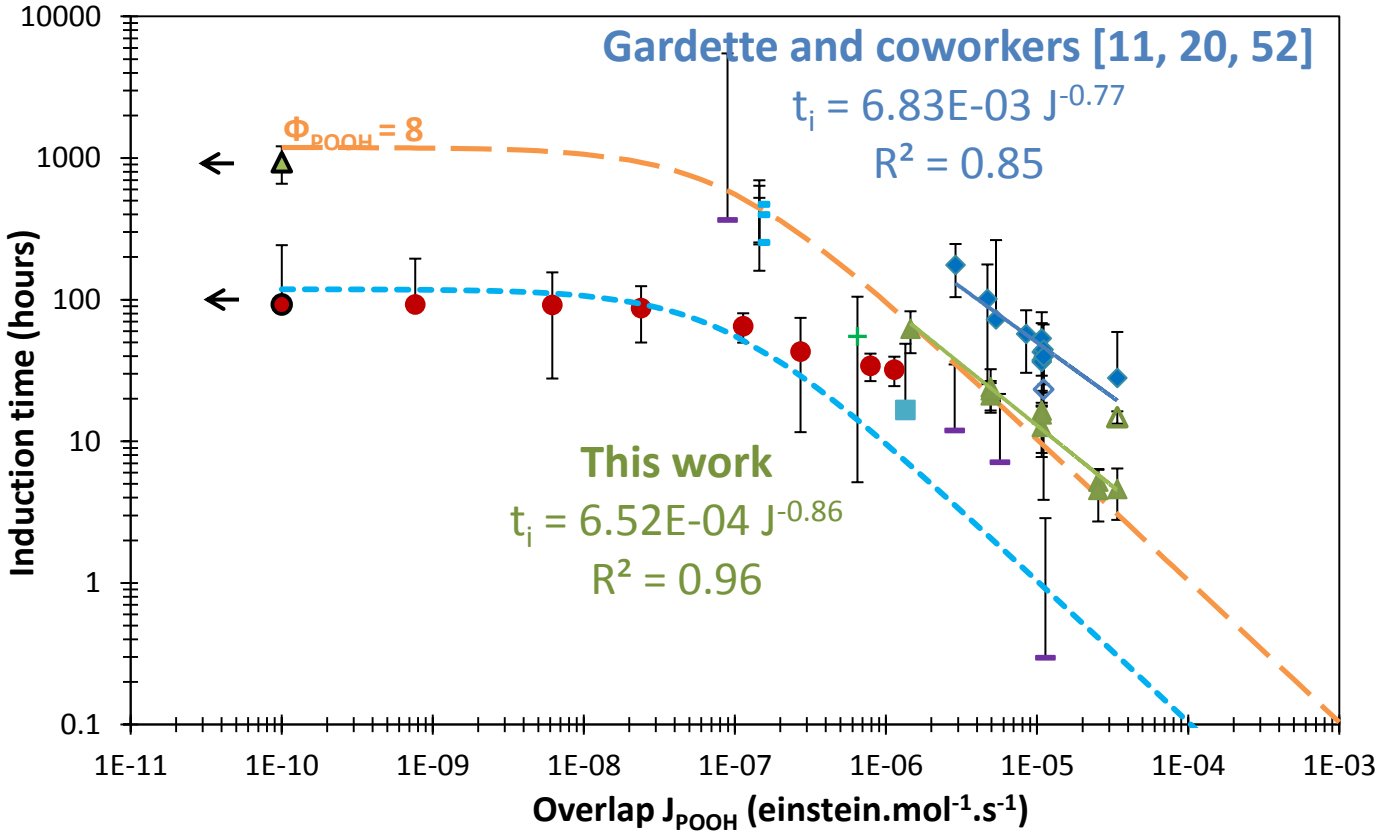

Figure **5**: Induction time as a function of the overlap function J accounting for the absorbed energy. The arrows indicate the experimental asymptotic values reached by the induction times in the case of a pure thermal aging. Legend: ▲ This work. △ This work, dismissed value. ◆ Gardette [11, 20, 53], ◇ Gardette, purified material [11], + Gijsman [50], ■ Elvira [52], ▪ Girois [1], — Yang [51], ● Zhenfeng [19]. Solid lines apply to the Schwarzschild's law for this work (blue) and Gardette and co-workers (green) (see equation 6). Dotted line apply to the kinetic model (equation 8) with λ=1 (in orange) and λ=10 (in cyan).

At this standpoint, it is notable that the introduction of the spectral overlap integral in the Schwarzschild's law enables to describe the oxidative behavior of our iPP in both SEPAP and WeatherOmeter devices. Various results on premumably free-additive polypropylenes have been also compiled from the literature in order to check this relationship ([50], [52],[1], [51], [19]). However, it was only possible to confirm the trend because of the high scattering of induction periods, which was attributed to various amounts of structural defaults (such as catalysis residues) or the uncertainty on input data –e.g. sources' emission spectra.

Nonetheless, when decreasing the value of J, the induction period seems to reach a plateau which is not modeled by the Schwarzschild's law. This can be connected to the lower activation energy of photothermal oxidation (i.e. 27 kJ.mol^{-1}) in comparison with thermal oxidation (about 100 kJ.mol^{-1}) as observed in this work and the literature [57-60] (appendix A). This fact clearly evidences that this empirical law would be only valid in a restricted range of aging conditions whose boundaries remain to be established.

3.4. Interpretation using a semi-empirical kinetic approach

3.4.1. Theory

Audouin et al. [1] used the closed-loop scheme to determine the expression of the oxidation induction time in the case of the photothermal oxidation of PP, assuming that both thermal and photochemical initiation processes were unimolecular:

$$t_{ind} = \frac{C}{\Phi J + k_{1u}{}^{0} \exp(\frac{-Ea_{1u}}{RT})} \qquad \textbf{Eq. 7}$$

with C a universal constant depending upon the monitored chemical species (C = 3 for carbonyl species and C = 0.383 for hydroperoxides),

Φ the quantum yield, J the spectral overlap integral, $k_{1u}{}^{0}$ and Ea_{1u} the preexponential factor and activation energy respectively for a unimolecular thermal initiation.

Actually, this amounts to consider that the photothermal oxidation applies to the case of the thermal oxidation, but taking into account an additional initiation, i.e the photolysis of a given chromophore. This approach constitutes a foundation for the general kinetic approach initiated by Tolbolsky and Mesrobian [61, 62]. The induction period before oxidation t_{ind} would thus result

from the competition of two modes of initiation: the photolysis and thermolysis of the relevant photosensitive species (namely hydroperoxides in the closed-loop scheme) [63].

It is noteworthy that a correction is implemented here as compared with the original model [1]: the spectral overlap integral (i.e. the amount of absorbed quanta) is substituted to the UV-light intensity measured by actinometry. Thereby, the absorbed intensity is normalized by the concentration in the considered photosensitive species (e.g. hydroperoxide or ketone). In this way, the photoinitiation term is effectively homogeneous to a kinetic rate constant for a unimolecular reaction (s^{-1}). This is the reason why both the thermolysis and photolysis of hydroperoxides are assumed to be unimolecular. Otherwise, the analytical kinetic treatment would be significantly complexified. The unimolecularity is commonly accepted for the photochemical initiation (see [23] for instance). It is also acceptable for thermal initiation, that allows to simplify considerably the analytical kinetic treatment since, in this case, the induction time only obeys a reciprocal dependence with the initiation rate constant (see Ref. [60] for instance).

It is also important to precise that the kinetic law would be anyway applicable for modeling the induction times of both hydroperoxides and ketones, by only changing the value of the constant C. Indeed, the kinetic law is independent of the specificity of their accumulation mode in the polymer matrix. It only differs by the value of C because the formations of both species are finally correlated considering that the latter results from the decomposition of the former (the detailed kinetic treatment of the closed-loop mechanistic scheme can be found elsehere [63]).

The determination of the model's parameters is operated stepwise. First, the apparent Arrhenius parameters for k_{1u} were determined from thermal oxidation experiments (monitoring of carbonyl species). Their values are: $k_{1u}^{0} = 2.45\ 10^{-9}\ s^{-1}$ and $Ea_{1u} = 99.2\ kJ.mol^{-1}$ (appendix A).
Then, the quantum yields were determined from the regression straight-lines of figure 6. They are found equal to $\Phi_{POOH} = 8.5 \pm 1.7$ and $\Phi_{C=O} = 0.54 \pm 0.11\ mol.Einstein^{-1}$ for hydroperoxides and ketones respectively.

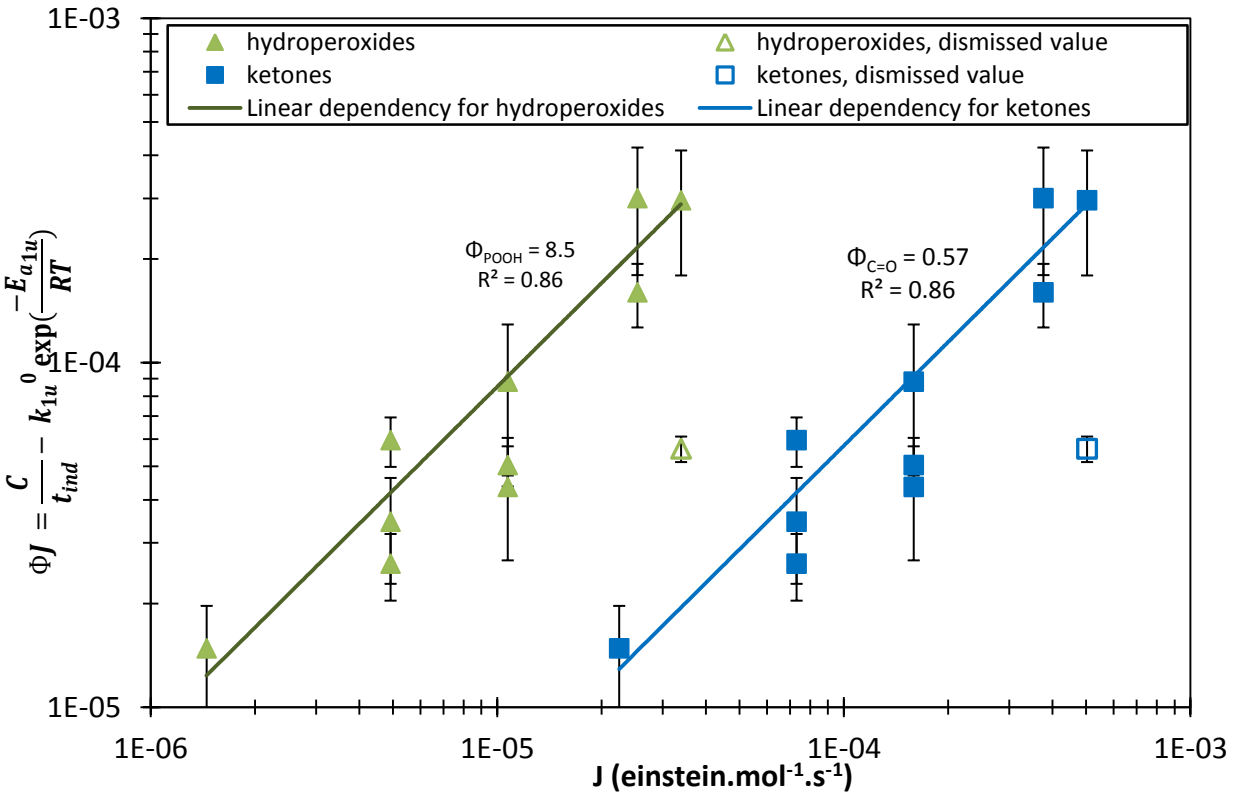

Figure 6: Kinetic correlation between the photolysis initiation rate and the overlap function J. The slope of the curve corresponds to the quantum yield.

Correlation coefficients are equal for both chemical species, presumably due to their similar wavelength sensitivities as shown in figure 4.

3.4.2. Comparison of both analytical models

The light dependence described by equation 7 has been plotted in figure 5 in order to compare both the Schwarzschild's and the kinetic models. The lower coefficient of correlation (equal to 0.86) indicates that the kinetic model does not provide a better fit of our experimental data in photothermal aging (the reverse is even observed). This is not surprising given the simplifying assumptions of the model, namely the unicity of the initiation species (hydroperoxides) and its unimolecular thermal and photochemical decompositions.

Instead, it can be considered that the kinetic model offers a "better" description of the oxidation behavior as far as it is valid whatever the exposure conditions (in terms of temperature and UV-light intensity). More particularly, when the light intensity tends towards 0, it generates a plateau describing the thermal oxidation regime, whose existence is attested by the asymptotic

experimental value indicated by an arrow. This trend is particularly well evidenced by the results obtained by Zhenfeng et al. [19] obtained for very low radiation intensities despite the vertical shift of the trend curve. This shift would be presumably due to the presence of a higher content of impurities in PP samples such as catalysis residues or prodegradant additives. By assuming that the kinetic parameters k_{1u} and ΦJ are proportional to the concentration of impurities, the equation 7 becomes:

$$t_{ind} = \frac{1}{\lambda} \frac{C}{\Phi J + k_{1u}{}^{0} \exp(\frac{-E_{a_{1u}}}{RT})} \qquad \textbf{Eq. 8}$$

It is thus possible to apply the kinetic model to the experimental data of Zhenfeng [19] by adjusting the parameter λ accounting for the material variability. This latter kinetic trend is depicted in figure 5.

As for radiothermal aging, the polymer lifetime results here from the competition between two different initiation reactions respectively induced by temperature (intrinsic mode) and radiation (extrinsic mode) [64, 65].

3.4.3. A powerful investigation tool for the competition of light and thermal effects

Therefore, the previous kinetic model enables to determine the ranges of relative predominance of UV-light and temperature to initiate oxidation in unstabilized PP. Different combinations of exposure conditions, in terms of light –as described by the spectral overlap integral J– and temperature, apply to a same balance between both sources of initiation. These equivalent combinations are given through the equation 8, for a ratio θ between both terms fixed from 0 to +∞:

$$\Phi J = \theta \, k_{1u}{}^{0} \exp(\frac{-E_{a_{1u}}}{RT}) \qquad \textbf{Eq. 9}$$

According to the kinetic model (equation 7), the induction period would be proportional to the reciprocal rate of initiation (either by thermolysis or photolysis). Thus, aging by thermal and photochemical oxidation can be considered as equivalent in terms mechanisms, at least those concerning primary processes (those determining the induction period). It is thus possible to plot the curves of iso-lifetime. Theoretically, this model would also suggest that the chemistries of thermal and photochemical oxidation would be identical, i.e. that a same conversion degree

induces the same alteration level of the polymer properties). If this statement was always fulfilled, curves of iso-lifetime would be analogous to curves of iso-damages.

However, this is not exactly the case and it is generally recommended to maintain the balance between both kinds of initiation processes (thermal and photochemical). In such conditions, an accelerated aging test will be considered as representative of the natural aging, which means situated on a same representativity curve. All the exposure conditions which apply to a same balance between both kinds of initiation (i.e. representative one another) and plot a so-called "representativity curve" can be obtained by solving equation 8 for a given θ value.

These operations allow to build an abacus for the relative predominance of UV-light and temperature on the photothermal aging of unstabilized PP, as depicted in figure 7. Domains of predominance are directly obtained from equation 9 with the corresponding inequalities. To draw the boundaries, the photochemical and thermal initiations were alternatively considered as predominant so long as the effect of the minor initiation source on the induction time would be lower than 10%.

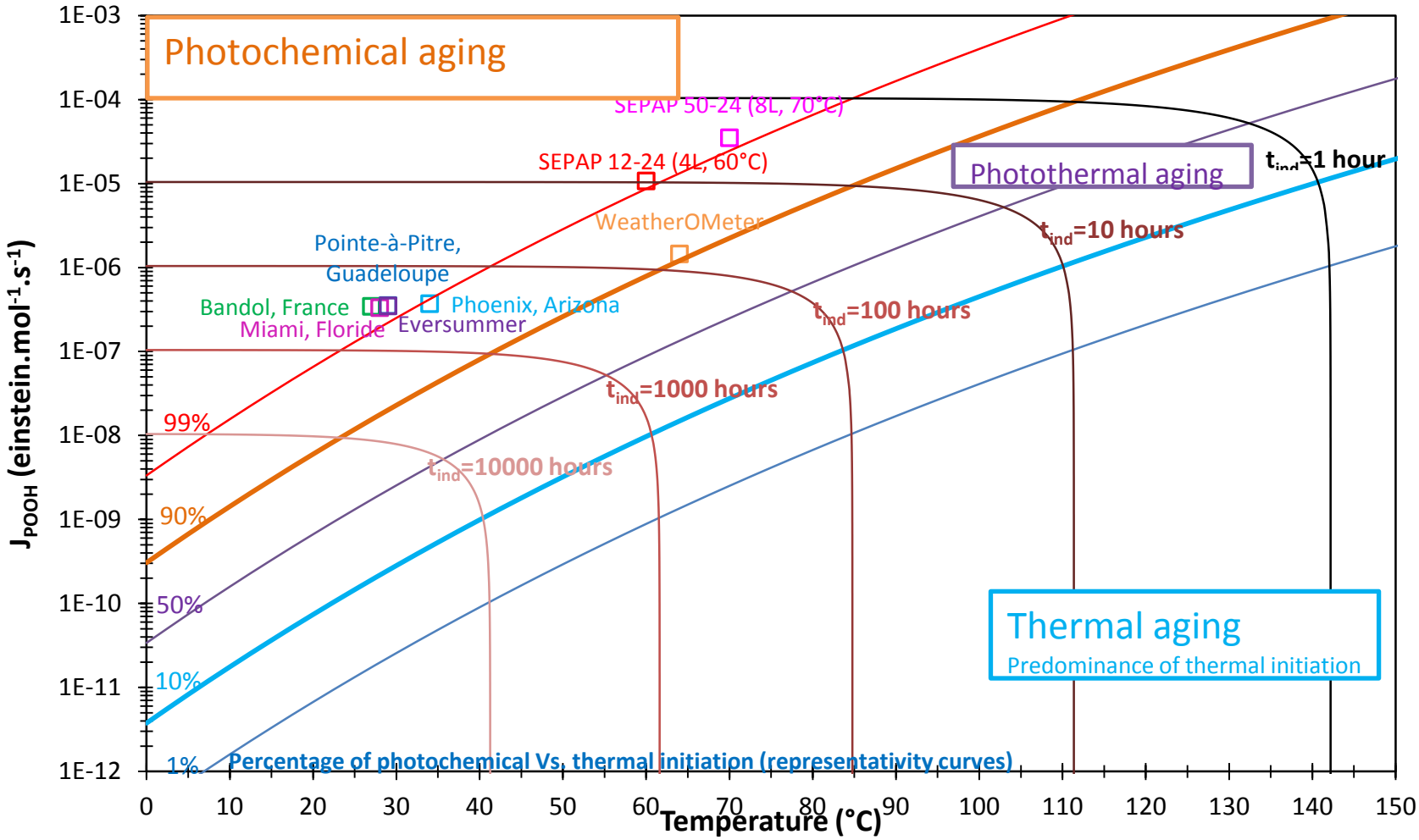

Figure 7: Abacus of relative predominance of temperature and UV light on the photochemical aging of unstabilized polypropylene (from the kinetic model in equation 7). The frontiers of the photochemical and thermal aging domains are in bold to be differentiated among the curves of representative aging tests. Iso-lifetime (or iso-damage) curves allow visualization of the acceleration factor between two aging methods. Symbols indicate exposure conditions in reference testing methods or weathering sites.

The abacus thus allows to evaluate how relevant are the exposure conditions used in a given test method, in terms of light and temperature. It includes all the conditions of the tested methods as well as those of common validation ones, both in artificial and outdoor weathering. For this latter, submitted to seasonal variations, average values were estimated from the cumulated light dosage for different reference weathering sites (there is here a small approximation). According to the representativity curve applying to 99% of photochemical initiation, the SEPAP 12-24 method would be more representative of natural aging conditions than the WOM method applying to "only" 90% of photochemical initiation. Practically, both SEPAP and WOM methods are acceptable because they belong to the domain of predominance of photochemical initiation according to the chosen boundaries.

When moving on the representativity curve, it is possible to visualize the acceleration factor by using the iso-lifetime curves. The lifetime in real aging conditions was thus calculated to be about 290 ± 15 h with equation 7. The acceleration factor would thus be of 18 ± 1 in respect to the experimental value obtained though an accelerated test in a SEPAP 12-24 device and 29 ± 2 in respect to the value returned by the model (the gap applies to the error of fit). These values are of the same order of magnitude as those experimentally determined by Arnaud et al. for unstabilized PP, which are generally ranged between 8 and 22 [66].

3.4.4. The heuristic value of the kinetic model

The main issue in the proposed kinetic model consists in the unrealistic value for the quantum yield of hydroperoxide photolysis. This one is found equal to more than 8 whereas it should not theoretically worth more than unity –i.e. 100 %– in the case of elementary initiation reactions. However, this finding can be compared to the values determined from photolysis experiments of polypropylene hydroperoxides in inert conditions. Thus, Carlsson and Wiles determined apparent quantum yields up to 4.8 (4 ± 1 on average) [30, 31] and a value of about 4.2 was calculated from experiments of Commereuc et al. [67]. Eventually, the experimental quantum yield of $\Phi_{POOH} = 4$ must be considered as the target value since obtained by photolysis and its excessive value would be due to "internal effects", i.e. specific mechanisms induced by hydroperoxide decomposition itself (and thus strongly correlated) or unsuitable hypothesis about its photosensitive features. The possible underestimation of the spectral cross sections for photosensitive species has been already envisaged by Carlsson, whose data have been reused here. It is however unimportant on the results since spectral cross sections of various hydroperoxides or ketones have been shown to be homothetic depending on model compounds (figure 2 and 3).

However, the factor 2 between the model's and the target values could result from unsuitable simplifying hypotheses used for determining analytical equation 7:

(i) The hypothesis of unimolecular thermal initiation, while decomposition of hydroperoxides was shown to be mostly bimolecular at these temperatures [68];

(ii) The hypothesis of a unique chromophoric species.

It is noteworthy that the model is theoretically designed for describing the UV-light initiation on a single photosensitive species. Practically, initiation is assumed to come from mostly hydroperoxide photolysis because of the high cleavability of the corresponding O-O bond [31]. Theoretically, it would be possible to consider several sources of photo-initiation provided that the balance reactions are of a similar form. Therefore, the equation 7 becomes:

$$t_{ind} = \frac{c}{\sum_{j\ chromophoric\ species} \Phi_j J_j + k_{1u}{}^0 \exp\left(\frac{-E_{a_{1u}}}{RT}\right)} \qquad \textbf{Eq. 10}$$

This condition is fulfilled with the two photosensitive species under investigation, namely hydroperoxides (or even alkyl peroxides) and ketones since:

POOH → 2P° + inactives products
P=O → 2P° + inactives products

Moreover, the spectral sensitivity of hydroperoxides and ketones are almost homothetic and consequently, equation 10 can be rewritten as:

$$t_{ind} = \frac{c}{(1+\beta)\,\Phi_{POOH}\,J + k_{1u}{}^0 \exp\left(\frac{-E_{a_{1u}}}{RT}\right)} \qquad \textbf{Eq. 11}$$

Finally, the overall quantum yield which is determined experimentally by an inverse method (see figure 7) would be a composite value accounting for various photochemical initiating species.

Otherwise, explanations would lie in the higher complexity of the involved reactions and phenomena:

(i) Potential energy transfer reactions via keto-hydroperoxides complexes –or exciplexes– to benefit from both high quantum yield (cleavable bonds) of hydroperoxides and high cross section of ketones (powerful chromophores) [69-72].

(ii) Involvement of other photochemical reactions, not belonging to the initiation step, would have dramatic effects on PP lifetime.

4. Conclusion

First of all, the spectral overlap integral J was proposed as a relevant criterion to describe the effect of the spectral distribution of light, and so, to establish a heuristic correlation between the common light sources in artificial and outdoor weathering. This quantity, derived from the quantum theory (i.e. band gap theory in electronics), applies to the energy absorbed by the photosensitive species whose photolysis will produce radicals and initiate photodegradation. This was checked to be consistent with the literature activation spectra defined as the light wavelength domain which will be efficient for generating damages. The criterion J is defined in such a way that it is independent of the specificity of the chromophores accumulation mode in the polymer matrix. Therefore, it can be introduced with relevancy in analytical models (namely the Schwarzschild's law and kinetic model) in order to describe the impact of exposure factors (temperature and UV-light) on the induction period whatever the light source under consideration (including xenon and medium pressure mercury lamps).

Secondly, this study enables to apprehend the limitations of both types of analytic approaches in order to describe the competitive effects of light and temperature. While the Schwarzschild's law was slightly better for modeling the results in photothermal aging, only the kinetic model would be valid in the whole light intensity range under study (including the pure thermal oxidation) under study. In fact, the kinetic model is particularly indicated for describing the competition between UV-light and temperature on the initiation of oxidation (at least, in terms of primary processes). This second model thus allows determination of the restricted domain where the Schwarzschild's law is presumably valid, i.e. the domain where photochemical initiation is predominant. It also constitutes a tool to compare different aging testing methods in accelerated and natural exposure conditions. It turns out that, as expected, the Xenon lamp provides a better description of the effect of the light wavelength on degradation, but it is finally off topic provided that this effect is properly described (which is the case through the spectral overlap integral). What matters is the suitable description of the competitive effects of UV-light and temperature.

Theoretically, the kinetic model states that temperature and UV-light would have analogous impact on the PP degradation. This approximation, coming from simplifying assumptions such as the unimolecular decomposition of hydroperoxides, the unicity of initiating species (neglecting ketones) or the neglect of the small differences in chemistry, leads to a questionable value for the quantum yield. Indeed, this latter is about twice higher than the expected value although of the right order of magnitude. For these reasons, it is recommended

to position the accelerated testing methods in representative conditions of natural weathering (i.e. for the same ratio of photochemical initiation). Clearly, the kinetic model provides interesting trends for describing the effects of the exposure conditions on the induction period but another important oxidation indicator, the maximal oxidation rate, has been left aside. It is also noteworthy that the kinetic model was only established for unstabilized PP and parameters would probably differ for stabilized materials (as established for the Schwarzschild's law in introduction). Finally, neither its accuracy nor its physical substantiations lead to recommend this analytical model for lifetime prediction.

Its translation into a numerical form will allow us to eradicate all the simplifying hypotheses and to check the validity of some complex phenomena (such as multiple initiating species, termolecular processes or energy transfers) as well as the interaction with additional components, particularly stabilizers.

5. Appendix A: Thermal aging results

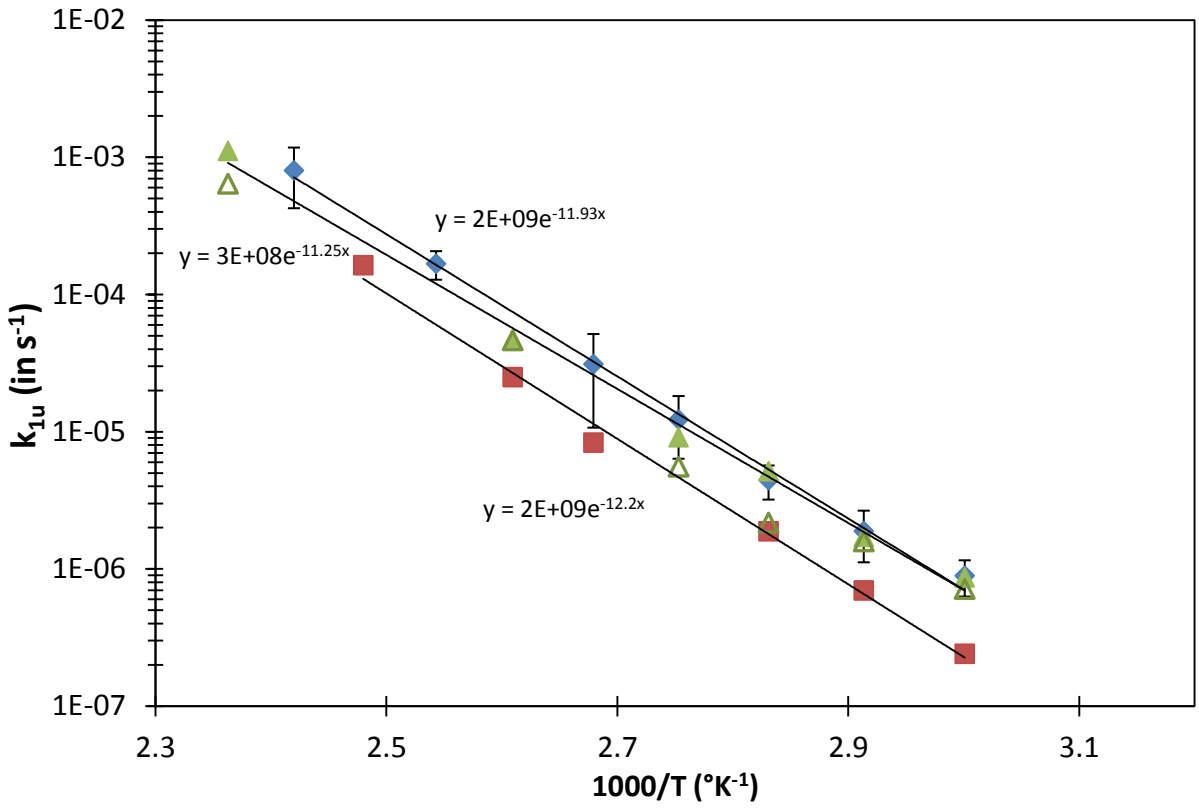

Figure 1: Arrhenius graphs of the thermal initiation rate constant for: ◆ This work., ■ Richaud et al [58], ▲ Achimsky [59], △ Achimsky et al [57]. The value of pseudo-unimolecular kinetic rate constants are determined from the induction times using $t_{ind}=3/k_{1u}$.

Table A.1: Arrhenius parameters of the initiation rate constant in thermal oxidation.

	Ea_{1u} (kJ.mol^{-1})	k_{1u}^0 (s^{-1})
This work	99.2 ± 6.5	(2.45 ± 5.27) 10^9
Achimsky [57, 59]	93.5 ± 9.9	(3.16 ± 10.30) 10^8
Richaud [58]	101.2 ± 13.5	(1.8 ± 8.0) 10^9

Acknowledgements

Dr. Narcisse Siampiringue from the *Centre National d'Evaluation de Photoprotection (Clermont-Ferrand, France)* is greatly acknowledged for the carrying out of radiation exposure experiments.

References

[1] L. Audouin, S. Girois, L. Achimsky, J. Verdu, Effect of temperature on the photooxidation of polypropylene films, Polymer Degradation and Stability, 60 (1998) 137-143.
[2] O.N. Karpukhin, E.M. Slobodetskaya, Photooxidation of polyolefins and their light stability, Journal of Polymer Science: Polymer Chemistry Edition, 17 (1979) 3687-3694.
[3] J.W. Chin, T. Nguyen, X. Gu, E. Byrd, J. Martin, Accelerated UV weathering of polymeric systems: Recent innovations and new perspectives, JCT CoatingsTech, 3 (2006) 20-26.
[4] P.A. Christensen, A. Dilks, T.A. Egerton, J. Temperley, Infrared spectroscopic evaluation of the photodegradation of paint: Part II: The effect of UV intensity & wavelength on the degradation of acrylic films pigmented with titanium dioxide, Journal of Materials Science, 35 (2000) 5353-5358.
[5] M. Diepens, P. Gijsman, Influence of light intensity on the photodegradation of bisphenol A polycarbonate, Polymer Degradation and Stability, 94 (2009) 34-38.
[6] G. Jorgensen, C. Bingham, D. King, A. Lewandowski, J. Netter, K. Terwilliger, K. Adamsons, Use of Uniformly Distributed Concentrated Sunlight for Highly Accelerated Testing of Coatings, in: Service Life Prediction, American Chemical Society, 2001, pp. 100-118.
[7] J.E. Pickett, D.A. Gibson, M.M. Gardner, Effects of irradiation conditions on the weathering of engineering thermoplastics, Polymer Degradation and Stability, 93 (2008) 1597-1606.
[8] D. Braun, S. Kull, Photoabbau von PVC-folien. I. Einfluß von bestrahlungsstärke und temperature, Die Angewandte Makromolekulare Chemie, 85 (1980) 79-90.
[9] L. Balabán, J. Majer, K. Vesely, Photooxidative Degradation of Polypropylene, Journal of Polymer Science Part C: Polymer Symposia, 22 (1969) 1059-1071.
[10] O.N. Karpukhin, Y.M. Slobodetskaya, The photo-oxidation of polypropylene and the changes in its physico-mechanical characteristics, Polymer Science U.S.S.R., 18 (1976) 3084-3090.
[11] Philippart, L. J, Sinturel, C, Gardette, Influence of light intensity on the photooxidation of polypropylene, Polymer Degradation and Stability, 58 (1997) 261-268.
[12] P. Vink, T.J. Van Veen, The mechanism of u.v. stabilization of polypropylene films by 2-hydroxy-4-octyloxybenzophenone, European Polymer Journal, 14 (1978) 533-537.
[13] T.M. Kollmann, D.G.M. Wood, Effects of variations in light intensity on the photooxidation of polypropylene, Polymer Engineering and Science, 20 (1980) 684-687.
[14] S.W. Bigger, J. Scheirs, O. Delatycki, Effect of light intensity on the photooxidation kinetics of high-density polyethylene, Journal of Polymer Science, Part A: Polymer Chemistry, 30 (1992) 2277-2280.

[15] J.W. Martin, J.W. Chin, T. Nguyen, Reciprocity law experiments in polymeric photodegradation: a critical review, Progress in Organic Coatings, 47 (2003) 292-311.
[16] P. Vink, Photooxidation of polypropylene Journal of Applied Polymer Science: Applied Polymer Symposium, 35 (1979) 265-273.
[17] N.D. Searle, Activation Spectra of Polymers and Their Application to Stabilization and Stability Testing, in: Handbook of Polymer Degradation, Second Edition, S. H. Hamid, Ed., Marcel Dekker, Inc., New York,, 2000, pp. 605-643.
[18] A.L. Andrady, Wavelength Sensitivity in Polymer Photodegradation, in: Advances in Polymer Science, 1997, pp. 46-94.
[19] Z. Zhenfeng, H. Xingzhou, L. Zubo, Wavelength sensitivity of photooxidation of polypropylene, Polymer Degradation and Stability, 51 (1996) 93-97.
[20] Philippart, L. J, Sinturel, C, Arnaud, R, Gardette, Influence of the exposure parameters on the mechanism of photooxidation of polypropylene, Polymer Degradation and Stability, 64 (1999) 213-225.
[21] A. Geburtig, V. Wachtendorf, Determination of the spectral sensitivity and temperature dependence of polypropylene crack formation caused by UV-irradiation, Polymer Degradation and Stability, 95 2118-2123.
[22] J.F.R. B. Rånby, Photodegradation, photo-oxidation, and photostabilization of polymers principles and applications 1975.
[23] J.G. Calvert, J.N.J. Pitts, Photochemistry American Chemical Society, 1966.
[24] J.W. Martin, Quantitative characterization of spectral ultraviolet radiation-induced photodegradation in coating systems exposed in the laboratory and the field, Progress in Organic Coatings, 23 (1993) 49-70.
[25] J.W. Martin, J.A. Lechner, R.N. Varner, Quantitative characterization of photodegradation effects of polymeric materials exposed in weathering environment, in: W.D. Ketola, D. Grossman (Eds.) Accelerated and outdoor durability testing of organic materials 1994, pp. pp27-51.
[26] Bauer, R. D, Interpreting weathering acceleration factors for automotive coatings using exposure models, Polymer Degradation and Stability, 69 (2000) 307–316.
[27] D.R. Bauer, Global exposure models for automotive coating photo-oxidation, Polymer Degradation and Stability, 69 (2000) 297-306.
[28] G.J. Jorgensen, A phenomenological approach to obtaining correlation between accelerated and outdoor exposure test results for organic materials, West Conshohocken, PA, 2003.
[29] D.J. Carlsson, D.M. Wiles, The Photodegradation of Polypropylene Films. II. Photolysis of Ketonic Oxidation Products, Macromolecules, 2 (1969) 587-597.
[30] D.J. Carlsson, D.M. Wiles, The Photooxidative Degradation of Polypropylene. Part I. Photooxidation and Photoinitiation Processes, Journal of Macromolecular Science, Part C, Polymer Reviews 14 (1976) 65 - 106.
[31] D.J. Carlsson, D.M. Wiles, The photodegradation of Polypropylene Films. III. Photolysis of polypropylene hydroperoxydes, Macromolecules, 2 (1969) 597-606.
[32] J.T. Martin, R.G.W. Norrish, The photochemical decomposition of tert-butyl hydroperoxyde, Proceeding of the Royal society of London. Serie A. Mathematical and physical sciences, 220 (1953) 322(339.
[33] F.o. Jorand, L. Kerhoas, A. Heiss, J. Einhorn, K. Sahetchian, Determination of the ultra violet absorption cross section of hexyl-ketohydroperoxides in solution in acetonitrile, Journal of Photochemistry and Photobiology A: Chemistry, 134 (2000) 119-125.
[34] Blitz, A. Mark, Heard, E. Dwayne, Pilling, J. Michael, Wavelength dependent photodissociation of CH[3]OOH quantum yields for CH[3]O and OH, and measurement of the OH + CH[3]OOH rate coefficient, Elsevier, Kidlington, ROYAUME-UNI, 2005.
[35] J. Matthews, A. Sinha, J.S. Francisco, The importance of weak absorption features in promoting tropospheric radical production, in: Proceedings of the National Academy of Sciences of the United States of America, 2005, pp. 7449.
[36] M.J. Molina, G. Arguello, Ultraviolet absorption spectrum of methylhydroperoxide vapor, Geophys. Res. Lett., 6 (1979) 953-955.
[37] G. Vaghjiani, L., A.R. Ravishankara, Photodissociation of H_2O_2 and CH_3OOH at 248 nm and 298 K: Quantum yields for OH, $O(^3P)$ and $H(^2S)$, The Journal of Chemical Physics, 92 (1990) 996-1003.

[38] C.M. Roehl, Z. Marka, J.L. Fry, P.O. Wennberg, Near-UV photolysis cross sections of CH3OOH and HOCH2OOH determined via action spectroscopy., Atmospheric Chemistry and Physics Discussions, 6 (2006) pp. 11597-11620.
[39] Y. Takezaki, T. Miyazaki, N. Nakahara, Photolysis of Dimethyl Peroxide, The Journal of Chemical Physics, 25 (1956) 536-542.
[40] R.A. Cox, G.S. Tyndall, Rate constants for reactions of CH3O2 in the gas phase, Chemical Physics Letters, 65 (1979) 357-360.
[41] M. Yujing, A. Mellouki, The near-UV absorption cross sections for several ketones, Journal of Photochemistry and Photobiology A: Chemistry, 134 (2000) 31-36.
[42] T. Gierczak, J.B. Burkholder, S. Bauerle, A.R. Ravishankara, Photochemistry of acetone under tropospheric conditions, Chemical Physics, 231 (1998) 229-244.
[43] R.D. Martinez, A.A. Buitrago, N.W. Howell, C.H. Hearn, J.A. Joens, The near U.V. absorption spectra of several aliphatic aldehydes and ketones at 300 K, Atmospheric Environment. Part A. General Topics, 26 (1992) 785-792.
[44] E. Guillet J, J. Dhanraj, J. Golemba F, H. Hartley G, Fundamental Processes in the Photodegradation of Polymers, in: Stabilization of Polymers and Stabilizer Processes, AMERICAN CHEMICAL SOCIETY, 1968, pp. 272-286.
[45] D.M. Mowery, R.A. Assink, D.K. Derzon, S.B. Klamo, R.L. Clough, R. Bernstein, Solid-State 13C NMR Investigation of the Oxidative Degradation of Selectively Labeled Polypropylene by Thermal Aging and Î³-Irradiation, Macromolecules, 38 (2005) 5035-5046.
[46] Tadic, Jovan, Juranic, Ivan, Moortgat, K. Geert, Pressure dependence of the photooxidation of selected carbonyl compounds in air : n-butanal and n-pentanal, Elsevier, Amsterdam, PAYS-BAS, 2001.
[47] L. Zhu, Y. Tang, Y. Chen, T. Cronin, Wavelength-Dependent Photolysis of C3-C7 Aldehydes in the 280-330 nm Region, Spectroscopy Letters, 42 (2009) 467-478.
[48] A.L. Andrady, S.H. Hamid, X. Hu, A. Torikai, Effects of increased solar ultraviolet radiation on materials, Journal of Photochemistry and Photobiology B: Biology, 46 (1998) 96-103.
[49] P. Gijsman, M. Kroon, M. van Oorschot, The role of peroxides in the thermooxidative degradation of polypropylene, Polymer Degradation and Stability, 51 (1996) 3-13.
[50] P. Gijsman, G. Meijers, G. Vitarelli, Comparison of the UV-degradation chemistry of polypropylene, polyethylene, polyamide 6 and polybutylene terephthalate, Polymer Degradation and Stability, 65 (1999) 433-441.
[51] X. Yang, X. Ding, Prediction of outdoor weathering performance of polypropylene filaments by accelerated weathering tests, Geotextiles and Geomembranes, 24 (2006) 103-109.
[52] M.L. Castejon, P. Tiemblo, J.M. Gomez-Elvira, Photo-oxidation of thick isotactic polypropylene films I. Characterisation of the heterogeneous degradation kinetics, Polymer Degradation and Stability, 70 (2000) 357-364.
[53] J.-L. Gardette, C. Sinturel, J. Lemaire, Photooxidation of fire retarded polypropylene, Polymer Degradation and Stability, 64 (1999) 411-417.
[54] K. Tomiita, Hardware and software for weathering simulation of polymeric used outdoors, in: T. Reichert (Ed.) 3rd European weathering symposium, Krakow, 2007, pp. 221-230.
[55] P.S. Tobias, D.C. Trindade, Applied Reliability, New York, 1995.
[56] F.R. Mayo, Relative reactivities in oxidations of polypropylene and polypropylene models, Macromolecules, 11 (1978) 942-946.
[57] L. Achimsky, L. Audouin, J. Verdu, J. Rychly, L. Matisova-Rychla, On a transition at 80 °C in polypropylene oxidation kinetics, Polymer Degradation and Stability, 58 (1997) 283-289.
[58] E. Richaud, F. Farcas, P. Bartoloméo, B. Fayolle, L. Audouin, J. Verdu, Effect of oxygen pressure on the oxidation kinetics of unstabilised polypropylene, Polymer Degradation and Stability, 91 (2006) 398-405.
[59] L. Achimsky, Etude cinétique de la thermooxydation du polypropylène, in: Mécanique et Matériaux, Université Pierre et Marie-Curie (Paris VI), Paris, 1996.
[60] L. Achimsky, L. Audouin, J. Verdu, Kinetic study of the thermal oxidation of polypropylene, Polymer Degradation and Stability, 57 (1997) 231-240.
[61] A.V. Tobolsky, Oxidative degradation of polymeric material, Discussions of the Faraday Society, 2 (1947) 384-388.

[62] A.V. Tobolsky, D.J. Metz, R.B. Mesrobian, Low temperature autoxidation of hydrocarbons: The phenomenon of maximum rates, Journal of the American Chemical Society, 72 (1950) 1942-1952.
[63] L. Audouin, L. Achimsky, J. Verdu, Kinetic modelling of low-temperature oxidation of hydrocarbon polymers., in: e. Hamid SH (Ed.) Handbook of polymer degradation. 2nd ed, Marcel Dekker, New York, 2000, pp. 734.
[64] N. Khelidj, X. Colin, L. Audouin, J. Verdu, A simplified approach for the lifetime prediction of PE in nuclear environments, Nuclear Instruments and Methods in Physics Research Section B: Beam Interactions with Materials and Atoms, 236 (2005) 88-94.
[65] N. Khelidj, X. Colin, L. Audouin, J. Verdu, C. Monchy-Leroy, V. Prunier, Oxidation of polyethylene under irradiation at low temperature and low dose rate. Part II. Low temperature thermal oxidation, Polymer Degradation and Stability, 91 (2006) 1598-1605.
[66] R. Arnaud, J.-L. Gardette, J. Lacoste, A. Rivaton, Evolution photochimique des macromolécules organiques naturelles et synthétiques- Photoprotection des matériaux polymères synthétiques, L'Actualité Chimique [In french], N°7 (suppl.) (12/94) (1994) 132-210.
[67] S. Commereuc, D. Vaillant, J.L. Philippart, J. Lacoste, J. Lemaire, D.J. Carlsson, Photo and thermal decomposition of iPP hydroperoxides, Polymer Degradation and Stability, 57 (1997) 175-182.
[68] N.C. Billingham, E.T.H. Then, A. Kron, Chemiluminescence from peroxides in polypropylene: II. Luminescence and kinetics of peroxide decomposition, Polymer Degradation and Stability, 55 (1997) 339-346.
[69] G. Geuskens, F. Debie, M.S. Kabamba, G. Nedelkos, New aspects of the photooxidation of polyolefins, Polymer Photochemistry, 5 (1984) 313-331.
[70] G. Geuskens, M.S. Kabamba, Photo-oxidation of polymers--Part V: A new chain scission mechanism in polyolefins, Polymer Degradation and Stability, 4 (1982) 69-76.
[71] G. Geuskens, M.S. Kabamba, Photo-oxidation of polymers: Part IX--Additional comments about a new chain scission mechanism in polyolefins, Polymer Degradation and Stability, 5 (1983) 399-401.
[72] E. Guillet J, Studies of energy transfer and molecular mobility in polymer photochemistry, Pure and Applied Chemistry, 49 (1977) 249-258.

CHAPTER VII. A general kinetic model for the photothermal oxidation of polypropylene

A. François-Heude[a,b 5], E. Richaud[a], E. Desnoux[b], X. Colin[a]
[a]PIMM Laboratory, CNRS UMR 8006, Arts et Metiers ParisTech, Paris, France
[b]Renault, Research Department, Guyancourt, France

Abstract

A general kinetic model for the photothermal oxidation of polypropylene has been derived from the basic auto-oxidation mechanistic scheme in which the main sources of radicals are the thermolysis and photolysis of the most unstable species, i.e hydroperoxides. Thermolysis is a uni- or bi-molecular reaction whose rate constant obeys an Arrhenius law. In contrast, photolysis is exclusively a unimolecular reaction and its rate constant is independent of temperature. According to the quantum theory, this latter is proportional to the energy absorbed by photosensitive species and thus, accounts for the impact of UV-light intensity and wavelength on the global oxidation kinetics.

The validity of this model has been checked on iPP films homogeneously oxidized in air over a wide range of temperatures and UV-light sources. It gives access to the concentration changes of: (i) primary (hydroperoxides) and secondary(carbonyls) oxidation products, (ii) double bonds, (iii) chain scissions and crosslinking nodes, but also to the subsequent changes in molecular masses. These calculations are in full agreement with the photolysis results reported by Carlsson and Wiles in the 70's [1-3]. However, the model seems to be only valid for UV-light energies equivalent to about 10 suns as upper boundary, presumably because of multiphotonic excitations or chromophores photosensitization (i.e. termolecular photo-physical reactions), both enhanced at high irradiances.

Keywords

[5] Corresponding author : Email: Alexandre.FRANCOIS-HEUDE@ensam.eu
Tel/ Fax: +33 1 44 24 64 13/ +33 1 44 24 63 82

Polypropylene; Photochemistry; Photothermal Oxidation; Diffusion limited oxidation; Screen effect; Kinetic modeling.

1. Introduction

The first attempts to model the oxidation kinetics of hydrocarbon polymeric substrates were done by Tobolsky et al. [4, 5] with the perspective of predicting their long-term behavior. Their analytical model was derived from an oversimplified mechanistic scheme in which the radical chain oxidation was composed of only four elementary chemical steps. Initiation consisted in the formation of radical species either from the thermal decomposition of hydroperoxides or from the effect of extrinsic factors (e.g. a radiation source). Propagation took place in two successive stages: the rapid addition of oxygen onto alkyl radicals followed by the slower hydrogen abstraction on polymer substrate by peroxy radicals. Finally, termination consisted only in the bimolecular combination of peroxy radicals. Thus, according to these authors, thermal and photochemical oxidation could be described by a very close mechanistic scheme differing only by their initiation step. A mathematical expression for oxidation rate was obtained through the conventional concepts of chemical kinetics by making four simplifying assumptions: 1) Unicity of reactive site, i.e. oxidation occurs exclusively on the most labile CH bond; 2) Low conversion ratios of oxidation process, i.e. concentration of reactive sites remains virtually constant; 3) Constancy of initiation rate in the case of oxidation induced by an extrinsic factor; 4) And steady-state for radicals concentrations in all oxidation cases, but also for hydroperoxides concentration in the case of pure thermal oxidation. This kinetic modeling approach turned out to be astonishingly efficient despite its apparent simplicity. It allowed predicting accurately the homogeneous thermo-, photo- and radio-oxidation of thin polymer films (typically 100 µm thick) exposed under a sufficiently high oxygen partial pressure to fully saturate the sample in oxygen, i.e. to reach the so-called regime of oxygen excess.

Kinetic developments were then made by Bolland and Gee [6], Reich and Stivala [7, 8], Furneaux and Davis [9, 10] and Audouin et al. [11], but also by Gillen and Clough [12], with the objective to describe other oxidation regimes of lower oxygen concentration than oxygen excess. These authors added other possible termination reactions, namely bimolecular combinations of alkyl-alkyl and alkyl-peroxy radicals, to the previous mechanistic scheme. They obtained a hyperbolic expression for oxidation rate by making two additional simplifying assumptions (in

addition to the previous four assumptions): 5) Long kinetic chain; 6) And existence of an interrelationship between termination rate constants. This model allowed to describe the oxygen concentration dependence of the oxidation rate of thin polymer films and to determine the critical value of the oxygen partial pressure above which oxygen is in excess. Moreover, when coupled with the Fick's second law (for oxygen diffusion) into an oxygen balance equation, this model allowed also to accurately predict the concentration profiles of oxygen and oxidation products in thick polymer samples (typically few mm thick).

Since then, new kinetic developments were made by Gillen et al. [12] and Colin et al. [13, 14] to reduce the number of questionable simplifying assumptions and thus, increase the robustness of the analytical kinetic model.

In the eighties, the advances of the previous decades in the elucidation of chain radical oxidation reactions and the emergence of new numerical algorithms especially adapted for solving stiff problems of chemical kinetics enabled Sommersal and Guillet to envisage the development of a numerical model for polyolefins photooxidation [15]. Their approach consisted in considering all the possible elementary chemical steps (up to sixty) and assigning them a rate constant whose value was determined on model compounds, when possible. Such an exhaustive approach was very attractive since it enabled to eradicate all the questionable simplifying assumptions (except assumption 1), but it failed because the numerical problem to be solved was largely oversized. Indeed, for most oxidation cases, too many rate constants were unknown and some of them were experimentally out-of-reach.

This observation encouraged our research team to propose an alternative approach of kinetic modeling. It consists in deriving a kinetic model from a simplified, but realistic, oxidation mechanistic schemeby focused on the critical oxidation path, i.e. constituted of the main contributory reactions to photothermal oxidation. In the case of pure thermal oxidation, it is called the "Closed Looped Mechanistic Scheme" (CLMS) [16, 17] [18], since the main source of radicals is the thermal decomposition of its main propagation products, i.e. hydroperoxides**.**

In the early 2000's, this numerical tool has been extended to solve oxidation problems initiated by extrinsic species or factors, in particular gamma-irradiation in a nuclear environment [19]. Now, it remains to extent this approach to the case of photothermal oxidation. However, the quantitative impact of UV-light on the initiation step of oxidation has not been clearly formalized. The introduction of a term of photo-induced initiation in a numerical model has been

performed by Kiil in the case of the photooxidation of epoxy coatings, but the corresponding initiation rate has been described through an empirical law [20], whereas it would be possible to use the quantum theory. A criterion, based on the absorbed energy by photosensitive species, was recently proposed in this purpose and tested through an analytical model [21]. This theory allowed describing the competition between thermal and photochemical initiations during polypropylene oxidation. However, the analytical treatment prevented from introducing photochemical initiation by multiple photosensitive species, and the values of quantum yields were excessive compared with the experimental values reported by Carlsson and Wiles [1-3, 22].

The objective of the present publication is to extend the numerical kinetic model, beforehand established for pure thermal oxidation, to the photothermal oxidation of iPP by taking into account the additional effect of UV-light sources. After having checked its validity, this model will be used for investigating the relative predominance of two important photosensitive species (namely peroxide type species and ketones) in the initiation step of photothermal oxidation which, still today, remains a controversial topic in the literature.

2. Experimental part

2.1. Materials

The isotactic polypropylene under investigation was supplied as pellets by Aldrich (under the reference 427888). Its main physico-chemical characteristics are: MFI [230°C, 2.16 kg] = 12 g/10min, M_w = 250 kg.mol^{-1}, M_n = 67 kg.mol^{-1} and PI = 3.7. Films of 80-135 µm thick were processed by compression molding in a Gibitre laboratory press during 1 min at 200°C under 20 MPa, and then purified from their stabilizers by Soxhlet extraction for 48 hours using dichloromethane as solvent prior to aging experiments.

2.2. Photothermal aging

In order to decouple UV-light from thermal effects, PP films were exposed under different light intensities and temperatures, always in dry conditions. Photothermal aging experiments were mostly performed on films of 80 µm thick in a series of SEPAP devices equipped with 80 W medium pressure arc mercury lamps having a borosilicate filter. To vary the light intensity, the number of lamps was changed from 2 to 4 lamps in a SEPAP 12-24 device, and from 6 to 8 lamps in a SEPAP 50-24 device. Both light intensity and emission spectrum were measured using

a IL390C radiometer in the 295-415 nm range and a Avantes spectro-radiometer (AvaSpec 2048x14-USB2, 0.7 nm resolution) in the 250-750 nm range respectively. Temperature was fixed at 45°C, 60°C or 80°C according to the apparatus specifications and directly monitored on sample surfaces using a thermo-button temperature logger. A photothermal aging test was also performed on films of 135 µm thick in a WeatherO'Meter device (WOM) equipped with a Xenon Lamp and Borosilicate S/S filters. The black (BPT) and white standard (WST, i.e. chamber) temperatures were fixed at 70°C and 55°C respectively. The temperature of the sample was found to be intermediary at 64°C, whereas the irradiance at 340 nm was measured at 0.46 $W.m^{-2}.nm^{-1}$, without water spraying. The thermal oxidation (in the absence of UV-light) was also investigated in air-ventilated ovens for temperatures ranging from 60°C to 140°C.

To ensure the test reproducibility (between samples stemming from different batches during their purification from stabilizers) and to determine a sampling frequency suitable for an accurate description of the oxidation kinetics (particularly fast under the harsher aging conditions), it was decided to proceed in two stages:

- A non-destructive monitoring of carbonyl oxidation products by FTIR spectrophotometry, repeated for all aging conditions on samples coming from three different batches.
- Both destructive (hydroperoxide titration, Gel Permeation Chromatography, DSC, etc…) and non-destructive analyses (FTIR spectrophotometry) on samples from different batches, periodically removed from the aging devices.

This is the reason why different datasets are depicted for carbonyl products in most of the aging conditions.

2.3. FTIR analyses

FTIR analyses were performed using a Perkin-Elmer spectrophotometer (16 scans, 4 cm^{-1} resolution) in order to monitor aging by basing on the peak of carbonyl at 1713 cm^{-1} accounting for the stretching (or valence vibration) of the C=O bond with a molar extinction coefficient fixed at $\varepsilon = 300\ L.mol^{-1}.cm^{-1}$. Actually, the FTIR absorbance only enables to perform semi-quantitative titration of the different carbonyl species due to overlapping of multiple carbonyl peaks (assigned to ketones, acids, esters, etc.).

The C=C ethylenic unsaturations were also tentatively monitored using the peak at 1645 cm^{-1} which results from the stretching or valence vibration υ of vinyl, vinylidene and cis-vinylene groups (peaks are assigned according to reference [23]). This mode of vibration appears at 1680 cm^{-1} for trans-vinylene and tri- or tetra-substituted olefins, and thus is partially overlapped by the increasing carbonyl peaks of oxidation products. All the other characteristic peaks identified for vinyl (at 910 and 990 cm^{-1}), vinylidene (890 cm^{-1}), cis-vinylene (690 ± 40 cm^{-1}), trans-vinylene (965 cm^{-1}) and tri-substituted olefins (815 ± 25 cm^{-1}) turns out to be unemployable either because of insufficient absorption or because of overlap with polypropylene characteristic peaks. In such conditions, only the peak at 1645 cm^{-1} is relevant for monitoring the double bonds formed during the course of photothermal oxidation, in particular vinylidenes or tri-substituted olefins by disproportionation (see further termination steps 4 and 5), or cis- and trans- vinylene as well as vinyl groups by the Norrish 2 reaction. Although only a part of these species are titrated at 1645 cm^{-1}, a value of ε = 20 $L.mol^{-1}.cm^{-1}$ [24] was chosen for the molar extinction coefficient, after having checked that it successfully accounts for the concentration of C=C double bonds, at least for those generated by disproportionation during thermal oxidation.

2.4. Hydroperoxides titration

The iodine method was chosen to perform hydroperoxides titration, instead of the sulfide dioxide or ferrous cyanate reactive methods, due to its better reliability for polypropylene [25, 26]. This former is based on the reduction of hydroperoxides by sodium iodide in an acidic medium according to the reaction:

$$R_3COOH + 3I^- + 2H^+ \rightarrow R_3COH + I_3^- + H_2O$$

The concentration of I_3^- ions was titrated by UV spectrophotometry at 355 nm using a Perkin-Elmer Lambda 35 device and a molar extinction coefficient of ε = 25000 $L.mol^{-1}.cm^{-1}$. About 10 mg of PP sample and 7 ml of a solution of isopropanol and acetic acid solvents mixture (10:1) were introduced into a two neck glass flask equipped with a bulb condenser. When refluxing, 2 ml of sodium iodide dissolved in isopropanol (200 $g.L^{-1}$) was added with a syringe throughout the side neck. After 10 minutes, the mixture was quenched up to room temperature with 25 ml of distilled water. It is noteworthy that the previous iodometry procedure does not enable discrimining between hydroperoxides, peracids and peresters. Dialkyl peroxides would not be

titrated in theory except if chlorhydric acid is used instead of acetic acid as catalyst. The accuracy on concentration measurement was estimated to be ± 7.5 mol%.

2.5. Molecular weight measurement

Gel Permeation Chromatography (GPC) experiments were performed with a PL-GPC 220 high temperature device commercialized by Agilent Technologies. The GPC was equipped with a guard column and two columns branded PLGel Olexis as well as a refractive index detector. The eluent was 1,2,4-trichlorobenzene (Chromasolv, Sigma-Aldrich) stabilized with 0.03 wt% of 2,6-di-*tert*-butyl-4-methylphenol (BHT, Fluka). It was filtered with a 0.2 µm pore size membrane (in PTFE, Whatman) before use. The injection volume was 200 µl and the flow rate was 1.0 ml/min. PP samples were dissolved in 1,2,4-trichlorobenzene/BHT (0.3 wt%) using a PL-SP 260-VS high temperature sample preparation system (PL Ltd.) at 135 °C during 20 minutes. The calibration curve was established from four Polystyrene Shodex narrow standards of respective molecular weights of 1470000, 257000, 46500 and 7210 $g.mol^{-1}$. Results were then corrected using the so-called "universal calibration", based on the well-known Mark-Houwink's relationship (Eq. 1) with the coefficient values reported in table 1.

$$[\eta] = K \bullet M^{\alpha} \qquad \textbf{Eq. 1}$$

Table 1: Coefficients used for the universal calibration

Materials	**K (10^3 $ml.g^{-1}$)**	**α**	**References**
Polystyrene standards	13.8	0.70	[27, 28]
Polypropylene	15.2	0.76	[29]

2.6. Crystallinity ratios measurement

Differential scanning calorimetry (DSC) was performed on 10 mg sample weight with a TA Q1000 calorimeter under a nitrogen flow. A temperature ramp of $10°C.min^{-1}$ from 30 to 200°C was applied in order to minimize the annealing phenomena. Crystallinity ratios were calculated taking a melting enthalpy for crystalline lamellae of ΔH_m^0 = 209 $J.g^{-1}$. The initial crystallinity value was 45 ± 3 %wt.

3. Theory

3.1. Multi-Closed-Loop Mechanistic Scheme (MCLMS)

The basic idea of the kinetic modeling approach, first formulated by Tobolsky [4, 5], is that the different kinds of oxidative aging (i.e. thermo-, radio- and photo-oxidation) differ exclusively by the nature of their initiation step. Thus, the mechanistic scheme of photothermal oxidation can be obtained by introducing, into the now common "Closed-Loop Mechanistic Scheme" (CLMS) previously established for pure iPP thermal oxidation [30, 31], additional initiation steps due to the effect of UV-light, in particular the photolysis of cleavable photosensitive species (i.e. chromophores). The CLMS has been recently updated for iPP [30, 31]. It is briefly reminded in the next section.

3.1.1. Thermal nucleus

Initiation

(1u) $POOH \rightarrow 2P^{\bullet} + (1 - \gamma_1)POH + \gamma_1 P{=}O + H_2O + \gamma_s S$ (- 2PH) (k_{1u})

(1b) $2POOH \rightarrow P^{\bullet} + PO_2^{\bullet} + (1 - \gamma_1)POH + \gamma_1 P{=}O + H_2O + \gamma_s S$ (- PH) (k_{1b})

Propagation

(2) $P^{\bullet} + O_2 \rightarrow PO_2^{\bullet}$ (k_2)

(3) $PO_2^{\bullet} + PH \rightarrow POOH + P^{\bullet}$ (k_3)

Termination

(4) $P^{\bullet} + P^{\bullet} \rightarrow \gamma_4 P\text{-}P + (1 - \gamma_4)PH + (1 - \gamma_4)F + \gamma_4 B$ (k_4)

(5) $P^{\bullet} + PO_2^{\bullet} \rightarrow \gamma_5 POOP + (1 - \gamma_5)POOH + (1 - \gamma_5)F + \gamma_5 B$ (k_5)

(6a) $PO_2^{\bullet} + PO_2^{\bullet} \rightarrow [PO^{\bullet}\ {}^{\bullet}OP]_{cage} + O_2$ (k_{6a})

(6b) $[PO^{\bullet}\ {}^{\bullet}OP]_{cage} \rightarrow POOP + B$ (k_{6b})

(6d) $[PO^{\bullet}\ {}^{\bullet}OP]_{cage} \rightarrow 2P^{\bullet} + 2(1 - \gamma_1)POH + 2\gamma_1 P{=}O + 2\gamma_s S$ (- 2PH) (k_{6d})

The CLMS consitutes the thermal nucleus of the mechanistic scheme for the photothermal oxidation of iPP. The main source of radicals is the thermal decomposition of hydroperoxides (POOH) which are the primary oxidation products generated in the propagation step. Thereby, hydroperoxides govern the oxidation kinetics and determine the length of the induction period.

In this scheme, PH accounts for tertiary CH groups (i.e. methynes) which are considered as the unique oxidation site of polymer chain. Their radical attack leads to a large variety of degradation products, in particular:

(i) Reactive species formed in addition to POOH, such as alkyl $P^{\bullet}$ and peroxy radicals $PO_2^{\bullet}$.

(ii) Inactive products accumulating in the polymer matrix during the course of oxidation, such as: peroxides POOP, alcohols P-OH, double-bonds or unsaturations F, and ketones or assimilated carbonyl products P=O. They are all denoted as secondary oxidation products since they result from the decomposition of primary oxidation products (POOH).

(iii) Macromolecular events contributing to the modification of polymer physical and mechanical properties, such as chain scissions S on the main polymer chain and crosslinks B (i.e. chemical bridges) between two adjacent polymer chains.

Different stoichiometric coefficients have been introduced as yields for describing the competition between several elementary reactions in balance reactions. For instance, γ_4 and γ_5 are the respective yields of recombination by coupling of alkyl-alkyl and alkyl-peroxy radicals versus disproportionation in termination steps.

Moreover, γ_1 is the yield in β-scission (leading to ketones) face to hydrogen abstraction (leading to alcohols) in both unimolecular (1u) and bimolecular initiation steps (1b). For a sake of simplicity, γ_s accounts for to β-scissions on the main polymer chain (denoted S), which significantly impact the molecular mass, contrarily to β-scissions on side-chain and end-chain groups which generate small volatile organic compounds..

From a practical point of view, it is more convenient to consider an apparent yield γ_1 for carbonyl products owing to the high uncertainty on their nature and the value of their molar extinction coefficients at 1713 cm^{-1}.

Finally, it is likely that formalizing the competition between propagation (by hydrogen abstraction) and recombination of alkoxy radicals through a cage reports the thermolabile feature of peroxide bridges.

3.1.2. Photochemically induced initiation processes

To account for the effect of UV-light, several important photo-induced reactions have to be considered. Since UV-light is an extrinsic source of radicals, the decomposition reactions of all photosensitive species (i.e. chromophores) identified as cleavable have been introduced into the previous CLMS. These reactions are: (i) The photolysis of hydroperoxides, through the scission

of O-O bond, (ii) The analogous photolysis of peroxide bridges, since these latter are still more photosensitive than hydroperoxides, (iii) The homolytic scission (in α-position) of ketones, also named Norrish I reaction, (iv) And the Norrish II reaction, through a concerted mechanism involving a six centers rearrangement.

These reactions are all the more relevant to consider that they have been identified as the main sources of chain-scission and thus, appear as critical in order to simulate the subsequent changes in mechanical and aspect properties.

It is noteworthy that the amount of ketones has been properly formalized here by differentiating them from other carbonyl species, since they do not accumulate in the polymer matrix anymore: ketones are now submitted to photolysis processes (in particular, Norrish 1 reaction) because they absorb UV-light above 290 nm, unlike other carbonyl products such as esters or carboxylic acids. Besides, it has been necessary to differentiate middle-chain from end-chain ketones (i.e. methyl ketones), denoted as ketones A (K_A) and ketones B (K_B) respectively, since their formation (by photolysis of alkyl- and hydro-peroxides) and decomposition (by Norrish 1 and 2 reactions) do not involve the same scission position along the polymer chain. Indeed, ketones K_B are formed by β-scissions on the main polymer chain, whereas ketones K_A result from β-scissions on side-chain methyl groups. Their respective yields were written γ'_1 and γ''_1. They satisfy the following equality: $\gamma_1 = \gamma'_1 + \gamma''_1$. Moreover, only Norrish type reactions on ketones K_A lead to scissions on main polymer chain, unlike those on ketones K_B which induce scissions near chain extremities.

Hydroperoxides decomposition can be written through the following sequence of elementary chemical steps:

$$POOH + h\nu \rightarrow PO^{\bullet} + HO^{\bullet} \qquad (k_{1h})$$
$$\gamma'_1\ PO^{\bullet} \rightarrow \gamma'_1\ K_A + P^{\bullet}_{\text{non tertiary}}$$
$$\gamma''_1\ PO^{\bullet} \rightarrow \gamma''_1\ K_B + P^{\bullet}_{\text{non tertiary}} + \gamma_s\ S$$
$$P^{\bullet}_{\text{non tertiary}} + PH \rightarrow PH_{\text{non tertiary}} + P^{\bullet}$$
$$(1 - \gamma'_1 - \gamma''_1)PO^{\bullet} + PH \rightarrow (1 - \gamma'_1 - \gamma''_1)P\text{-}OH + P^{\bullet}$$
$$HO^{\bullet} + PH \rightarrow H_2O + P^{\bullet}$$

Then, the balance reaction is:

$$\text{(1h)}\quad POOH + h\nu \rightarrow 2P^{\bullet} + (1 - \gamma'_1 - \gamma''_1)P\text{-}OH + \gamma'_1\ K_A + \gamma''_1\ K_B + H_2O + \gamma_s S \quad (-2PH)\ (k_{1h})$$

Its rate is governed by the slowest step, i.e. the scission of O-O bond. Thus, hydroperoxides decomposition by UV-light is assumed to be exclusively unimolecular. Indeed, from a photophysical point of view, the photo-induced bimolecular decomposition of hydroperoxides would apply to a termolecular process whose probability of occurrence would be very low in most of cases. This assumption will be discussed further in a section dedicated to termolecular processes in general.

Regarding all peroxide type species, the photolysis of peroxide bridges must be also considered. Indeed, these latter are known to be more photosensitive (due to their higher molar extinction coefficient) than and almost as cleavable as hydroperoxides [1, 3]. The sequence of elementary chemical steps is similar as for hydroperoxides, except that photolysis generates two alkoxy radicals instead of one alkoxy and one hydroxy radicals. Thus, the writing of the balance reaction is immediate:

(1p) $POOP + h\nu \rightarrow 2P^{\bullet} + 2(1 - \gamma'_1 - \gamma''_1)P\text{-}OH + 2\gamma'_1 K_A + 2\gamma''_1 K_B + 2\gamma_s S$ (-2PH)
(k_{1p})

Norrish 1 reaction generates an acyl radical which is assumed to undergo a total decarbonylation to give finally an alkyl radical.

$K_A + h\nu \rightarrow P{=}O^{\bullet} + P^{\bullet}_{\text{non tertiary}} + S$ (k_{N1A})
$K_B + h\nu \rightarrow P{=}O^{\bullet} + P^{\bullet}_{\text{non tertiary}}$ (k_{N1B})
$P{=}O^{\bullet} \rightarrow P^{\bullet}_{\text{non tertiary}} + CO\nearrow$
$P^{\bullet}_{\text{non tertiary}} + PH \rightarrow P^{\bullet} + PH_{\text{non tertiary}}$

Hence, the corresponding balance reactions for ketones A and B are:

(N1A) $K_A + h\nu \rightarrow 2P^{\bullet} + CO\nearrow + S$ (- 2PH) (k_{N1A})
(N1B) $K_B + h\nu \rightarrow 2P^{\bullet} + CO\nearrow$ (- 2PH) (k_{N1B})

Norrish 2 reaction consists in a six-membered mechanism which does not produce radicals, but transforms the middle-chain ketone K_A intoan end-chain ketone K_B (methyl ketone). In contrast, it eliminates ketone K_B in the form of a volatile product (acetone).

(N2A) $K_A + h\nu \rightarrow K_B + F + S$ (k_{N2A})
(N2B) $K_B + h\nu \rightarrow F + Ac\nearrow$ (k_{N2B})

where F designates a vinylene double bond.

Therefore, the general mechanistic scheme for the photothermal oxidation of polypropylene potentially involves several closed loops, since peroxide type species and ketones are all 'critical species' which decompose into radicals meanwhile they are produced during the oxidation process. Thereafter, it will be called "Multi-Closed Loops Mechanistic Scheme" (MCLMS).

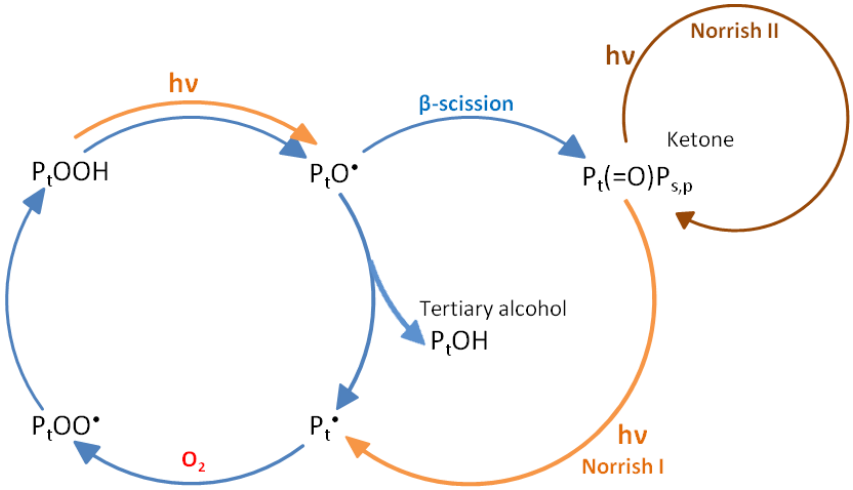

Figure 1: Multi-Closed-Loops Mechanistic Scheme for the photothermal oxidation of polypropylene

3.2. Kinetics in photochemistry

3.2.1. Quantum theory (the reader may refer to Calvert and Pitts [32] or Ranby and Rabek [33] for more details)

According to the first law of photochemistry (Grotthus, 1817 and Drapper, 1843), only the UV-light absorbed by a molecule can lead to photochemical changes. According to the second law of photochemistry (Stark-Einstein, 1908), this is a one-quantum process. In the case of hydroperoxides photolysis, the absorption of light is attributed to the forbidden σ*←n transition from a non-bonding orbital to an anti-bonding valence orbital. As a consequence, the excited state is not stable and its absorption spectrum (i.e. the spectral distribution of molar extinction coefficient) is very diffuse. This result thereby explained both the high cleavability and the relatively low value of the molar extinction coefficient of hydroperoxides. At this stage, it is

valuable to precise that the molar extinction coefficient accounts for the probability that an incident quantum will be absorbed by a molecule after a collision.

In the case of ketones, the main absorption band, whose maximum appears between 280 and 320 nm in the UV-visible range, corresponds to the excitation of an electron from a nonbonding to an antibonding orbital ($\pi^* \leftarrow$ n transition), mainly localized on the carbonyl group. The absorption in the far UV-range corresponds to the $\pi^* \leftarrow \pi$ transition for the excited electron, which is delocalized over the entire molecule.

Once excited from ground state S_0 to singlet excited state S_1, the molecule can desexcite though different elementary steps (bond dissociation, intramolecular isomerization, fluorescence, phosphorescence, internal conversion or vibrational (i.e. non-radiative) relaxation), denoted as kinds of primary processes since they result from the immediate effect of light on the absorbing molecule. In contrast, the secondary processes consist in subsequent chemical reactions undergone by excited molecules or in the production of radicals by the primary processes. It is thus possible to calculate the efficiency, i.e. the probability of occurrence, of the bond dissociation (by photolysis) compared with other competitive primary processes. Since it is a one-quantum mechanism, the sum of the quantum yields of all these elementary photochemical processes is equal to unity (Stark-Bodenstein, 1913). On the contrary, when secondary processes are involved, the quantum yield of this phenomenon can be greater than unity. This is the case, for instance, for chain scission processes.

3.2.2. Formalism and calculation of the rate constants of photo-induced reactions

The temperature dependence of thermal oxidation is described by applying the Arrhenius law to the rate constant k_i of each elementary reaction (i):

$$k_i = k_i^0 \exp\frac{-Ea_i}{RT} \qquad \textbf{Eq. 2}$$

with k_i^0 the preexponential factor and Ea_i the activation energy

Analogeously, a suitable formalism must be found to report the kinetic dependence of photo-induced reactions with the amount of "radiant" UV-visible energy. According to the quantum theory, the initiation rate by a given photosensitive species X (i.e. a chromophore) can be written

as the product of the energy absorbed by the photolysis efficiency, i.e. the probability that an absorbed photon triggers the chemical bond dissociation:

$$\left.\frac{d[X]}{dt}\right]^{photolysis} = -\Phi(\lambda)_X \times I_{abs_v} \quad \textbf{Eq. 3}$$

with [X] the concentration of the chemical species X (in mol.L^{-1}),

$I_{abs.v}$ the volumic absorbed energy (in Einstein.L^{-1}.s^{-1}),

and $\Phi(\lambda)_X$ the quantum yield of photolysis efficiency (in mol.Einstein^{-1}, dimensionless).

This energy absorbed by the photosensitive species consists in the overall quanta energy satisfying the authorized electronic transitions. It can be thus deduced by calculating the overlap between the spectral distribution of molar extinction coefficient and the energy emitted by the UV-light source. It can be written as:

$$I_{abs_v} = \int_{\lambda_{min}}^{\lambda_{max}} \frac{\ln(10)}{10} \frac{E(\lambda)}{N_a} \frac{\lambda}{hc} \frac{\varepsilon_X(\lambda)\ \Delta z\ [X]}{\Delta z}\, d\lambda \qquad \textbf{Eq. 4}$$

with E(λ) the spectral irradiance of the light source including filters (in W.m^{-2}.nm^{-1}),

N_a the Avogadro's number,

h the Planck constant equal to 6.623·10^{-34} J.s,

c the light celerity (in m.s^{-1}), λ the wavelength (in m),

$\varepsilon_X(\lambda)$ the spectral distribution of the molar extinction coefficient (in L.mol^{-1}.cm^{-1}),

[X] the concentration of the photosensitive species X (in mol.L^{-1}),

and Δz the sample thickness (in m).

Since the concentration *[X]* is a separate variable, it is possible to calculate the spectral overlap integral of light absorption J_X (in Einstein.mol^{-1}.s^{-1}), chosen here as the relevant criterion independent of concentration to describe oxidation, and defined as:

$$J_X = \frac{I_{abs_v}}{[X]} = \int_{\lambda_{min}}^{\lambda_{max}} \frac{\ln(10)}{10} \frac{E(\lambda)}{N_a} \frac{\lambda}{hc} \varepsilon_X(\lambda)\ d\lambda \qquad \textbf{Eq. 5}$$

It is thus noteworthy that the product $\Phi \cdot J$ is homogeneous to the rate constant of a unimolecular decomposition (i.e. expressed in s^{-1}). If k_{1x} designates the corresponding rate constant, it can be thus written, for a given chemical species X: $k_{1x} = \Phi_X \cdot J_X$.

3.2.3. Domains of validity

Thus, the presented theory of quantum photochemistry only deals with the "bimolecular" interaction of a UV-light quantum with a molecule, i.e. an unimolecular photo-induced bond dissociation. In other words, this is not suitable for treating the case of termolecular reactions (involving two molecules and a quantum). The probability of collision between three species is usually considered as very low, but could occur in several cases: two molecules would be associated in a relative stable complex, whose lifetime would be long enough to allow a quantum absorption. This is all the more likely for high density (concentration) of quanta and so, high irradiance. Applying the quantum theory would be theoretically possible by formalizing the transient state for a molecule in a complex, but the absorption features of such an intermediate species are unclear and experimental data are very scarce.

The other complication for high UV-light intensities would be the occurrence of biphotonic (or multiphotonic) excitations, which consist in a quantum absorption by a molecule already excited by a previous absorption. Such a phenomenon is considered as negligible for sufficiently low irradiances regarding at the short lifetime of excited states. Admittedly, it remains possible to consider the notion of three-states quantum yields in order to account for the excitation of the excited states higher than S_1, but this problem would be practically out-of-reach because of the overcomplexity of phenomena. As a result, it will be considered that the validity of the kinetic model is restricted to monophotonic excitations.

3.2.4. Application to kinetic modeling

Solving a problem of photothermal oxidation requires beforehand the determination of unknown kinetic parameters, in particular Φ and J, as well as the setting of several simplifying assumptions:

(i) The quantum yield must be independent of temperature. This is theoretically true for primary processes according to Calvert and Pitts [32]. Guillet et al. [34] measured the temperature dependence of the quantum yield of Norrish type reactions. They found an activation energy of 3.5 $kJ.mol^{-1}$ for Φ_{N2} in the case of 8-

pentanedecanone, which is a rather moderate value. They observed activation energies of 20 and 21.7 kJ.mol^{-1} for Φ_{N2} in the case of 8-pentanedecanone and polyethylene-co-carbon monoxide (PE-co-CO) respectively. This latter temperature dependence was presumably assigned to a radical diffusion facilitated at high temperature, thereby promoting cleavage according to the Frank-Rabinowitch's principle (cage effect). Besides, it is noteworthy that this quantum yield was measured basing on the emission of carbon monoxide, whereas decarbonylation is expected to be thermally activated [35].

(ii) The quantum yield must be independent of the molecular weight of photosensitive species. Otherwise, it would change with the amount of chain scissions and thus, would be time-dependent. This assumption has been investigated by Guillet et al. in the case of Norrish 1 reaction for model compounds, again basing on the yield in carbon monoxide [34, 36]. They found no change with molar mass in the case of molecules containing more than 30 carbon atoms.

The quantum yield must remain unchanged along time, i.e. must be independent of the conversion degree of oxidation. To apprehend this issue, it is relevant to carefully study photochemical processes, especially Norrish type reactions. For instance, Norrish 2 rearrangement would happen from both singlet S_1 and triplet T_1 excited states [37]. In a non-polar solvent, such as hexane, this reaction would be twice more likely to occur from T_1 than S_1 for both aliphatic and acyclic ketones according to studies made on poly(ethylene-co-carbon monoxide) [37] and molecular model compounds [38, 39]. However, only rearrangements from singlet state would be independent of the solvent polarity. These results suggest that the quantum yield for the Norrish 2 reaction is prone to change with the polymer polarity, thus restraining the validity of the kinetic model to low conversion degrees of oxidation for which polarity changes are negligible.

(iii) Theoretically, the quantum yield is wavelength dependent, so its spectral distribution $\Phi(\lambda)$ should be considered. This dependence can be explained, for instance, by the settlement of higher excited states than S_1. Their direct determination can be tentatively performed on model compounds by using monochromatic UV-light sources, for instance lasers, in the case of flash

photolysis techniques. These spectral distributions have been compiled for tert-butyl hydroperoxide [40] and various ketonic products [41, 42], as depicted in appendix B. The photolysis of macromolecular photosensitive species could also be investigated by using other types of monochromatic UV-light source, such as LED, or polychromatic sources with filters of narrow bandwidth [43, 44]. In practice, it is more convenient to consider that the quantum yield is constant in the whole spectral range, i.e. that its spectral distribution can be neglected. Such a hypothesis is not unrealistic, considering that the efficient wavelength range is restricted to few decades of nanometers in current photochemical aging conditions.

3.3. Model equations

3.3.1. System of differential equations (SDE)

The MCLMS can be translated into a system of ordinary differential equations (SDE) describing the local concentration changes in relevant chemical species by using the classical concepts of chemical kinetics. This SDE can be written as (**Eq. 6-14)**:

$$\frac{d[P^\bullet]}{dt} = 2k_{1u}[POOH] + k_{1b}[POOH]^2 - k_2[P^\bullet][O_2] + k_3[PO_2^\bullet][PH] - 2k_4[P^\bullet]^2 - k_5[P^\bullet][PO_2^\bullet] + 2k_{6d}[PO^{\bullet\bullet}OP] + 2\phi_{POOH}\,J_{POOH}\,[POOH] + 2\phi_{N1a}\,J_K\,[K_A] + 2\phi_{N1b}\,J_K\,[K_B] + \; 2\phi_{POOP}\,J_{POOP}\,[POOP] \quad \textbf{Eq. 6}$$

$$\frac{d[PO_2^\bullet]}{dt} = k_{1b}[POOH]^2 + k_2[P^\bullet][O_2] - k_3[PO_2^\bullet][PH] - k_5[P^\bullet][PO_2^\bullet] - 2k_{6a}[PO_2^\bullet]^2 \quad \textbf{Eq. 7}$$

$$\frac{d[POOH]}{dt} = -k_{1u}[POOH] - 2k_{1b}[POOH]^2 + k_3[PO_2^\bullet][PH] + (1-\gamma_5)k_5[P^\bullet][PO_2^\bullet] - \phi_{POOH}\,J_{POOH}\,[POOH] \quad \textbf{Eq. 8}$$

$$\frac{d[PH]}{dt} = -2k_{1u}[POOH] - k_{1b}[POOH]^2 - k_3[PO_2^\bullet][PH] + (1-\gamma_4)k_4[P^\bullet]^2 - 2k_{6d}[PO^{\bullet\bullet}OP] - 2\phi_{POOH}\,J_{POOH}\,[POOH] - 2\phi_{N1}\,J_K\,[K_A] - 2\phi_{N1}\,J_K\,[K_B] - \; 2\phi_{POOP}\,J_{POOP}\,[POOP] \quad \textbf{Eq. 9}$$

$$\frac{d[PO^{\bullet\bullet}OP]}{dt} = k_{60}[PO_2^\bullet]^2 - (k_{6b}+k_{6d})[PO^{\bullet\bullet}OP] \quad \textbf{Eq. 10}$$

$$\partial[O_2]/_{\partial t} = D_{O_2}\,\partial^2[O_2]/_{\partial z^2} - k_2[P^\bullet][O_2] - k_{6a}[PO_2^\bullet]^2 \quad \textbf{Eq. 11}$$

$$\frac{d[K_A]}{dt} = \gamma_{1a}(k_{1u}[POOH] + k_{1b}[POOH]^2 + 2k_{6d}[PO^{\bullet\bullet}OP] + \phi_{POOH}\,J_{POOH}\,[POOH] + 2\phi_{POOP}\,J_{POOP}\,[POOP]) - \phi_{N1}\,J_K\,[K_A] - \phi_{N2}\,J_K\,[K_A] \quad \textbf{Eq. 12}$$

$$\frac{d[K_B]}{dt} = \gamma_{1b}(k_{1u}[POOH] + k_{1b}[POOH]^2 + 2k_{6d}[PO^{\bullet\bullet}OP] + \phi_{POOH}\,J_{POOH}\,[POOH] + 2\phi_{POOP}\,J_{POOP}\,[POOP]) - \phi_{N1}\,J_K\,[K_B] - \phi_{N2}\,J_K\,[K_B] + \phi_{N2}\,J_K\,[K_A]) \quad \textbf{Eq. 13}$$

$$\frac{d[POOP]}{dt} = \gamma_5 k_5[P^\bullet][PO_2^\bullet] + k_{6b}[PO^{\bullet\bullet}OP] - \phi_{POOP}\,J_{POOP}\,[POOP] \quad \textbf{Eq. 14}$$

where $[P^\bullet]$, $[PO_2^\bullet]$, $[POOH]$, $[PH]$, $[PO^{\bullet\bullet}OP]$, $[O_2]$, K_A, K_B and $[POOP]$ are the respective concentrations in alkyl and peroxy radicals, hydroperoxides, tertiary CH groups, cage paired alkoxy radicals, oxygen, ketones of type A (middle-chain ketones) and B (end-chain or methyl ketones), and peroxide bridges. D_{O2} is the coefficient of oxygen diffusion into the semi-crystalline polymer, here considered constant and independent of time (i.e. of conversion degree of oxidation).

Although the present study is only focused on homogeneously oxidized iPP films, the Fick's second law (for oxygen diffusion) has been directly introduced into the oxygen balance equation (i.e. equation 11) in order to take into account the possible effects, even small, of the diffusion-limited oxidation (DLO).

From this SDE, it is also possible to calculate the local concentrations in chain scissions S and crosslinks B (covalent bridges), or even in double bonds F (unsaturations):

$$\frac{dS}{dt} = \gamma_{1b}(k_{1u}[POOH] + k_{1b}[POOH]^2 + 2k_{6d}[PO^{\bullet\bullet}OP] + \phi_{POOH}\,J_{POOH}\,[POOH] + 2\phi_{POOP}\,J_{POOP}\,[POOP]) + \phi_{N1}\,J_K\,[K_A] + \phi_{N2}\,J_K\,[K_A] \quad \textbf{Eq. 15}$$

$$\frac{dB}{dt} = \gamma_4 k_4[P^\bullet]^2 + \gamma_5 k_5[P^\bullet][PO_2^\bullet] + k_{6b}[PO^{\bullet\bullet}OP] - \phi_{POOP}\,J_{POOP}\,[POOP] \quad \textbf{Eq. 16}$$

$$\frac{dF}{dt} = \gamma_4 k_4 [P^\bullet]^2 + \gamma_5 k_5 [P^\bullet][PO_2^\bullet] + \phi_{N2}\, J_K\, [K_A] + \phi_{N2}\, J_K\, [K_B] \qquad \textbf{Eq. 17}$$

3.1.2. Initial and boundary conditions

Initial conditions are the same throughout the sample thickness. Thus, at t = 0, and ∀ z ∈ [0 ; L]:

$$[P^\bullet]\,(0, z) = [PO_2^\bullet]\,(0, z) = [PO^\bullet{}^\bullet OP]\,(0, z) = 0 \text{ mol.L}^{-1}$$

$$[PH]\,(0, z) = [PH]_0 \approx 20.3 \text{ mol.L}^{-1}$$

$$[POOH]\,(0, z) = [POOH]_0 = 4 \cdot 10^{-3} \text{ mol.L}^{-1}$$

$$[P{=}O]\,(0, z) = [P{=}O]_0 = 10^{-4} \text{ mol.L}^{-1}$$

$$[O_2]\,(0, z) = C_s$$

Boundary conditions at the film surfaces (i.e. at z = 0 and z = L) are:

$$\forall\ t > 0, \qquad [O_2]\,(t, 0) = [O_2]\,(t, L) = C_s$$

with C_s the oxygen concentration (in mol.L^{-1}) in the polymer in equilibrium with the atmosphere under an oxygen partial pressure P_{O2} given by the Henry's law:

$$C_s = P_{O_2} \times S_{O_2}^{am} \qquad \textbf{Eq. 18}$$

where S_{O2}^{am} is the coefficient of oxygen solubility in the polymer (in mol.L^{-1}.Pa^{-1}) here taken in the amorphous phase, i.e. only where oxygen is soluble [37, 38].

3.1.3. Boundary conditions due to aspects of geometrical optics

In photothermal oxidation, oxidation profiles does not results from the unique control of chemical reaction by oxygen diffusion (see equation 8), but also from the UV-light attenuation in the sample thickness, also called "screen effect". This effect results from: (i) the opacity of the semi-crystalline polymer, largely due to scattering or diffraction phenomena, (ii) the absorption of light by photosensitive species.

Opacity remains almost constant along the course of oxidation provided that morphology does not undergo noticeable changes (i.e. that chemi-crystallization remains negligible). On the contrary, the light absorption by chromophores increases with the conversion degree of oxidation since chromophores are oxidation products. In this case, the light attenuation factor is decoupled into a constant component accounting for opacity, i.e. into a wavelength dependent coefficient α(λ) of lineic absorption, and a variable component describing the light absorption by

chromophores using the Beer-Lambert's law. When only one sample face is exposed to UV-light, it comes:

∀ t,

Eq. 19

$$E_{z+dz}(\lambda) = E_z(\lambda)\left[1 - \left(\alpha(\lambda) + \ln(10) \sum_{\substack{j \\ chromophoric \\ species}} \varepsilon_j(\lambda)\,[X_j]\right)\Delta z\right]$$

with $E_z(\lambda)$ the spectral irradiance (in $W.m^{-2}.nm^{-1}$) at a depth z (in m) beneath the irradiated surface, $\alpha(\lambda)$ the coefficient of lineic absorption (in m^{-1}), $\varepsilon_j(\lambda)$ the spectral distribution of molar extinction coefficient (in $L.mol^{-1}.m^{-1}$) and $[X_j]$ the concentration of a given photosensitive species X_j (in $mol.L^{-1}$).

The spectral irradiance on the sample surface exposed to UV-light is equal to the intensity of the light source:

∀ t, for z=0: $E_{z\to 0}(\lambda) = E_\lambda^{source}$

In a first approach, no reflectance coefficient is introduced since most of the reflected light would not be specular but rather diffuse, which means that the reflected light would have penetrated in the material depth. These aspects would be discussed in the second part of this study dedicated to thicker specimens and optical phenomena.

3.1.4. Numerical resolution and computation

The coupling between oxygen diffusion and its chemical consumption by the polymer in the sample thickness was directly introduced into the SDE by using a finite difference method. The sample thickness was discretized into N-1 elementary sublayers of thickness Δz. The second derivative of the Fick's second law (for oxygen diffusion) was approximated by a central difference expression. In contrast, the coupling of the SDE with the algebraic equation 19, describing the UV-light attenuation in the sample thickness, is much more complex and cannot be treated with the common Matlab's algorithms recommended for solving stiff problems of

chemical kinetics [45]. It requires the use of more suitable algorithms which will be presented in a next publication. In a first approach, it was assumed that the contribution of oxidation products such as chromophores to UV-light attenuation is minority compared with the contribution of opacity (in films of 100 µm thick, their respective contributions are less than 0.3% and ~ 6%). Thus, the SDE was solved numerically, using the ODE15s or ODE23s Matlab's algorithms and applying the initial and boundary conditions given in equations 18 and 19.

Let us remind that the value of oxygen solubility was taken in the amorphous phase. Then, the real concentrations of all chemical species in the semi-crystalline polymer were deduced from the concentrations calculated in the amorphous phase by multiplying them by the volumic fraction of amorphous phase V_a:

$$V_a = (1 - \chi_c) \times \frac{\rho_p}{\rho_a} \qquad \textbf{Eq. 20}$$

with χ_c the crystallinity ratio (as measured by DSC), ρ_p and ρ_a the respective densities of the semi-crystalline polymer (910 g.L^{-1}) and amorphous phase (854 g.L^{-1})

Since most of the physico-chemical analyses were done throughout the sample thickness such as, for instance, FTIR monitoring in transmission mode, the global concentrations of all chemical species were averaged from the local values of the N-1 computational sublayers:

$$[X]_{global}(t) = \frac{1}{N-1}\int_{z=0}^{z=N}[X](z,t)dz \qquad \textbf{Eq. 21}$$

4. Experimental results

4.1. Photothermal oxidation results

This work reports a substantial experimental campaign of photothermal oxidation results (figures 2 to 6). These results are unprecedented by the variety of both exposure conditions and multiscale characterizations, all obtained on a unique reference iPP whose specimens have been cautiously prepared. This last specificity is of a great interest since it enables to minimize the material variability which might prevent from studying accurately the effect of exposure conditions. The experimental campaign includes exposures under different UV-light sources, namely arc xenon

and mercury lamps whose intensities vary in a ratio from 1 to 35 in terms of efficient energy for damaging the material (i.e. in terms of absorbed energy). It also includes the use of complementary analytical techniques, giving an overall view of the oxidation chemistry, in order to follow:

(i) Hydroperoxides involved in the main loop of the MCLMS,

(ii) Carbonyl species, involved in the secondary loops of the MCLMS and currently chosen as a relevant oxidation indicator in the literature,

(iii) Double bonds (unsaturations) generated by disproportionation in termination steps.

(iv) And weight and number average molecular masses related to the concentrations of chain scissions S and crosslinks B via the common Saito's equations [46]:

$$\overline{M_w} = \left(\frac{S}{2} - 2B + \frac{1}{\overline{M_{wO}}}\right)^{-1} \qquad \textbf{Eq. 22}$$

And

$$\overline{M_n} = \left(S - B + \frac{1}{\overline{M_{nO}}}\right)^{-1} \qquad \textbf{Eq. 23}$$

It is relevant to precise here that chain scissions are often considered as responsible for the alteration of both fracture and aspect (in terms of whitening and loss of gloss) properties.

The kinetic modeling approach has been chosen here to study the impact of exposure conditions (i.e. temperature and UV-light) on the relative predominance of the oxidation mechanisms proposed in the literature for describing the photothermal oxidation of iPP.

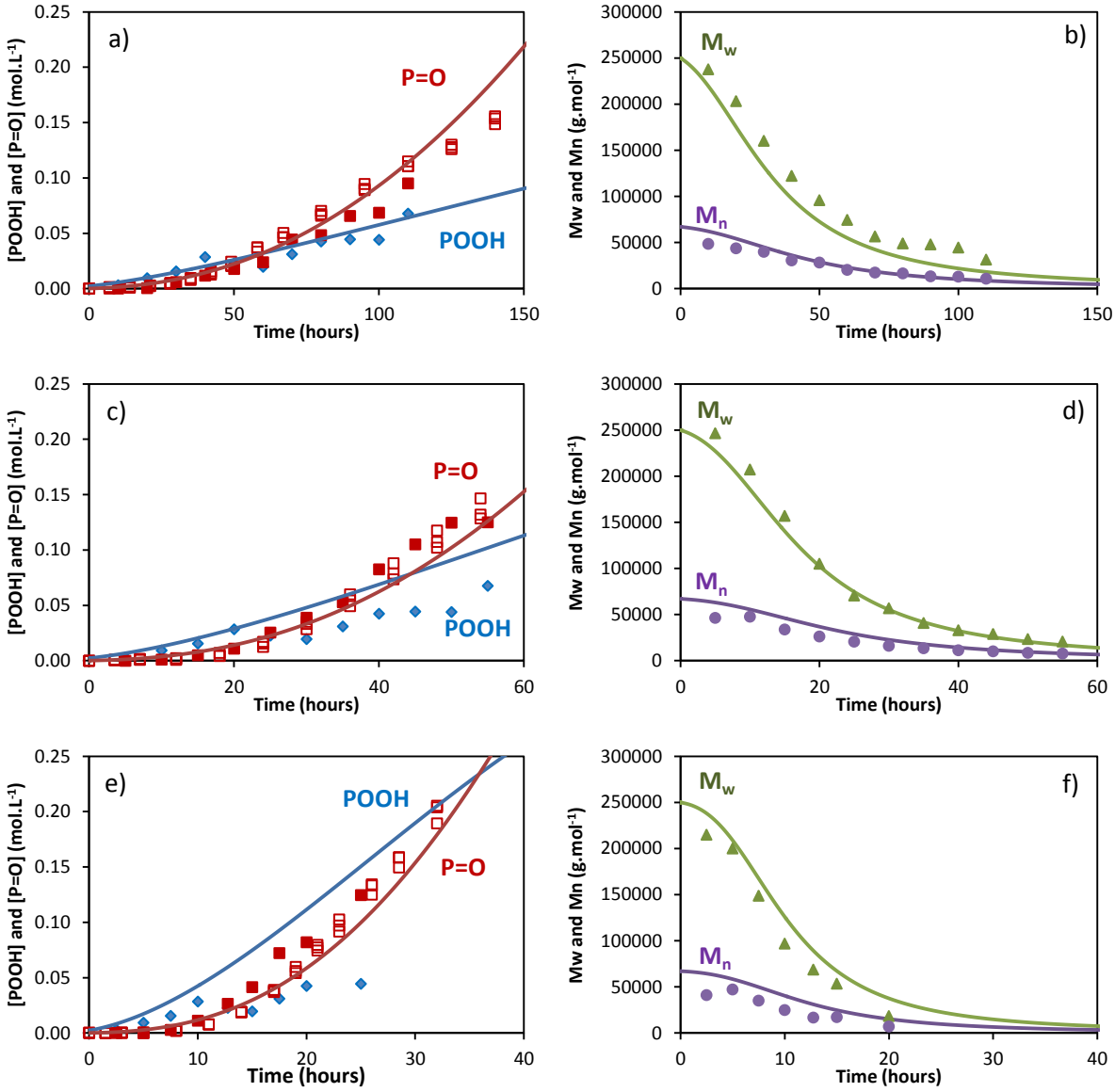

Figure 2: Simulation of iPP photothermal oxidation in SEPAP with 2 UV-lamps at 45°C (a), 60°C (b) and 80°C (c). Symbols: experimental data; ◆ hydroperoxides; ■□ carbonyl products; ▲weight and ●number average molecular masses. Solid lines: kinetic modeling.

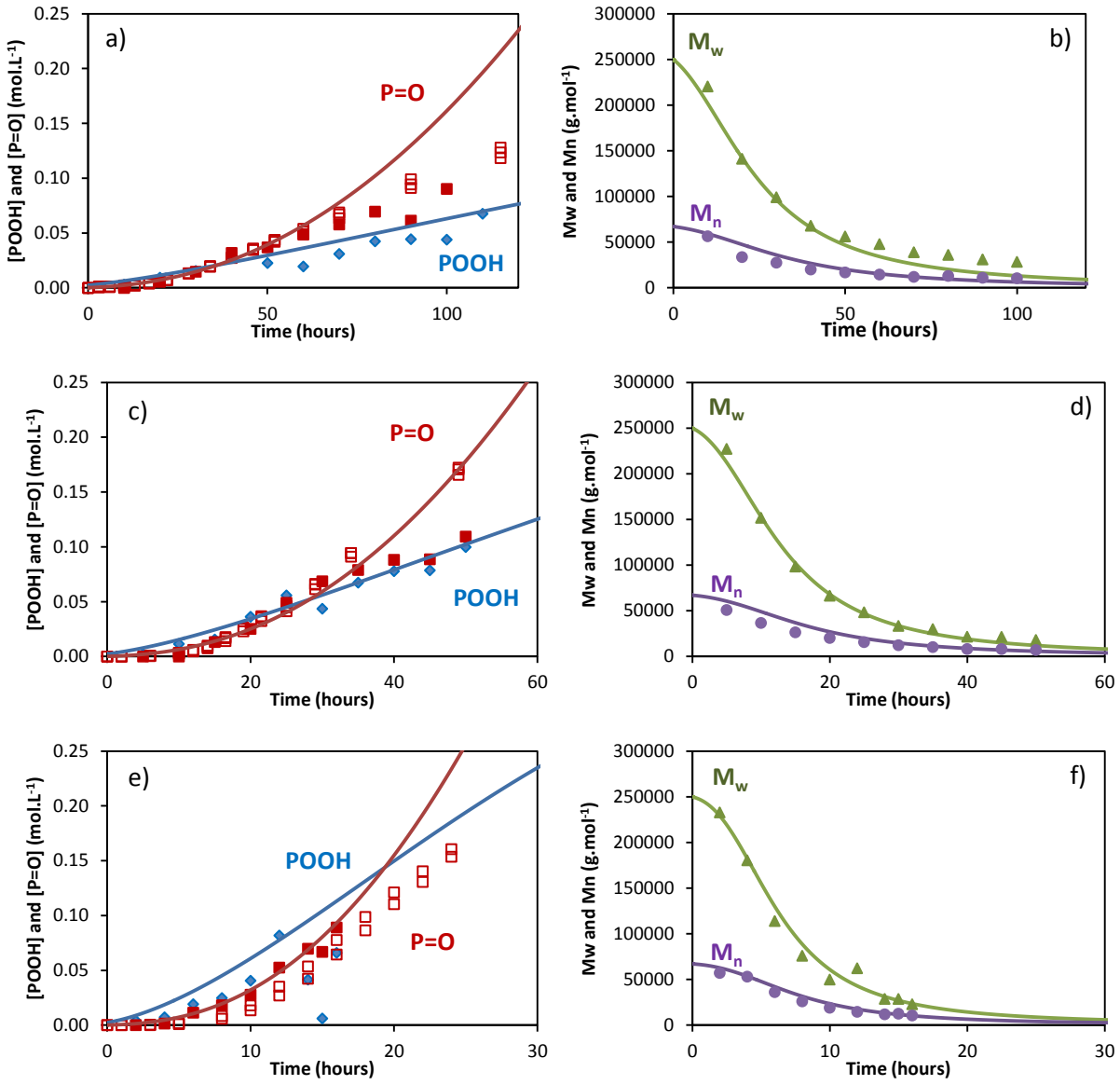

Figure 3: Simulation of iPP photothermal oxidation in SEPAP with 4 UV-lamps at 45°C (a), 60°C (b) and 80°C (c). Symbols: experimental data; ◆ hydroperoxides; ■□ carbonyl products; ▲weight and ●number average molecular masses. Solid lines: kinetic modeling.

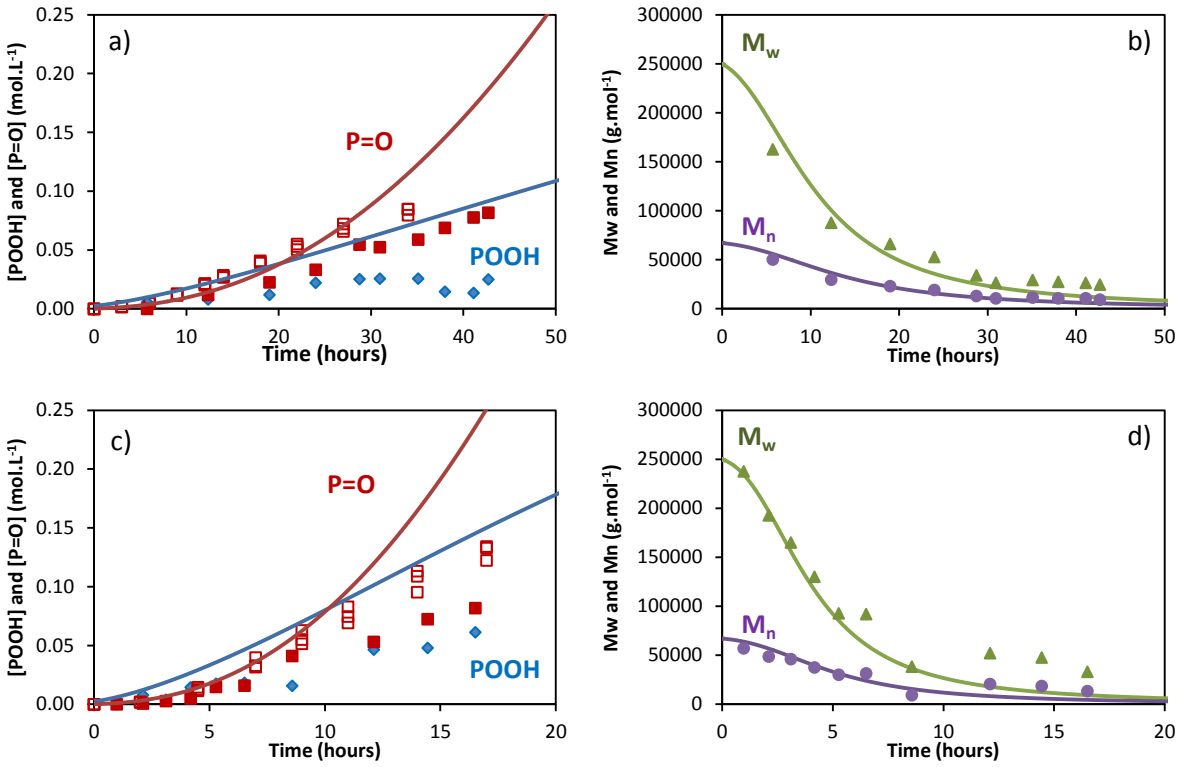

Figure 4: Simulation of iPP photothermal oxidation in SEPAP with 6 UV-lamps at 60°C (a), 80°C (b). Symbols: experimental data; ◆ hydroperoxides; ■□ carbonyl products; ▲weight and ●number average molecular masses. Solid lines: kinetic modeling.

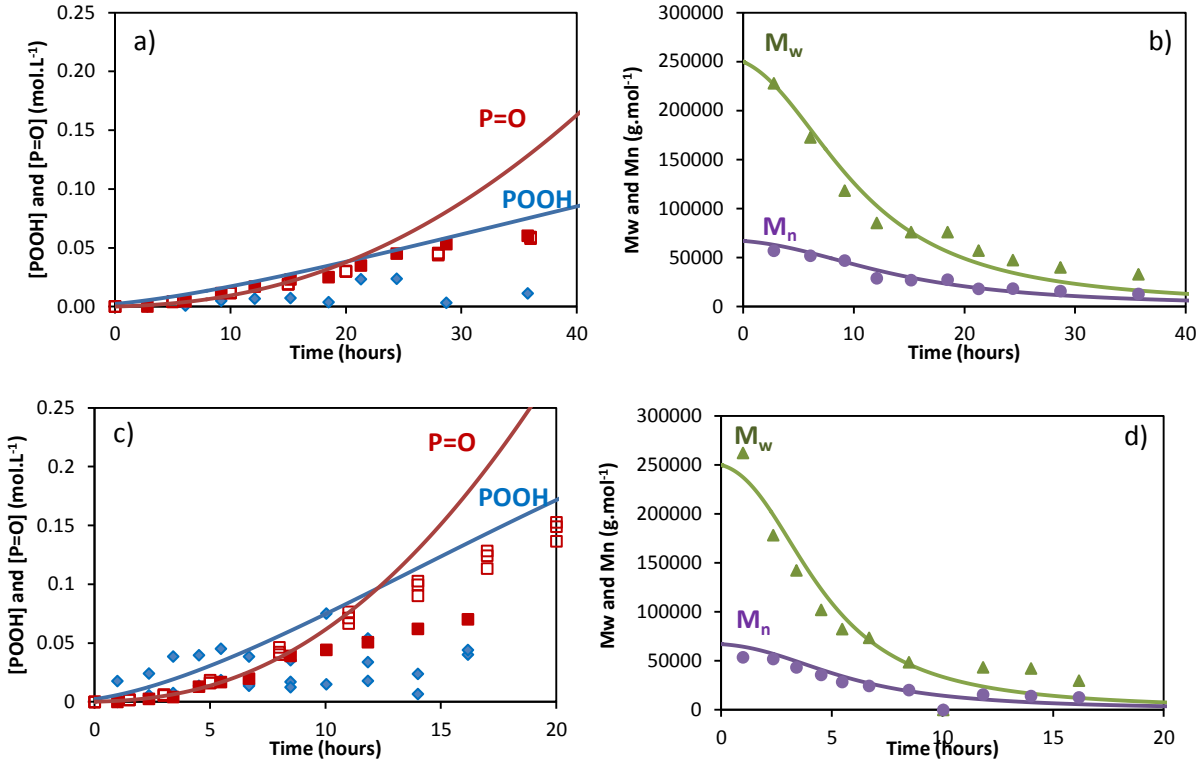

Figure 5: Simulation of iPP photothermal oxidation in SEPAP with 8 UV-lamps at 60°C (a), 80°C (b). Symbols: experimental data; ◆ hydroperoxides; ■□ carbonyl products; ▲weight and ●number average molecular masses. Solid lines: kinetic modeling.

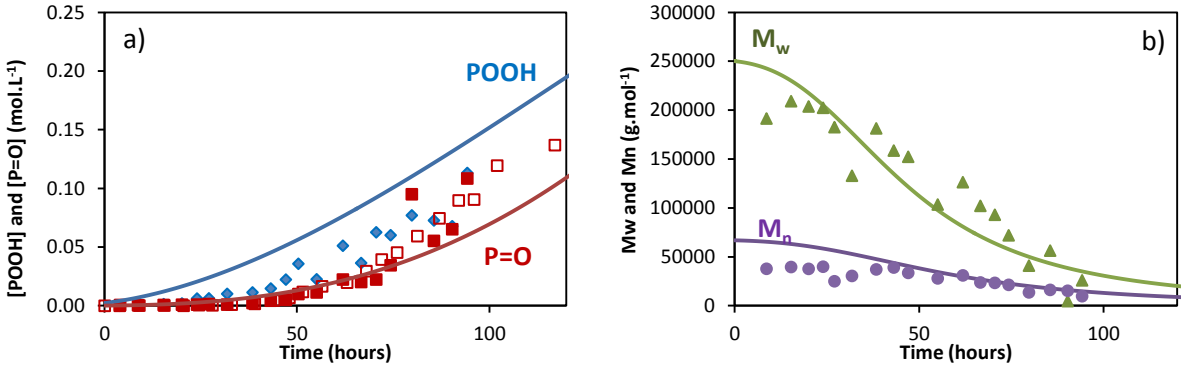

Figure 6: Simulation of iPP photothermal oxidation in in Weather O'Meter (Xenon lamp) at 64°C: experimental data; ◆ hydroperoxides; ■□ carbonyl products; ▲weight and ●number average molecular masses. Solid lines: kinetic modeling.

4.2. Comparison with pure thermal oxidation

From figures 2 to 6, several comments can be made on the shape of kinetic curves:

(i) Contrarily to pure thermal oxidation at the same temperature, one can observe a very low value, and even sometimes the absence, of induction period. Moreover, the extent of oxidative degradation is an increasing function of both temperature and UV-light intensity (i.e. number of UV-lamps in SEPAP devices), although the impact of temperature seems to be much more pronounced. No doubt, this complex combination between the effects of temperature and UV-light intensity will constitute an important validity criterion for the kinetic model.

(ii) The carbonyls concentration gradually grows with exposure time up to the film embrittlement. This final value corresponds approximately to that found for pure thermal oxidation at the same temperature. This result suggests that ketones photolysis (by Norrish 1 and 2 reactions) would be minority against other initiation steps for all the exposure conditions under study.

(iii) In the same way, hydroperoxides accumulate over time, but their concentration reaches a much lower final value, typically ranged between 0.05 and 0.10 $mol.L^{-1}$ whatever the exposure conditions. This value is much lower than the steady concentration of hydroperoxides found for pure thermal oxidation at the same temperature. Indeed, their steady concentration is a decreasing function of temperature [30, 47]: in air, it is 0.6, 0.5 and 0.4 $mol.L^{-1}$ at 80, 60 and 45°C respectively. This result suggests that hydroperoxides photolysis would be a source of radicals as important as hydroperoxides thermolysis for all the exposure conditions under study. Thereby, it justifies the MCLMS (figure 1) proposed for describing the photothermal oxidation of polypropylene.

(iv) In contrast, M_n and M_w decrease continuously over time, with a sharpest drop at the end of the induction period. Contrarily to pure thermal oxidation, where a shoulder was observed in the molecular mass distribution at the end of the induction period, especially at 60°C [30], there is no sign of crosslinking or branching process. This result confirms that the relative predominance of chain scission over crosslinking is accentuated for all the exposure conditions under study by the existence of the additional initiation step of hydroperoxides photolysis.

A first interesting characteristic of the photothermal oxidation is the concentration ratio between chain scissions (on main polymer chain) and carbonyl products: S / [P=O], i.e. γ_s / γ_1. It is noteworthy that for sufficient conversion degrees of oxidation (i.e. typically for [P=O] > 0.01 mol.L^{-1}, a critical value above which the sensitivity of spectrophotometry techniques does not generate high experimental scattering), all datasets overlap irrespectively to exposure conditions, including temperature, UV-light intensity and sources (see figure 7). It was found that: $\gamma_s / \gamma_1 = 0.97 \pm 0.05$. When neglecting crosslinking, this ratio decreases to 0.70 ± 0.04, a value to be compared with the value of 0.75 found in the case of pure thermal oxidation for the same reference iPP, but also for a compilation of literature data (see table 4 in reference [30]).

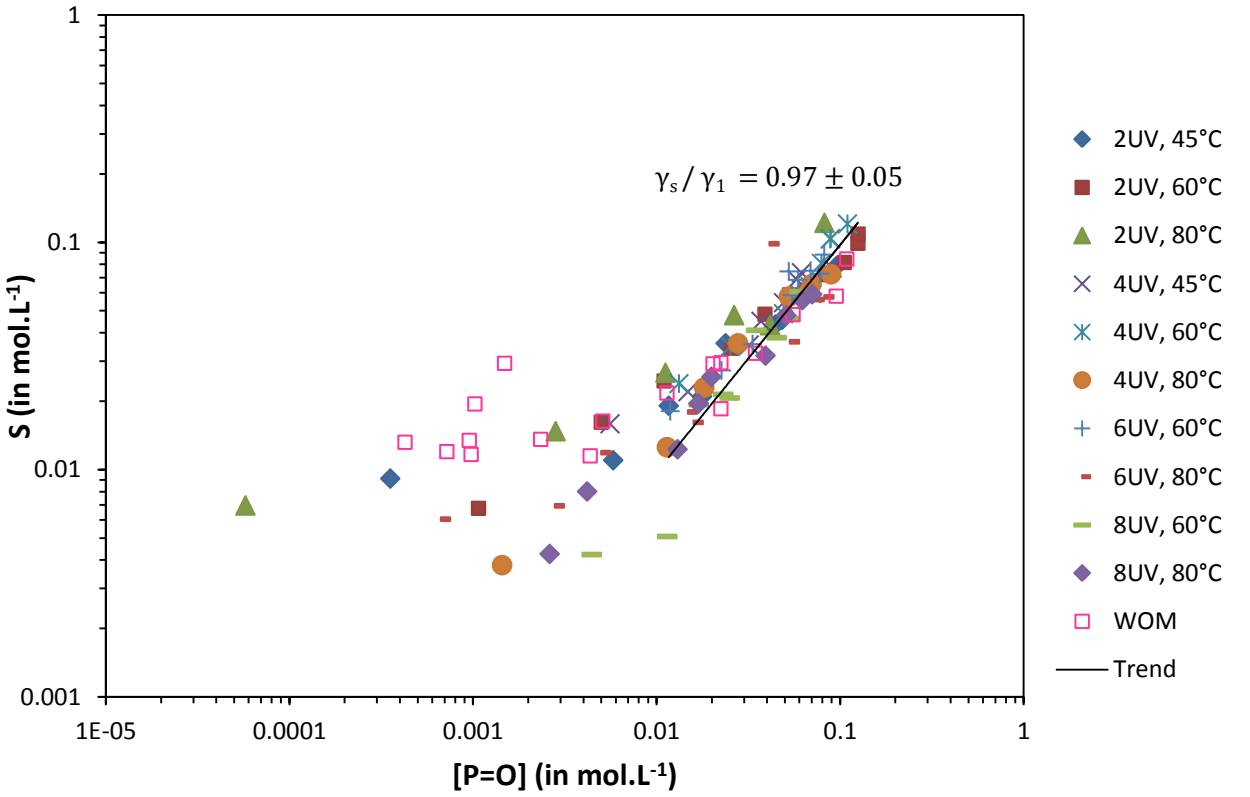

Figure 7: Concentration of chain scissions S (determined by solving equation 22 and 23) versus concentration of carbonyl products (titrated by FTIR spectrophotometry at 1713 cm^{-1}) for iPP exposed in SEPAP (with 2, 4, 6 or 8 UV-lamps) at 45, 60 and 80°C, and in WOM (Xenon lamp) at 64°C.

A second interesting characteristic of the photothermal oxidation is the concentration ratio between chain scissions (on main polymer chain) and crosslinks: S/B (figure 8). It is found that S/B = 10.6 ± 1.0, a value to be compared to the value of 9.6 ± 2.7 found in the case of pure thermal oxidation for the same reference iPP [30]. This result tends to temper the role played by the additional chain scissions on the embrittlement process of iPP under UV-light exposure, especially at high irradiances.

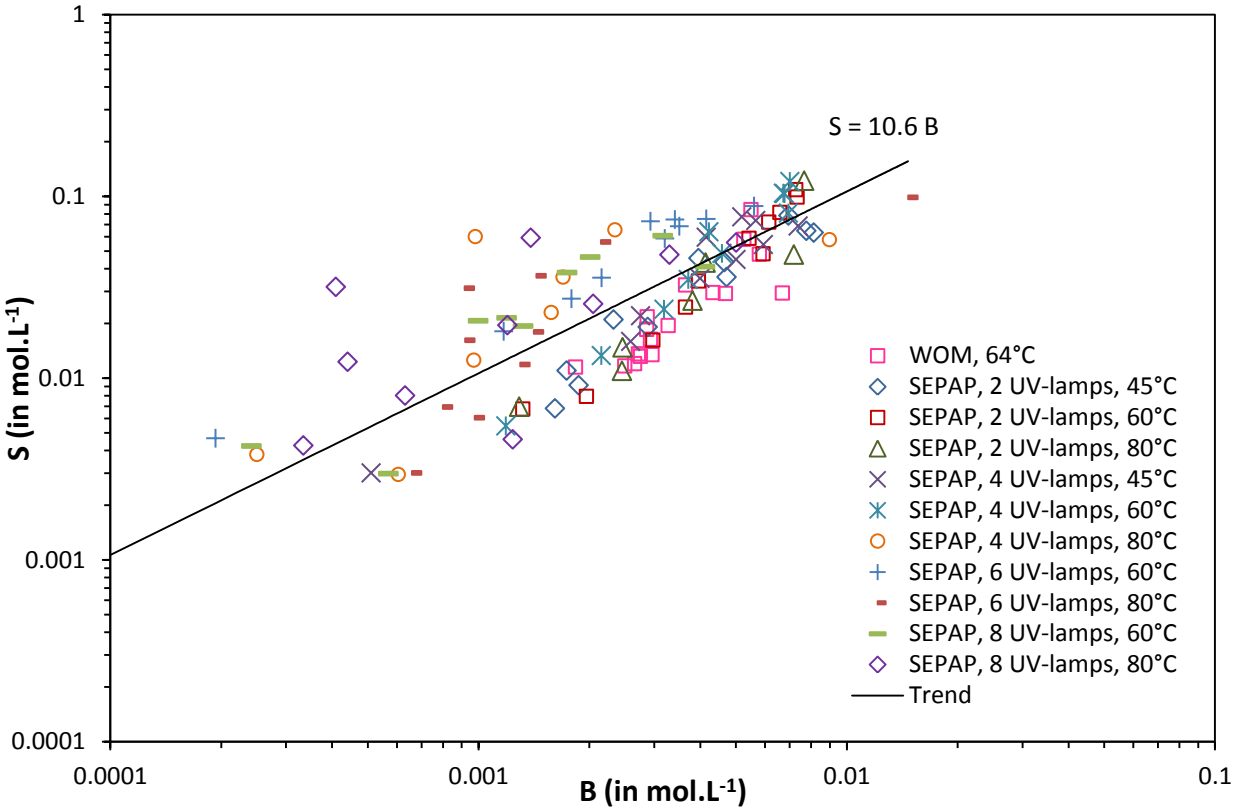

Figure 8: Concentration of chain scissions S versus concentration of crosslinks B (determined by solving equations 22 and 23) for iPP exposed in SEPAP (with 2, 4, 6 or 8 UV-lamps) at 45, 60 and 80°C, and in WOM (Xenon lamp) at 64°C.

4.3. Data scattering

The quality of experimental data can also be criticized. First of all, the different datasets obtained by carbonyls monitoring enable to apprehend the aging reproducibility, i.e. the suitable control of both material variability and exposure conditions. Both datasets are usually overlapped, except

for certain samples, typically for concentrations above 0.07 mol.L^{-1} (i.e. for moderate conversion degrees of oxidation). Therefore, oxidation rate can suffer slight deviations, presumably owing to the diffusion control of oxidation (DLO) for the thickest samples exposed in the harshest conditions.

Hydroperoxides titrations were also reproducible and consistent over exposure time, but showed a higher experimental scattering. This results can potentially come from: (i) the material variability, (ii) the poor accuracy of the titration method or procedure, given the low values of hydroperoxides concentration to be determined, (iii) a waiting time not long enough to allow the titration reagent to diffuse until the core of the thickest samples, and (iv) a partial titration of all the hydroperoxide type species responsible for the initiation of photothermal oxidation. Among other types of hydroperoxides, one could mention peracids, whose fast decomposition could govern the oxidation rate, but not the length of the induction period [48, 49].

5. Kinetic modeling and discussion

5.1. Optimization procedure - Numerical simulations and determination of unknown parameters

Many parameters are involved in the kinetic model for photothermal oxidation of iPP. Those appearing only in the CLMS (i.e. rate constants and yields of reactions 1u, 1b, and 2 to 6d) were determined in a previous study from thermal aging experiments in a large range of temperatures (60-140°C) and oxygen partial pressures (0.02 to 5 MPa) [30]. Their values are reminded in table 2.

Table 2: Parameters used for kinetic modeling of iPP photothermal oxidation

Parameters	***Units***	P^0	***Ea (kJ.mol^{-1})***
$[POOH]_0$	mol.L^{-1}	$4 \cdot 10^{-3}$	-
S_{O2}^{am}	mol.L^{-1}.Pa^{-1}	$2.5 \cdot 10^{-6}$	6.7
D_{O2}	m^2.s^{-1}	$8.6 \cdot 10^{-6}$	36.4
Pe_{O2}	cm^3.cm.cm^{-2}.Pa^{-1}.s^{-1}	$2.9 \cdot 10^{-6}$	43.0
k_{1u}	s^{-1}	$2.9 \cdot 10^{13}$	140.7
k_{1b}	L.mol^{-1}.s^{-1}	$9.2 \cdot 10^{8}$	95.0

k_2	$L.mol^{-1}.s^{-1}$	$3.0 \cdot 10^9$	10.0
k_3	$L.mol^{-1}.s^{-1}$	$5.1 \cdot 10^7$	62.2
k_4	$L.mol^{-1}.s^{-1}$	$1.0 \cdot 10^{12}$	0
k_5	$L.mol^{-1}.s^{-1}$	$4.5 \cdot 10^{10}$	0
k_{6a}	$L.mol^{-1}.s^{-1}$	$2.0 \cdot 10^{17}$	90.0
k_{6b}	s^{-1}	$6.7 \cdot 10^6$	5.0
k_{6d}	s^{-1}	$1.4 \cdot 10^{12}$	41.0
γ_1	%	60	-
γ'_1	%	27	-
γ''_1	%	33	-
γ_4	%	0	-
γ_5	%	0	-
γ_s	%	50	-

It is important to precise that middle-chain (K_A) and end-chain ketones (K_B) have not been differentiated from each other in the previous study [30]. Indeed, the concentration changes in carbonyl products were modeled by using an apparent yield γ_1 stemming from FTIR monitoring at 1713 cm^{-1}. Obviously, the value of γ_1 should be kept unchanged at 0.5 in the present study in order to ensure a perfect continuity with the thermal oxidation model. For the same reason, the yield in chain scissions (on main polymer chain) γ_S should be also kept unchanged at 0.5. In a first approach, their values can be deduced from the ratio: $\gamma_S / \gamma_1 = 0.97 \pm 0.06$ determined experimentally (see figure 7). Taking $\gamma_1 = 0.5$, it comes effectively: $\gamma_s = 0.48 \pm 0.03$, which is very close to 0.5.

If this first value of γ_s allowed simulating satisfactorily all the kinetic curves of hydroperoxides concentration and average molecular masses shown on figures 2 to 6, in contrast, the value of γ_1 underestimated largely the concentrations of carbonyl products (assumed to be exclusively composed of ketones). A possible explanation could be that the distribution of carbonyl products is different from pure thermal to photothermal oxidation, due to a partial photolysis of ketones (by Norrish 1 and 2 reactions). In such a case, the value of molar extinction coefficient $\varepsilon^{P=O}$ conventionally (but arbitrarily) fixed at 300 $mol.L^{-1}.cm^{-1}$ at 1713 cm^{-1} in pure thermal oxidation, should be reconsidered in photothermal oxidation. Indeed, it should not be forgotten that, if the molar extinction coefficients of ketones is relatively low (typically between 200 and 400 $mol.L^{-1}.cm^{-1}$), whereas those of carboxylic acids (650-850 $mol.L^{-1}.cm^{-1}$) and esters are much higher (450-600 $mol.L^{-1}.cm^{-1}$).

For this reason, in a second approach, the values of γ_1 was fixed in agreement with the distribution of carbonyl products determined in the literature in photothermal oxidation [30, 50-53], in particular from the results of Carlsson and Wiles [1-3]. First of all, γ_1 was increased was up to 0.6 since it was reported that more than half the alkoxy radicals undergo β scission [1, 2]. Then, γ'_1 and γ''_1 were respectively fixed at 0.27 and 0.33 knowing the concentration ratio of 0.82 was determined between ketones A and B [1, 2].

Once known the parameters of the CLMS, the objective was to determine the additional effects of UV-light and their corresponding parameters. Since the rate constants k_i of the photo-induced reactions can be written as follows: $k_i = \Phi_i \cdot J_i$, the spectral overlap integrals J_i were calculated for each chromophore i under consideration (according to the calculation procedure given in section 3.2.2), prior to determine the quantum yields Φ_i. There was no additional adjustable parameter. The values of J_i are reported in Table 3.

Table 3: Values Values of spectral overlap integrals (in Einstein.mol^{-1}-s^{-1}) of hydroperoxides, ketones and alkyl peroxides and Ti catalysts for exposures to different UV-light sources (calculated from absorption spectra given in references [1, 54], [2], [1] and [1] respectively)

Light source	**J_{POOH}**	**$J_{P=O}$**	**J_{POOP}**	**J_{Ti} catalyst**
SEPAP 12-24, 2 arc mercury lamps	4.92E-06	7.31E-05	8.40E-06	5.23E-03
SEPAP 12-24, 4 arc mercury lamps	1.07E-05	1.46E-04	1.68E-05	1.05E-02
SEPAP 50-24, 6 arc mercury lamps	2.54E-05	3.77E-04	4.33E-05	2.69E-02
SEPAP 50-24, 8 arc mercury lamps	5.53E-05	7.53E-04	8.67E-05	5.39E-02
WeatherOMeter, xenon lamp	1.45E-06	2.25E-05	4.19E-06	1.49E-03
Philips TLK 05 lamp fluorescent lamp [9]	1.45E-07	2.31E-06	4.71E-07	1.45E-04

Then, the quantum yields of peroxide type species (i.e. $\Phi_{POOH,}$ and Φ_{POOP}) and ketones photolysis (i.e. Φ_{N1A}, $\Phi_{N1B,}$ $\Phi_{N2A,}$ Φ_{N2B}), were determined by adjusting the concentration changes in hydroperoxides, ketones/carbonyls and double bonds, but also the changes in molecular masses. The value of Φ_{POOH} was fixed first, since hydroperoxides are considred as the primary oxidation products [3, 55, 56].

5.2. Relative predominance of initiating species

5.2.1. Hydroperoxides Vs. ketones contribution

Surprisingly, small variations in Φ_{POOH} around its optimal value have almost no effect on the kinetic curves of hydroperoxides. This is presumably due to the presence of several imbricated closed-loops in the MCLMS, which makes the photothermal oxidation behavior hardly predicable. Φ_{POOH} was thus adjusted basing mainly on the changes in carbonyl products and molecular masses. Since ketones K_A and K_B have been differentiated in the MCLMS, it was then possible to study the impact of their respective quantum yields on the overall photothermal oxidation kinetics. As observed experimentally by Carlsson and Wiles [2], Norrish 1 and 2 reactions would not have the same degree of sensitivity on ketones K_A and K_B.

The absence of Norrish 2 reaction on ketones A is understandable because it requires a peculiar chain conformation for having a six-membered rearrangement. Indeed, this reaction would be constrained in middle-chain due to bond tension, but favored at chain extremities where methyl substituents could promote more mobility. This assumption is in perfect agreement with the literature [2, 15, 34, 44, 51, 57-59] which generally reports values of Φ_{N2} varying in the following order: End-chain > Middle-chain > Side-chain, except for ketones formed in PE [15] (see figure A2 in appendix A). As an example, Φ_{N2} is twice higher for end-chain (Φ_{N2}=0.22) than for middle-chain ketones (Φ_{N2} = 0.11) in 8-pentadecanone [60]. This result would be independent of temperature or physical state (film, solution, etc.) because of the relatively high lifetime of the transient triplet state.

The lower value of Φ_{N1} for ketones K_B than for ketones K_A is also in good agreement with the values reported in the literature [2, 15, 58-62] for end-chain and middle-chain ketones (see figure A1 in appendix A), but more difficult to understand particularly when considering that aldehydes also undergo Norrish 1 reaction. The selective quenching of end-chain ketones can be envisaged, but it would also prevent Norrish 2 reaction. These quantum yields were thus assumed to be independent from each other for the different kinds of ketones.

From this standpoint, a parametric study involving different combinations of Φ_{POOH} on one side, and Φ_{N1A}, Φ_{N1B}, Φ_{N2A} and Φ_{N2B} on the other side, has been performed with values ranging from 1 to 10 for POOH photolysis and 0 to 0.03 for Norrish type reactions. The parametric study has been led preferentially in exposure conditions where photochemical initiation is predominant

over thermal initiation, in order to enhance the sensitivity of quantum yields. This optimization procedure was thus performed on the SEPAP results obtained with 4 UV-lamps at 45°C.
Results are depicted in figure 9, for Φ_{N1B} and Φ_{N2A} set at zero. Hydroperoxides concentration was highly sensitive to Norrish 1 reaction, unlike carbonyls concentration. From the changes in hydroperoxides concentration, it can be concluded that Φ_{N1} must be kept lower than 0.01. Similarly, all the ethylenic unsaturations would come from termination reactions (in particular, disproportionation) and therefore, Φ_{N2} would be also lower than 0.01. It also appears that the changes in molecular masses are weakly sensitive to ketones photolysis with such low values of quantum yields. All these results are consistent with the compilation of literature data (see figures A1 and A2 in appendix A).

Before concluding that the contribution of Norrish type reactions can be neglected compared with hydroperoxides photolysis, it remained to check that this result does not depend on the way whose kinetic model is initialized, i.e. on the choice of the initial concentrations in hydroperoxides $[POOH]_0$ and ketones $[K_A]_0$ and $[K_B]_0$. Indeed, in the previous kinetic submodel for pure thermal oxidation [29], the initial amount of structural defects responsible for the extrinsic initiation, that only predominates in the early stages of oxidation, was successfully accounted by an (kinetically equivalent) initial concentration in hydroperoxides $[POOH]_0$. In contrast, in the kinetic models of pure photooxidation developed by Sommersal and Guillet [15] and Geuskens et al [56], these defects were replaced by an initial concentration in ketones. In the present case of photothermal oxidation, both types of initiating species have to be considered. Given the large number of parameters involved in the kinetic model of photothermal oxidation, the problem of determining the most relevant chemical species appears as badly conditioned. In order to ensure the continuity with the submodel of pure thermal oxidation (and thus, the relevancy of the kinetic modeling approach), the following strategy has been adopted. The initial concentration in hydroperoxides was kept unchanged at $[POOH]_0 = 4 \cdot 10^{-3}$ mol.L^{-1} for the same reference iPP. Thus, the initial concentration in ketones was determined so as to account for the potential surplus of the extrinsic initiation, induced by the photosensitive species. In our case, it was checked that values ranged from 0 to 10^{-3} mol.L^{-1} for this last concentration has no influence on simulations, presumably because the contribution of Norrish type reactions to oxidation is negligible compared with hydroperoxides photolysis.

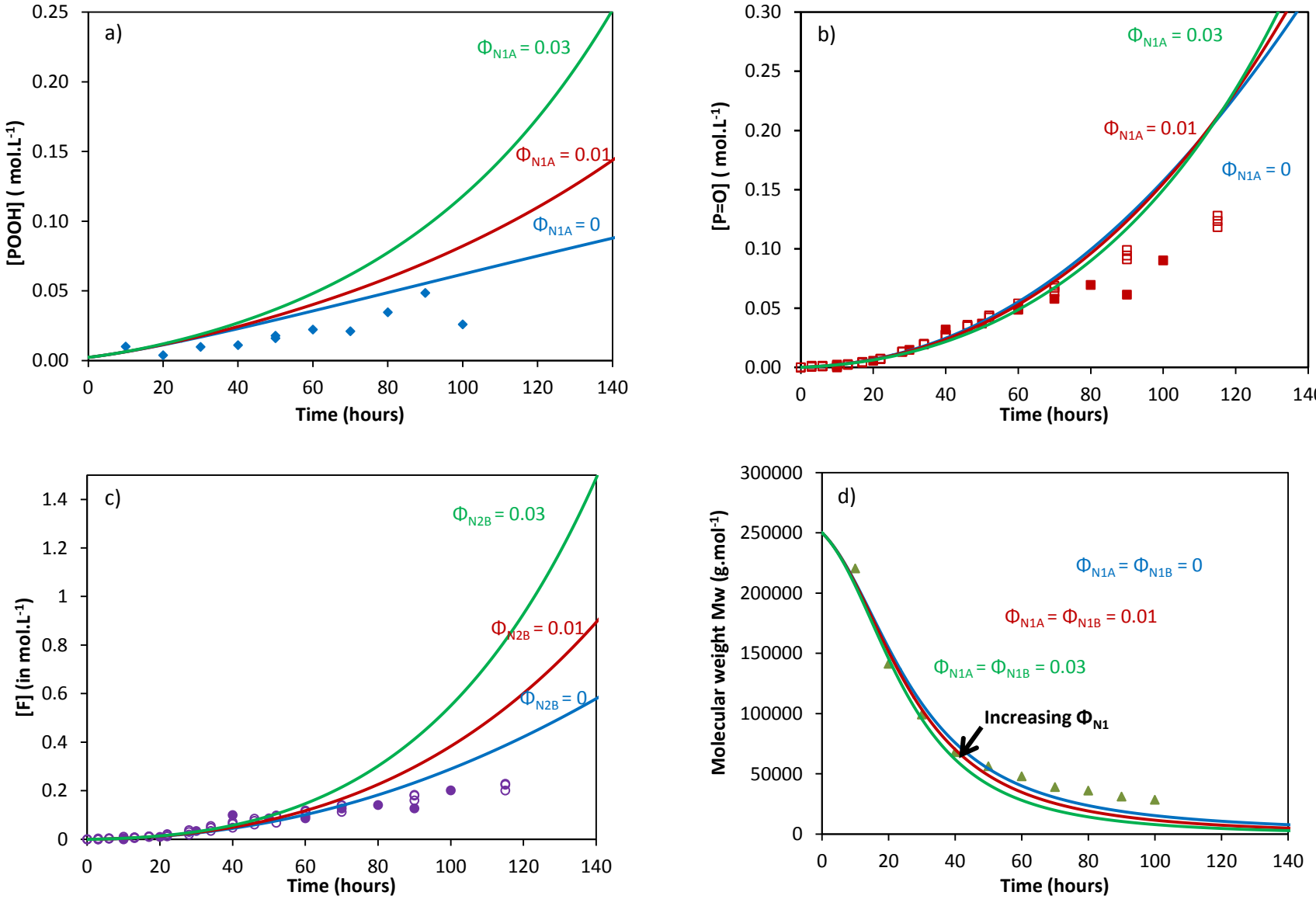

Figure 9: Optimization of quantum yields for Norrish 1 and 2 reactions. Symbols: experimental data. Solid lines: kinetic modeling.

5.2.2. Contribution of the photolysis of peroxide bridges (alkyl peroxides)

In a previous paper [21], it was shown that alkyl-peroxides are more photosensitive than hydroperoxides while their O-O bond is almost as cleavable. Then, their photolysis must also occur. In a first approach, the value of Φ_{POOP} was set between 1 and the value previously determined for Φ_{POOH} as upper boundary. As expected, the introduction of the alkyl-peroxides photolysis induces a slight decrease in the quantum yield of hydroperoxides photolysis Φ_{POOH}, but has no influence on the quantum yields of Norrish type reactions.

From all these results, it can be concluded that:

(i) The contribution of Norrish type reactions to iPP photothermal oxidation is almost negligible. The findings with 4 UV-lamps at 45°C can be extended to the whole photothermal aging conditions under investigation, since primary processes are independent of temperature as long as the quantum theory is valid (i.e. for moderate UV-light intensities for which termolecular reactions and multiphotonic excitations are negligible).

(ii) The consideration of alkyl-peroxides photolysis enables to slightly decrease the value of Φ_{POOH}, but it is not indispensable for simulating the experimental data.

5.3. Validity of the kinetic model

A single set of quantum yields was determined using the kinetic model of photothermal oxidation as an inverse approach for all the exposure conditions under study. However, it is relevant to precise that these latter conditions cover a domain where photochemical initiation largely predominates (above 90%) over thermal initiation, even in WOM device. This is the reason why the validity of the kinetic model was also tested in intermediary exposure conditions where both thermolysis and photolysis contribute to initiation with a similar order of magnitude (as evidenced in previous work [21]). As an example, the simulation of the kinetic curves of carbonyl products reported by Audouin et al. [55] for iPP exposed to fluorescent lamp between 40 and 70°C is presented in figure 10.

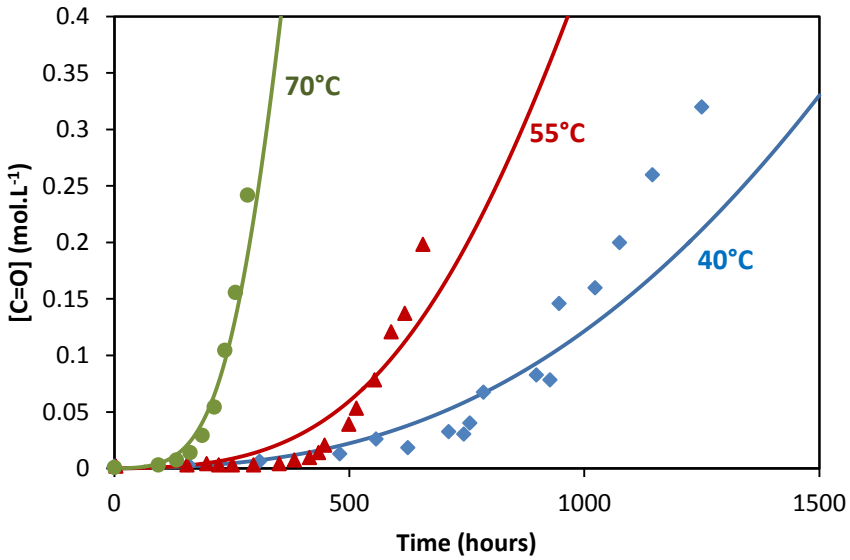

Figure 10: Simulation of carbonyl products build-up in iPP exposed to Philips TLK 05 fluorescent lamp (spectral distribution with maximum at 365 nm) at 40, 55 and 70°C. Symbols: experimental data [55]. Solid lines: kinetic modeling.

It is found that Φ_{POOH} ranges between 1.5 and 5.5 in the whole domain of exposure conditions under investigation. The different values are depicted in figure 11 in function of the spectral overlap integral as abscissa. In most of cases, Φ_{POOH} belongs to the variation domain of 4 ± 1 (colored in red), in agreement with the experimental findings of Carlsson and Wiles [1] and in general agreement with the literature (see table A1 in appendix A). This is an important result in favor of our kinetic modeling approach. Indeed, it confirms that the photo-thermal oxidation of iPP can be satisfactorily described by extending the common CLMS, in particular by introducing additional initiation steps corresponding to the photolysis of peroxide type species.

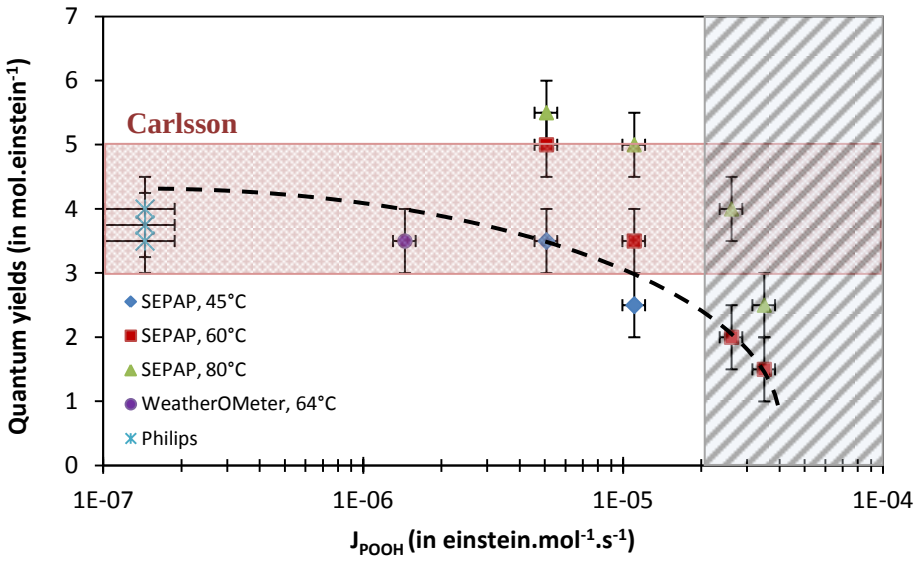

Figure 11: Quantum yields of hydroperoxides photolysis determined by inverse resolution method. The domain colored in pink applies to the value proposed by Carlsson and Wiles [1]. The hachured domain applies to the domain where the kinetic model is presumably not valid anymore.

It is also noteworthy that this value of Φ_{POOH} is twice lower than the value found by using the analytical kinetic model (Φ_{POOH} = 8) in a previous publication [21]. Since ketones and peroxide bridges photolysis have been found to have negligible contribution to the photothermal oxidation kinetics, most of the modeling improvement comes from a better description of the coupling between temperature and UV-light effects in the numerical kinetic model. This is also noteworthy that this value is in perfect agreement with the experimental findings of Carlsson and Wiles [1] whose photochemical (e.g. molar absorptivity) and mechanistic characteristics (e.g. concentration ratio of oxidation products) have been reused in this study. Despite this improvement, values of Φ_{POOH} are still too high since they should not theoretically exceed unity in the case of primary processes such as bond dissociation, thus questioning on their physical meaning. Different explanations were discussed by Carlsson and Wiles [1]:

(i) The probable underestimation of the corresponding molar extinction coefficient, which was estimated from model compounds. These authors particularly highlighted the difficulty to measure this quantity in hydrocarbon polymers, but also the lack of knowledge on the impact of the polymer chain length and polarity of reactive medium.

(ii) The existence of energy transfers, i.e. the photosensitization of the hydroperoxides decomposition by ketones or catalyst residues.

Both options could also explain the trend of Φ_{POOH} to decrease when increasing the UV-light intensity (i.e. J_{POOH}), as materialized by the dashed line in figure 11. Different other explanations can be envisaged:

(i) The experimental data would not be enough accurate or reliable for the highest irradiances (ultra-acceleration) despite the careful control of exposure conditions. Indeed, the temperature regulation turned out to be awkward, in particular because of the fast oxidation kinetics. However, this possibility is considered as unlikely since the decreasing trend of Φ_{POOH} is too obvious to be coincidental.

(ii) The occurrence of multiphotonic excitations (electronic transitions up to orbitals higher than the LUMO) which would finally reduce the average efficiency of quanta. This kind of excitation would predominate above a critical value of light intensity, which could potentially set an intrinsic validity frontier for the kinetic model.

(iii) Other mechanistic considerations would be necessary in order to properly describe the experimental results, particularly in terms of nature and molecularity of chemical reactions.

Moreover, one can observe that the kinetic model hardly accounts for the curvatures of the kinetic curves of carbonyl products at the end of the induction period. This auto-accelerated character of photothermal oxidation is more particularly highlighted at low (see, for instance, results of Girois [55] at 40 and 55°C in figure 10) and high irradiances (figures 5 and 6). It is generally attributed to a predominant initiation by the bimolecular decomposition of hydroperoxides. In photooxidation, this bimolecular decomposition is a termolecular process (two molecules with one quantum), and thus is usually thought to have a low probability of occurrence except in the case of high irradiances (where quanta are in large excess compared with molecular species), or in the case of formation of relatively stable associations between two molecular species such as excimers/exciplexes, or charge transfer complex (CT). Such molecular edifices, stabilized by hydrogen bonding as reversible interactions, would include in the present case:

(i) Energy transfers from the highly photosensitive ketones to very cleavable hydroperoxides, since associated in complexes. This would be an argument in favor of the mechanism proposed by Geuskens and Kabamba [63, 64];

(ii) Photosensitization of hydroperoxides decomposition by catalyst residues;

(iii) Bimolecular decomposition of hydroperoxides, associated in pairs or constituting longer sequences, was shown to predominate in the case of pure thermal oxidation at low temperature. However, the yield in water formation would suggest an unimolecular instead of a bimolecular hydroperoxides decomposition by photolysis (this argument was already used by Carlsson to dismiss the assumption of radicals induced hydroperoxides decomposition) [1].

Although their complete kinetic treatment remains awkward, our first implementations of these reactions into the kinetic model enable to dismiss the former option.

Furthermore, the kinetic model enables to calculate the maximal rate of oxygen consumption, i.e. the steady oxidation rate R_s. Unlike carbonyl products, oxygen is directly involved in the MCLMS and its concentration does not depend on the choice of apparent yields. The values of R_s were determined by the kinetic model for all photothermal aging conditions under study. Then, they were plotted versus the spectral overlap integral relative to hydroperoxides J_{POOH} in figure 12 in logarithm-logarithm coordinates. It can be seen that these values are of the same order of magnitude as those deduced from oxygen uptake measurements in the literature [65-70].

A mean-square optimization procedure was applied to determine the activation energy of photothermal oxidation: 71 kJ.mol^{-1}.This value is slightly lower than the activation energy found for pure thermal oxidation in a previous study: 91 kJ.mol^{-1} (see literature compilation in reference [30]).

Finally, a trend curve was tentatively determined. It was found that the steady oxidation rate is proportional to spectral overlap integral (i.e. UV-light intensity) at a power close to ½, in close agreement with the usual analytical solution determined from the basic auto-oxidation scheme in the literature [67, 69, 71]. It can be thus written:

$$R_s = K \cdot J^{1/2} \cdot \exp\left(-Ea/RT\right) \qquad \text{Eq.24}$$

These results confirm the validity and good predictive value of the kinetic model.

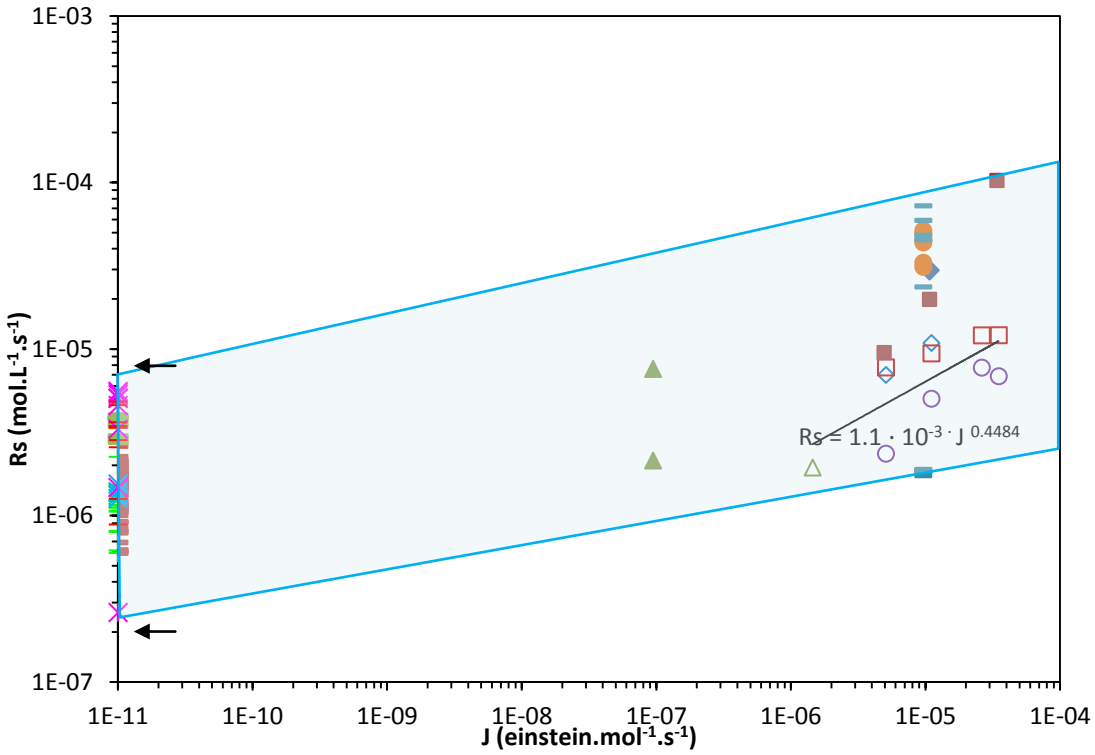

Figure 12: Master curve at 60°C for the steady oxidation rates plotted as a function of the spectral overlap integral of hydroperoxides. Open symbols: kinetic model by inverse resolution method; ◇ SEPAP (ML), 45°C; □ SEPAP (ML), 60°C; ○ SEPAP (ML), 80°C △WOM (XL), 64°C. Filled symbols: Oxygen uptake measurements from the literature in photothermal oxidation: ◆ SEPAP 12-24 (ML), 60°C [66]; ▲ SunTester (XL), 45°C [70]; ■ SEPAP (ML) at 40, 60, 65°C respectively [72]. ● High Pressure Mercury Lamps (ML), 70°C [69]; ▬ High Pressure Mercury Lamps (ML), between 60 and 75°C, [68]; and in thermal oxidation: + 50-130°C [73]; - 50-130°C [74]; ▬ 110-140°C [75]; ×130°C, [76]; ✳ 80 and 130°C [77, 78] ; + 120-140°C [79-82]. Arrows indicate the variation range of steady oxidation rate in the case of pure thermal aging.

6. Conclusion

A general kinetic model has been proposed in order to describe the oxidative degradation of polypropylene under the combined effects of UV-light and temperature. The approach consists in modeling the chemical changes of the material and then, to deduce the subsequent changes in physico-chemical and mechanical properties at upper scales by using suitable structure/property

relationships. The photochemical processes undergone by photosensitive species, namely peroxide type species and ketones photolysis, were added into the CLMS in order to introduce the effect of UV-light. The photolysis kinetics was expressed by using the spectral overlap integral, which accounts for the energy absorbed by chromophores and initiates oxidation. The resulting kinetic model couples chemical reactions with physical phenomena, such as the oxygen diffusion and light attenuation (screen effect) due to sample opacity and formation of photo-sensitive species. It aims to be fully consistent from a physical point of view and valid for polychromatic UV-light sources and thick specimens.

Currently, this model is used as a research tool based on formal kinetics. The consistency of the different photothermal aging scenarios has been tested. The model parameters have been determined by using the model as an inverse resolution method in order to simulate, as well as possible, the concentration changes in hydroperoxides, carbonyls and double bonds, but also the changes in molecular masses. The model validity has been checked from a substantial aging campaign involving tests on thin films (100 µm of average thickness) in two devices equipped with distinct UV-light sources, namely SEPAP and WeatherO'Meter. Thus, it has been possible to investigate:

(i) The competition between multiple initiating species. Norrish 1 and 2 reactions were shown to be negligible compared with hydroperoxides photolysis.

(ii) The occurrence of energy transfers between these different chemical species. Using the formal kinetic approach, it has been shown that the experimental data are compatible with the photosensitization of hydroperoxides by metal chelates (catalyst residues), but not by ketones.

(iii) The consistency of assumptions on oxidation mechanisms, photochemistry (independence of quantum yields upon temperature, molecular weight of photosensitive species and UV-light wavelength) and initial concentrations of initiating species.

Finally, the optimization procedure has led to quantum yields of hydroperoxides photolysis which are consistent with the experimental findings of Carlsson and Wiles. In a first approach, it can be considered that the CLMS can be successfully extended to the case of photothermal oxidation, but only in a restricted domain were the quantum theory provides a suitable description of

photochemistry, i.e. for UV-light intensities not involving multiphotonic excitations or termolecular processes.

This result suggests the existence of an upper boundary in the validity range of the kinetic model corresponding to a critical UV-light intensity of about $2 \cdot 10^{-5}$ Einstein.L^{-1}.s^{-1}, i.e. ten times the UV-light intensity of sunlight (zenith, filtered by the atmosphere).

Irrespectively to the photothermal aging conditions, the value of Φ_{POOH} exceeds the theoretical maximum for primary processes ($\Phi_{POOH} > 1$), which is presumably ascribed to a misestimation of the molar extinction coefficient of hydroperoxides, or the ephotosensitization of hydroperoxides by catalyst residues. The decrease in Φ_{POOH} with UV-light intensity, as well as some evidences of bimolecular photochemical decomposition of hydroperoxides (termolecular photophysical process), suggest that the kinetic model can still be improved.

The main advantage of the kinetic modeling approach is its upgradability, which can be discussed regarding at the formal kinetic approach. For instance, if some energy transfers occur, it would be necessary to consider how they may be impacted by the introduction of the effects of other chemical compounds such as stabilizers like quenchers.

Clearly, similar models can be established for all types of polyolefins, but it would involve the same kind of difficulty, i.e. the uncertainty on the nature and relative contribution of structural defects to the initiation step of oxidation. Obviously, this kind of kinetic model of photothermal oxidation would be advantageously applied to other polymers for which the chromophores are clearly identified and their photochemical characteristics measurable with accuracy.

Acknowledgements

The authors gratefully acknowledge the *Carnot-Arts Institute* for its financial support to acquire an Agilent Technologies PL-GPC 220 high temperature device and the *Centre National d'Evaluation de Photoprotection* (Clermont-Ferrand, France) for photothermal aging tests and careful control of exposure conditions.

7. Appendices

7.1. Quantum yields from the literature

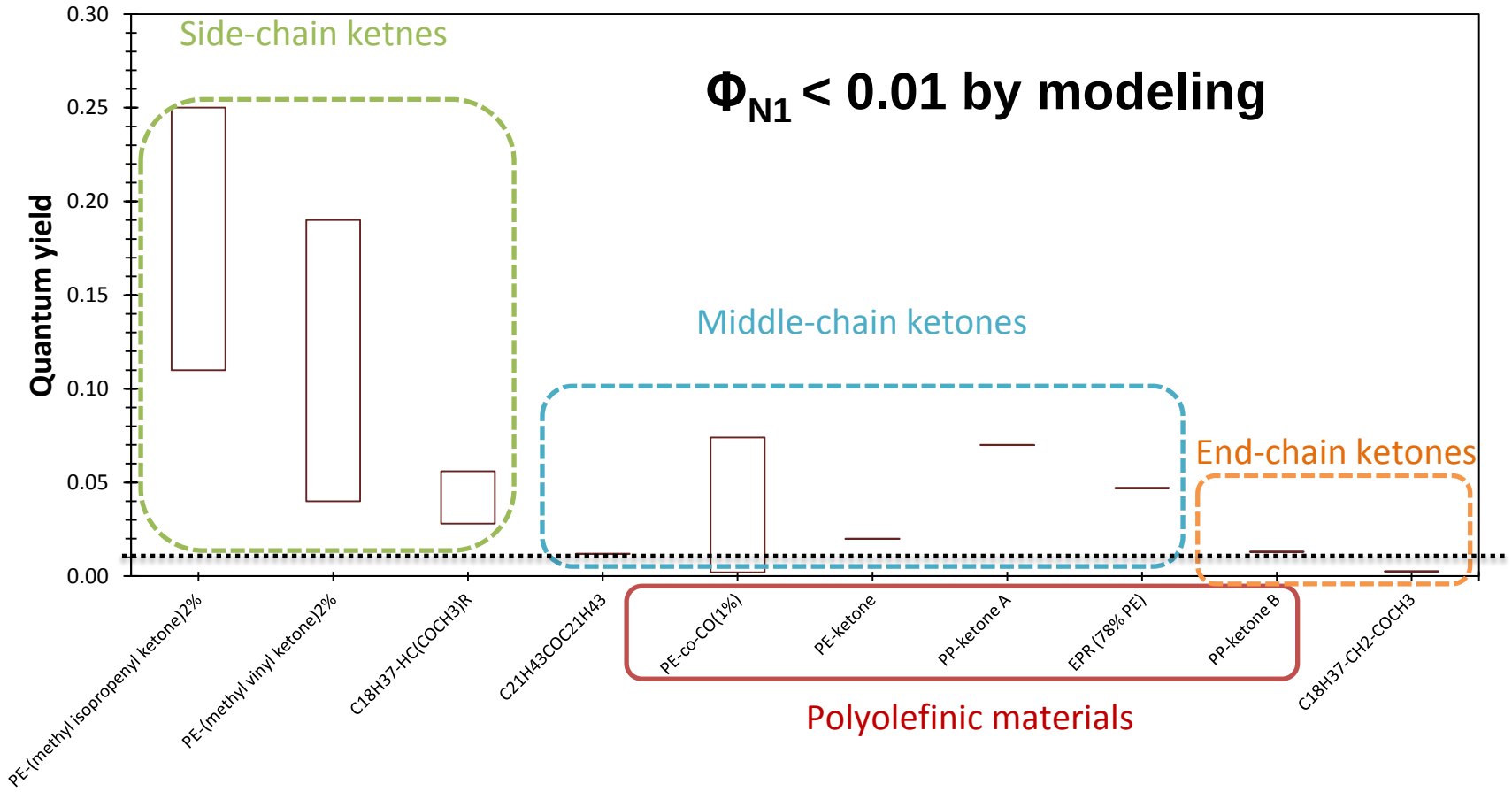

Figure A1: Compilation of quantum yields of Norrish 1 reaction for various ketones compounds including (Poly(methyl)vinyl or poly(methylisopropyl) ketone [60]; molecular side-chain [60]; in-chain and end-chain model compounds [61]; PE-co-carbon monoxide [58, 59, 62]; oxidized polyethylene [15]; polypropylene [2] and EPR [59].

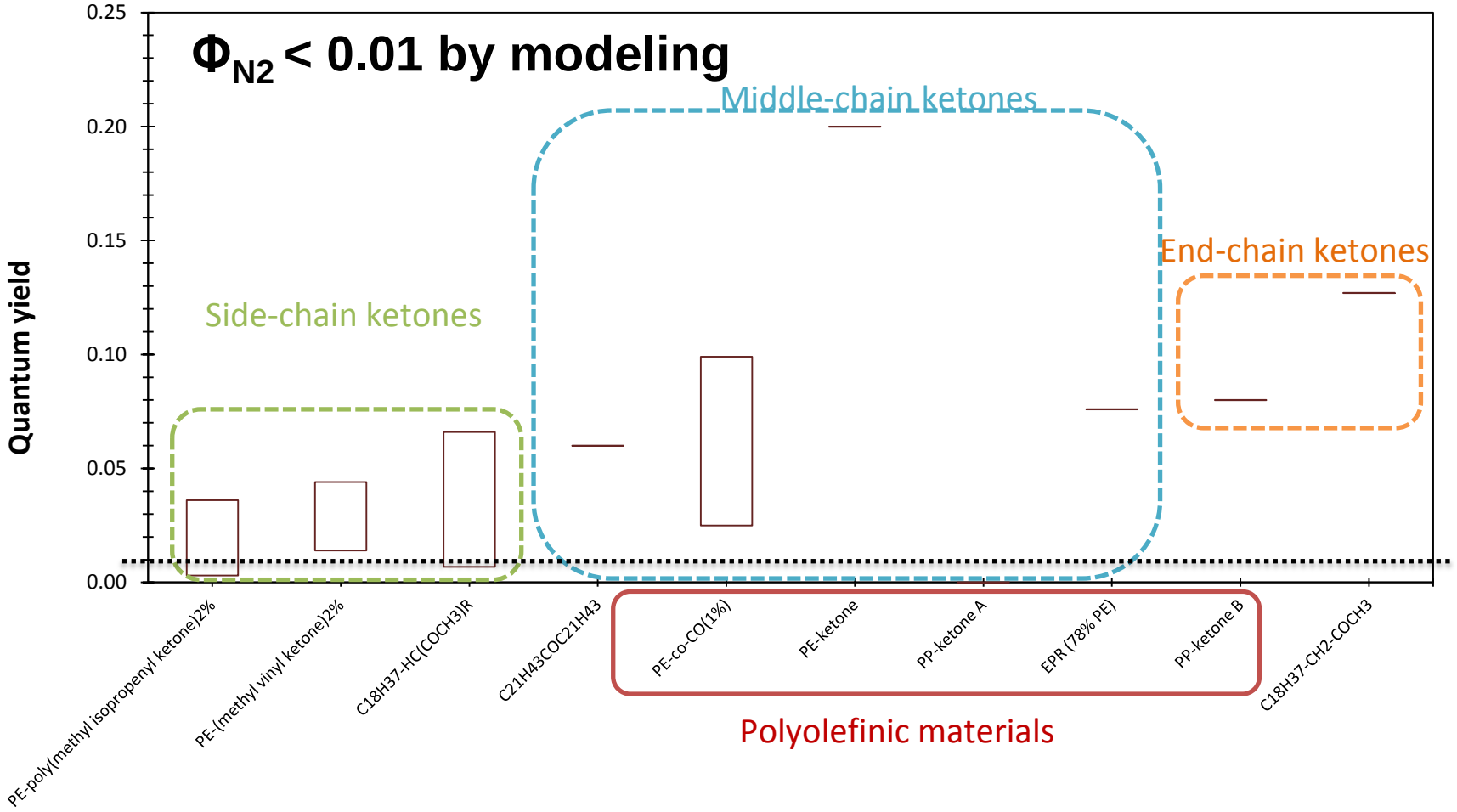

Figure A2: Compilation of quantum yields of Norrish 2 reaction for various ketones compounds including (Poly(methyl)vinyl or poly(methylisopropyl) ketone [44]; molecular side-chain [44]; in-chain and end-chain model compounds [51]; PE-co-carbon monoxide [34, 57-59]; oxidized polyethylene [15]; polypropylene [2] and EPR [59].

Table A1: Compilation of quantum yields for hydroperoxides photolysis

Type of hydroperoxide	**Wavelength**	**Φ_{POOH}**	**References**
cis-1,4-polyisoprene hydroperoxide	313 nm	5 to 30	[83]
cis-1,4-polyisoprene hydroperoxide	313 nm	2.5 to 7.5	[34]
cis-1,4-polyisoprene hydroperoxide	313 nm	5.5 to 7.6	[62]
PP hydroperoxide	365 nm	3.4 to 4.8	[1]
PP hydroperoxide	SEPAP 12/24	4.2	Calculated from [84]
PP alkyl peroxide	365 nm	2	[3]

7.2. Spectral distributions of quantum yields

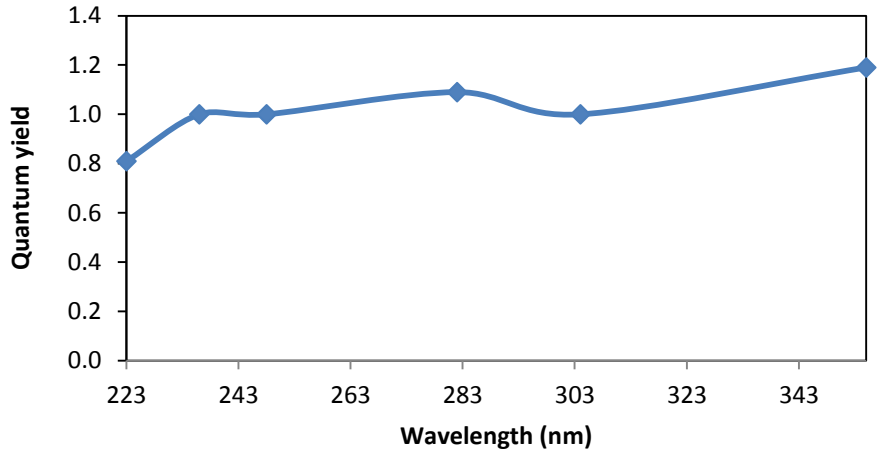

Figure B1: Spectral distribution of the quantum yield of tert-butyl hydroperoxide photolysis according to Vaghjani et al. [40]

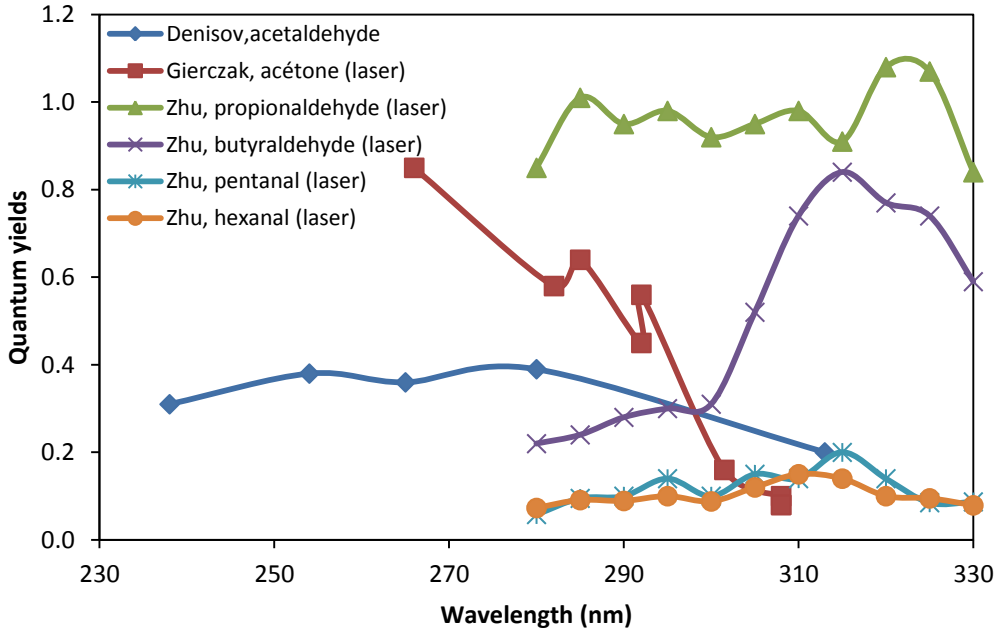

Figure B2: Spectral distribution of the quantum yield ketones photolysis according to Norrish 1 reaction (with UV-lamp or lasers) [41, 42]

References

[1] D.J. Carlsson, D.M. Wiles, The photodegradation of Polypropylene Films. III. Photolysis of polypropylene hydroperoxydes, Macromolecules, 2 (1969) 597-606.
[2] D.J. Carlsson, D.M. Wiles, The Photodegradation of Polypropylene Films. II. Photolysis of Ketonic Oxidation Products, Macromolecules, 2 (1969) 587-597.
[3] D.J. Carlsson, D.M. Wiles, The Photooxidative Degradation of Polypropylene. Part I. Photooxidation and Photoinitiation Processes, Journal of Macromolecular Science, Part C, Polymer Reviews 14 (1976) 65 - 106.
[4] A.V. Tobolsky, Oxidative degradation of polymeric material, Discussions of the Faraday Society, 2 (1947) 384-388.
[5] A.V. Tobolsky, D.J. Metz, R.B. Mesrobian, Low temperature autoxidation of hydrocarbons: The phenomenon of maximum rates, Journal of the American Chemical Society, 72 (1950) 1942-1952.
[6] J.L. Bolland, G. Gee, Kinetic studies in the chemistry of rubber and related materials. II. The kinetics of oxidation of unconjugated olefins, Transactions of the Faraday Society, 42 (1946) 236-243.
[7] L. Reich, S.S. Stivala, Kinetics and mechanism of oxidative degradation of polymers, in: McGraw-Hill (Ed.) Elements of polymer degradation 1971, pp. 229-293.
[8] S.S. Stivala, J. Kimura, S.M. Gabbay, Thermal degradation and oxidative processes, in: N.S. Allen (Ed.) Degradation and Stabilization of Polyolefins, Appl. Sci. Publ., London, 1983, pp. 63–185.
[9] A.V. Cunliffe, A. Davis, Photo-oxidation of thick polymer samples" Part II: The influence of oxygen diffusion on the natural and artificial weathering of polyolefins, Polymer Degradation and Stability, 4 (1982) 17-37.
[10] G.C. Furneaux, K.J. Ledbury, A. Davis, Photo-oxidation of thick polymer samples" Part I: The variation of photo-oxidation with depth in naturally and artificially weathered low density polyethylene, Polymer Degradation and Stability, 3 (1981) 431-442.
[11] L. Audouin, V. Langlois, J. Verdu, J.C.M. de Bruijn, Role of oxygen diffusion in polymer ageing: kinetic and mechanical aspects, Journal of Materials Science, 29 (1994) 569-583.
[12] K.T. Gillen, J. Wise, R.L. Clough, General solution for the basic autoxidation scheme, Polymer Degradation and Stability, 47 (1995) 149-161.
[13] X. Colin, C. Marais, J. Verdu, A new method for predicting the thermal oxidation of thermoset matrices: Application to an amine crosslinked epoxy, Polymer Testing, 20 (2001) 795-803.
[14] X. Colin, C. Marais, J. Verdu, Thermal oxidation kinetics for a poly(bismaleimide), Journal of Applied Polymer Science, 82 (2001) 3418-3430.
[15] A. Somersall, C., J. Guillet, E., Computer Modeling Studies of Polymer Photooxidation and Stabilization, in: Polymer Stabilization and Degradation, American Chemical Society, 1985, pp. 211-234.
[16] L. Audouin, V. Gueguen, A. Tcharkhtchi, J. Verdu, "Closed loop" mechanistic schemes for hydrocarbon polymer oxidation, Journal of Polymer Science Part A: Polymer Chemistry, 33 (1995) 921-927.
[17] S. Verdu, J. Verdu, A new kinetic model for polypropylene thermal oxidation at moderate temperatures, Macromolecules, 30 (1997) 2262-2267.
[18] L. Achimsky, L. Audouin, J. Verdu, Kinetic study of the thermal oxidation of polypropylene, Polymer Degradation and Stability, 57 (1997) 231-240.
[19] N. Khelidj, X. Colin, L. Audouin, J. Verdu, C. Monchy-Leroy, V. Prunier, Oxidation of polyethylene under irradiation at low temperature and low dose rate. Part I. The case of "pure" radiochemical initiation, Polymer Degradation and Stability, 91 (2006) 1593-1597.
[20] S.r. Kiil, Model-based analysis of photoinitiated coating degradation under artificial exposure conditions, Journal of Coatings Technology and Research, 9 375-398.
[21] A. François-Heude, E. Richaud, E. Desnoux, X. Colin, Influence of temperature, UV-light wavelength and intensity on polypropylene photothermal oxidation, Polymer Degradation and Stability, 100 (2014) 10-20.
[22] J.-L. Gardette, C. Sinturel, J. Lemaire, Photooxidation of fire retarded polypropylene, Polymer Degradation and Stability, 64 (1999) 411-417.

[23] D.W. Mayo, F.A. Miller, R.W. Hannah, Infrared Spectra of Polymers: Introduction, John Wiley & Sons, Inc., 2004.
[24] F.M. Rugg, J.J. Smith, R.C. Bacon, Infrared spectrophotometric studies on polyethylene. II. Oxidation, Journal of Polymer Science, 13 (1954) 535-547.
[25] D.J. Carlsson, R. Brousseau, D.M. Wiles, Reactions of sulfur dioxide with oxidized polyolefins, Polymer Degradation and Stability, 15 (1986) 67-79.
[26] D.J. Carlsson, J. Lacoste, A critical comparison of methods for hydroperoxide measurement in oxidized polyolefins, Polymer Degradation and Stability, 32 (1991) 377-386.
[27] J.M. Evans, Gel permeation chromatography: A guide to data interpretation, Polymer Engineering & Science, 13 (1973) 401-408.
[28] W.W. Yau, J.J. Kirkland, D.D. Bly, Modern Size-Exclusion Liquid Chromatography: Practice of Gel Permeation and Gel Filtration Chromatography, 2nd Edition, John Wiley and Sons, 1979.
[29] S. Mori, H.G. Barth, Size Exclusion Chromatography, Springer, 1999.
[30] A. François-Heude, E. Richaud, A. Guinault, E. Desnoux, X. Colin, On the impact of oxygen transport properties on the polypropylene thermal oxidation. Part I: Effect of oxygen solubility Submitted in: Journal of Applied Polymer Science, (2014).
[31] A. François-Heude, E. Richaud, A. Guinault, E. Desnoux, X. Colin, On the impact of oxygen transport properties on the polypropylene thermal oxidation. Part II: Effect of oxygen diffusivity, Submitted in: Journal of Applied Polymer Science, (2014).
[32] J.G. Calvert, J.N.J. Pitts, Photochemistry American Chemical Society, 1966.
[33] B. Rånby, J.F. Rabek, Photodegradation, photo-oxidation, and photostabilization of polymers principles and applications 1975.
[34] E. Guillet J, J. Dhanraj, J. Golemba F, H. Hartley G, Fundamental Processes in the Photodegradation of Polymers, in: Stabilization of Polymers and Stabilizer Processes, American Chemical Society, 1968, pp. 272-286.
[35] C. Chatgilialoglu, D. Crich, M. Komatsu, I. Ryu, Chemistry of Acyl Radicals, Chemical Reviews, 99 (1999) 1991-2070.
[36] J.E. Guillet, Photochemistry in macromolecular systems, Naturwissenschaften, 59 (1972) 503-509.
[37] J.C. Dalton, N.J. Turro, Photoreactivity of n,pi* Excited States of Alkyl Ketones, Annual Review of Physical Chemistry, 21 (1970) 499-560.
[38] J.E. Guillet, Fundamental processes in the UV degradation and stabilization of polymers Pure and Applied Chemistry, 30 (1972) 135-144.
[39] M. Heskins, J.E. Guillet, Photochemistry of Ketone Polymers. III. Energy Transfer in Ethylene-Carbon Monoxide Polymers, Macromolecules, 3 (1970) 224-231.
[40] G. Vaghjiani, L., A.R. Ravishankara, Photodissociation of H_2O_2 and CH_3OOH at 248 nm and 298 K: Quantum yields for OH, O(^{3}P) and H(^{2}S), The Journal of Chemical Physics, 92 (1990) 996-1003.
[41] T. Gierczak, J.B. Burkholder, S. Bauerle, A.R. Ravishankara, Photochemistry of acetone under tropospheric conditions, Chemical Physics, 231 (1998) 229-244.
[42] L. Zhu, Y. Tang, Y. Chen, T. Cronin, Wavelength-Dependent Photolysis of C3-C7 Aldehydes in the 280-330 nm Region, Spectroscopy Letters, 42 (2009) 467-478.
[43] Searle, Activation spectra : the activation spectrum and its significance to weathering of polymeric materials, Atlas SunSpots, 14 (1984).
[44] Z. Zhenfeng, H. Xingzhou, L. Zubo, Wavelength sensitivity of photooxidation of polypropylene, Polymer Degradation and Stability, 51 (1996) 93-97.
[45] E. Hairer, G. Wanner, Stiff and Differential-Algebraic Problems, 1996.
[46] O. Saito, The Radiation Chemistry of Macromolecules, ed. M. Dole ed., Academic Press, New-York, 1972.
[47] E. Richaud, F. Farcas, B. Fayolle, L. Audouin, J. Verdu, Hydroperoxide build-up in the thermal oxidation of polypropylene - A kinetic study, Polymer Degradation and Stability, 92 (2007) 118-124.
[48] P. Gijsman, J. Hennekens, J. Vincent, The mechanism of the low-temperature oxidation of polypropylene, Polymer Degradation and Stability, 42 (1993) 95-105.
[49] P. Gijsman, M. Kroon, M. van Oorschot, The role of peroxides in the thermooxidative degradation of polypropylene, Polymer Degradation and Stability, 51 (1996) 3-13.

[50] J.H. Adams, Analysis of the nonvolatile oxidation products of polypropylene I. Thermal oxidation, Journal of Polymer Science Part A-1: Polymer Chemistry, 8 (1970) 1077-1090.
[51] J.H. Adams, Analysis of nonvolatile oxidation products of polypropylene. III. Photodegradation, Journal of Polymer Science Part A-1: Polymer Chemistry, 8 (1970) 1279-1288.
[52] J. Lacoste, D. Vaillant, D.J. Carlsson, Gamma-, photo-, and thermally-initiated oxidation of isotactic polypropylene, Journal of Polymer Science Part A: Polymer Chemistry, 31 (1993) 715-722.
[53] D.M. Mowery, R.A. Assink, D.K. Derzon, S.B. Klamo, R.L. Clough, R. Bernstein, Solid-State 13C NMR Investigation of the Oxidative Degradation of Selectively Labeled Polypropylene by Thermal Aging and Î³-Irradiation, Macromolecules, 38 (2005) 5035-5046.
[54] J.T. Martin, R.G.W. Norrish, The photochemical decomposition of tert-butyl hydroperoxyde, Proceeding of the Royal society of London. Serie A. Mathematical and physical sciences, 220 (1953) 322(339.
[55] L. Audouin, S. Girois, L. Achimsky, J. Verdu, Effect of temperature on the photooxidation of polypropylene films, Polymer Degradation and Stability, 60 (1998) 137-143.
[56] G. Geuskens, F. Debie, M.S. Kabamba, G. Nedelkos, New aspects of the photooxidation of polyolefins, Polymer Photochemistry, 5 (1984) 313-331.
[57] C.H. Bamford, C.F.H. Tipper, Degradation of polymers, in: Comprehensive chemical kinetics, Elsevier, Amsterdam ; Oxford ; New York 1975.
[58] G.H. Hartley, J.E. Guillet, Photochemistry of Ketone Polymers. I. Studies of Ethylene-Carbon Monoxide Copolymers, Macromolecules, 1 (1968) 165-170.
[59] S.K.L. Li, J.E. Guillet, Photochemistry of ketone polymers. 17. Photodegradation of an amorphous ethylene-propylene copolymer, Macromolecules, 17 (1984) 41-50.
[60] E. Guillet J, Studies of the mechanism of polyolefin photodegradation, Pure and Applied Chemistry, 52 (1980) 295-294.
[61] G.H. Hartley, J.E. Guillet, Photochemistry of Ketone Polymers. II. Studies of Model Compounds, Macromolecules, 1 (1968) 413-417.
[62] J.E. Guillet, Fundamental Processes in the Photodegradation of Polyolefins, in: Stabilization and Degradation of Polymers, American Chemical Society, 1978, pp. 1-10.
[63] G. Geuskens, M.S. Kabamba, Photo-oxidation of polymers--Part V: A new chain scission mechanism in polyolefins, Polymer Degradation and Stability, 4 (1982) 69-76.
[64] G. Geuskens, M.S. Kabamba, Photo-oxidation of polymers: Part IX--Additional comments about a new chain scission mechanism in polyolefins, Polymer Degradation and Stability, 5 (1983) 399-401.
[65] Philippart, L. J, Sinturel, C, Arnaud, R, Gardette, Influence of the exposure parameters on the mechanism of photooxidation of polypropylene, Polymer Degradation and Stability, 64 (1999) 213-225.
[66] C. Sinturel, J.-L. Philippart, J. Lemaire, J.-L. Gardette, Photooxidation of fire retarded polypropylene. I. Photoageing in accelerated conditions, European Polymer Journal, 35 (1999) 1773-1781.
[67] P. Vink, Photooxidation of polypropylene Journal of Applied Polymer Science: Applied Polymer Symposium, 35 (1979) 265-273.
[68] P. Vink, The Photo-Oxidation of Polyolefins - Structural and Morphological Aspects, in: e.N.S. Allen (Ed.) Degradation and Stabilisation of Polyolefins, Applied Science Publishers, London, 1983, pp. 213-246.
[69] P. Vink, T.J. Van Veen, The mechanism of u.v. stabilization of polypropylene films by 2-hydroxy-4-octyloxybenzophenone, European Polymer Journal, 14 (1978) 533-537.
[70] P. Gijsman, A. Dozeman, Comparison of the UV-degradation chemistry of unstabilized and HALS-stabilized polyethylene and polypropylene, Polymer Degradation and Stability, 53 (1996) 45-50.
[71] L. Balabán, J. Majer, K. Vesely, Photooxidative Degradation of Polypropylene, Journal of Polymer Science Part C: Polymer Symposia, 22 (1969) 1059-1071.
[72] Philippart, L. J, Sinturel, C, Gardette, Influence of light intensity on the photooxidation of polypropylene, Polymer Degradation and Stability, 58 (1997) 261-268.
[73] P. Gijsman, J. Hennekens, J. Vincent, The influence of temperature and catalyst residues on the degradation of unstabilized polypropylene, Polymer Degradation and Stability, 39 (1993) 271-277.

[74] P. Gijsman, The Long-Term Stability of Polyolefins. Wibro Dissertatiedrukkerij, Helmond., in, Technische Universiteit Eindhoven 1994, pp. 176 p.
[75] C.R. Boss, J.C.W. Chien, Oxygen diffusion limitation in autoxidation of polypropylene, Journal of Polymer Science Part A-1: Polymer Chemistry, 4 (1966) 1543-1551.
[76] N.Y. Rapoport, S.I. Berulava, A.L. Kovarskii, I.N. Musayelyan, Y.A. Yershov, V.B. Miller, The kinetics of thermo-oxidative degradation of oriented polypropylene in relation to the structure and molecular mobility of the polymer, Polymer Science U.S.S.R., 17 (1975) 2901-2909.
[77] N.Y. Rapoport, A.S. Goniashvili, M.S. Akutin, V.B. Miller, Vysokomol. Soed., 21A (1979) 2071.
[78] N.Y. Rapoport, N.M. Livanova, V.B. Miller, On the influence of internal stress on the kinetics of oxidation of oriented polypropylene, Polymer Science U.S.S.R., 18 (1976) 2336-2341.
[79] M. Iring, S. László-Hedvig, K. Barabás, T. Kelen, F. Tüdos, Study of the thermal oxidation of polyolefins--IX : Some differences in the oxidation of polyethylene and polypropylene, European Polymer Journal, 14 (1978) 439-442.
[80] M. Iring, S. Laszlo-Hedvig, T. Kelen, F. Tudos, L. Fuzes, G. Gamey, G. Bodor, Journal of Polymer Science, 57 (1976) 55-63.
[81] M. Iring, S. László-Hedvig, F. Tüdos, T. Kelen, Study of the thermal oxidation of polyolefins--XII : Thermal oxidation of isotactic and atactic polypropylene in the condensed phase and in solution, Polymer Degradation and Stability, 5 (1983) 467-480.
[82] F. Tüdos, M. Iring, T. Kelen, Oxidation of Polyolefins, in: E.A.V. Patsis (Ed.) International conference on advances in the stabilization and controlled degradation of polymers, 1985.
[83] H.C. Ng, J.E. Guillet, Photochemistry of Ketone Polymers. 13. Quenching of Excited Ketone Carbonyls by Hydroperoxides and Peroxides, Macromolecules, 11 (1978) 937-942.
[84] S. Commereuc, D. Vaillant, J.L. Philippart, J. Lacoste, J. Lemaire, D.J. Carlsson, Photo and thermal decomposition of iPP hydroperoxides, Polymer Degradation and Stability, 57 (1997) 175-182.

CHAPTER VIII. Challenges in the numerical simulation of photodegradation profiles

Alexandre François-Heude[a,b] [6], Emmanuel Richaud[a], Alain Guinault[a], Eric Desnoux[b], Xavier Colin[a]

[a]PIMM Laboratory, CNRS UMR 8006, Arts et Metiers ParisTech, Paris, France

[b]Renault, DETC-A, Guyancourt, France

Abstract

A general framework is given for the numerical simulation of the photothermal oxidation profiles of polypropylene. The kinetics of photothermal oxidation reaction is coupled into a system of differential equations with the transport phenomena of molecular reactants, in particular with oxygen diffusion and UV-light attenuation in the sample thickness due to sample opacity and light absorption by chromophores. The resulting kinetic model is used as an inverse method to determine unknown parameters, that are difficult to access experimentally, but also as an efficient tool for interpreting the experimental results obtained in the present study and collected in the literature. In particular, this model allows investigating the reciprocal effects of oxidation kinetics and oxygen transport properties. It is found that oxidation induces a dramatic drop in oxygen permeability, even at very low conversion degrees, well beyond expectations by considering only the effects of chemi-crystallization.

Keywords

Polypropylene; Photothermal oxidation profiles; Screen effect; Diffusion limited oxidation; Numerical resolution methods.

[6] Corresponding author : Email: Alexandre.FRANCOIS-HEUDE@ensam.eu
Tel/ Fax: +33 1 44 24 64 13/ +33 1 44 24 63 82

1. Introduction

Understanding and predicting the formation of a superficial oxidized layer during the natural weathering of polymer parts is of a great interest for the scientific and industrial communities since this layer is responsible for the alteration of both their aspect (early cracking, whitening and loss of gloss) and mechanical properties (increase in stiffness and hardness; decrease in ductility, toughness and impact resistance) [1].

Oxidation products profiles result from the diffusion control of oxidation kinetics, but also from the UV-light attenuation in the sample thickness due to sample opacity and light absorption by photosensitive species (namely chromophores). These profiles are generally predicted by introducing the Fick's second law (for describing the oxygen supply by the diffusive process) into the balance equation governing the oxygen chemical consumption by the polymer:

$$\partial[O_2]/\partial t = D_{O_2}\,\partial^2[O_2]/\partial z^2 - r([O_2]) \qquad \textbf{Eq. 1}$$

where D_{O2} is the coefficient of oxygen diffusion (in $m^2.s^{-1}$) and $r([O_2])$ is the rate of oxygen chemical consumption (in $mol.L^{-1}.s^{-1}$), whose mathematical expression is derived from a mechanistic scheme.

The numerical solving of equation 1 gives access to the changes, with exposure time t, in oxygen concentration $[O_2]$ in an elementary sublayer located at the depth z beneath the sample surface.

Here, the key issue is to provide a suitable kinetic description of $r([O_2])$ depending on both intensive (temperature and oxygen partial pressure) and extensive (UV-light energy and wavelength) variables. In the case of pure thermo-oxidation [2-6] and pure photo-oxidation [7-9], most of the analytical expressions were derived from the basic autooxidation scheme proposed for hydrocarbon polymers by Bolland and Gee [10]. However, these expressions were established by setting a series of very restrictive simplifying assumptions, for instance: low conversion ratios of oxidation process, constancy of initiation rate, steady-state for radicals concentrations, long kinetic chain, existence of an interrelationship between termination rate constants, etc., that can

lead to serious inaccuracies in extrapolation. The most popular are hyperbolic relationships [4-6, 8, 9] of the type:

$$r([O_2]) = \frac{\alpha[O_2]}{1 + \beta[O_2]} \quad \textbf{Eq. 2}$$

where α and β are parameters expressed as a function of the elementary rate constants of initiation, propagation and termination steps.

In the case of pure thermo-oxidation [4-6], α and β obey an Arrhenius law (as elementary rate constants). In addition, in the case of pure photo-oxidation [8, 9], α varies as the square root of the UV-light intensity I, as confirmed by UV-light irradiations on iPP samples with both filtered high pressure mercury [11] and fluorescent lamps [12]. Thus, α depends on exposure conditions according to:

$$\alpha = \alpha_0 \cdot I^{\gamma} \cdot \exp\left(-\frac{Ea_\alpha}{RT}\right) \qquad \textbf{Eq. 3}$$

with α_0 and Ea_α the pre-exponential factor and activation energy respectively, and γ an exponent such as: $\gamma = 0$ for pure thermo-oxidation and $\gamma = ½$ for pure photo-oxidation.

The maximal value of the thickness of oxidized layer (TOL), reached in the steady-state regime, can be predicted by a simple scaling law highlighting the competition between oxygen diffusivity and polymer reactivity towards oxygen [2]:

$$TOL = \left(D_{O2}/\alpha\right)^{1/2} \quad \textbf{Eq. 4}$$

Since, in a given physical state (i.e. in glassy or rubbery state), D_{O2} obeys also an Arrhenius law:

$$D_{O2} = D_0 \exp\left(-\frac{Ea_D}{RT}\right) \quad \textbf{Eq. 5}$$

with D_0 and Ea_D the pre-exponential factor and activation energy respectively,

it comes finally:

$$TOL = TOL_0 \cdot I^{-\gamma/2} \cdot \exp\left(-\frac{Ea_{TOL}}{RT}\right) \qquad \textbf{Eq. 6}$$

$$with\ TOL_0 = {D_0}^{1/2}.\alpha_0^{-1/2}\ \ and\ \ Ea_{TOL} = Ea_D - Ea_\alpha$$

Thus, TOL would depend also on photothermal exposure conditions, i.e. on temperature and UV-light intensity (usually at the power -¼).

If such analytical models (equations 2 to 6) appear as very helpful for evaluating the depth penetration of oxidation into thick polymer plates in the boundary cases of pure thermo-oxidation and pure photo-oxidation, in contrast, they are totally unsuitable for treating the most general case of photothermal oxidation, in which two distinct types of (thermal and photochemical) initiation coexist. The most restrictive assumption is, by far, the constancy of the initiation rate which does not allow the simulation of induction periods and implies that such models are only valid in a restricted range of UV-light intensities [13].

Besides, if these models describe almost satisfyingly the impact of UV-light intensity on the oxidation kinetics, in contrast, they consider a simple exponential decay in the specimen thickness for accounting for UV-light attenuation due to the presence of chromophores (including additives such as UV-light absorbers), crystalline lamellae and spherulites, or even fillers and pigments [14, 15]:

$$I_z = I_0 \cdot e^{-\kappa z} \qquad \textbf{Eq. 7}$$

This attenuation factor was frequently considered constant irrespectively to: (i) radiations wavelength, i.e. the type of UV-light source, and (ii) time, i.e. the concentration changes of photosensitive species such as peroxide type species, carbonyl products and UV-absorbers. Sometimes, this factor was even neglected because oxidation profiles were reported to be almost symmetrical for unstabilized polyolefin samples of few millimeters thick [8, 9, 16], which is surprising even for translucent materials.

In the case of photothermal oxidation, analytical solutions are out-of-reach due to the hypercomplexity of the corresponding mechanistic scheme. The system of differential equations, derived from the mechanistic scheme, must be solved numerically using the semi-implicit

algorithms recommended for stiff problems of chemical kinetics. This numerical solving will allow to eradicate all the usual simplifying assumptions (except unicity of reactive site), and to describe more rigorously all physico-chemical couplings existing between oxygen chemical consumption, oxygen transport properties, sample opacity and light absorption by chromophores.

This approach was first applied to polypropylene thermal oxidation with the objective to refine the values of oxygen transport properties, namely oxygen solubility and diffusivity, and to describe the large variety of thermal oxidation behaviors reported in the literature among the whole iPP family [17]. This kinetic model was then extended to polypropylene photothermal oxidation by adding other sources of radicals than the thermal decomposition of hydroperoxidesinto the mechanistic scheme, namely the photo-induced decomposition of chromophores [18]. The photolysis kinetics have been formalized by using concept of spectral overlap integral, which enables to account for the quantitative effect of UV-light including its spectral selectivity towards chromophores decomposition. In practice, it enables to model the differences existing between different UV-light sources.

In this upgraded kinetic model, UV-light attenuation was tentatively described more precisely by decomposing the attenuation factor κ(λ) into time-dependent and time-independent components accounting respectively for the semi-crystalline polymer opacity and the light absorption by chromophores:

$$\kappa(\lambda) = \alpha(\lambda) + \ln(10) \sum_{\substack{j \\ chromophoric \\ species\ X_j}} \varepsilon_j(\lambda)\,[X_j] \qquad \textbf{Eq. 8}$$

In a first approach, the spectral distribution of α(λ) was considered as constant with exposure time, but this parameter could vary during photothermal oxidation for instance, because of surface aspect alteration (loss of gloss) or morphological changes impacting multiple scattering. In this latter case, it is noteworthy that the optical path of the UV-light beam would be modified, thus inducing a change in the quantum yield.

This model allows simulating faithfully the local concentration changes in primary (hydroperoxides) and secondary (carbonyls) oxidation products, double bonds, chain scissions and crosslinking nodes in a wide range of temperatures and UV-light intensities whatever the light source [1]. Moreover, when used in an inverse method, it constitutes an efficient tool for investigating the reciprocal effects of oxidation kinetics and oxygen transport properties. Main results can be summarized as follows:

i) The variability of oxygen solubility allows accounting for the large scattering of induction periods and oxidation rates, but also for the oxygen pressure dependence of both quantities, reported in the literature for the whole iPP family [18]. This variability is presumably due to iPP polymorphism in the temperature range where oxygen permeability is commonly measured.

ii) There is a change in oxygen diffusivity with the conversion degree of oxidation [19, 20]. This phenomenon has been ascribed to chemi-crystallization or, potentially, to polarity changes due to oxygen grafting (change in oxygen solubility).

In contrast, Schoolenberg et al. have reported the formation of spontaneous cracks at surface of thick polymer plates [16] revealing the existence of a tensile stress field induced by the densification of the superficial oxidized layer. This latter phenomenon is expected to modify the shape of oxidation profiles, since favoring oxygen penetration into deeper layers, thus increasing the apparent value of D_{O2}. It would be materialized on the profiles of oxidation products by the appearance of a plateau near to the sample surface [21] for carbonyl concentrations higher than typically 0.1 $mol.L^{-1}$ (i.e. a carbonyl index of 0.7) [16]. Such profiles must be differentiated from similar ones evidenced when oxygen becomes in excess near the sample surface [4].

In the present paper, it is proposed to investigate the validity range of the kinetic model [18] when it is applied to thicker specimens (typically few mm thick), and to highlight the main specific hurdles in the kinetic modeling of photothermal degradation profiles. A peculiar attention will be drawn to the changes in oxygen transport and optical properties during the course of oxidation. In this perspective, the model will be used as a research tool for estimating the importance of these phenomena on the photothermal oxidation kinetics. A particular attention will be also paid on numerical issues, i.e. methods and solvers, and future challenges for accurately simulating photothermal oxidation profiles.

2. Model theory and numerical resolution

2.1. Mechanistic scheme

The kinetic modeling approach developed in our laboratory consists in deriving a kinetic model from a simplified, but realistic, oxidation mechanistic scheme focused on the critical oxidation path, i.e. constituted of the main contributory reactions to photothermal oxidation. This scheme must describe satisfyingly the macromolecular changes responsible for the alteration of both the aspect and mechanical properties of polymers, i.e. chain scissions.

In this scheme, oxidation is mainly initiated by the decomposition of the most thermally and photochemically unstable species i.e. peroxide type species, owing to the high cleavability of their O-O bond, which presents a dissociation energy of about 150 $kJ.mol^{-1}$ against more than 330 $kJ.mol^{-1}$ for all other polymer bonds (i.e. C-C and C-H). Indeed, it was found that Norrish 1 and 2 reactions are negligible sources of radicals and chain scissions, in agreement with the literature [22-25]. As a result, hydroperoxides are the key species in photothermal oxidation, since they decompose under the combined effects of temperature and UV-light, to produce radicals and chain scissions, meanwhile they are produced during the propagation step. They govern the oxidation kinetics and are responsible for the sharp auto-acceleration of oxidation at the end of the induction period. This is the basic idea of the so-called "Closed-Loop Mechanistic Scheme" (CLMS).

One of the major obstacles when simulating the photothermal oxidation kinetics lays in the multiplicity of the decomposition modes of hydroperoxides:

(i) Thermal initiation can be unimolecular or bimolecular [5, 50], the bimolecular mode being favored when hydroperoxides are associated in pairs or constitute longer sequences [45, 47-49];

(ii) Photochemical initiation is only unimolecular since the reaction of a quantum with two chemical species applies to a termolecular process whose probability is expected to be very low [26, 27].

However, the fact that the resulting kinetic model hardly accounts for the steep curvature of the kinetic curves of carbonyl products at the end of the induction period would suggest a higher bimolecular character. This observation could result from the fact that termolecular processes are not negligible anymore for high irradiances (i.e. high concentrations in quanta), or the occurrence of energy transfers from ketones to hydroperoxides through complexes as intermediates. These aspects can be only investigated theoretically using a specific, but non-trivial, mathematical formalism.

The resulting CLMS can be summarized as follows. It is composed of 11 elementary reactions grouped into three main stages: initiation, propagation and termination:

Initiation

(1u)	$POOH \rightarrow 2P^{\bullet} + (1 - \gamma_1)POH + \gamma_1 P{=}O + H_2O + \gamma_s S$	(- 2PH)	(k_{1u})
(1b)	$2POOH \rightarrow P^{\bullet} + PO_2^{\bullet} + (1 - \gamma_1)POH + \gamma_1 P{=}O + H_2O + \gamma_s S$	(- PH)	(k_{1b})
(1h)	$POOH + h\nu \rightarrow 2P^{\bullet} + (1 - \gamma_1)POH + \gamma_1 P{=}O + H_2O + \gamma_s S$	(-2PH)	(k_{1h})
(1p)	$POOP + h\nu \rightarrow 2P^{\bullet} + 2(1 - \gamma_1)POH + 2\gamma_1 P{=}O + 2H_2O + 2\gamma_s S$	(-2PH)	(k_{1p})

Propagation

(2)	$P^{\bullet} + O_2 \rightarrow PO_2^{\bullet}$	(k_2)
(3)	$PO_2^{\bullet} + PH \rightarrow POOH + P^{\bullet}$ (k_3)	

Termination

(4)	$P^{\bullet} + P^{\bullet} \rightarrow \gamma_4 P\text{-}P + (1 - \gamma_4)PH + (1 - \gamma_4)F + \gamma_4 B$		(k_4)
(5)	$P^{\bullet} + PO_2^{\bullet} \rightarrow \gamma_5 POOP + (1 - \gamma_5)POOH + (1 - \gamma_5)F + \gamma_5 B$		(k_5)
(6a)	$PO_2^{\bullet} + PO_2^{\bullet} \rightarrow [PO^{\bullet}\ {}^{\bullet}OP]_{cage} + O_2$ (k_{6a})		
(6b)	$[PO^{\bullet}\ {}^{\bullet}OP]_{cage} \rightarrow POOP + B$		(k_{6b})
(6d)	$[PO^{\bullet}\ {}^{\bullet}OP]_{cage} \rightarrow 2P^{\bullet} + 2(1 - \gamma_1)POH + 2\gamma_1 P{=}O + 2\gamma_s S$	(- 2PH)	(k_{6d})

In this scheme, PH accounts for tertiary CH groups (i.e. methynes) which are considered as the unique oxidation site of the polymer chain. Its radical attack leads to a large variety of degradation products, in particular:

(iv) Reactive species formed in addition to hydroperoxides POOH, such as alkyl $P^{\bullet}$ and peroxy radicals $PO_2^{\bullet}$.

(v) Inactive products accumulating in the polymer matrix during the course of oxidation, such as: peroxides POOP, alcohols P-OH, double-bonds or unsaturations F and ketones or assimilated carbonyl products P=O. They are denoted as secondary oxidation products since they result from the decomposition of primary oxidation products (POOH).

(vi) Macromolecular events contributing to the modification of polymer physical and mechanical properties, such as chain scissions S on the main polymer chain and crosslinks B (i.e. chemical bridges).

Different stoichiometric coefficients have been introduced as yields for describing the competition between several elementary reactions in balance reactions. For instance, γ_4 and γ_5 are the respective yields of recombination by coupling of alkyl-alkyl and alkyl-peroxy radicals versus disproportionation in termination steps.

Moreover, γ_s is the yield in β-scission (leading to ketones) face to hydrogen abstraction (leading to alcohols) in both unimolecular (1u, 1h and 1p) and bimolecular initiation steps (1b). For a sake of simplicity, it was assigned to β-scissions on the main polymer chain (denoted S), which significantly impact the molecular mass, contrarily to β-scissions on side-chain and end-chain groups which generate only small volatile organic compounds. From a practical point of view, it is more convenient to consider an apparent yield γ_1 for carbonyl products owing to the high uncertainty on their nature and the value of their molar extinction coefficients at 1713 cm^{-1}.

2.2. **Photochemical kinetics**

The temperature dependence of thermal oxidation is described by applying the Arrhenius law to the rate constant k_i of each elementary reaction (i):

$$k_i = k_i^0 \exp\frac{-Ea_i}{RT} \qquad \textbf{Eq. 9}$$

with k_i^0 the preexponential factor and Ea_i the activation energy

Analogeously, a suitable formalism must be found to report the kinetic dependence of photo-induced reactions with the amount of "radiant" UV-visible energy. According to the quantum theory, the initiation rate by a given photosensitive species X (i.e. a chromophore) can be written as the product of the energy absorbed by the photolysis efficiency, i.e. the probability that an absorbed photon triggers the chemical bond dissociation:

$$\left.\frac{d[X]}{dt}\right|^{photolysis} = -\Phi(\lambda)_X \times I_{abs_v} \quad \textbf{Eq. 10}$$

with [X] the concentration of the chemical species X (in mol.L^{-1}),

$I_{abs.v}$ the volumic absorbed energy (in Einstein.L^{-1}.s^{-1}),

and $\Phi(\lambda)_X$ the quantum yield of photolysis efficiency (in mol.Einstein^{-1}, dimensionless).

This energy absorbed by the photosensitive species consists in the overall quanta energy satisfying the authorized electronic transitions. It can be thus deduced by calculating the overlap between the spectral distribution of molar extinction coefficient and the energy emitted by the UV-light source. It can be written as:

$$I_{abs_v} = \int_{\lambda_{min}}^{\lambda_{max}} \frac{\ln(10)}{10} \frac{E(\lambda)}{N_a} \frac{\lambda}{hc} \frac{\varepsilon_X(\lambda)\ \Delta z\ [X]}{\Delta z}\ d\lambda \qquad \textbf{Eq. 11}$$

with E (λ) the spectral irradiance of the light source including filters (in W.m^{-2}.nm^{-1}),

N_a the Avogadro's number,

h the Planck constant equal to 6.623·10^{-34} J.s,

c the light celerity (in m.s^{-1}), λ the wavelength (in m),

$\varepsilon_X(\lambda)$ the spectral distribution of the molar extinction coefficient (in L.mol^{-1}.cm^{-1}),

[X] the concentration in the photosensitive species X (in mol.L^{-1}),

and Δz the sample thickness (in m).

Since the concentration *[X]* is a separate variable, it is possible to calculate the spectral overlap integral of light absorption J_X (in Einstein.mol^{-1}.s^{-1}), chosen here as the relevant criterion independent of concentration to describe oxidation, and defined as:

$$J_X = \frac{I_{abs_v}}{[X]} = \int_{\lambda_{min}}^{\lambda_{max}} \frac{\ln(10)}{10} \frac{E(\lambda)}{N_a} \frac{\lambda}{hc} \varepsilon_X(\lambda)\ d\lambda \qquad \textbf{Eq. 12}$$

It is thus noteworthy that the product $\Phi \cdot J$ is homogeneous to the rate constant of a unimolecular decomposition (i.e. expressed in s^{-1}). If k_{1x} designates the corresponding rate constant, it can be thus written, for a given chemical species X: $k_{1x} = \Phi_X \cdot J_X$.

2.3. **Screening effect**

In addition to photochemical aspects, the UV-light attenuation in the sample thickness -i.e. the so-called "screen effect"- has also a significant impact on the photothermal degradation profiles.

In a first approach, it is relevant to start from the simplest equation available for describing such an effect, i.e. the single flux Beer-Lambert's law. This equation applies to the exponential decay of UV-light intensity previously considered by Furneaux and Cunliffe [9]. In the framework of an upgradable and general kinetic model for photothermal oxidation, the attenuation of light intensity has been decomposed into time-independent and time-dependent terms accounting respectively for:

(i) The opacity of the polymer described by the lineic absorption coefficient α(λ), which is largely due to scattering or diffraction phenomena in unfilled polyolefins. This term can also account for the opacifying action of pigments such as titanium dioxide, talc or even UV-absorbers such as carbon black.

(ii) The absorption of light by photosensitive species such as oxidation products or additives (UV-absorbers, stabilizers and their degradation products), whose concentrations are prone to changes with exposure time owing to their chemical consumption by the oxidation reaction, or their physical loss by diffusion and/or evaporation when their molecular mass is low enough.

Therefore, after discretization of the sample thickness into thin elementary sublayers of thickness Δz, the irradiance E can be written:

$$E_{z+dz}(\lambda) = E_z(\lambda)\left[1 - \left(\alpha(\lambda) + \ln(10) \sum_{\substack{j \\ chromophoric \\ species\ X_j}} \varepsilon_j(\lambda)\,[X_j]\right)\Delta z\right] \qquad \textbf{Eq. 13}$$

with $E_z(\lambda)$ the spectral irradiance (in $W.m^{-2}.nm^{-1}$) at a depth z(in m) beneath the irradiated surface, $\alpha(\lambda)$ the coefficient of lineic absorption (in m^{-1}), $\varepsilon_j(\lambda)$ the spectral distribution of molar extinction coefficient (in $L.mol^{-1}.m^{-1}$) and $[X_j]$ the concentration of a given photosensitive species X_j (in $mol.L^{-1}$).

This kind of approach was previously used by various authors [28-31] for describing the attenuation of a laser beam (monochromatic and collimated radiations) during the monitoring of polypropylene crystallization kinetics. It must be noteworthy that second order phenomena, such

as light reflection at the specimen surface, as well as multiple scattering or diffraction, have been neglected in equation 13. Nevertheless, it is relatively easy to include the description of the specular component of the reflectance as a boundary condition fulfilled by the irradiance at the specimen surface.

If UV-light is partly reflected by the specimen surface, the spectral irradiance in this position is equal to:

$\forall$ t, for z=0 $\quad E_\lambda(t, 0) = (1-r^{specular}) \bullet E_\lambda^{source}$ **Eq. 14**

where $r^{specular}$ is the specular component of the reflectance, which depends on the surface finish.

In practice, it is considered that most of the reflectance is diffuse and not specular for such semi-crystalline materials, i.e. that the reflection on the surface finish is negligible compared with the reflection due multiple scattering.

However, equation 13 cannot be used in the present form to be coupled with the kinetic model and calculate the photothermal oxidation profiles in the sample thickness. The light attenuation in the sample thickness must be determined by using the concept of spectral overlaps integral, i.e. by applying the previous transform (see equation 12):

$$J_{z+dz} = J_z - J_z^{\alpha} \Delta z - \ln(10) \left(\sum_{\substack{j \\ chromophoric \\ species\ X_j}} J_z^{\varepsilon_j} [X_j] \right) \Delta z \qquad \textbf{Eq. 14}$$

where J_z is the spectral overlap integral for the photosensitive species X_j under consideration and J_z^{α} and $J_z^{\varepsilon j}$ are the respective contributions to opacity and light absorption

$$J_z^{\alpha} = \int_{\lambda_{min}}^{\lambda_{max}} \frac{\ln(10)}{10} \frac{E(\lambda)}{N_a} \frac{\lambda}{hc} \varepsilon_i(\lambda)\, \alpha(\lambda)\, d\lambda \qquad \textbf{Eq. 16}$$

and

$$J_z^{\varepsilon_j} = \int_{\lambda_{min}}^{\lambda_{max}} \frac{100 \ln(10)}{10} \frac{E(\lambda)}{N_a} \frac{\lambda}{hc} \varepsilon_i(\lambda)\, \varepsilon_j(\lambda)\, d\lambda \qquad \textbf{Eq. 17}$$

The spectral overlap integrals J_z^{α} *and* $J_z^{\varepsilon j}$ are given in Einstein.mol^{-2}.L.s^{-1} m^{-1} provided that $\alpha(\lambda)$ and $\varepsilon_j(\lambda)$ are respectively given in m^{-1} and L.mol^{-1}.m^{-1}.

All these attenuation factors can be calculated independently. As an example, coefficient $\alpha(\lambda)$, relative to opacity, can be assumed constant (i.e. independent of exposure time) when the morphological changes due to recrystallization or chemicrystallization are neglected.

Finally, such an approach was also used for saving calculation time.

2.4. **Formalizing the problem**

The CLMS can be translated into a system of ordinary differential equations (SDE) describing the local concentration changes in relevant chemical species by using the classical concepts of chemical kinetics. This SDE can be written as (**Eq. 18-25**):

$$\frac{d[P^{\bullet}]}{dt} = 2k_{1u}[POOH] + k_{1b}[POOH]^2 - k_2[P^{\bullet}][O_2] + k_3[PO_2^{\bullet}][PH] - 2k_4[P^{\bullet}]^2 - k_5[P^{\bullet}][PO_2^{\bullet}] + 2k_{6d}[PO^{\bullet\bullet}OP] + 2\phi_{POOH}\,J_{POOH}\,[POOH] + 2\phi_{POOP}\,J_{POOP}\,[POOP] \quad \textbf{Eq. 18}$$

$$\frac{d[PO_2^{\bullet}]}{dt} = k_{1b}[POOH]^2 + k_2[P^{\bullet}][O_2] - k_3[PO_2^{\bullet}][PH] - k_5[P^{\bullet}][PO_2^{\bullet}] - 2k_{6a}[PO_2^{\bullet}]^2 \quad \textbf{Eq. 19}$$

$$\frac{d[POOH]}{dt} = -k_{1u}[POOH] - 2k_{1b}[POOH]^2 + k_3[PO_2^{\bullet}][PH] + (1-\gamma_5)k_5[P^{\bullet}][PO_2^{\bullet}] - \phi_{POOH}\,J_{POOH}\,[POOH] \quad \textbf{Eq. 20}$$

$$\frac{d[PH]}{dt} = -2k_{1u}[POOH] - k_{1b}[POOH]^2 - k_3[PO_2^{\bullet}][PH] + (1-\gamma_4)k_4[P^{\bullet}]^2 - 2k_{6d}[PO^{\bullet\bullet}OP] - 2\phi_{POOH}\,J_{POOH}\,[POOH] - -\,2\phi_{POOP}\,J_{POOP}\,[POOP] \quad \textbf{Eq. 21}$$

$$\frac{d[PO^{\bullet\bullet}OP]}{dt} = k_{60}[PO_2^{\bullet}]^2 - (k_{6b}+k_{6d})[PO^{\bullet\bullet}OP] \quad \textbf{Eq. 22}$$

$$\partial[O_2]/_{\partial t} = D_{O_2}\,\partial^2[O_2]/_{\partial z^2} - k_2[P^{\bullet}][O_2] - k_{6a}[PO_2^{\bullet}]^2 \quad \textbf{Eq. 23}$$

$$\frac{d[P=O]}{dt} = \gamma_1(k_{1u}[POOH] + k_{1b}[POOH]^2 + 2k_{6d}[PO^{\bullet\bullet}OP] + \phi_{POOH}\,J_{POOH}\,[POOH] + 2\phi_{POOP}\,J_{POOP}\,[POOP]) \quad \textbf{Eq. 24}$$

$$\frac{d[POOP]}{dt} = \gamma_5 k_5 [P^\bullet][PO_2^\bullet] + k_{6b}[PO^{\bullet\bullet}OP] - \phi_{POOP} J_{POOP} [POOP] \quad \textbf{Eq. 25}$$

where [$P^\bullet$], [$PO_2^\bullet$], [POOH], [PH], [$PO^{\bullet\bullet}OP$], [O_2] and [POOP] are the respective concentrations in alkyl and peroxy radicals, hydroperoxides, tertiary CH groups, cage paired alkoxy radicals, oxygen and peroxide bridges. D_{O2} is the coefficient of oxygen diffusion into the semi-crystalline polymer, here considered as constant and independent of time (i.e. of conversion degree of oxidation).

It must be noteworthy that the second derivative of the Fick's law, accounting for the oxygen diffusion (see equation 23), was approximated by a central difference expression. Moreover, the introduction of equation 15 into the SDE, for computing UV-light attenuation in the sample thickness, leads to a system of differential-algebraic equations (SDAE) whose numerical solving requires the use of specific algorithms (see next section).

When light attenuation by chromophores absorption can be neglected (i.e. in the case of iPP films sufficiently thin to be homogeneously oxidized throughout their thickness), it was shown that the ODE15s and ODE23s algorithms of Matlab software, recommended for stiff problem of chemical kinetics [32, 33], allow to solve efficiently the SDE.

From this SDAE, it is also possible to calculate the local concentration changes in chain scissions S and crosslinks B (i.e. covalent bridges):

$$\frac{dS}{dt} = \gamma_{1b}(k_{1u}[POOH] + k_{1b}[POOH]^2 + 2k_{6d}[PO^{\bullet\bullet}OP] + \phi_{POOH} J_{POOH} [POOH] + 2\phi_{POOP} J_{POOP} [POOP]) \quad \textbf{Eq. 25}$$

$$\frac{dB}{dt} = \gamma_4 k_4 [P^\bullet]^2 + \gamma_5 k_5 [P^\bullet][PO_2^\bullet] + k_{6b}[PO^{\bullet\bullet}OP] - \phi_{POOP} J_{POOP} [POOP] \quad \textbf{Eq. 26}$$

2.4.1. Initial and boundary conditions

Initial conditions are the same throughout the sample thickness. Thus, at t = 0, and ∀ z ∈ [0 ; L]:

$$[P^\bullet](0, z) = [PO_2^\bullet](0, z) = [PO^{\bullet\bullet}OP](0, z) = 0 \text{ mol.L}^{-1}$$

$$[PH](0, z) = [PH]_0 \approx 20.3 \text{ mol.L}^{-1}$$

$$[POOH](0, z) = [POOH]_0 = 4 \cdot 10^{-3} \text{ mol.L}^{-1}$$

$$[P{=}O]\ (0, z) = [P{=}O]_0 = 10^{-4}\ mol.L^{-1}$$

$$[O_2]\ (0, z) = C_s$$

Boundary conditions at the plate surfaces (i.e. at z = 0 or z = L) are:

$\forall\ t > 0$, $[O_2]\ (t, 0) = [O_2]\ (t, L) = C_s$

with C_s the oxygen concentration (in mol.L^{-1}) in the polymer in equilibrium with the atmosphere under an oxygen partial pressure P_{O2} given by the Henry's law:

$$C_s = P_{O_2} \times S_{O_2}^{am} \qquad \textbf{Eq. 28}$$

where S_{O2}^{am} is the coefficient of oxygen solubility in the polymer (in mol.L^{-1}.Pa^{-1}) here taken in the amorphous phase, i.e. only where oxygen is soluble [34, 35].

2.4.2. Numerical resolution and computation

The SDAE was solved numerically using the Open Modelica's routine based on the DASSL method [32, 33] and the Pantelides index reduction algorithm [36]. For iPP plates typically lower than 1 mm, it was possible to check that the time-dependent term of light attenuation can be neglected. In contrast, for thickest samples, the numerical tool must be still improved in order to provide efficient and reliable simulations. This approximation was then used for saving calculation time, but it is no longer valid for iPP matrices containing UV-stabilizers, carbon blacks or other types of efficient absorber additives.

The SDAE was solved applying the initial and boundary conditions given in equation 28. Let us remind that the value of oxygen solubility was taken in the amorphous phase. Then, the real concentrations of all chemical species in the semi-crystalline polymer were deduced from the concentrations calculated in the amorphous phase by multiplying them by the volumic fraction of amorphous phase V_a:

$$V_a = (1 - \chi_c) \times \frac{\rho_p}{\rho_a} \qquad \textbf{Eq. 29}$$

with χ_c the crystallinity ratio (as measured by DSC), ρ_p and ρ_a the respective densities of the semi-crystalline polymer (910 g.L^{-1}) and amorphous phase (854 g.L^{-1})

Since most of the physico-chemical analyses were done throughout the sample thickness such as, for instance, FTIR monitoring in a transmission mode, the global concentrations of all chemical species were averaged from the local values of the N-1 computational sublayers:

$$[X]_{global}(t) = \frac{1}{N-1}\int_{z=0}^{z=N}[X](z,t)dz \qquad \textbf{Eq. 30}$$

3. Experimental part

3.1. Materials

The isotactic polypropylene under investigation was supplied by Aldrich (under the reference 427888). Its main physico-chemical characteristics are: MFI [230°C, 2.16 kg] = 12 g/10min, M_w = 250 kg.mol^{-1}, M_n = 67 kg.mol^{-1} and PI = 3.7. This polymer is formulated with about 0.3 wt% of a thioester (Irganox PS 800) as thermal stabilizer.

For determination of optical properties only, plates of about 3 mm thick were molded by DK CODIM 175-400 injection machine from as-received iPP pellets using the following processing conditions: T molten polymer = 210°C, screw speed = 60 rev.min^{-1}, injection rate = 40 mm.min^{-1}, commutation pressure =500 bars, hold pressure = 500 bars, hold time = 6 s and cooling time at 40°C = 25 s.

For photothermal aging studies, films of about 80-100 µm thick were processed by compression molding in a Gibitre laboratory press during 1 min at 200°C under 20 MPa, then purified from their stabilizers by Soxhlet extraction for 48 hours using dichloromethane as solvent. Plates of free additive iPP of about 2 mm thick were then elaborated by stacking about 25 films in the Gibitre laboratory press during 2 min at 140°C under 20 MPa.

All these processed materials were translucent without bubble and thus, expected to have similar morphologies throughout their thickness, as confirmed by differential calorimetric analyses. It was found that their average thermal characteristics are: crystallinity ratio of 45 ± 3 %wt and melting temperature of 165 ± 2°C.

3.2. **Photothermal aging**

Free additive films and plates were then exposed in a WeatherO'Meter device (WOM) equipped with a Xenon Lamp and Borosilicate S/S filters. The black (BPT) and white standard (WST, i.e. chamber) temperatures were fixed at 70°C and 55°C respectively. The temperature of the sample was found to be intermediary at 64°C, whereas the irradiance at 340 nm was measured at 0.46 $W.m^{-2}.nm^{-1}$, without water spraying.

3.3. **Oxidation profiles**

Oxidation profiles in the plate thickness were determined by FTIR cartography in a transmission mode with a space increment of 20 µm using a Perkin-Elmer Spotlight device (32 scans, 4 cm^{-1}). This analytical method consists in coupling a FTIR spectrophotometer with an optical microscope equipped by a motorized and scaled X-Y table. After photothermal aging, iPP plates were embedded in a commercial methacrylate resin (crosslinked at room temperature), then thin cross-sectioned slices of a constant thickness of 100 µm were cut with a diamond wire saw in order to be analyzed by FTIR cartography. The concentration profiles of carbonyl products were determined from the changes in optical density of the absorption band monitored at 1713 cm^{-1} throughout the sample thickness applying the classical Beer-Lambert's law with a coefficient of molar absorptivity of 300 $L.mol^{-1}.cm^{-1}$.

As complementary analysis method, the elementary films were delaminated from the plates with a cutter to be analyzed separately by FTIR spectrophotometry in a transmission mode (Perkin-Elmer spectrophotometer, 16 scans, resolution of 4 cm^{-1}).

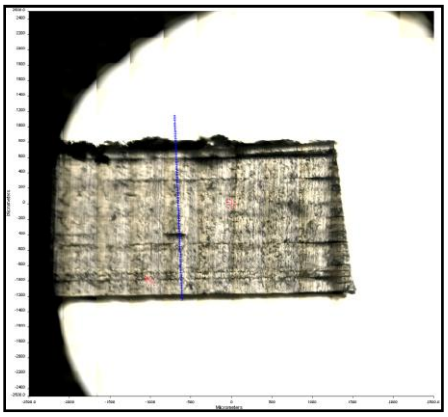

Figure 1: Optical photography of the cross section of an aged iPP plate.

3.4. **Measurements of opacity and reflectance**

Optical properties -i.e. reflectance and opacity- of an iPP plate were measured using a Lambda 900 Perkin-Elmer UV-visible spectrophotometer equipped with a PELA-1000 integration sphere. The respective illumination geometries were 8°/hemispherical in reflectance and 0°/hemispherical in transmittance. Results are reported in Figure 2. Since stabilizers were not removed from the injection molded plates before measurements, the peak corresponding to the UV absorption of the residual phenol ring was visible at 280 nm, but it was removed by mathematical treatment for subsequent analyses.

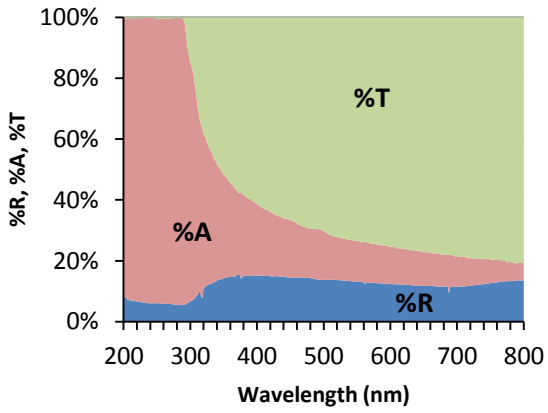

Figure 2: Geometric repartition of UV-light in the injection molded iPP plates of about 3 mm thick (b). %R: reflected part. %A: absorbed part. %T: transmitted part.

The use of an integration sphere is indispensable to get a reliable and quantitative value of the lineic absorption coefficient α(λ) which was calculated from the absorbed part of UV-light (figure 3). It is supposed that the spectral distribution of α(λ) is valid for all translucent samples.

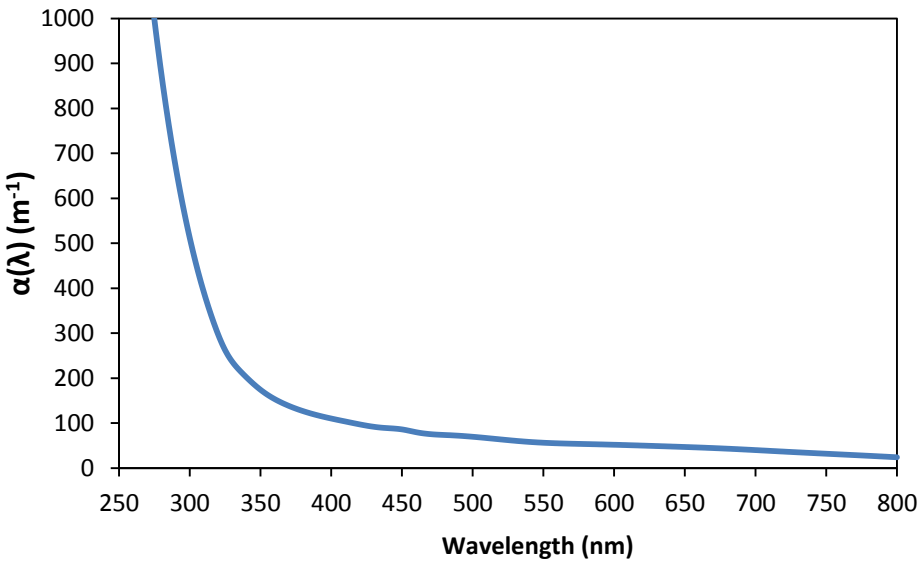

Figure 3: Spectral distribution of the lineic absorption coefficient of unstabilised iPP samples

When experiments were performed in a Perkin-Elmer UV-visible spectrophotometer without an integration sphere (i.e. with specimens of various thicknesses), the values of α(λ) were obtained by linear regression as described in the procedure of White and coworkers [14]. In this case, these values were consistent with those reported by Rabello and White [14], but they were about 5 times higher than those obtained with the integration sphere, which evidences multiple scattering (figure 2). However, this second method was checked to be a relevant alternative for determining the reflectance R by extrapolating the values determined at the specimen surface (i.e. *by using the Albuma method*).

$$\ln(1-R) = \ln\left(\frac{I}{I_0}\right)_{z=0} = ln\left(\frac{I_0 - I_r}{I_0}\right) \qquad \textbf{Eq. 31}$$

All results are summarized in table 1.

Table 1: Determination of the average values of reflectance for all iPP samples under study according to two distinct methods (values averaged over the visible range since they are weakly dependent on wavelength)

iPP samples	***Integration sphere Method***	***Albuma method***
Films	10 ± 1 %	1 ± 14 %
Plates	15 ± 2 %	14 ± 2 %

It appears that the reflectance increases with the specimen thickness. In parallel, the specular component of the reflectance was checked to be negligible according to the previous assumption. That is the reason why the previous observation was attributed to the "state of the surface", in particular to the existence of multiple scattering in media with certain turbidity. In free additive iPP matrices, this phenomenon is ascribed to the semi-crystalline nature of polypropylene (i.e. the existence of crystallites structures such as spherulithes). This phenomenon should be more marked in the case of filled iPP matrices, thus having a higher turbidity. It is noteworthy that crystallites and fillers would be also responsible for a higher sample opacity, thus increasing the value of $\alpha(\lambda)$.

4. Results and Discussion

4.1. Potentialities of the improved numerical tool for simulating photothermal oxidation profiles.

4.1.1. Determination of model parameters

Theoretically, the model could be used to generate all the photothermal oxidation profiles since its parameters have been determined in previous studies from either thermal oxidation experiments made on thin films [17] and thick plates [20], or photothermal oxidation experiments on thin films [18]. The values of all these parameters are reminded in table 1.

Table 2: Parameters used for kinetic modeling of iPP photothermal oxidation

Parameters	***Units***	P^0	***Ea (kJ.mol^{-1})***
$[POOH]_0$	$mol.L^{-1}$	$4 \cdot 10^{-3}$	-
S_{O2}^{am}	$mol.L^{-1}.Pa^{-1}$	$2.5 \cdot 10^{-6}$	6.7
D_{O2}	$m^2.s^{-1}$	$8.6 \cdot 10^{-6}$	36.4
Pe_{O2}	$cm^3.cm.cm^{-2}.Pa^{-1}.s^{-1}$	$2.9 \cdot 10^{-6}$	43.0
k_{1u}	s^{-1}	$2.9 \cdot 10^{13}$	140.7
k_{1b}	$L.mol^{-1}.s^{-1}$	$9.2 \cdot 10^{8}$	95.0
k_2	$L.mol^{-1}.s^{-1}$	$3.0 \cdot 10^{9}$	10.0
k_3	$L.mol^{-1}.s^{-1}$	$5.1 \cdot 10^{7}$	62.2
k_4	$L.mol^{-1}.s^{-1}$	$1.0 \cdot 10^{12}$	0
k_5	$L.mol^{-1}.s^{-1}$	$4.5 \cdot 10^{10}$	0
k_{6a}	$L.mol^{-1}.s^{-1}$	$2.0 \cdot 10^{17}$	90.0
k_{6b}	s^{-1}	$6.7 \cdot 10^{6}$	5.0

k_{6d}	s^{-1}	$1.4 \cdot 10^{12}$	41.0
γ_1	%	60	-
γ'_1	%	27	-
γ''_1	%	33	-
γ_4	%	0	-
γ_5	%	0	-
γ_s	%	50	-

Similarly, the values of spectral overlap integrals and their associated quantities are reported in tables 3 to 5.

Table 3: Values of the spectral overlap integrals (in Einstein.mol^{-1}.s^{-1}) of hydroperoxides, ketones, alkyl peroxides and Ti catalysts for exposures to different UV-light sources (calculated from the absorption spectra of [23, 37], [38], [23] and [39] respectively)

Light source	$\mathbf{J_{POOH}}$	$\mathbf{J_{P=O}}$	$\mathbf{J_{POOP}}$	$\mathbf{J_{Ti\ catalyst}}$
SEPAP 12-24, 2 arc mercury lamps	4.92E-06	7.31E-05	8.40E-06	5.23E-03
SEPAP 12-24, 4 arc mercury lamps	1.07E-05	1.46E-04	1.68E-05	1.05E-02
SEPAP 50-24, 6 arc mercury lamps	2.54E-05	3.77E-04	4.33E-05	2.69E-02
SEPAP 50-24, 8 arc mercury lamps	5.53E-05	7.53E-04	8.67E-05	5.39E-02
WeatherOMeter, xenon lamp	1.45E-06	2.25E-05	4.19E-06	1.49E-03
Philips TLK 05 fluorescent lamp [9]	1.45E-07	2.31E-06	4.71E-07	1.45E-04

Table 4 Values of the quantity J^{α} (in Einstein.mol^{-2}.L.s^{-1}.m^{-1}) accounting for the effect of the opacity on the spectral overlap integrals relative to hydroperoxides, ketones and alkyl peroxides and Ti catalysts for exposures to different UV-light sources (calculated from the absorption spectra of [23, 37], [38], [23] and [39] respectively)

Light source	$\mathbf{J^{\alpha}_{POOH}}$	$\mathbf{J^{\alpha}_{P=O}}$	$\mathbf{J^{\alpha}_{POOP}}$	$\mathbf{J^{\alpha}_{Ti\ catalyst}}$
SEPAP 12-24, 2 arc mercury lamps	3.55E-06	3.44E-05	3.99E-06	2.93E-03
SEPAP 12-24, 4 arc mercury lamps	7.73E-06	7.49E-05	8.68E-06	6.37E-03
SEPAP 50-24, 6 arc mercury lamps	1.83E-05	1.77E-04	2.05E-05	1.51E-02
SEPAP 50-24, 8 arc mercury lamps	2.44E-05	2.37E-04	2.75E-05	2.02E-02
WeatherOMeter, xenon lamp	4.97E-07	7.71E-06	1.15E-06	5.30E-04
Philips TLK 05 fluorescent lamp [9]	3.87E-08	6.90E-07	1.13E-07	4.27E-05

Table 5: Values of the quantity $J^{\varepsilon}_{Xi/Xj}$ (in Einstein.mol^{-2}.L.s^{-1} m^{-1}) accounting for the screening effect of photosensitive species X_j on the UV-light absorption of species X_i for exposures to different UV-light sources (including hydroperoxides, ketones and alkyl peroxides and Ti catalysts whose respective absorption spectra were collected in [23, 37], [38], [23] and [39] respectively).

Light source	$\mathbf{J_{POOH/POOH}}$	$\mathbf{J_{P=O/P=O}}$	$\mathbf{J_{POOP/POOP}}$	$\mathbf{J_{Ti/Ti}}$	$\mathbf{J_{POOH/P=O}}$	$\mathbf{J_{P=O/POOP}}$	$\mathbf{J_{POOH/POOP}}$	$\mathbf{J_{POOH/Ti}}$	$\mathbf{J_{P=O/Ti}}$	$\mathbf{J_{POOP/Ti}}$
SEPAP 12-24, 2 lamps	2.69E-04	1.08E-01	7.86E-04	4.03E-03	5.17E-03	8.90E-03	4.45E-04	1.01E-03	2.05E-02	1.77E-03
SEPAP 12-24, 4 lamps	5.85E-04	2.36E-01	1.71E-03	8.77E-03	1.13E-02	1.94E-02	9.69E-04	2.20E-03	4.46E-02	3.85E-03
SEPAP 50-24, lamps	1.38E-03	5.58E-01	4.05E-03	2.08E-02	2.66E-02	4.58E-02	2.29E-03	5.22E-03	1.05E-01	9.11E-03
SEPAP 50-24, 8 lamps	1.85E-03	7.45E-01	5.41E-03	2.77E-02	3.56E-02	6.13E-02	3.06E-03	6.97E-03	1.41E-01	1.22E-02
WeatherOMeter, xenon lamp	8.76E-05	1.84E-02	2.39E-04	9.75E-04	1.16E-03	1.96E-03	1.31E-04	2.74E-04	4.14E-03	4.73E-04
Philips TLK 05 fluorescent lamp [9]	3.28E-06	1.45E-03	1.86E-05	6.95E-05	6.80E-05	1.47E-04	7.40E-06	1.49E-05	3.07E-04	3.48E-05

4.1.2. Test with Open Modelica and limitations

Since the numerical tools for solving the SDAE problems are still limited to simpler systems with a lower number of equations, they cannot be used for simulating the photothermal oxidation of too thick specimens (typically of few millimeters thick). That is the reason why it was checked with Open Modelica if it was possible to neglect the time-dependent term of UV-light attenuation on thinner samples (typically of 500 µm thick).

The resulting kinetic curves of carbonyl products averaged over the whole sample thickness are depicted in figure 4.

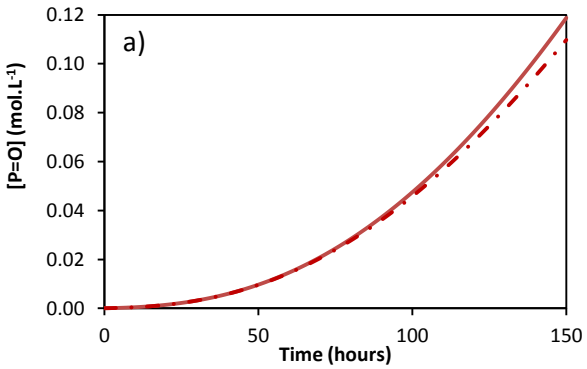

Figure 4: Concentration changes in carbonyl products for iPP plates of 500 µm thick in WeatherOMeter at 64°C . Dashed and solid lines account respectively for simulations with and without UV-light attenuation by chromophores.

It is clear that these effects are clearly negligible up to the end of the induction period. Then, a small divergence can be observed between both simulations. To know the origin of such a discrepancy, the normalized oxidation profiles determined for a moderate oxidation conversion ratio (typically for [P=O] = 0.05 mol.L^{-1} at the surface exposed to UV-light) have been depicted in figure 5. It can be seen that the gap between both simulations is more important at the surface unexposed to UV-light where it does not exceed 7%. This result is in full agreement with the assumption made in the previous paper to facilitate numerical solving [18].

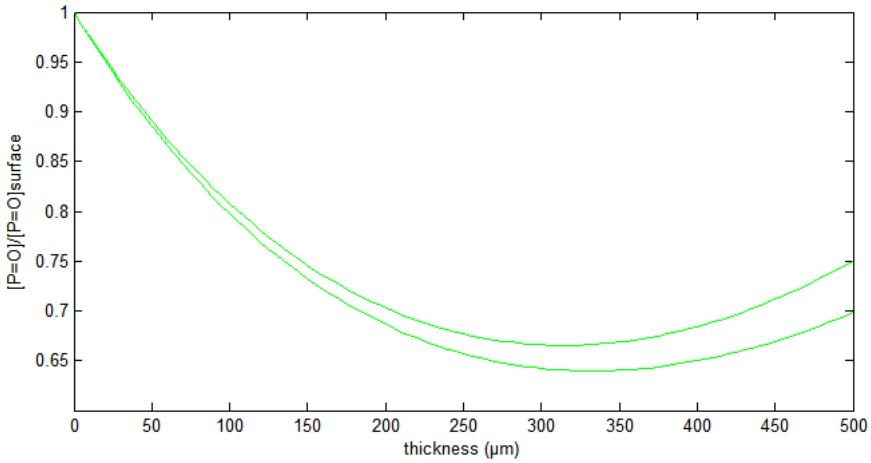

Figure 5: Normalized profiles of carbonyl products by their maximal value at the surface exposed to UV-light for an iPP plate of 500µm thick after 100 hours in a WeatherOMeter at 64°C. Dashed and solid lines account respectively for simulations with and without UV-light attenuation by chromophores.

4.1.3. Trends and comparison between thermal and photothermal oxidation

Taking these parameters and assuming that they remain unchanged during photothermal exposure, the oxidation profiles in the sample thickness and their change with exposure time have been simulated and reported in figure 6.

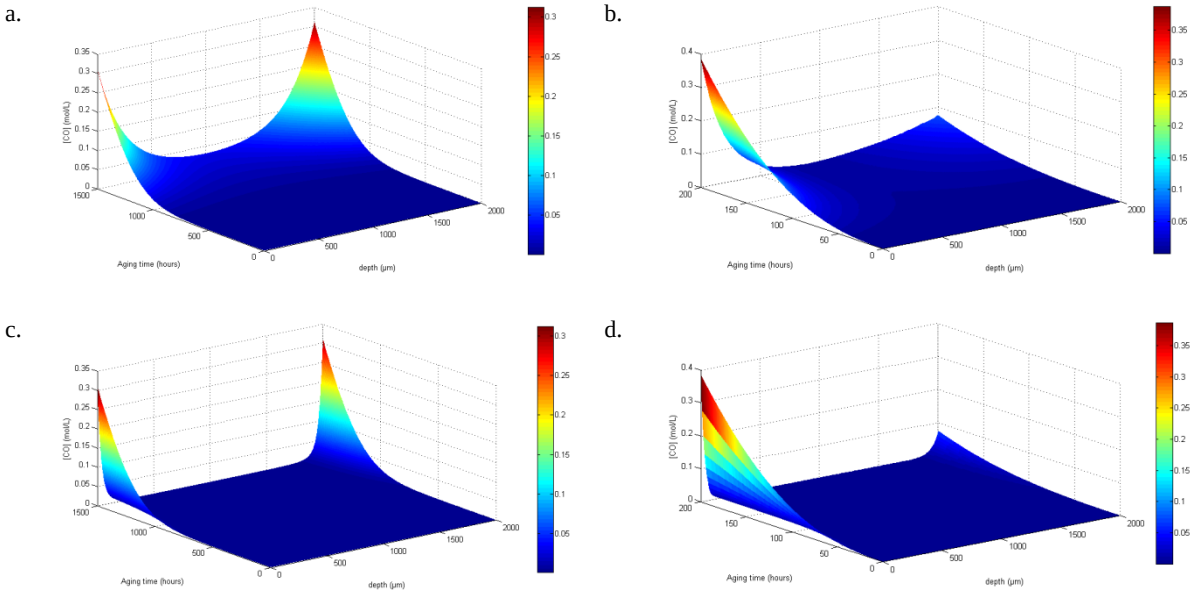

Figure 6: Changes in carbonyl products profileswith exposure time for iPP plates of 2mm thick in air ventilated ovens at 60°C (Fig. a and c) and in a WeatherOMeter device at 64°C (Fig. b and d).

Numerical simulations have been performed with $D_{O2}=1.7\cdot10^{-11}$ $m^2.s^{-1}$ (top) and $D_{O2}=3.4\cdot10^{-13}$ $m^2.s^{-1}$ (bottom).

These results are particularly valuable in order to understand the main impact of UV-light on both oxygen diffusion and chemical consumption by the polymer substrate. As expected, the photothermal oxidation profiles are sharper than the thermo-oxidation ones due to a higher oxidation rate, but also are clearly asymmetric because the sample was submitted to one-side UV-light exposure. It is concluded that the model generates the main trends of the photothermal oxidation kinetics.

4.2. Implementation for simulating experimental data

4.2.1. Procedure of Inverse Resolution Method

At this stage of investigations, the model can be used as an inverse resolution method to determine accurately the values of some parameters whose constancy during photothermal exposure remains highly questionable, such as:

(i) Oxygen transport properties which could be significantly impacted by molecular and morphological changes [17, 20].

(ii) Optical properties, namely the specular reflectance $r^{specular}$ and lineic absorption coefficients both describing light ability to penetrate into the material depth, since loss of gloss occurs at moderate conversion ratios of oxidation.

(iii) But also, quantum yield of hydroperoxide decomposition, which can be determined from the experimental kinetics curves of oxidation products of thin films (homogeneously oxidized throughout their thickness) or at the surface of thick specimens.

It is necessary to precise that numerical simulation requires a rigorous control and knowledge of exposure conditions. In particular, temperature and UV-light intensity must be carefully controlled according to space and time variables, since only small fluctuations of these latter could have dramatic effects on the photothermal degradation kinetics. To date, only experimental results from static exposure conditions can be simulated accurately by the kinetic model, which implies a homogeneous illumination of the specimen surface, the absence of temperature gradients and a constancy of all the exposure conditions during the

photothermal exposure. Indeed, in dynamic exposure conditions (i.e. weathering cycles), the highly clocked UV-light (on/off) and spraying cycles trigger noticeable temperature fluctuations. Similarly, the presence of atmospheric gaseous contaminants (considered as chromophores) contaminating the outer microns of superficial layers [40] increases the photooxidation rate at the surface of polyolefin samples [41, 42].

These conditions severely restrain the amount of experimental data which can be simulated. That is the reason why no alternating day/night or spraying cycles have been applied during photothermal aging in WOM. Because of the precise control of exposure conditions in the current aging methods, tests in SEPAP devices constitute good candidates for numerical simulation. In some cases, it has been possible to estimate the exposure conditions beforehand by neglecting the exposure duration in absence of UV-light atvery low temperature in comparison with the harshest conditions of weathering cycles.

Thus, the possible changes with exposure time in oxygen permeability Pe_{O2} (show to govern the shape of oxidation profiles in thermal oxidation) and coefficient $\alpha(\lambda)$ have been investigated from a large number of experimental data determined in our laboratory or collected in the literature [16, 43-45] for a wide variety of photothermal exposure conditions, including SEPAP, Xenon and fluorescent lamps..

In the optimization procedure, the problem must be initialized properly, which means that the parameters of material variability, i.e. the initial concentration in hydroperoxides $[POOH]_0$ and the oxygen solubility S_{O2}, are required. These parameters, accounting respectively for residual concentrations in stabilizers or prodegradant species and differences in crystalline morphology, can be ideally determine from thermal oxidation experiments.

These parameters have been determined in our laboratory in previous studies dedicated to the thermal oxidation of our iPP [17]. They have been also determined from the experimental results reported by Singh, Mani and coworkers and Girois and coworkers on the thermal [46] and photothermal oxidation [43] of thin iPP films, and by Schoolenberg et al. on the photothermal oxidation of thick iPP plates [16].

It has turned out possible to simulate oxidation profiles with different types of UV-light sources. Examples of simulations of carbonyl products profiles determined during iPP photothermal oxidation are reported in figures 7 and 8. Analogous simulations made on experimental results reported by Singh at al. [43] and Schoolenerg et al. [16] are depicted in figures 9 and 10.

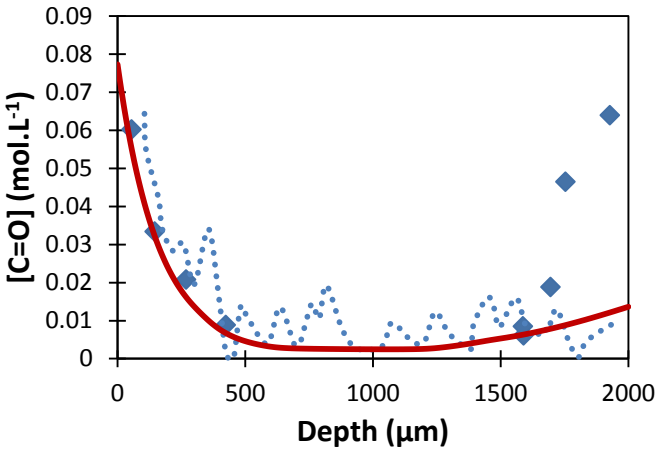

Figure 7: Carbonyl products profile for an iPP plate of 2 mm thick after 48 hours in a WeatherOMeter at 64°C. Symbols: FTIR spectrophotometry on delaminated elementary sublayers. Dotted line: FTIR cartography on thin crosssectioned slices. Solid line: kinetic modeling.

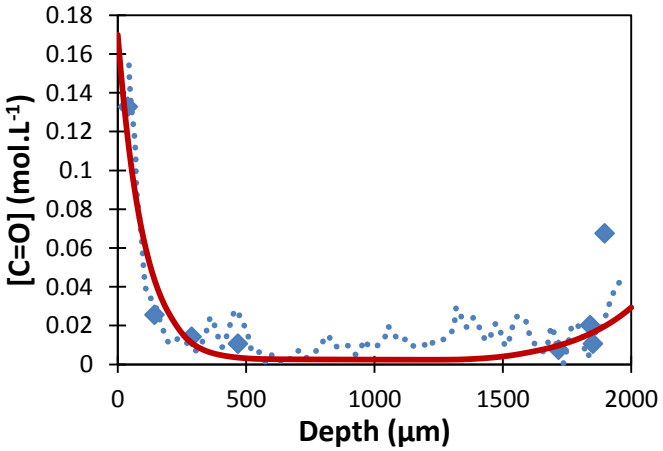

Figure 8: Carbonyl products profile for an iPP plate of 2 mm thick after 115 hours in a WeatherOMeter at 64°C. Symbols: FTIR spectrophotometry on delaminated elementary sublayers. Dotted line: FTIR cartography on thin crosssectioned slices. Solid line: kinetic modeling.

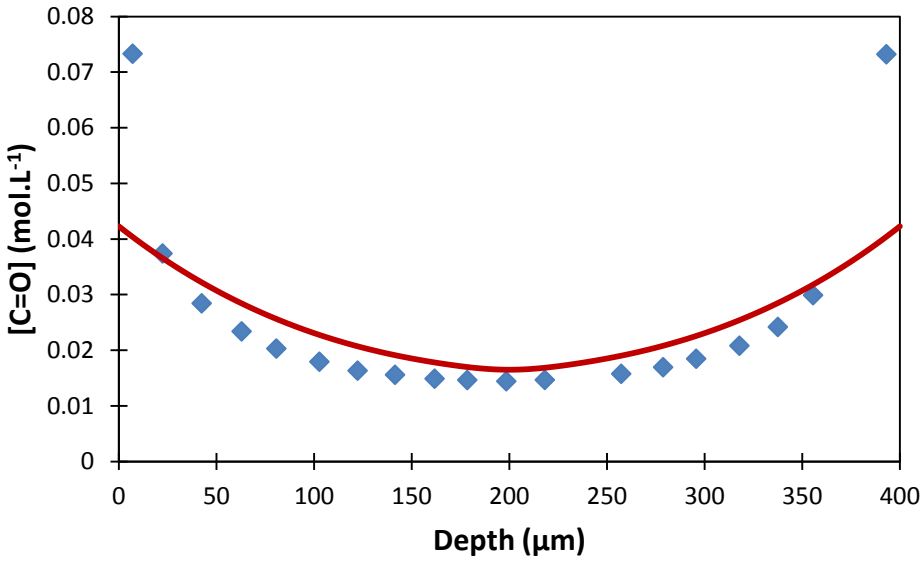

Figure 9: Carbonyl products profile for an iPP plate of 400 µm thick after 50 hours in a SEPAP 12-24 device at 60°C. Symbols: FTIR cartography on thin cross-sectioned slices; Solid line: kinetic modeling.

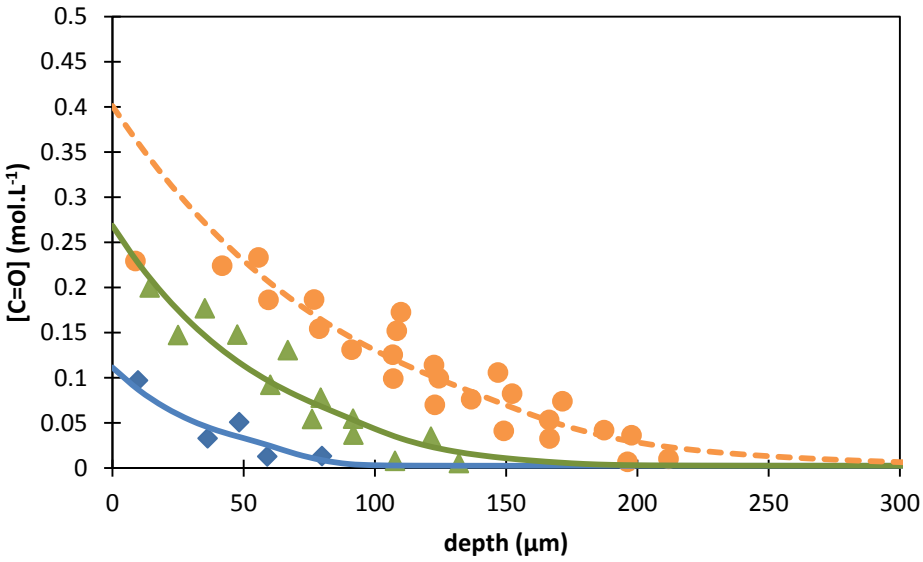

Figure 10: Carbonyl products profiles for an iPP plate of 4 mm thick after 100, 200 and 300 hours in a Xenotest 1200 device at 25°C. Symbols: FTIR cartography on thin cross-sectioned slices; Lines: kinetic modeling.

The most relevant set of kinetic parameters allowing the simulations of experimental data are reported in table 6. They will thus be compared each other to identify some particular dependence with exposure conditions.

Table 6: Parameters determined by inverse resolution method for simulating the photothermal oxidation profiles. The values obtained in a previous study for pure thermal oxidation in air-ventiled ovens have been added in the last lines.

Light source	***T (°C)***	**Aging time (hours)**	***[C=O] in surface***	S_{O2} ***(mol.L^{-1}.Pa^{-1})***	S_{O2} ***(cc[STP]. cm^{-3}.Pa^{-1})***	D_{O2} ***(m^2.s^{-1})***	Pe_{O2} ***(cm^3.cm.cm^{-2}.Pa^{-1}.s^{-1})***	Pe_{O2} ***(cm^3.cm.cm^{-2}.cmHg^{-1}.s^{-1})***	Φ_{POOH}	Φ_{POOH}.J_{POOH}	**Ref.**
WOM	64	48	0.08	2.30E-07	5.14E-06	9.95E-12	5.12E-13	6.83E-10	13	3.25	This study
WOM	64	115	0.17	2.30E-07	5.14E-06	3.98E-12	2.05E-13	2.73E-10	5	1.25	This study
Philips TLK 05 florescent lamp	40	625	0.09	4.35E-15	4.28E-06	4.91E-14	2.10E-15	4.36E-12	8	2	[44, 45]
Philips TLK 05 florescent lamp	55	350	0.05	2.15E-07	4.82E-06	9.30E-14	4.48E-15	5.97E-12	6	1.5	[44, 45]
Philips TLK 05 florescent lamp	70	211	0.05	2.39E-07	5.36E-06	1.67E-13	8.93E-15	1.19E-11	4	1	[44, 45]
Xenotest 150 S	60	120	0.07	2.23E-07	5.00E-06	3.41E-13	1.70E-14	2.27E-11	6	1.5	[44, 45]
WOM (dry)	64	97	0.07	2.30E-07	5.14E-06	1.99E-12	1.02E-13	1.37E-10	6	1.5	[44, 45]
WOM (wet)	40	81	0.01	1.91E-07	4.28E-06	1.47E-13	6.31E-15	8.41E-12	7	1.75	[44, 45]
Xenotest 1200	25	50	0.11	1.91E-07	4.28E-06	4.91E-13	2.10E-14	2.80E-11	4	1	[16]
Xenotest 1200	25	100	0.24	1.91E-07	4.28E-06	7.36E-13	3.15E-14	4.20E-11	4	1	[16]
SEPAP 12/24	60	503	0.05	4.46E-08	1.00E-06	9.73E-12	9.73E-14	1.30E-10	3.5	0.875	[43]
-	60	1400	0.22	2.23E-07	5.00E-06	5.70E-12	2.85E-13	2.56E-10	-	-	[17]
-	80	300	0.50	2.56E-07	5.73E-06	1.24E-11	7.10E-13	6.38E-10	-	-	[17]
-	100	70	0.70	2.89E-07	6.48E-06	2.47E-11	1.60E-12	1.44E-09	-	-	[17]
-	140	3.5	0.50	3.57E-07	7.99E-06	8.07E-11	6.45E-12	5.79E-09	-	-	[17]

Basically, several irregularities can be observed from these results in respect to either oxygen transport properties or optical features.

4.2.2. Changes in oxygen transport properties

The values of oxygen permeability required for simulating the experimental photothermal oxidation profiles determined in different studies (table 6) have been reported in an Arrhenius graph (figure 11) and compared with the experimental values determined by permeametry (on both neat and aged materials) [19]. At this stage of investigations, we have at disposal two relevant datasets coming from our own investigations and the collection of papers of Lemaire and coworkers [19, 43, 46, 47] dedicated to both thermal and photothermal oxidation. Both of them highlight a drop in oxygen transport properties during the course of oxidation.

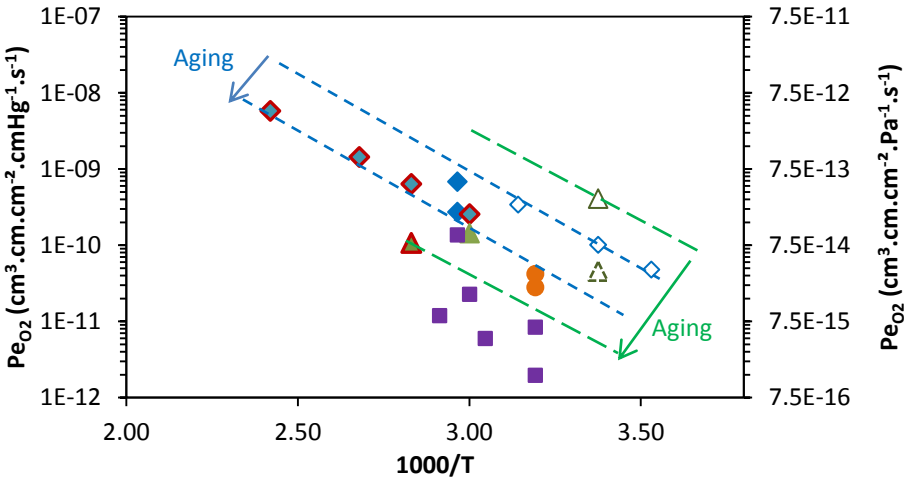

Figure 11: Arrhenius graph of oxygen permeability between 23 and 140°C for iPP before and after photothermal exposure. The first dataset correspond to values for our iPP determined by: ◇ permeametry at 10, 23, and 45°C and inverse resolution method in ◆ photothermal oxidation in WOM at 64°C (This work); ◆ thermal oxidation between 60 and 140°C [18]. Second dataset from: permeametry at 23°C of △ non-aged and ⧋ photooxidized iPP [46] and inverse resolution method from: ▲ photothermal oxidation in SEPAP 12-24 at 60°C [43]; ▲ thermal oxidation at 60°C [46]. ■ Girois et al. with xenon and florescent lamps [44, 45]. ● Schoolenberg with a xenon lamp at 25°C [16].

Therefore, the coefficients of oxygen permeability have been extrapolated at a reference temperature of 23°C by assuming that the permeability obeys an Arrhenius law with activation energy of 42 kJ.mol^{-1} in the whole temperature range under investigation. These values have been plotted as a function of the conversion degree of oxidation, materialized by the concentration in carbonyl products at the sample surface (obtained from FTIR monitoring

at 1713 cm^{-1}). The first dataset includes values obtained before and after photothermal exposure by permeametry between 10 and 45°C, by inverse resolution method in thermal oxidation between 60 and 140°C and after photothermal oxidation in WOM at 64°C. The second dataset was obtained from permeametry at 23°C on both neat and photooxidized iPP as well as inverse resolution method in thermal aging at 80°C and photothermal aging in SEPAP 12-24 at 60°C. The resulting master curves (at 23°C) are depicted in figure 8. It is noteworthy that all these values are consistent one another although determined by different techniques and in very different aging conditions.

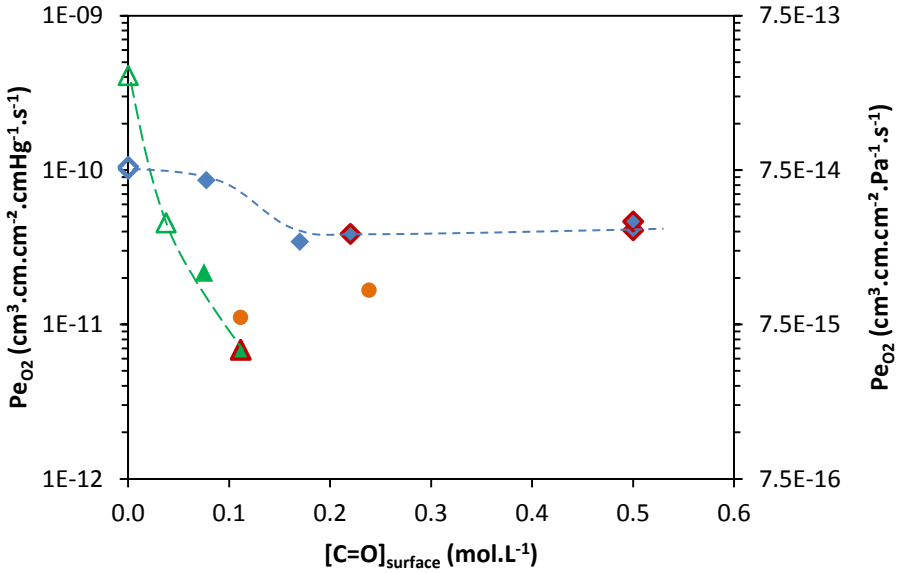

Figure 12: Oxygen permeability during the course of iPP photothermal oxidation versus concentration of carbonyl products determined at the surface of the specimen. Arrhenius graph of oxygen permeability between 23 and 140°C for iPP before and after photothermal exposure.

The first dataset correspond to values for our iPP determined by: ◇ permeametry at 10, 23, and 45°C and inverse resolution method in ◆ photothermal oxidation in WOM at 64°C (This work); ◆ thermal oxidation between 60 and 140°C [18]. Second dataset from: permeametry at 23°C of △ non-aged and △ photooxidized iPP [46] and inverse resolution method from: ▲ photothermal oxidation in SEPAP 12-24 at 60°C [43]; ▲ thermal oxidation at 60°C [46]. ● Schoolenberg et al; with a xenon lamp at 25°C [16].

Two distinct behaviors are clearly put in evidence. For our iPP sample, oxygen permeability undergoes a dramatic decrease with exposure time (i.e. at very low conversion ratios of oxidation) and then reaches a plateau. The drop for the second dataset is still more acute and occurs right from the end of the induction period.

In contrast, the appearance of cracks and the associated shoulder on oxidation profiles, reported by Schoolenberg et al. [16], were also undoubtedly observed right from a critical value of oxidation products concentration: [C=O] > 0.2 mol.L^{-1} in the results of Girois et al. [44]. Their deleterious effects on the oxygen permeability would be decoupled of the drop in oxygen permeability up to this threshold.

However, it is noteworthy that inverse resolution method only enables to determine apparent parameters, i.e. apparent oxygen permeability (or diffusivity) values which are averaged over the whole thickness of the oxidized layer. There is probably gradients of these properties in the oxidized layer. As a result, the quickness of the oxygen drop property would depend on the thickness of oxidized layer That is the reason why, in a second approach, these permeability values has been plotted as a function of the concentration in carbonyl products averaged in the whole thickness of oxidized layer.

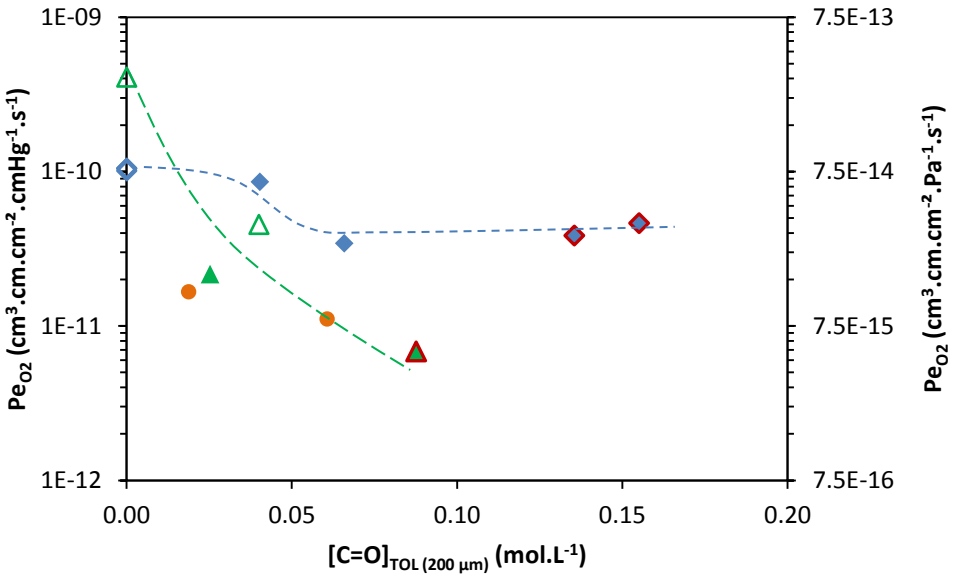

Figure 13: Oxygen permeability during the course of iPP photothermal oxidation versus concentration of carbonyl products averaged for a TOL of 200 µm.

The first dataset correspond to values for our iPP determined by: ◇ permeametry at 10, 23, and 45°C and inverse resolution method in ◆ photothermal oxidation in WOM at 64°C (This work); ◆ thermal oxidation between 60 and 140°C [18]. Second dataset from: permeametry at 23°C of △ non-aged and ⧋ photooxidized iPP [46] and inverse resolution method from: ▲ photothermal oxidation in SEPAP 12-24 at 60°C [43]; ▲ thermal oxidation at 60°C [46]. ● Schoolenberg et al; with a xenon lamp at 25°C [16].

In thermal oxidation, it has been checked that the drop in oxygen permeability cannot be explained in terms of crystallinity changes alone by the existing models [20]. Here, it has been attempted to correlate the drop in oxygen permeability and the crystallinity ratio via the

concentration in carbonyl products as relevant oxidation indicator basing on the studies of Mani et al. [19, 47].

It is clear that the drop in oxygen permeability is of several decades as order of magnitude which cannot be only ascribed to crystalline rearrangements such as chemicrystallization.

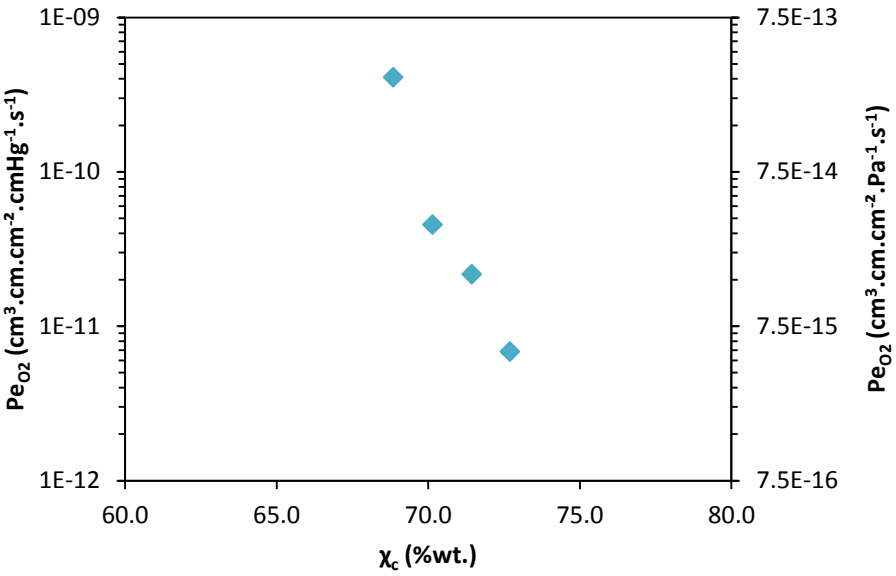

Figure 14: Oxygen permeability versus crystallinity ratio during the course of iPP photothermal oxidation from the results of Mani et al. [19, 47].

5. Conclusion

In the present paper, a numerical model has been proposed for simulating photothermal oxidation profiles of polypropylene. It has been derived from a mechanistic scheme where oxidation is initiated by the combined effects of temperature and UV-light in the presence of oxygen. It has been coupled with oxygen diffusion and UV-light attenuation in the sample thickness order to account respectively for the diffusion-limited oxidation and screen effect.

Its main parameters have been determined in previous studies as well from thermal as photothermal oxidation expriments in order to calibrate the different rate constants and yields separately.

The numerical approach noticeably facilitates the solving of such complex multiphysical problems including thermochemistry, photochemistry, and physics of species diffusion and optics, since it enhances accuracy of results and demonstrates its versatility by allowing

calculation of any property changes from the state of degradation provided that the structure-properties relationship has been beforehand determined. The proposed general kinetic model thus enables to generate the major trends of the photothermal oxidation kinetics, in particular the sharper and asymmetric shape of photothermaloxidation profiles compared with purely thermal ones.

This model has been used here in an inverse resolution method in order to investigate changes in some parameters which can vary during exposure, in particular oxygen permeability. This latter has been evidence to decrease with the conversion degree of oxidation in a similar way for photothermal as for thermal oxidation. This result substantiates relevancy of describing photothermal oxidation by starting from a thermally initiated oxidation mechanistic scheme and adding additional reactions of initiation by photolysis. Besides, the coefficient of lineic absorption $\alpha(\lambda)$ could also undergo changes during aging, although expected minor compared with oxygen permeability Pe_{O2}. Also, both optical and oxygen transport properties would be impacted by the formation and development of cracks at the sample surface, thus moves the front of oxygen supply towards deeper layers.

From this standpoint, it is even relevant to precise that it is unwise to envisage the simulation of oxidation profiles above a moderated conversion ratio. It is also noteworthy that the use of the current numerical tool is restricted to tests performed in static exposure conditions, i.e. without weathering cycle, which considerably induce uncertainty on exposure conditions.

All these phenomena, namely time-change of polymer properties, kinetics of cracks formation and propagation, dynamic exposure conditions, could be tentatively introduced into such a kinetic model, but it would first required extended investigations. Then, the harshest challenges probably lay in numerical issues for such a purpose, in terms of (i) mathematical formalization of the problem through systems of Differential-Algebric Equations (SDAE) or Partial Derivative Equations (SPDE) and, (ii) their solving in respect to time and space variables by checking carefully their convergence, stability or calculation cost.

References

[1] G.E. Schoolenberg, H.D.F. Meijer, Ultra-violet degradation of polypropylene: 2. Residual strength and failure mode in relation to the degraded surface layer, Polymer, 32 (1991) 438-444.
[2] L. Audouin, V. Langlois, J. Verdu, J.C.M. de Bruijn, Role of oxygen diffusion in polymer ageing: kinetic and mechanical aspects, Journal of Materials Science, 29 (1994) 569-583.
[3] K.T. Gillen, R.L. Clough, Rigorous experimental confirmation of a theoretical model for diffusion-limited oxidation, Polymer, 33 (1992) 4358-4365.

[4] K.T. Gillen, J. Wise, R.L. Clough, General solution for the basic autoxidation scheme, Polymer Degradation and Stability, 47 (1995) 149-161.
[5] L. Reich, S.S. Stivala, Autoxidation of hydrocarbons and polyolefins: kinetics and mechanisms, Marcel Dekker, Inc., New York, 1969.
[6] L. Reich, S.S. Stivala, Kinetics and mechanism of oxidative degradation of polymers, in: McGraw-Hill (Ed.) Elements of polymer degradation 1971, pp. 229-293.
[7] G.C. Furneaux, K.J. Ledbury, A. Davis, Photo-oxidation of thick polymer samples" Part I: The variation of photo-oxidation with depth in naturally and artificially weathered low density polyethylene, Polymer Degradation and Stability, 3 (1981) 431-442.
[8] K.M.B. Jansen, Analytical approximation of degradation profiles in polymer products, Polymer Engineering & Science, 34 (1994) 1619-1627.
[9] A.V. Cunliffe, A. Davis, Photo-oxidation of thick polymer samples" Part II: The influence of oxygen diffusion on the natural and artificial weathering of polyolefins, Polymer Degradation and Stability, 4 (1982) 17-37.
[10] J.L. Bolland, G. Gee, Kinetic studies in the chemistry of rubber and related materials. II. The kinetics of oxidation of unconjugated olefins, Transactions of the Faraday Society, 42 (1946) 236-243.
[11] P. Vink, T.J. Van Veen, The mechanism of u.v. stabilization of polypropylene films by 2-hydroxy-4-octyloxybenzophenone, European Polymer Journal, 14 (1978) 533-537.
[12] T.M. Kollmann, D.G.M. Wood, Effects of variations in light intensity on the photooxidation of polypropylene, Polymer Engineering and Science, 20 (1980) 684-687.
[13] A. François-Heude, E. Richaud, E. Desnoux, X. Colin, Influence of temperature, UV-light wavelength and intensity on polypropylene photothermal oxidation, Polymer Degradation and Stability, 100 (2014) 10-20.
[14] T.J. Turton, J.R. White, Effect of stabilizer and pigment on photo-degradation depth profiles in polypropylene, Polymer Degradation and Stability, 74 (2001) 559-568.
[15] J.R. White, A.V. Shyichuk, T.J. Turton, I.D. Syrotynska, Effect of stabilizer and pigment on photodegradation of polypropylene as revealed by macromolecule scission and crosslinking measurements, Polymer Degradation and Stability, 91 (2006) 1755-1760.
[16] G.E. Schoolenberg, P. Vink, Ultra-violet degradation of polypropylene: 1. Degradation profile and thickness of the embrittled surface layer, Polymer, 32 (1991) 432-437.
[17] A. François-Heude, E. Richaud, A. Guinault, E. Desnoux, X. Colin, On the impact of oxygen transport properties on the polypropylene thermal oxidation. Part I: Effect of oxygen solubility Submitted in: Journal of Applied Polymer Science, (2014).
[18] A. François-Heude, E. Richaud, E. Desnoux, X. Colin, A general kinetic model for the photothermal oxidation of polypropylene, Submitted in Journal of Photochemistry and Photobiology, Part A: chemistry, (2014).
[19] R. Mani, R.P. Singh, S. Sivaram, J. Lacoste, J. Lemaire, Effect of UV irradiation on gas permeability in heterophasic ethylene-propylene copolymer films, Journal of Macromolecular Science - Pure and Applied Chemistry, 33 (1996) 783-787.
[20] A. François-Heude, E. Richaud, A. Guinault, E. Desnoux, X. Colin, On the impact of oxygen transport properties on the polypropylene thermal oxidation. Part II: Effect of oxygen diffusivity, Submitted in: Journal of Applied Polymer Science, (2014).
[21] J.C.M. De Bruijn, Degradation profiles of thick high-density polyethylene samples after outdoor and artificial weathering, Advances in Chemistry Series, 249 (1996) 596-598.
[22] L. Bateman, G. Gee, A Kinetic Investigation of the Photochemical Oxidation of Certain Non-Conjugated Olefins, Proceedings of the Royal Society of London. Series A. Mathematical and Physical Sciences, 195 (1948) 376-391.
[23] D.J. Carlsson, D.M. Wiles, The photodegradation of Polypropylene Films. III. Photolysis of polypropylene hydroperoxydes, Macromolecules, 2 (1969) 597-606.
[24] G. Geuskens, F. Debie, M.S. Kabamba, G. Nedelkos, New aspects of the photooxidation of polyolefins, Polymer Photochemistry, 5 (1984) 313-331.
[25] L. Bateman, H. Hughes, A.L. Morris, Hydroperoxide decomposition in relation to the initiation of radical chain reactions, Discussions of the Faraday Society, 14 (1953) 190-199.
[26] J.G. Calvert, J.N. Pitts, Jr., Photochemistry, American Chemical Society, 1966.

[27] S. Girois, Photooxydation du polypropylène : aspects cinétiques in: Mécanique et Matériaux, Ecole Nationale Supérieure des Arts et Métiers, 2001.
[28] G. Lamberti, F. De Santis, V. Brucato, G. Titomanlio, Modeling the interactions between light and crystallizing polymer during fast cooling, Applied Physics A: Materials Science & Processing, 78 (2004) 895-901.
[29] G. Lamberti, G. Titomanlio, Interaction between light and crystallizing polymer: a simulation study, European Polymer Journal, 41 (2005) 2055-2066.
[30] R.S. Stein, Studies of Polymers with Radiation, MRS Bulletin, 25 (2000) 19-26.
[31] A. Perlin, Structured polymer properties, The identification, interpretation, and application of crystalline polymer structure, Robert Joel Samuels, Wiley-Interscience, New York, 1974, 251 pp. $19.95, Journal of Polymer Science: Polymer Letters Edition, 13 (1975) 61-62.
[32] C. Gear, L. Petzold, ODE Methods for the Solution of Differential/Algebraic Systems, SIAM Journal on Numerical Analysis, 21 (1984) 716-728.
[33] L. Petzold, Differential/Algebraic Equations are not ODE's, SIAM Journal on Scientific and Statistical Computing, 3 (1982) 367-384.
[34] J.B. Knight, P.D. Calvert, N.C. Billingham, Localization of oxidation in polypropylene, Polymer, 26 (1985) 1713-1718.
[35] A.K. Taraiya, G.A.J. Orchard, I.M. Ward, The effect of amorphous orientation on the oxygen permeability of polypropylene films, Journal of Polymer Science Part B: Polymer Physics, 31 (1993) 641-645.
[36] C. Pantelides, The Consistent Initialization of Differential-Algebraic Systems, SIAM Journal on Scientific and Statistical Computing, 9 (1988) 213-231.
[37] J.T. Martin, R.G.W. Norrish, The photochemical decomposition of tert-butyl hydroperoxyde, Proceeding of the Royal society of London. Serie A. Mathematical and physical sciences, 220 (1953) 322(339.
[38] D.J. Carlsson, D.M. Wiles, The Photodegradation of Polypropylene Films. II. Photolysis of Ketonic Oxidation Products, Macromolecules, 2 (1969) 587-597.
[39] O. Cicchetti, F. Gratani, The effect of titanium compounds on photo-oxidation of 2,4,6,8-tetramethylnonane (a liquid model of polypropylene), European Polymer Journal, 8 (1972) 561-573.
[40] D.J. Carlsson, D.M. Wiles, Photooxidation of Polypropylene Films. V. Origin of Preferential Surface Oxidation, Macromolecules, 4 (1971) 179-184.
[41] D.J. Carlsson, D.M. Wiles, Photooxidation of Polypropylene Films. IV. Surface Changes Studied by Attenuated Total Reflection Spectroscopy, Macromolecules, 4 (1971) 174-179.
[42] F.H. Winslow, C.J. Aloisio, W.L. Hawkins, W. Matreyek, Chem. Ind., (1963) 1465.
[43] R.P. Singh, R. Mani, S. Sivaram, J. Locoste, D. Vaillant, Photoinitiated oxidation of heterophasic ethylene-propylene copolymers. I. Comparison of oxidation products, Journal of Applied Polymer Science, 50 (1993) 1871-1881.
[44] S. Girois, P. Delprat, L. Audouin, J. Verdu, Oxidation thickness profiles during photooxidation of non-photostabilized polypropylene, Polymer Degradation and Stability, 56 (1997) 169-177.
[45] S. Girois, L. Audouin, J. Verdu, P. Delprat, G. Marot, Molecular weight changes during the photooxidation of isotactic polypropylene, Polymer Degradation and Stability, 51 (1996) 125-132.
[46] R.P. Singh, R. Mani, S. Sivaram, J. Lacoste, J. Lemaire, Thermo-oxidative degradation of heterophasic ethylene-propylene copolymers and their fractions, Polymer International, 32 (1993) 189-196.
[47] R. Mani, R.P. Singh, S. Sivaram, J. Lacoste, Effect of UV irradiation on the structure of heterophasic ethylene-propylene copolymers, Polymer Journal, 26 (1994) 1132-1141.

CHAPTER IX. General discussion

1. Introduction

In the perspective of establishing an effective numerical tool for the lifetime prediction of commercial materials, a key advantage of the kinetic modeling approach is its upgradability. Indeed, new differential or algebraic equations can be added to the basic system of differential equations in order to account for the chemical reactivity of additional constituents or physical phenomena, such as the effects of extrinsic sources of radicals, the diffusion limited oxidation and UV-light attenuation in the sample thickness by its own opacity and absorption by chomophoric species.

In this study, the purpose was clearly to propose a better description of the polypropylene oxidation kinetics in a wide range of photothermal exposure conditions, i.e. of temperature, UV light intensity and wavelength. Although critical in the modeling of macroscopic properties, the establishment of the structure-property relationships as well as the relevance assessment of the end-of-life criteria have been left side for two reasons: (i) the macroscopic properties can be calculated *a posteriori* from the concentration changes in chemical species, (ii) critical values of carbonyl products concentrations or molecular masses are considered as sufficient in a first approach.

Due to the high number of adjustable parameters, the inverse resolution method constitutes an awkward optimization problem which has required the development of a rigorous strategy, starting from the simpler aging problem and introducing stepwise additional reactions or coupled physical phenomena. This strategy has consisted in studying first the thermal core of the kinetic model, and then additional layers have been added around the thermal core in order to describe:

- The impact of additional environmental factors or stresses, for instance UV-light in photothermal oxidation
- The impact of reactants transport when extending the model to thick specimens
- The impact of new constituents in industrial formulations.

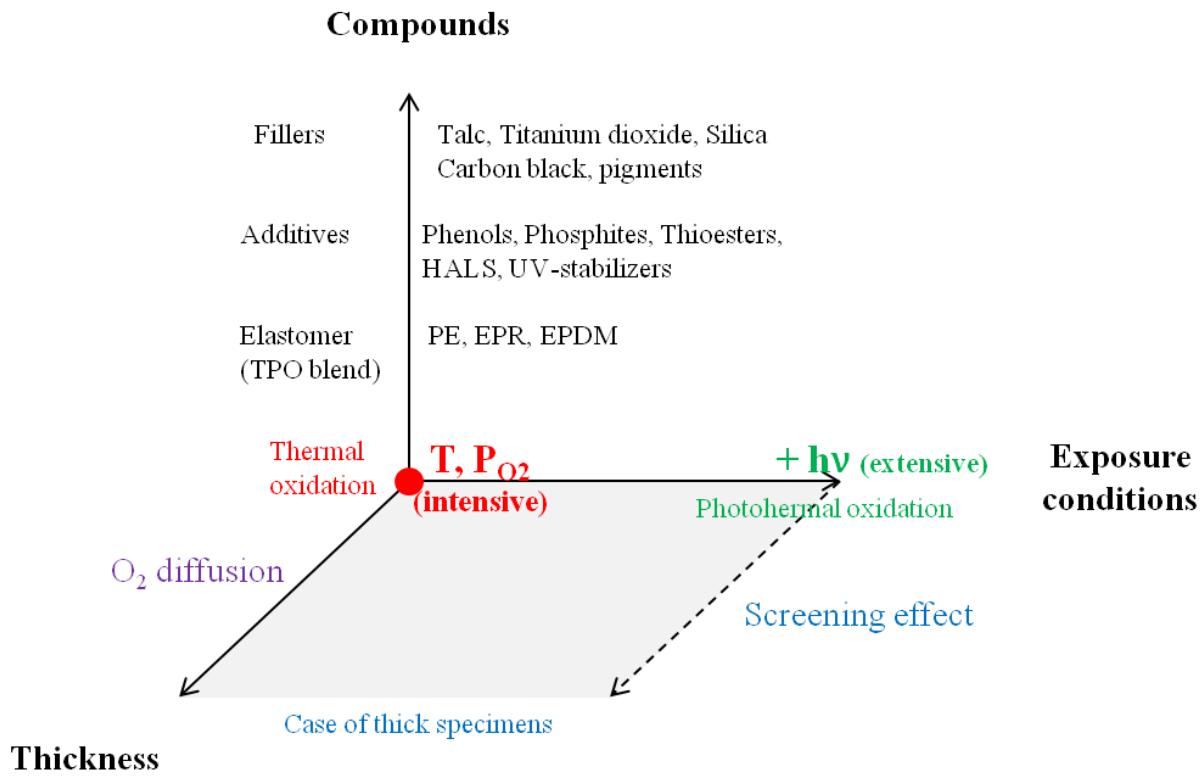

Figure 1: Strategy of implementation of the kinetic model

2. Advances in the kinetic modeling of photothermal oxidation

2.1. Towards a universal model for the thermal oxidation of iPP

In our stepwise optimization procedure, it was critical to calibrate accurately the thermal core of the kinetic model, i.e. to predict accurately the variability of thermal oxidation behaviors among the whole iPP family This has been performed by refining the oxygen transport parameters, in particular kinetics with oxygen solubility, whose variability has been connected to the dependence of the oxidation behavior on the oxygen partial pressure as unarguable evidence. Therefore, the resulting model enables to explain the scattering of induction times and oxidation rates among the whole iPP family.

This model universality constitutes a major advance in respect to the purpose since it has enabled to envisage the model extension to photothermal oxidation. However, one could wonder the meaning of such a variability on the oxygen solubility parameter. Our exhaustive review of the literature has enabled to shown a strong correlation between the variability of

oxygen solubility and polymer morphology [1-5], especially its polymorphism [6-9]. Two explanations can be envisaged depending on whether the expected variations of oxygen solubility are real or only apparent:

(i) In the first case, oxygen solubility would be governed by polymer morphology, which enables to introduce into the kinetic model the direct impact of polymer morphology on induction times, i.e. lifetime, and oxidation rates. This result is very interesting because it reports the necessity of investigating both chemical and morphological changes during photothermal aging, in relation with the material and tprocess (thermal history) characteristics. It is noteworthy that the impact of oxygen solubility on induction times has been already made for other materials [10].

(ii) In the second case, variations of oxygen solubility would account for differences in reactivity with oxygen between different iPP substrates, depending especially on the tacticity [11-13].

However, it is difficult to discriminate between both options since these structural and morphological features are closely intertwined. Indeed, it is well-known that a high isotacticity favors PP crystallization, particularly in a α-monoclinic lattice. From a practical point of view, this issue has a major implication on the manner the model can be used. If discrepancies between iPP samples are attributed to structural rather than morphological features, the solubility becomes at the present time an apparent and so, an adjustable parameter, instead of being easily measurable by permeametry prior to be introduced as input data into the kinetic model. It is also noteworthy that specific shapes of melting endotherms peaks have been observed by Differential Scanning Calorimetry during the photothermal oxidation of iPP. These latter were ascribed to a multiplicity of crystal lattices [14-17] or lengths of crystallisable isotactic sequences (i.e. stereodefects distribution) rather than to isotacticity itself [18-23]. Both changes would impact oxygen solubility along the course of oxidation. This finding is in agreement with the drop in oxygen permeability which cannot be explained by the simple effect of morphological changes on oxygen diffusivity, as evidenced in chapter 5.

2.2. **Validity of the CLMS in photothermal oxidation**

In order to account for the effect of UV-light, it has been first necessary to define a quantity which describes the UV-light contribution to oxidation in terms of both intensity and wavelength. This quantity was derived from the energy absorbed by each photosensitive species by calculating the overlap between the absorption and the emission spectra of the light source, thus obeying the first law of photochemistry. The difficulty was that this quantity, the so-called "spectral overlap integral", required a suitable dimension in order to be introduced into kinetic model, i.e. not to depend on the species accumulation in the matrix. Its relevancy was demonstrated by checking its consistency (for arc xenon or mercury UV-light sources) with two analytical models, namely the Schwarzschild's law and the kinetic model, establishing relationships between the induction period and exposure conditions.

This latter model was shown to remain valid whatever the amount of absorbed UV-light compared with the former which is only valid in the range where photochemical initiation predominates over thermal initiation. However, the apparent quantum yield of hydroperoxide photolysis, which is the parameter which accounts for the photochemical initiation in the latter model, was about twice than measured experimentally by Carlsson and Wiles [24]. This finding result from the use of simplifying assumptions required in the analytical model, but then eradicated in the numerical model. Although very useful for establishing simple behavior law giving directly access to lifetime, the analytical resolution was abandoned since leading to serious inaccuracies.

By numerical simulation, the hydroperoxide photolysis was thus shown to be the predominant source of radicals compared with Norrish type reactions. Moreover, the quantum yield of hydroperoxide photolysis Φ_{POOH} has been found approximately equal to 4 ± 1 in a large domain of UV-light irradiances, in full agreement with the results of Carlsson and Wiles [24-26]. It is noteworthy that most of parameters, including oxygen transport properties, kinetic rate constants and yields in chain scissions have been kept identical between the thermal and photothermal oxidation models to ensure perfect continuity. This result confirms the validity of our strategy of kinetic modeling.

Only the apparent yield in carbonyl products was slightly increased from 50% to 60% to account for small stoichiometry changes in the distribution of oxidation products. It has been

also attempted to correlate the true yield in ketones (i.e. a heuristic yield for γ_1) with the yield in chain scission. Indeed, the theoretical mechanistic scheme indicates that "effective" macromolecular chain scissions result essentially from β-scission leading to ketone of type B (methyl or end-chain ketones). Therefore the yield in chain scission should be equal to the yield in ketones B. According to the proportions proposed by Carlsson and Wiles [24-26], it would mean that the true yield in ketones γ_1 is equal to 0.9, which is positioned in the upper range of the literature [27-31]. It is noticeable that this latter range is very scattered owing to the large variety of experimental procedure and justifies the introduction of an apparent yield in carbonyl products (see chapter 3 for VOCs emissions and chapter 4 for complete listing of reasons).

2.3. Attempts for extending the validity range of the photothermal oxidation model

Despite its very wide validity range, the value of Φ_{POOH} determined by numerical simulation displays a decrease with the amount of absorbed energy above a critical UV-light intensity equivalent to ten suns. Actually, this trend could be ascribed to multiphotonic excitations or the "termolecular" (from a photophysical point of view) feature of photolysis reactions. This latter explanation seems to be more likely since the curvature of the carbonyl build-up is clearly higher experimentally than numerically. These termolecular processes would consist in:

(i) The photosensitization of hydroperoxides by ketones. Indeed, it is noteworthy that only 15% of the overall energy absorbed by ketones would be sufficient to make φ_{POOH} equal to unity. This would involve either an exciplexe [32], [33] or a complex formed between adjacent hydroperoxides and ketones, distant from not more than one nanometer [34, 35]. As a point of comparison, the energy transfer can be estimated at about 60% by assuming hydroperoxide concentrations of about 0.4 $mol.L^{-1}$, as done by Geuskens and David [34], but its value drops at only 12% for more realistic concentrations of 0.05 $mol.L^{-1}$. It enables to question the relevancy of this scenario. Moreover, such an energy transfer does not occur in the case of molecular ketones randomly distributed in a rigid matrix [24] unlike liquid state [36, 37].

(ii) The hydroperoxides photosensitization by catalyst residues,

(iii) The photolysis of hydroperoxides associated in pairs or longer sequences.

The consistency of these different scenarios was tentatively checked by using a formal kinetic approach whose kinetic treatment, based on the framework given by Turro for energy transfers [38], has been detailed in appendix A.

The photosensitization of hydroperoxides decomposition by ketones can be written:

$$\left.\frac{d[POOH]}{dt}\right|^{photolysis} = -\Phi_{POOH}(\lambda)\cdot\left(J_{POOH}[POOH] + \psi_{K^*\rightarrow POOH}\, J_{P=O}[P=O][POOH]\right) \quad \textbf{Eq. 1}$$

where $\psi_{K^*\rightarrow POOH}$ is a function describing the energy transfer from excited ketones to hydroperoxides (see equation A.3 in appendix A)

The introduction of this energy transfer effectively confers a bimolecular feature to the oxidation behavior since enhances the curvature of carbonyl build-up. However, the value of the overlap between hydroperoxide absorptivity and ketones phosphorescence emission spectra, i.e. $\psi_{K^*\rightarrow POOH}$, would be very low. Therefore, this assumption would not explain the high value of Φ_{POOH} compared with its theoretical maximum ($\Phi_{POOH} \leq 1$).

In contrast, hydroperoxides photosensitization by catalyst residues (metal chelate) would be more likely since the spectral overlap integral $\psi_{M^*\rightarrow POOH}$ would be higher owing to their presumed high absorptivity ($\varepsilon_M \approx 1000$ L.mol^{-1}.cm^{-1} according to [39]) and emissivity, and despite their relatively low concentration ([M] $\leq 10^{-4}$ mol.L^{-1}) applying to inter-particle length of about 50 to 100 nm. However, they are not expected to change the molecularity of the hydroperoxide decomposition if one considers that its concentration remains unchanged along exposure time since they are regenerated such as a catalyst:

$$\left.\frac{d[POOH]}{dt}\right|^{photolysis} = -\Phi_{POOH}(\lambda)\cdot\left(J_{POOH}[POOH] + \psi_{M^*\rightarrow POOH}\, J_M[M][POOH]\right) = -\Phi_{POOH}(\lambda)\cdot(J_{POOH} + \psi')[POOH] \quad \textbf{Eq. 2}$$

with $\psi_{M^*\rightarrow POOH}$ a function describing the energy transfer from metal catalyst to hydroperoxides and $\psi' = \psi_{M^*\rightarrow POOH}\cdot J_M \cdot [M]$ a constant (independent of time).

Moreover, the mechanism of action of catalyst residues is not fully understood in photooxidation since ascribed either to energy transfer, radical transfer due to the "ligand" oxidation, or catalysis of hydroperoxides decomposition.

Finally, the last option would consist in energy transfer between hydroperoxides and ketones associated in complexes. This case corresponds to energy transfer through exchange mechanisms whose probability of occurrence is a function of the distance between the donor and acceptor. It is thereby interesting to highlight that the improvement of the numerical model consistency compared with the analytical model is presumably ascribed to a better description of the thermal core by introducing of the bimolecular decomposition of hydroperoxides, attributed to the role of associated hydroperoxides.

3. Limitations of the kinetic modeling approach

3.1. Implication of simplifying assumptions in formal and homogeneous kinetics

Obviously, it is legitimate to wonder in which extent the kinetic model remains valid in terms of:

(i) Exposure conditions (oxygen partial pressure, temperature, UV-light intensity and wavelength distribution), particularly for extrapolation outside of investigated range.
(ii) Time domain.

In both thermal and photothermal oxidation, the kinetic model has been shown to simulate accurately the concentration changes in primary oxidation products (hydroperoxides) which govern the induction period without involving additional adjustable parameters. In contrast, the modeling of the concentration changes in both secondary oxidation products (carbonyl species) and chain scissions involves apparent yields which could be connected to:

(i) Assumptions inherent to the formal kinetic approach which have been discussed in the first chapter of this study, i.e. the unicity of the reactive site (most labile hydrogen, i.e. methyne unit) and the complete isomerization of the non tertiary radicals potentially generated, which also imply to neglect the decomposition of a fraction of peroxide type species (peracids).
(ii) The generation of volatile compounds (VOCs) and particularly of volatile fragments such carbon monoxide and dioxide which account for a large part of the overall VOCs emissions and impact the maximal oxidation rate.

These yields have been checked to be independent of temperature in the range under investigation. Their values are also consistent and show that only the chain scissions occurring in the polymer middle-chain are effective for decreasing the molecular masses, unlike those occurring on the side-chain or end-chain which generates volatile compounds.

Besides, the distribution of molecular masses remains monomodal and the polydispersity index decreases towards the asymptotic value of 2 in both thermal and photothermal oxidation, as depicted in figure 2. This result is in perfect agreement with the Saito's laws predictions assuming a random chain scission, which constitutes an unarguable evidence for the homogeneity of the oxidation process and thus justifies the use of chemical kinetics for establishing models for lifetime prediction. This observation is only highlighted here because it only confirms previous experimental results obtained in the laboratory [40, 41].

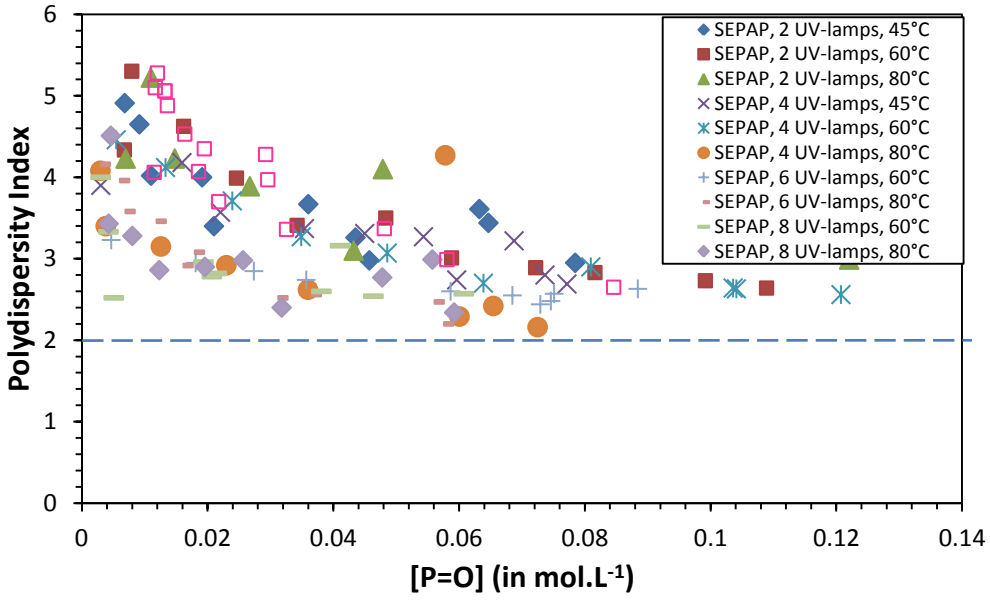

Figure 2: Changes in polydispersity Index during the course of photothermal oxidation materialized by the carbonyl products concentration

3.2. A complex multiphysical problem: insight from the case of thick specimens

Through this approach, it has been attempted to decompose the complex aging process into a combination of competing chemical and physical elementary phenomena, including chemical reactions, transport of molecular species into polymer substrates and its dependence with polymer morphology, interactions between UV-light and matter, concepts of fracture

mechanics, etc... This ability to investigate their relative predominance is a key advantage of the modeling approach, and is of a particular interest in testing methodology. Indeed, it is recommended to keep unchanged the relative weight of the involved phenomena in accelerated aging testing methods compared with natural weathering to ensure representativity.

The formal kinetic approach translated into its numerical form has enabled to test the consistency by comparing their simulations with experimental data, and eventually, to dismiss those which are incompatible or involve negligible phenomena Thus, the kinetic model appears as a powerful research tool for testing aging scenarios out of reach experimentally and determining their corresponding kinetics.

Thus, the numerical simulation of photodegradation profiles has highlighted additional phenomena:

(iii) The changes in polymer properties along the course of oxidation owing to molecular (oxygen grafting) and morphological changes (e.g. chemi-crystallization), especially in terms of permeability or optical properties.

(iv) The formation of of cracks at the sample surface which modify its geometry.

Eventually, it can be noticed that the difficulties emerges from the complex coupling between physical and chemical phenomena as well as from the hypercomplexity of chemical processes which has been partially got around through the formal kinetic approach.

3.3. **Expectations from kinetic modeling**

Clearly, kinetic modeling is a compromise between the model accuracy (i.e. goodness-of-fit), its predictive value (i.e. reliability of extrapolations in different exposure than those investigated), and its legibility. For favoring this latter feature, it is clear that the input data must be available or easily measurable experimentally in order to reduce the number of adjustable parameters. In order to increase the heuristic value of the kinetic model, parameters must be determined according to physico-chemical relationships. Failing that, it is possible to deduce them from empiric relationships whose validity is highly questionable outside the experimental domain under study.

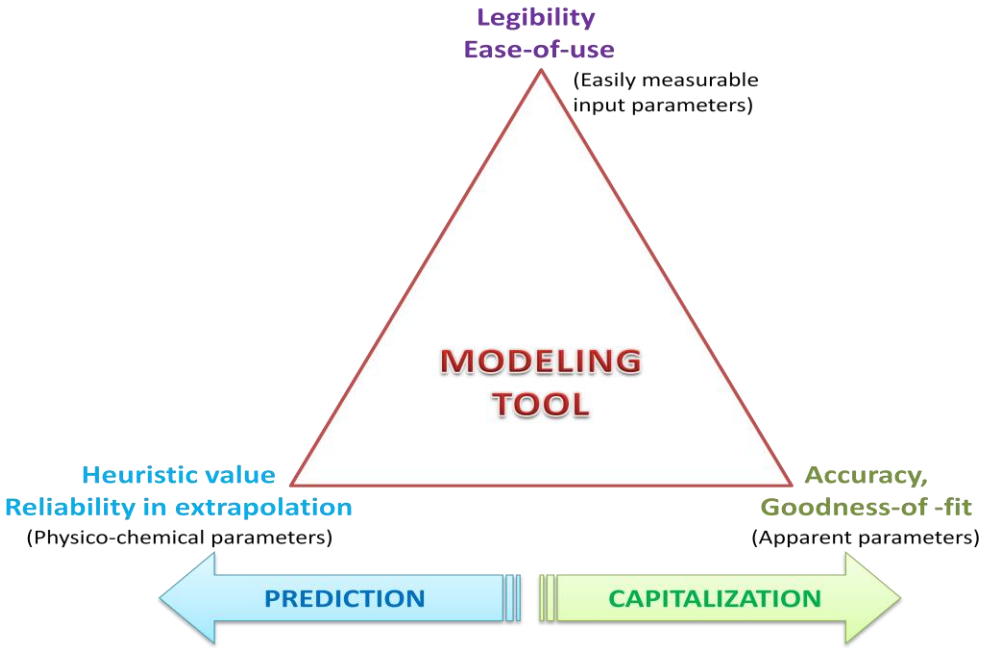

Figure 3: Compromise in kinetic modeling

Currently, the photothermal oxidation model has been shown to be predictive in terms of induction time, i.e. from the early periods of exposure until a moderate conversion degree of oxidation whose maximal value would correspond to a critical concentration in carbonyl products not exceeding [C=O] = 0.1 $mol.L^{-1}$. Despite this apparent success, a series of improvements can be envisaged for enhancing the model validity to higher conversion degrees:

(i) Introducing termolecular reactions in the mechanistic scheme which requires awkward calculation of the energy absorbed by complexes of photosensitive species;

(ii) Determining non-empirical relationships to describe changes in oxygen transport and optical properties along the course of oxidation;

(iii) Predicting cracks initiation at the sample surface and coupling oxidation and cracks propagation kinetics

(iv) Considering the mechanistic paths for the formation of volatile products.

However, their cost has been thought to be incommensurate compared with their expected return.

4. Towards a kinetic model for predicting the lifetime of TPO blends

Actually, the current industrial material that we have to study is in a Thermoplastic PolyOlefins (TPO) blends supplied by Borealis under the reference WH107AE which aims at being used in automotive parts such as bumpers and side protectors. So, EPR or EPDM nodules have been introduced into the iPP matrix in order to confer an impact resistance to the final product. They are called heterophasic ethylene propylene copolymers (HEPC) or polypropylene impact copolymers. They are obtained by multi-stage polymerization in fluidized beds involving up to four reactors. The impact of these rubbery nodules must be investigated in terms of polymer matrix resistance, oxygen transport properties and interaction between UV-light and microstructure. Two important issues must be considered:

(i) The reactivity of TPO blends towards oxygen in the absence of UV-light, i.e. in the case of pure thermal oxidation. As evidenced in previous chapters, this issue must be investigated at the local scale (i.e. on homogeneously oxidized TPO films) in terms of oxygen solubility and kinetic rate constants.

(ii) TPO opacity.

The main challenge, here, will be to investigate in which extent our kinetic modeling approach can be applied to multi-phase materials, considered now as markedly heterogeneous. It implies to apply a homogenization approach which raises several issues, in particular to determine the relevant scale of homogenization for obtaining a predictive tool. Shall we consider multiple phases or even interphases with their respective oxidation sites? How boundary conditions must be written to account for potential interactions between the different phases?

4.1. Describing the thermal oxidation of multiphase materials

4.1.1. A singular behavior

As reviewed by Pospíšil [42], polymer blends generally oxidize with a different rate than their elementary constituents because of the existence of co-reactions at the interfaces. These co-reactions can be of different natures: (i) chain branching or crosslinking, (ii) transport of degradation products across the interface, and (iii) effects of additives, contaminants or

compatibilizers, which generally accumulate in the interfacial region. They are usually impacted by the blend morphology, particularly the nodules size (depending itself on the phases compatibility), since occurring at the interfaces.

However, in scarce cases, co-reactions and co-oxidation reactions would be negligible and the overall oxidation of the blend applies to the independent oxidation of each phase. This type of behavior, qualified as "additive", was sometimes reported for polyolefines blends [43-46], in particular for PP/PE or PP/EPR blends, since no co-reaction had been observed except in presence of significant amount of peroxides or compatibilizing agent such as butadiene [Krulis, 1998]. Anymore, Tochacek and co-workers [47, 48] observed no change of the size and spatial distribution of EPR inclusions (rubbery domains) along extrusion/degradation which would suggest the absence of interaction between phases.

Besides, it was shown that oxidation is mostly localized in the iPP phase rather than the rubbery nodules by using various techniques such as TEM-EDX [44] or blend fractionation [15, 49, 50]. It was also reported that blend lifetime would be impacted by the amount and nature of metal catalyst residues [43, 48], and their spatial distribution inducing potentially oxidation heterogeneity in the PP phase itself [51].

The additivity behavior has been checked by performing a fractionation of the blend into the iPP and EPR phases, basic compared with those obtained by multiple extractions [49] or Temperature Rising Elution Fractionation [50], into its iPP and rubbery phase in order to study the oxidation of each separate phase besides the blend. The blend and its different phases have been then characterized in terms of composition and blend morphology (see table 1).

Table 1: Blend characterization

	Method				
Property	***FTIR (1)***	***^{1}H NMR (2)***	***^{13}C NMR (2)***	***Fractionation (3)***	***STEM (4)***
EPR volume fraction (%Vol.)	35 ± 3	-	-	35 ± 2	30-35
Ehtylene content (%mol.)	80 ± 3	79.5 ± 3.0	78†	-	-
Feret Diameter (µm)	-	-	-	-	2.18 ± 0.35
Min Feret Diameter (µm)	-	-	-	-	1.34 ± 0.26
Circularity	-	-	-	-	0.74 ± 0.05

(1) FT-IR titration of ethylene content according to the Wei's and Fan's laws [52] in a Perkin-Elmer

(2) ^{1}H-NMR (512 scans) and ^{13}C-NMR (16000 scans) analyses using a Bruker Avance Ultrashied 400 MHz device with a Broad band Inverse probe (BBI-Z, Atma, 5mm). NMR titrations by using the peaks assignments given in references [53, 54] in ^{1}H-NMR and [55] in ^{13}C-NMR.

(3) Fractionation according to ISO 9193: 1987-10

(4) S-TEM (Jeol JSM-6700 F; 10 mA; voltage of 30 kV) perfomed on 40-100 nm slices obtained with an ultramicrotome at -100°C and placed on carbon membranes.

Purified PP and EPR films -beforehand squeezed on KBr windows- and unpurified TPO films were then submitted separately to thermal exposures in air-ventilated ovens between 60 and 140°C. Their thermal oxidation was followed by FTIR spectrophotometry using the carbonyl absorbance at 1713 cm^{-1}.

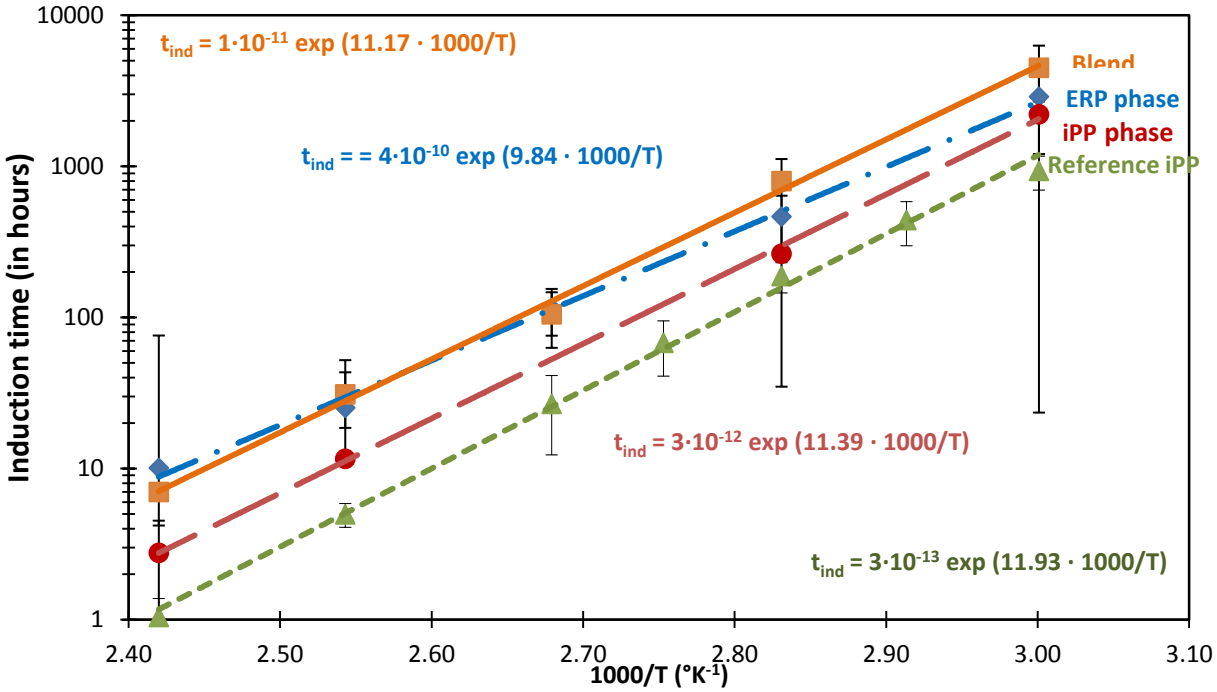

Figure 4: Induction times of the reference iPP, TPO blend and fractionnated iPP and EPR phases between 60°C and 140°C in air

As shown in figure 4, the blend clearly displays a much higher oxidation induction times than those of the iPP and EPR phases taken separatelybelow 110°C. Above 120°C, the blend and EPR phase have close oxidation induction times. Such a global oxidation behavior clearly does not result from the additivity of the elementary oxidation behaviors.

Alternative explanations for a synergistic effect on the induction time of blend must be envisaged:

(i) Co-oxidation reactions can explain the longer induction period of the blend than for its most oxidizable phase if its oxidation kinetics is comprised between those of each phase separately. When monitoring the oxidation kinetics of TPOs and their fractions, Mani and coworkers observed a delayed induction time for the blend compared to the iPP phase at 140°C but did not report results at lower temperatures [56]. It was thus postulated that polyethylene acts as a moderator of oxygen consumption, and later this result was ascribed to cooxidation reactions [57]. In our case, this argument would be valid for explaining the synergistic

effects at 140°C but not at lower temperatures where blend oxidation are much slower than for its fractioned phases.

Besides, describing co-oxidation reactions in ethylene-propylene copolymers is a very difficult task because of the numerous kinetic parameters, which has only been attempted at 45°C [58].

(ii) A residual concentration in stabilizers in the purified blend can explain its longer induction period compared to both phases. Indeed, blend specimens have only been purified by solvent extraction whereas fractionated phases were dissolved and reprecipitated. The resulting experimental scattering for the blend leads to temper the experimental findings, although the temperature dependence of induction times is consistent. However, it is noteworthy that steady-state oxidation rate of the blend were surprisingly low compared with reference iPP, whereas thermal stabilizer such as hindered phenol should not impact this quantity.

(iii) A last explanation, although difficult to check, would be the changes in oxygen permeabilities due to the incorporation of a small fraction of polyethylene, thus inducing micro-structural effects. In particular, the incorporation of ethylene into the iPP matrix during the multistage synthesis of TPO can trigger a dramatic decrease in oxygen solubility and thus, would lead to the observed delay of induction time if considering a similar dependence on morphology as for the various types of iPP. To explain the higher stability of the blend, it is suspected that EPR nodules cause local oxygen depletion in the iPP phase, presumably owing to physical interactions.

This last assumption would imply the absence of chemical but not physical interactions.

4.1.2. Theory

For a sake of simplicity, the blend was represented by a series of ERP nodules regularly spaced in a PP matrix and arranged according to a centered face cubic lattice. The corresponding elementary cell, represented in figure 5, was used in kinetic modeling to describe the material at the local scale though a homogenization approach.

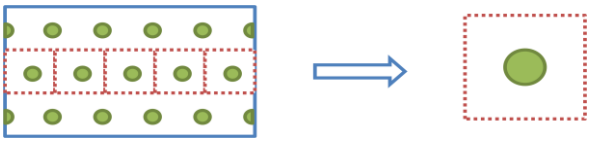

Figure 5: Schematization of the microstructure of an ERP/PP blend and the corresponding elementary cell.

In a first approach, it was assumed that each polymer phase degrades independently, i.e. that cooxidation reactions are negligible at the interface. Their respective thermal oxidation kinetics were simulated by a general kinetic model established for pure polypropylene [29] and pure polyethylene [59] in previous studies. Indeed, the EPR phase appears to have oxidation behavior very similar to the PE one, in agreement with its high ethylene fraction, typically higher than 80 %mol. (this was also the case in the work of Mani [56]).

Both PE and iPP thermal oxidations have been described by the Close-Loop Mechanistic Scheme (CLMS) in which only one type of reactive site is considered: the methyne group for PP and methylene group for EPR.

The only difference in terms of mechanistic scheme lays in the existence of the Russel's reaction (6c) for recombination of peroxy radicals, competitive with reaction (6b) and (6d). This reaction enables to account for the generation of oxidation products without involving chain scission. In term of kinetic formalism, it is equivalent to the recombination of alkoxy and hydroxy radicals in a cage. It is expected to be significant in PE [59, 60] but absent in iPP since the presence of methyl side groups prevents disproportionation. The scheme can be written with subscript i = t for PP and i = s for PE:

(1u) $P_iOOH \rightarrow 2P_i^\bullet + (1 - \gamma_1)\, P_iOH + \gamma_1 P_i{=}O + H_2O + \gamma_s S$ $(-2P_iH)$ (k_{1u})

(1b) $2P_iOOH \rightarrow P_i^\bullet + P_iO_2^\bullet + (1 - \gamma_1)\, P_iOH + \gamma_1 P_i{=}O + H_2O + \gamma_s S$ $(-P_iH)$ (k_{1b})

(2) $P_i^\bullet + O_2 \rightarrow P_iO_2^\bullet$ (k_2)

(3) $P_iO_2^\bullet + P_iH \rightarrow P_iOOH + P_i^\bullet$ (k_3)

(4) $P_i^\bullet + P_i^\bullet \rightarrow \gamma_4 P_i\text{-}P_i + (1 - \gamma_4)\, P_iH + (1 - \gamma_4)F + \gamma_4 B$ (k_4)

(5) $P_i^\bullet + P_iO_2^\bullet \rightarrow \gamma_5 P_iOOP_i + (1 - \gamma_5)\, P_iOOH + (1 - \gamma_5)F + \gamma_5 B$ (k_5)

(6a) $P_iO_2^\bullet + P_iO_2^\bullet \rightarrow [P_iO^\bullet\ {}^\bullet OP_i]_{cage} + O_2$ (k_{6a})

(6b) $[P_iO^\bullet\ {}^\bullet OP_i]_{cage} \rightarrow P_iOOP_i + B$ (k_{6b})

(6c) $[P_iO^\bullet\ {}^\bullet OP_i]_{cage} \rightarrow P_iOH + P_i{=}O$ (k_{6c})

(6d) $[P_iO^\bullet\ {}^\bullet OP_i]_{cage} \rightarrow 2P_i^\bullet + 2(1 - \gamma_1)\, P_iOH + 2\gamma_1 P_i{=}O + 2\gamma_s S$ $(-2P_iH)$ (k_{6d})

The initial conditions are:

$$[P_i^{\bullet}]_0 = [P_iO_2^{\bullet}]_0 = [P_iO^{\bullet}\ {}^{\bullet}OP_i]_0 = 0 \text{ mol.L}^{-1}$$

$$[P_sH]_0 = 60 \text{ mol.L}^{-1} \quad \text{(concentration of methylene } CH_2 \text{ groups)}$$

$$[P_tH]_0 = 20.3 \text{ mol.L}^{-1} \quad \text{(concentration of methyne CH groups)}$$

$$[P_iOOH]_0 = 10^{-5}–10^{-1} \text{ mol.L}^{-1}$$

Since cooxidation reactions are assumed to be negligible, no corresponding additional step has been added into the mechanistic scheme, but physical interactions are expected to occur. The challenge lies in boundary conditions, especially in terms of oxygen supply. The equilibrium oxygen concentration can be obtained from the classical Henry's law applied to pure iPP and pure EPR:

$$[O_2]^{pure\ PP} = s_{O_2}^{PP} \cdot P_{O_2} \qquad \textbf{Eq. 3}$$

and

$$[O_2]^{pure\ EPR} = s_{O_2}^{EPR} \cdot P_{O_2} \qquad \textbf{Eq. 4}$$

with $s_{O_2}^{PP}$ and $s_{O_2}^{ERP}$ the respective oxygen solubility coefficients in each phase and P_{O2} the oxygen partial pressure in the environment.

If these conditions are fulfilled in the whole sample thickness (scheme a, figure 6), both phases will oxidize independently in the blend, i.e. in a similar way as in pure materials. However, the peculiar microstructure of the blend (EPR nodules included into an iPP matrix) would change the relative concentration in oxygen in both phases. The overall amount of oxygen in the blend would be limited by the amount of oxygen soluble and thus, available in the iPP phase due to its own oxygen transport properties (see permeability measurements farther).

In a first approach, it was assumed that the EPR/iPP interface is highly permeable, i.e. that the rate of the oxygen transfer between both phases is much faster than all the other phenomena impacting the variation of oxygen concentration in each phase. It implies that the reactions in the EPR nodules are not limited by the oxygen supply from the iPP phase.

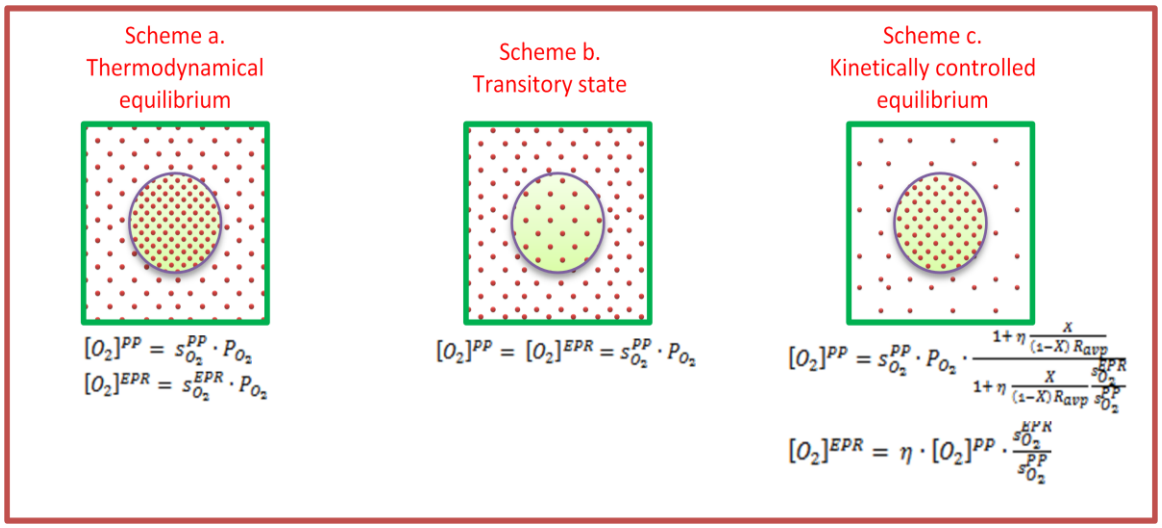

Figure 6: Scheme explaining the oxygen repartition between the iPP and EPR phases, i.e. oxygen solubility boundary conditions

As a consequence, the oxygen concentration in the EPR phase is given by a continuity equation:

$$[O_2]^{PP} = \eta \cdot [O_2]^{EPR} \cdot \frac{s_{O_2}^{EPR}}{s_{O_2}^{PP}} \qquad \textbf{Eq. 5}$$

with η the efficiency of the oxygen transfer from PP to EPR phases

Also, the number of oxygen moles which is supplied to the elementary cell by permeation is equal to:

$$n_{O_2}^{TOT} = s_{O_2}^{PP} \cdot P_{O_2} \cdot (1 - X) \cdot V_a \cdot V^{TOT} + s_{O_2}^{PP} \cdot P_{O_2} \cdot \eta \cdot X \cdot V^{TOT}$$

$$n_{O_2}^{TOT} = s_{O_2}^{PP} \cdot P_{O_2} \cdot [1 - X \cdot (1 - \eta)] \cdot V^{TOT} \qquad \textbf{Eq. 6}$$

with $n_{O2}{}^{TOT}$ the number of oxygen moles supplied to the elementary cell, and V^{TOT} their volume its volume and X the volume fraction of nodules in the PP matrix: $X = \omega_{EPR} \frac{\rho_{blend}}{\rho_{ERP}}$

The conservation law of matter implies that the total amount of oxygen is divided between the entire EPR phase (fully amorphous) and the amorphous fraction V_a of the iPP phase (where oxygen is soluble [61]) so:

$$n_{O_2}^{TOT} = n_{O_2}^{EPR} + n_{O_2}^{PP} = [O_2]^{EPR} \cdot X \cdot V^{TOT} + [O_2]^{PP} \cdot (1 - X) \cdot V_a \cdot V^{TOT} \qquad \textbf{Eq. 7}$$

Hence, from equations 5, 6 and 7, it comes:

$$[O_2]^{PP} = s_{O_2}^{PP} \cdot P_{O_2} \cdot \frac{1+\eta \frac{X}{(1-X)\,V_a}}{1+\eta \frac{X}{(1-X)\,V_a}\frac{s_{O_2}^{EPR}}{s_{O_2}^{PP}}} \quad \textbf{Eq. 8}$$

Concentrations of chemicals species or physico-chemical properties in the blend can be then calculated by summing the elementary contributions of both phases, which has been preliminary corrected by the amount of amorphous phase as multiplier. For instance, the overall oxidation rate of the blend rate corresponds to the average value of the elementary oxidation rates:

$$r_{ox}^{blend} = X.r_{ox}^{EPR} + (1-X).r_{ox}^{PP} \qquad \textbf{Eq. 9}$$

In a similar way, the results by oxygen permeametry measurements, including permeability (figure 7), solubility (figure 8) and diffusivity (figure 9) data, can be reported and compared to those obtained for the reference iPP and the pure EPR phase (at 23°C).

It is noteworthy that the permeability is higher for the blend than for the reference iPP, but different conclusions are drawn for solubility and diffusivity. The solubility is much lower for the blend than for the reference iPP. In contrast, the diffusivity is much higher which is not surprising when considering the lower content in crystallites, resulting in a lower tortuosity of diffusion paths i.e. a lower value of the shape factor in the Michaels and Bixler's theory [62, 63].

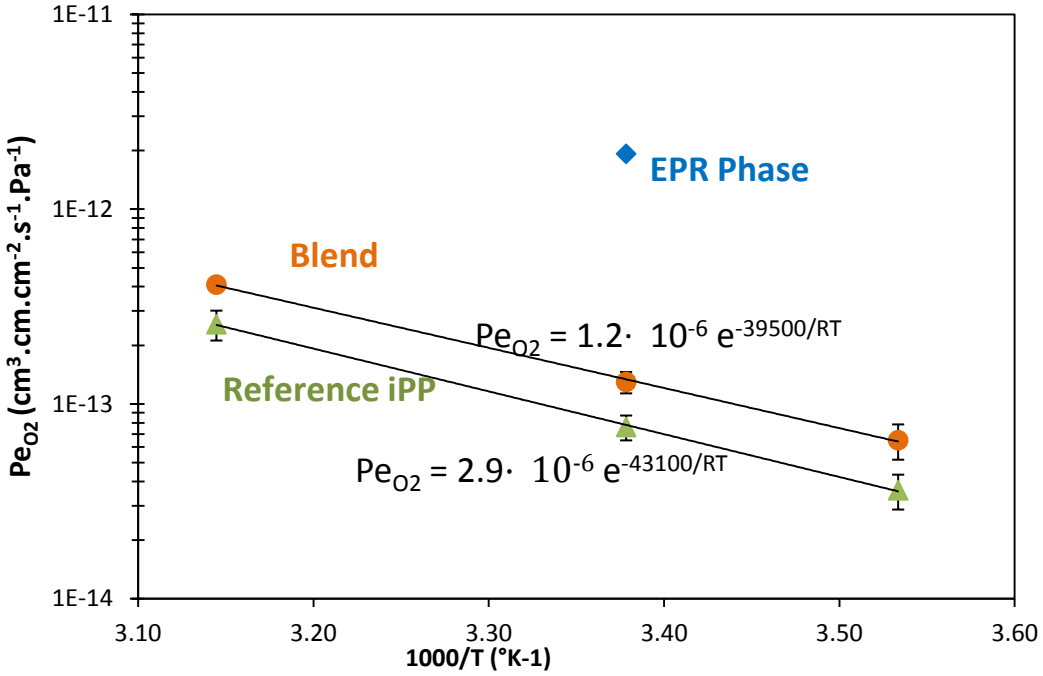

Figure 7: Arrhenius graph of oxygen permeability for the reference iPP, blend and pure ERP phase

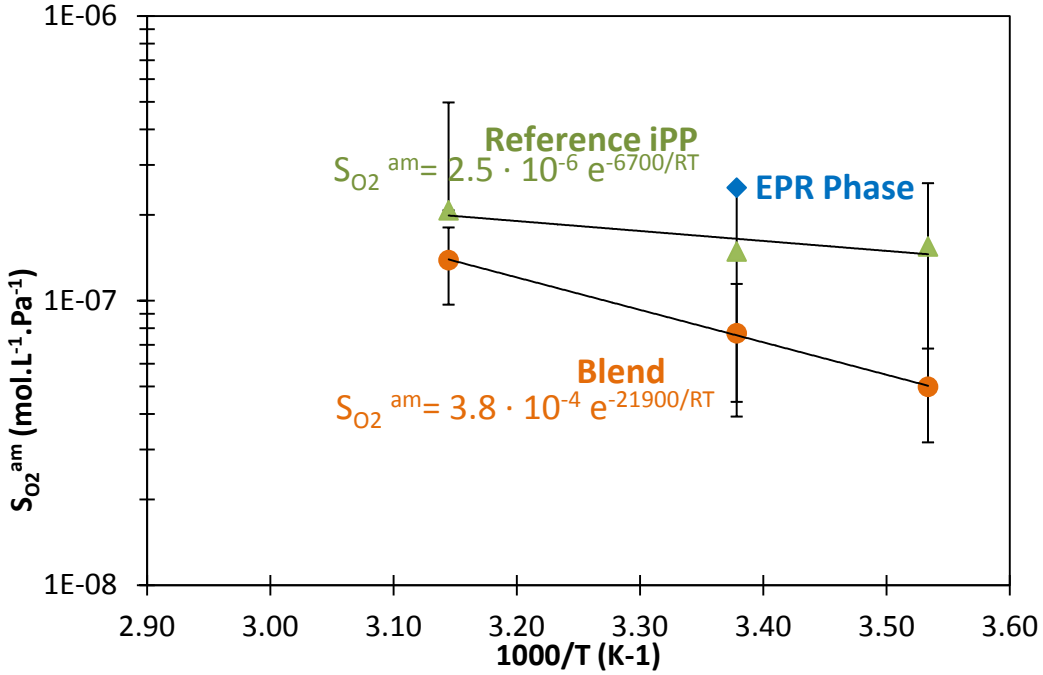

Figure 8: Data Arrhenius graph of oxygen solubility for the reference iPP, blend and pure ERP phase

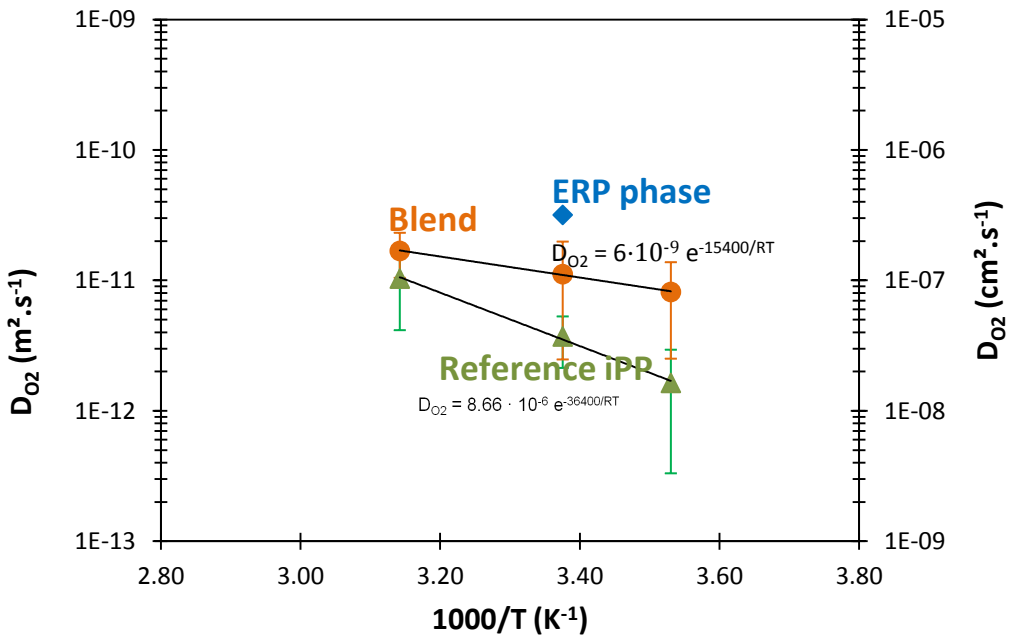

Figure 9: Arrhenius graph of oxygen diffusivity for the reference iPP, blend and pure ERP phase

4.1.3. Kinetic modeling of the EPR phase

In order to perfectly describe the EPR thermal oxidation behavior, the corresponding parameters (i.e. rate constants and yields) must be adjusted from experimental data since they presumably depend on the fraction of propylene units. Since its oxygen solubility is high, the EPR phase is expected to be almost fully saturated in oxygen, i.e. close to oxygen excess. In this case, simulations would weakly depend on the kinetic rate constants k_4 and k_5. This fact considerably facilitates the optimization procedure for simulating accurately the oxidation behavior of the EPR phase alone. However, these latter rate constants must be eventually determined because of the decrease in oxygen concentration when introducing EPR nodules into the iPP matrix the blend, thus coming nearer of oxygen default conditions. Parameters k_4 and γ_4 would only have an influence for very low oxygen pressures and can be neglected here. On the contrary, parameters k_5 and γ_5 would enable to describe the oxygen pressure dependence at intermediary oxygen concentration between oxygen default and excess. The kinetic modeling of the EPR phase was finally done using the following set of parameters (Table 2).

Table 2: Parameters for modeling the thermal oxidation of EPR phase

Parameters	***Units***	k_i^0	***Ea (kJ.mol^{-1})***
$[POOH]_0$	$mol.L^{-1}$	$1 \cdot 10^{-2}$	-
S_{O2}^{am}	$mol.L^{-1}.Pa^{-1}$	$2.5 \cdot 10^{-7}$	0
k_{1u}	s^{-1}	$8.0 \cdot 10^{12}$	140
k_{1b}	$L.mol^{-1}.s^{-1}$	$6.2 \cdot 10^{5}$	80
k_2	$L.mol^{-1}.s^{-1}$	$1.0 \cdot 10^{8}$	0
k_3	$L.mol^{-1}.s^{-1}$	$1.5 \cdot 10^{10}$	73
k_4	$L.mol^{-1}.s^{-1}$	$8.0 \cdot 10^{11}$	0
k_5	$L.mol^{-1}.s^{-1}$	$8.0 \cdot 10^{11}$	0
k_{6a}	$L.mol^{-1}.s^{-1}$	$4.9 \cdot 10^{19}$	80
k_{6b}	s^{-1}	$2.0 \cdot 10^{6}$	0
k_{6c}	s^{-1}	$1.2 \cdot 10^{6}$	5
k_{6d}	s^{-1}	$8.0 \cdot 10^{12}$	50
γ_1	%	57	-
γ_4	%	50	-
γ_5	%	50	-

As depicted in figure 10, simulations are in rather good agreements with experimental data over the whole temperature range under study.

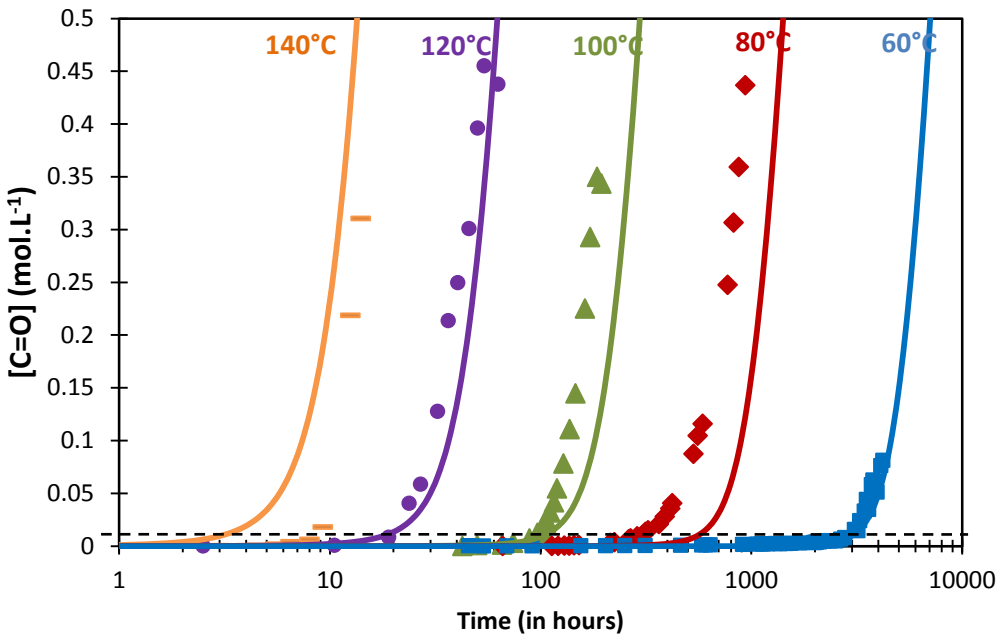

Figure 10: Carbonyl products build-up in the pure EPR phase in air between 60 and 140°C. Symbols: experimental data, lines: kinetic modeling

4.1.4. Kinetic modeling of the iPP phase

According to our previous publications, oxygen solubility and initial concentrations of hydroperoxides constitute adjustable parameters in the general model of thermal oxidation [29]. Basically, $[POOH]_0$ has only a minor effect on induction times and no effect on maximal oxidation rates, whereas S_{O2} has a strong impact on both parameters. In order to simulate the material at best, a quick parametric study was done, fixing the boundary modalities for $[POOH]_0$ and ψ and adjusting S_{O2} on the results.

The set of adjustable parameters was optimized accordingly with tolerance previously reported. By a simple parametric study, these parameters where determined at $[POOH]_0 = 10^{-2}$ $mol.L^{-1}$ and S_{O2}^{am} was found to be equal to the minimal value (iPP2 in ref. [29]). It is notable that the $[POOH]_0$ chosen value is the same as in EPR simulations which would suggest a similar amount of structural defaults or catalysis residues in both phases.

Table 3: Set of kinetic parameters for the iPP phase

Parameters	***Units***	k_i^0	***Ea (kJ.mol^{-1})***
$[POOH]_0$	$mol.L^{-1}$	10^{-2}	-
S_{O2}^{am}	$mol.L^{-1}.Pa^{-1}$	$4.2 \cdot 10^{-7}$	6.7
D_{O2}	$m^2.s^{-1}$	$8.7 \cdot 10^{-6}$	36.4
Pe_{O2}	$cm^3.cm.cm^{-2}.Pa^{-1}.s^{-1}$	$4.8 \cdot 10^{-7}$	43
k_{1u}	s^{-1}	$1.9 \cdot 10^{13}$	140.7
k_{1b}	$L.mol^{-1}.s^{-1}$	$6.2 \cdot 10^{8}$	95
k_2	$L.mol^{-1}.s^{-1}$	$3.0 \cdot 10^{9}$	10
k_3	$L.mol^{-1}.s^{-1}$	$5.1 \cdot 10^{7}$	62.2
k_4	$L.mol^{-1}.s^{-1}$	$1.0 \cdot 10^{12}$	0
k_5	$L.mol^{-1}.s^{-1}$	$4.5 \cdot 10^{10}$	0
k_{6a}	$L.mol^{-1}.s^{-1}$	$2.0 \cdot 10^{17}$	90
k_{6b}	s^{-1}	$6.7 \cdot 10^{6}$	5
k_{6d}	s^{-1}	$1.4 \cdot 10^{12}$	41
γ_1	%	50	-
γ_4	%	0	-
γ_5	%	0	-

Simulations are reported in figure 11 and show a perfect agreement with experimental results, which substantiates the kinetic model for iPP thermal oxidation.

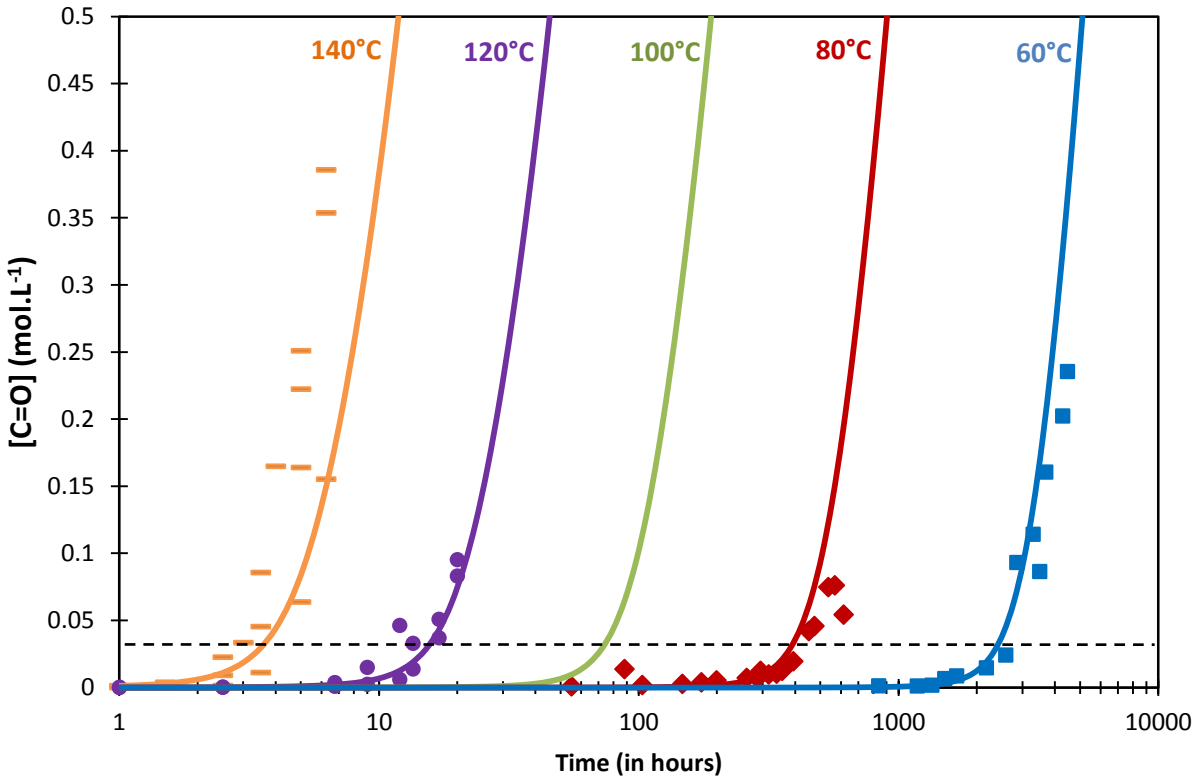

Figure 11: Carbonyl products build-up in the pure iPP phase in air between 60 and 140°C. Symbols: experimental data, lines: kinetic modeling

4.1.5. Kinetic modeling of the blend behavior

The proposed numerical tool is composed of the juxtaposition of both elementary models relative to each phase with specific boundary conditions. It enables to simulate the thermal oxidation behavior of the blend in the whole temperature range under investigation without using additional adjustable parameter. Results are presented in figure 12. In a general manner, it can be concluded that the oxygen solubility is lower of the blend than for each phase considered separately. However, the model must explain the synergistic effect observed for the blend, i.e. an induction time longer for the blend than for the iPP and the EPR phases. This result seems to demonstrate the validity of the numerical tool.

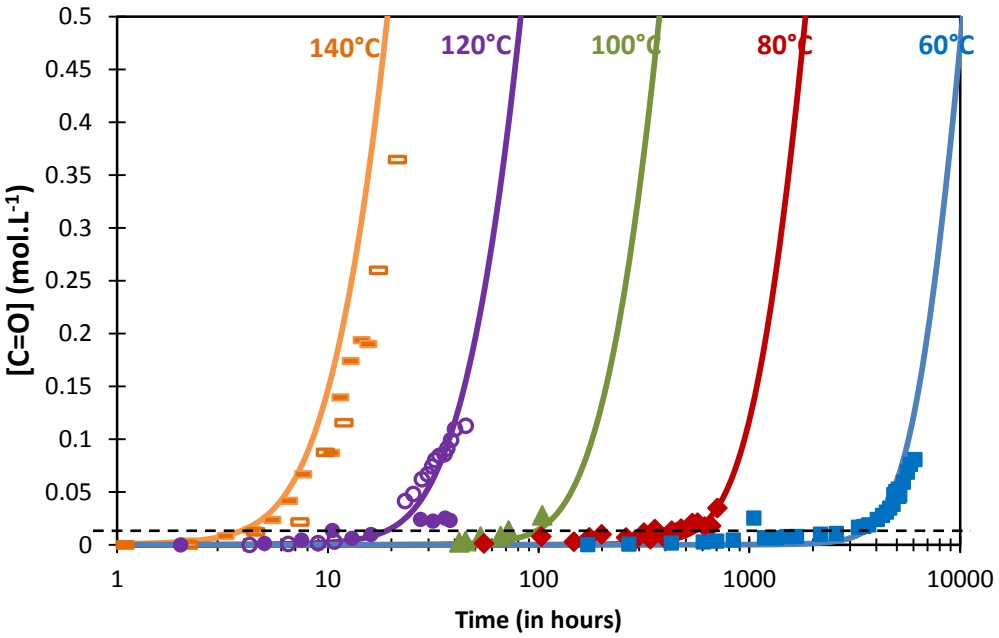

Figure 12: Carbonyl products build-up in the blend in air between 60 and 140°C. Symbols: experimental data, lines: kinetic modeling

Since boundary conditions concern the physics of oxygen transport properties, the model's relevancy must be discussed regarding at the permeability data of the materials under investigation.

The oxygen transport properties, determined by inverse resolution method for the blend, have been compared to the values calculated by the Maxwell's or Voigt's compositions laws [64].

Theoretically, the solubility is proportional to the overall number of Henry sites in the amorphous iPP and EPR:

$$s_{O_2}^{blend} = s_{O_2}^{PP} \cdot R_{avp} \cdot v^{PP} + s_{O_2}^{EPR} \cdot v^{EPR} \quad \textbf{Eq. 10}$$

with v^{EPR} and v^{PP} the respective volume fractions of EPR nodules and iPP matrix and V_a the volume fraction of amorphous phase in the iPP matrix.

At 23°C, it comes:

$$s_{O_2}^{blend} = 0.312 \cdot 4.2 \cdot 10^{-7} \exp\left(-6700/RT\right) + 0.35 \cdot 2.51 \cdot 10^{-7}$$
$$= 9.64 \cdot 10^{-8} \text{ mol. L}^{-1}\text{. Pa}^{-1}$$

This theoretical values is of the same order of magnitude than the experimental value of $7.7 \cdot 10^{-8}$ mol.L^{-1}.Pa^{-1} determined by permeametry. It comes essentially from the EPR contribution (91%).

The connection between the polymer morphology and the coefficient of oxygen solubility has been also observed in the case of a commercial PP matrices modified by elastomeric nodules (TPO). The oxidative behavior of the blend (particularly its induction period) has been simulated by assuming only physical interactions between its different phases, instead of cooxidation reactions. Its low oxygen solubility is the direct consequence of blending, which has been modeled by a homogenization approach with specific boundary conditions at the nodule matrix interface. Thus, here also, the oxygen solubility appears as a relevant property to measure in order to describe accurately the impact of polymer morphology on lifetime.

4.2. Light attenuation issues in photothermal oxidation of TPO blends

4.2.1. Comparison of optical properties between the reference iPP and TPO blend

Similarly as for iPP plates, TPO plates of about 3 mm thick were molded by DK CODIM 175-400 injection machine from as-received pellets using the same processing conditions (T molten polymer = 210°C, screw speed = 60 rev.min^{-1}, injection rate = 40 mm.min^{-1}, commutation pressure =500 bars, hold pressure = 500 bars, hold time = 6 s, cooling time at 40°C = 25 s). Both reflectance and opacity (lineic absorption coefficient) were measured by using the two methods described in chapter 8, i.e.; (i) a Lambda 900 Perkin-Elmer UV-visible spectrophotometer equipped with a PELA-1000 integration sphere whose illumination geometries were 8°/hemispherical in reflectance and 0°/hemispherical in transmittance; (ii) the Albuma method decribed by Rabello and White [65] whose formula is reminded in equation 11.

$$\ln(1-R) = \ln\left(\frac{I}{I_0}\right)_{z=0} = ln\left(\frac{I_0-I_r}{I_0}\right) \qquad \textbf{Eq. 11}$$

Results obtained with the integration sphere (first method) are depicted in figure 13. Since stabilizers were not removed from the injection molded plates before measurements, the peak visible at 280 nm and corresponding to the UV absorption of the residual phenol ring was removed by mathematical treatment for subsequent analyses.

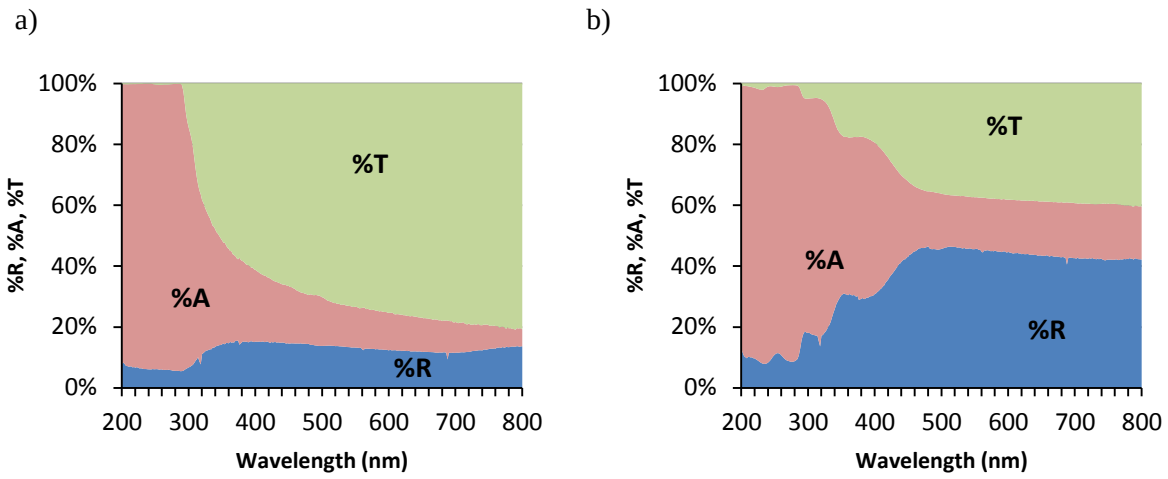

Figure 13: Geometric repartition of UV-visible light in 3 mm thick plates of iPP (a) and EPR/PP (b) and 3 mm thick plates of iPP %R: reflected part. %A: absorbed part. %T: transmitted part.

From the former measurements, it was possible to determine the lineic absorption coefficient for the TPO blend depicted in figure 14, as well as the iPP for comparison:

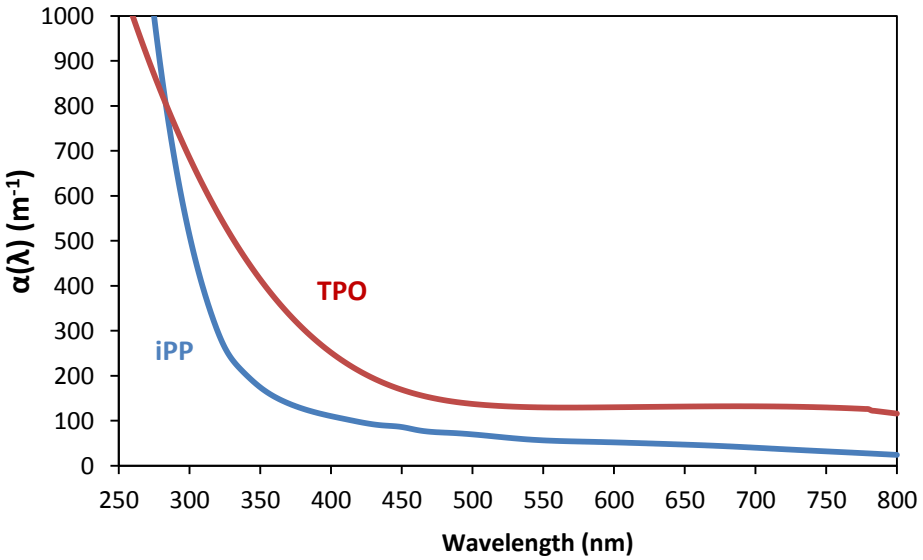

Figure 14: Spectral distribution of the lineic absorption coefficient of unstabilised iPP and TPO samples

All the results with both methods are summarized in table 4.

Table 4: Determination of the average values of reflectance for polypropylene based materials according to these different methods

Samples	***Integration sphere Method***	***Albuma method***
iPP film	10 ± 1 %	1 ± 14 %
iPP plate	15 ± 2 %	14 ± 2 %
TPO film	10 ± 1 %	12 ± 1 %
TPO plate	40 ± 2 %	37 ± 6 %

It appears that the reflectance increases with the specimen thickness, particularly in the case of the blend. In parallel, the specular component of the reflectance was found to be negligible in all cases. Thus, this phenomenon is attributed to the "state of the surface". It would be due to the existence of multiple scatterings in the case of media with a certain turbidity. In the reference iPP, it is ascribed to the semi-crystalline nature of polypropylene (i.e. the existence of crystallites structures such as spherulithes). This phenomenon is still reinforced in the blend because of the presence of EPR nodules (rubbery domains). It is noteworthy that they are also responsible of a higher material opacity, as evidenced by the value of the lineic absorption coefficient (figure 14).

4.2.2. Modeling by using the Kubleka-Munk's theory

In order to account for double side exposure to irradiation and multiple scatterings, it is relevant to promote multi-flux models based on radiative transfer equations instead of the single flux Beer-Lambert's law describing only light attenuation. These theories were mostly applied to the plane parallel layers geometry with infinite horizontal extension, thus neglecting edge effects (one dimension model applied in the perpendicular direction to the illuminated side).

The simplest model requires at least two light fluxes propagating in opposite directions, i.e. forward and a backward light beams, as for instance the Kubelka-Munk's (KM) model [66-68]. The set of coupled differential equations is:

$$\begin{cases} \frac{dI}{dz} = -(K+S)I + SJ \\ \\ \frac{dJ}{dz} = (K+S)J - SI \end{cases}$$ **Eq. 12 and 13**

where I and J are the forward and backward fluxes respectively, and K and S are the respective KM's coefficients of absorption and scattering (in m^{-1})

It is also noteworthy that the absorption K and scattering S parameters of the KM's model have no direct physical meaning, unlike the corresponding intrinsic parameters which represent the probability of light being absorbed and scattered UV-light per unit path length isotropically. However, various linear relationships have been established between the former and the latter depending on the illumination geometry (See for instance [69-71]).

4.2.3. Determination of K and S as model parameters

Instead, these coefficients will be here tentatively determined, basing on the measurements performed with the integrating sphere, by solving the equations established for the reflectance R and transmittance T established from the KM's theory [66, 67]:

$$T_{KM} = \frac{b}{a\sinh(bSh) - b\cosh(bSh)}$$ **Eq. 14**

$$R_{KM} = \frac{1 - R_g[a - b\coth(bSh)]}{a - b\coth(bSh) - R_g}$$ **Eq. 15**

with $a = (S + K) / S$, $b = (a^2 - 1)^{1/2}$, R_g the diffuse reflectance of the backing (here $R_g = 0$ as for black substrate in the absence of backing), and h the specimen thickness.

This determination included several assumptions:

(i) Structural irregularities (inducing absorption and scattering) are much smaller than the specimen thickness and randomly distributed;

(ii) Forward and backward light beam would be perfectly diffused (scattered according to semi-isotropic distributions) and to occur without change of frequency;

(iii) Illumination must be perfectly diffuse or collimated with an incidence angle of 60° (only applicable to diffuse/diffuse or 60°/diffuse geometries).

Assumptions relative to the analytical integration of the differential equations were also added to these restrictive hypotheses. Most of them could be got around by implementing a numerical treatment, in particular:

(iv) Radiation is assumed to be spectrally homogeneous or monochromatic in order to avoid polychromatic complications.

(v) The material is perfectly dull, i.e. without specular component of the reflectance;

(vi) Boundary conditions would be independent of time and space at the top and bottom surfaces.

The original KM's theory has been also completed by the Saunderson's approximation, in order to correct the surface optical properties by the changes of refractive index, by using the Fresnel-Descartes' relationship [72]:

$$T = (1 - r_c)^2 \frac{T_{KM}}{1 - r_c^2 T_{KM}^2} \qquad \textbf{Eq. 16}$$

$$R = r_c + (1 - r_c)(1 - r_d) \frac{R_{KM}}{1 - r_c T_{KM}^2} F \qquad \textbf{Eq. 17}$$

with $r_c = (n-1)^2/(n+1)^2$ the collimated reflectance (i.e. the specular component), which is a function of the refraction index at the surface of the iPP specimen. The internal diffuse reflectance r_d is assumed equal to 0.4.

The term F is a correction factor which has been introduced by Vargas [71] [70, 71] in order to use the previous equations in the case of collimated beam irradiance (see assumption (iii)). In the present case, this factor is assumed to be equal to unity. This assumption constitutes an approximation in the case of an integrating sphere. It is acceptable here since this study only aims at estimating the relative importance of phenomena, but not to provide an accurate modeling.

The resulting spectral distribution of K and S are reported in figure 15.

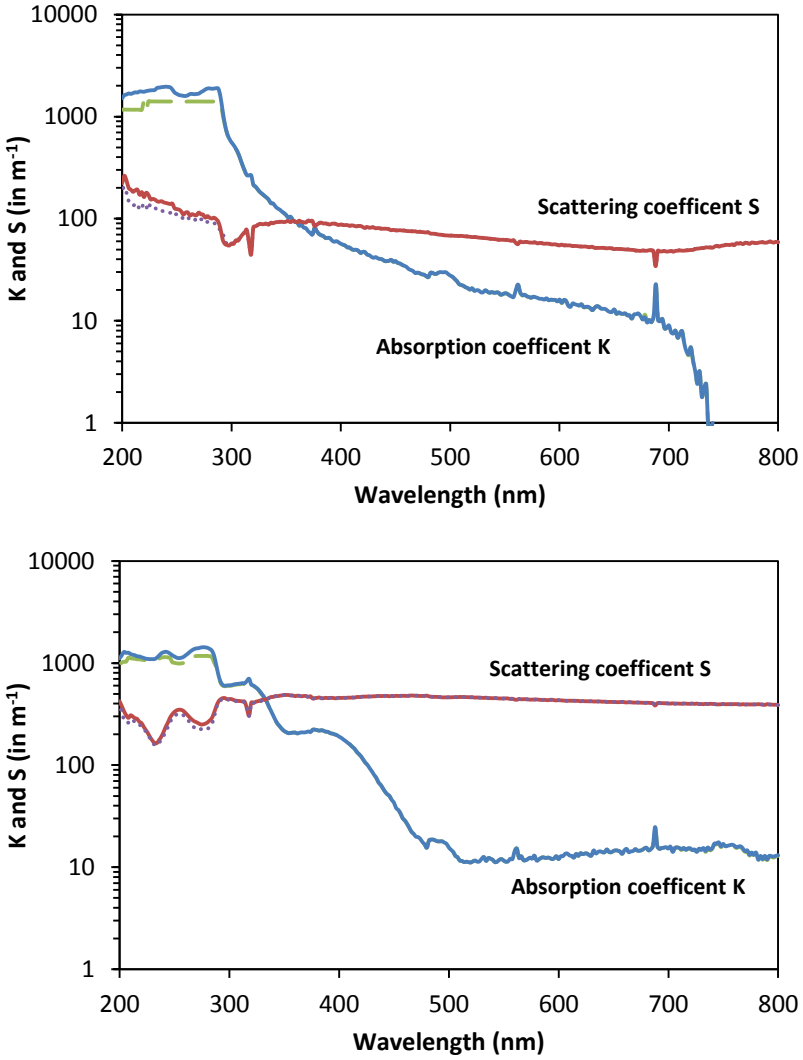

Figure 15: Spectral distribution of the of absorption K and scattering S coefficients in the reference iPP (Fig. a) and TPO blend (Fig. b)

In the original Kubelka-Munk's model, only monochromatic radiations were considered. In the present work, it is proposed to consider polychromatic radiations in the same way than for opacity, i.e. by calculating the quantities J^S and J^K (by analogy with J^α). Then, some composite values of K^{comp} and S^{comp} will be calculated for accounting for the spectral distribution of K and S, according to:

$$K^{comp} = \frac{J_X^K}{J_X} = \frac{\int_{\lambda_{min}}^{\lambda_{max}} \frac{\ln(10)}{10} \frac{E_\lambda}{N_a} \frac{\lambda}{hc} \varepsilon_i(\lambda)\, K(\lambda)\, d\lambda}{\int_{\lambda_{min}}^{\lambda_{max}} \frac{\ln(10)}{10} \frac{E_\lambda}{N_a} \frac{\lambda}{hc} \varepsilon_X(\lambda)\, d\lambda} \quad \textbf{Eq. 18}$$

$$S^{comp} = \frac{J_X^S}{J_X} = \frac{\int_{\lambda_{min}}^{\lambda_{max}} \frac{\ln(10)}{10} \frac{E_\lambda}{N_a} \frac{\lambda}{hc} \varepsilon_i(\lambda)\, S(\lambda)\, d\lambda}{\int_{\lambda_{min}}^{\lambda_{max}} \frac{\ln(10)}{10} \frac{E_\lambda}{N_a} \frac{\lambda}{hc} \varepsilon_X(\lambda)\, d\lambda} \quad \textbf{Eq. 19}$$

Since these composite coefficients depend on the UV-light source, they have been calculated for the different climatic devices used in this study (table 5):

Table 5: Composite values K^{comp} and $S^{\wedge comp}$ for various light sources

Light source	**K_{POOH} in iPP (in m^{-1})**	**S_{POOH} in iPP (in m^{-1})**	**$K_{POOH\ in}$ in TPO (in m^{-1})**	**S_{POOH} in TPO (in m^{-1})**
SEPAP 12-24, 4 arc mercury lamps	815	83	797	394
WeatherOMeter, xenon lamp	436	83	570	420
Philips TLK 05 lamp fluorescent lamp [9]	212	82	448	441

It is noteworthy that the absorption coefficients K^{comp} are rather similar but the scattering coefficient S^{comp} is noticeably higher for the TPO blend than for the reference iPP, in agreement with the literature [73]. Moreover, S^{comp} does not depend on the light source since it is almost independent of wavelength unlike K^{comp}.

4.2.4. Numerical simulation of UV-light attenuation profiles

In the case of a one-side exposure originally treated by Kubelka and Munk, the backward light beam only accounts for the part of the light which is retro-diffused or scattered. However, it is easily modifiable in order to introduce irradiance at the back face of the specimen.

The initialization of the problem is ensured through the following boundary conditions:

$$\begin{cases} I_{z=0}(\lambda) = E_{foreward}(\lambda) \\ \\ J_{z=l}(\lambda) = E_{backward}(\lambda) \end{cases} \qquad \textbf{Eq. 20 and 21}$$

with $E_{foreward}$ the irradiance directly emitted by the light source and $E_{backward}$ the secondary irradiance reflected by the wall of the climatic chamber in the opposite direction (whose spectral distribution is assumed to be similar as the primary source).

The resulting problem constrained by the boundary conditions has been solved by using the Matlab's routines bvp4c or bvp5c (based on the three stages Lobaltto IIIa formula).

In order to investigate the effect of multiple scatering alone, the backward irradiance was set at $E_{backward} = 0$. After calculation of the light attenuation profiles, it is possible to estimate the gain in UV-light at the surface owing to multiple reflections/scatterings (figure 16):

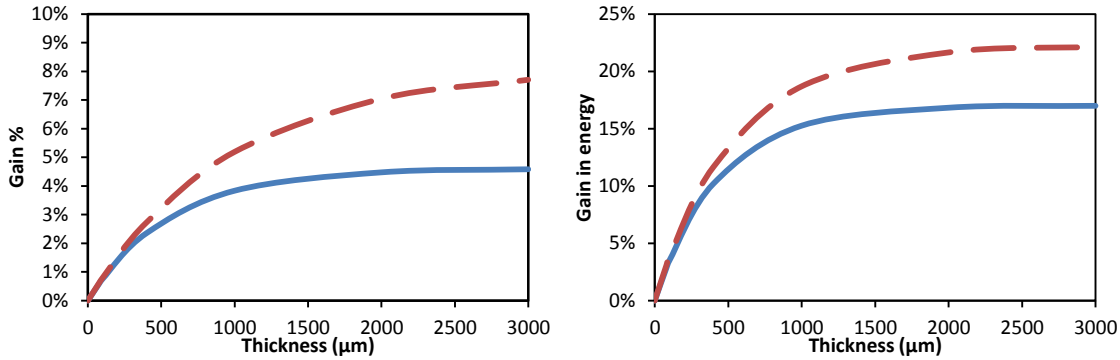

Figure 16: Gain in UV-light at the surface due to multiple scatterings in iPP (Fig. a) and TPO blend (Fig. b), for SEPAP 12-24 (solid line) and Weather O Meter (dotted line) climatic devices.

It is clear that the multiple scatterings are of a minor importance for the reference iPP materials but have to be considered in the case of TPO blends.

Similarly, it is possible to estimate the effect of double side exposure to irradiation (by setting $E_{backward} = E_{foreward}$ as worst-case) on the quantum yield at the surface:

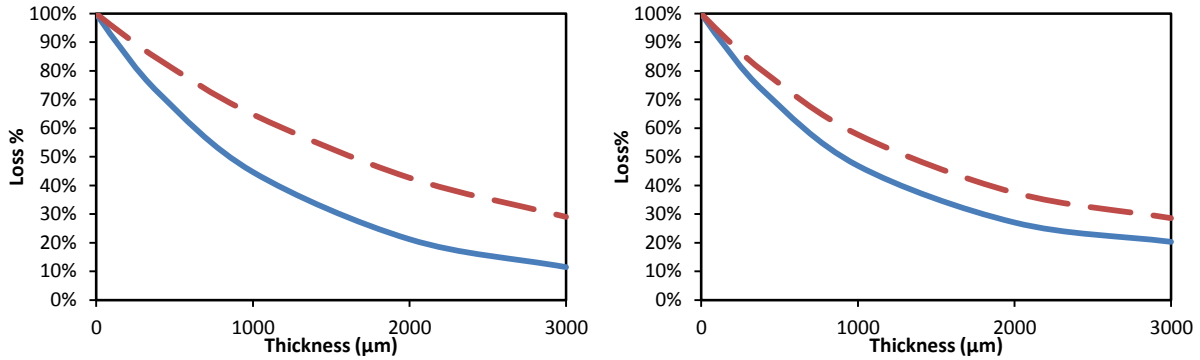

Figure 17: Loss in UV-light at the surface of plates compared with films in the case of double side exposure in iPP (Fig. a) and TPO (Fig. b), for SEPAP 12-24 (solid line) and Weather O Meter (dotted line) climatic devices.

The loss of efficiency is due to the attenuation of the backward beam with the material thickness owing to its opacity. Therefore, the apparent quantum yield would decrease with the thickness, while the reverse trend is observed. This explanation is consequently irrelevant in the case of our materials and should be dismissed.

A more sophisticated approach is the four flux theory of Maheu and coworkers [74, 75] which decomposes the total vertical streams into collimated and diffuse components. This model provides a suitable description of a wider range of illumination geometries (including the diffuse reflection in a specimen illuminated by a collimated beam as in an integrating sphere), as well as a better description of the scattering phenomena since it involves absorption and scattering coefficients which are directly computable from the Lorentz-Mie's parameters and thus, physically meaningful. This model is in good agreement with accurate numerical resolution of the radiative transfer equations by using Monte-Carlo's simulations [76] and is thus recommended in most cases [71, 77-79], including pigmented materials [80].

5. Designing an upgradable tool for complex formulations

Besides the establishment of a reliable model for the photothermal oxidation of unstabilized polypropylene, a prospection task has been performed in order to determine the feasibility of an efficient numerical tool for lifetime prediction, to quantity the required resources and to attempt proposing a strategic roadmap. In order to treat the industrial formulations for bumpers, the model should describe the effects of:

(i) So-called "elastomer-modified" matrixes, i.e. the previous TPO blends,
(ii) The introduction of fillers/pigments (talc, titanium dioxide, carbon black);
(iii) And, the incorporation of various antioxidants, including phosphites, phenols, Hindered Amine Light Stabilizers (HALS), UV-absorbers (benzotriazoles, benzophenones), and their potential degradation products.

These latter constituents would have various impacts on mechanical and/or aspects properties through various physico-chemical processes, in particular:

a. The inhibiting, retarding or prodegradant role of each additive on the oxidation process, which induces changes in both mechanical and aspect properties (whitening, gloss loss).
b. Polypropylene discoloration, i.e. yellowing, attributed to the formation of degradation products from either phenolic thermal stabilizers (quinone

methides) or triazine ring UV-absorbers (for instance, the Chimassorb 944 molecule, Ciba-Ceigy).

5.1. **Extension to complex formulations**

Such a purpose would practically imply to describe, for thermal stabilizers and/or their main degradation products:

(i) Their chemical reactivity, in particular the inhibiting effect of thermal stabilizers (hydrogen donors such as phenol and hydroperoxide decomposer such as thioester, and phosphites or the retarding effect of HALS,
(ii) Their physical loss by evaporation and/or water extraction (spaying),
(iii) Their diffusion in thick specimens,
(iv) Their photolysis,
(v) Their screening effect, in particular for UV-absorbers whose concentration varies along exposure time.

The two latter points are specific to the photothermal case. The impact of fillers will be also considered, in particular:

(vi) Their screening effect and the multiple scattering phenomena (UV-light attenuation)
(vii) Their direct effect on the oxygen diffusion by increasing the tortuosity of diffusion paths (shape factor)
(viii) Their additional effect on the stabilizers due to stabilizers adsorption at their surface.
(ix) The surface functionalization of fillers, for instance the presence of phenol groups at the surface of carbon blacks.

Each of these phenomena should be investigated deeply to generate a powerful numerical tool for lifetime prediction. Stabilization reactions (i) have been already studied in the laboratory but the corresponsing rate constants should be probably calibrated with the current set of parameters established for pure iPP. The general principles for treating items (ii) and (iii) have also been established but should be advantageously applied to generate antioxidant profiles in the case of HALS, and more particularly to investigate the potential synergisms between

migrants (of low molar mass such as Tinuvin 770) and non migrant molecules (of high molar mass such as Chimassorb 944). Items (iv) and (v) are specific to photooxidation. Among the remaining issues, the introduction of sorption model would be particularly valuable for understanding the effect of fillers on the migration of additives (viii).

5.2. **Risks and challenges in numerical simulation of aging**

The relevancy of the homogenization approach is questionable when microscopic or macroscopic heterogeneities are reported. In the case of stabilized materials, they can be reasonably ascribed to an improper incorporation of additives or to concentrations higher than their solubility threshold, implying blooming. Although markedly heterogeneous, the case of stabilized TPOs can still be envisaged by homogenization: similarly as for the unstabilized matrix, the concentrations in stabilizers in each phase would obey to the solubility ratios. In contrast, the case of fillers and particularly the points (xiii) and (ix) might require considering heterogeneous kinetics. The alternative would be to consider some "worst case" approach at the cost of substantial safety margins.

This kind of modeling approach focuses on the material properties, not on the car part. In this perspective, it would be necessary to apply the model by taking into account the residual levels of thermo-mechanical stresses coming from processing and the specific geometry of the car part, i.e. to extend the model to the three spatial dimensions. Admittedly, the development of a whole modeling line would be noticeably valuable for reducing the certification time but this is obviously a long term goal.

5.3. **Numerical issues**

If numerical simulation considerably enriches the perspectives of the kinetic model, its specific issues must not be occulted. Indeed, the introduction of new chemical, physical or optical phenomena into the kinetic model requires first their suitable mathematical translation in equations (e.g. the spectral overlap integral for describing the selectivity of UV-light sources) and then requires their numerical solving, an issue rather pertaining to numericians.

First of all, it is necessary to precise that numerical solving of systems of ordinary differential equations (SDE) can be very awkward because of their high stiffness: owing to the very different characteristic times of the elementary processes, mass matrices are very sparse.

Moreover, it requires satisfying the consistency of initialization conditions. These difficulties typically happen when solving problems with high numbers of spatial discretization steps (> 1000), or when introducing many phenomena such as the effects of several stabilizers.

The mathematical formalism of the problem can also involve different kinds of equations including Differential Algebraic Equations (DAE) or systems of Partial Derivative Equations (PDE). The former has appeared for describing the UV-light attenuation in the sample thickness through the Beer-Lambert's law whose attenuation factor contains a time-dependent term. This improvement enabled introducing the screening effect of chromophoric species whose concentration varies along exposure time. These species consist in oxidation products in unstabilized iPP and, in future developments, in additives dissipating UV-light (e.g. UV stabilizers). The latter PDE systems would be encountered for describing the specific issues of UV-light attenuation, such as double-side exposure, or multiple scatterings, by using multi-flux methods. Previously, these phenomena have been described only for initial materials, which has required to solve ODE systems with boundary conditions. Describing their coupling with the aging process is expected to be still more awkward, since would imply to solve PDE systems very constrained by boundary conditions.

Since this approach requires a powerful numerical tool, it has been decided to use robust algorithms proposed in existing libraries. However, each algorithm can be used only in a restricted perimeter of validity: for instance, the ODE23s and ODE15s Matlab algorithms are not suitable for most of DAE systems (of index higher than unity). To overpass such a difficulty, it can be envisaged to use other solvers and/or any specific software since:

(i) Additional routines implemented in Matlab are supplied by numerical groups (see for instance http://www.unige.ch/~hairer/software.html)
(ii) Higher index methods are also available in other software.
(iii) Fully integrated software with graphical interfaces are available (e.g. COMSOL)

In the present work, solving has been performed by using DASSL methods implemented in Open Modelica whose solutions have been exported and post-treated in Matlab.

No doubt that improving the robustness of integration methods constitutes a major challenge but pertaining to numericians. It is likely that the use a single general solver for every cases is

illusory and that specific solvers have to be selected depending on the exposure conditions and polymeric formulations under investigation.

However, this work has enabled to highlight several numerical challenges which arise in homogeneous kinetics. Long-term model improvements would also require developments of numerical tools for describing heterogeneous kinetics (i.e. three dimensions problems) in industrial parts.

6. Appendix: A general framework for the kinetic treatment of photosensitization reactions

The review of Turro [38] gives us an extremely relevant framework for the conceptualization and the quantitative introduction of energy transfers into the kinetic model. Basically, different kinds of energy transfers can occur:

(i) Radiative energy transfers, so-called “Trivial emission-reabsorption mechanism”, occurring over large distances between the donor and the acceptor molecules.

By opposition, other energy transfers basically result from radiationless interactions between the molecular orbitals (wave functions) describing the initial (excited donor and ground state acceptor molecules) and final electronic configurations. These latter can be approximed as the sum of a resonance (or coulombic) and exchange terms.

(ii) Resonance excitation involves coulombic interactions between the electrons and nuclei of two molecular systems. It can be considered as a “dipole-dipole” interaction.

(iii) Exchange energy transfer in which electrostatic interactions involve exchange or crossed transitions of valence electrons between the two molecular systems. This requires finite overlapping of their respective electronic clouds and so, only occurs over short wavelength ranges, typically not exceeding twice the collisional diameter.

(iv) True molecules collisions or so-called dynamic quenching. This can be neglected in the case of rigid media such as polymers.

In all cases, the rate constant of energy transfer k_{ET} must satisfy structural and energetic requirements and would obey to a law of the form:

$$k_{ET} \propto f(R_{DA}) \cdot J \qquad \textbf{Eq. A. 1}$$

Here, f(R_{DA}) is function of the distance between the donor and acceptor, specific to the type of energy transfer. It is noteworthy that these dependence can be particularly complex when involving molecules diffusion or energy migration (sequences of highly efficient energy transfers). The term J is the normalized spectral overlap integral between the emission spectrum of the donor and the absorption spectrum of the acceptor. This term constitutes an energetic requirement of energy transfer and accounts for the density of transitions which are energetically allowed including the Franck-Condon's effect:

$$J = \int_{\lambda_{min}}^{\lambda_{max}} \frac{\varphi_{D^*}(\lambda)}{\varphi_{D^*}^{max}} \cdot \frac{\varepsilon_A(\lambda)}{\varepsilon_A^{max}} \, d\lambda = \int_{\lambda_{min}}^{\lambda_{max}} f_D \cdot f_A \, d\lambda \qquad \textbf{Eq. A. 2}$$

with f_D and f_A the respective spectral distribution of the donor emission and acceptor absorption.

More specifically, it can be relevant to write the complete spectral overlap integral of energy transfer $J_{D^*\rightarrow A}^{ET}$ (in einstein.L^{-1}.s^{-1}), without any normalization, which well describes the resonance (or Coulombic) and radiative –but not exchange- energy transfers, since an oscillating electronic dipole can describe the electric field of a light wave.

$$J_{D^*\rightarrow A}^{ET} = \int_{\lambda_{min}}^{\lambda_{max}} \varphi_{D^*}(\lambda) \, J_D \, [D] \cdot \ln(10) \, \varepsilon_A(\lambda) \, \Delta z \, [A] \, d\lambda$$
$$= [A] \cdot \left(\int_{\lambda_{min}}^{\lambda_{max}} \ln(10) \, \varphi_{D^*}(\lambda) \, \varepsilon_A(\lambda) \, \Delta z \, d\lambda \right) \cdot J_D \, [D] \qquad \textbf{Eq. A. 3}$$

with $\varphi_D(\lambda)$ the spectral distribution of the quantum yield of luminescence (or light emission), including all types of fluorescences and phosphorescences (in Einstein.einstein^{-1}.nm^{-1}), $\varepsilon_A(\lambda)$ the spectral distribution of the molar extinction coefficient (in L.mol^{-1}.cm^{-1}), [D] and [A] the respective concentrations of donor and acceptor molecules (in mol.L^{-1}), $J_D$the spectral overlap integral of light absorption (in einstein.mol^{-1}.s^{-1}) such as the overall light absorbed by the donor is equal to J_D [D].

This equation has the advantage of making explicit the dependence of the energy transfer to the concentrations of both the donor and acceptor molecules, in good agreement with a generalized formalism explicating the efficiency of the energy transfer φ_{ET}:

$$I_{D*\rightarrow A}^{ET} = \Phi_{ET} \cdot J_D\,[D] = \frac{k_{ET}\,[A]}{k_{ET}\,[A] + k_D} \cdot J_D\,[D] \qquad \textbf{Eq. A. 4}$$

with [A] the concentration of donor molecules (in mol.L^{-1}), k_{ET} and k_D the rate constants of energy transfer and energy decay of the donor molecules.

Structural considerations must also be taken into account in terms of spin multiplicity (Wigner's spin rule). The elementary processes involving a change in spin multiplicity ($\Delta S \neq 0$), for instance singlet-triplet or triplet-singlet processes, are noticeably slower than the others and thereby considered as spin-forbidden (as the opposite of spin-allowed). However, even spin-forbidden processes can occur, provided that the donor excited state has very long lifetime (their probability is small but finite), usually only through an exchange energy transfer.

Eventually, the main goal in the present formal kinetic approach consists in making explicit the main time-dependent terms. Then the transferred energy would be of the form:

$$I_{D*\rightarrow A}^{ET} = \psi \cdot [A] \cdot J_D\,[D] \qquad \textbf{Eq. A. 5}$$

with ψ a constant independent of concentration for the given couple of acceptor and donor molecules, such as:

$$\psi \propto f(R_{DA}) \cdot \int_{\lambda_{min}}^{\lambda_{max}} \ln(10)\ \varphi_D(\lambda)\ \varepsilon_A(\lambda)\ \Delta z\ d\lambda \qquad \textbf{Eq. A. 6}$$

In this latter expression, the key variable is probably the quantum yield of luminescence $\varphi_{D*}(\lambda)$, since it accounts for the competition of the energy transfer with other primary processes of energy decay, when using this formalism. No doubt it is the more difficult to obtain (because of scarce literature data), which makes thereby the calculation of ψ very difficult. Eventually, this was anyway off-topic since it is not indispensable for introducing the energy transfers into the kinetic model. Thus, it appears as an adjustable parameter in the optimization procedure (by inverse resolution method).

In the case of an energy transfer from ketones to hydroperoxides, the coexistence of both singlet and triplet excited states implies several peculiarities:

(i) The subsequent transfers (i.e. singlet-singlet or triplet-singlet) obey to different spin multiplicities and thus, occur potentially through different kinds of energy transfers. The triplet-singlet energy transfer is thus spin-forbidden but conceivable due to the rather high lifetime of its triplet state.

(ii) The quenching of the triplet state by singlet oxygen, as reported by Trozollo and Winslow [81], or another metal chelates can be envisaged [82]. This would impact the values of $\varphi_{D^*}(\lambda)$ and φ_{ET} (Ψ in our formalism).

(iii) The value of the spectral overlap integral $J_{D^*\rightarrow A}^{ET}$ is expected to be very low when considering the low absorptivity and emissivity of ketones, and the low absorptivity of hydroperoxides. Resonance mechanisms would thereby prevail but they require a small distance between the donor and acceptor molecules, in agreement with the estimation of 1 nm for the oxidation of neighboring monomer units (intramolecular energy transfer) [34].

References

[1] F.H. McTigue , M. Blumberg, Modern Plastics, 44 (1967) 145.
[2] P. Vink, Photooxidation of polypropylene Journal of Applied Polymer Science: Applied Polymer Symposium, 35 (1979) 265-273.
[3] T.A. Bogayevskaya, B.A. Gromov, V.B. Miller, T.V. Monakhova, Y.A. Shlyapnikov, Effect of the supermolecular structure of polypropylene on its oxidation kinetics, Polymer Science U.S.S.R., 14 (1972) 1741-1746.
[4] N.Y. Rapoport, S.I. Berulava, A.L. Kovarskii, I.N. Musayelyan, Y.A. Yershov, V.B. Miller, The kinetics of thermo-oxidative degradation of oriented polypropylene in relation to the structure and molecular mobility of the polymer, Polymer Science U.S.S.R., 17 (1975) 2901-2909.
[5] P. Vink, The Photo-Oxidation of Polyolefins - Structural and Morphological Aspects, in: e.N.S. Allen (Ed.) Degradation and Stabilisation of Polyolefins, Applied Science Publishers, London, 1983, pp. 213-246.
[6] W. Vieth, W.F. Wuerth, Transport properties and their correlation with the morphology of thermally conditioned polypropylene, Journal of Applied Polymer Science, 13 (1969) 685-712.
[7] S. Nishimoto, T. Kagiya, Y. Watanabe, M. Kato, Material design of radiation resistant polypropylene: Part II-Importance of the smectic structure produced by quenching treatment, Polymer Degradation and Stability, 14 (1986) 199-208.
[8] M. Obadal, R. Cermak, M. Raab, V. Verney, S. Commereuc, F. Fraïsse, Structure evolution of □-and beta-polypropylenes upon UV irradiation: A multiscale comparison, Polymer Degradation and Stability, 88 (2005) 532-539.
[9] M. Obadal, R. Cermak, M. Raab, V. Verney, S. Commereuc, F. Fraïsse, Study on photodegradation of injection-moulded Î²-polypropylenes, Polymer Degradation and Stability, 91 (2006) 459-463.
[10] T. Scherzer, H. Langguth, Temperature Dependence of the Oxygen Solubility in Acrylates and its Effect on the Induction Period in UV Photopolymerization, Macromolecular Chemistry and Physics, 206 (2005) 240-245.
[11] Y. Kato, D.J. Carlsson, D.M. Wiles, The photo-oxidation of polypropylene: Some effects of molecular order, Journal of Applied Polymer Science, 13 (1969) 1447-1458.
[12] H. Nakatani, S. Suzuki, T. Tanaka, M. Terano, New kinetic aspects on the mechanism of thermal oxidative degradation of polypropylenes with various tacticities, Polymer, 46 (2005) 12366-12371.
[13] S. Suzuki, Y. Nakamura, A.T.M.K. Hasan, B. Liu, M. Terano, H. Nakatani, Dependence of tacticity distribution in thermal oxidative degradation of polypropylene, Polymer Bulletin, 54 (2005) 311-319.
[14] M.S. Rabello, J.R. White, Crystallization and melting behaviour of photodegraded polypropylene -- I. Chemi-crystallization, Polymer, 38 (1997) 6379-6387.

[15] R. Mani, R.P. Singh, S. Sivaram, J. Lacoste, Effect of UV irradiation on the structure of heterophasic ethylene-propylene copolymers, Polymer Journal, 26 (1994) 1132-1141.
[16] M. Elvira, P. Tiemblo, J.M. Gómez-Elvira, Changes in the crystalline phase during the thermo-oxidation of a metallocene isotactic polypropylene. A DSC study, Polymer Degradation and Stability, 83 (2004) 509-518.
[17] P. Tiemblo, J.M. Gómez-Elvira, S. García Beltrán, L. Matisova-Rychla, J. Rychly, Melting and α relaxation effects on the kinetics of polypropylene thermooxidation in the range 80-170°C, Macromolecules, 35 (2002) 5922-5926.
[18] J.J. Janimak, S.Z.D. Cheng, A. Zhang, E.T. Hsieh, Isotacticity effect on crystallization and melting in polypropylene fractions: 3. Overall crystallization and melting behaviour, Polymer, 33 (1992) 728-735.
[19] V. Virkkunen, P. Laari, P. Pitkänen, F. Sundholm, Tacticity distribution of isotactic polypropylene prepared with heterogeneous Ziegler-Natta catalyst. 2. Application and analysis of SSA data for polypropylene, Polymer, 45 (2004) 4623-4631.
[20] V. Virkkunen, P. Laari, P. Pitkänen, F. Sundholm, Tacticity distribution of isotactic polypropylene prepared with heterogeneous Ziegler-Natta catalyst. 1. Fractionation of polypropylene, Polymer, 45 (2004) 3091-3098.
[21] R. Paukkeri, A. Lehtinen, Thermal behaviour of polypropylene fractions: 1. Influence of tacticity and molecular weight on crystallization and melting behaviour, Polymer, 34 (1993) 4075-4082.
[22] S. Qian, T. Igarashi, K.-H. Nitta, Influence of Thermo-degradation on the Crystallization Kinetics of Isotactic Polypropylene with a Beta□Nucleating Agent, Journal of Macromolecular Science, Part B, 52 (2013) 48-64.
[23] J. Kang, J. Li, S. Chen, H. Peng, B. Wang, Y. Cao, H. Li, J. Chen, J. Gai, F. Yang, M. Xiang, Investigation of the crystallization behavior of isotactic polypropylene polymerized with different Ziegler-Natta catalysts, Journal of Applied Polymer Science, 129 (2013) 2663-2670.
[24] D.J. Carlsson, D.M. Wiles, The photodegradation of Polypropylene Films. III. Photolysis of polypropylene hydroperoxydes, Macromolecules, 2 (1969) 597-606.
[25] D.J. Carlsson, D.M. Wiles, The Photodegradation of Polypropylene Films. II. Photolysis of Ketonic Oxidation Products, Macromolecules, 2 (1969) 587-597.
[26] D.J. Carlsson, D.M. Wiles, The Photooxidative Degradation of Polypropylene. Part I. Photooxidation and Photoinitiation Processes, Journal of Macromolecular Science, Part C, Polymer Reviews 14 (1976) 65 - 106.
[27] J.H. Adams, Analysis of the nonvolatile oxidation products of polypropylene I. Thermal oxidation, Journal of Polymer Science Part A-1: Polymer Chemistry, 8 (1970) 1077-1090.
[28] J.H. Adams, Analysis of nonvolatile oxidation products of polypropylene. III. Photodegradation, Journal of Polymer Science Part A-1: Polymer Chemistry, 8 (1970) 1279-1288.
[29] A. François-Heude, E. Richaud, A. Guinault, E. Desnoux, X. Colin, On the impact of oxygen transport properties on the polypropylene thermal oxidation. Part I: Effect of oxygen solubility Submitted in: Journal of Applied Polymer Science, (2014).
[30] J. Lacoste, D. Vaillant, D.J. Carlsson, Gamma-, photo-, and thermally-initiated oxidation of isotactic polypropylene, Journal of Polymer Science Part A: Polymer Chemistry, 31 (1993) 715-722.
[31] D.M. Mowery, R.A. Assink, D.K. Derzon, S.B. Klamo, R.L. Clough, R. Bernstein, Solid-State 13C NMR Investigation of the Oxidative Degradation of Selectively Labeled Polypropylene by Thermal Aging and Î³-Irradiation, Macromolecules, 38 (2005) 5035-5046.
[32] E. Guillet J, Studies of the mechanism of polyolefin photodegradation, Pure and Applied Chemistry, 52 (1980) 295-294.
[33] E. Guillet J, Studies of energy transfer and molecular mobility in polymer photochemistry, Pure and Applied Chemistry, 49 (1977) 249-258.
[34] G. Geuskens, C. David, The photo-oxidation of polymers. A comparison with low molecular weight compounds Pure and Applied Chemistry 51 (1979) 233-240.
[35] N.L. Maecker, D.B. Priddy, Photodegradation of ethylene–propylene copolymer and ethylene–propylene–ethylidene norbornene terpolymer, Journal of Applied Polymer Science, 42 (1991) 21-33.
[36] K. Tokumaru, Complications in photochemistry of organic peroxides, Research on Chemical Intermediates, 22 (1996) 255-273.

[37] C. Walling, M.J. Gibian, The photosensitized decomposition of peroxides, Journal of the American Chemical Society, 87 (1965) 3413-3417.
[38] N.J. Turro, Energy Transfer Processes, Pure and Applied Chemistry, 49 (1977) 405-429.
[39] O. Cicchetti, F. Gratani, The effect of titanium compounds on photo-oxidation of 2,4,6,8-tetramethylnonane (a liquid model of polypropylene), European Polymer Journal, 8 (1972) 561-573.
[40] L. Achimsky, Etude cinétique de la thermooxydation du polypropylène, in: Mécanique et Matériaux, Université Pierre et Marie-Curie (Paris VI), Paris, 1996.
[41] S. Girois, Photooxydation du polypropylène : aspects cinétiques in: Mécanique et Matériaux, Ecole Nationale Supérieure des Arts et Métiers, 2001.
[42] J. Pospisil, Z. Horak, Z. Kruliis, S. Nespurrek, S.-i. Kuroda, Degradation and aging of polymer blends I. Thermomechanical and thermal degradation, Polymer Degradation and Stability, 65 (1999) 405-414.
[43] J. Tocháček, J. Jančář, J. Kalfus, P. Zbořilováa, Z. Buráňa, Degradation of polypropylene impact-copolymer during processing, Polymer Degradation and Stability, 93 (2008) 770-775.
[44] N. Manabe, Y. Yokota, H. Nakatani, S. Suzuki, L. Boping, M. Terano, Study of local oxidative degradation in polypropylene impact copolymer by energy dispersive X-ray system, Polymer Bulletin, 54 (2005) 141-145.
[45] F.P. La Mantia, A. Valenza, D. Acierno, Thermomechanical degradation of blends of isotactic polypropylene and high density polyethylene, Polymer Degradation and Stability, 13 (1985) 1-9.
[46] R. Arnaud, J. Lemaire, A. Jevanoff, Photo-oxidation of ethylene-propylene copolymers in the solid state, Polymer Degradation and Stability, 15 (1986) 205-218.
[47] J. Tocháček, J. Jančář, J. Kalfus, S. Hermanová, Processing stability of polypropylene impact-copolymer during multiple extrusion â€“ Effect of polymerization technology, Polymer Degradation and Stability, 96 (2011) 491-498.
[48] J. Jancar, J. Tochacek, Effect of thermal history on the mechanical properties of three polypropylene impact-copolymers, Polymer Degradation and Stability, 96 (2011) 1546-1556.
[49] S. Hermanová, J. Tocháček, J. Jančář, J. Kalfus, Effect of multiple extrusion on molecular structure of polypropylene impact copolymer, Polymer Degradation and Stability, 94 (2009) 1722-1727.
[50] H. Nakatani, N. Manabe, Y. Yokota, H. Minami, S. Suzuki, F. Yamaguchi, M. Terano, Studies of thermal oxidative degradation of polypropylene impact copolymer using the temperature rising elution fractionation method, Polymer International, 56 (2007) 1152-1158.
[51] N. Manabe, Y. Yokota, H. Nakatani, S. Suzuki, B. Liu, M. Terano, Local thermal degradation behavior of heterophasic polypropylene copolymers, Journal of Applied Polymer Science, 100 (2006) 1831-1835.
[52] Z.-q. Fan, Y.-q. Zhang, J.-t. Xu, H.-t. Wang, L.-x. Feng, Structure and properties of polypropylene/poly(ethylene-co-propylene) in-situ blends synthesized by spherical Zieglerâ€“Natta catalyst, Polymer, 42 (2001) 5559-5566.
[53] H.N. Cheng, G.H. Lee, Two-dimensional NMR studies of polypropylene tacticity, Polymer Bulletin, 13 (1985) 549-556.
[54] G. Monaco, A. Zambelli, Simple Trends in NMR Spectra of Vinyl Polymers: The 1H NMR Spectrum of Poly(propylene), Macromolecular Chemistry and Physics, 206 (2005) 203-209.
[55] H.N. Cheng, Carbon-13 NMR analysis of ethylene-propylene rubbers, Macromolecules, 17 (1984) 1950-1955.
[56] R. Mani, R.P. Singh, S. Sivaram, Kinetics of thermal decomposition of heterophasic ethylene-propylene copolymers, Journal of Macromolecular Science - Pure and Applied Chemistry, A31 (1994) 413-425.
[57] R.P. Singh, A. Singh, Photodegradation of heterophasic ethylene-propylene copolymers in the solid state, Journal of macromolecular science. Chemistry, A28 (1991) 487-502.
[58] X. Colin, E. Richaud, J. Verdu, C. Monchy-Leroy, Kinetic modelling of radiochemical ageing of ethylene-propylene copolymers, in: I.R.a. Polymers (Ed.) Proceedings of the 8th International Symposium on Ionizing Radiation and Polymers, Elsevier, Angra dos Reis, Rio de Janeiro, Brazil, 12-17 October 2008, 2008, pp. 6.

[59] N. Khelidj, X. Colin, L. Audouin, J. Verdu, C. Monchy-Leroy, V. Prunier, Oxidation of polyethylene under irradiation at low temperature and low dose rate. Part II. Low temperature thermal oxidation, Polymer Degradation and Stability, 91 (2006) 1598-1605.
[60] N. Khelidj, X. Colin, L. Audouin, J. Verdu, C. Monchy-Leroy, V. Prunier, Oxidation of polyethylene under irradiation at low temperature and low dose rate. Part I. The case of "pure" radiochemical initiation, Polymer Degradation and Stability, 91 (2006) 1593-1597.
[61] J.B. Knight, P.D. Calvert, N.C. Billingham, Localization of oxidation in polypropylene, Polymer, 26 (1985) 1713-1718.
[62] A.S. Michaels, H.J. Bixler, Solubility of gases in polyethylene, Journal of Polymer Science, 50 (1961) 393-412.
[63] A.S. Michaels, H.J. Bixler, Flow of gases through polyethylene, Journal of Polymer Science, 50 (1961) 413-439.
[64] J. Kolařk, Simultaneous prediction of the modulus, tensile strength and gas permeability of binary polymer blends, European Polymer Journal, 34 (1998) 585-590.
[65] T.J. Turton, J.R. White, Effect of stabilizer and pigment on photo-degradation depth profiles in polypropylene, Polymer Degradation and Stability, 74 (2001) 559-568.
[66] P. Kubelka, Errata: New Contributions to the Optics of Intensely Light-ScatteringMaterials. Part I, Journal of the Optical Society of America, 38 (1948) 1067-1067.
[67] P. Kubelka, New Contributions to the Optics of Intensely Light-Scattering Materials. Part I, Journal of the Optical Society of America, 38 (1948) 448-448.
[68] P. Kubelka, New Contributions to the Optics of Intensely Light-Scattering Materials. Part II: Nonhomogeneous Layers, Journal of the Optical Society of America, 44 (1954) 330-334.
[69] S.N. Thennadil, Relationship between the Kubelka-Munk scattering and radiative transfer coefficients, Journal of the Optical Society of America A, 25 (2008) 1480-1485.
[70] W.E. Vargas, Two-Flux Radiative Transfer Model Under Nonisotropic Propagating Diffuse Radiation, Applied Optics, 38 (1999) 1077-1085.
[71] W.E. Vargas, G.A. Niklasson, Applicability conditions of the Kubelka-Munk theory, Applied Optics, 36 (1997) 5580-5586.
[72] J.L. Saunderson, Calculation of the Color of Pigmented Plastics, Journal of the Optical Society of America, 32 (1942) 727-729.
[73] J. Holoubek, Light scattering and reflectance of optically heterogeneous polymers in multiple scattering regime, Polymer, 40 (1999) 277-280.
[74] B. Maheu, G. Gouesbet, Four-flux models to solve the scattering transfer equation: special cases, Applied Optics, 25 (1986) 1122-1128.
[75] B. Maheu, J.N. Letoulouzan, G. Gouesbet, Four-flux models to solve the scattering transfer equation in terms of Lorenz-Mie parameters, Applied Optics, 23 (1984) 3353-3362.
[76] B. Maheu, J.P. Briton, G. Gouesbet, Four-flux model and a Monte Carlo code: comparisons between two simple, complementary tools for multiple scattering calculations, Applied Optics, 28 (1989) 22-24.
[77] P.S. Mudgett, L.W. Richards, Multiple scattering calculations for technology II, Journal of Colloid and Interface Science, 39 (1972) 551-567.
[78] P. Edström, Examination of the revised Kubelka-Munk theory: considerations of modeling strategies, Journal of the Optical Society of America A, 24 (2007) 548-556.
[79] G.A. Niklasson, Comparison between four flux theory and multiple scattering theory, Applied Optics, 26 (1987) 4034-4036.
[80] P. Callet, Pertinent data for modelling pigmented materials in realistic rendering, Computer Graphics Forum, 15 (1996) 119-127.
[81] A.M. Trozzolo, F.H. Winslow, A Mechanism for the Oxidative Photodegradation of Polyethylene, Macromolecules, 1 (1968) 98-100.
[82] E. Guillet J, J. Dhanraj, J. Golemba F, H. Hartley G, Fundamental Processes in the Photodegradation of Polymers, in: Stabilization of Polymers and Stabilizer Processes, American Chemical Society, 1968, pp. 272-286.

General conclusions

1. Photothermal oxidation model

The original purpose of this PhD thesis was to design a numerical tool for the lifetime prediction of polypropylene-based automotive materials in terms of both mechanical and aspect properties whose origins is well-known to be the chain scissions. Since this degradation process results essentially from oxidation reactions, the model couples their kinetic with physical phenomena into a system of differential equations. The main advantage of such a kind of model is its upgradability, since additional physicochemical processes can be progressively introduced. As a result, the kinetic model has been established stepwise with developments according to three main axes: (i) exposure conditions, from thermal to photothermal ageing conditions, (ii) extension to thick specimens and (ii) large variety of additives, from unstabilized iPP to industrial formulations.

For developing a reliable numerical tool, the model parameters must be calibrated properly in order to avoid inaccuracies in extrapolation. The first stage has consisted in obtaining a universal kinetic model for thermal oxidation of iPP, i.e. describing the variability of thermal oxidation behaviors among the whole iPP familly in terms of both induction time and oxidation rate. Oxygen transport properties have been evidenced to be critical parameters accounting for the impact of both the molecular and morphological iPP features.

Then, the impact of UV-light has been introduced into the kinetic model to extent it to photothermal oxidation. This stage has required the proposal of a suitable kinetic formalism accounting for the impact of UV-light intensity and wavelength, i.e. UV-light selectivity in triggering damages. This development was mandatory in order to understand the quantitative differences between the different climatic devices commonly used for accelerating the natural ageing of polymers. As major result of this development, it has been evidenced that the photothermal oxidation can be effectively described by the “Closed-Loop Mechanistic Scheme” (CLMS) completed with additional photochemical initiation steps.

The model extension to thick specimens implies to focus on the competition between the chemical consumption and transport of - reactants, to which oxygen diffusion and and UV-light attenuation can be assimilated. Their respective behaviors have been described by the

second Fick's law and the Beer-Lambert law (i.e. an exponential decay) whose attenuation coeffiecient has been decomposed into time-dependent and independent terms.

2. Validity range

The model has thus been cautiously calibrated on a reference iPP whose characteristics has been determined in a large range of temperatures (from 45 to 230°C) and UV-light intensities (from 0.1 to 30 times the daily sunlight) with various types of light sources. Its validity has been checked without complacency in terms of self-consistency from our own experimental data, but also from literature data. These latter have been collected because the such a readjustment-based model requires lots of these datas whose determination is very time-consuming. Moreover, they have allowed checking the model universality on the whole iPP family.

This procedure has resulted in highlighting the validity domains of the kinetic model in terms of:

(i) Exposure conditions. For instance, the kinetic model would be valid up to about ten sunlight intensity presumably owing to the existence of multi-photonic excitations and/or termolecular reactions. This finding asks the relevancy of so-called ultra-accelerated testing procedures whose representativeness of natural weathering would not be ensured.

(ii) Time-validity. Currently, the kinetic model is calibrated in priority on species directly involved in the CLMS which ensures an accurate prediction of induction times. In contrast, oxidation rates would be impacted by several physical phenomena occurring at moderate conversion degrees of oxidation (i.e. just after the end of the induction period) such as VOCs emission, morphological heterogeneities (e.g. "skin/core structure") and rearrangements (e.g. chemi-crystallization or annealing) and early cracking at the sample surface which moves the front of oxygen supply towards deeper layers.

All these limitations result from simplifying assumptions introduced into the kinetic model, in particular formal kinetics because of the postulated unicity of reactive site, and the neglect of some physical phenomena (such as UV-light attenuation in the sample thickness due to light absorption by chromophores compared to opacity). Because of these simplifying assumptions, it is noteworthy that only the primary oxidation reactions can be modeled in a predictive manner.

Finally, the homogeneous kinetic approach would be suitable for unstabilized and unfilled iPP, at least for chain scissions, despite the unarguable multiphasic feature of semicrystalline polymers. This issue will have to be considered again for markedly heterogenous materials such as TPO blends.

3. Implications for industrial use

As immediate implication, the model predictivity in extrapolation will be only ensured up to the end of the induction period. For longer durations, the model validity is restricted to the range of photothermal exposures under investigation. At this stage of our research, the model reliability should be satisfactory for thin films, but not for thick plates in which relative importance of physical phenomena is higher. The existence of adjustable parameters (e.g. $[POOH]_0$ and, potentially, S_{O2}) also restrains our expectations in kinetic modeling. If these parameters are connected to measurable molecular or morphological characteristics, the kinetic modeling approach will provide trial-free tools for lifetime prediction. Otherwise, the kinetic modeling alone will not constitute a credible alternative to accelerated ageing tests.

From a practical point of view, the material certification by numerical simulation alone will require developing:

(i) Models accepting dynamic testing programs accounting for the daily or seasonal variations of environmental stresses (e.g. temperature, UV-light intensity, etc.), whereas current models only consider static exposure conditions.

(ii) A complete computer modeling chain for certifying the final automotive parts, i.e. including the influence of processing conditions. This procedure would require cartography of thermal stresses during processing, but also developments of 3D solving tools.

However, such a numerical tool is perfectly suitable for investigating competition between phenomena (e.g. thermal vs. photochemical initiation, chemical consumption vs. diffusion of molecular reagents) and thus, for testing and improving the quality of climatic devices aimed at simply accelerating the natural weathering. In addition to discuss about exposure conditions, such a kinetic model would also be valuable for optimizing the commercial polymer formulations, for instance by selecting a suitable package of antioxidants for given photothermal exposure conditions.

4. Numerical issues

Numerical issues must not be occulted since calculation with the available solvers during a reasonable time requires: (i) The translation of the physicochemical problem into equations in a suitable formalism, (ii) The choice of relevant initialization conditions, (iii) The selection of the most adequate and powerful solvers from the commercially available softwares.

The present work has only permitted to highlight challenges and needs in the kinetic modelling of photothermal processes. Next studies in this field will undoubtedly require the help and expertise of numericians, especially if one envisages treating the case of heterogeneous kinetics, which will require solving the kinetic model in the three spatial dimensions.

5. Transverse theoretical developments

Although specifically dedicated to polypropylene photothermal degradation, this PhD thesis has necessitated several theoretical developments which can be reused for other polymeric substrates or fields of research.

Firstly, the kinetic analytical development describing the oxygen partial pressure dependence of the oxidation kinetics has been considered in order to establish a common referential for determining the critical oxygen pressure. It has enabled comparing accurately the values coming from different authors.

Secondly, a framework has been proposed for formalizing the impact of both UV-light intensity and wavelength on the photothermal oxidation kinetics in both analytical and numerical models. These effects have been integrated into a single equation based on the calculation of various spectral overlap integrals. It allows envisaging numerical modeling the effects of UV-light characteristics on photochemical reactions encountered in photothermal degradation, but also in photo-polymerization with potential benefits in additive manufacturing. Moreover, it is likely that the proposed approach would result in better results for polymers containing intrinsic structural defects (i.e. included in monomer units themselves) whose concentrations and photochemical features would be clearly known. It would enable not to resort to formal kinetics.

Finally, the implementation of the Kulkelka-Munk's model with polychromatic radiations constitutes an innovative development and enables envisaging the investigation of UV-light attenuation in multiphasic materials.

6. Conclusion Générale [Translation in French]

Modèle d'oxydation photothermique

L'objectif original de cette these était de concevoir un outil numérique de prediction de la durée de vie de matériaux automobiles à base de polypropylene, en termes de propriétés mécaniques et d'aspect dont l'altération résulte des coupures de chaines macromoléculaires. Puisque ce processus de dégradation résulte essentiellement des réactions d'oxydation, le modèle couple leur cinétique avec des phénomènes physiques en un système d'équations différentielles. Le principale d'un tel modèle est son évolutivité, puisque des phénomènes physico-chimiques peuvent être progressivement introduits. Par conséquent, le modèle cinétique a été établi par étapes avec des améliorations selon trois directions : (i) les conditions d'exposition, allant du thermique vers le photothermique, (ii) le passage à la pièce épaisse, et (iii) la multiplication des constituants, en allant de l'iPP vers les formulations industrielles.

Dans l'optique d'établir un outil numérique fiable, les paramètres du modèle doivent être calibrés ave soin de manière à prévenir les imprécisions lors d'extrapolations. La première étape a consisté à obtenir un modèle cinétique universel pour la thermooxydation de l'iPP, c'est-à-dire décrivant la variabilité des comportements au sein de la famille des iPP à la fois en termes de temps d'induction et de vitesse d'oxydation. Les propriétés de transport du dioxygène ont été mises en évidence comme des paramètres critiques traduisant l'impact des caractéristiques moléculaires et morphologiques des iPP.

Ensuite, l'impact de la lumière UV a été introduit dans le modèle cinétique pour l'étendre au cas de la photo-thermo-oxydation. Cette étape a nécessité de proposer un formalisme adéquat traduisant à la fois l'influence de l'intensité et de la longueur d'onde des rayonnements, c'est-à-dire la sélectivité de la lumière sur l'endommagement. Ces développements étaient indispensables pour comprendre les différences quantitatives engendrées selon les différents équipements climatiques utilisés couramment pour accélérer le vieillissement naturel des polymères. L'une des résultats majeurs de cette étude est que l'oxydation photo-thermique peut effectivement être décrite par le schéma mécanistique en éboucle ferméeé, complété de réactions d'amorçage photochimique.

L'extension du modèle aux pièces épaisses implique de se concentrer sur la compétition entre la consommation chimique et le transport des réactifs migrants auxquels peuvent être assimilés le dioxygène, diffusant dans le matériau et la lumière UV, atténuée dans l'épaisseur sous l'effet de l'opacité et des composés chromophores. Leurs comportements respectifs ont

été décrits au moyen de la seconde loi de Fick et une loi de Beer-Lambert, i.e. une loi de décroissance exponentielle dont le coefficient d'atténuation a été composé en deux termes, l'un dépendant et l'autre indépendant du temps.

Domaine de validité

Le modèle a été calibré avec soin sur un iPP de reference dont les caractéristiques ont été déterminées dans un large domaine de temperature (de 45 à 230°C), d'intensités lumineuses (allant d'environ 1/10^{e} à 30 fois l'énergie solaire) sous différentes sources lumineuses. Sa validité a été vérifié sans complaisance en termes d'autocohérence avec nos données expérimentales, mais également à partir des données de la litérature. Ces dernières ont été récupérées car le recalage de modèle nécessite un grand nombre de ces données expérimentales dont la détermination est très chronophage. De plus, elles ont permiss de vérifier l'universalité du modèle pour la famille des iPP. Cette procédure a conduit à mettre en lumière les domaines de validité du modèle en termes de:

(iii) Conditions d'exposition. Par exemple, le modèle cinétique serait valide jusqu'à environ 10 intensités solaires, probablement à cause d'excitations multiphotoniques et/ou de réactions termoléculaires. Ce résultat questionne la pertinence des méthodes de vieillissement dites « ultra-accélérées » dont la représentativité par rapport au vieillissement naturel n'est pas assurée.

(iv) Validité temporelle. Actuellement, le modèle cinétique est calibré en priorité sur les espèces impliquées directement dans le schéma mécanistique en boucle fermée, ce qui garantit une prédiction fiable des temps d'induction. Toutefois les vitesses d'oxydation seraient impactées par divers phénomènes physiques se produisant à des taux d'avancement modérés (peu après la période d'induction) tels que les émissions de produits volatils, les hétérogénéités morphologiques (e.g. structure « cœur/peau »), les réarrangements macromoléculaires (par exemple, la chimicristallisation et le recuit) et la fissuration précoce en surface de l'échantillon qui déplace le front d'alimentation en oxygène vers les couches inférieures du matériau.

Toutes ces limitations résultent d'hypothèses simplificatrices introduites dans le modèle cinétique, en particulier le postulat d'unicité du site réactif en cinétique formelle, ou au fait de négliger les phénomènes physiques (telle que l'atténuation due aux chromophores comparée à celle due à l'opacité). A cause de ces hypothèses simplificatrices, il est notable que seules les réactions d'oxydation primaires peuvent être modélisées de manière prédictive.

Finalement, l'approche de cinétique homogène serait adéquate pour des iPP non additivés et non charges, du moins en termes de coupures de chaînes, en dépit du caractère multiphasique indéniable des matériaux semi-cristallins. Cette problématique est à reconsidérer pour des matériaux ouvertement hétérogènes comme les alliages TPO.

Implications sur l'usage industriel

Comme implication immédiate, il apparaît que la prédictivité du modèle en extrapolation va être uniquement assure jusqu'à la fin de la période d'induction. Sur des durées plus longues, la validité du modèle est restreinte au domaine de conditions étudiées. A cette étape de nos recherches, la fiabilité du modèle devrait être satisfaisante pour des films minces, mais pas pour des plaques épaisses dans lesquelles l'importance des phénomènes physiques est accentuée. L'existence de paramètres ajustables (par exemple $[POOH]_0$ et S_{O2}) modèrent également nos attentes vis-à-vis de la modélisation cinétique. Si ces paramètres reliés à des caractéristiques moléculaires ou morphologiques mesurables, la modélisation cinétique apportera des outils/lois sans essais de prédiction de durée de vie. A défaut, la modélisation cinétique ne constituera pas à elle seule une alternative crédible aux essais de vieillissement accélérés.

D'un point de vue pratique, la certification des matériaux par seule simulation numérique nécessiterait de développer :

(iii) Des modèles acceptant des programmes d'essais dynamiques traduisant les variations quotidiennes et saisonnières de contraintes environnementales (dont la température, l'intensité en lumière UV, etc.), tandis que les modèles actuels ne considèrent que des conditions d'exposition statiques.

(iv) Une chaîne complète de modélisation pour certifier les pièces automobiles finies, c'est-à-dire incluant l'influence de la mise en œuvre. Cela requiert une cartographie des contraintes thermiques appliquées au matériau durant sa mise en œuvre (simulation du processus d'injection avec *Moldflow*) ainsi que le développement d'outils de résolution dans les trois dimensions de l'espace.

Toutefois, l'outil numérique propose est parfaitement adéquate pour étudier la compétition des phénomènes (telle l'amorçage thermique vs. photochimique, la consommation chimique vs. la diffusion des réactifs moléculaires) et ainsi, pour tester et améliorer la qualité des moyens d'essais visant à accélérer simplement le vieillissement naturel. De plus de discuter les conditions d'exposition, un tel modèle cinétique est aussi valorisable pour optimiser les

formulations commerciales de polymères, par exemple en sélectionnant un mélange adéquat d'antioxydants pour des conditions d'exposition photothermique données.

Problématiques numériques

Les problématiques numériques ne doivent pas être occultées car les calculs au moyen des solveurs à disposition en un temps raisonnable requiert: (i) La mise en équations du problème physico-chimique avec un formalism adéquat, (ii) le choix de conditions d'initialisation pertinentes, (iii) la sélection des solveurs les plus adaptés et performants parmi ceux proposés dans les logiciels commerciaux.

Le travail présent n'a permis que de mettre en lumière les défis et les besoins en modélisation cinétique des processus photothermiques. Les prochaines études dans le domaine vont indubitablement nécessiter l'assistance et l'expertise de numériciens, tout spécialement si l'on envisage de traiter le cas de cinétiques hétérogènes, qui vont impliquer des résolutions dans les trios dimensions de l'espace.

Développements théoriques transverses

Bien que dédié spécifiquement à la dégradation photothermique du polypropylène, cette thèse de doctorat a nécessité plusieurs développements théoriques qui peuvent être réutilisés pour d'autres substrats polymériques ou d'autres domaines de recherche. D'abord, le développent cinétique analytique décrivant la dépendance des cinétiques d'oxydation à la pression partielle en dioxygène a été considérée de manière à établir un référentiel commun pour déterminer les pressions critiques. Cela a permis de comparer efficacement les résultats de divers auteurs.

Ensuite, un cadre a été propose pour formaliser l'impact de l'intensité et de la distribution spectral d la lumière UV sur les cinétiques d'oxydation photo-thermiques dans les modèles analytiques et numériques. Ces effets ont été intégrés dans une simple relation basée sur le calcul des intégrales de recouvrement spectral. Cela permet d'envisager la prise en compte des caractéristiques de la source lumineuse sur les réactions photochimiques rencontrées en dégradation photothermique, mais aussi en photopolymerisation avec des retombées éventuelles en fabrication additive. De plus, il est probable que l'approche proposée se traduise par de meilleurs résultats pour les polymères contenant des défauts de structure intrinsèques (c'est-à-dire faisant partie intégrante de l'unité monomère) dont les concentrations et les caractéristiques photochimiques seraient clairement établies, permettant ainsi un recours moindre à la cinétique formelle. Enfin, l'implémentation du modèle de Kubelka-Munk au cas des rayonnements polychromatiques constitue une innovation et permet d'envisager une description précise de l'atténuation de la lumière UV dans les matériaux multiphasiques ou des géométries plus complexes.

Figures and tables captions

Chapter 1

Chapter2

Part1 :

Chapter3

Chapter4

Chapter5

Part2 :

Chapter6

Chapter7

Chapter8

General discussion : Chapter9

MODELISATION CINETIQUE DE LA PHOTO-THERMO-OXYDATION DU POLYPROPYLENE

Le développement d'outils numériques de prédiction de la durée de vie des polymères constitue un levier prometteur pour réduire les durées des processus de certification de ces matériaux dans le domaine automobile sans sacrifier leur fiabilité. Cette thèse s'applique à la modélisation de la photo-thermo-oxydation du polypropylène isotactique (iPP), laquelle est responsable de l'altération de ses propriétés mécaniques et d'aspect. L'approche adoptée consiste à coupler la cinétique des réactions de photo- et thermo-oxydation avec des phénomènes physiques, comme le transport du dioxygène et l'atténuation de la lumière UV dans l'épaisseur du matériau, pour décrire l'ensemble des évolutions physico-chimiques. Les propriétés aux échelles supérieures, sur lesquelles seront définis les critères de fin de vie, seront calculées *a posteriori* en appliquant les relations structure-propriété adéquates. Le principal enjeu était d'étendre le modèle cinétique de vieillissement thermique préexistant au vieillissement photo-thermique en prenant en compte les réactions d'amorçage photolytique. De lourdes campagnes d'essais de vieillissement et de caractérisation menées sur un iPP de référence, ainsi qu'une capitalisation exhaustive des données de la littérature d'autres iPPs, ont permis de mettre au point un modèle cinétique de photo-thermo-oxydation et de le généraliser à l'ensemble de la famille des iPPs dans de larges domaines de pression partielle d'oxygène (de 0.2 à 50 bars), de température (de 40 à 230°C) et d'exposition à la lumière UV (intensités et sources lumineuses variables) décrivant des conditions de vieillissements naturels et accélérés. La validation expérimentale du modèle a permis d'étayer l'approche cinétique et de montrer ses limites, mais aussi de révéler un certain nombre d'enjeux numériques. Le modèle a été conçu pour être un outil numérique évolutif qui permettra, à terme, d'optimiser la représentativité des méthodes d'essais de vieillissement et la performance des formulations commerciales d'iPP. L'ensemble de ces développements théoriques et numériques peut être appliqué à la photo-thermo-dégradation d'autres types de polymères, mais aussi dans d'autres champs d'application de la photochimie macromoléculaire telle que la photo-polymérisation UV.
Mots-Clés : Polypropylène, photo-thermo-oxydation, contrôle par la diffusion d'oxygène, effet d'écran, modélisation cinétique, prédiction de durée de vie.

KINETIC MODELING OF THE POLYPROPYLENE PHOTOTHERMAL OXIDATION

Developing numerical tools for polymer lifetime prediction constitutes a promising opportunity for shortening the duration of material certification procedures in the automotive industry without decreasing their reliability. This PhD thesis aims at modeling the photothermal oxidation of isotactic polypropylene (iPP), which is responsible for the alteration of both its mechanical and aspect properties. The adopted approach consists in coupling the kinetics of photo- and thermo-oxidation reactions with physical phenomena, such as oxygen transport and UV-light attenuation in the material thickness, in order to describe all the physico-chemical changes. Upper-scale properties, from which will be defined the end-of-life criteria, will be calculated afterwards by applying the suitable structure-property relationships. The main challenge was to extend the pre-existing kinetic model of thermal ageing to photothermal ageing by taking into account initiation reactions of photolysis. Heavy campaigns of ageing and characterization tests made on a reference iPP, as well as an exhaustive capitalization of literature data of other iPPs, have allowed elaborating a kinetic model of photothermal oxidation and to generalize it to the whole iPP family in large domains of oxygen partial pressure (from 0.2 to 50 bars), temperature (from 40 to 230°C) and UV-light exposure (variable intensities and light sources) describing both natural and accelerated ageing conditions. The experimental validation of the model has allowed substantiating the kinetic approach and showing its limitations, as well as highlighting some numerical issues. The model has been designed in order to be an upgradable numerical tool which will allow, at term, optimizing the representativeness of the ageing testing devices and the performance of commercial iPP formulations. All these theoretical and numerical developments are prone to be applied to the photothermal degradation of other types of polymer substrates, but also in other application fields of the macromolecular photochemistry such as UV-photopolymerization.
Keywords: Polypropylene, photothermal oxidation, oxygen diffusion control, screen effect, kinetic modeling, lifetime prediction.

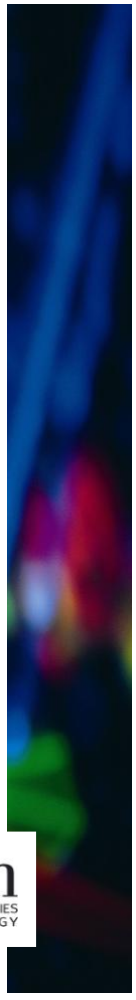

ARTS ET MÉTIERS ParisTech

ParisTech
INSTITUT DES SCIENCES ET TECHNOLOGIES
PARIS INSTITUTE OF TECHNOLOGY